SHEAR TRANSFER IN CRACKED REINFORCED CONCRETE UNDER MONOTONIC AND REPEATED LOAD

By

MOHAMED AYMAN FAREED ABD EL-KHALIK

A thesis submitted for the degree of

Doctor of Philosophy

Department of Civil Engineering

University of Glasgow

November 1987

To my parents

and

my uncle

ACKNOWLEDGEMENT

The work presented in this thesis was carried out in the department of Civil Engineering at the University of Glasgow under the general direction of Professor A. Coull whose help and encouragement is gratefully acknowledged.

I wish to express my thanks to Dr. D. R. Green, Head of the department of Civil Engineering for the facilities provided for this work.

I wish to express my indebtedness to my supervisor Dr. D. V. Phillips for his appreciated involvement in this work and for his matchless supervision as manifested in useful criticisms, sincere efforts, valuable guidance and admirable interests.

Many thanks are due to

The computor staff of the Department of Civil Engineering, in particular, Mr. G. Irving, for their help.

The staff of the concrete laboratory, in particular, the late Mr. J. Love, Mr. A. Burnett, Mr. J. Thomson, and Mr. I. Todd for their assistance in the experimental work.

My colleagues, in paricular, Dr. T. N. Megahid, Dr. M. S. Mohamed, and Mr. M. S. Bari for their useful discussions.

Mrs. J. Lawn and Mrs. A. Cunningham for their efficient typing.

Finally my thanks are reserved for my family, particularly, my parents and my uncle for their full financial support, boundless patience and continual encouragemnet through the years.

SUMMARY

This thesis presents an experimental and analytical study of the behaviour of shear transfer across cracked reinforced concrete subject to monotonic and repeated loading.

The experiments used push off specimens to produce pure shear forces along a shear plane which had a total area of 45000 mm^2. The experimental program consisted of two main test series which evaluated the transfer of shear forces by (a) dowel action alone, and (b) the combination of interface shear transfer and dowel action mechanisms. The average shear displacement, crack width, and reinforcement strains were measured for all load increments.The reinforcement ratios provided across the shear plane, the initial crack width, the type of transverse reinforcement, and the type of shear load were the main variables studied.

Assessments were also made of (a) the relative contribution of the interface shear transfer and dowel action mechanisms to the total shear, (b) shear transfer design presented in British standard BS:8110 and American Code ACI 318-83, and (c) the representation of shear transfer in nonlinear finite element analysis of structural concrete.

The research concluded that shear transfer is significantly influenced by initial crack width, reinforcement ratio and repeated load. Shear forces can be efficiently transferred across cracked surfaces by the combination of the interface shear transfer and dowel action mechanisms. The interface shear transfer mechanism sustained between 70% to 82% of the total applied shear, while the dowel action was responsible for 30% to 18% of the total shear.

The shear stiffnesses of cracked reinforced concrete degrades nonlinearly when the load is first applied and depend on both lateral and shear strains.

The current methods of BS:8110 and ACI 318—83 gave a too conservative shear transfer strength for design purpose in monotonic case of loading. An alternative formulation derived from the test results of this study agreed reasonably well with other available experimental data. The ultimate shear transfer under repeated load can be taken as 0.7— 0.9 of the shear transfer strength under monotonic load. Also formulation derived from the test results under repeated load showed safe prediction for the other experimental results under reversed cyclic load .

CONTENTS

NOTATIONS

Major symbols used in the text are listed below, others are defined as they first appear. Some symbols have different meaning in different contexts; these are clearly defined.

A_c	total area of shear or crack plane
A_s	area of reinforcing bars crossing the shear plane
A_x	projection on the y-plane of the total contact area, obtained over a unite crack area
a_x	projection of a contact length in a z-plane on the x-axis
A_y	projection on the x-plane of the total contact area, obtained over a unite crack area
a_y	projection of a contact length in a z-plane on the y-axis
D_{max}	maximum diameter of aggregate particle
d_j	maximum deflection of loaded slab
d_j'	maximum deflection of unloaded slab
E	load transfer effectiveness coefficient
E_s	Yong's modulus of steel
f_c	cylinder compressive stress of concrete
f_{cu}	cube compressive stress of concrete
f_t	tensile stress of concrete
f_y	yield stress of steel
G	shear modulus of uncracked concrete
G'	shear modulus of cracked concrete
G_f	foundation modulus of concrete

K_1^a to K_3^a interface shear transfer stiffness coefficients for the idealized hysteris loop.

K_1^d to K_3^d dowel stiffness coefficients for the idealized hysteris loop

K_i initial dowel stiffness

K_s secant shear stiffness

K_T tangent shear stiffness

L length between the plastic hinges on each side of shear plane

M_p plastic moment

N number of load cycles

n number of bars

P_K ratio between the total volume of aggregate and the concrete volume

V shear load

v shear stress

V_d dowel load

v_d dowel stress

V_{du} ultimate dowel load

v_{du} ultimate dowel stress

V_{dUR} ultimate repeated dowel load

v_{dUR} ultimate repeated dowel stress

V_u ultimate shear load

vu ultimate shear stress

V_{UR} ultimate repeated shear load

v_{UR} ultimate repeated shear stress

w crack width

w_o initial crack width

α ratio of axial stress to yield stress of steel bar

β shear retention factor

γ shear strain

γ_u ultimate shear strain

γ, θ percentage of maximum interface shear transfer or dowel stresses, respectively, at which a change in loading or unloading stiffness is accompanied under reversible cyclic load.

δ, Ψ percentage of the maximum interface shear transfer or dowel action displacements, respectively, at which a change in loading stiffness is accompanied under reversible cyclic load.

w percentage of the maximum interface shear transfer displacement exhibited when the specimen is completely unloaded under reversible cyclic load.

Δ shear displacement

Δ_d dowel displacement

Δ_p change in bar tension caused by increase in crack width.

Δ_u ultimate shear displacement

Φ bar diameter

Φ_{kr} function which accounts for variations in the axial restraining stiffness.

$\Phi_d(n)$ functional which accounts for variations in the number of loading cycles applied for the dowel action under reversible cyclic load.

ρ reinforcement ratio $= \frac{As}{bh}$

σ normal stress

σ_{pu} normal stress at which plastic deformation of the matrix occurs.

ϵ lateral or normal strain

ϵ_B measured strain at the bottom surface of steel bar

ϵ_{cr} strain for which cracking occurs

ϵ_{d} direct strain

ϵ_{f} flexure strain

ϵ_{T} measured strain at the top surface of steel bar

ϵ_{U} ultimate lateral or normal strain

μ friction coefficient

τ_{pu} shear stress plastic deformation of the matrix during sliding of the crack faces.

CHAPTER (1)

INTRODUCTION

1.1 Introduction

This work is primarily concerned with shear transfer across cracks in reinforced concrete. In many structural elements, shear forces have to be transferred across cracks formed by the applications of external normal forces, shrinkage or thermal stresses, or across inclined cracks caused by diagonal tensile stresses exceeding the tensile strength of the concrete.

Several examples where shear forces are often transferred across cracks are provided by reinforced concrete deep beams, corbels, pavement and construction joints, connection joints in precast construction and by nuclear containment vessels see Figure (1.1). In these examples failure has mainly occurred due to shear distress and although each member exhibits different mode of cracking, the mechanisms by which shear is transferred within the member may be similar.

The understanding and knowledge of the shear transfer mechanisms has progressed significantly since the joint ACI-ASCE Committee 326 issued its report 1962[1]. The motivation behind this report was the possible lack of safety by 1951 design procedures and general lack of knowledge regarding the fundamental nature of effect of shear and diagonal tension on the behaviour of reinforced concrete members. A few structural failures added momentum to intensive efforts devoted to the solution of the problem involved. The main purpose of this report was to consolidate thoughts and knowledge gained from various

experimental and analytical investigations into a form useful to practicing engineers, and also to formulate safe and workable design procedures for shear and diagonal tension in reinforced concrete beams, frames, slabs and footings. The same joint committee issued a second report in 1973[2] which reviewed recent research results and design proposal until that date in an attempt to establish a state-of-the-art knowledge of shear transfer in reinforced concrete structures. Although specific design recommendations were not presented, it was hoped that this report would help designers, researchers, and specification writers to arrive at simple, universal design concepts.

Despite a large number of references on this subject up to 1973 the question of shear strength of reinforced concrete was far from being settled. In some instances the explanations of behaviour and the design concepts that were presented were somewhat speculative. It seemed from the Joint Committee's second report[2] that the understanding of shear transfer had improved and the main types of shear transfer had been identified. However, appreciation of some of the principle shear mechanisms was relatively recent and therefore the evaluation of the contribution of those shear carrying components was only tentative.

Experimental evidence had indicated that shear forces can be effectively transferred across cracks by the bearing and frictional forces generated between the crack surfaces and by dowel action of the reinforcement crossing the crack.

The frictional and bearing forces generated by the occurrence of tangential shear displacements along a crack are shown schematically in Figure (1.2). These forces are generally known as interface shear transfer or aggregate interlock forces. The first term is adopted herein because aggregate interlock forces represent primarily the bearing action generated between the protruding particles of the cracked surfaces as they come into contact and does not reflect the additional frictional forces that are generated between the crack surfaces. There also tend to be an increase on frictional resistance due to normal forces in reinforcement both applied and as concrete cracks widen due to shear displacement.

Dowel action denotes the shear forces that can be resisted by the reinforcing bars, crossing the crack plane, normal to their longitudinal axis, see Figure (1.3).

The relative importance of these mechanisms and their interaction depend on several factors including the type and the properties of the structural member, the nature and level of loading, the extent of cracking and crack width, the size and arrangement of the reinforcement, amongst others.

In the past 15 years the aim of many studies has been to investigate the effect of such parameters on each mechanism but have been mainly concerned with monotonic loading and on the ultimate shear strength. Less attention has been paid to studying overall behaviour and other important loading cases such as reversing and repeated cyclic loadings. Such loadings frequently exist in practical situations such as offshore structures subject to wind and wave, or the high

intensity cyclic loading resulting from traffic or seismic conditions.

For example, crack planes can form in the concrete wall of a nuclear containment vessel in horizontal and vertical directions due to the internal pressure as shown in Figure (1.4). The cyclic shearing forces due to a seismic excitation must then be transmitted along these planes. In the USA current design criteria[3] for reinforced concrete nuclear containment vessels require that the structure be designed to withstand the simultaneous occurrence of internal pressurisation and the inertia forces generated by a strong motion earthquake.

In general due to insufficient information concerning shear transfer phenomena, the current international design codes such as BS:8110:Part 1:1985 Section 5[4] for design and detailing of precast, composite construction and ACI 318-83[5] Section 11.7 for shear friction,have not changed much from earlier versions which base their methods of design on the shear friction hypothesis[6] developed by Mast[7] in 1968. However, it has been stated [8],[9] that the use of this simplified theory results in conservative prediction of shear transfer strength.

In recent years the use of computational methods, such as the finite element method, for the analysis of reinforced concrete structures, has increased considerably. In fact the finite element method, which is still being refined, is now recognised as a powerful method of analysis and a future tool of design. New applications are being developed continually, particularly in nonlinear analysis. An

important aspect which has a significant effect on the nonlinear finite element analysis of reinforced concrete is the modelling of the behaviour of cracked concrete under shear stresses. Due to the insufficient information on shear transfer phenomena, its modelling is still not well established.

1.2 Scope and objectives

The detailed objectives of this work are described in Chapter (3) after a review of current knowledge is presented in Chapter (2).

In general this work is primarily an experimental investigation of shear transfer properties across cracks in reinforced concrete under both monotonic and repeated cases of loadings. Its general objectives include

- studying the difference between the behaviour of shear transfer under monotonic and repeated loadings,

- establishing the relative contributions of dowel action and interface shear transfer mechanism,

- obtaining fundamental hysteretic relationships under repeated load,

- enhancing shear transfer design provisions presented in major codes of practices such as ACI 318-83[3] and British Standard BS:8110[4] by offering additional design recommendations,

- and providing information that might help to improve the representation of shear transfer in nonlinear finite element analysis of structural concrete.

1.3 Layout of thesis

A thorough and critical review of the research conducted to date on shear transfer by dowel action, interface shear transfer mechanism and their combined actions under monotonic and repated loadings is presented in Chapter (2).

Chapter (3) presents the scope and objectives of the experimental study and the reasons for them. The experimental programme is also described showing the number of test series and main aim of each one. Details of test specimens, materials used, frame work and construction, instrumentation, testing arrangement and test procedures are described in Chapter (4).

Chapter (5) presents the results of shear transfer by the dowel action only (dowel tests) under monotonic and repeated loadings. The test results of shear transfer by the combination of dowel action and interface shear transfer mechanism (combined action tests) are presented in Chapter (6).

In Chapters (7) and (8) the experimental results and general observations obtained from Chapters (5) and (6), are thoroughly discussed and analysed according to the scope and the objectives of this study.

The main conclusions drawn from the various aspects of this study are compiled in Chapter (9) and recommendations for further work are made.

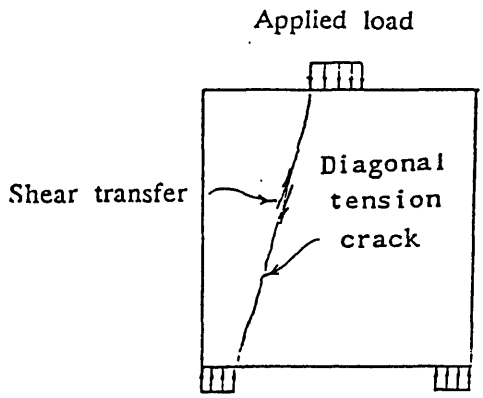

(a) Deep beam

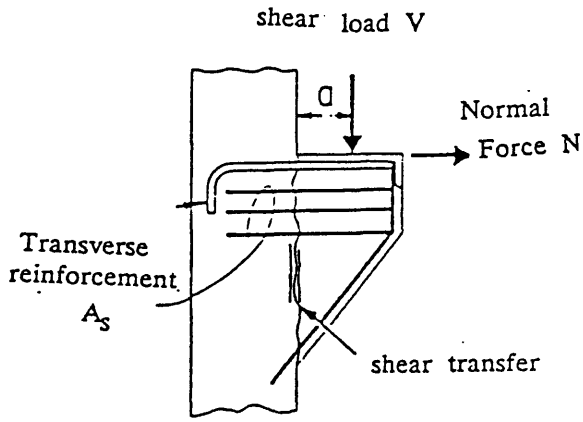

(b) Corbel

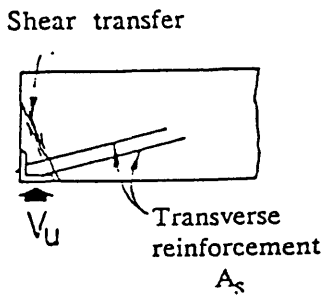

(c) Precast beam bearing

Figure(1.1) Application of shear transfer

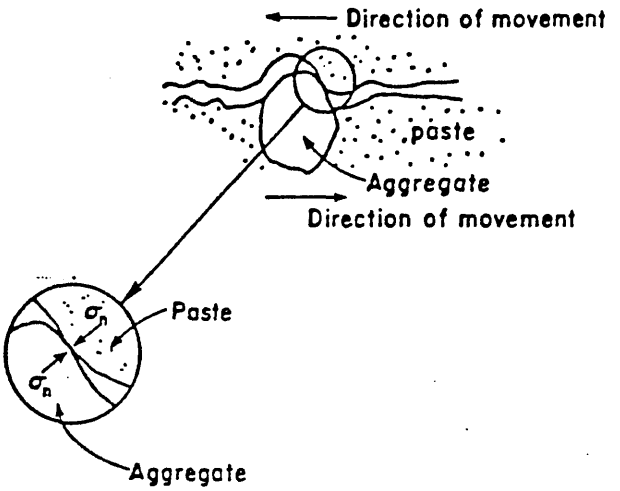

(a) Bearing action mechanism

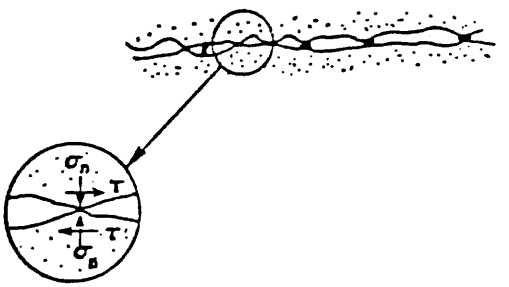

(b) Frictional mechanism

Figure (1.2) Interface shear transfer mechanism

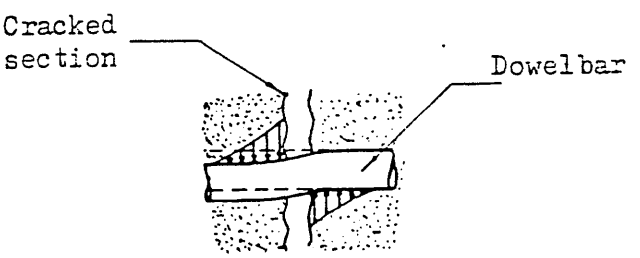

Figure (1.3) Dowel action mechanism

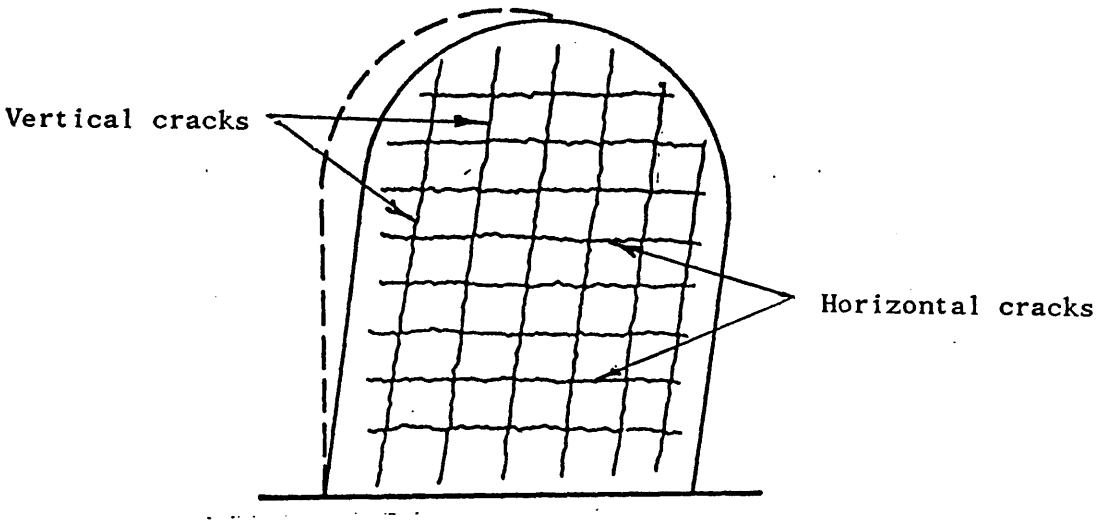

Figure (1.4) Cracking of vessel under internal pressure and seismic shear load

REFERENCES

(1) ACI-ASCE Committee 326, "Shear and Diagonal Tension", Proceedings, American Concrete Institute, Vol.59, Jan., Feb., and Mar., 1962, pp.1-30, 277-334 and 353-396.

(2) ACI-ASCE Committee 426, "The Shear Strength of Reinforced Concrete Members", Proceedings, ASCE, Vol.99, No. ST6, June 1973, pp.1091-1187.

(3) "Criteria for reinforced concrete nuclear power containment structures", ACI Committee 349 Report, Journal of the American Concrete Institute, January 1972.

(4) British Standard Institution, BS:8110-1985, "The British Standard Structural Use of Concrete", Part 1, Code of practice for design and construction.

(5) ACI Standard 318-83 "Building Code Requirement for Reinforced Concrete", American Concrete Institute, Detroit, 1983.

(6) Birkeland, P.W. and Birkeland, H.W., "Connections in precast concrete constructions", Jnl. ACI., Vol.63, No.3, March 1966, pp. 345-368.

(7) Mast, R.F., "Auxiliary reinforcement in concrete connections", Proceedings of the American Society of Civil Engineers, Vol.194, No.ST6, June 1968, pp.1485-1504.

(8) ACI 318R-83 Commentary on Building Code Requirements for Reinforced Concrete", ACI 318-83, American Concrete Institute, Detroit, 1983, pp.318R-71, 318R-72.

(9) Handbook to British Standard. BS:8110:1985, "Structural Use of Concrete", A Viewpoint Publication, 1987.

CHAPTER (2)

LITERATURE REVIEW

2.1 Introduction

This chapter presents a critical review of the previous experimental and theoretical studies of interface shear transfer and dowel action as separate mechanisms, as well as their combined action, under both monotonic and cyclic load.

2.2 Interface shear transfer under monotonic loading

2.2.1 Experimental investigations

The main aim of previous studies can be summarised as follows:

(a) To determine the internal shear force distributions in reinforced concrete beams [1],[3],[4], [5].

(b) To assess the contribution of the interface shear transfer mechanism to the total shear load [6],[7], [8].

(c) To determine the shear load-displacement relationship of interface shear transfer [11,(15),(20)].

(d) To evaluate the effect of several parameters on the interface shear transfer mechanism [8],[9],[10],[11],[12].

Early researchers such as Jones [3], Watstein and Mathey [5], Kani [4] and Archary and Kemp [2] conducted extensive experimental studies to determine the internal shear force distribution in reinforced concrete beams by means of elaborate test setups and specimens. However, most of these tests did not take into account the shear

forces that may be transferred by the interface shear transfer mechanism across the diagonal cracks and thus overestimated severely the contribution of dowel action and concrete in compression zone.

Taylor[1] presented what is probably the first rational description of the mobilisation of the interface shear forces and their influence on diagonal cracking in beams. He suggested that after a shear crack is formed, as shown in Figure (2.1), any further increase in load will displace the beam section marked B relative to beam section A, causing it to rotates about point X. Since the crack follows a curved path, the rotation between the beam sections will interlock the aggregate particles protruding from each cracked plane and will generate a tangential force across the crack. Other diagonal cracks, shown by the dotted line in Figure (2.1), will initiate if stresses induced by the tangential force exceed the concrete tensile capacity.

To test this hypothesis, Taylor performed a test on the special beam shown in Figure (2.2), in which thin plastic sheeting was inserted in preformanced cracks on the central sections of the shear span in order to eliminate the interface shear transfer forces. The ultimate shear strength of the special beam was 22% smaller than that observed on a control beam in which the interface shear transfer forces were not eliminated. The collapse mechanism observed in the special beam was caused by an extension of the preformed crack to the loading blocks and by splitting of the concrete along the reinforcement axis.

Taylor concluded that the interface shear transfer mechanism can sustain considerable forces and consequently, cannot be neglected when the internal force distribution of a crack beam is analysed.

Fenwick and Paulay[6], Taylor[8] and Sharma[7] also tested special beam specimens to assess the contribution of the interface shear transfer mechanism. All of these investigations concluded that the interface shear transfer mechanism resisted between 33% to 50% of the total shear applied to the section.

These investigations, however, did not enable the researchers to determine fundamental shear load-displacement relationships. Beam specimens do not permit a systematic evaluation of the effect of several important parameters such as initial crack width, concrete strength, aggregate size, and the restraining effect of the reinforcement crossing the crack. (i.e. normal restraining stiffness). The cracked area over which the shear force is transferred is not well defined since the crack width varies and hence the magnitude of the shear stress will vary over the cracked plane.

Direct shear tests aim to overcome these difficulties by applying a constant shear over a given plane section of known dimensions.The systematic evaluation of the parameters can be made, because these tests can better isolate the effect of a given variable on the overall behaviour. Such tests have been conducted by Fenwick and Paulay[6], Houde and Mirza[10], Paulay and Loeber[11], White and Holley[9], Laible et al[12], Millard and Johnson[15], and Walraven [20]. A variety of test specimens and setups have been employed.

Fenwick and Paulay[6] conducted tests on plain concrete specimens as shown in Figure (2.3). The tests were designed to study the effect of initial crack width and concrete strength on the interface shear transfer mechanism. Initial crack widths were varied between 0.06mm

and 0.36mm, while the concrete strength, as measured by 4" concrete cubes, ranged between 19 N/mm^2 to 56 N/mm^2. The specimen was cracked prior to testing by an external tensile force. The crack plane was predetermined by a groove along the outline of the specimen. After cracking the crack width was kept constant, by adjusting it after every load increment by means of an external force normal to the crack plane. Values for this force were not given. The shear displacements as well as the width of the crack were measured. In the first series of tests the concrete strength was kept constant on 33 N/mm^2, and the initial width of the preformed crack was varied. The average curves obtained are presented in Figure (2.4). In the second series of tests the influence of the concrete strength was investigated for a constant crack width 0.199 mm. The results of this series are shown in Figure (2.5).

All specimens failed as a result of flexural tension cracking of the concrete, see Figure (2.3). In no case was the interface shear transfer action observed to break down, so that the relations are only valid for a restricted range shown by the dotted line in Figure (2.4.) in which the blocks did not exhibit flexural cracks. It was found that the shear stiffness of the specimens increased with decreasing initial crack width and increasing concrete strength. From Figures (2.4) and (2.5) it is obvious that the crack width had a larger influence on the shear stiffness rather than the concrete strength.

Houde and Mirza[10] carried out an investigation on specimens which were to a certain extent comparable with those of Fenwick and Paulay. Direct shear tests were performed on precracked concrete block specimens, Figure (2.6). After the concrete blocks were cracked

along the shear plane and the initial crack width was set to a predetermined value, the specimens were sheared monotonically to failure.

The influence of the crack width (0.050mm - 0.50mm), the concrete compressive strength (16.5 - 51 N/mm^2) and the maximum aggregate particle size (10 - 19mm) were the object of the investigation. A set of the experimentally obtained shear stress-displacement curves is presented in Figure *(2.7)*. Specimens failed as a result of flexural tension cracking of concrete similar to those of Fenwick and Paulay[6].

The results obtained indicated that the variation of the shear stiffness of cracked concrete with compressive concrete strength was similar to that found by Fenwick and Paulay[6], i.e. proportional to the square root of concrete compressive strength. Within the range of the maximum aggregate sizes tested the influence of the maximum aggregate size was found to be negligible compared to the effect of the crack width and the concrete strength.

Paulay and Loeber[11] avoided in their experiments the disadvantages concerned with the test arrangements used by Fenwick/Paulay and Houd/Mirza by using the direct shear specimens shown in Figure (2.8). The specimen was highly reinforced with ties and flexural steel in order to avoid any premature flexural or diagonal cracks near the shear plane. Crack width and shear displacement were measured at both sides of the specimen. The test results were not influenced by the development of secondary cracks in the specimens.

The tests were carried out with a constant concrete strength equal to 37 N/mm^2, since the influence of the concrete strength was established in the earlier program already described[6]. The test series was designed to investigate the effect of the aggregate shape and size, and of initial crack width under monotonic and cyclic loading. Paulay and Loeber observed that the shear stress-displacement relation essentially depending on the crack width. Shape and size of the aggregate particles had for the range tested (9.5mm-19mm, round and crushed) no significant influence. The relation between shear stress-shear displacement for monotonic loading is represented in Figure (2.9). A bilinear shear stress-shear displacement curve was observed. Paulay and Loeber attributed the increase in shear stiffness to the bearing between the aggregate particles projecting across the crack and the matrix of the opposite face. Houde and Mirza[10] attributed this trend to the increase of the contact area of the two crack faces due to the localised crushing of concrete on each crack face at the higher stress level which causes the shear stiffness to increase.

Taylor[8] devised a test setup, illustrated in Figure (2.10) which permitted the simultaneous occurrence of shear and normal displacements. The test specimen, an unreinforced concrete block with a precracked section was bolted to a pair of linked crossheads. The lower crosshead was bolted to the floor and upper crosshead was pulled horizontally. The effect of the crack width to shear displacement ratio, the concrete strength and aggregate type were investigated. The ratio of normal to shear displacement was kept constant throughout the test to simulate the real crack behaviour in beams.

However, experiments[13], in which measurements were taken across and along a crack in actual beam from the beginning of loading, revealed an increasing ratio between shear and normal displacements of the cracked interfaces, as the load was increased.

However, it was concluded from the different test results that both the ultimate shear stress and ultimate crack width decreased as a function of crack width to shear displacement ratio, Figures (2.11) and (2.12). Taylor's results also showed that the type of aggregate is important but that the parameter is probably the relative strength of aggregate to cement matrix. If the aggregate is relatively weak compared with the matrix, the aggregate fails when the crack is formed, which results in a smoother crack surface than would be obtained if the aggregate were stronger than the matrix. In the latter case bond between the aggregate and the matrix fails when the crack is formed, which results in the maximum roughness possible. This was demonstrated by means of a concrete with a relatively weak aggregate (Limestone). Figure (2.13) shows that for approximately equal concrete strengths (49-53 N/mm^2) lower ultimate shear values were observed for Limestone than for a concrete with a stronger aggregate. It could also be observed that a reduction of the strength of the Limestone concrete to 30 N/mm^2 resulted in a higher shear resistance since in this case the aggregate-matrix bond failed before the aggregate itself was split and a rougher crack surface was obtained.

Millard/Johnson[15] devised tests of a new type to examine independently the interface shear transfer mechanism. The specimens used for testing consisted of rectangular concrete prisms with dimensions as shown in Figure (2.14). Dowel action effects were

eliminated from tests by placing the reinforcement within ducts with diameters larger than the diameters of the reinforcement. The size of the reinforcing bars used were 8mm, 12mm, 16mm and 25mm diameter to provide different normal stiffnesses.Millard/Johnson claimed that the dowel stiffness resulting from flexure of the bars over their entire length was negligible. The test specimens were precracked before applying the shear load by means of direct forces acting through knife-edge bearings adjacent to the crack. Two additional forces were applied at the ends of the specimens via distribution beams, needle roller bearings and knife-edge bearing to maintain equilibrium, see Figure (2.15). Crack opening was allowed to occur naturally and was only controlled by the restraint provided by the normal stiffness of the reinforcing bars.

The principal parameters investigated were:

(1) The initial crack width, from 0.063 to 0.75mm.

(2) The cube strength of concrete, from 29 to 52 N/mm^2.

(3) The direct stiffness normal to the crack plane.

For the range of initial crack widths investigated, the shear stiffness across the crack and the ultimate shear stress both decreased as the initial crack width was increased, see Figure (2.16). The shear stiffness also diminished with increasing shear displacement.

Irrespective of the initial crack width, an increase in the axial stiffness restraining crack widening resulted in a reduction in the ratio of crack widening to shear displacement and an increase in the shear stiffness and ultimate shear stress, Figure (2.17).

Also, from the test results it was concluded that an increase in the strength of the concrete from 30 to 52.1 N/mm^2 had only a small effect upon the behaviour.

In one test in which the crack width was restored to its initial value after each increment of shear load, there was much higher shear stiffness than when the crack width was allowed to increase. This behaviour was similar to that observed in the Paulay/Loeber[11] and Houd/Mirza[10] investigations, Figure (2.18) and shows that caution must be used in applying the results of such tests to situations where the crack width does not remain constant. Millard/Johnson pointed out that the differences between these test results may be related to the difference of the concrete mix designs and strengths used.

2.2.2 Theoretical models

Local and global roughness :

Laible, White and Gergly[12], proposed a model to explain the behaviour of the interface shear transfer mechanism according to the test results. They subdivided the roughness of the crack surfaces into a local and global roughness as illustrated in Figure (2.19). It was stated that there are two modes of behaviour:

(1) bearing and crushing due to local roughness (i.e. interlocking of the fine aggregate particles).

(2) Sliding and overriding action (frictional mode) due to global roughness (i.e. interlocking of the coarse aggregate particles).

It was claimed that bearing mode dominates the behaviour when the initial crack width is less than approximately 0.25mm,local concrete crushing occurs and there is relatively little overriding. Consequently the increase in the crack width and the normal forces to the crack plane are not as large as in the frictional mode of behaviour. The resistance in this mode is highly dependent on the local roughness of the surface and the amount of the initial crack width and less dependent on the amount of the normal restraint. The fricitional mode of behaviour predominate when initial crack width is 0.50mm or greater. There is a little crushing of concrete and appreciable overriding. Consequently, the increase in crack width and normal forces is larger than in the bearing mode of behaviour.

Sawtooth crack model

Jimenez et al[16] presented an analytical model to explain the results obtained. The crack profile was modelled as sawtooth with a mean slope θ (Figure 2.20). Upon the application of shear forces V, the top and bottom block displace horizontally until contact is established between the inclined faces. Up to this stage the only resistance to sliding is provided by the dowel action of the reinforcement crossing the crack if any. Once contact between the inclined faces is obtained, the stiffness of the system increases considerably. The forces are transferred across the crack by the normal and frictional stresses generated at the surface contact area as shown in Figure (2.20). The following equilibrium equations in the horizontal and vertical planes can be established:

$$V = A_o [\sigma_n \cos\theta + \tau \sin\theta] \quad (2.1)$$

$$\Delta_p = A_o [\sigma_n \sin\theta - \tau \cos\theta] \quad (2.2)$$

where

V = shear force transferred across cracks

σ_n = normal stress at the contact area

τ = frictional stress generated at contact area

θ = angle of inclination of contact plane with respect to the horizontal plane

A_o = contact area across which the bearing and frictional stresses are transferred

Δ_p = change in bar tension caused by increase in crack width.

In the above equation the shear forces taken by the dowel have been neglected, although it is assumed that a normal restraint stiffness is provided by the reinforcement crossing the crack. The angle of inclination θ is a function of the aggregate size, angularity, and the relative strength of the aggregate and cement paste. In a cracked plane the angle of inclination of the protruding particles on the surface can vary, but for the purpose of derivation it is assumed constant throughout the shear plane. The contact area A_o is also a function of the aggregate size and relative strength between aggregate and cement paste.

Solving Equation 2.2 results in

$$\sigma_n = \left[\frac{\Delta_p}{A_o} + \tau \cos\theta\right] \cdot \frac{1}{\sin\theta} \qquad (2.3)$$

Substituting Equation (2.3) into Equation (2.1) yields

$$V = \Delta_p \cot\theta + \frac{A_o \tau}{\sin\theta} \qquad (2.4)$$

Thus the total shear transferred across a shear plane is a function of the change in the bar tension, and the frictional stress generated

at the crack surface.

Jimenez et al stated that the change in bar tension measured experimentally was small and hence the contribution of the first term in equation (2.4) can be ignored.

The shear displacement is then related to the frictional and bearing stresses described by Laible et al[12].

$$\Delta = A_0 [\beta_1 \tau + \beta_2 \sigma_n] \qquad (2.5)$$

where β_1 and β_2 are empirically derived flexibility coefficients for the friction and bearing actions.

A dimensionally inconsistent expression was then formulated relating the interface shear stiffness to the crack width and stiffness normal to the plane of the cracking.

This model was reasonably criticised by Millard[15]. Firstly, the elimination of the first term in equation (2.4) is not a rational assumption. In aggregate interlock tests the reinforcement is unbonded and the normal restraining stiffness will be quite low. But, in the practical case of the reinforced crack the normal restraining stiffness will be quite high due to local anchorage and the bond between the concrete and the reinforcing bars. In such circumstances the term Δp can not be neglected. Secondly, it is assumed that the crack faces are rigid and the ratio of crack widening to shear displacement is constant, regardless of the forces restraining the crack from widening. This contradicts experimental evidence. Thirdly, the ratio of crack widening to shear

displacement will be influenced by the crack width because of the possibility of the change of the contact angle.

Fardis and Buyukozturk (17) Model:

Figure (2.21) shows the crack configuration considered by Fardis and Buyukozturk. The random function that describes the stochastic shape of the global roughness is assumed to have a constant mean value. The positive stress resultants, N and V caused by external loading acting on the concrete block are shown in Figure (2.21). In the absence of these internal forces the two faces of the crack have identical shapes and they are separated by an "initial crack width" $w_o(x)$. With the existence of the internal forces the crack width increases by $\Delta w(x)$ and the "shear displacement" Δ, of the upper block with respect to the lower one develops along the x direction. During the relative movement of the two blocks the lower block is considered fixed. Furthermore, the global roughness of both faces of the crack is assumed to retain its shape during this relative movement, whereas the local roughness is allowed to be ground and diminished in the contact areas between the two faces, giving rise to finite contact areas. For mathematical convenience the finite contact areas of the two faces are idealised as points of contact between the concrete blocks along the global roughness. As shown in Figure (2.22), the shape of the crack face was expressed as a series of parabolic segments given by

$$y = a_k - b_k + b \left[1 - \frac{2(x_k - x)}{L_k} \right]^2 \quad \text{if } x_k - \frac{L_k}{2} < x < x_k \qquad (2.6)$$

$$y = a_k - b_k + b_k \left[1 - \frac{2(x - x_k)}{L_k} \right]^2 \quad \text{if } x_k < x < x_k + \frac{L_k}{2} \qquad (2.7)$$

For a two dimensional problem, it is assumed that there are two points of contact over a finite concrete length. At each contact point the tangent of the upper and lower curve will have the same slope, Figure (2.23). From the above assumptions and the overall equilibrium an expression for the shear strength could be derived.

$$V = A_d\Delta + b_a A_n w_o + e' A_n \Delta \qquad (2.8)$$

where

A_d, A_n are the dowel and extension stiffnesses of the reinforcement

Δ is shear displacement

b_a, e' are frictional coefficients derived from equations (2.6) and (2.7).

w_o is initial crack width.

It was then argued that because any crack path is inherently stochastic it is not possible to evaluate the terms in Equations (2.6) and (2.7) and hence b_a and e'. However, it was inferred from the qualitative form of the expression that an increase in the initial crack width will result in a decrease in the shear stiffness. These trends agree with the experimental observations.

Having developed the model but being unable to evaluate it, the authors then suggest that the shear stress-shear displacement relationship is bilinear. At low slip values, when the crack surfaces have not made contact, only dowel action is resisting shear. At high values of shear displacement a linear interface shear transfer stiffness is proposed. However, this proposal is

inconsistent with fundamental interface shear transfer model described. The shear stiffness is dependent upon the contact angle between the two crack surfaces. As shear displacement occurs the contact angle must diminish and hence cause a reduction in the interface shear transfer stiffness.

Two Phase Model by Walraven[20],[21]

Walraven assumed that concrete can be represented as a two-phase system: in a matrix (hardened cement paste) a collection of aggregate particles are embedded. Generally the strength and stiffness of the aggregate particles are greater than those of the matrix. However, the contact area between the two materials, the bond zone, is the weakest link of the system. Hence, cracking occurs commonly through the matrix, but along the circumference of the aggregate particles. These particles are simplified to spheres, which can be intersected by the crack plane at all depths with the same probability. This results in a crack structure as represented in Figure (2.24).

Hardened cement paste is a visco-elastic material: the deformations provoked by stresses are only partially elastic, for the other part they are plastic. Under multi-axial stresses, in the area between the aggregate particles in concrete, large plastic deformations can occur as a result of pore-volume reduction. Since plastic deformations are expected to predominate over elastic deformations, the stress-strain relation of the matrix material, consisting of hardened cement paste with aggregate particles smaller than 0.25 mm, is assumed to be rigid-plastic, as represented in Figure (2.25). The stress at which plastic deformation occurs is denoted by σ_{pu}. Hence it can be expected that, during shear displacement of the crack

faces, contact areas develop on the surface of the particles, with interlocking between the crack faces, due to plastic deformation of the matrix.

Figure (2.26) shows the formation of this type of area as a result of shear displacement in the direction of the X-axis. The stresses at these contact areas produce reactions in the directions of all principal axes. On the assumption of spherical particles, the resulting component in the z-direction is zero, just as for a real crack face, if the crack area is not too small. As a result it is possible to consider a cracked concrete body, as presented in Figure (2.27a), as an assembly of a large number of slices each of finite width, Figure (2.27c), and it is possible to deduce the overall behaviour of the crack by first studying the properties of this thin slice.

Figure (2.28) shows a cross section through a particle lying in a Z-plane in which there is a line of contact between the opposite crack faces. The projection of this line of contact on the X and Y directions are a_x and a_y. The shaded area represents that part of the matrix which has disappeared due to plastic deformation of the matrix.

If the shear load on the plane of cracking is increased and crack opening is countered by restraining forces, a mechanism will develop which can be described as follows.

The contact areas tend initially to slide, and as a result of this sliding, the contact area is reduced, so that too high contact stresses occur. Hence, further plastic deformation occurs, until

equilibrium of forces is obtained in the X and Y directions. The stresses at the contact area are resolved into a stress σ_{pu}, normal to the contact area, and a stress τ_{pu}, tangential to this area. The stresses σ_{pu} and τ_{pu} are interrelated by the condition that the contact areas are about to slide. Therefore, the equilibrium conditions are formulated based on a uniform critical stress combination (σ_{pu}, τ_{pu}), with

$$\tau_{pu} = \mu.\sigma_{pu} \qquad (2.9)$$

where u is coefficient of friction.

Based on the previous assumptions, the components of the contact forces in the X and Y directions can be derived. Figure (2.28b) shows the equilibrium conditions at a particle surface. The reactions in X and Y directions can be formulated as:

$$F_y = \sigma_{pu}.a_x - \tau_{pu}.a_y \qquad (2.10a)$$

$$F_x = \sigma_{pu}.a_y + \tau_{pu}.a_x \qquad (2.10b)$$

Inserting τ_{pu} from equation (2.9) into these equations and subsequently summing all particles contributions, the total resistance of the crack area considered (with a unit width dz = 1, figure (2.27c) can be formulated as:

$$\Sigma F_y = \sigma_{pu} (\Sigma a_x - \mu \underline{\Sigma a_y}) \qquad (2.11a)$$

$$\Sigma F_x = \sigma_{pu} (\Sigma a_y + \mu \underline{\Sigma a_x}) \qquad (2.11b)$$

Expressions for the total projected areas $A_x = \Sigma a_x$ and $A_y = \Sigma a_y$ as a function of the crack width w, and shear displacement Δ were derived

and are represented graphically as shown in Figure (2.29).

Tests were then carried out by Walraven for two reasons to:

(a) establish expressions for σ_{pu} and μ

(b) establish the reliability of the model.

The set-up of the tests is shown in Figure (2.30). The specimens were precracked before the actual testing. Crack opening during the actual shear test was counteracted by external restraining bars, clamping the two specimen halves together. The parameters σ_{pu}, the matrix yielding strength, and μ, the coefficient of friction, were established by fitting equations (2.11a) and (2.11b) to the experimental results. Walraven found that the best results were obtained for a friction coefficient $\mu = 0.40$ and matrix yield stress $\sigma_{pu} = 6.39\ f_{cu}^{0.56}$ (see Figures 2.31 and 2.32).

As the proposed model was in adequate agreement with the experimental results, it was then used for parametric studies to obtain a better insight into the fundamental mechanism of interface shear transfer and the following parameters were investigated:

(a) The role of the friction between aggregate and matrix.

It was shown that a friction coefficient equal to 0.4 resulted in the best fitting of the curves to the experimental results.In order to visualise the influence of friction calculations were carried out for mix with maximum aggregate size D_{max} = 16mm, σ_{pu} = 50 N/mm^2 corresponding with f_{cu} = 40 N/mm^2, P_k = 0.75 (ratio between the total volume of the aggregate and the concrete volume) and μ = 0,and 0.4.

The results are shown in Figure (2.33) for crack widths of w = 0.2, 0.6 and 1.0mm. This figure shows that for large values of shear displacement the frictional forces on the aggregate contributed to about 50% of the total shear resistance. For low shear displacement the friction did not contribute much and most of the shear resistance was due to bearing action and crushing of the cement paste.

(b) The effect of aggregate size.

To study the effect of the aggregate size, two mixtures were compared. Both had the same properties, except for the maximum particle diameter, which was 16mm and 32mm respectively. The results of this comparison are shown in Figure (2.34). It is seen that the normal stress σ is not very susceptible to this variation, but that the shear stress τ is more affected as the crack width becomes greater.

The expressions derived to give the projected contact area A_x and A_y in Figure (2.29) are complex and so the following linear regression equations were derived by Walraven to describe the experimental results

$$\tau = \frac{f_{cu}}{30} + \left[1.8\, w^{-0.8} + \left[0.234\, w^{0.707} - 0.20 \right] . f_{cu} \right] \Delta \quad (\tau \geq 0) \qquad (2.12a)$$

$$\sigma = -\frac{f_{cu}}{20} + \left[1.35\, w^{-0.63} + \left[0.191\, w^{0.552} - 0.15 \right] . f_{cu} \right] \Delta \quad (\sigma \geq 0) \qquad (2.12b)$$

where

τ = shear stress across the crack plane (N/mm^2)

σ = normal stress to the crack plane (N/mm^2)

f_{cu} = cube compressive strength of concrete (N/mm^2)

w = crack width (mm)

Δ = shear displacement (mm)

2.2.3 Summary of research on interface shear transfer under monotonic loading

Summarizing the work on interface shear transfer under monotonic loading the following points have been observed:

1. Interface shear transfer stiffness increased with decreasing initial crack width and increasing concrete strength. The initial crack width has a greater influence compared to concrete strength.

2. Within the range of maximum aggregate size tested (10-19 mm) the influence of the maximum aggregate size was found insignificant compared to the effect of initial crack width and concrete strength.

3. The relative strengths of aggregate and concrete can exert a major influence on the interface shear transfer stiffness but the absolute strengths are of lesser importance.

4. An increase in the axial stiffness restraining crack widening resulted in an increase in the shear stiffness and ultimate shear stress.

5. Laible et al[12] presented a simple model of interface shear transfer mechanism as a combination of crushing and friction. The

relative importance of these actions would appear to depend upon the initial crack width.

6. Walraven[20] presented a more sophisticated and detailed model considering concrete as a two phase material with rigid/plastic components. The shear forces can be transferred by the combination of both crushing and sliding actions. However, contact between any rigid aggregate particles protruding from opposite sides of the crack was not considered.

2.3 Dowel action under monotonic loading

2.3.1 Experimental investigations

The tests on dowel action which have been carried out can be subdivided into four groups:-

(1) Pavement joints
(2) Divided beam tests
(3) Beam end tests
(4) Direct tests.

(1) Pavement joints

The earlier experimental investigations on dowel action mechanisms were performed on contraction joints by Marcus[22], Finney[23] and Teller/Cashell[24]. The main interest of these investigators was directed towards the assessment of an experimental value for the modulus of subgrade reaction (G_f) offered by the concrete which could be used in a beam on elastic foundation model presented by Friberg[25]. Another major objective of this research was to determine the dowel effectiveness of the longitudinal rebars in

transferring the load from the loaded slab to the adjacent slab. These investigations did not concentrate on the development of fundamental load-displacement relationships for the dowel mechanism.

The research revealed that the modulus of subgrade reaction decreased with increasing bar diameter but it must be noted, however, that for a given bar diameter a considerable variation of G_f was observed. Typical values ranged between 81 to 2334 N/mm^3 with average values between 271 to 678.6 N/mm^3. This scatter in value of G_f can be attributed to the quality of the concrete immediately under the bar. So, even when the same concrete composition is used, a scatter is obtained, depending on the position of the bar during casting. When the direction of the bar is parallel to the direction of casting, Figure (2.35a) a greater value of G_f can be expected than the case of a bar perpendicular to this direction, Figure (2.35b), since during vibration local segregation of water under the bar can be expected resulting in lower concrete quality. Also for bars situated nearer to the bottom of a construction, Figure (2.35c), a greater value for G_f may be expected, since the density of the concrete increases from the top to the bottom.

From the research on pavement joints, it was also concluded that the dowel load transfer capacity increased with increasing bar diameter and with reduced joint width. Failure of the specimens occurred by the development of a vertical crack below the dowel, indicating that high circumferential tensile stresses generated by the bearing dowel.

The results from the pavement joints investigation, however, cannot be directly applied to other structural problems where significant nonlinear response, as induced by concrete cracking and other

material nonlinearities, are observed.

(2) Divided Beam Tests

Divided beam tests are designed to study the dowel action mechanism when little or no tension exists in the reinforcement. These types of tests were conducted by Krefeld and Thurston[27], Bauman[28] and Taylor[29]. Krefeld and Thurston[27] tested nine beam specimens as shown in Figure (2.36), as a part of study on the shear strength of reinforced concrete beams. The specimens, reinforced with either 2#7 (2 @ 22mm) or 2#9 (2 @ 28mm) bars, were loaded on the central portion of the beam. This section of the beam was cast independently of the remaining section and was connected to it only by the longitudinal reinforcement. Thus, the loading applied to the central beam section was resisted by the dowel action of the longitudinal reinforcement.

The investigtion considered the effect of the concrete cover provided to the reinforcement, the bar diameter, the beam width, and the distance of the preformed crack from the support.

The load-displacement relationships, shown in Figure (2.37), exhibited approximately linear response up to the formation of a major splitting crack along the reinforcement. The splitting cracks formed gradually and eventually propagated to the support, increasing significantly the dowel displacement. The propogation can be minimised by the presence of stirrups in the shear span of the beam.

It was also concluded that the ultimate force decreased with increasing distance from the crack to the support and that resistance increased with larger concrete covers to the reinforcement. The

contribution of the dowel was estimated as 33% of the total shear carried by the beam.

Bauman[28] used specimen designed by Krefeld and Thurston to extend the investigation into dowel behaviour. The main test program evaluated the effects on the dowel strength of the crack width of the preformed crack, the beam dimensions, the location and number of stirrups, the diameter of the dowel, the layers of the reinforcement present in the beam and the concrete strength.

From these experiments, Bauman was able to establish the dowel stiffness relationships shown in Figure (2.38). The dowel stiffness is essentially linear up to the splitting cracking load v_{do}. After this cracking, a sudden increase in dowel displacement will occur and if there are no stirrups in the vicinity of the crack, the load displacement curve will follow curve 2 in Figure (2.38). If a stirrup is placed close to the crack, the reinforcement will be able to sustain additional loads as shown in the same figure, and will follow curve 3

Bauman concluded that the dowel splitting load increased with increasing beam width, bar diameter, and the concrete strength. The beam depth, concrete cover, and the width of the preformed crack did not affect the dowel capacity of the reinforcement. The presence of two layers of reinforcement of the same total area increased the dowel strength compared to the specimens with only one layer by approximately 40%. After the occurrence of splitting cracks in the beams, stirrups were beneficial in increasing the dowel capacity if they were within one inch of the diagonal crack. Stirrups placed further than one inch did not provide significant support to the

longitudinal reinforcement.

Taylor[29] also used the divided beam test setup for model and prototype tests of the dowel action mechanism. The model beam loading arrangement permitted the measurement of the load displacement curves after dowel splitting occurred. Taylor also studied the effect on the dowel strength and stiffness of the concrete strength, the distance from the support to the inclined crack, the concrete cover and spacing of the bars within the beam, the layers of reinforcement provided, and the distance from the crack to the closest stirrup.

A typical dowel load-displacement curve is given in Figure (2.39). The stiffness is essentially linear at very low loads, but as the cracking load is approached, increasing nonlinear behaviour is exhibited. After cracking, the dowel load drops suddenly to approximately half the dowel cracking load, and remains constant thereafter. Taylor idealized the load-displacement curves after cracking by the curve shown in Figure (2.40). The load-displacement curves for specimens with stirrups in the crack vicinity are also shown in Figure (2.41). The shapes of the curves agree with the results presented by Bauman, where the stirrups increased the dowel capacity of the reinforcement after dowel splitting. Their effectiveness increased significantly as the stirrup approached the diagonal crack.

Taylor concluded that the dowel capacity of the reinforcement increased with increasing concrete tensile strength, beam net width, and to a lesser degree, with increasing concrete cover provided to the reinforcement. Failure was always caused by concrete splitting

in a horizontal plane through the reinforcement. Variations in the distance between the support and the diagonal crack also affected the dowel capacity. Taylor also found that stirrups are effective after cracking if they are placed within one inch of the diagonal crack.

(3) Beam-end tests

Beam end tests enabled researchers to study the effect of the interaction between tensile and dowel forces on the stiffness relations and ultimate dowel strength. Beam end tests can also be used to examine the anchorage properties of the reinforcement with and without dowel forces present. Sharma[7], Houde[30], Kemp and Wilhelm[31] used the specimen shown in Figure (2.42).

In general, failure occurred by concrete splitting along the reinforcement longitudinal axis, on either a vertical or horizontal plane. The test results generally revealed that a significant reduction in the dowel stiffness and capacity is observed as the axial stress in the reinforcement exceeds 80% of the axial yield stress, but otherwise had little influence.

(4) Direct dowel tests:

In direct dowel tests failure may occur either by splitting along the reinforcement axis as in the tests conducted by Eleiott[32] and Stanton[33] or by yielding of the reinforcement and by bearing failure of the concrete as those reported by Dulaska[34], Hofbeck et al[35], Paulay et al[26], Walraven[20] and Millard[15].

Dulacsk[34], performed direct dowel tests using the specimen shown in Figure (2.43). The interface shear transfer was eliminated by means

of two layers of brass sheets placed at the shear plane. The major parameters considered included

(a) the effect of the angle inclination of the reinforcement with respect to the horizontal plane
(b) the dowel diameter
(c) the concrete tensile strength.

The typical load displacement relationship, Figure (2.44), exhibits elasto-plastic behaviour for the dowel action mechanism.

Dulacska concluded that the ultimate dowel force increased in an approximately linear manner with increasing bar diameter and concrete strength. The angle of inclination of the dowel bar did not show any influence on the ultimate dowel capacity.

Hofbeck et al[35], reported a limited investigation on dowel action using a specimen similar to that used by Dulaska. However, instead of eliminating the interface shear transfer action, Hofbeck used rubber sleeves 50mm long and 3.2mm thick secured around the legs of the stirrups where they crossed the crack to eliminate the dowel action. The effectiveness of the dowel action mode was then assessed by comparing these test series with other series in which dowel action was not eliminated. It was concluded that dowel action of reinforcing bars crossing the shear plane is insignificant in uncracked concrete, but is substantial in concrete with a pre-existing crack along the shear plane.

Paulay, Park and Phillips[26] conducted a limited investigation on the dowel action of the reinforcement using the test specimen and

setup shown in Figure (2.45). The interface shear transfer mechanism was eliminated by means of smooth waxed surfaces. The parameters evaluated were the reinforcement percentage and bar diameter.

Typical results for the dowel load-displacement relationship are presented in Figure (2.46). The dowel stiffness curve is highly nonlinear and its shape is similar to that determined by Dulacska. Figure (2.46a) shows the load-displacement curves for constant reinforcement ratio provided by different bar diameters. These curves lie within a narrow range, suggesting that the shear resistance provided by the dowel is proportional to the bar area. It has been claimed that the direct shear and kinking marks are the principle mechanism of the dowel action. From Figure (2.46), it can be concluded that the bar diameter has much lesser effect than that of the reinforcement area on both dowel stiffness and dowel capacity of the test specimens.

Millard and Johnson[15] used the specimen shown in Figure (2.47). Interface shear transfer mechanism was eliminated by the construction of a smooth, low friction crack passing through the centre of the specimen. The principal parameters investigated were:

(1) the reinforcement diameter from 8mm to 16mm

(2) the concrete strength from 27.6 to 54 N/mm^2

(3) the axial stress in the reinforcement from zero to 344 N/mm^2

Both dowel displacement and crack width were measured during the test. Strain gauges were used to measure the strains in the dowel bars at the crack plane. Unfortunately, during five tests out of

seven, no consistent pattern was observed from the reading of the strain gauges. This was attributed to

(1) asymmetry due to imperfect location of the gauges at the point of the contraflexure or to non homogenity of the concrete,

(2) movement of the point of contraflexure as the concrete was damaged during testing.

Millard and Johnson concluded that increasing the diameter of the reinforcement resulted in a higher dowel stiffness and ultimate stress. There was also an increasing tendency for the smooth crack to widen as shown in Figure (2.48). A splitting failure was observed in specimens with 12mm or 16mm diameter bars, but also there was more spalling associated with larger bars (see Figure 2.49). It was suggested that this expansive spalling may explain the tendency for the crack to widen. Also, it was concluded that an increase in the concrete strength from 27.6 N/mm^2 to 54 N/mm^2 had a relatively small effect upon the behaviour. Increasing axial tensile force in the reinforcement resulted in lower dowel stiffnesses and ultimate shear stress and was accompanied by an increased tendency for the crack to widen (see Figure 2.50). Failure occurred not by splitting but by crushing of the concrete as shown in Figure (2.51).

2.3.2 Failure modes of dowel action

Based on the results of the many different types of dowel action tests, various failure modes can be identified as illustrated by the dowel load-displacement relationships presented in Figure (2.52). At low applied loads the dowel stiffness is given by the initial portion

of curve A. At this stage, the dowel load is transferred across the crack mainly by the shear deformations of the reinforcement. As the dowel force increases, splitting cracks may form in any radial direction as the circumferential tensile stress exceeds the concrete tensile strength. The circumferential stress is induced by the bearing stresses between the dowel and the concrete, by the wedging effect of the bar deformations once cracks have been initiated and by concrete shrinkage.

As the load increases, the radial cracks propagate in an outward direction until the splitting crack is formed on a vertical or horizontal plane through the reinforcement axis. This plane will depend on the spacing between bars and the concrete cover. At this stage, the load-displacement curve is given by curve B in Figure (2.52). The presence of large axial stresses in the reinforcement will shift the load displacement curve downward as shown by curve D, because bond breakdown is caused which reduces the effectiveness of the dowel action.

If the crack propagation is arrested by a stirrup place close to the crack, the dowel load can be increased and the displacement curve follows the path marked C. The longitudinal reinforcement is supported by the stirrup and the dowel forces are transferred across the shear plane mainly by bending of the reinforcement. The dowel load can be increased until either the stirrups or the longitudinal reinforcement reaches their yield strength. If the radial cracks do not develop into splitting cracks, the load displacement curve follows curve A.

The dowel stiffness decreases as the concrete beneath the reinforcement begins to deteriorate due to high localised bearing stresses. The dowel unbonded length of the dowel increases and the main load transfer mechanism is most probably provided by the bending action of the reinforcement. The ultimate capacity of the dowel may be attained if the dowel does not fail prematurely by concrete crushing or axial yielding of the reinforcement. It must be noted, however, that the dowel ultimate capacity is accompanied by the occurrence of excessive shear displacements.

2.3.3 Dowel action mechanisms

Paulay, Park and Phillips[26] identified three separate mechanisms by which shear can be transferred across crack by the reinforcement.

(1) Direct Shear of the Reinforcement

This is the primary deformation mode which occurs when the span to depth ratio of a fixed-ended beam is less than unity, Figure (2.53a). Although the bar diameter may be two orders of magnitude greater than the crack width, direct shear is not considered to be an important mode of deformation. The concrete surrounding the bar is not rigid and hence the effective span of the bar will be much greater than the crack width. Failure is more likely to occur by crushing of the concrete beneath the bar or by tensile splitting rather than a shear failure of the steel.

(2) Kinking of the reinforcement

If the shear displacement causes a large deformation of the reinforcement, the reinforcement may kink and the component of the reinforcement axial force parallel to the crack will resist shear,

Figure (2.53b). If the reinforcement is not normal to the direction of cracking there will be considerable shear transfer through the axial forces in the reinforcement, without kinking. However, there has been controversy over whether sufficient kinking of the reinforcement occurs across a crack for it to be significant. For example the original yield line theory for slabs, Johanson[36] ignored kinking of reinforcment passing obliquely across a crack. Wood[37] found that this assumption gave over conservative results for the ultimate strength of a one way reinforced concrete slab and proposed a "complex kinking" theory. Hence the ultimate force normal to the crack was given by $A_s f_y$ and not $A_s f_y \cos\theta$ as suggested by Johansen.

Further tests by Kwiecinski [38], Prince and Kemp[39] and Mills[40] suggest that there is partial kinking of the reinforcement across cracks. However, Morley[41] did not find significant distortion of the reinforcement across cracks but suggested that this might be because the crack often tends to travel parallel to the reinforcement when it is close to the reinforcement. Thus for a given crack width, the distortion of the reinforcement from its original orientation becomes insignificent.

All these studies have been carried out by observing the flexural behaviour of a slab with reinforcement oblique to the axis of the principle moment. In a situation where tensile forces cause cracking in a slab and shear is subsequently applied to the crack, kinking may be more significant. However, it is still necessary to develop large shear displacements across the crack before the reinforcement will deviate substantially from its original line. This will again be limited by concrete strength and, like shearing,

kinking is not generally considered to be an important mode of shear transfer.

(3) Flexure of the Reinforcement

This deformation mode becomes significant when the span of fixed-ended beam is greater than its depth, Figure (2.53c). The relatively low stiffness of concrete and the degradation of the concrete around a bar as the shear increased means that this is probably the most important mode of behaviour of a dowel bar.

2.3.4 Theoretical models

The description of the dowel load-displacement relation can be based on the theory of beams on elastic foundation, as published by Timoshenko and Lessels [44].

Den Hartog [42] analysed a semi-finite beam on elastic foundation with a point load, V_d, at the end, Figure (2.54). The end deflection is given by

$$\Delta_d = \frac{2\beta V_d}{k} \qquad (2.13)$$

where

$$\beta = \left[\frac{k}{4E_s I_s} \right]^{1/4}$$

and k is the stiffness of the spring foundation, per unit length of beam, and is uniform along the beam. Now if the beam is considered as a cylindrical bar,

$$I_S = \frac{\pi \Phi^4}{64}$$

If G_f is the foundation modulus for concrete (in units of force x length ^{3}) then assuming that K is a linear function of the bar diameter $K = G_f.\Phi$

Hence,

$$V_d = C\ \Delta_d \Phi^{1.75}\ G_f^{0.75}\ E_s^{0.25} \qquad (2.14)$$

where

V_d = dowel force

C = constant

Δ_d = dowel displacement

Φ = bar diameter

G_f = foundation modulus

E_s = Young's modulus of the reinforcing bar

This theory would explain why the curves in Figure (2.46a) have similar initial stiffness. However, the model predicts a linear-displacement behaviour and hence will not predict the failure mode or the ultimate load of dowel bar.

Eleiott[32], Stanton[33] and Jimenez et al[16] noted that the early part of the load-deflection curve for dowel bars could be modelled quite clearly by the beam on elastic foundation theory. However, this analysis was in each case found to give a poor correlation with experimental results after the onset of the concrete crushing beneath the dowel bars.

A simplified beam on elastic foundation model was developed by Dalaska[34] to predict the ultimate failure load. The beam on elastic foundation theory predicts that distribution of reaction loads supporting the beam is that of damped sinusoidal curve, Figure

(2.55a). This was simplified to a triangular distribution, Figure (2.55b).

Based on this load distribution and taking into account the test results, Dulaska suggested the following expression to predict the ultimate dowel force.

$$V_{du} = 0.20 \ \phi^2 \ f_y \sin\theta \left[\sqrt{1 + \frac{f_{cu}}{.03 \ f_y \sin^2\theta}} - 1 \right] \qquad (2.15a)$$

where

V_{du} = ultimate dowel force (N)

ϕ = bar diameter (mm)

f_y = yield stress of the reinforcement (N/mm^2)

f_{cu} = cube compressive stress of concrete (N/mm^2

θ = angle of inclination of the dowel bars with respect to the horizontal plane

when

$\theta=0$ = this equation can be simplified to

$$V_{du} = 1.16 \ \phi^2 \ f_y^{0.5} \ f_{cu}^{0.5} \qquad (2.15b)$$

No simple basic relationship similar in form to the static equilibrium equations for load capacity could be found for the deformations by Dulaska. Instead an imperical expression was found to fit the test data.

A similar expression to equation (2.15) was derived by Rasmussen[43] to predict the ultimate capacity of the reinforcement or bolts embedded in concrete. The stiffness of the conrete is assumed to diminish once the compressive strength is reached at the face of the

crack. The load is, therefore, redistributed to the concrete further away from crack Figure (2.56), until plastic hinge ultimately forms in the bar at some distance remote from the crack face.

The theoretical model of dowel failure proposed by Daluska and Rumssen agrees quite closely with experimental results. However, it should be realised that this type of failure will only occur if the concrete is sufficiently well restrained not to fail first in splitting. The model does not consider what the predicted failure load will be if the dowel force is combined with axial tension. It is clear that the ultimate plastic moment of the bar will be reduced by any axial force. It is reasonable to expect, however, that axial tension in the bar may also damage the concrete supporting the dowel bar. This would cause a more rapid redistribution of the bearing stress resultants away from the crack and hence cause a reduction in the initial dowel stiffness and in the ultimate dowel force. White and Gergely[19] found that with zero axial stress a foundation modulus of 820 N/mm^3 was present. As the axial stress increased, the foundation modulus decreased linearly until with an axial stress of 350 N/mm^2 the foundation modulus was 40 N/mm^3.

Walraven[20] derived a semi-imperical expression, based on the beam on elastic foundation equation (2.14), in which the effect of the tensile force and the degradation of foundation modulus G_f were incorporated and was based upon the test data from[26],[32]. This expression predicts that the dowel force is a function of crack width, shear displacement, bar diameter and concrete quality as follows:

$$V_d = 10\ (w + 0.20)^{-1}\ \Delta_d^{.36}\ \phi^{1.75}\ f_{cu}^{.38} \qquad (2.16)$$

where

V_d = dowel force (N)

Δ = dowel displacement (mm)

w = crack width (mm)

Φ = dowel bar diameter (mm)

f_{cu} = cube compressive stress of concrete (N/mm^2).

This equation, however, was not examined by Walraven to predict any other test results. Recently, Millard and Johnson[15] used this equation to predict their dowel test results but it did not show good correlation.

Millard and Johnson admitted that the actual deterioration of the concrete beneath the reinforcement and the resulting redistribution of internal forces is too complex to permit a realistic analytical modelling without considerably more experimental data than is presently available. Therefore, they selected an exponential function to describe the nonlinear dowel force-displacement relationship which is given by

$$V_d = V_{du}\left[1 - \exp\frac{K_i \Delta_d}{V_{du}}\right] \qquad (2.17)$$

where

V_d = dowel force

V_{du} = ultimate dowel force

K_i = initial dowel stiffness given by equation (2.14)

Δ_d = dowel displacement.

To calculate the ultimate dowel force for a dowel bar with an axial force of αf_y, equation (2.15b) was modified by Millard and Johnson to

$$V_{du} = 1.3\ \phi^2\ f_{cu}^{0.5}\ [f_y\ (1-\alpha^2)]^{0.5} \qquad (2.18)$$

where

ϕ = bar diameter

f_{cu} = cube compressive stress of concrete

f_y = yield stress of dowel bar

α = ratio of axial stress to the yield stress of the dowel bar.

Although equation (2.17) showed good agreement with Millard and Johnson's test results, they recommended that more test results would be helpful in establishing the general applicability of the equation.

2.3.5 Summary of research on dowel action under monotonic loading

1. Dowel tests on pavement joint showed that the foundation modulus of concrete G_f decreases with increasing bar diameter. For a given bar diameter a considerable variation was observed of G_f. The research also revealed that the dowel load increased with increasing bar diameter and with reduced joint width.

2. Failure in the divided beam test and beam end test occurred by formation of a splitting crack, propagating along the axis of the reinforcing bar. This crack would occur on the side or the soffit of the beam depending on the relative cover in each direction.

3. Splitting load increased with increasing beam width, bar diameter and concrete strength. The beam depth and concrete cover did not affect the dowel capacity of the reinforcement. After the occurrence of splitting crack in the beams, stirrups were beneficial in increasing the dowel capacity if they were close to the diagonal crack.

4. The beam end test results revealed that a significant reduction in the dowel stiffness and dowel capacity as the axial stress in the reinforcement exceeded 80% of the axial yield stress.

5. In direct dowel tests when small diameter of dowel bars were used failure occurred by yielding of the dowel bars or by bearing failure of the concrete. Angle of inclination of the dowel bar to the crack plane did not show any significant influence on the dowel capacity. Also an increase in compressive concrete strength from 27 to 54 N/mm^2 had a small effect upon the dowel behaviour. Increasing the axial tensile force in the reinforcement resulted in a lower dowel stiffness and ultimate dowel stress accompanied by an increasing tendency for the crack to widen.

6. Three mechanisms by which shear can transfer across a crack by dowel action have been identified, i.e. direct shear, kinking, and flexure of reinforcement. It seems that the flexure mode is the most important, whereas kinking might have a small influence in some circumstances.

7. It seems that the beam on elastic foundation model can predict with reasonably accuracy the initial stiffness of a dowel bar

whilst the concrete is still elastic. However, once the concrete starts to crush or split locally the model is no longer realistic. It may be possible to model this localized damage by reducing the foundation modulus of concrete G_f, but at best this will only be an empirical approximation which is unlikely to be generally applicable. In the absence of tensile splitting causing ultimate failure, equation (2.15b) gives a reasonable prediction of the ultimate dowel force. This equation has the advantage that its derivation does not rely upon any assumptions about the stiffness of locally damaged concrete.

2.4 Combined action under monotonic loading

In the practical situations where shear forces have to be transferred across a crack, both interface shear transfer and dowel action will be simultaneously activated. As Millard [46] stated, there is an interaction between the two mechanisms which makes the combined effect in reinforced concrete more complex than might first appear. In dowel action tests, interface shear transfer is removed by the artificial creation of a smooth crack, so that there was no tendency for crack faces to override.

In normal reinforced concrete, the interface shear transfer action causes widening of the crack, with a resulting increase in the axial tensile force in the reinforcement. This has been shown to cause local tensile damage to the concrete and hence soften the dowel stiffness. There are also compressive forces over the whole crack face, balancing the tensile force in the reinforcement, which may also influence the dowel stiffness. These forces are not present in dowel action tests with a simultaneous axial tensile force in the reinforcement.

In interface shear transfer tests, dowel action is eliminated by placing a soft sleeve around the reinforcement or by removing the reinforcement from the concrete and providing an external restraint normal to the plane of cracking. The difficulty with both these methods is that, in removing the dowel action effects, the local bond between the reinforcement and the concrete has also been removed. One problem this causes is that the axial restraint stiffness of sleeved or external reinforcement is much less than that of fully bonded reinforcement. Another problem caused by the removal of local bond is that the crack width in the interface shear transfer test was uniform through the depth of the section. Previous research on reinforced concrete[47,45] has suggested that local bond causes the width of the crack to diminish in the vicinity of each reinforcing bar. So, if the shear stiffness due to interface shear transfer is dependent upon the width of the crack, two specimens with the same crack width at the surface can not be expected to have similar shear stiffness if their internal crack widths are not similar. Because of this complexity, most experiments of combined actions have been carried out in order to establish the ultimate shear capacity and not much attenion has been paid to studying the overall behaviour of the combined mechanisms.

2.4.1 Experimental investigations

Mattock[34],[49-51] conducted several investigations on shear transfer in cracked and uncracked reinforced concrete using push off type of specimens. Attention was focused mainly on prediction of the ultimate shear stress rather than the behaviour of the specimens. His investigations studied the effect of the following parameters on the ultimate shear strength:

(a) percentage of reinforcement crossing the shear plane

(b) the yield strength of reinforcing bars

(c) the strength of the concrete normal to the shear plane

(d) the presence of moments and forces normal to the shear plane

(e) the aggregate type.

As shown in Figure (2.57), he found that there were approximately linear relationships between stress and the reinforcement parameter pfy, for both the initially cracked and uncracked concrete. For values of the reinforcement parameter larger than 1000 psi, there was a lower but constant rate of increase in the ultimate strength for the initially uncracked concrete until the strength approximated that of the initially cracked specimens. At this stage the strength of the shear plane is controlled more by the concrete compressive strength and is not dependent on variations in the reinforcement parameter. The effect of different bar diameters, spacing and yield stress are accounted for by the reinforcement parameter pfy.

Direct compressive stresses normal to the shear plane increased the shear strength whereas direct tensile normal stresses reduced it. Applied moments smaller than the ultimate flexural moment of the cracked section did not reduce the shear strength of the specimens.

Figure (2.58) shows the effect of aggregate type on the ultimate shear strength of initially cracked specimens. It can be seen that the shear transfer strength of the sand and gravel concrete is consistently greater than that of the lightweight concretes for the same degree of reinforcement. It can also be seen that while the rate of the increase of shear transfer strength with pfy is about the same for all four concretes for moderate pfy, the shear transfer strength

of lightweight concretes commences to increase at a lesser rate at a lower value of pfy than does the sand and gravel concrete.

Reinhard/Walraven[52] used specimens similar to those tested by Mattock. The variables studied in these tests included

(a) the reinforcement ratio,

(b) the concrete strength,

(c) the roughness of the crack plane,

(d) and angle of inclination of the reinforcing bars crossing the crack.

It was found that with more reinforcement and with smaller bar diameters the stiffness of embedded steel increased due to increased steel area and bond. Concrete strength and roughness of the crack plane affected the interlock resistance and the crack opening during sliding. The shear capacity increases if the reinforcing bars intersect the crack plane at angles smaller than 90 degrees.

2.4.2 Theoretical models

Prediction of ultimate shear load

The shear friction model presented by Birkeland and Birkeland[53] was the first to be used for shear transfer and has been incorporated in the ACI Building Code 318-83[54] and British Standard BS:8110:1985 (60).

The model employed is shown in Figure (2.59). Dowel action is assumed to contribute a negligible proportion of the total shear. The roughness of the crack is visualised as a series of frictionless sawtooth ramps of slope tanϕ. The applied shear load is assumed to

produce tangential and normal displacements at the shear plane (m-m). The normal displacement will develop axial tensile stresses in the reinforcement crossing the crack, which will induce vertical compressive stresses on the concrete. The resistance to sliding will then be provided by the frictional force generated by the vertical compressive stress. From vertical equilibrium and assuming failure occurs when the reinforcement crossing the crack yields then

$$V_u = A_s f_y \tan\phi \qquad (2.19)$$

where

V_u = ultimate shear load

f_y = yield stress of reinforcing bars crossing the shear plane

A_s = area of reinforcement crossing the shear plane

$\tan\phi = \mu$ = coefficient of friction.

A fictiously high value of the coefficient μ is used to compensate for neglect of dowel action. Birkeland and Birkeland suggested three values for the shear friction coefficient as follows:

μ = 1.70 for monolithic concrete

= 1.40 for artifically roughened construction joints

= 0.8 to 1.0 for ordinary construction joints and for concrete to steel interfaces.

The shear friction hypothesis is a simplified theory for design purposes, which has been shown to lead to a conservative estimate of shear transfer strength in normal weight concrete made from natural

aggregates and subject to monotonic shear loading. It does not reflect the true mechanics of shear transfer in cracked sections, and neglects such effects as dowel action.

Much higher values of the ultimate shear strength can be developed with the appropriate combinations of the reinforcement crossing the crack plane and concrete strength. This can be seen in Figure (2.60), which compares the shear friction equation with measured shear transfer strength of monolithic reinforced concrete made from natural gravel and containing a crack in the shear plane. Section 6.1.9 of the PCI Design Handbook[55] attempts to take advantage of the higher ultimate shear transfer strength which can be attained by removing the upper limit on V of 800 psi, Figure (2.60) and substituting it with a new linear relationship in which the shear friction coefficient is modified to

$$\left(\frac{300}{pfy} + 0.5\right) \qquad (2.19a)$$

if pfy exceeds 600 psi. This is shown by the broken line in Figure (2.60), which can be seen to follow the trend of test data. A deficiency in this proposal is that no upper limit on either pfy or V_u is specified.

Another modification to the shear friction equation is proposed by Mattock[50],[51], for predicting the ultimate shear strength of a cracked section. The following equations were suggested by Mattock as a lower bound and mean value to the ultimate shear strength observed in the experiments.

$$V_u = 0.80\ (A_s f_y + N) + 200 \qquad (2.20)$$

$$V_u = 0.80 (A_s f_y + N) + 400 \qquad (2.21)$$

where

V_u = ultimate shear load. (Ib)

A_s = area of reinforcement crossing the crack plane. (in^2)

f_y = yield stress of the reinforcing bars crossing the crack plane. (psi)

N = normal force to the crack plane. (Ib).

The use of these equations was claimed to be applicable for pfy < 0.15 f_{cu} and for f_{cu} < 4000 psi (≈28 N/mm^2).

In these equations, the first term represents the contribution of friction to shear transfer resistance, whereas the second term represents the sum of two additional contributions to shear transfer resistance (1) dowel action of the reinforcement and (2) resistance to shearing off of protusions on the crack faces.

The last modification to the shear friction equation was proposed by Walraven[52]. The effect of the concrete strength is taken into account as an influence variable and not as an upper limit as used before in Equation (2.19) and the Mattock Equations (2.20) and (2.21). The ultimate shear strength suggested by Walraven is given by

$$v_u = C_1 (p f_y)^{C2} \qquad (2.22)$$

where

v_u = ultimate shear stress (N/mm^2)

p = ratio of reinforcement crossing crack plane

f_y = yield stress of the reinforcement crossing crack plane (N/mm^2)

C_1, C_2 = constants which can be calculated from the following expressions

$C_1 = f_{cu}^{0.36}$ (N/mm^2)

$C_2 = 0.09\, f_{cu}^{0.46}$ (N/mm^2)

Figure (2.61) shows comparisons between the modified shear friction Equation, i.e. Equation (2.21), and Walraven's Equation (2.22). It is seen that the modified shear friction Equation is rather conservative for higher concrete strength.

Prediction of shear transfer behaviour

Walraven[56] noticed that there was a fundamental difference between the behaviour of interface shear transfer specimens and that of reinforced concrete specimens. With interface shear transfer specimens the crack opening path, i.e. shear displacement vs crack width curve, was dependent upon the stiffness restraining the crack from widening. With reinforced concrete specimens there was a critical crack opening path which was quite steep and was independent of the amount of the reinforcing bar embedded in the concrete and crossing the crack plane. For high values of ρ the stiffness of the reinforced concrete specimens was found to be greater than the stiffness obtained by summing the individual components of interface shear transfer and dowel action mechanisms. However, in case of the low reinforcement ratio a better agreement was obtained. In this case, the crack opening path of interface shear transfer tests was similar to the critical crack opening path of the reinforced concrete tests and the stiffness could be predicted by summing the separate components as shown in Figure (2.62).

The following hypothesis was proposed by Walraven to explain these observations. When reinforced concrete specimens crack in tension, internal crack of the type observed by Goto [45], were initiated by reinforcement ribs adjacent to the primary crack, Figure (2.63). If these internal cracks propagate to the primary crack, a conical region of loose concrete is formed as shown in Figure (2.64). If there is a subsequent shear displacement with a low level of crack widening the conical region will lockup and form strut which forces the crack to open in a characteristic direction as shown in Figure (2.65). The strut is considered to be rigid and hence the amount of the reinforcement does not affect the direction of the critical crack opening path. The strut also provides the compressive force required to complete the equilibrium of the internal and the external forces (see Figure 2.66). The mechanism of force transmission is schematically shown in Figure (2.67).

Millard and Johnson[46] found from their investigation that the ratio of crack widening to shear slip was less than that predicted by the equation proposed by Walraven in nine of the thirteen shear tests. When the crack faces were examined after completion of the shear test, there were signs of crushing and sliding over the face, but there was no evidence of localized damage to the concrete adjacent to the reinforcing bars. This result is contrary to that reported by Walraven, where conical regions of cracked concrete were found around each bar. Millard and Johnson thought that this damage might have been produced by the method used previously to expose the crack faces, which was to stress the reinforcement to yield in tension after completion of the test. In one test of their investigation, axial tension was applied to the reinforcement subsequent to shear testing until fracture occurred. There was still no sign of any

conical regions of damaged concrete adjacent to the reinforcement. Because of such differences between Walraven's hypothesis and Millard and Johnson's findings, any final conclusion can not be made until further studies are carried out.

2.4.3 Summary of research on combined action under monotonic loading

It is possible to note the following points from the research on shear transfer by combined action under monotonic loading:

1. The ultimate shear load increased with the reinforcement parameter pfy.

2. Direct compressive stresses normal to the shear plane increased the shear strength and decreased it with presence of direct tensile stresses normal to the crack plane.

3. Applied moments smaller than the ultimate flexure moments of the cracked section will not reduce the shear strength.

4. Shear transfer strength of the sand and gravel concrete is greater than that of lightweight concrete.

5. Initial crack width has a major influence on the ultimate shear strength.

6. The ultimate shear strength increases if the reinforcing bars intersect the crack plane at angles smaller than 90^{o}.

7. The shear friction model presents a simple model which does not attempt to describe the mechanism of shear transfer and shows a

conservative estimate of ultimate shear strength in normal weight concrete. Design equations of shear transfer of ACI Building Code 318-83 and BS8110:1985 are based on this model. The other equations, which are mainly based on the development of shear friction model, still need to be examined to be used confidently for design purpose.

2.5 Interface shear transfer under cyclic loading

2.5.1 Experimental investigations

Several experimental studies have been concerned with the effect of repeated traffic loads on pavement joints.

Colley and Humphrey [57] studied the effectiveness of the interface shear transfer mechanism under repeated cyclic loading using the specimen shown in Figure (2.68a). The repetitive motion of the truck wheels as they moved across the joint was simulated by the loading shown in figure (2.68b), where the heavy line shows the load applied to the approach slab, and the dotted line represent the load applied to the approach slab. The time interval between the maximum loads was only 0.02 sec, and the total loading cycle lasted for 1.5 sec. The maximum concentrated load applied to the slabs caused an average shear stress on the concrete section of 39 psi for the 7" (177mm) thick slabs and 28 psi (0.24 N/mm^2) for the 9" (228mm) thick slab. Deflections were automatically recorded at the different locations indicated in Figure (2.68a).

The independent variables studied in this investigation were the joint width, the modulus of subgrade reaction, the maximum shear stress intensity, i.e. the level of the applied repeated load, and

the aggregate shape and hardness. The effect of each parameter was evaluated by a coefficient by the following equation,

$$E\% = \frac{2dj}{dj' + dj} \times 100 \qquad (2.23)$$

where dj' = maximum deflection of loaded slab, dj = maximum deflection of unloaded slab, E = effectiveness coefficient.

They concluded that for a given load,slab thickness, and modulus of subgrade reaction, the joint effectiveness decreased with increasing number and load level of loading cycles. The joint effectiveness increased, however with increasing modulus of subgrade reaction. Also for aggregates of the same hardness,the joint effectiveness increased with larger particle angularity.

Nowlen [58] also conducted joint tests similar to those of Colley and Humphrey but extended the investigation to consider the effect of the aggregate size, hardness, and the age of concrete at joint cracking. Equation (2.23) was also used to evaluate the relative performance of the variables considered.

Nowlen concluded that the joint effectiveness parameter increases with increasing aggregate size, especially for joints with the larger initial openings. It also increases for joints which had cracked at an early concrete age, and for cracked surfaces with increasing aggregate angularity or hardness.

Although the applied shear stresses were small and crack widths large the results appear to show that the interface shear transfer is a viable shear transfer mechanism under cyclic loading.

Tests with higher stress intensities were carried out by White and Holley [9], who developed an experimental program to study the effect of seismic loading on the behaviour of cracks. These tests produced a valuable preliminary assessment of the behaviour of the cracks and established a valuable testing scheme, which was later used by Laible, White and Gergely [12] to extend the test programme. The experimental results obtained had to be directly applicable to the design and calculation of concrete nuclear containment vessels.

The tests were carried out on specimens as shown in Figure (2.69). Dowel action was excluded by using external restraint bars. These bars had a negligible shear stiffness but acted to hold the specimen halves together when shearing and overriding occurs. The specimens were cracked at mid-depth prior to testing. The desired initial crack width was then set by positioning the upper half of the specimen with respect to the lower half by adjustment of the nuts on the restraint rods that passed through the upper beams.

The horizontal shearing surface had a net cross-sectional area of 19400mm . Fully reversing cyclic shear stress of about 1.24 N/mm^2 were applied across initial crack widths of 0.25, 0.51 and 0.76mm. Most of the specimens were subjected to 25 cycles of shear. Two types of loading were performed. Firstly, incremental, where the load was increased in increments of about 15% of the peak load and, secondly, direct loading and unloading to and from the peak stress level. The incremental type of loading was done for the first and fifteenth cycles on nearly all tests while the direct loading was used for all other cycles.

The variables studied were the initial crack width,the concrete

strength,the aggregate size and quality and the degree of tranverse reinforcement restraint.

Results for an initial crack width of 0.76mm and a restraint stiffness of 600 kN/mm, is shown in Figure (2.70). These results are representative of the generally observed behaviour, although there was a marked difference in behaviour between the specimen with 0.25mm initial crack widths and the other groups.

The most significant aspect of the behaviour is that during any of the load cycles the total load-shear displacement relationship was highly non-linear except the first cycle.A considerable amount of hysteresis existed when the initial crack width was 0.51 or 0.76mm (see Figure 2.70a). In only a few cases did the shear displacement freely return to as little as 50% of the maximum value. Usually the return shear displacement was in the range of 0.20% of the maximum shear displacement, which was believed to be caused by the locking effect of contact areas, creating a high degree of resistance.

However, since hardly any shear stress was necessary to bring the specimen to the original position, it seems to be more likely that this irreversability is due to local crushing of the concrete.

Figure (2.70d) illustrates that the maximum shear displacement in each cycle increased most rapidly during the initial cycles but the increase tended to stabilize as the cycling proceeded. However, both maximum shear displacement and crack width Figure (2.70e) were still increasing even after 25 cycles.

Figure (2.71) shows the influence of the initial crack width on the

specimen behaviour. It appears that specimens with initial crack widths of 0.25mm behave much differently from the other specimens, in that both the initial ratio of shear displacement to crack width and the rate of increase of this value with cycling are much less severe than for specimens with initial crack widths of 0.51mm or higher. This difference can be explained by the hypothesis that for lower values of crack widths, shear resistance is dominated by bearing action and little overriding and grinding action results.

The effect of concrete strength was particularly evident in the first cycle when the lower strength cement paste leads to easier crushing. It was also observed that the shear capacity was enhanced substantially by the use of large aggregate size.

The effect the restraint stiffness normal to the cracked plane for the cycle 1 and 15 is given in Figure (2.72) for specimens with initial crack width 0.76 mm. It can be seen from this figure that although increased restraining stiffness decreases shear displacement it becomes less effective at higher levels, i.e. above 2000 Kip/in.

Loeber and Paulay (11) studied the interface shear transfer mechanism under repeated loading using a push-off specimen. A series of nine test specimens was designed to study the effect of the initial crack width (0.127mm, 0.25mm and 0.50mm) and size of aggregate (19mm and 10mm). The 10mm aggregate size specimen was tested with a crack width of 0.25mm only.

In this study, load intensities more likely to be encountered during severe seismic disturbances were applied to the specimen. Therefore, shear stress over 5.5 N/mm^2 were applied 33 times and then the

specimens were loaded to failure. No attempt, however, was made to measure this failure load.

From this study it was concluded that the magnitude of the initial crack width dominate the response of test specimens. The accumulation of the residual shear displacement after each load cycle was proportional to the preselected crack width. The stiffness of interface shear transfer mechanism during the repeated load was two to three times the stiffness during first loading (see Figures 2.73, b, c).

As in the monotonic shear tests no significant difference in the behaviour of the specimen with different aggregate size was observed (see Figures 2.73,b,d).

From Figure (2.73) it seems that the number of cycles of loading applied was insufficient to show all the trends of interface shear transfer behaviour nor was it possible to see if the two different types of loadings affected the results.

2.5.2 Theoretical model

Based on Laible et al [12] results, an analytical model was developed by Jimenez et al [16] to predict the shear load-shear displacement relation under cyclic loading. The typical response of the test specimens is shown previously in Figure (2.70a) for the first and 15th shear loading cycles. This response was idealized by Jimenez et al [16] as shown in Figure (2.74). The shear stress and displacement at which the change in loading stiffness occurs was expressed as a proportion of the shear stress, θ, and the maximum shear displacement, δ, taken by interface shear transfer mechanism

during the cycle considered. The residual displacement exhibited when the specimen is unloaded is also expressed as a proportion, ω, of the maximum shear displacement for a particular cycle.

Referring to Figure (2.74), it can be shown that the interface shear transfer stiffnesses for the hysteresis idealization were given by the following equations:

$$k_1{}^a = \Phi_{kr} A_c / \sigma_n \qquad (2.24a)$$

$$k_2{}^a = k_1{}^a/(1-\omega) \qquad (2.24b)$$

$$k_3{}^a = k_1\theta/(\omega+\theta) \qquad (2.24c)$$

$$k_4{}^a = \theta V_a{}^n/(\omega\ \Delta_a{}^{n-1} + \delta\Delta_a{}^n \qquad (2.24d)$$

$$k_5{}^a = (1-\theta)V_a{}^n/[(1-\delta)\Delta_a{}^n] \qquad (2.24e)$$

$$k_6{}^a = k_5(1-\delta)/[(1-\theta)(1-\omega)] \qquad (2.24f)$$

The disadvantage of this analytical model however is that it is based on the idealization of certain test results which are only relevant to a similar history of loading. Therefore, it can not be directly used for any other loading history.

The "Two-Phase" model [20], explained previously in section 2.2.2, was also used by Walraven to describe the behaviour of interface shear transfer under cyclic shear loading. A fictitious specimen is considered as shown in Figure (2.75a). The specimen consists of two parts, separated by a crack. The two halves are loaded by shear forces, while an enlargement of crack width is counteracted by external restraint rods.

The theoretical shear load-shear displacement curves shown in figure (2.75b) could be explained with the aid of Figure (2.76). The

position of the crack faces before loading is represented in Figure (2.76a). At peak stress level the crack width has been increased by Δw and the shear displacement by Δ.

As a result of the rigid-plastic character of the matrix material a cavitation has been formed (shaded area in Figure 2.76b). Due to this cavitation the "no contact phase" after unloading is reached before the shear displacement is back to zero, Figure (2.76c) and point C in Figure (2.75b). To bring the two halves of the specimen back to their original position a small shear force may be necessary, since the rubble between the crack faces due to the deterioration of matrix material during loading, may cause some frictional resistance (point D in Figure 2.75b).

If the shear force is imposed in the other direction the same type of behaviour can be expected, Figure (2.75b) A', B', C', D'. Also, it was stated that in the subsequent loading cycles the presence of the cavitations, worn down in the first cycle of loading, influence the behaviour of the specimen considerably. At first a shear displacement will occur under a low shear force, until contact between the opposing areas is obtained [point E in Figure (2.75b)]. Then in a short interval of shear displacement full contact between the cavitations will be obtained. In this short interval a process of wearing off will take place at points of high contact stresses, point X in Figure (2.76). Hence a steeply ascending branch [EFG - figure (2.75b)] may be expected. During unloading similar behaviour to the first cycle may be expected [(GHI - Figure (2.75b)].

A comparison of shear load-shear displacement curves based on the two phase model, Figure (2.75b), with experiments carried out by Laible,

White and Gergely [12], Figure (2.70a), shows fairly good agreement. Therefore, it appears that the two phase model could be suitable as a basis for general use. However, the complexity of the calculations required for the two phase model seems to be a severe disadvantage.

2.5.3 Summary of research on interface shear transfer under cyclic loading

Summarizing the reseach on interface shear transfer mechanism under cyclic loading the following points can be made:

1. The efficiency of the interface shear transfer mechanism increases with increasing aggregate angularity, hardness and aggregate size.

2. Large initial crack width of the joints or cracked sections decrease the effectiveness of the shear transfer mechanism.

3. The effectiveness of interface shear transfer increases with the increase of normal restraining force.

4. The most significant aspect of interface shear transfer behaviour during any load cycle, except the first was that the shear load-shear displacement relationship was highly nonlinear. The first cycle exhibited a more linear trend.

5. Residual shear displacement is noticed at the end of any load cycle. This residual is increased considerably near the failure.

6. The two phase model seems to show general applicability whereas

the analytical model proposed by Jimenez et al was only applicable to predict their own test results.

2.6 Dowel action under cyclic loading

2.6.1 Experimental investigations

Eleiott[32] performed small scale experiments using the specimen shown in Figure (2.77). This test setup permitted the application of both tensile and dowel forces to #4 (12.7 mm) or #6 (19.5 mm) bars. The interface shear transfer mode was eliminated by means of greased plates placed at the shear plane. The variation in dowel stiffness and ultimate strength were studied for different bar diameters and varying levels of axial tension in the reinforcement and applied shear forces under cyclic loading.

Eleiott concluded that the presence of tensile stresses in reinforcement above 50 Ksi (172 N/mm^2) induces bond cracking in the specimen which decreased the integrity and axial stiffness of the concrete surrounding the reinforcement. Consequently, under the action of dowel forces, higher displacements and a reduced dowel stiffness are observed. Reversing cyclic shear stresses at any given load level further deteriorates the concrete and decreases the dowel stiffness.

Stanton[33] conducted an investigation on the dowel action of large diameter reinforcement bars under cyclic loading. The specimen, shown in Figure (2.78), contained two shear planes crossed by a number 11 bar (i.e. 34 mm diameter). Failure on all specimens occurred by concrete splitting on either a horizontal or vertical plane.

The main objectives of the investigation was to obtain a dowel stiffness relationship that could be employed in an analytical formulation. Typical results for the load displcement relationships obtained are represented in Figure (2.79). It can be seen that the stiffness is essentially linear in the first cycle, but increases with applied dowel load in subsequent cycles. This was attributed to concrete crushing beneath the reinforcement or the initiation of splitting cracks. The increase of maximum dowel displacement with both cycling and increasing dowel forces was also observed.

Jimenez et al [16] also conducted an experimental investigation on the dowel cyclic loading. Specimens similar to that of Laible[12] was used to study the dowel capacity in a reinforced concrete reactor vessel. In general, the same behaviour as that noticed in Stanton's investigation was found.

It should be noted that these experimental investigations [32],[33],[16] studied the dowel action under reversible cycle loading where failure occurred due to splitting of concrete using large diameter dowel bars. No investigations have been done to study dowel action under repeated loading similar to the interface shear transfer mechanism. Also, no attempt was made to investigate dowel action if small diameter dowel bars are used and if failure occurred due to yielding of reinforcement either under reversible or repeated cyclic loadings.

2.6.2 Theoretical model

Jimenez et al[16] presented an analytical model to describe the dowel action behaviour under cyclic loading.

From their previous experimental investigations, it was observed that the first cycle stiffness for all specimens was roughly linear during loading in the positive and negative directions. Unloading stiffness was nonlinear and a residual shear displacement was observed at zero load. For subsequent loading cycles at the same shear stress, the loading exhibits a hardening type of behaviour. It was claimed that the nonlinearity of the dowel stiffness was caused mainly by the reduction in the bar's unbonded length which occurs as the bars come into firm contact with the surrounding mortar. A reduction in the area enclosed by the hysteresis loop was also observed with cycling (see Figure 2.80). This area increased only when the specimen was cycled at shear stress close to its failure.

Based on the previous observations and beam on elastic foundation model, the first cycle dowel stiffness was given by

$$k_1^d = 312\, n_b \phi^{1.75} \qquad (2.25)$$

where

k_1^d = the first cycle dowel stiffness

n_b = number of bars

ϕ = bar diameter

The increase in the first cycle dowel displacement caused by cyclic loading was evaulated by a function, $\phi_d^{(n)}$, designed as the ratio of the dowel displacement at cycle n, $\Delta_d^{(n)}$, to the shear displacement of the first cycle, $\Delta_d^{(1)}$. From the limited experimental data obtained in these tests, the expression for $\phi_d^{(n)}$ was given by

$$\Phi_d^{(n)} = 0.03n + 0.97 \qquad (2.26)$$

where

n = number of cycle.

The peak dowel displacement at any cycle "n", $\Delta_d^{(n)}$, was given by

$$\Delta_d^{(n)} = \Phi_d^{(n)} \Delta_d^{(1)} \qquad (2.27)$$

The dowel shear force-dowel displacement relationship was idealized as shown in Figure (2.81). The dowel stiffness for the first cycle is linear, while for the subsequent loading cycles it is idealized by a bilinear representation. Due to the small area enclosed by hysteresis loop, the unloading stiffness is assumed equal to the loading stiffness. For subsequent cycles, the change in the loading or unloading stiffness is expressed as a proportion of the total dowel force applied, γ, and of the maximum dowel displacement, ψ, experienced during the cycle considered.

Referring to Figure (2.81), it can be shown that the dowel stiffnesses for the hysteresis idealization are given by the following equations

$$k_2^d = \gamma V_d^n / (\psi \Delta_d^n) \qquad (2.28a)$$

$$k_3^d = (1-\gamma) V_d^n / [(1-\psi) - \Delta_d^n] \qquad (2.28b)$$

In fact, this dowel action model is mainly related to cases in which failure occurred due to splitting of concrete and where large diameter of dowel bars were used. Also, because it was not based on the principle mechanisms of dowel action it is not applicable for

general use.

2.6.3 Summary of research on dowel action under cyclic loading

Based on previous research on dowel action under cyclic loading the following notes can be made.

1. The presence of tensile stress in the dowel bars resulted in a reduction in the dowel stiffness.

2. Failure occurred by concrete splitting when using dowel bars with large diameter.

3. The dowel stiffness is essentially linear for the first cycle and nonlinear for subsequent cycles.

4. No advanced model to predict the dowel action behaviour, such as the two phase model in the case of interface shear transfer, has been produced, most probably because of the few studies which have been carried out so far.

5. No investigation has been carried out to study the dowel action of smaller diameter bars, or when failure occurs due to the yielding of the dowel bars, either in the case of cyclic or repeated loadings.

2.7 Combined action under cyclic loading

Only two investigations appear to have been conducted to study shear transfer across reinforced cracks under cyclic loading, those by Mattock[59] and Jimenez et al[16].

Mattock[59] used the specimen and set-up shown in Figures (2.82) and (2.83). The shear plane area was 50 in (32,260 mm^2). The main variables studied were loading history, initial crack width, amount of reinforcement and aggregate type. The development of recommendations for shear transfer design in reinforced concrete subject to cyclically reversing shear was a major purpose of this study.

Two reinforcement ratios were investigated 0.88% and 1.32% by using reinforcing bars with diameters of No.3 (9.5 mm) and No.2 (6.4 mm). The initial crack widths investigated in test program were 0.010" (0.25 mm), 0.016" (0.40) and 0.025" (0.64 mm).

The specimens were subjected to the following history of cyclic loading. The shear was first continuously increased to 50% of the ultimate calculated shear strength under monotonic loading after which it was reduced to zero. Shear of opposite sign was then applied to the specimen, again being increased to 50% of the calculated shear transfer. Each specimen was subjected to ten such cycles of loading. The maximum positive and negative shears were increased by 8% of the calculated shear strength (i.e. 58% of the calculated ultimate shear strength) for the next five loading cycles. After each succeeding five cycles of load the maximum shears are increased by the same amount. This process was continued until failure of specimen occurred. Failure was considered to have occurred when the shear could not be increased to the planned maximum shear for the last cycle. The calculated ultimate shear strength was based on the previous equation derived for monotonic loading.

$$V_u = (0.80\ pfy + 400)Ac$$

In these tests, the response of the specimens changed as the number of cycles of loading and the level of loading increased. This is illustrated in Figures (2.84) and (2.85), which show typical shear load-shear displacement and shear displacement-crack width curves at different stages of loading. Response to the first cycle of loading is characterised by a gradual reduction in shear stiffness as the shear is increased in both positive and negative directions and by retention of almost all of the shear displacement caused by the maximum shear until the shear reduces to abouthalf its maximum value Figure (2.84a).

Response to succeeding cycles of loading is characterized by a low shear stiffness at low load values and a gradual increase in shear stiffness with increase in shear in positive and in negative directions. As the number of load cycles increases, the shear stiffness at low shears decreases and the increase in stiffness with increase in shear becomes greater. This results in the shear load-shear displacement curve for a complete cycle of load assuming a more and more pinched appearance as the nubmer of load cycles increases, as may be seen in Figure (2.84).

The shear displacement at maximum shear tended to increase slightly after each cycle for about the first five cycles. Thereafter, specimens having an initial crack width 0.010" (0.25 mm) responded in a stable manner. The shear displacement at maximum shear and the shape of the shear load-shear displacement curve remained essentially constant for a given maximum shear, until the maximum shear reached a value equal to about 90% of the load which was to cause failure. At and above this load, the shear displacement at maximum shear increased with each cycle, and by progressively increasing amounts.

The characteristic shape of the shear load-shear displacement curve also changed, in that after increasing as the shear increased, the shear stiffness decreased again as the maximum shear was approached, Figure (2.84c).

Failure occurred when the shear stiffness under increasing load reduced to zero and then the shear displacement increased rapidly under a declining shear. No big change was found in the shear load-shear displacement in the other specimens.

Based on the test data the following conclusions were drawn:

(1) Initially, most of the resistance to shear appears to be derived from the direct bearing of the asperities. At high values of shear a major part of the shear resistance is probably developed by friction between the crack faces, with remaining contribution coming from direct bearing of asperities and from dowel action of the reinforcement.

(2) An increase in the initial crack width results in a reduction in the ultimate shear load and the shear stiffness and an increase in shear displacement at all levels of load.

(3) For design purposes, the shear transfer strength under cyclically reversing loading should be taken as 0.80 of the calculated shear transfer strength under monotonic loading.

Jimenez et at[16] investigation was originally motivated by the need to understand the transfer of membrane shear stresses induced by seismic activity across precracked concrete surfaces in secondary containment vessels. They used the same specimen of Liable, but the

net cross sectional shearing areas was 225 in^2 (145.161 mm^2). This study was limited to two reinforcement ratios of 1% and 2% only using large diameter bars of 22 mm and 44 mm.

The research concluded that cyclic shear forces can be efficiently transferred across cracked surfaces by the combined action of interface shear transfer and dowel actions mechanisms. For the specimens tested, interface shear transfer sustained between 65% and 80% of the total applied load, while the dowel action mechanism was responsible for 32% to 20% of the total shear.

Cyclic loading increased the shear displacement, the crack width, and bar strains. The rates of increase, however, are highly dependent on the reinforcement ratio and on the applied shear stress. Large diameter bars enhanced the probability of concrete splitting along the reinforcement longitudinal axis.

Although the previous research[59],[16] on shear transfer by combined action under cyclic loading produced useful information, the studies were fairly limited in scope. Some aspects were not covered include (a) the effect of cyclic loading on the contribution of dowel action and interface shear transfer mechanism compared to the case of monotonic loading, (b) the behaviour of combined action under repeated loads and other loading histories (c) the theoretical development of general shear transfer models, i.e. shear load-shear displacement relationships, for cyclic and repeated loading.

2.8 Conclusions

In this section, some general conclusions regarding the state-of-art

of shear transfer in cracked reinforced concrete which might be led to this present work are drawn.

1. The most important parameters which have a significant influence on the behaviour and the ultimate strength of shear transfer across a cracked section are the initial crack width, the reinforcement ratio crossing the crack and type of shear loading. Other parameters such as scale and type of aggregate size and concrete strength are of less importance.

2. The different methods of testing used to study the interface shear transfer mechanism individually did not simulate the actual mechanism in the practical situation of a reinforced cracked section. However, these tests were important to evaluate the influence of the different parameters on the interface shear transfer mechanism.

3. The method of eliminating the roughness of the crack surfaces to study the dowel action seemed to be more realistic. The advantage of this method is that beside studying the dowel action individually the contribution of interface shear transfer can be evaluated.

4. Although available hypotheses and theoretical models proposed to describe the behaviour of shear transfer in a cracked section under monotonic loading are fairly satisfactory, some uncertainties still exist and more experimental evidence is required to check their validity.

5. More information is required upon the shape of the load-displacement relationship for dowel action once non-linearity starts to occur and up to ultimate loading.

6. It is obvious that few studies have been done on shear transfer under cyclic loading and in particular little attention has been paid to the case of repeated loading. It appears that more information is required in this area to obtain a better understanding of the behaviour and the mechanics of the shear transfer in the reinforced cracks with a view to developing recommendations for shear transfer design for those structures subjected to both reversible cyclic loadings and repeated loading.

7. Also, it is clear from the previous investigations on shear transfer under cyclic loading, that systematic investigations of the effective parameters are still necessary in order to clarify their influence. Parameters of importance include initial crack widths, reinforcement ratio crossing the crack plane and the loading history of the cycled loads, for example, the level of the repeated load and the number of cycles.

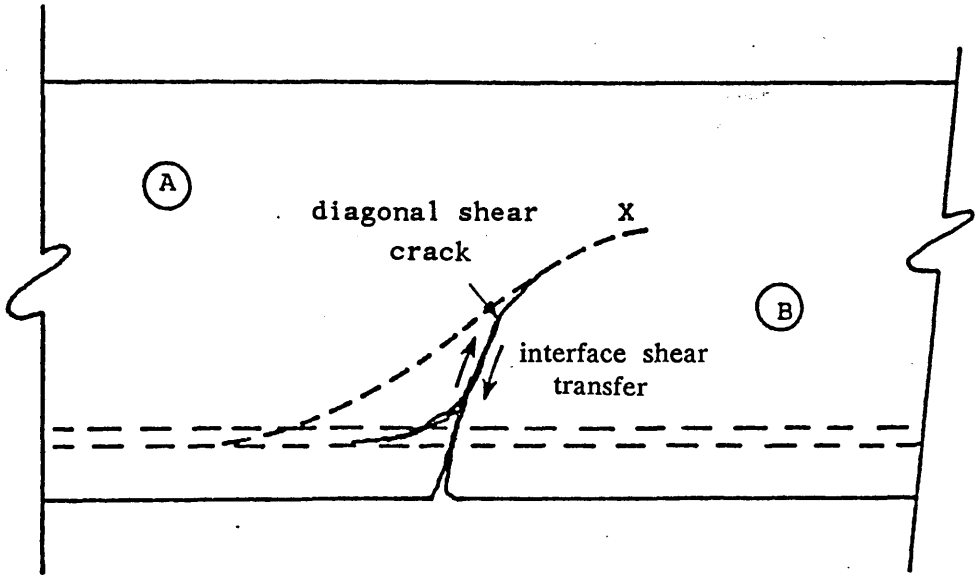

Figure (2.1) Stages in the development of diagonal cracking

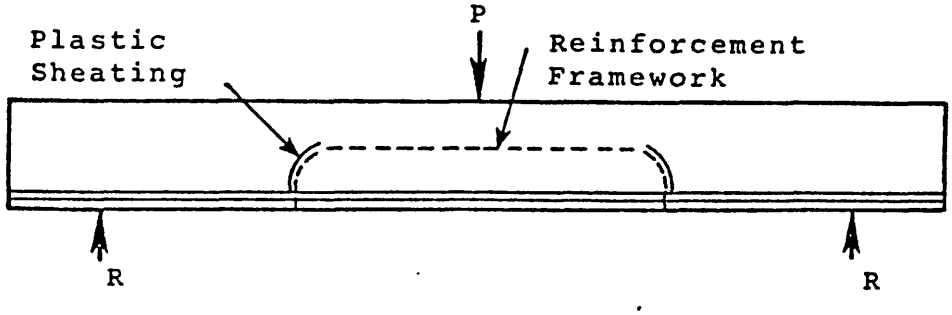

Figure (2.2) Test specimen used by Taylor (1)

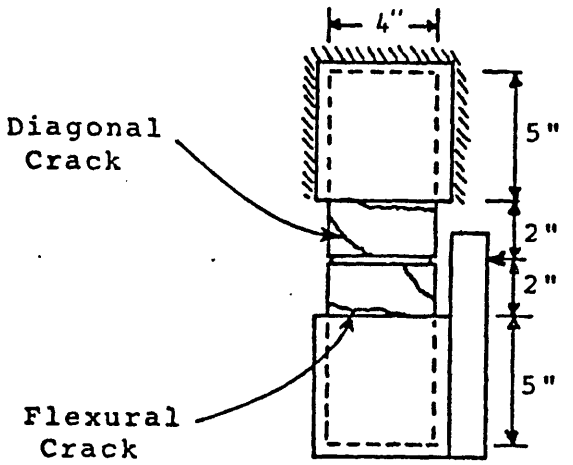

Figure (2.3) Direct test specimen used by Fenwick (6)

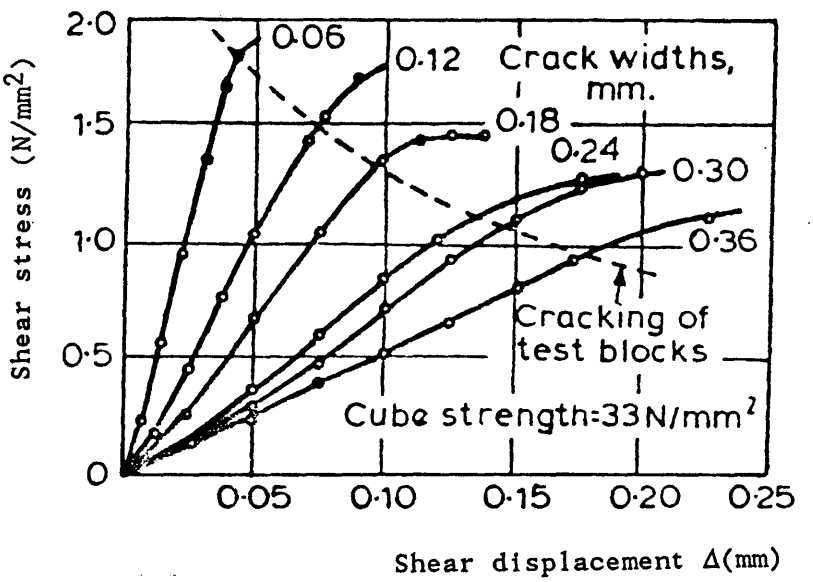

Figure (2.4) Effect of crack width on interface shear transfer (6)

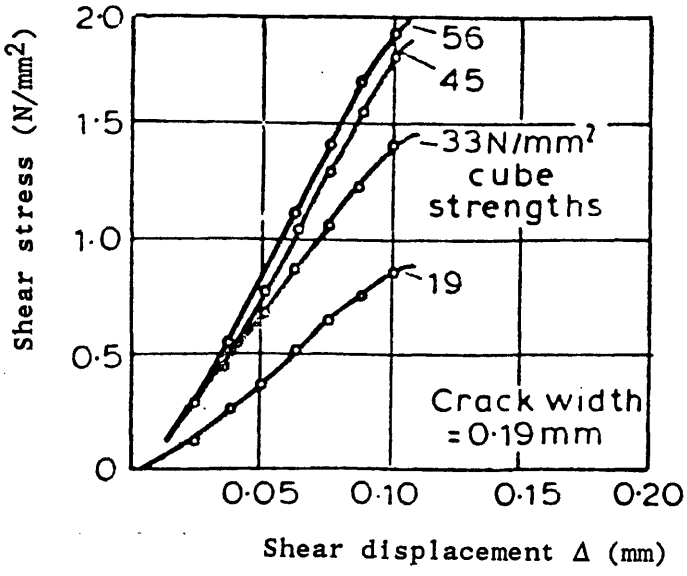

Figure (2.5) Effect of concrete strength on interface shear transfer (6)

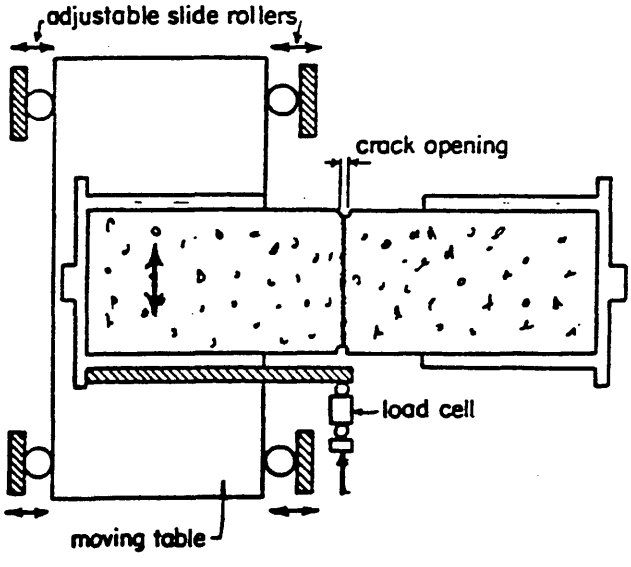

Figure (2.6) Test equipment as used by Houde and Mirza (10)

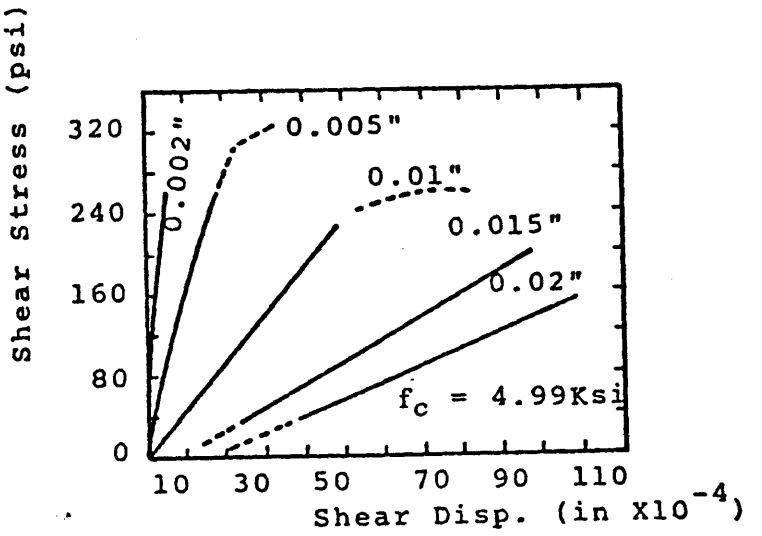

Figure (2.7) Shear load - shear displacement relations for constant crack widths according to Houde and Mirza (10)

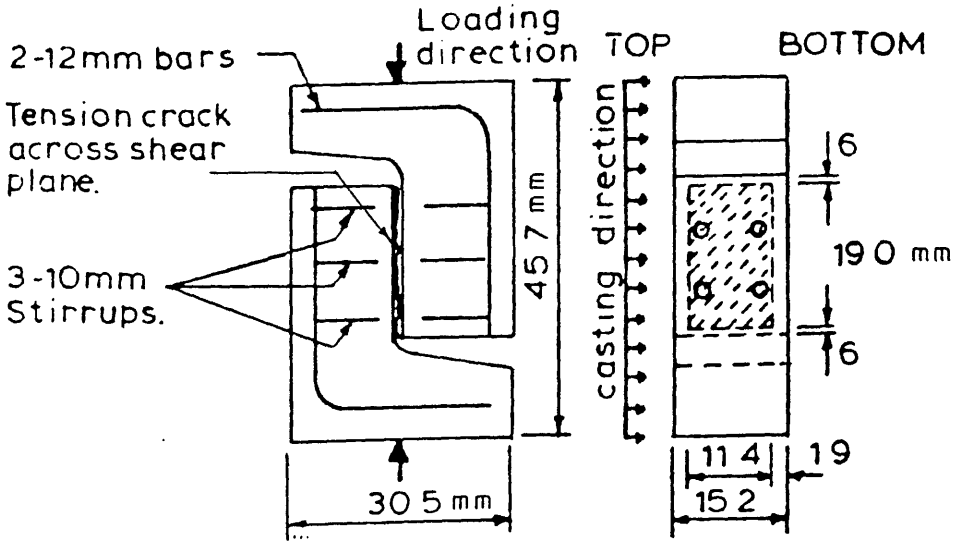

Figure (2.8) Typical test specimen used by Paulay and Loeber (11)

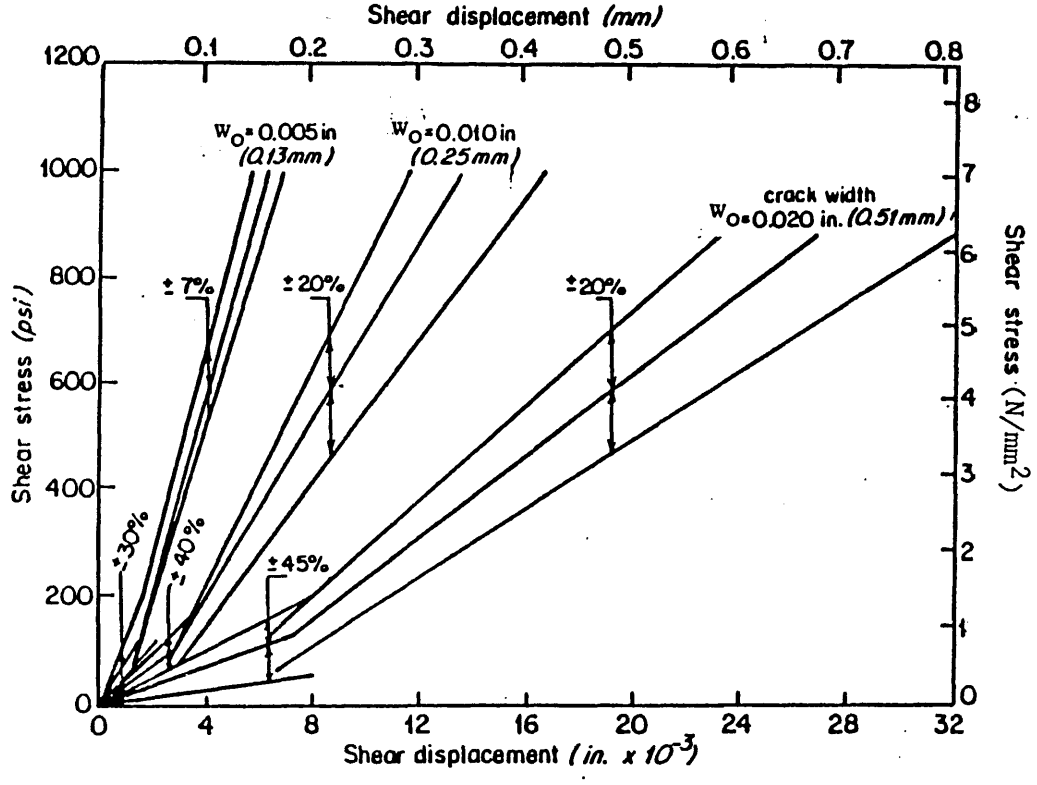

Figure (2.9) Shear stress - shear displacement relation for constant crack widths, according to (11)

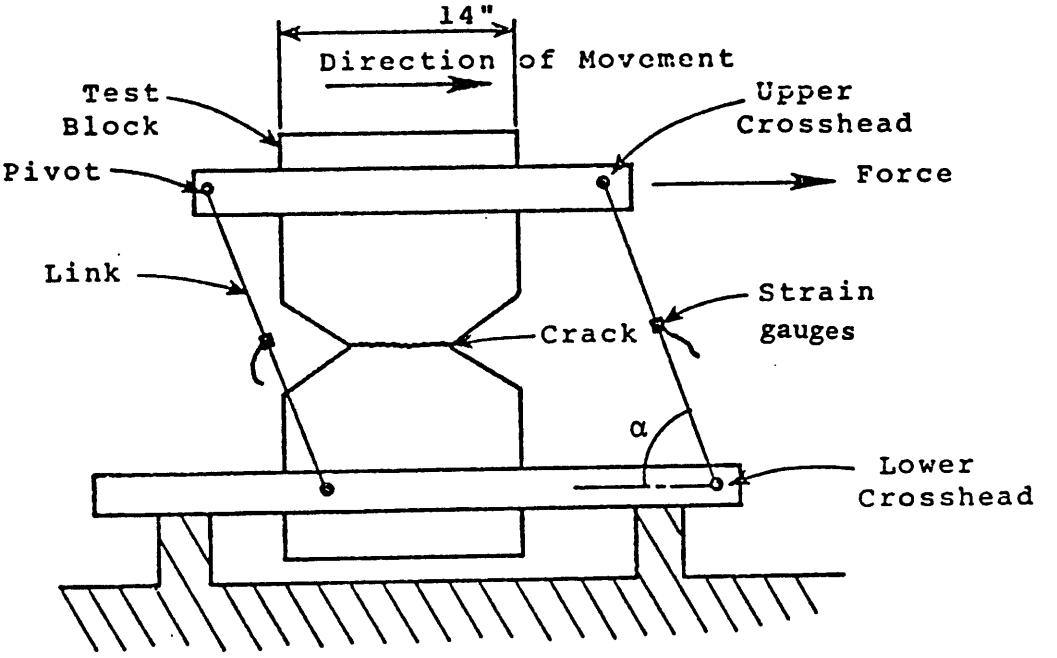

Figure (2.10) Direct shear test specimen used by Taylor (8)

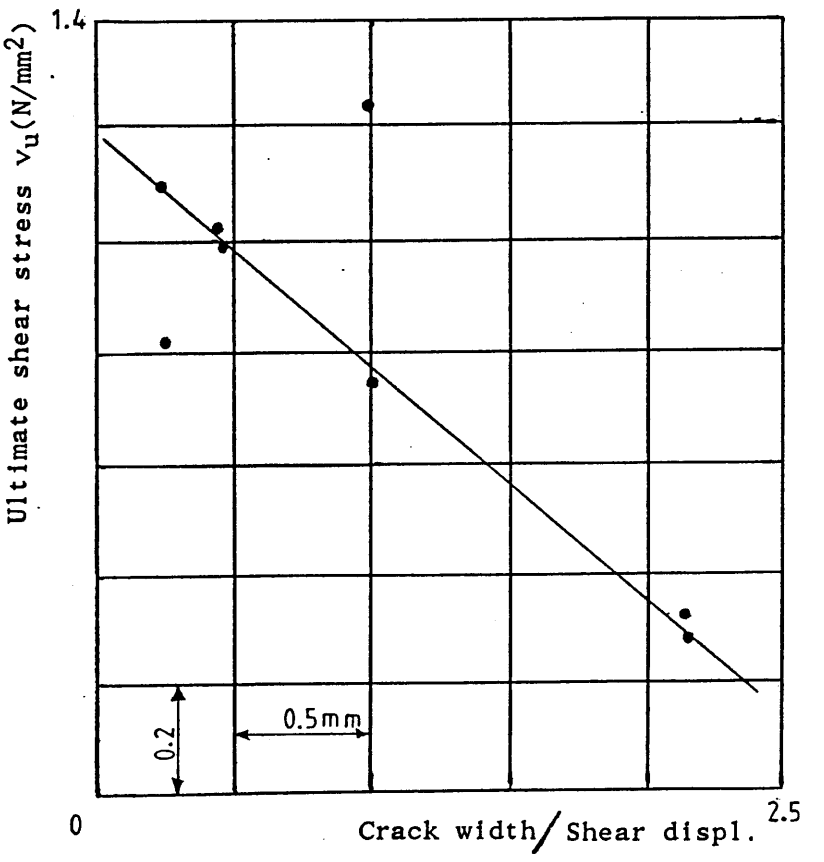

Figure (2.11) Relation between ultimate shear stress and crack width to shear displacement ratio (8)

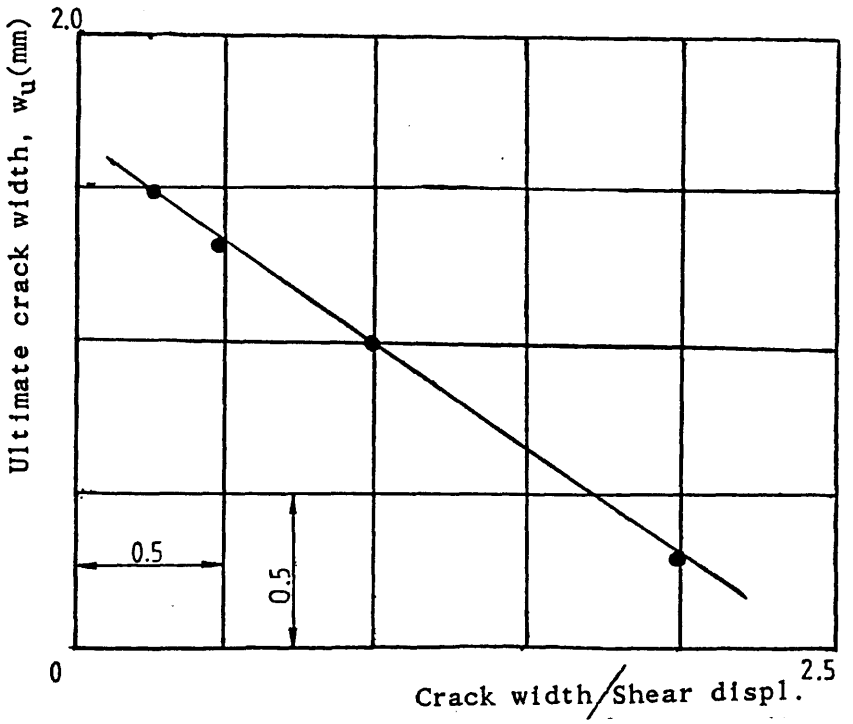

Figure (2.12) Crack width at ultimate shear stress as a function of the direction of crack opening according to Taylor (8)

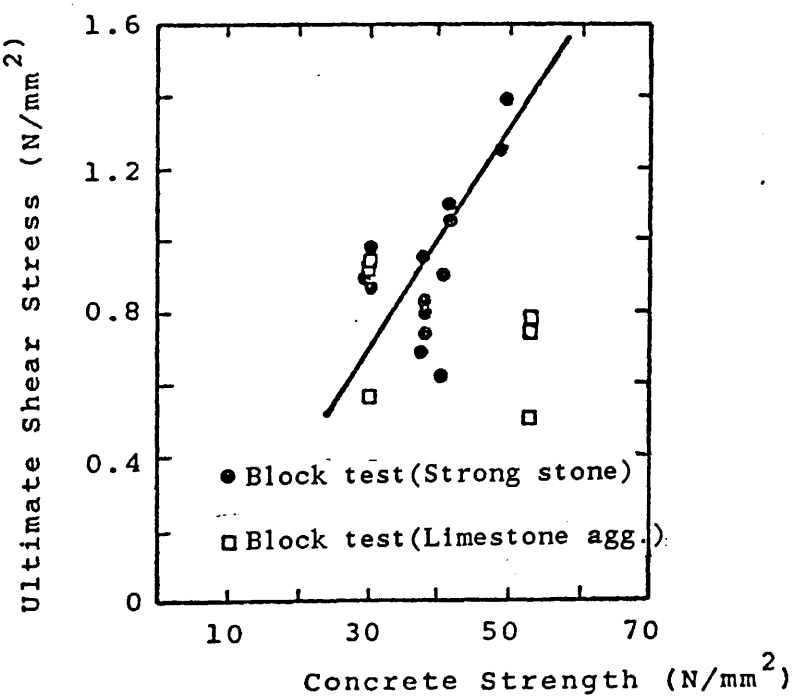

Figure (2.13) Ultimate shear stress vs concrete strength determined by Taylor (8)

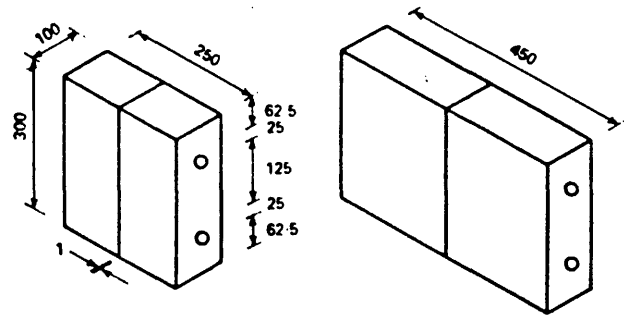

Figure (2.14) Dimensions of specimens for interface shear transfer tests used by Millard and Johnson (15)

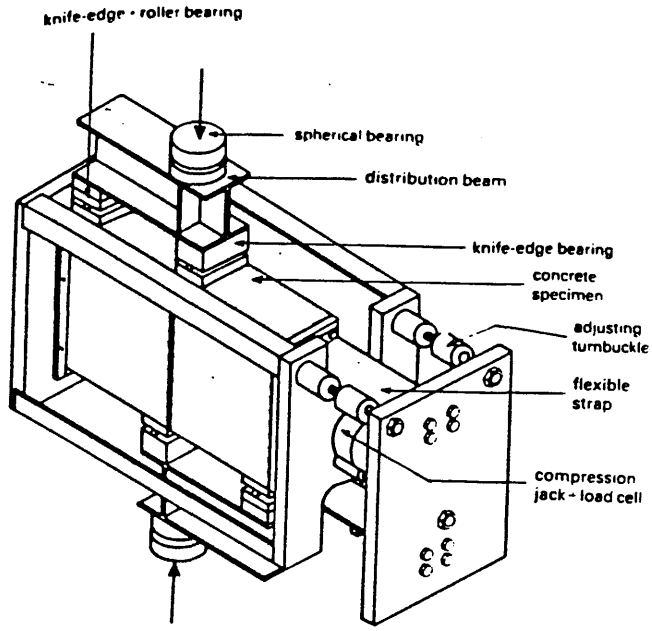

Figure (2.15) General arrangement of specimen and test rig (15)

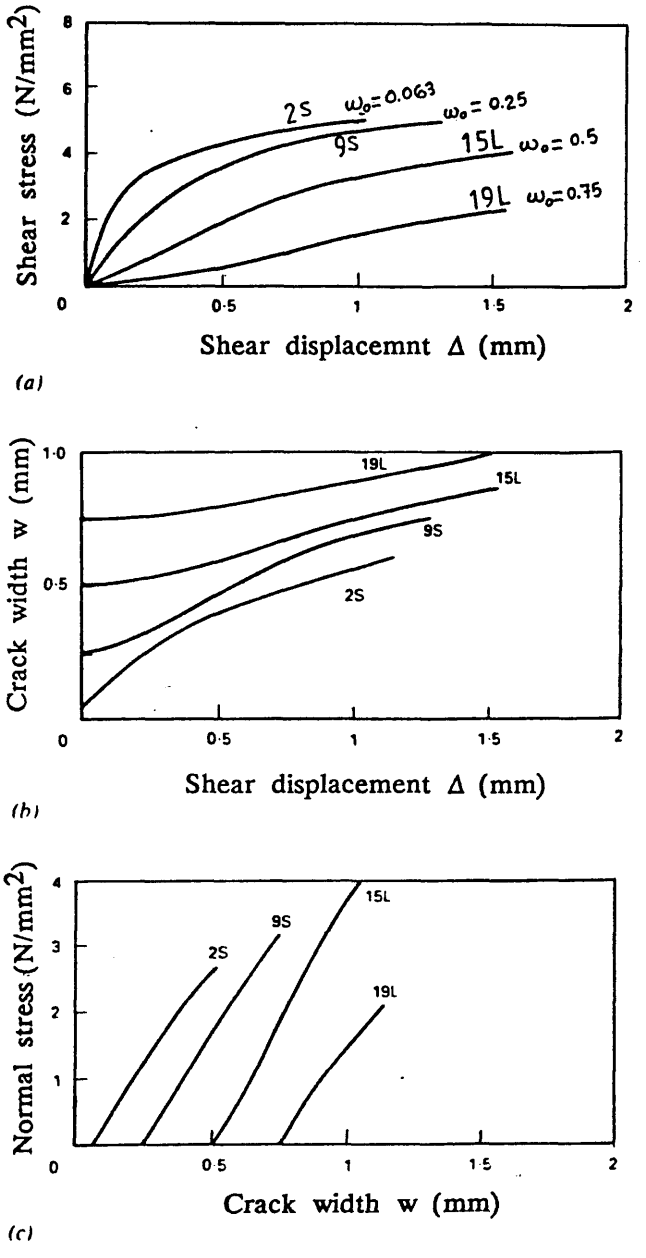

Figure (2.16) Behaviour of interface shear transfer specimens with different initial crack width (15)

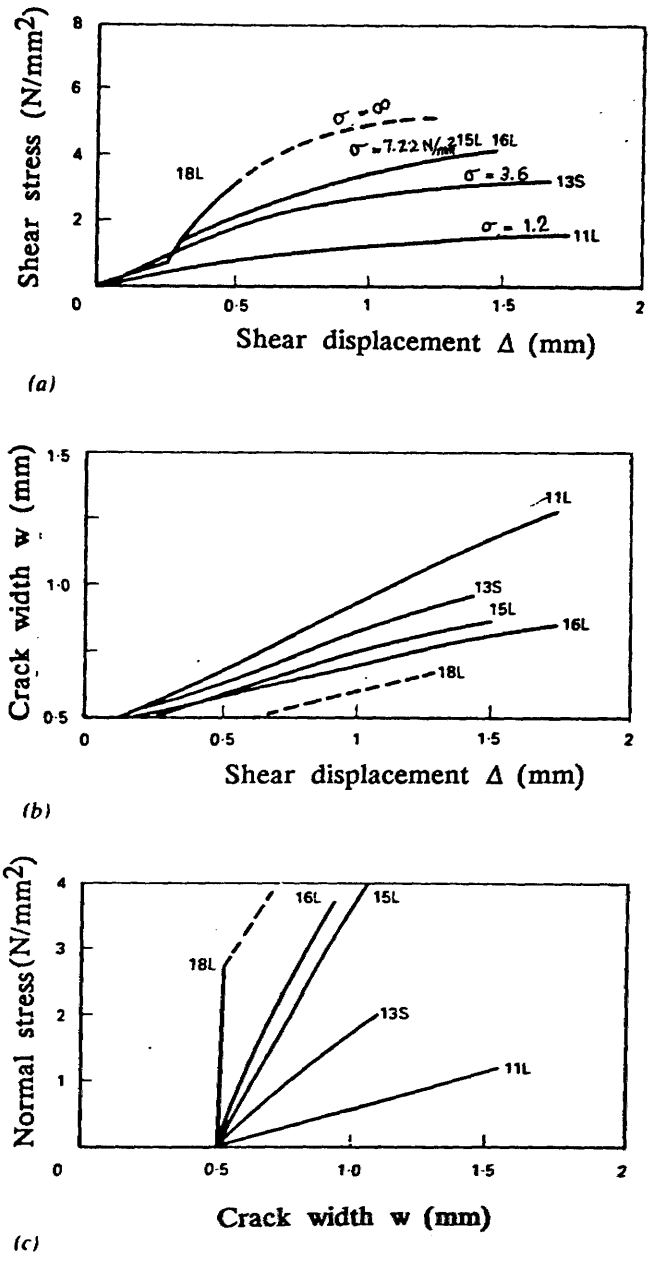

Figure (2.17) Behaviour of interface shear transfer specimens with different normal restraint stiffness (15)

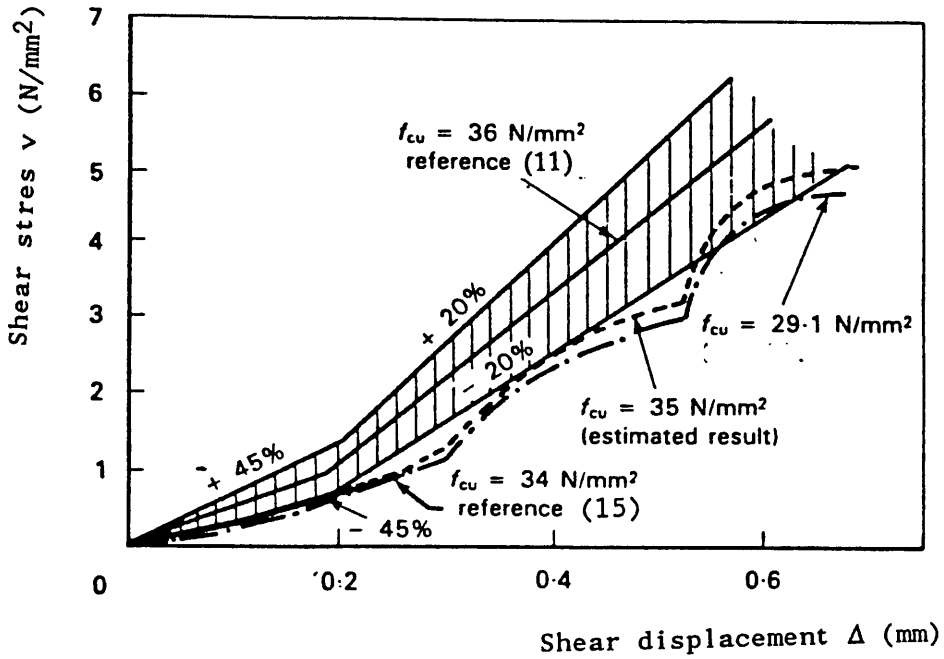

Figure (2.18) Comparison of interface shear transfer test results at constant crack width of 0.5 mm (15) and (11)

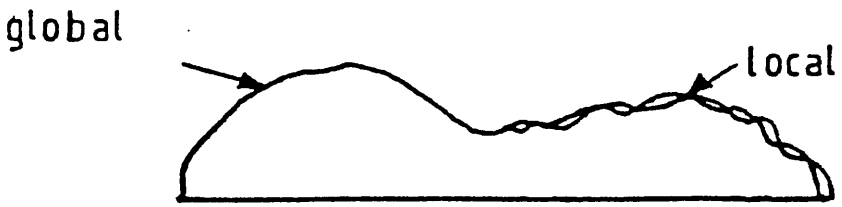

Figure (2.19) Subdivision of roughness (12)

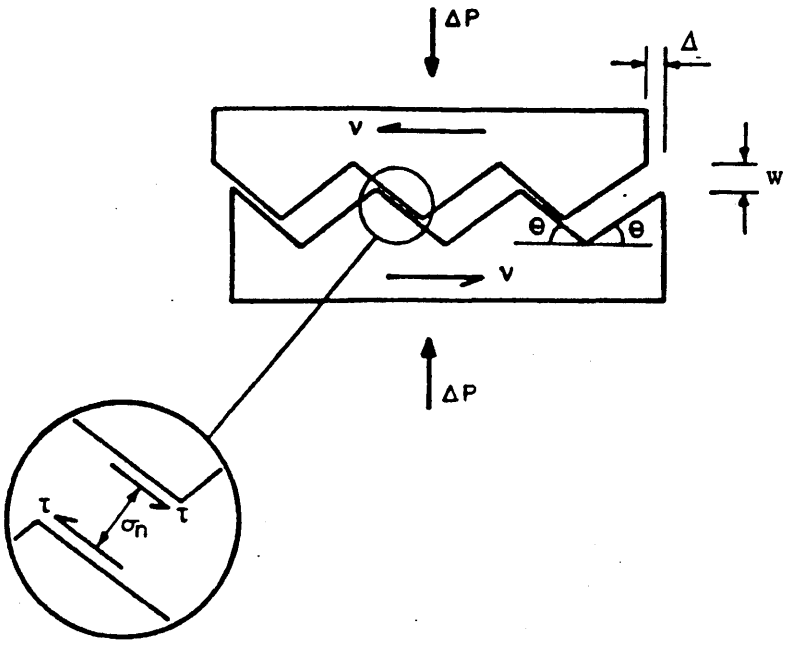

Figure (2.20) Interface shear transfer model (16)

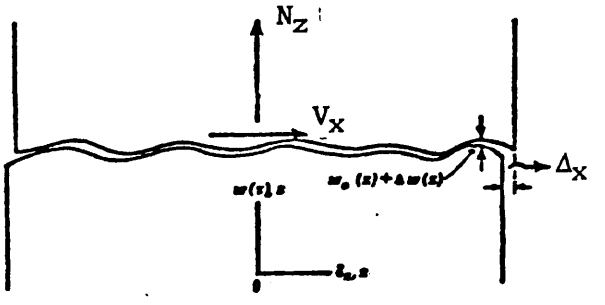

Figure (2.21) Two-dimensional crack configuration (17)

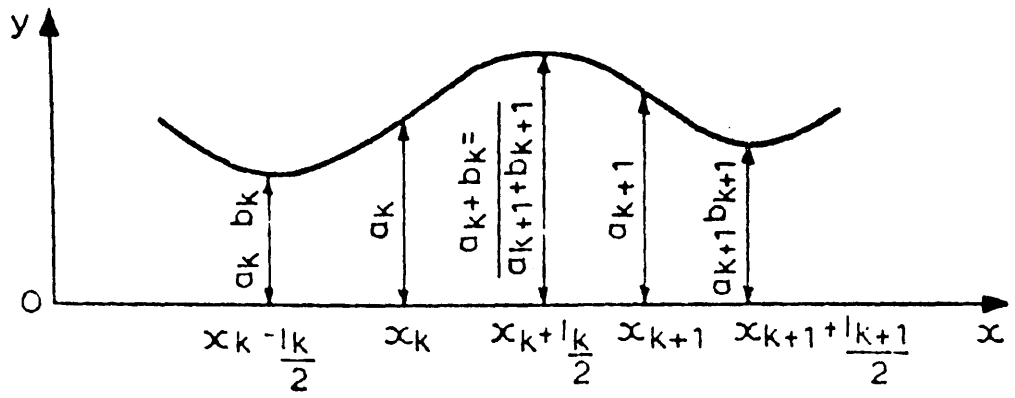

Figure (2.22) Profile of crack (Global roughness), y=f(x) (17)

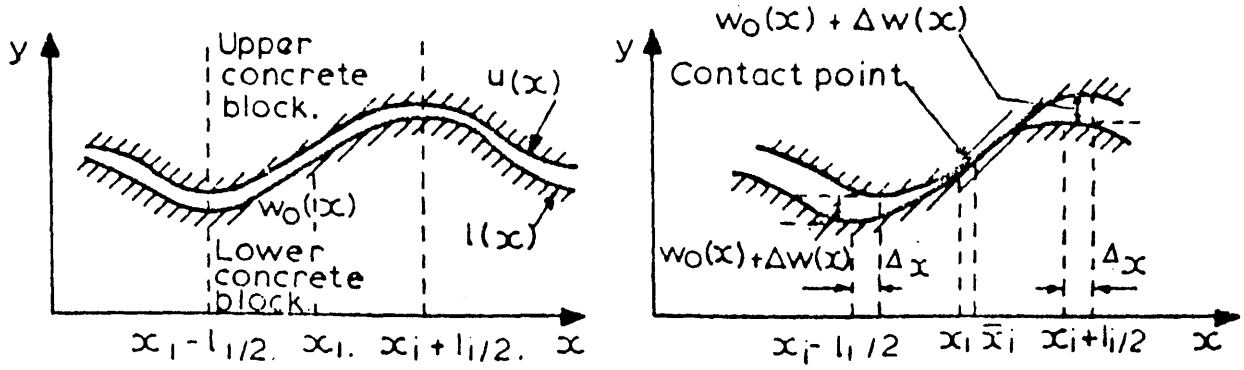

(a) Before shear displacement

(b) After shear displacement

Figure (2.23) Model for interface shear transfer (17)

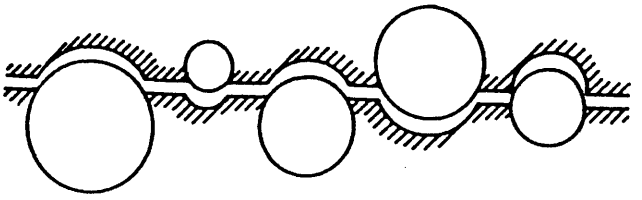

Figure (2.24) Generally observed structure of a crack plane

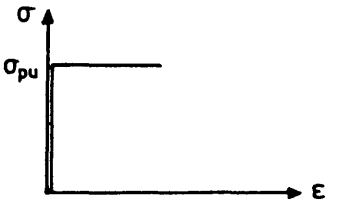

Figure (2.25) Rigid plastic stress–strain relation for the matrix material (20)

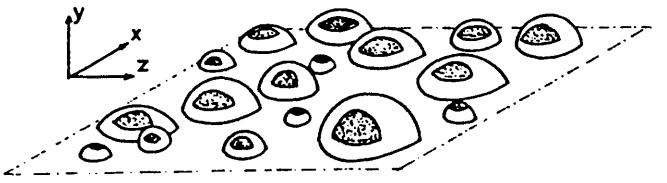

Figure (2.26) Contact areas during shear displacement

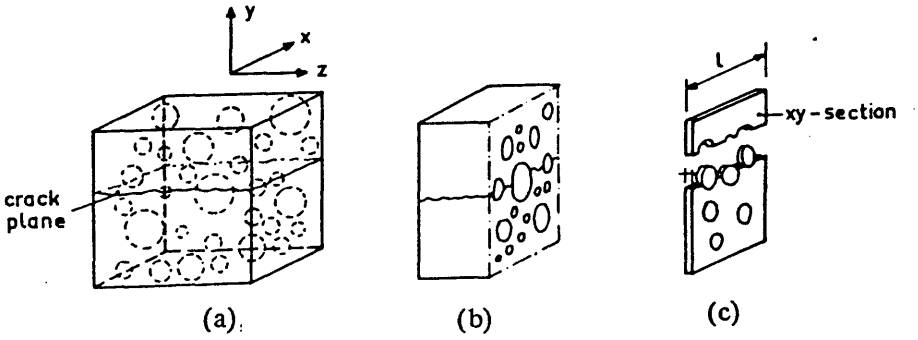

Figure (2.27) Cracked concrete body (a), intersected by Z-plane (b), and a representative slice (c) (20)

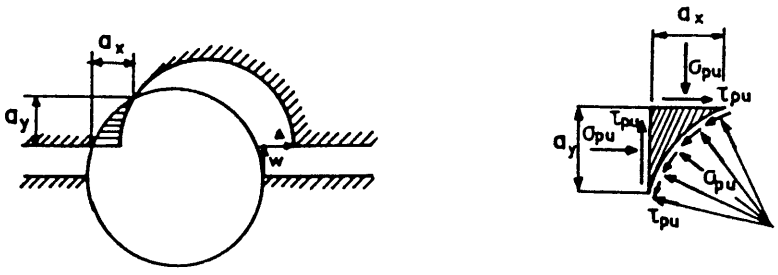

a. contact area between matrix and aggregate

b. stress conditions

Figure (2.28) Equilibrium conditions

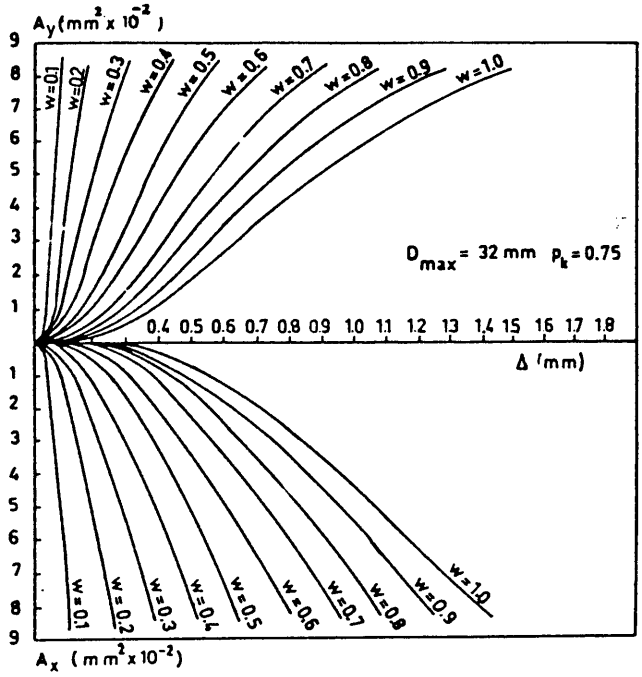

Figure (2.29) Total projected contact areas A_y and A_x for 1 mm^2 crack plane, as a function of crack width w and shear displacement Δ

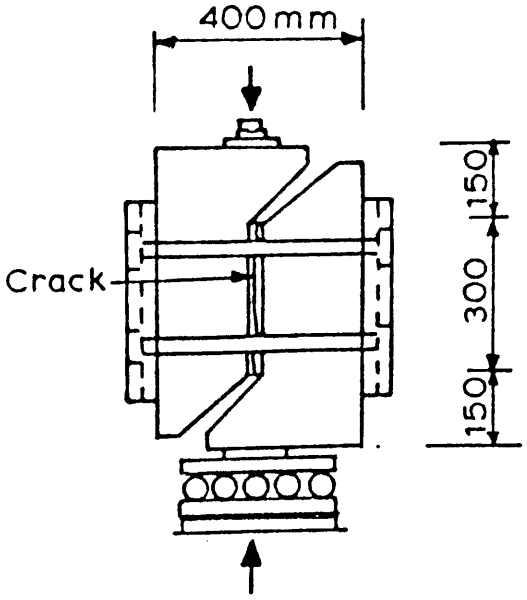

Figure (2.30) Geometry of test specimen used by Walraven (20)

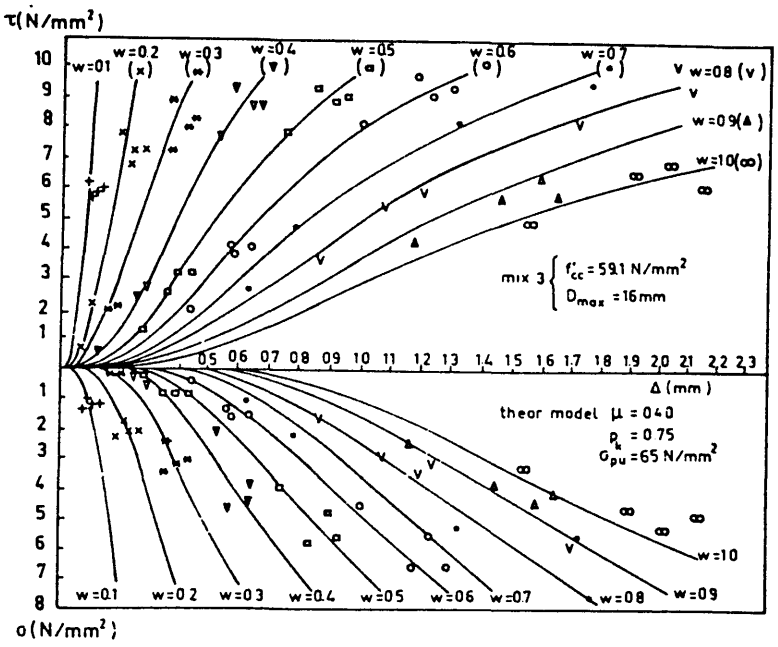

Figure (2.31) Comparison between experimental values for a concrete with $f'_{cc} = 59$ N/mm², $D_{max} = 16$ mm and theoretical values, with $p_k = 0.75$, $\mu = 0.40$ and $\sigma_{pu} = 65$ N/mm².

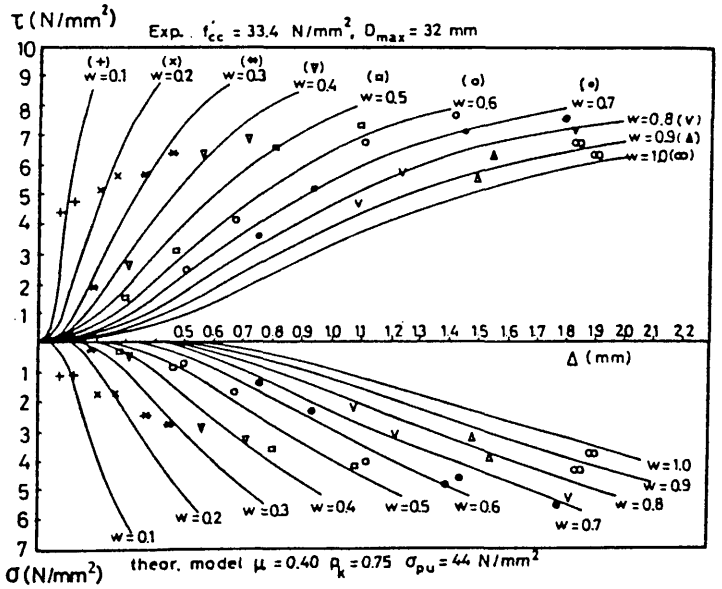

Figure (2.32) Comparison between experimental values for a concrete with $f'_{cc} = 33$ N/mm², $D_{max} = 32$ mm and theoretical values, with $p_k = 0.75$, $\mu = 0.40$ and $\sigma_{pu} = 44$ N/mm²

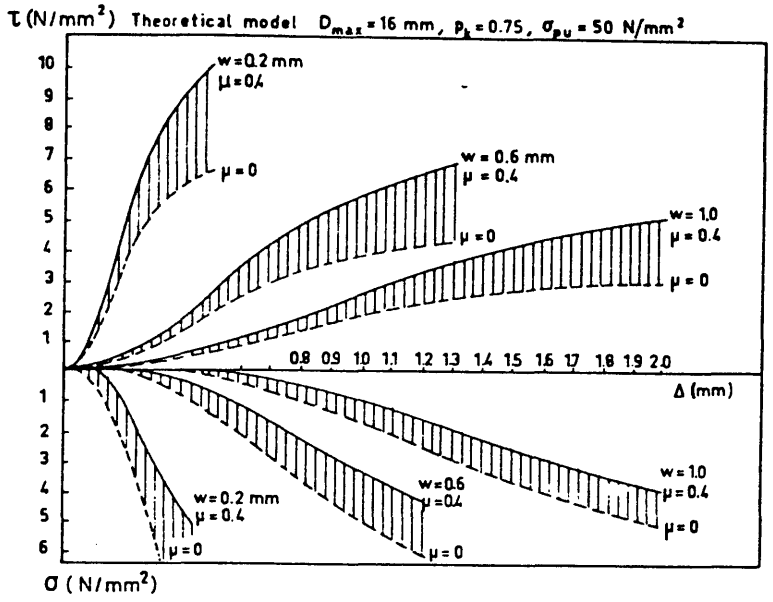

Figure (2.33) The role of friction between aggregate and matrix in the transfer of stresses in a crack, for a concrete with $D_{max} = 16$ mm and $f_{cc} = 40$ N/mm².

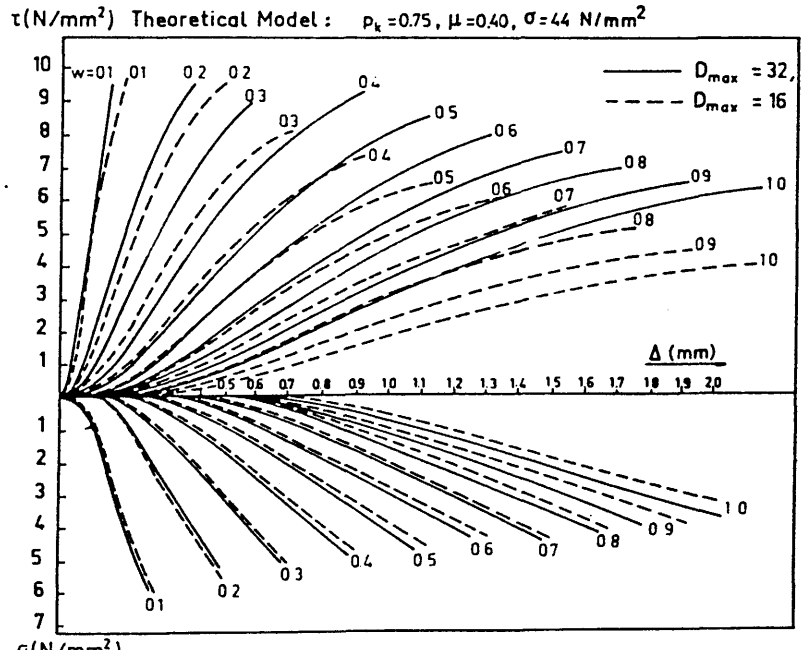

Figure (2.34) The effect of the maximum aggregate particle size on the transfer of stresses in a crack. Concrete strength $f_{cc} = 32$ N/mm², maximum diameter $D_{max} = 16$ and 32 mm.

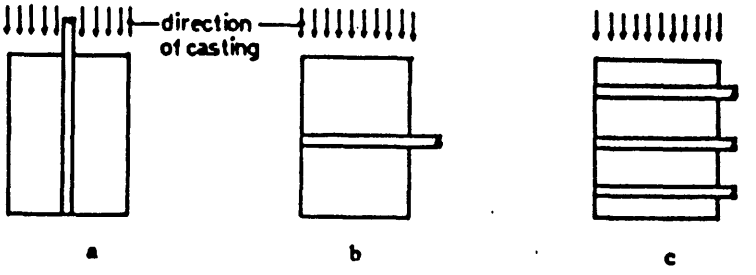

Figure (2.35) Various positions of bars influencing the value of G_f

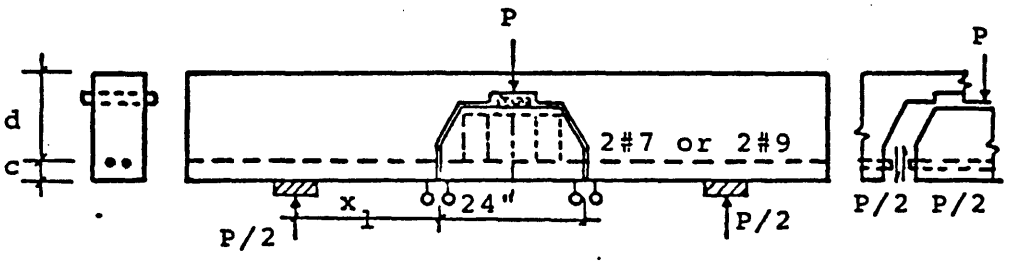

Figure (2.36) Krefeld and Thurston divided beam specimen (27)

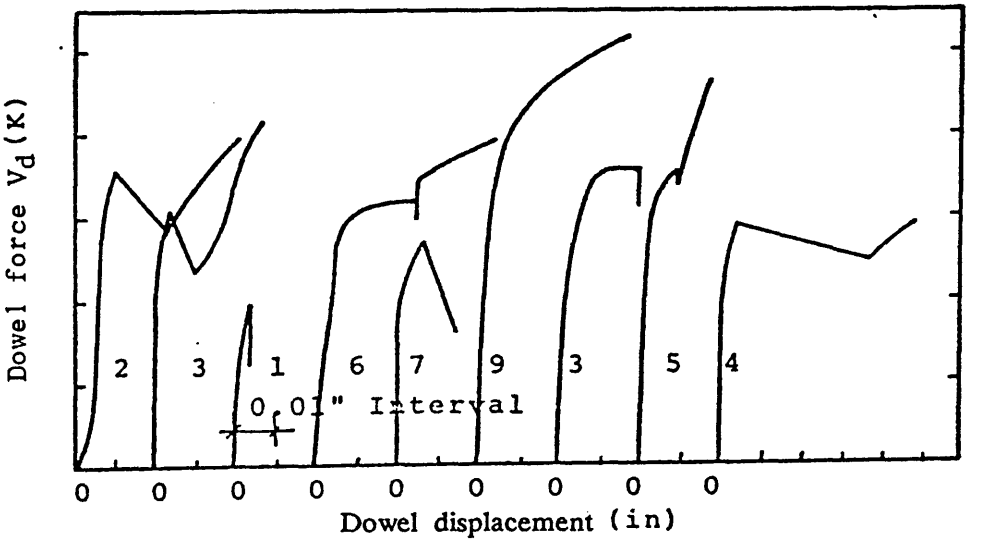

Figure (2.37) Load–displacement curves from Krefeld and Thurston tests (27)

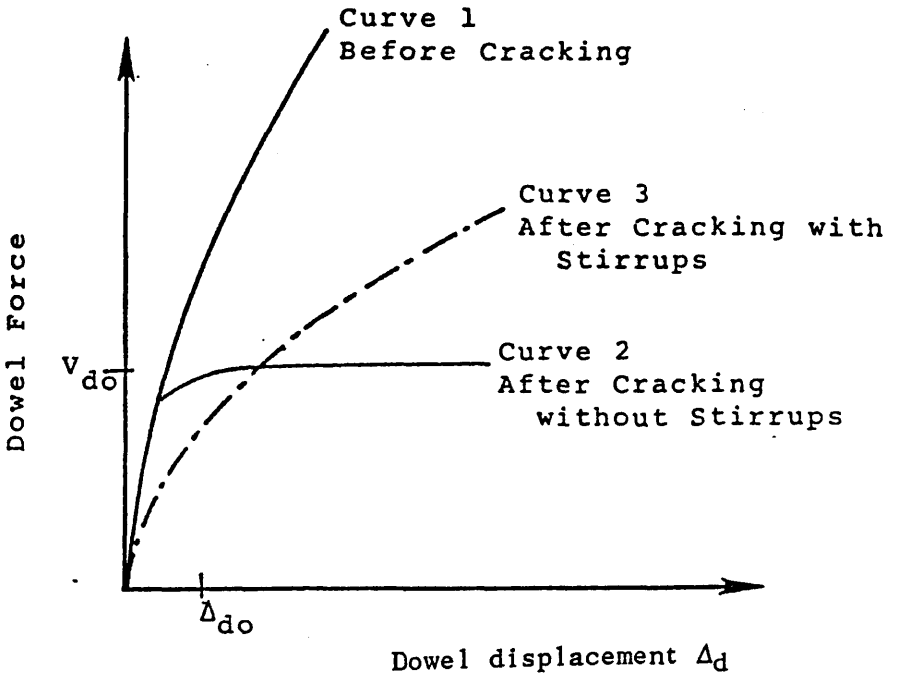

Figure (2.38) Dowel load–displacemnt curves proposed by Baumann (28)

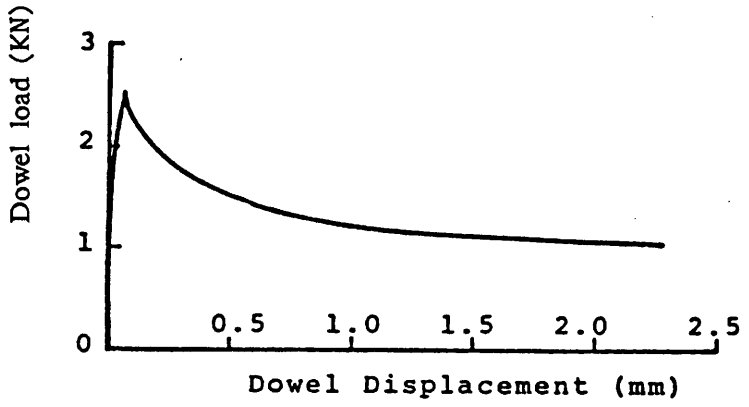

Figure (2.39) Experimental dowel stiffness curve determined by Taylor (29)

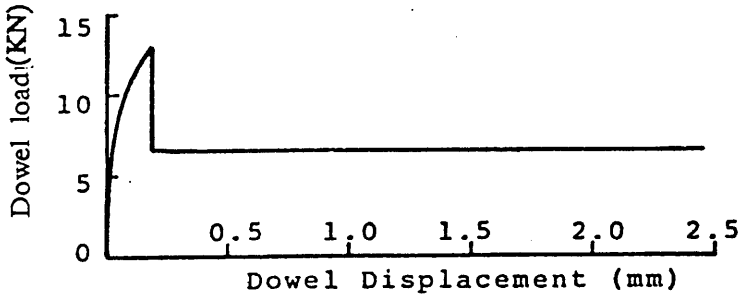

Figuer (2.40) Idealized dowel load–displacemnt curve (29)

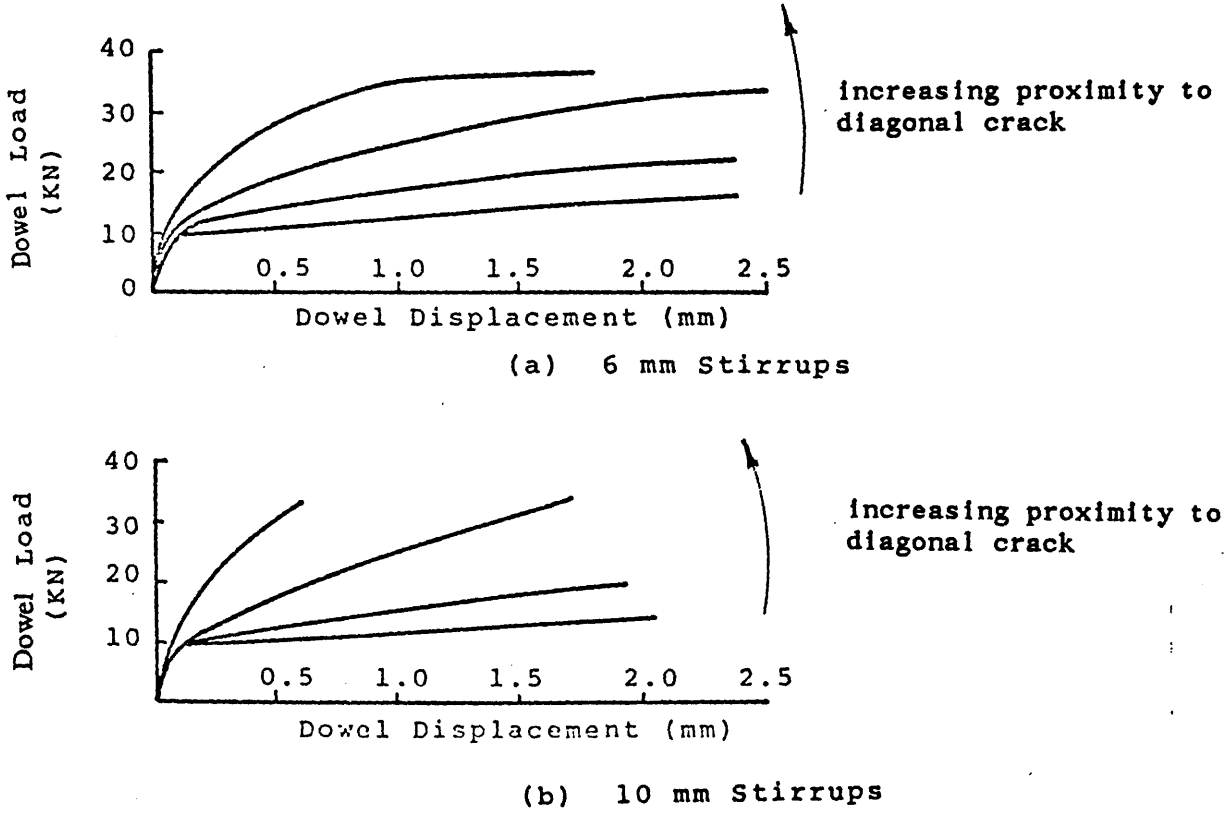

Figure (2.41) Dowel load – displacement curves for specimens with transverse reinforcement (29)

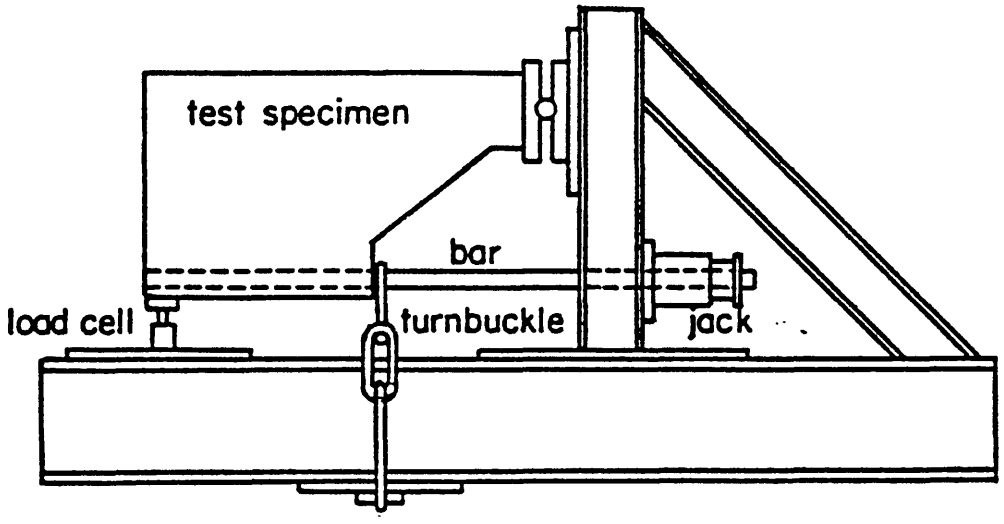

Figure (2.42) Beam end specimen

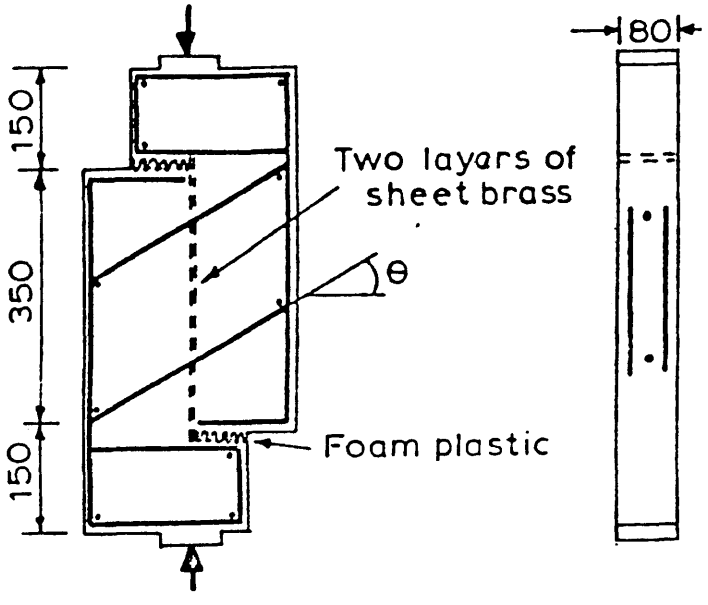

Figure (2.43) Dulacska's test specimen (34)

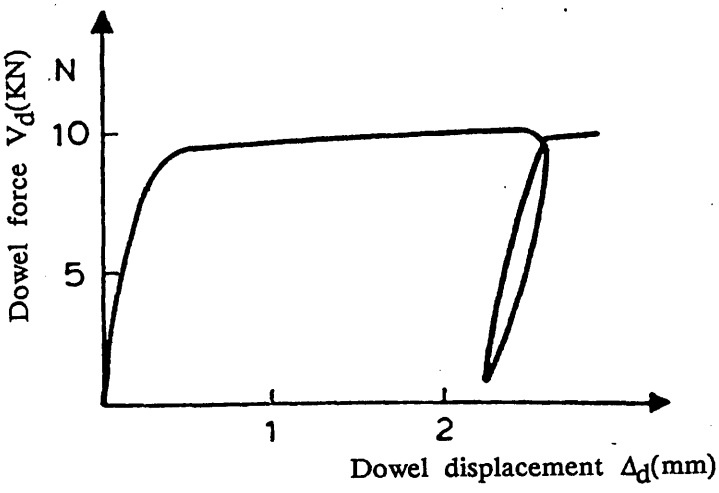

Figure (2.44) Typical dowel load – displacement curve (34)

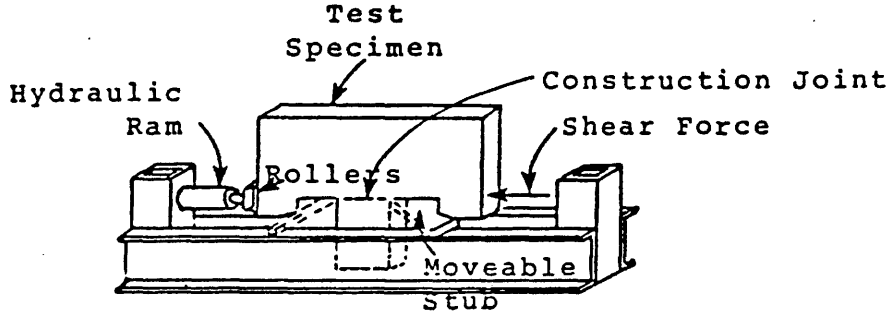

Figure (2.45) Phillips' test specimen (26)

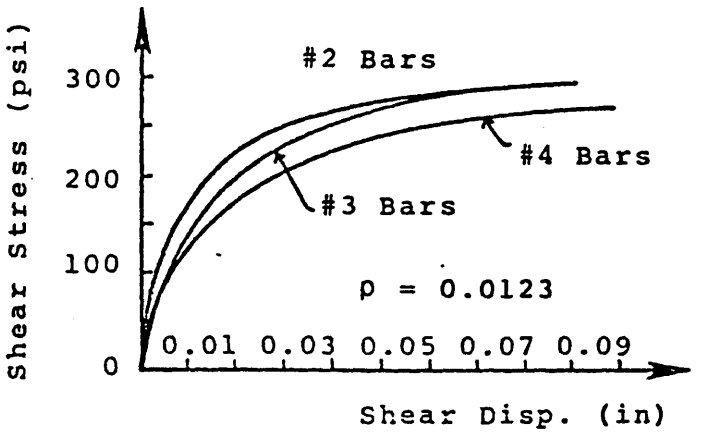

(a) Effect of Bar Diameter

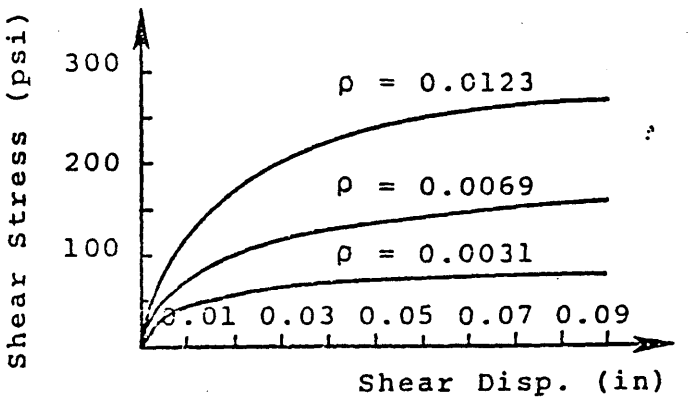

(b) Effect of Reinforcement Ratio

Figure (2.46) Dowel load – displacement curves (26)

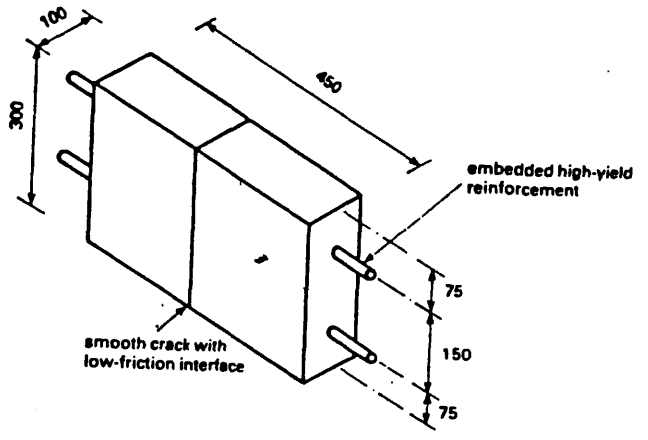

Figure (2.47) Dimensions of specimens for dowel action tests (15)

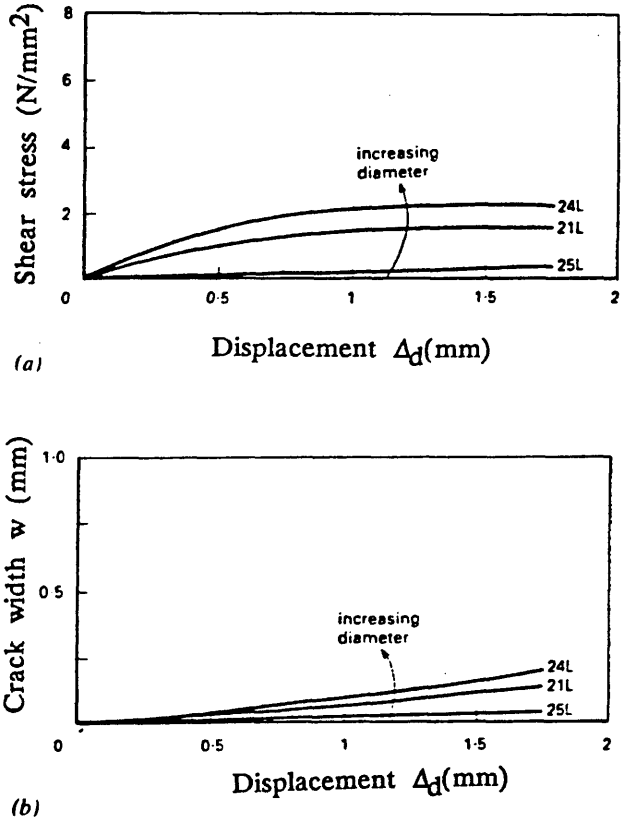

Figure (2.48) Behaviour of dowel action specimens with different reinforcement diameters (15)

(a) Specimen 24L. ϕ = 16 mm *(b) Both faces of specimen 21 L. ϕ = 12 mm* *(c) Both faces of specimen 25 L. ϕ = 8 mm*

Figure (2.49) Crack faces of dowel action specimens after shear testing (15)

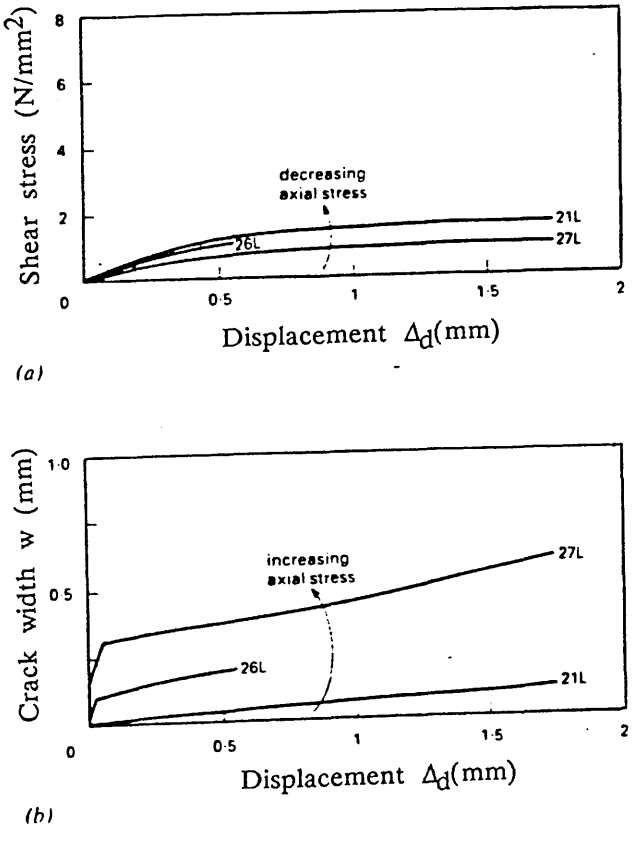

Figure (2.50) Behaviour of dowel action specimens with different axial reinforcement stresses (15)

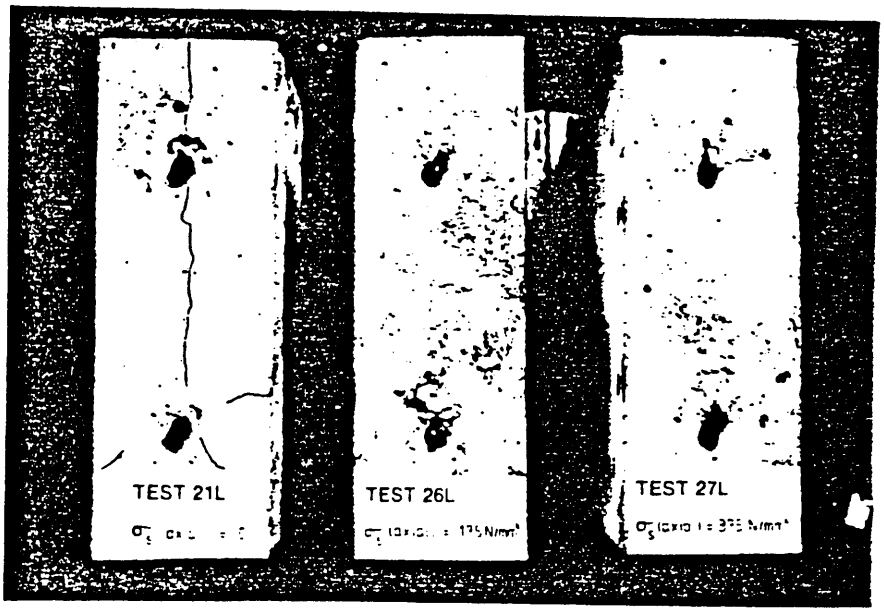

Figure (2.51) Crack faces of dowel action specimens with different axial loads after shear testing (15)

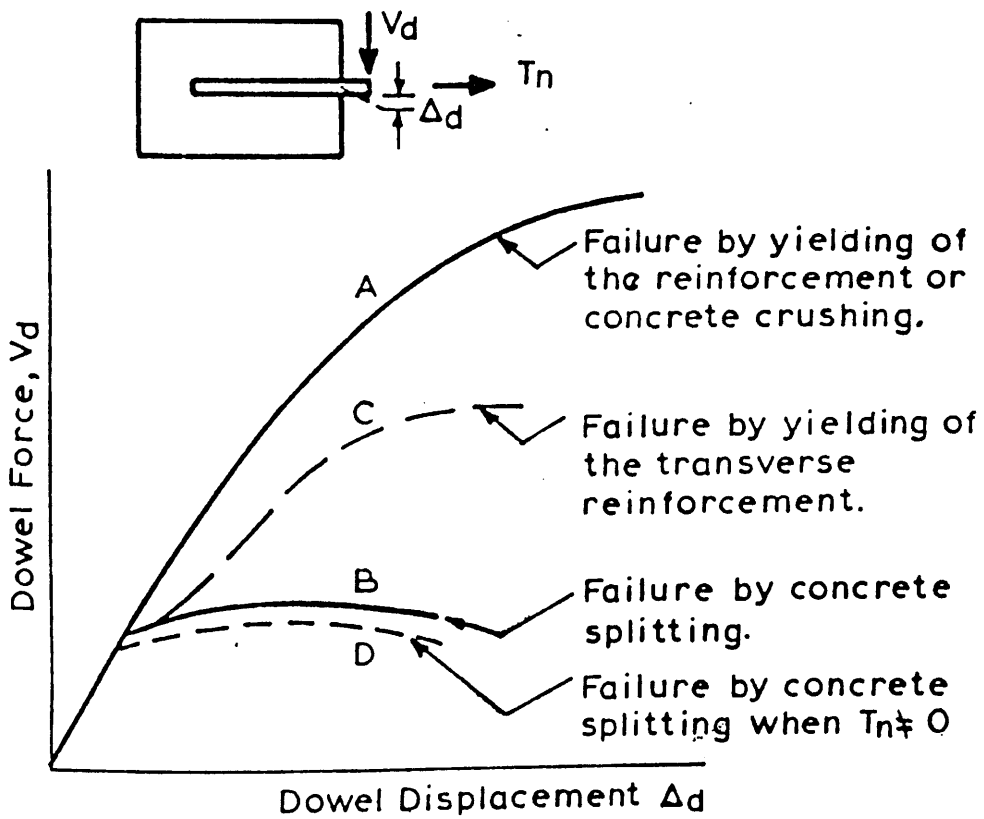

Figure (2.52) Possible relationship between dowel force and displacemnt

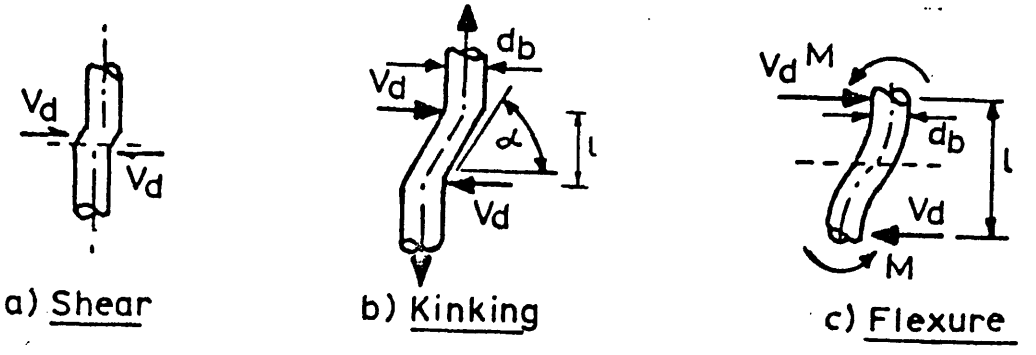

Figure (2.53) The mechanisms of dowel action (26)

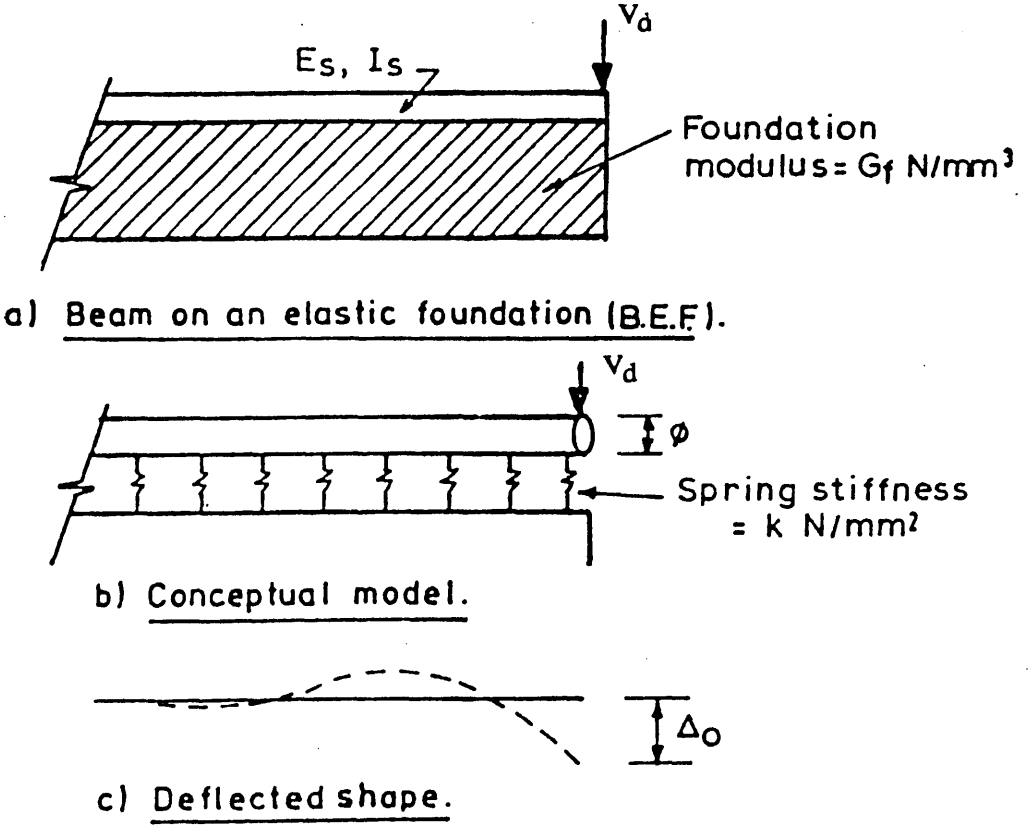

Figure (2.54) Dowel action model (42)

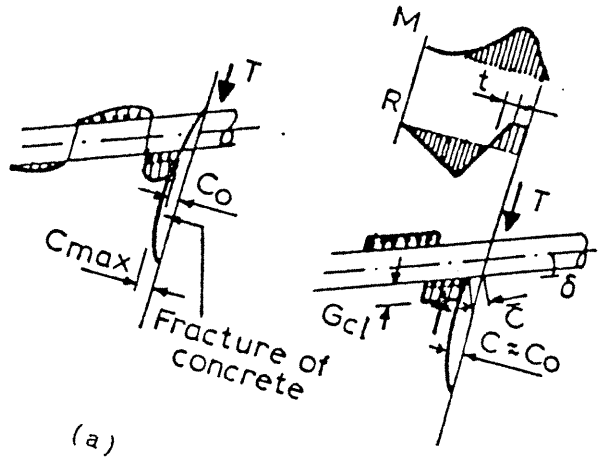

Figure (2.55) (a) Probable system of forces ; (b) assumed system of forces (34)

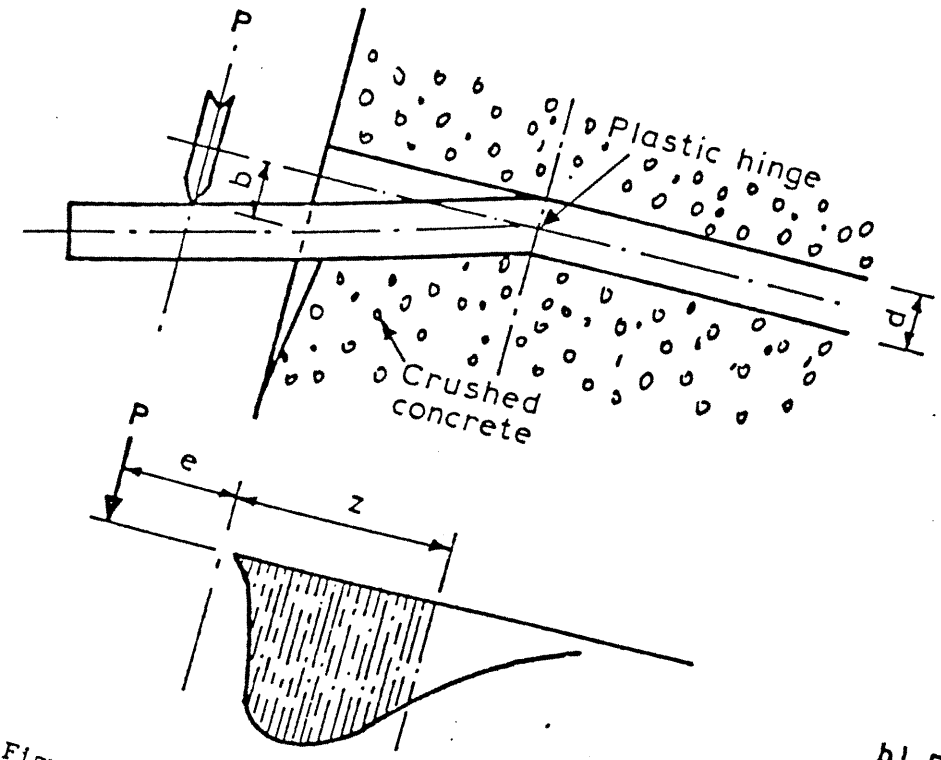

a) Deformation at ultimate loading.

b) Re-distributed reaction.

Figure (2.56) Mechanism to describe the bearing capacity for a dowel (43)

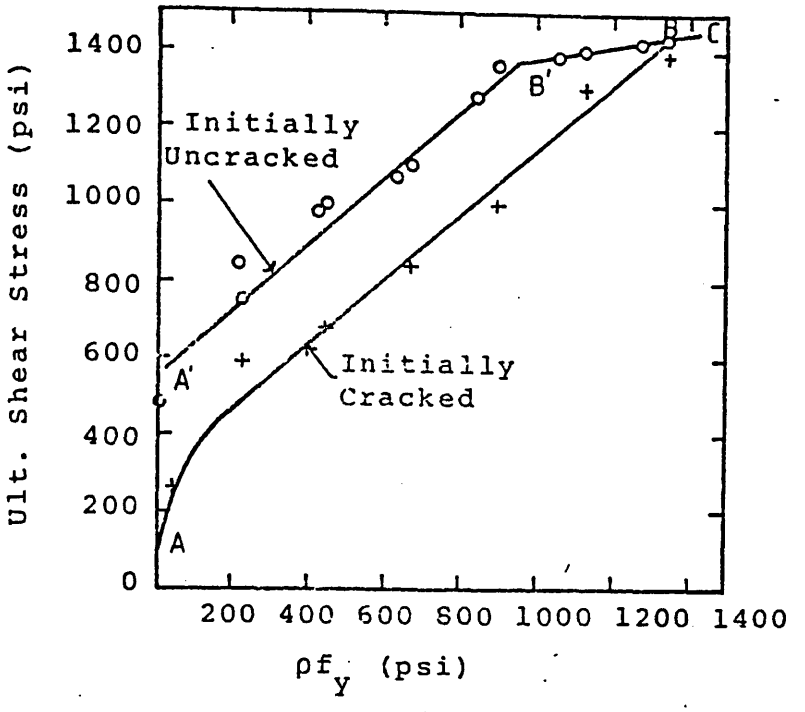

Figure (2.57) Ultimate shear stress vs reinforcement parameter for Mattock's tests (49)

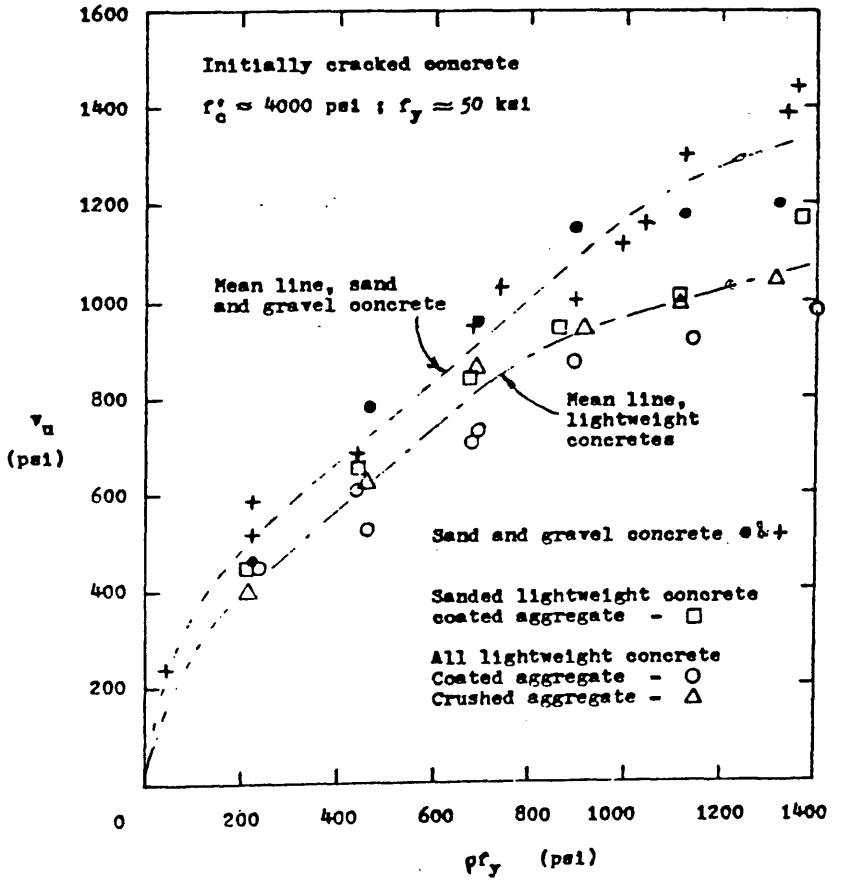

Figure (2.58) Effect of aggregate type on the shear transfer strength of initially cracked concete (51)

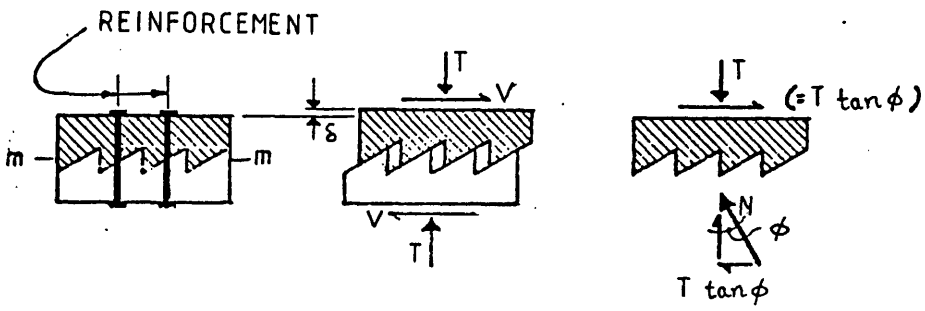

Figure (2.59) Shear friction hypothesis (53)

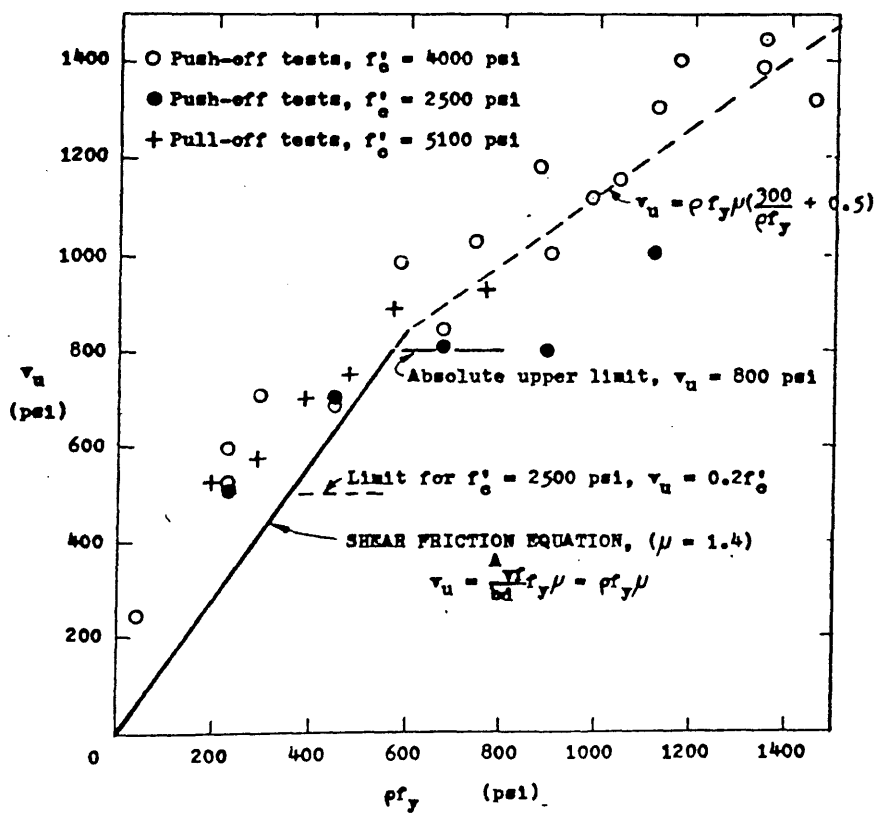

Figure (2.60) Comparison of shear transfer strength calculated using shear friction model and test results (51)

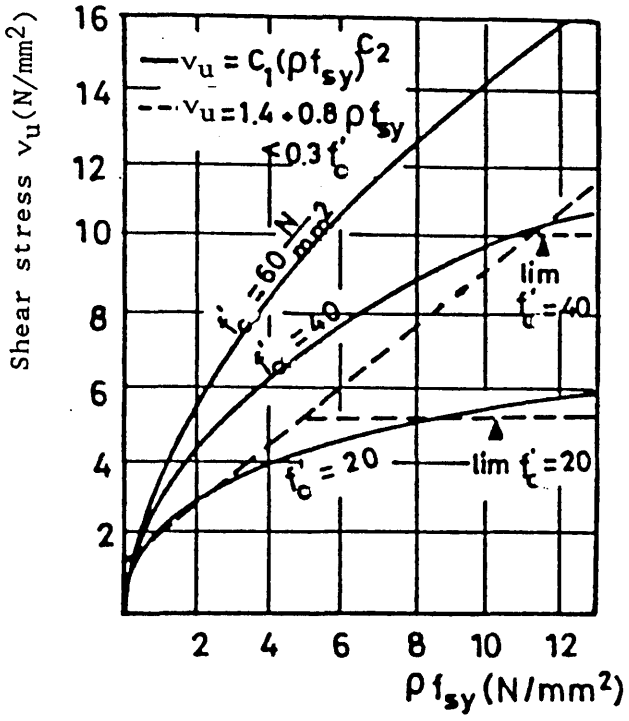

Figure (2.61) Comparison between Equations (2.21)and(2.22) for ultimate shear stress

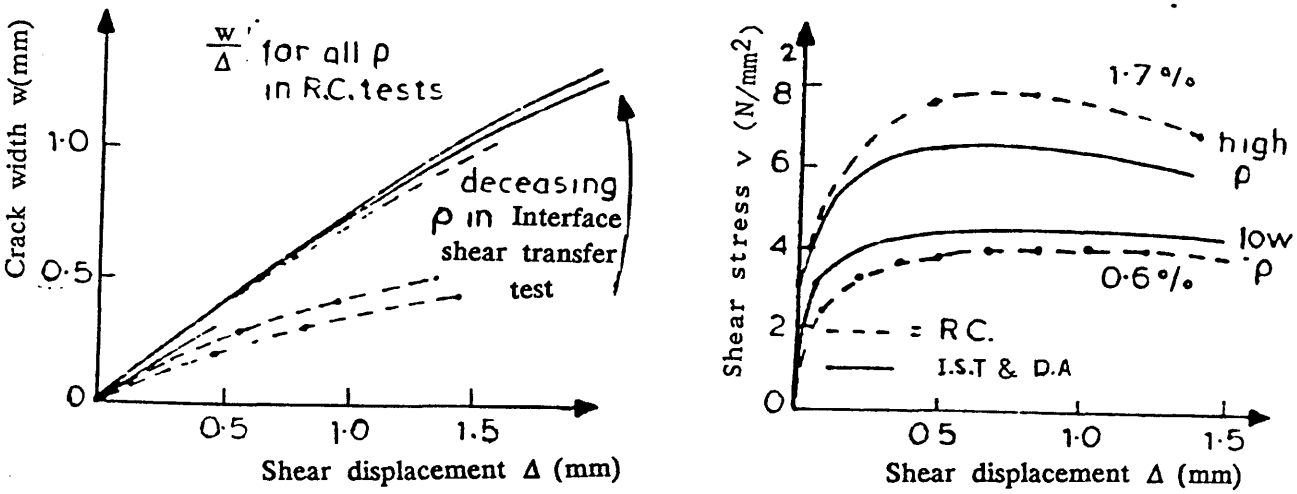

Figure (2.62) Comparison of R.C test results with results predicted from interface shear transfer and dowel action tests (56)

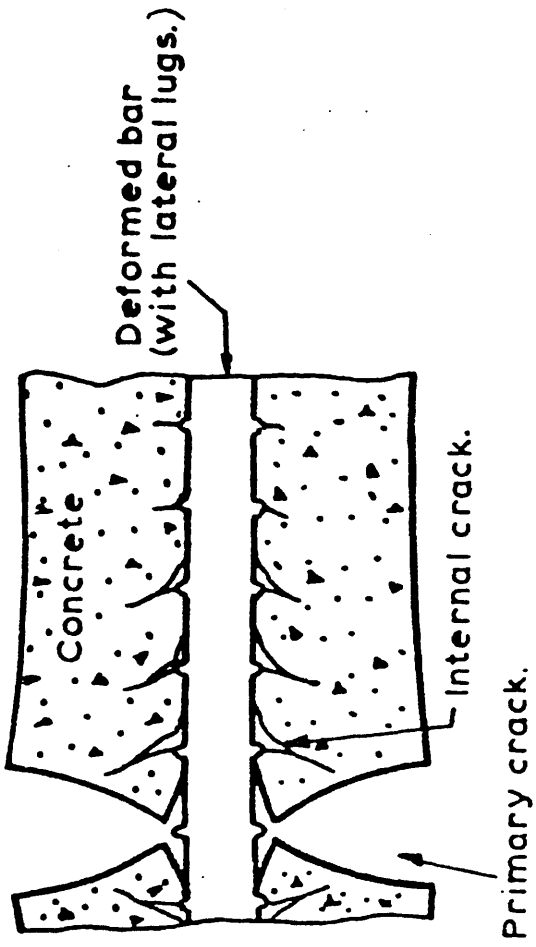

Figure (2.63) Internal crack pattern according to Goto (45)

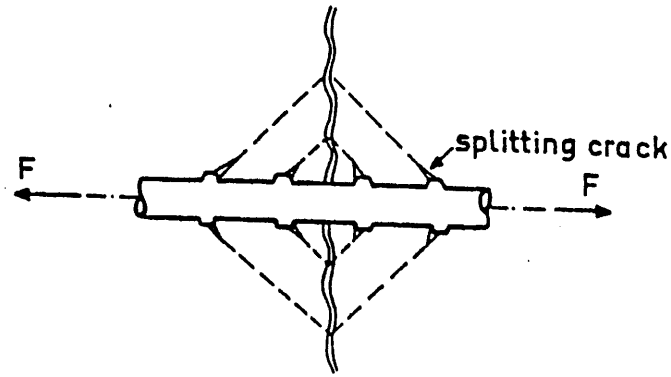

Figure (2.64) Deterioration of the concrete by splitting forces around a rebar

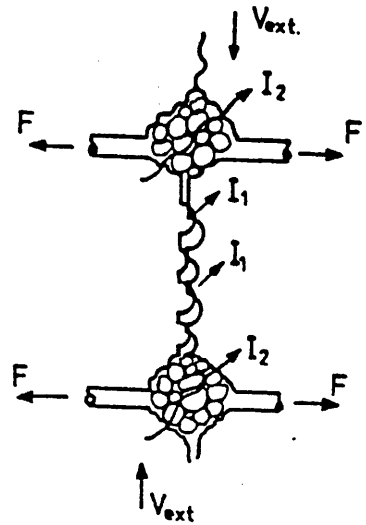

Figure (2.65) Two mechanisms of interface shear transfer in a crack, crossed by reinforcement

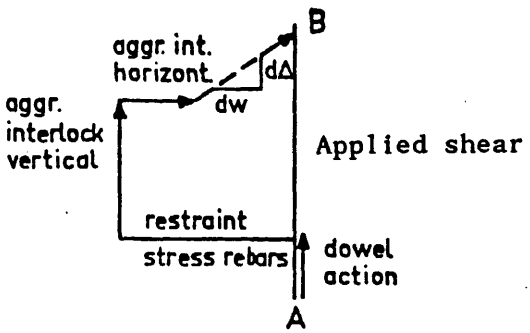

Figure (2.66) Polygon of forces (56)

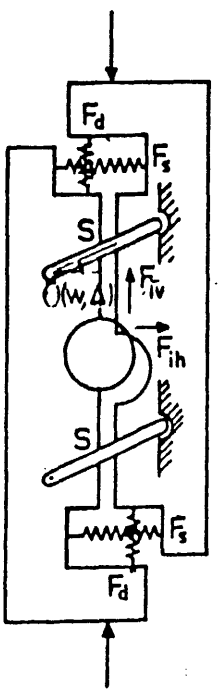

Figure (2.67) Schematical representation of forces in a reinforced crack (56)

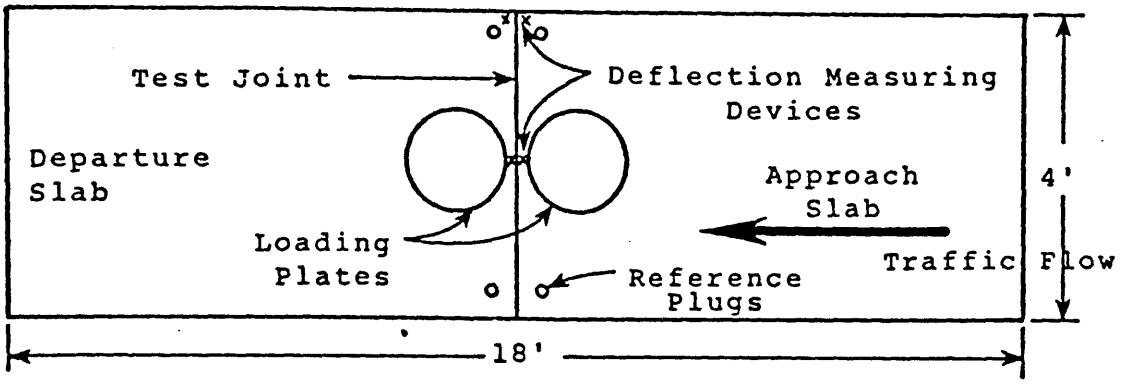

(a) Test specimen

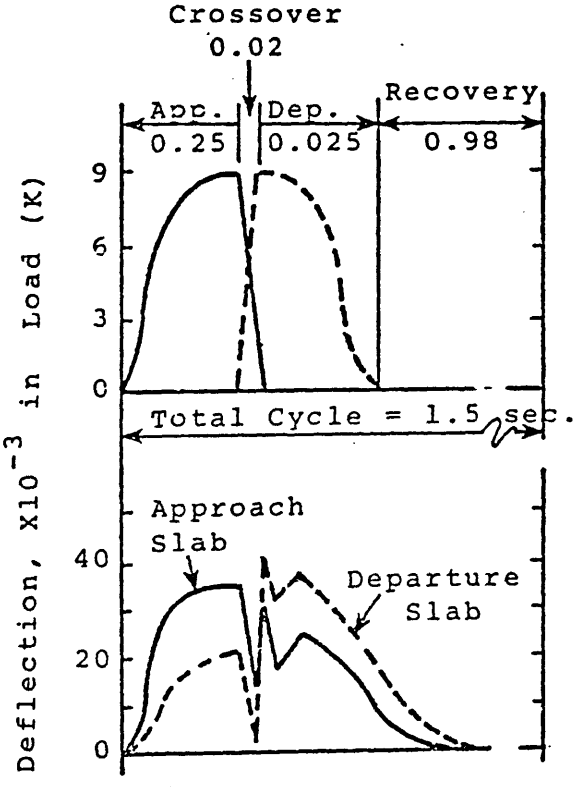

(b) Loading cycle

Figure (2.68) Colley and Humphey test specimen and loading details (57)

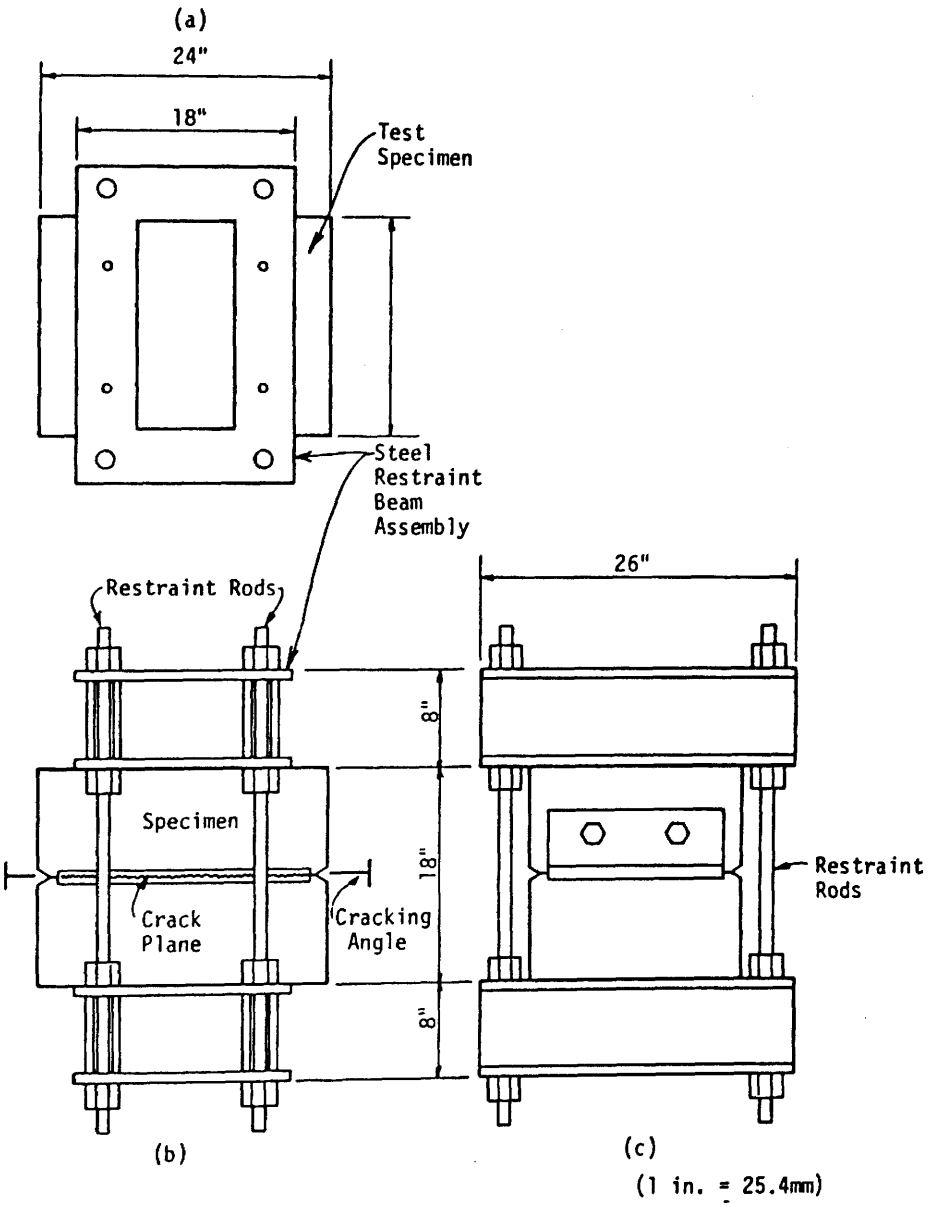

Figure (2.69) Test specimen (12)

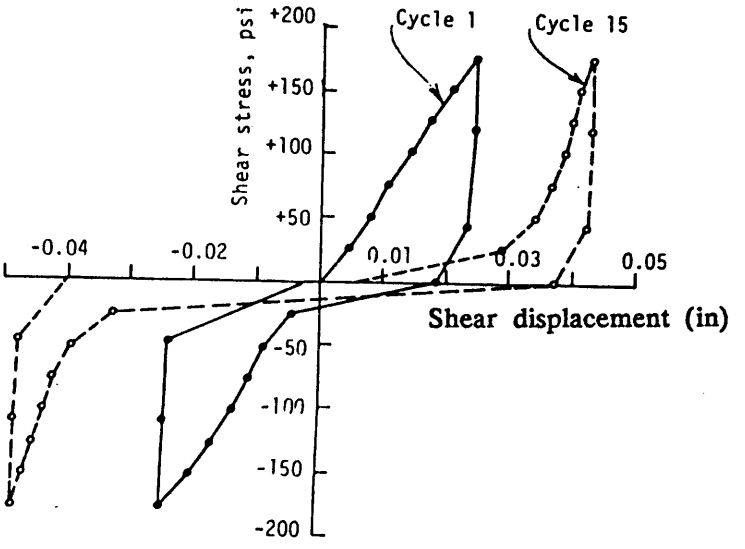

(a) Shear stress vs shear displacement

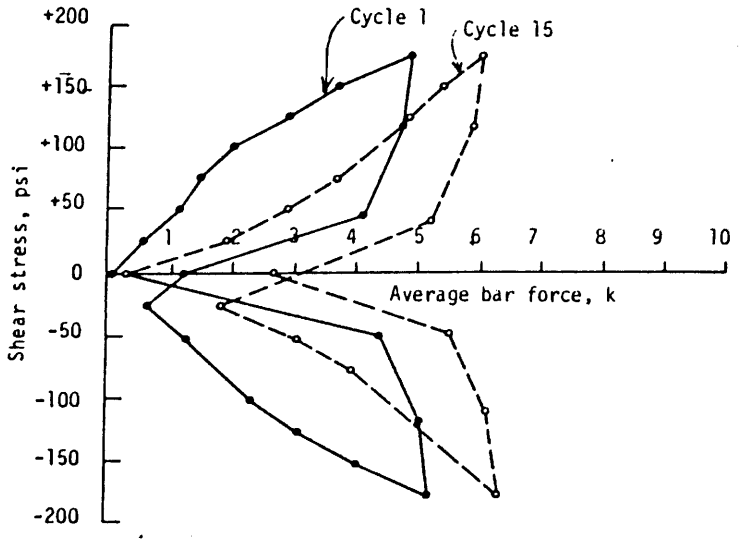

(b) Shear stress vs bar force

Figure (2.70) Typical test results : specimen A1 , initial crack width = 0.030 in. and restraint stiffness = 3420 kip/in(12)

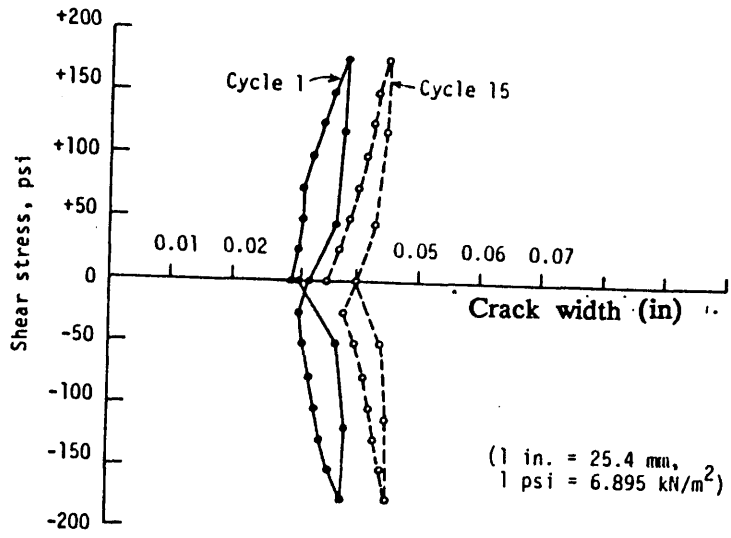

(c) Shear stress vs crack width

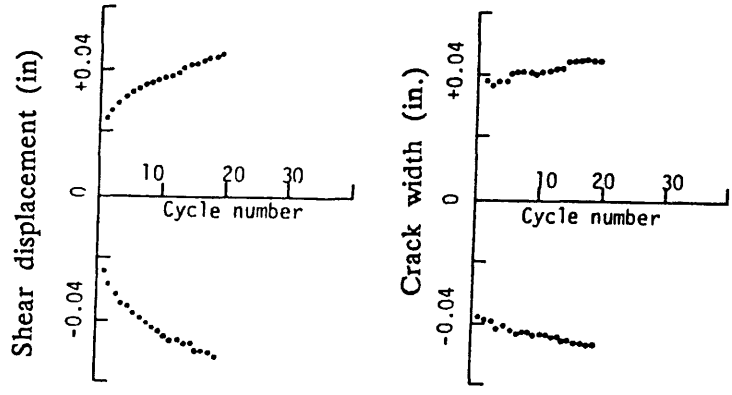

(d) Max. shear displacement vs cycle number

(e) Crack width vs cycle number

Figure (2.70) Typical test results : specimen A1 , initial crack width = 0.030 in. and restraint stiffness = 3420 kip/in(12)
(Cont.)

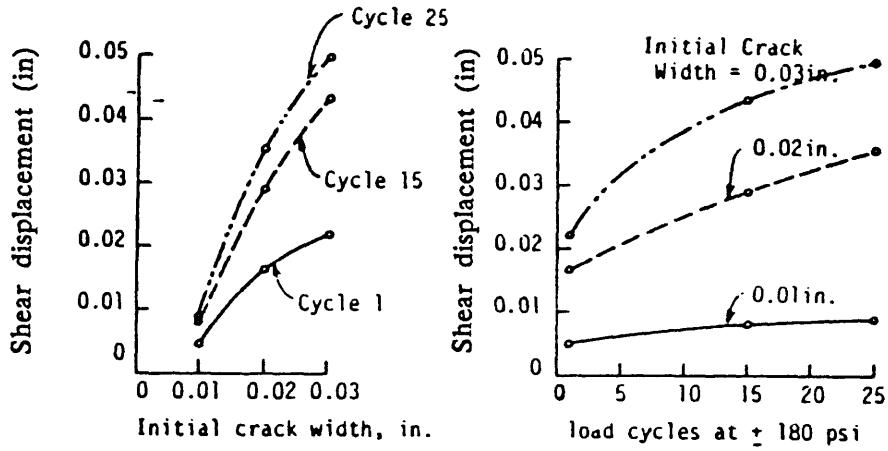

(a) Variation of shear displacemnt with initial crack width

(b) Variation of shear displacement with load cycles

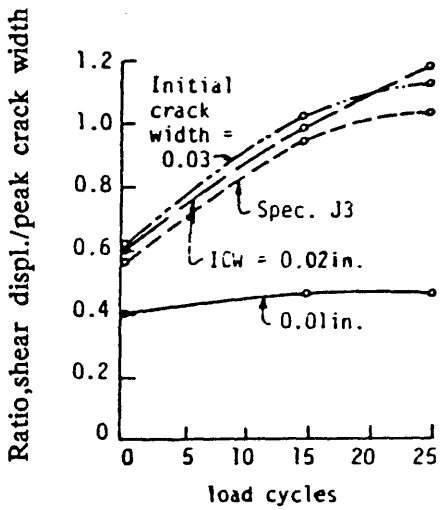

(c) Variation of shear displacement to peak crack width with load cycles

Figure (2.71) Shear displacement as a function of crack width and cycling restraint k = 3420 Kip/in. (12)

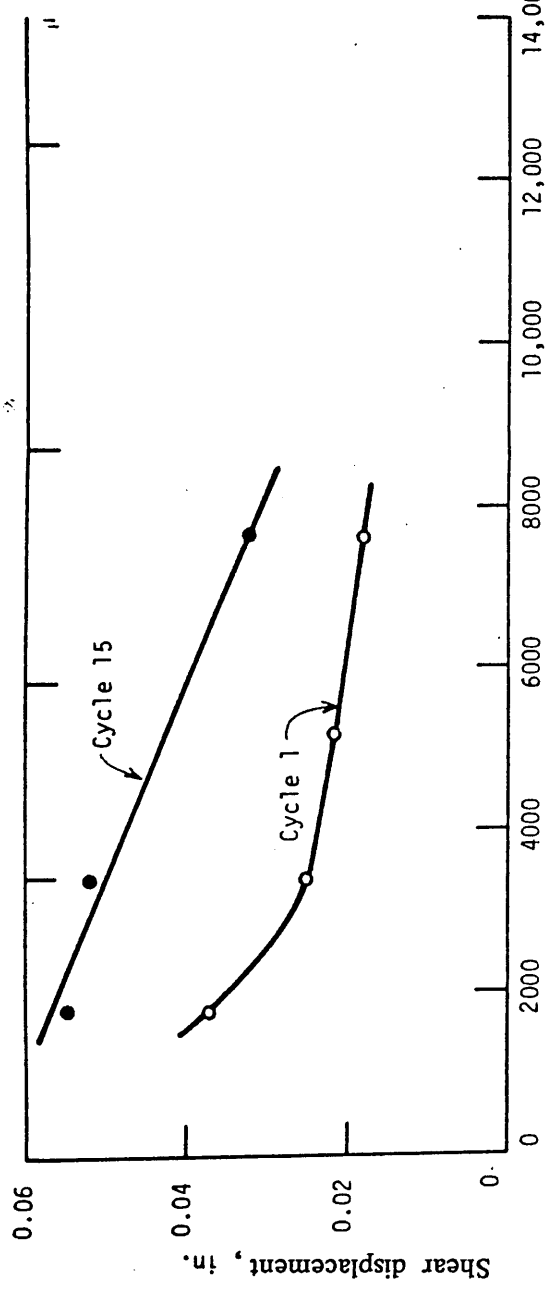

Figure (2.72) Shear displacement versus restraint stiffness, initial crack width = 0.030 in. , shear stress =±180 psi

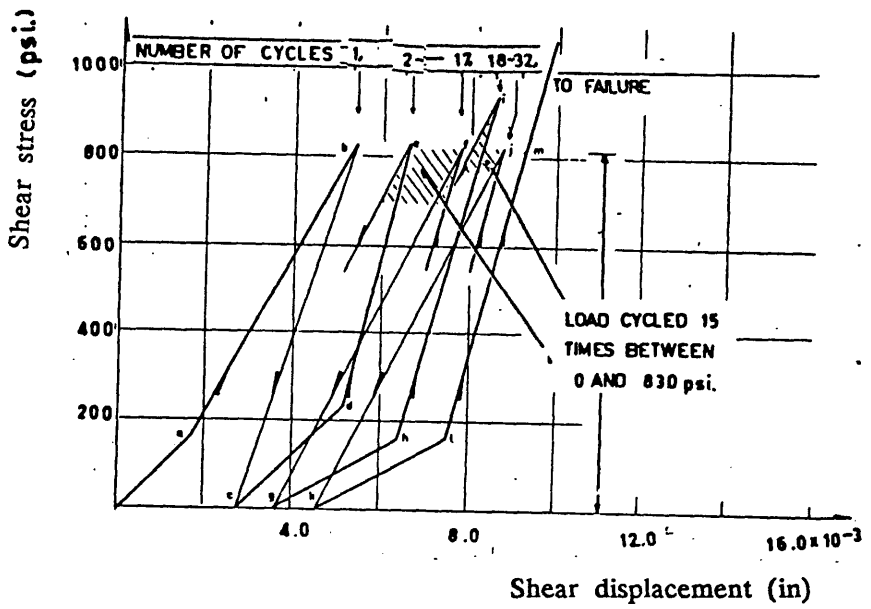

(a) Initial crack width = 0.005 in., max. aggregate size 3/4 in.(round)

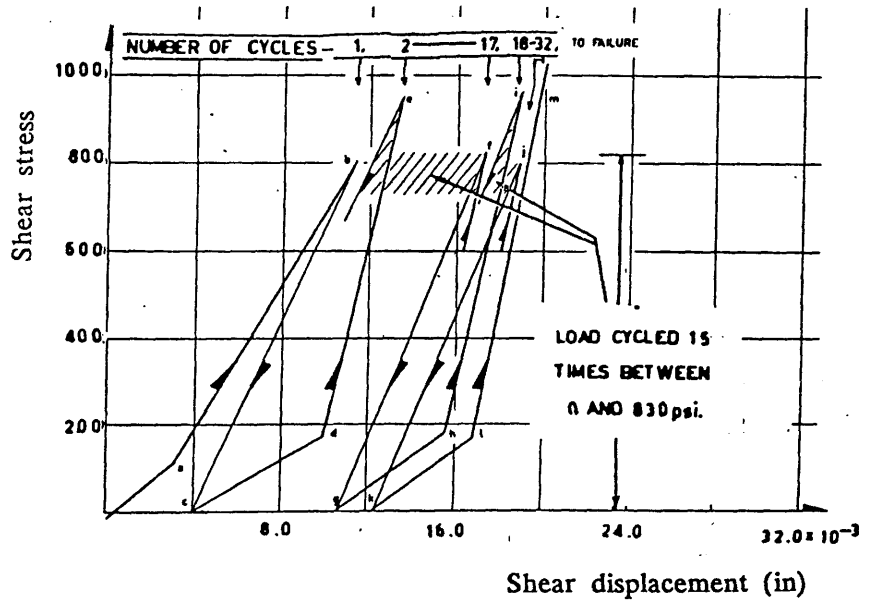

(b) Initial crack width = 0.010 in., max. aggregate size 3/4 in.(round)

Figure (2.73) Shear stress — shear displacement relationship for repeated loading (11)

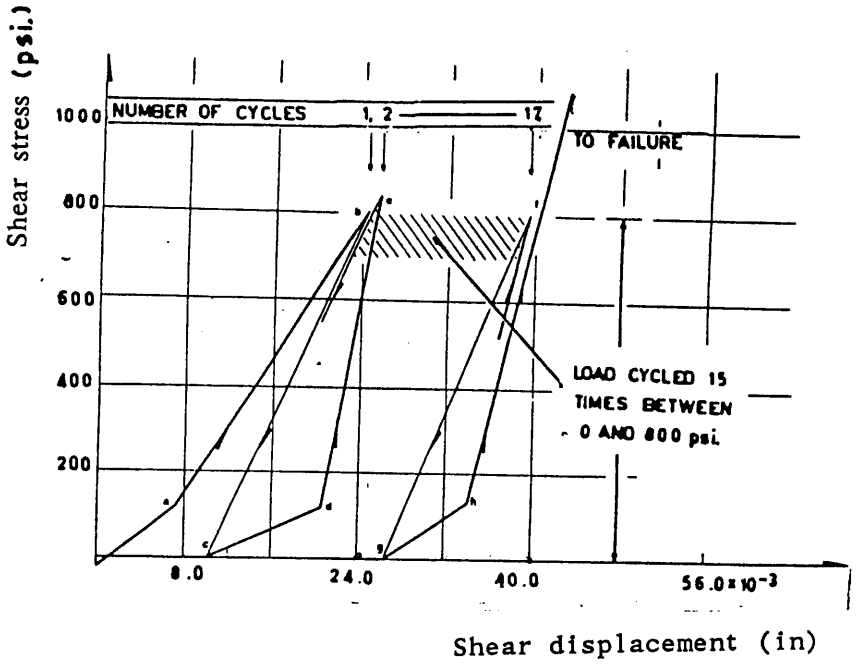

(c) Initial crack width = 0.020 in., max. aggregate size 3/4 in.(round)

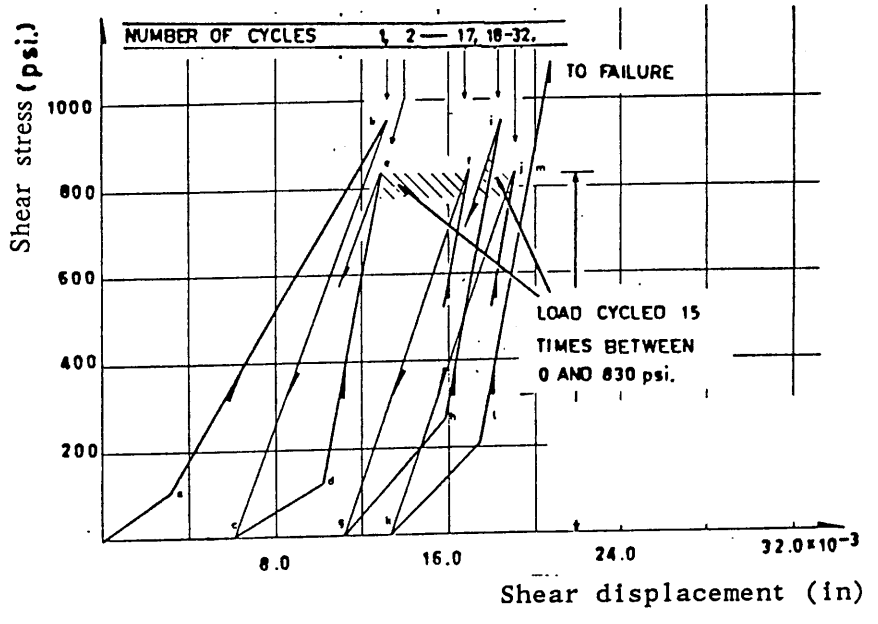

(d) Initial crack width = 0.010 in., max. aggregate size 3/8 in.(round)

Figure (2.73) Shear stress - shear displacement relationship for repeated loading (11)

(Cont.)

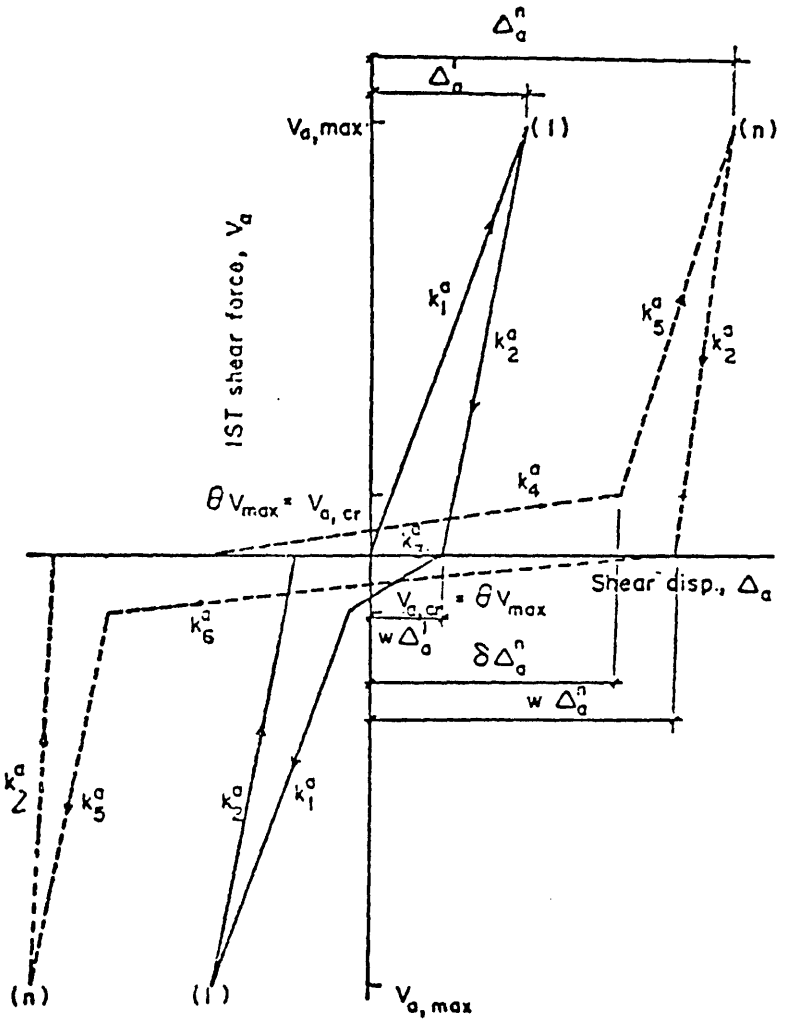

Figure (2.74) Idealization for interface shear transfer force versus shear displacemen (16)

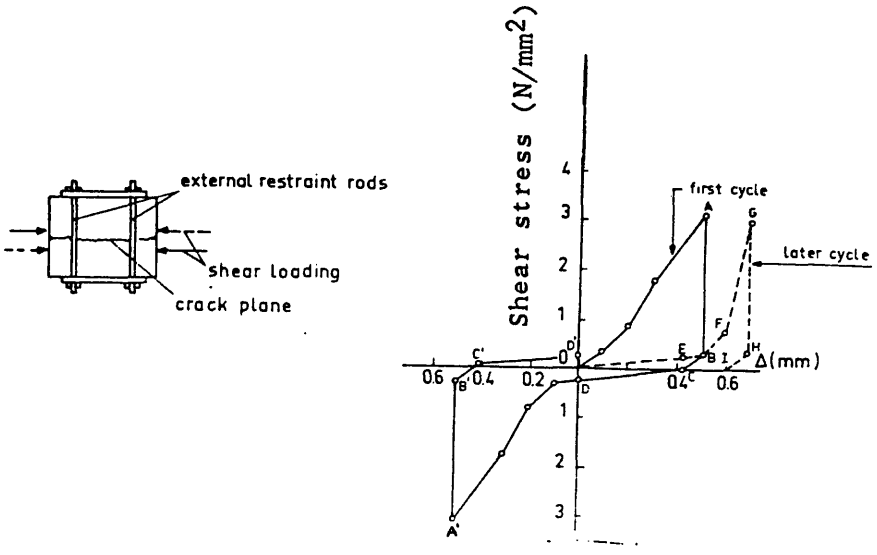

(a) Fictitious specimen

(b) Calculated response to cyclic loading

Figure (2.75) Response to cyclic loading of fictitious specimen calculated with theoretical model (20)

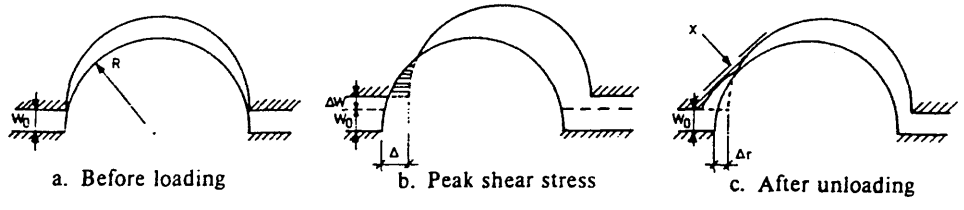

Figure (2.76) Three characteristic stages during the first loading cycle (20)

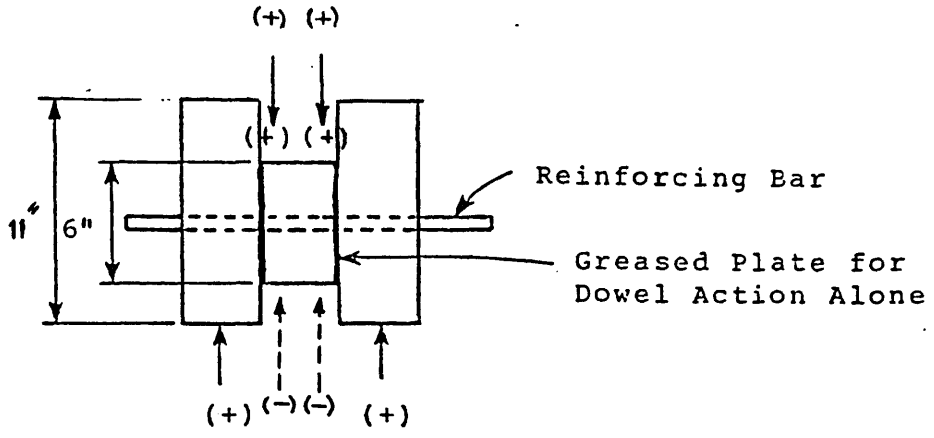

Figure (2.77) Eleiott's test specimen (32)

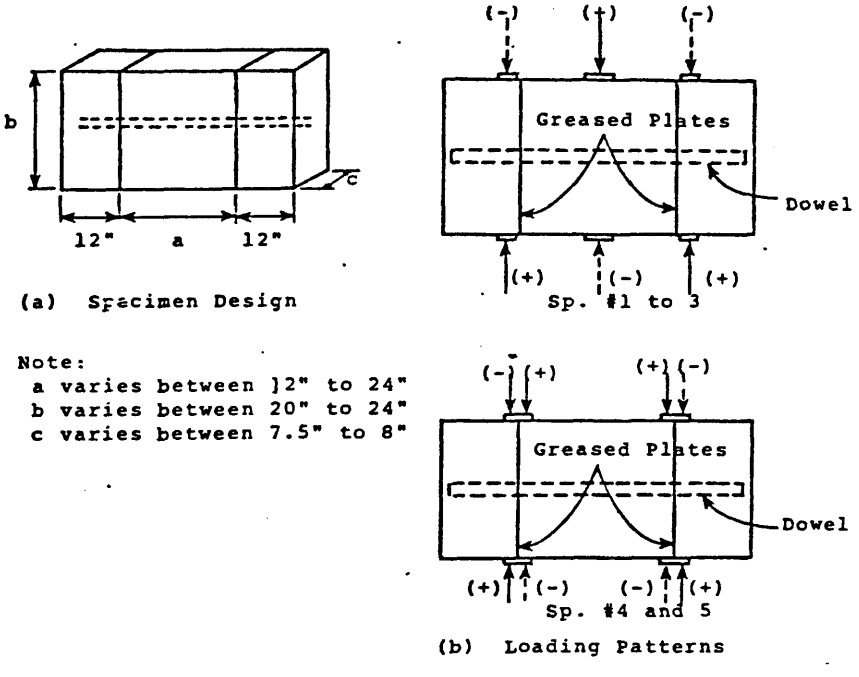

Figure (2.78) Stanton's test specimen (33)

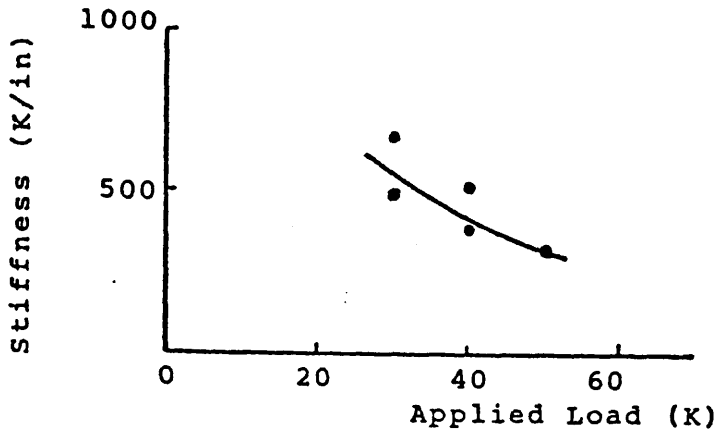

(a) Stiffness vs. Applied Load

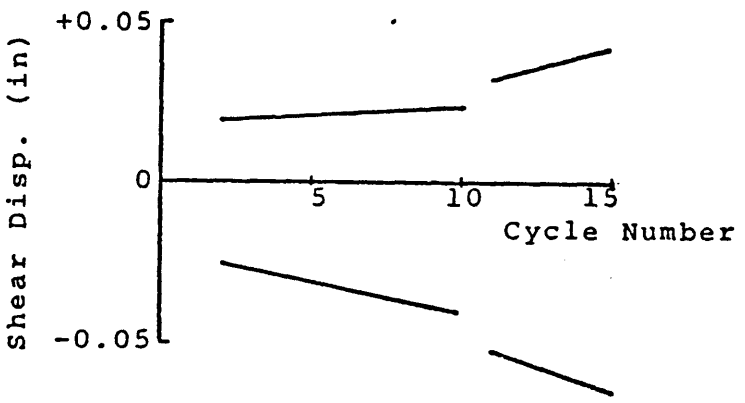

(b) Shear Disp. vs. Cycle Number

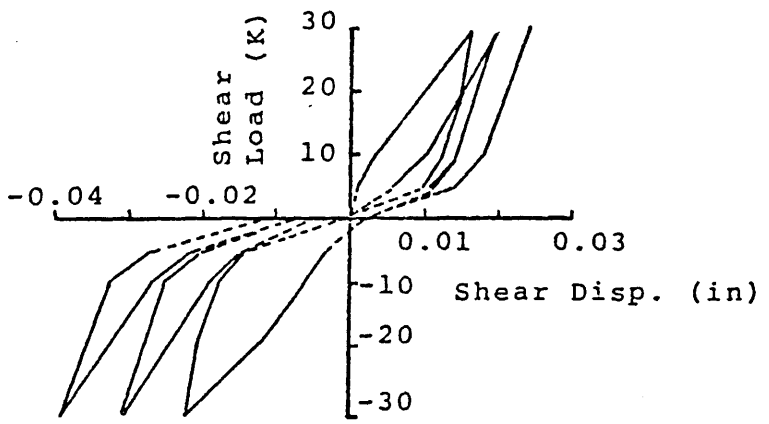

(c) Shear Load vs. Displacement

Figure (2.79) Typical results from Stanton's investigation

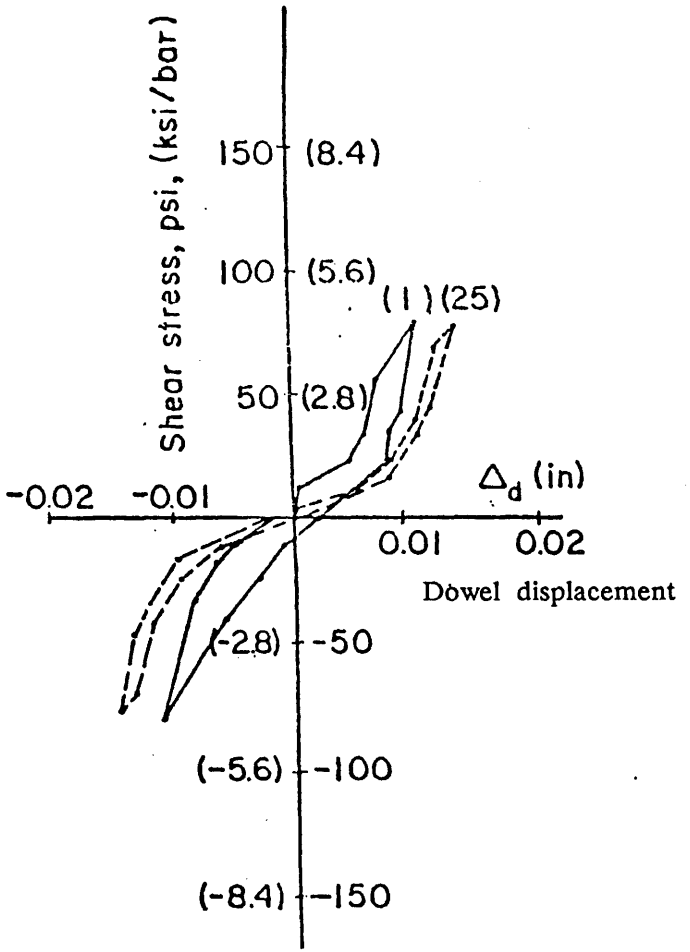

Figure (2.80) Typical results of dowel action tests (16)

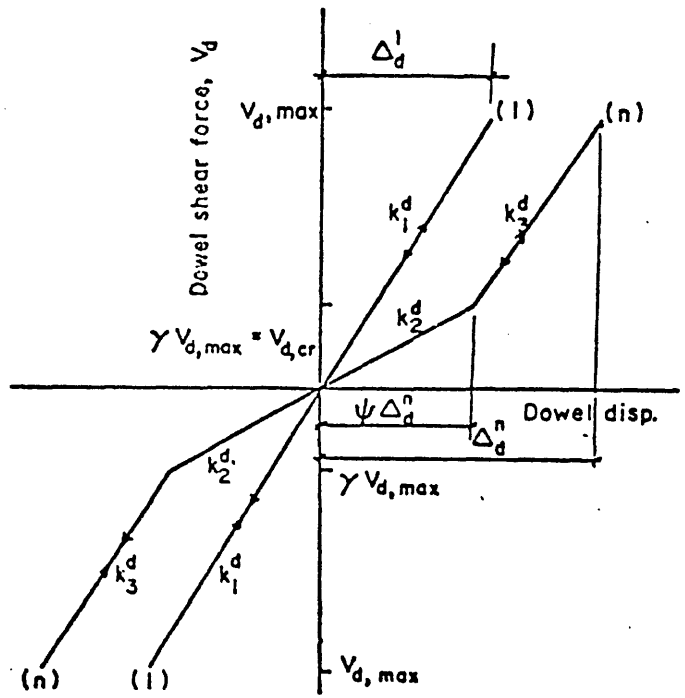

Figure (2.81) Idealization of dowel shear force - displacement relation (16)

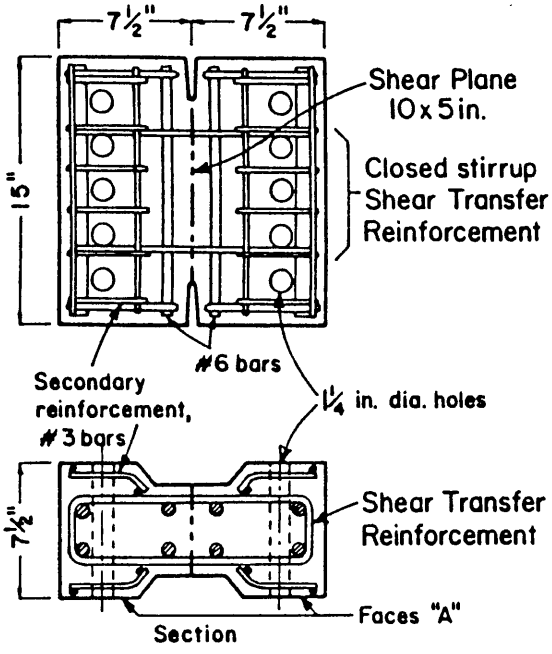

Figure (2.82) Typical specimen (59)

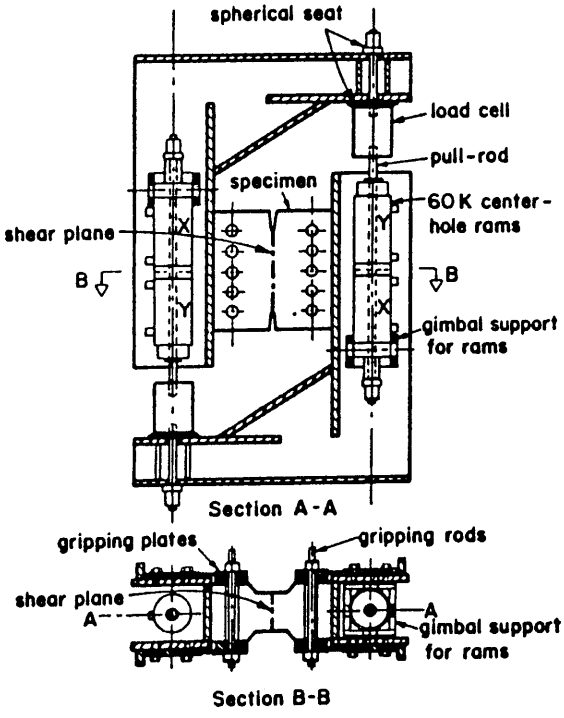

Figure (2.83) Arrangemnet for test (59) under cyclic loading

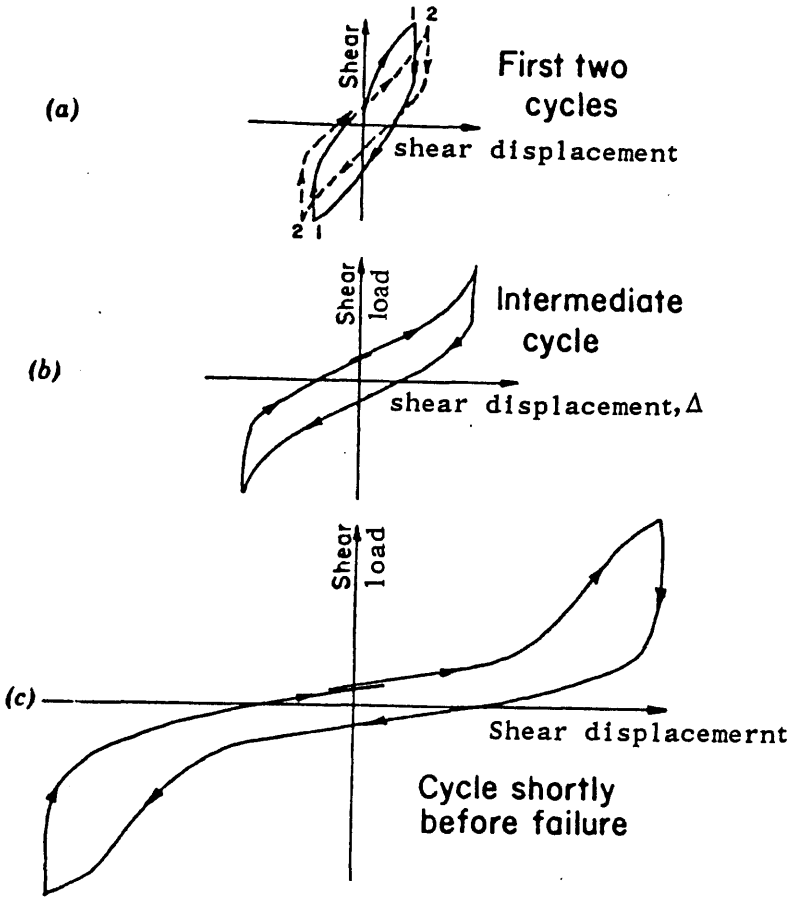

Figure (2.84) Typical shear load – shear displacement curves for cyclic loading (59)

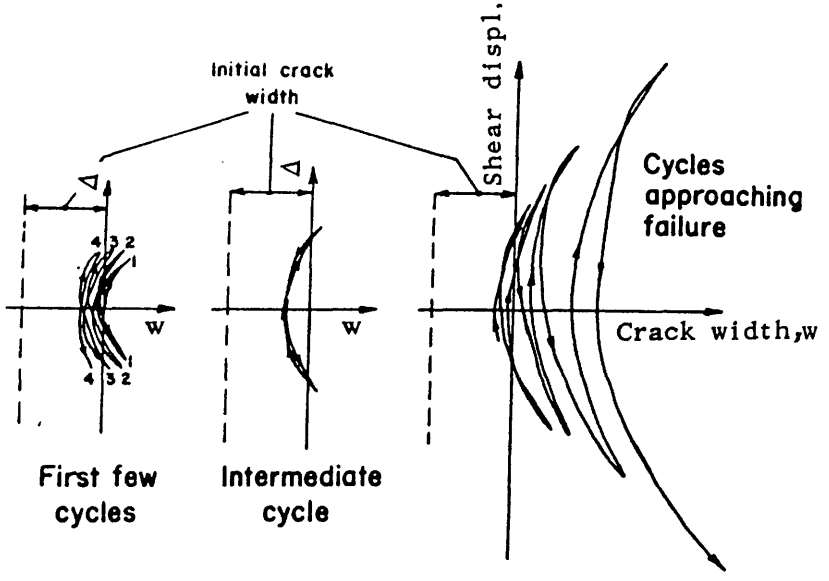

Figure (2.85) Typical shear displacement – crack width curves for cyclic loading (59)

REFERENCES

(1) Taylor, H.P.J. "A note on the mechanism of diagonal cracking in reinforcement" Magazine of Concrete Research, Vol.11, No. 31, March 1959, pp.151-158.

(2) Acharya, D.M. and Kemp, K.O., "Significance of dowel forces on the shear failure of rectangular reinforced concrete beams without web reinforcement", Journal of the American Concrete Institute, title No. 62-69, October 1965, pp.1265-1278.

(3) Jones, R. "The ultimate strength of reinforced concrete beams in shear", Magazine of Concrete Research, Vol.8, August 1956.

(4) Kani, G.N.J. "The riddle of shear failure and its solution", Journal of the American Concrete Institute, Vol. 61, No.4, April 1964.

(5) Watstein, D. and Mathey, R.G. "Strains in beams having diagonal cracks", Journal of the American Concrete Institute, Proceedings, Vol.55, No.4, December 1958.

(6) Fenwick, R.C. and Paulay, T., "Mechanism of shear resistance of concrete beams", Journal of the Structural Division, ASCE, Vol.94, No. ST10, Proceedings, paper 2325, October 1968, pp.2325-2350.

(7) Sharama, N.K., "Splitting failures in reinforced concrete members", Ph.D. Thesis, Department of Structural Engineering, Cornell University, New York, 1969.

(8) Taylor, H.P.T., "The fundamental behaviour of reinforced concrete beams in bending and shear", Shear in reinforced concrete, Vol.1, Special Publication SP-42, American Concrete Institute, Detroit, Michigan, 1974.

(9) White, R.N. and Holley, M.J. Jr., "Experimental studies of membrance shear transfer", Journal of the Structural Division, ASCE, Vol.98, No.914.ST8, Paper 9145, August 1972, pp.1835-1852.

(10)Houde, J. and Mirza, M.S. "A finite element analysis of shear strength of reinforced concrete beams", Shear in reinforced concrete, Vol.1, Special Publication SP-42, American Concrete Institute, Detroit, Michigan, 1974.

(11 Paulay, T. and Loeber, P.S. "Shear transfer by aggregate interlock", Shear in reinforced concrete, Vol.1, Special Publication, SP-42, American Concrete Institute, Detroit, Michigan, 1974.

(12)Laible, J.P., White, R.N. and Gergely, P., "An experimental investigation of seismic shear transfer across cracks in concrete nuclear containment vessels", Reinforced concrete structures in seismic zones, Special Publication, SP-53, American Concrete Institute, Detroit, Michigan 1977.

(13 Walraven, J.C. "The influence of depth on the shear strength of concrete beams without shear reinforcement", Report No. 5-78-4, May 1978, Stevin Laboratory, Delft University of Technology, Holland.

(14)Walraven, J.C., "The influence of depth on shear strength of lightweight concrete beams without shear reinforcement", Report 5-78-9, May 1978, Stevin Laboratory, Delft, University of Technology, Holland.

(15)Millard, S.G. and Johnson, R.P. "Shear transfer across cracks in reinforced concrete due to aggregate interlock and to dowel action". Magazine of Concrete Research, Vol.36, No.126, March 1984, pp.9-21.

(16)Jimenez, R., Gergely, P. and White, R.N., "Shear transfer across cracks in reinforced concrete", Cornell University, Report 78-4, August 1978.

(17)Fardis, M.N. and Buyukozturk, O., "Shear transfer model for reinforced concrete", Journal Mechanical Division, ASCE, April 1979, pp.255-275.

(18)Jimenez, R. et al "Interface shear transfer and dowel action in cracked reinforced concrete subjected to cyclic shear". Proceedings of the special conference on structural analysis, ASCE, August 1976.

(19)White, R.N. and Gergely, P. "Shear transfer in thick wall reinforced concrete structures under seismic loading", Report No. 75-10, Department of Structural Engineering, Cornell University, Ithaca, N.Y. 1975.

(20)Walraven, J.C. "Aggregate interlock: a theoretical and experimental analysis", Delft University Press, 1980.

(21)Walraven, J.C. "Experiment on shear transfer in cracks in concrete", Part 2: Analysis of test results, Report 5-79-10, Stevin Laboratory, Delft University of Technology, 1979.

(22)Marcus, H. "Load carrying capacity of dowels at transverse pavement joints", ACI Journal, Proc.V.48, No.2, October 1951.

(23)Finney, E.A. "Structural Design Considerations for Pavement Joints", ACI Journal, Proc.V.28, No.1, July 1956.

(24)Teller, L.W. and Cashell, H.D., "Performance of Doweled Joints under Repetitive Loading", Bureau of Technology, Groteborg, Sweden.

(25)Friberg, B.F. "Design of Dowels in Transverse Joints of Concrete Pavements", Transactions, American Society of Civil Engineering, V.105, 1940, pp.1809-1828.

(26)Paulay, T., Park, R. and Phillips, M.H. "Horizontal construction joints in cast in place reinforced concrete", ACI. Special Publication"SP.42", Shear in reinforced concrete, Vol.II, pp.599-616, 1974.

(27)Krefled, W.J. and Thurston, C.W. "Contribution of Longitudinal Steel to Shear Resistance of Reinforced Concrete Beams". Journal of the American Concrete Institute, Vol.63, No.3, March 1966.

(28)Baumann, T, " Versuche Zum Studium der Verdubelungswirking der Biegezugberwehrung eines Stahlbetonbalken" Material Priufungsamt fur das Vavwesen der Technischen Hochschule Munchen, Bericht, No.77.

(29)Taylor, H.P.J. "Investigation of the dowel shear force carried by the tensile steel in reinforced concrete beams", Cement and Concrete Association, TRA.431, November 1969.

(30)Houde, J. "Study of Force-Displacement Relationship for the Finite Element Analysis of Reinforced Concrete", Structural Concrete series, No,. 73.2, McGill University, Montreal, December 1973.

(31)Kemp, E.L. and Wilhelm, W.J. "An Investigation of the Parameters Influencing Bond Behaviour with a view towards Establishing Design Criteria", Report No. WVDOH 46-2, Dept. of Civil Engineering, West Virgina University, Morgantown, West Virginia, November 1977.

(32)Eleiott, A.F. "An Experimental Investigation of Shear Transfer Across Cracks in Reinforced Concrete" M.S. Thesis, Cornell University, June 1974.

(33)Stanton, J. "The Dowel Action of Reinforced and the Nonlinear Dynamic Analysis of Concrete Nuclear Containment Vessels", M.S. Thesis, Cornell University, August 1976.

(34)Dulacska, H. "Dowel Action of Reinforcement Crossing Cracks in Concrete", Journal of the American Institute, Vol.69, No.12, December 1972.

(35)Hofbeck, J.A., Ibrahim, I.O. and Mattock, A.H. "Shear Transfer in Reinforced Concrete", ACI Journal, Proc.V.66, No.2, February 1969.

(36)Johansen, K.W. "Yield-Line Theory", Cement and Concrete Association, London 1962, pp.181.

(37)Wood, R.H. "Plastic and elastic design of slabs and plates. Thames and Hudson, London 1961, pp. 344.

(38)Kwiecinski, M.W. "Yield Criterion for initially isotropic reinforced concrete slabs", Magazine of Concrete Research, Vol.17, No.51, June 1965, pp.97-100.

(39)Prince, M.R. and Kemp, K.O. "A new approach to the yield criterion for isotropically reinforced concrete slabs" Magazine of Concrete Research, Vol.20, No.62, March 1968, pp.13-20.

(40)Mills, G.M. "A partial kinking criterion for reinforced concrete slabs" Magazine of Concrete Research, Vol.27, No.90, March 1975, pp.13-11.

(41)Morley, C.T. "Experiments on the distortion of steel bars across cracks in reinforced concrete slabs". Magazine of Concrete Research, Vol.18, No.54, March 1966, pp.25-34.

(42)Den Harlog, J.P. "Advanced strength of materials" McGraw Hill, New York, 1952.

(43)Rasmussen, B.H. "Strength of transversely loaded bolts and dowels cast into concrete", Laboratoriet for Bygningsstalik, Dem,Tecn. Hoskde, Meddelelee, Vol.34, No.2, 1962 (in Danish).

(44)Timoshenko, S. and Lessels, J.M. "Applied Elasticity", Westinghouse Technical Night School Press, East Pittsburg, Pa.1925.

(45)Goto, Y. "Cracks formed in concrete around deformed tension bars", ACI Journal, Proceeding, Vol.68, No.4, April 1974, pp.244-251.

(46)Millard, S.G. "Shear transfer in cracked reinforced concrete". Magazine of Concrete Research: Vol.37, No.130, March 1985.

(47)Lutz, L.A. and Gergely, P. "Mechanics of bond and slip of deformed bars in concrete", Journal of the American Institute. Proceedings, Vol.64, No.11, November 1967, pp.711-721.

(48)Mattock, A.H. "Effect of moment and tension across the shear plane on single direction shear transfer strength in monolithic concrete", Report No. SM74-3, Department of Civil Engineering, University of Washington, October 1974.

(49)Mattock, A.H. "Shear transfer in concrete having reinforcements at an angle to the shear plane". Shear in Reinforced Concrete, Volume 1, Special Publication SP-42, American Concrete Institute, Detroit, Michigan, 1974.

(50)Mattock, A.H. and Hawkins, N.M. "Shear transfer in reinforced concrete- Recent Research", PCI Journal, Vol.17, March/April 1972.

(51)Mattock, A.H. "Effect of aggregate type on single direction shear transfer strength in monolithic concrete". Report SM.74-2, Department of Civil Engineering, University of Washington, August 1974.

(52)Reinhardt, H.W. and Walraven, J.C. "Shear transfer in reinforced concrete with small crack widths", Preprint 80-012, ASCE Convention, Portland, April 1980.

(53)Birkland, P.W. and Birkland, H.W. "Connection in precast concrete construction". ACI Journal, Proc. Vol.63, Nos.3, March 1966.

(54)Building Code Requirements for Reinforced Concrete", ACI 318-83, American Concrete Institute, 1983.

(55)"PCI Design Handbook", Prestressed Concrete Institute, 1971.

(56)Walraven, J.C. and Reinhardt, H.W. Concrete Mechanics, Part A: Theory and experiments on mechanical behviour of cracks in plain and reinforced concrete subject to shear loading. Heron, Vol.26, No.1A, 1981.

(57)Colley, B.E. and Humphrey, H.A. "Aggregate interlock at Joints in Concrete Pavements". Highway Research Record, No.189, 1967, pp.1-18.

(58)Nowlen, W.J. "Influence of aggregate properties on the effectiveness of interlock joints in concrete pavements". Portland Cement Association and Development Laboratories, Bulletin D-139.

(59)Mattock, A.H. "The shear transfer behaviour of cracked monolithic concrete subject to cyclically reversing shear". Report 74-4, Department of Civil Engineering, University of Washington, Seattle, Washington 1974.

(60)British Standard Institution, "The Structural Use of Concrete", Unified British Code for Structural use of Concrete in Building, BS8110, London 1985.

CHAPTER (3)

SCOPE AND OBJECTIVES OF EXPERIMENTAL STUDY

3.1 Introduction

In this chapter the scope of the experimental study is first presented explaining the object of tests and the variables to be studied. The experimental programme is then described showing the numbers of test series and the aim of each one.

3.2 Objectives of the present study

From the review in Chapter (2) it was seen that although many experimental results are available, they are still not sufficient to form an accurate and generally agreed formulation of the basic relationships under monotonic and repeated loadings. Moreover, much less attention has been paid towards shear transfer under cyclic loading, especially repeated loading, in spite of the fact that many structures are subjected to fluctuating effects. In addition, available data does not answer all the questions concerning the fundamental understanding of the phenomenon. It is therefore, necessary to carry out further experimental investigations to obtain more relevant data and to attain a better understanding of the mechanics and the behaviour of shear transfer. The ultimate purpose is to use this understanding to develop recommendations for shear transfer design and for use in analytical methods of reinforced concrete.

In particular, shear forces transferred across a reinforced cracked

section by dowel action only and by combined action, i.e. interface shear transfer and dowel action, under monotonic and repeated shear loads are investigated in this study. The most important variables which have a significant influence on the shear transfer behaviour i.e. initial crack width, reinforcement ratio, are included. In addition to these variables, the type of reinforcing bars crossing the crack plane, i.e. high tensile deformed steel and plain mild steel bars, is also considered because not enough information is known about its effects on the shear transfer compared with other variables like the bar diameter and aggregate size and shape.

In summary the objectives of this work were as follows:

(1) To investigate the effect of the type of loading on shear tranfer behaviour and ultimate strength, i.e. monotonic and repeated loadings, of both dowel action and combined action mechanisms.

(2) To investigate the influence of the following variables on shear transfer

   a) The reinforcement ratio
   b) The initial crack width
   c) Type of reinforcement

(3) To study the contribution of the different mechanisms in shear i.e. dowel action, interface shear transfer mechanism.

(4) To investigate the stress distribution in the reinforcing bars crossing the crack plane, to understand their internal

mechanisms.

(5) To determine whether shear strength equations based on monotonic loading should be modified when they are used in the design for repeated loading, or whether completely new equations and analytical models and explanation of behaviour need to be derived.

(6) To study the difference between the behaviour of the shear transfer in case of the reversible cyclic loading and repeated loading, by comparing the results obtained from this study and the available information on reversing cyclic load presented in Chapter (2).

(7) To develop recommendations for the design of shear transfer.

(8) To develop load-displacements and stiffness relationships for use in design and analytical procedures.

3.3 Selection of the studied parameters

3.3.1 Reinforcement ratios:

The range of the reinforcement ratios crossing the crack plane was selected to investigate if and how they affected the mode of shear failure, i.e. failure due to yielding of the steel bars or due to splitting of the concrete, and also to show any difference in the behaviour of shear transfer across the cracked sections, the contribution of difference mechanisms and the ultimate shear strength.

The different ratios were obtained by using different numbers of closed 8 mm diameter stirrups in a constant cross-section, i.e., one, two, four, and six stirrups were used giving reinforcement ratios of 0.28%, 0.56%, 1.12% and 1.68%.

In dowel action test specimens these reinforcement ratios were slightly different due to the change of the crack plane area, i.e. crack plane areas for the dowel action and combined action test specimens were 150x300&120x300 mm^2 respectively, thus the reinforcement ratios of dowel action specimens were 0.23%, 0.44%, 0.89% and 1.34%. The typical arrangement of these stirrups are shown in Figure (3.2).

3.3.2 Initial crack width

From previous work it was claimed that the behaviour at small initial crack width, i.e. less than approximately 0.25 mm, was different from that at larger crack widths. Therefore, it was decided to select two initial crack widths to represent both small and large crack widths as defined by the distinguishing value of 0.25 mm. These initial crack widths chosen were 0.125 mm and 0.40 mm.

3.3.3 History of loading

The history of loading in shear transfer tests under repeated loading was selected according to the following considerations:

(1) Enabling a systematic study of the effect of the different involved parameter.

(2) To find a direct relation between shear transfer across a cracked

section under both monotonic and repeated loadings.

(3) To simulate the severe conditions where the structures may be subjected to small cycling numbers of high intensity load.

(4) To compensate the difference between the reversible cyclic loading as used in the previous investigations and this non-reversible cyclic load.

In the combined action tests the applied load was cycled between zero shear load and 0.70 of the shear load calculated by Mattock's equation for monotonic loading for 43 cycles and then the specimens were loaded to failure.

Mattock's equation is given by

$$V_u = A_c\ (400 + 0.8\ \rho f_y) \text{lbs}$$

where V_u = ultimate shear load

ρ = reinforcement ratio crossing the crack plane (in^2)

f_y = yield stress of the reinforcing bars (psi)

A_c = area of the crack plane (psi)

This equation was selected because it showed good agreement with the results obtained from preliminary tests.

The typical history of loading is shown in Figure (3.3). From the previous investigation of shear transfer under reversible cyclic loading, failure occurred after 25 load cycles. Less effect on ultimate shear strength is expected under repeated loading.

Therefore, it is assumed that the number of repeated load cycles would be greater than that of the reversible cyclic loading to produce a similar ultimate shear strength. Also, from the previous investigation it was concluded that shear transfer behaviour at the first load cycle is different compared to the middle and final stages. Therefore, it was important to examine the behaviour of shear transfer under repeated load at these different stages. From the above, the number of 43 cycles was chosen which is approximately twice the number of reversible cyclic load. Also, this number divides the range between the second, middle and last repeated load cycles to two equal number of cycles, i.e. 20 load cycles as shown in Figure (3.3).

From Mattock's previous investigation[1] it was found that the ultimate shear load for a reinforced cracked section under reversible cyclic loading was about 0.6-0.8 of that ultimate shear trasnsfer calculated by the above equation. So, 70% of shear load was selected in this present study to investigate the applicability of such a relation between the shear failure due to the applied monotonic and repeated case of loadings.

According to the author's knowledge no such relation between dowel capacity under monotonic and repeated shear load has been established. Thus, it was difficult to know how the repeated shear load would affect the dowel action compared with the case of monotonic load. Therefore, it was decided to choose an arbitrary maximum repeated shear load as a percentage of the ultimate dowel load obtained from the dowel action tests under monotonic shear load.

The selected applied repeated loads were 18 kN for specimens with two and four stirrups crossing the crack plane and 54 kN for specimen with 6 stirrups. These loads give ratios of 0.35, 0.19 and 0.35 of the ultimate shear load of the monotonic dowel action specimens having a similar number of stirrups. Each load was applied for 43 cycles similar to the combined action before it was increased monotonically up to failure. The history of loading is schematically illustrated in Figure (3.3).

3.4 Test program

A test program designed to achieve this scope of work is schematically shown in Figure (3.1). It has been divided into three test series. The first series was considered as preliminary tests. The second and third series were designed to study the shear transfer across a cracked section under monotonic and repeated loads by dowel mechanism only and by combined action respectively.

The dimensions of the test specimen, materials, instrumentation, pre-cracking operation, testing arrangement and test procedures are explained in the next chapter. In this section the aim of each series is presented.

3.4.1 Series (1)

This first preliminary test series of 12 test specimens was designed for the following purposes:

(1) To examine different test specimens for determining the best shape, dimensions and reinforcement to get shear failure along

the shear plane and to avoid any local failures that might occur.

(2) To examine the testing arrangement and the instrumentations used for measuring the required parameters such as shear displacement, the change in the crack width and strain in the reinforcing bars crossing the crack plane.

3.4.2 Series 2 (Dowel action tests)

The aim of this test series was to investigate the following:

(1) The effect of the reinforcement ratio.
(2) The effect of the type of loading.
(3) The internal stresses in the dowel bars.

This series was divided into two groups, the number of specimens in the first and the second groups were seven and two respectively. The type of the closed stirrups and the concrete strength were kept constant. The first group is designed to study the first two aims whereas the second series is designed to study the third aim.

The summary of the test specimen details of this series is presented in Table (3.1).

3.4.3 Series 3 (combined action tests)

The main aims of this series were to study the following:

(1) Effect of the initial crack width
(2) Effect of the reinforcement ratios

(3) Effect of type of the shear reinforcement

(4) Effect of the type of loading

(5) The internal stresses in the shear transverse reinforcement.

This series was divided into five groups. Each of the first three groups consisted of eight test specimens. The last two groups included two test specimens each. In this series the target concrete strength was kept constant. In groups (1), (3) and (4) the average initial crack width was approximately 0.125 mm and in groups (2) and (5) the initial crack width was changed to 0.40 mm. Shear transverse reinforcement (i.e. reinforcement crossing the crack plane) of high tensile deformed bars were used in groups (1), (2), (4) and (5) and in group (3) mild steel bars with plain surface was used. The diameter of all shear transverse reinforcing bars was 8 mm.

A summary of test specimen details of this series is shown in Table (3.2).

Each specimen is designated by three numbers and sometimes by a letter the "A" at the end. The first three numbers indicate the series number, the group number and serial number. The letter "A" indicates shear tests under repeated load.

Table (3.1) Test specimens details of series 2.

Specimen No.	No.& size of stirrups	Reinf-ratio ρ%	Yield stress of reinf. f_y N/mm²	Cube comp. stress of conc. f_{cu} N/mm²	Cylinder comp.stress of concrete f'_c N/mm²	Concrete tensile of conc. f_t N/mm	Type of loading
Group 1							
2.1.1	1Y8	0.23		46	34.9	2.9	*M
2.1.2	2Y8	0.44		48	37.1	3.1	M
2.1.2A	2Y8	0.44		48	37.1	3.1	+R
2.1.3	4Y8	0.89	535 N/mm²	47	36.8	3.2	M
2.1.3A	4Y8	0.89		47	36.8	3.2	R
2.1.4	6Y8	1.34		45	34.7	3.1	M
2.1.4A	6Y8	1.34		45	34.7	3.1	R
Group 2							
2.2.1	2Y8	0.44	535	52	38	2.9	M
2.2.2	6Y8	1.34	N/mm²	60	45.2	3.21	M

* monotonic load

\+ repeated load

Table (3.2) Test specimens details of series 3.

Specimen No.	No.and size of stirrups	Reinf. ratio %	Yield stress of stirrups f_y N/mm^2	Cub. comp. stress of concrete f_{cu} N/mm^2	Cylinder comp. stress of concrete f_c N/mm^2	Tensile stress of concrete f_t N/mm^2	Initial crack width	Type of loading
Group 1								
3.1.1	1Y8	0.27		50	36.74	3.26	0.125	M
3.1.1A	1Y8	0.27		50	36.74	3.26	0.120	R
3.1.2	2Y8	0.56		52	35.39	3.3	0.130	M
3.1.2A	2Y8	0.56	535	52	35.39	3.3	0.136	R
3.1.3	4Y8	1.12	N/mm^2	47	34.2	3.2	0.120	M
3.1.3A	4Y8	1.12		47	34.2	3.2	0.125	R
3.1.4	6Y8	1.68		45	35.10	3.18	0.130	M
3.1.4A	6Y8	1.68		45	35.10	3.18	0.133	R
Group 2								
3.2.1	1Y8	0.27		53	38.78	2.97	0.39	M
3.2.1A	1Y8	0.27		53	38.78	2.97	0.39	R
3.2.2	2Y8	0.56	535	50	36.8	3.0	0.39	M
3.2.2A	2Y8	0.56	N/mm^2	50	36.8	3.0	0.41	R

Table (3.2) Test specimens details of series 3. contd.

Specimen No.	No.and size of stirrups	Reinf. ratio %	Yield stress of stirrups f_y N/mm^2	Cub. comp. stress of concrete f_{cu} N/mm^2	Cylinder comp. stress of concrete f_c N/mm^2	Tensile stress of concrete f_t N/mm^2	Initial crack width	Type of loading
Group 2 contd.								
3.2.3	4Y8	1.12		48	35.95	2.83	0.40	M
3.2.3A	4Y8	1.12		48	35.95	2.83	0.39	R
3.2.4	6Y8	1.68		50	38.5	3.1	0.38	M
3.2.4A	6Y8	1.68		50	38.5	3.1	0.40	R
Group (3)								
3.3.1	1Ø8	0.27		55	40.2	3.4	0.125	M
3.3.1A	1Ø8	0.27	475	55	40.2	3.4	0.125	R
3.3.2	2Ø8	0.56	N/mm^2	50	38.7	3.2	0.130	M
3.3.2A	2Ø8	0.56		50	38.7	3.2	0.130	R
3.3.3	4Ø8	1.12		49	37.4	3.1	6.125	M
3.3.3A	4Ø8	1.12	475	49	37.4	3.1	6.126	R
3.3.4	6Ø8	1.68	N/mm^2	47	35.1	2.9	0.125	M
3.3.4A	6Ø8	1.68		47	35.1	2.9	0.127	R

Table (3.2) Test specimens details of series 3. contd.

Specimen No.	No.and size of stirrups	Reinf. ratio %	Yield stress of stirrups f_y N/mm^2	Cub. comp. stress of concrete f_{cu} N/mm^2	Cylinder comp. stress of concrete f_c N/mm^2	Tensile stress of concrete f_t N/mm^2	Initial crack width	Type of loading
Group (4)								
3.4.1A	2Y8	0.56	535	46	35.2	2.76	0.125	R
3.4.2A	6Y8	1.68		45	34.7	2.9	0.125	R
Group (5)								
3.5.1	2Y8	0.56	535	50	37.9	3.1	0.40	M
3.5.2	6Y8	1.68		50	37.9	3.1	0.40	M

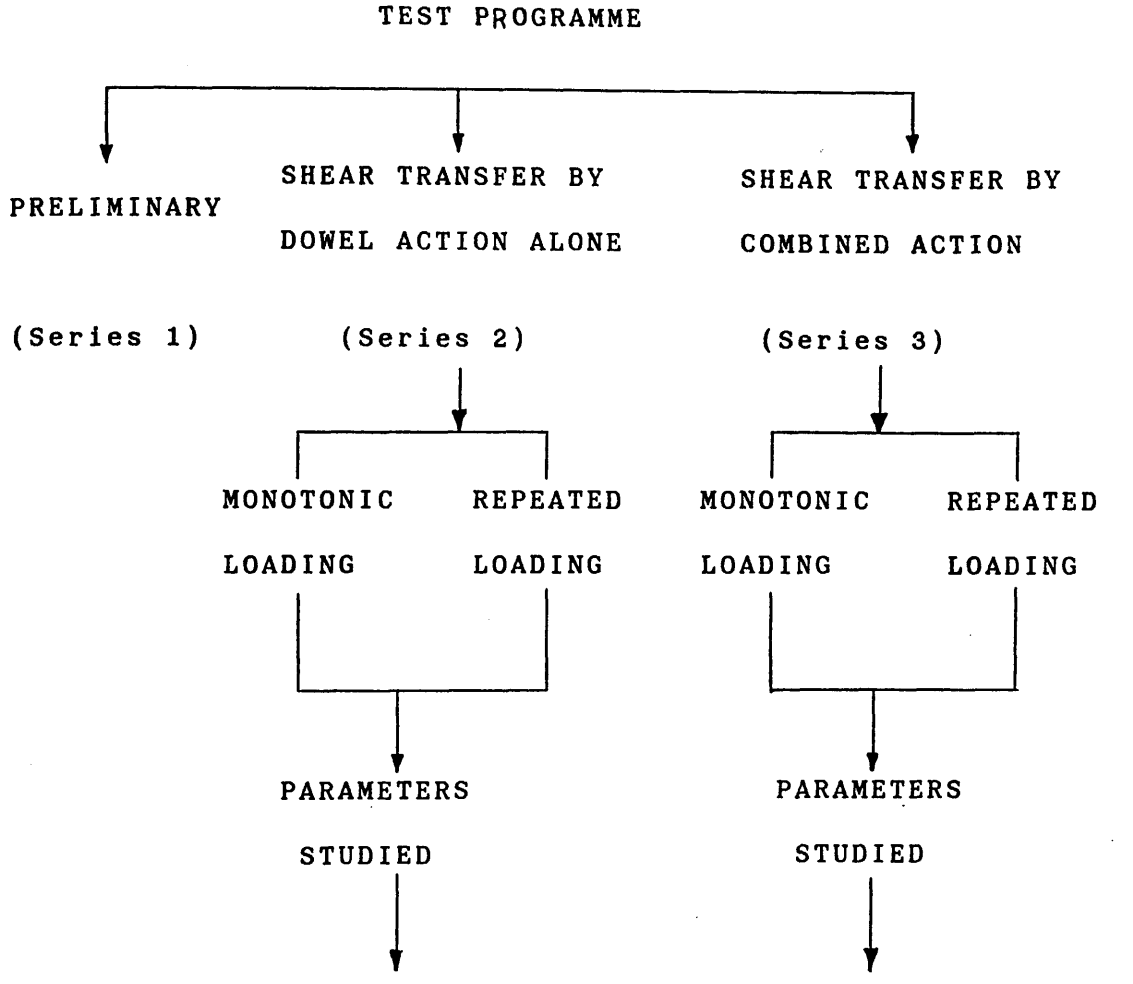

Figure (3.1) Summary of test programme

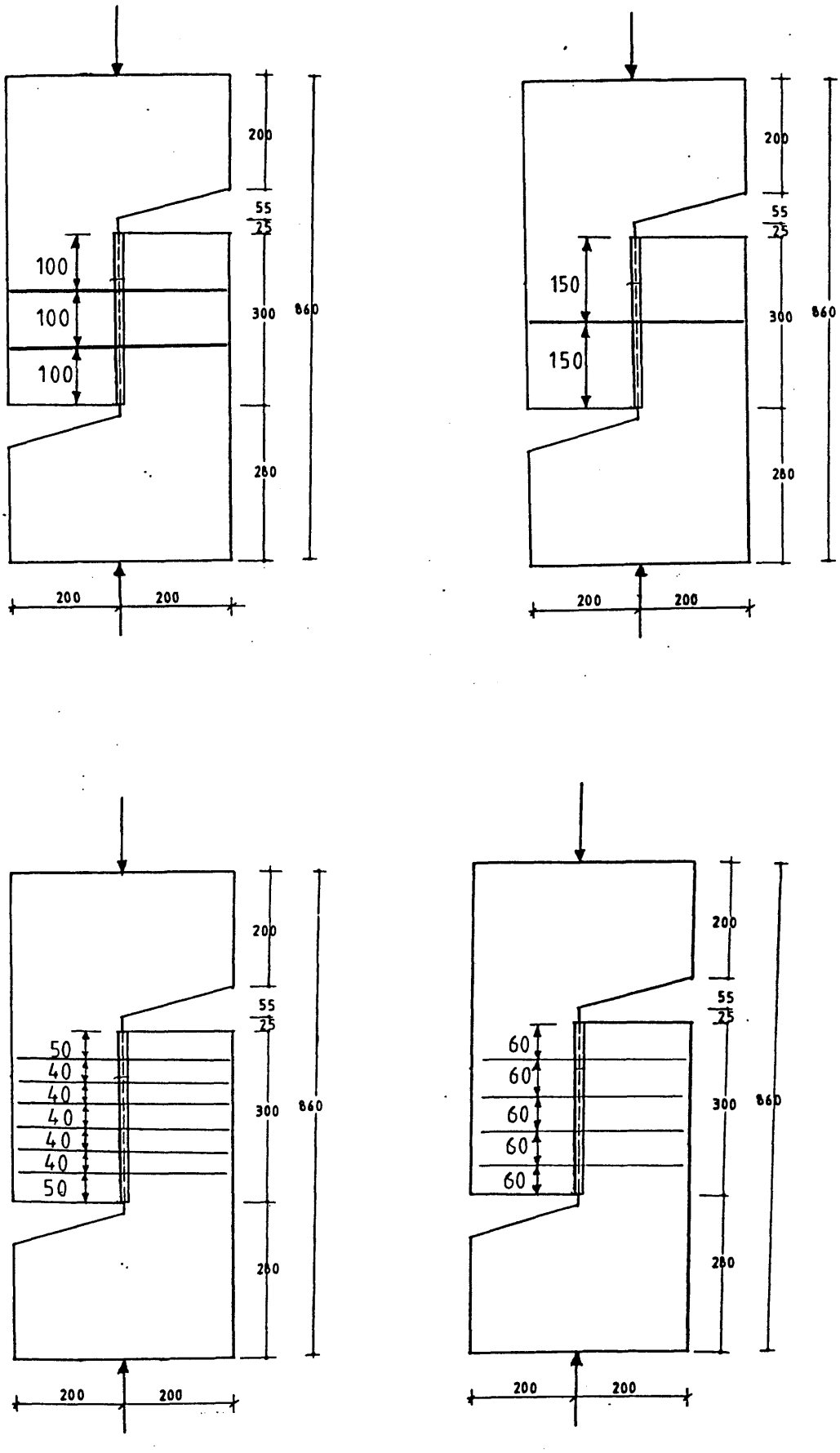

Figure (3.2) Arrangement of the reinforcement (closed stirrups) crossing the shear plane

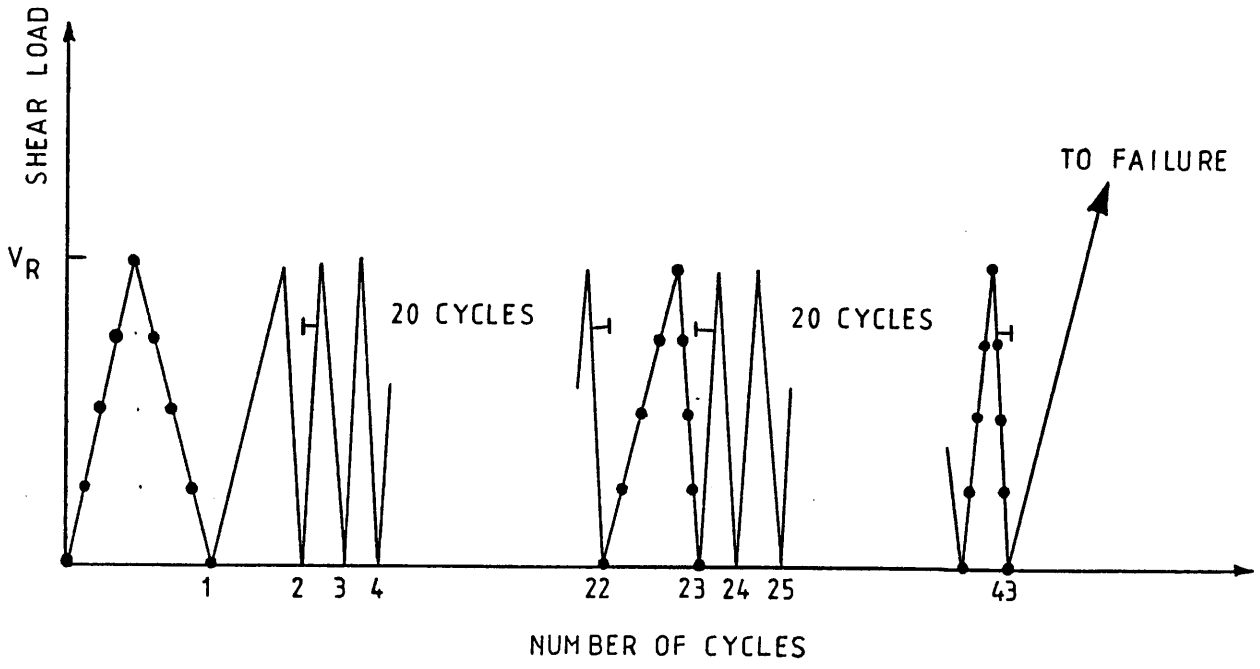

V_R (KN)	No. & Size of stirrups	Type of shear test
107	1Y8	
134	2Y8	Combined
209	4Y8	action
267	6Y8	
18	2Y8	Dowel
18	4Y8	action
54	6Y8	

Figure (3.3) Schematic diagram of load history for shear tests under repeated loading

REFERENCES

(1) Mattock, A.H. "The shear transfer behaviour of cracked monolithic concrete subject to cyclically reversing shear". Report 74-4, Dept. of Civil Engineering, University of Washington, Seattle, Washington 1974.

CHAPTER (4)

EXPERIMENTAL SETUP, MATERIALS AND INSTRUMENTATION

4.1 Introduction

This chapter explains the experimental setup used to study both dowel action and combined mechanisms of shear transfer in both monotonic and repeated case of loadings.

The details of the test specimens, materials used, frame work and construction, instrumentation, testing arrangement and test procedures are described.

4.2 Test Specimen

Since the present study is concerned with shear transfer across a single crack, it is necessary to use a specimen which will provide a pure shear without moment in the shear plane. Push-off specimens meet this requirement. This type of specimen is also suitable for a systematic study of the different parameters involved. Also by using this type of specimen a better comparison can be made between the results of this present investigation and previous results obtained by direct shear tests.

Two categories of specimens were used : one for the shear transfer mechanism across precracked surfaces by the combined action and one for the dowel action.

As a result of the preliminary tests, the final shape and dimensions of the test specimens used in the main programme are presented in

Figure (4.1).

The specimen cross-sectional dimensions were 150 mm by 300 mm with a net shear plane area of 36000 mm (120 mm x 300 mm) to suit the required arrangement of the reinforcement crossing the shear plane. The total height of the specimen was 860 mm. Specimens used for testing the combined action had a V-shaped groove in the middle of the front and the rear faces to initiate the crack width required as will be explained later. In the dowel action specimens, interface shear transfer was eliminated by constructing a smooth, low-friction crack passing through the centre of the specimen.

Typical reinforcement for one specimen is shown in Figure (4.2). The reinforcement crossing the shear plane was in the form of closed stirrups, overlapped on one of the short sides. This was to ensure the effective anchorage of the reinforcement on both sides of the shear plane. The other reinforcements were provided at the upper and lower parts of the specimen as well as at each side to the shear plane to prevent any local failure.

4.3 Fabrication of the specimen mould

The mould for a specimen was made of 20 mm plywood as shown in Figure (4.3).

The four sides of the mould were strengthened by nailing 50 mm x 50 mm timber battens at the corners and horizontally at the intersection of the sides with the bottom sheet. To form the upper and lower holes, two pieces of polystyrene of appropriate shape were fixed to the bottom wooden plate. By using such material local damage to the concrete during demoulding was prevented.

The V-shaped grooves in the middle of the front and rear faces were formed by two aluminium angles, the lower angle was fixed to the bottom plate and the upper one was fixed to a wooden strip fixed to the polystyrene pieces.

4.4 Materials

4.4.1 Concrete

Cement: Ordinary Portland and Rapid Hardening cements were used in this test programme.

Aggregate: Hyndford sand and uncrushed gravel obtained from Lanarkshire were used for all mixes. The maximum size of the uncrushed gravel used was 10 mm, and the grading of sand was in zone 2(1).

Concrete mix: the concrete mix was designed to give an average cube strength greater than 45 N/mm^2 at 28 days by using Ordinary Portland cement or at 14 days by using Rapid Hardening cement. For each batch 13 Kg of cement, 20.3 Kg of sand and 41 Kg of 10 mm aggregate (giving a mix ratio of 1 : 1.56 : 3.15) were mixed thoroughly for about two minutes in the concrete mixer and then 6.1 Kg of water was added, giving a water cement ratio of 0.47. It was allowed to mix for five more minutes to prepare the concrete of required consistency.

For each pair of test specimens, the control specimens were 6-100 mm cubes and 6-150 mm x 300 mm cylinders. All cubes and cylinders were removed from the main push-off specimens under the same condition. 4-cubes and 6-cylinders were tested on the same day as their respective test specimen.

Standard tests to determine the cube compressive strength, cylinder splitting test, and the static modulus of concrete were determined according to the British Standard No. BS.1881 : 1970 [2].
Average values for the concrete properties for each test specimen were calculated and are given in Tables (3.1) and (3.2).

A typical stress-strain curve for concrete is shown in Figure (4.4).

4.4.2 Reinforcement

The closed stirrups crossing the crack plane were of 8 mm diameter high yield deformed bars or mild steel plain bars.

The material properties of the reinforcement was obtained experimentally by testing three samples of each type in a 1000 kN Tinus-Olsen Class A testing machine taking an average of the three values. An S-type Olsen extensometer was attached to the bars near its centre to measure strain. The stress-strain curve was recorded automatically. An Olsen extensometer is an electronic strain instrument designed to operate in conjunction with the Olsen Model 51 Electronic Recorder. Tests were carried out in accordance with the recommendations of the "Panel for standard practices in Testing". DOE-TRRL[3].

For the high yield steel, the 0.2% proof strain was measured as shown in Figure (4.5) whereas for the mild steel bars a more precise yield stress was obtained. The modulus of elasticity was also calculated from the slope of the graph. Typical stress-strain curves for different reinforcing bars as shown in Figures (4.5) and (4.6). The properties are summarised in Table 4.1.

4.5 Casting and curing

All internal surfaces of the mould were oiled to facilitate easy removal. Thin soft iron wire was used for tying the reinforcement bars. 15 mm cover was obtained by using plastic spacers. Each specimen was cast in the horizontal wooden mould(i.e. shear plane was vertical) as shown in Figure (4.3). The concrete was placed and compacted in three layers by using a vibrating table to minimize segregation or water gain around the reinforcement.

After the concrete has set, the specimen together with the cubes and cylinders were cured under wet hessian for seven days. The concrete cubes and cylinders were demoulded one day afte casting. The mould of the main test specimens were removed after two or three days of the curing period. Cubes, cylinders and main test specimens were kept at the same place and condition until the day of testing.

The dowel action specimens were cast in two stages to achieve a smooth crack surface. The first half was cast against a flat plywood plate positioned across the centre of the mould (see Figure 4.7a). After one day the plate was removed and the exposed face covered with thin polythene sheeting. The second half of the specimen was then cast against this sheeting [see Figure (4.7b)]. For each half of the specimen 6-cubes and 3 cylinders were cast to determine the concrete properties.

4.6 Instrumentation

4.6.1 Strain measurement

Electrical resistance strain gauges were used to measure the strain in the steel stirrups crossing the crack plane. Depending on

availability, two different types of strain gauges were used, i.e. EA.06.240 LZ-120 and C 45 Ni. All gauges were 6 mm long with an elongation capacity of 3-5% at a temperature of 75 F and an internal resistance equal to 120 ± 3%. The difference betwen the gauges was the gauge factor, which was either 2.045 or 2.01.

For fixing the strain gauges to the steel, the ribs were first removed by filing and then smoothed with the help of 'smooth file single cut'. The surface was further smoothed with emery paper (care being taken not to remove too much area of the steel during the operation). It was then cleaned with conditioner (water based acidic surface cleaner) and afterwards with neutralizer (water based alkaline surface cleaner). The adhesive M-Bond-200 specially supplied for this purpose was smeared to the back of the strain gauge and it was then stuck to the steel at required position by pressing it firmly for about two minutes and then was covered with adhesive tape. After 24 hours the tape was removed, lead wires were connected and protective coating type M-Coat D was applied. To protect the gauges against moisture and mechanical damage during casting they were covered with a coat of Araldite reduced to a minimum thickness.

For all specimens the strain gauges were connected to the linear voltage processing minicomputer type Orion A data logger which directly recorded the strains.

Numbers, locations and arrangement of the strain gauges were varied according to the following considerations.

(a) To avoid as much as possible any damage that might occur to the strain gauges during the precracking operation.

(b) To be placed a sufficient distance from the crack plane in order to obtain steady strain readings, which might be prevented if the degrading concrete interfered with the strain gauge as the load was applied.

(c) To minimize the effect of the protecting coat (covering the strain gauges) on the bond condition between the reinforcing bars and the surrounding concrete.

The strain gauges arrangement for the varying specimens is illustrated in the next two chapters.

4.6.2 Calibration of steel strain measurement

Since the steel strains in the main shear test were measured by using two types of strain gauges while the strains in the tensile tests for samples of the steel bars were measured by an extensometer, a calibration between these three types of strain measurements was carried out.

This was done by conducting a tensile test for a sample of 8 mm high tensile deformed diameter bar using the Olsen machine with the same procedure described previously. Six strain gauges (three of each type) were affixed to the surface of the bar together with the extensometer clamped onto it. The positions of the strain gauges and the extensometer along the bar are shown in Figure (4.8).

It can be seen from Figure (4.9) that no significant differences were

observed between the strain gauges and the extensometer readings for the required range 0-6000 microstrain. Consequently no correction was required to the strain gauges readings obtained during the main shear tests.

4.6.3 Displacements Measurements

The displacements required to be measured were shear displacement (i.e. relative movement parallel to the shear plane) and crack width (i.e. relative motion normal to the shear plane of the two halves of a specimen). Because of the small range of both shear displacement and crack width, instruments with high accuracy and small range were required. For this reason special electrical transducers, Type SE355 Miniature DC/DC Linear Transducers with maximum range of ± 2.5 mm and with accuracy of 0.001 mm were used.

The transducers were connected to the data logger which automatically recorded the displacements in mm.

In the precrack operation the crack width along the shear plane was measured by using Demec gauges with gauge length of 100 mm. The locations of the Demec points bonded to the concrete surfaces of the two sides of the specimen are shown in Figure (4.11b).

4.7 Precracking Operation

All the reinforced concrete specimens were cracked in the shear plane before being subjected to shear loading. The crack was produced by applying line loads to the back and front faces of the specimen along the line of the shear plane in the Olsen Universal testing machine. To achieve this, the specimen was placed in a horizontal position and

the line loads were applied incrementally through a pair of steel rods positioned in a pair of steel angles placed in the V-shaped grooves in the middle of the specimen, as shown in Figures (4.10) and (4.11). After each load increment the crack was measured at 3 places along the centre line of each face of the specimen by using the Demec gauge [see Figure (4.11b)]. The Demec gauge readings were taken after releasing the load. The load application was stopped, when the required initial crack width was obtained. The initial crack width was taken as the average of the crack width of the two faces of the specimen.

4.8 Testing Arrangement

The push-off specimens were also testing using the Tinus-Olsen Universal testing machine. The arrangement is shown in Figure (4.12). At the bottom the specimens were supported by a roller bearing. The rollers ensured that separation of the two halves of the push-off specimen was not restrained by the testing machine itself. At the top the upper platen of the testing machine was applied to load the specimen through the hinge bearing [see Figure (4.13)]. Using such a loading arrangement shear without moment was produced in the shear plane.

In order to install the transducers at the proper positions to measure both the crack width and shear displacement on both sides of the specimen, special frames were designed and the transducers were fixed to them at the required points by using clamp brackets as shown in Figure (4.14). The vertical transducers measured the shear displacement and the horizontal ones measured the change in the crack width. The location of the transducers is shown schematically in Figure (4.15) where it can be seen that the shear displacement and

crack width were measured in two positions on each side of the specimen. The displacements were recorded directly using an "ORION A" data logger.

4.9 Test Procedure

4.9.1 Monotonic Loading

After initialization of all instruments to the data logger the load was increased incrementally until the failure of the specimen occurred. The value of the applied load was read directly by the Olsen machine but the test was conducted under displacement control. The ultimate failure load was defined as the maximum load that would be carried by the specimen. The time taken for a test varied between 20-50 minutes.

In the combined action tests the load increment was 13 kN whilst for the dowel action tests the increment was 5 kN. After each increment of load, the shear displacement, the crack widths and the steel strains were recorded. Short pauses were allowed as necessary to mark any cracks that might have occurred.

4.9.2 Repeated Loading

The testing arrangement was similar to that of the monotonic case of loading. In these repeated shear loading tests, the load on the specimens was cycled between zero load and a given stress level a prerequisite number of cycles and then the specimens were loaded until failure occurred.

The total number of loading cycles were 44 for all the specimens. For four cycles throughout the tests (cycles numbers 1, 2, 23 and 43)

the shear load was applied and released incrementally. In each increment, the shear displcement, crack width and steel strains were recorded. For other cycles, the load was applied to the specimen from zero to maximum shear load and then released to zero in two increments. Also for most of the specimens shear displacement, crack width and steel strain were recorded at the maximum and zero shear loads.

For the last cycle where the load was increased until failure the same procedures as for the monotonic case of loading were follows. The values of each load increments were the same as those mentioned in the monotonic load procedure.

Table 4.1 Properties of transverse reinforcement

Type of steel	Bar Size (mm)	Yield Stress (N/mm^2)	Yield Strain (microstrain)	Young's Modulus (kN/mm^2)
High tensile deformed bar	8	535*	0.002	205
Mild tensile plain bar	8	475	.0023	200

* Taken as the stress at which a line parallel to the initial slope of the curve from 0.20% proof strain intersects the curve as shown in Figure (4.5).

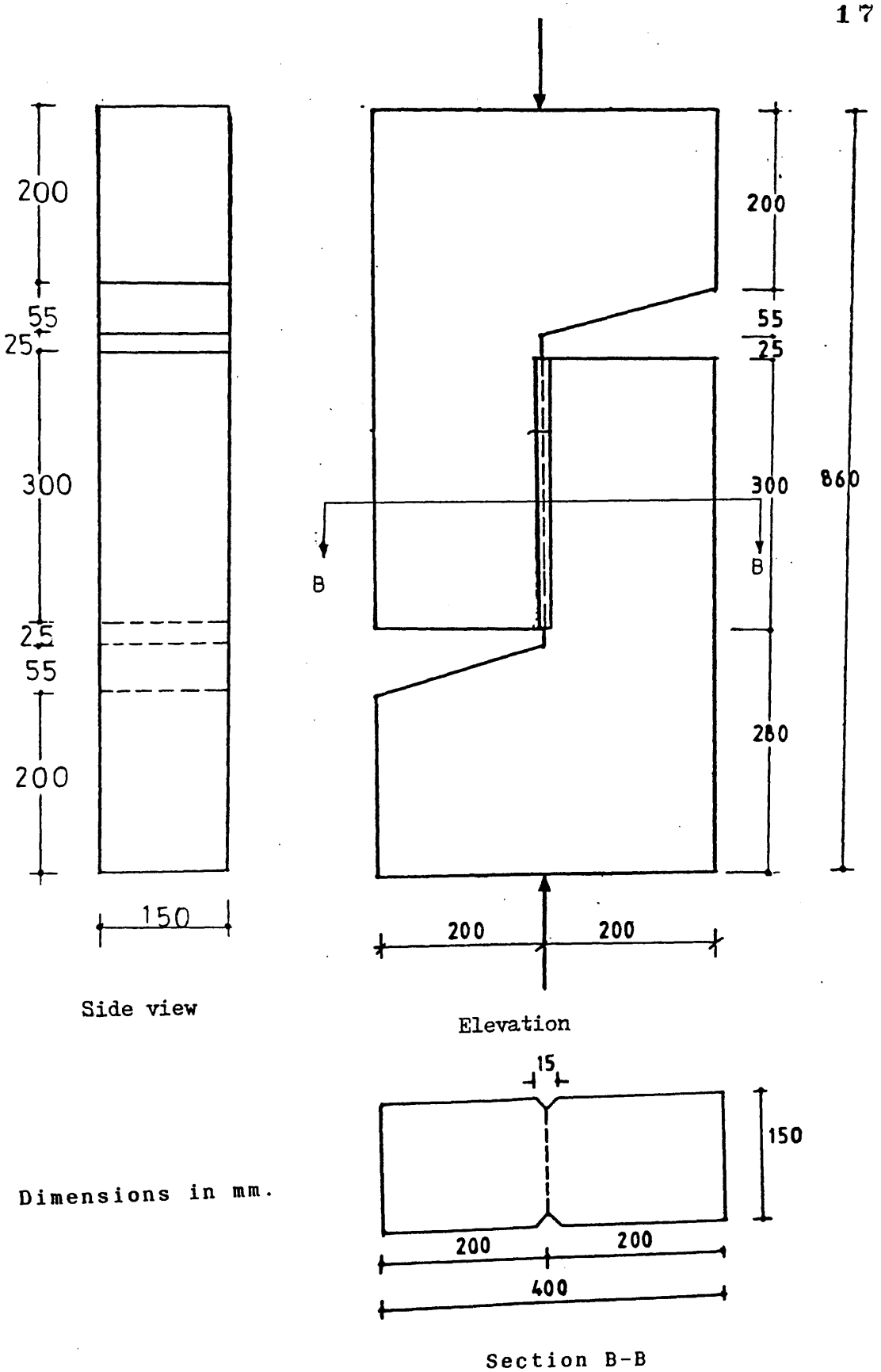

Figure (4.1) Geometry of a typical test specimen

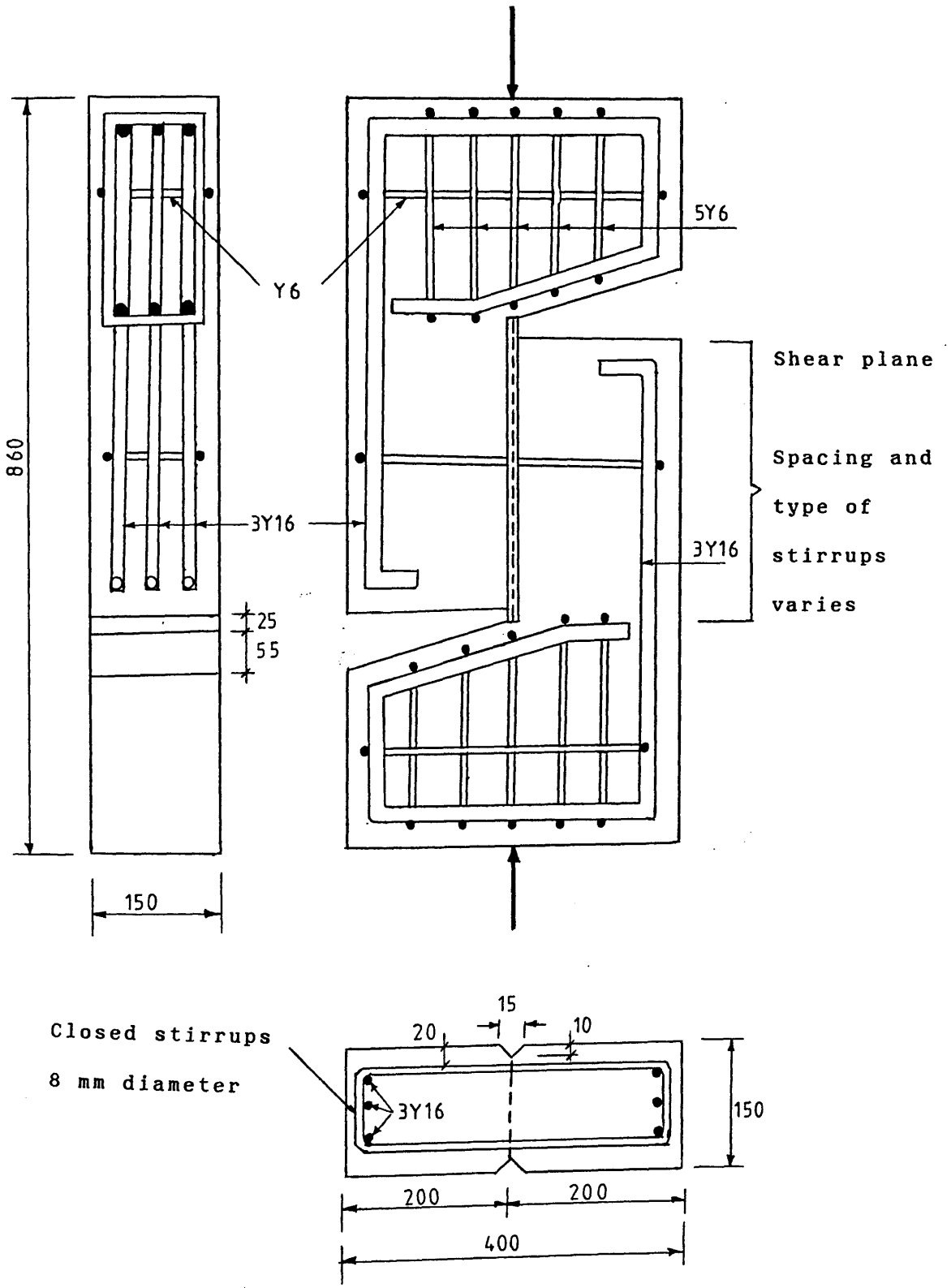

Figure(4.2) Reinforcement Details

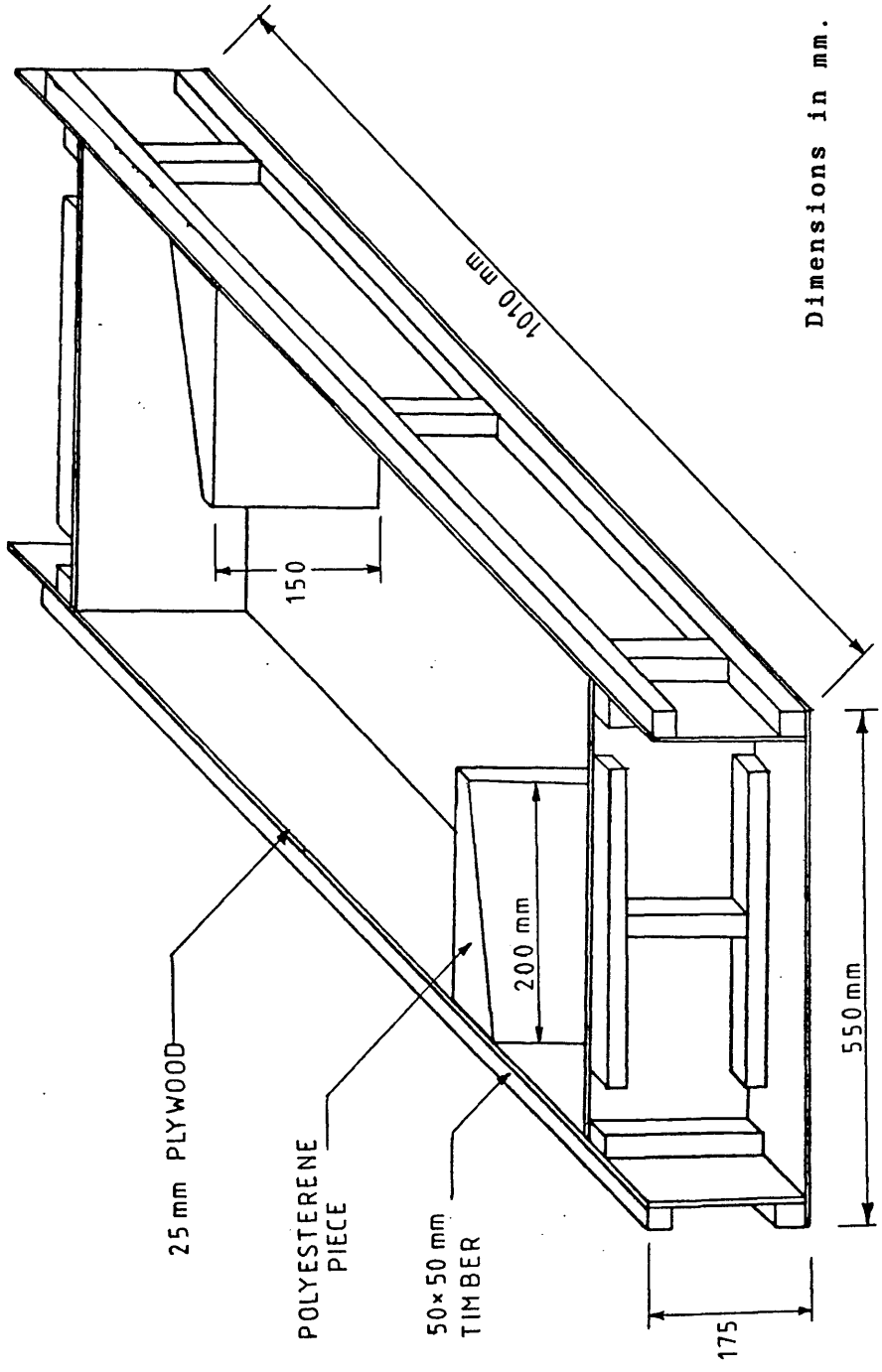

Figure(4.3) : Wooden formwork for a typical specimen

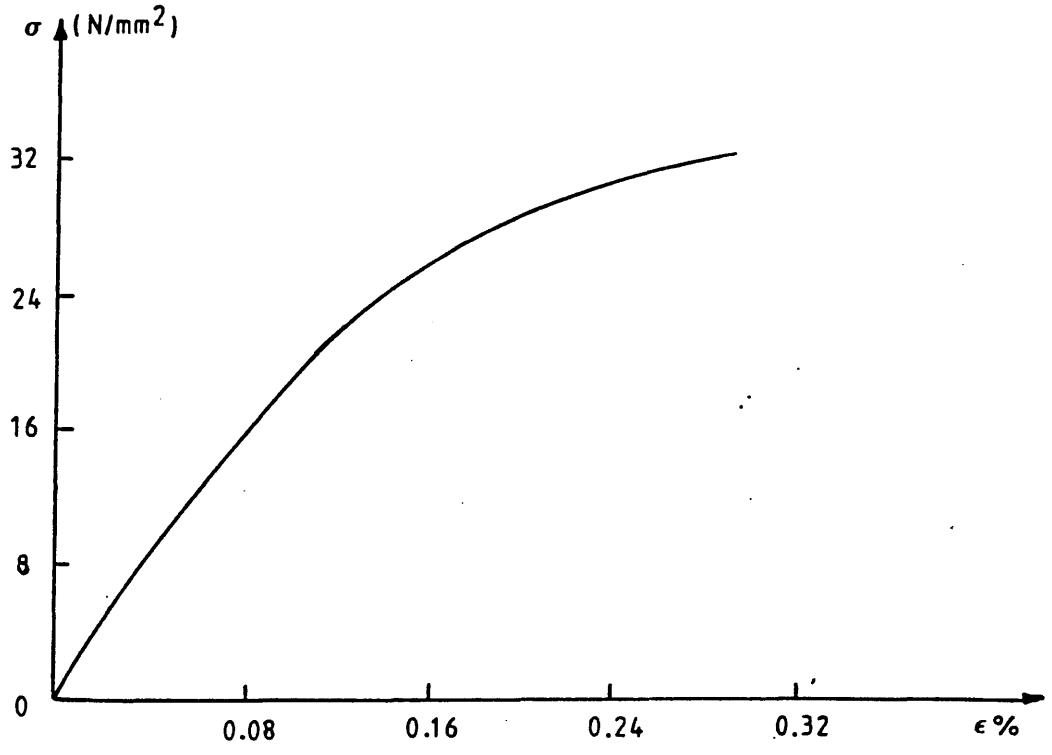

Figure (4.4) Typical stress-strain curve for concrete

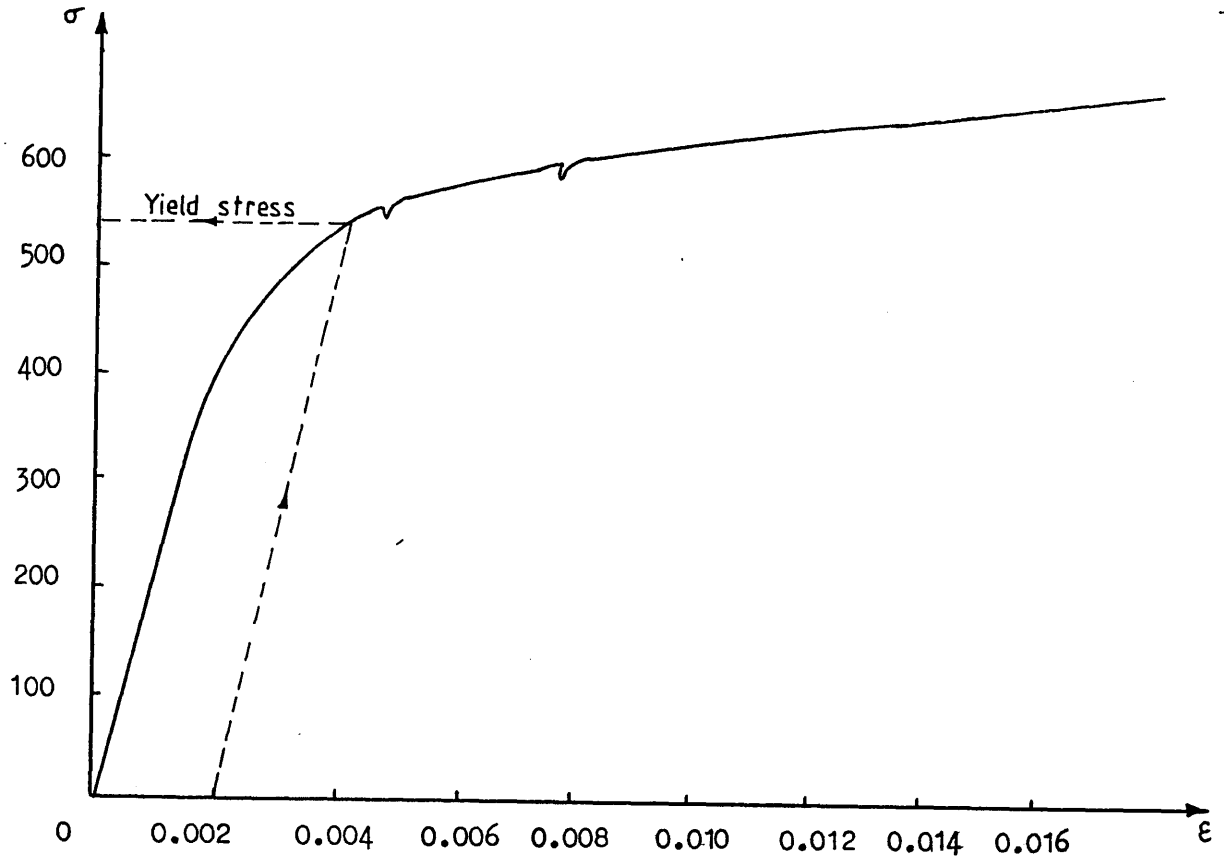

Figure (4.5) Typical stress-strain curve for high tensile deformed bar (8 mm dia.)

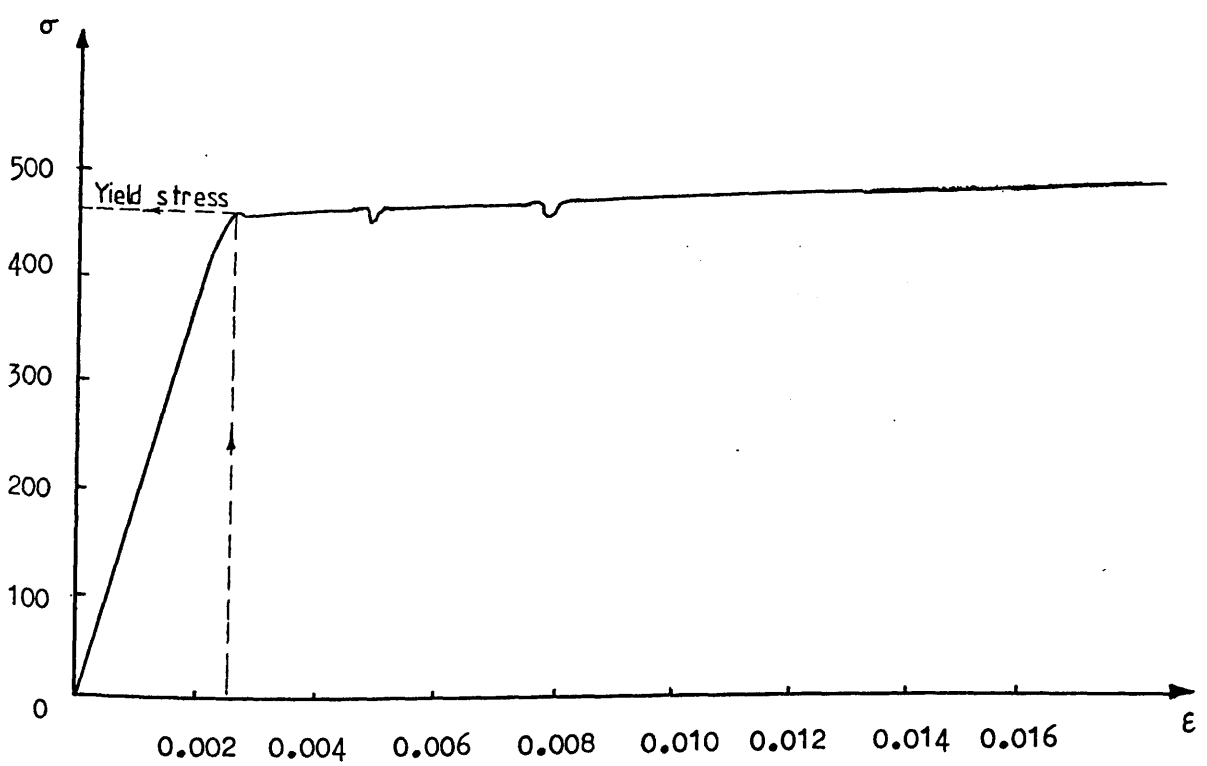

Figure (4.6) Typical stress-strain curve for a mild tensile plain bar (8 mm dia.)

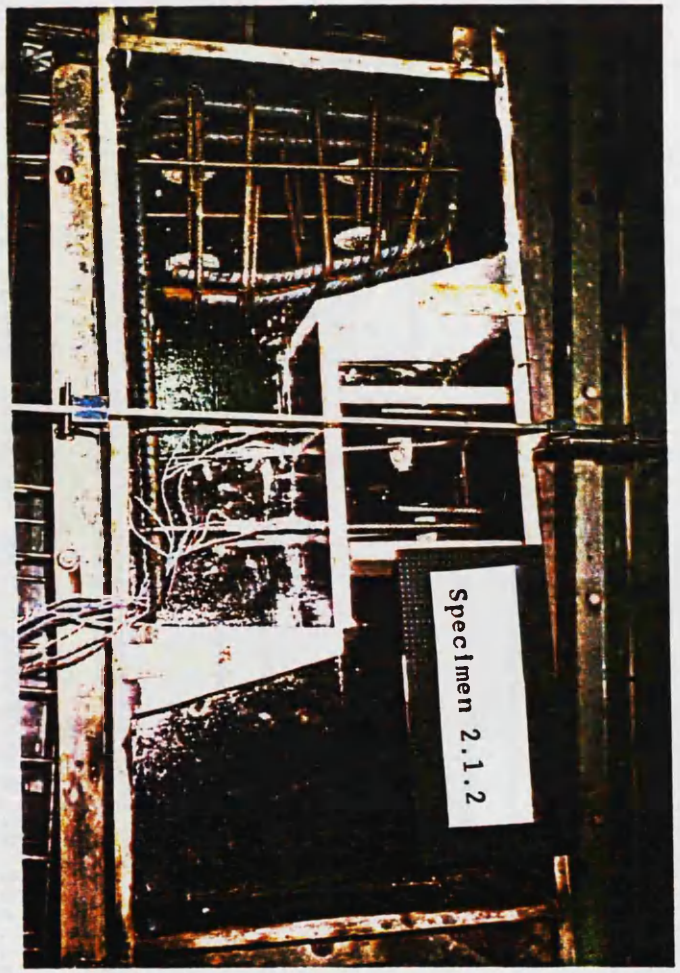

(a)

(b)

Figure (4.7) Procedure of casting a typical specimen for dowel action test

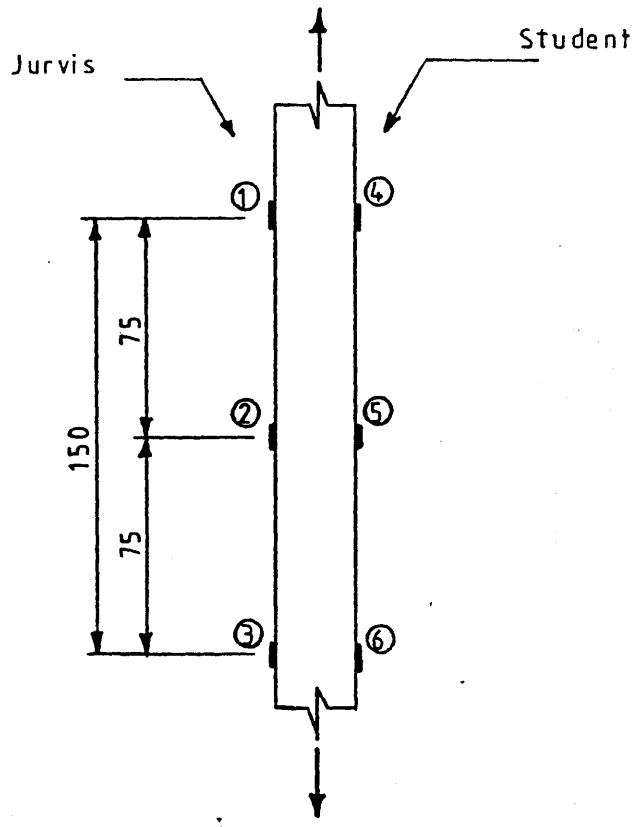

Figure (4.8) Arrangement of extensometer and strain gauges for comparison

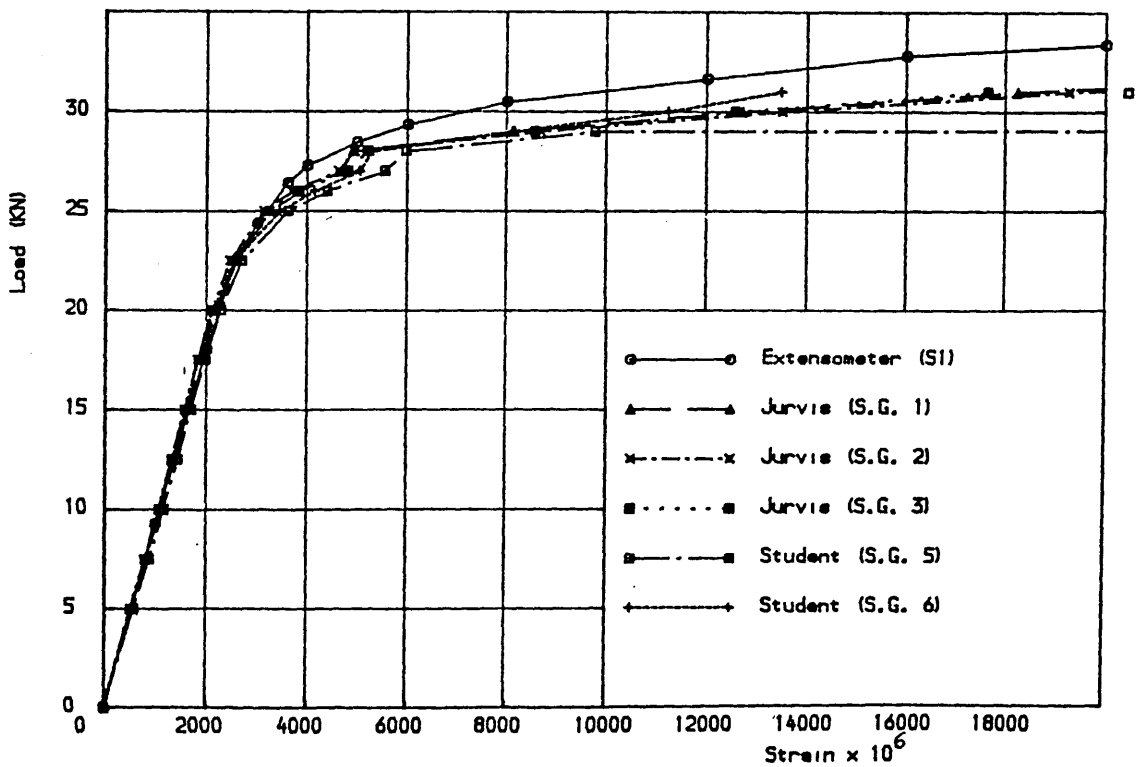

Figure (4.9) Comaprison of extensometer with the two types of strain gauges

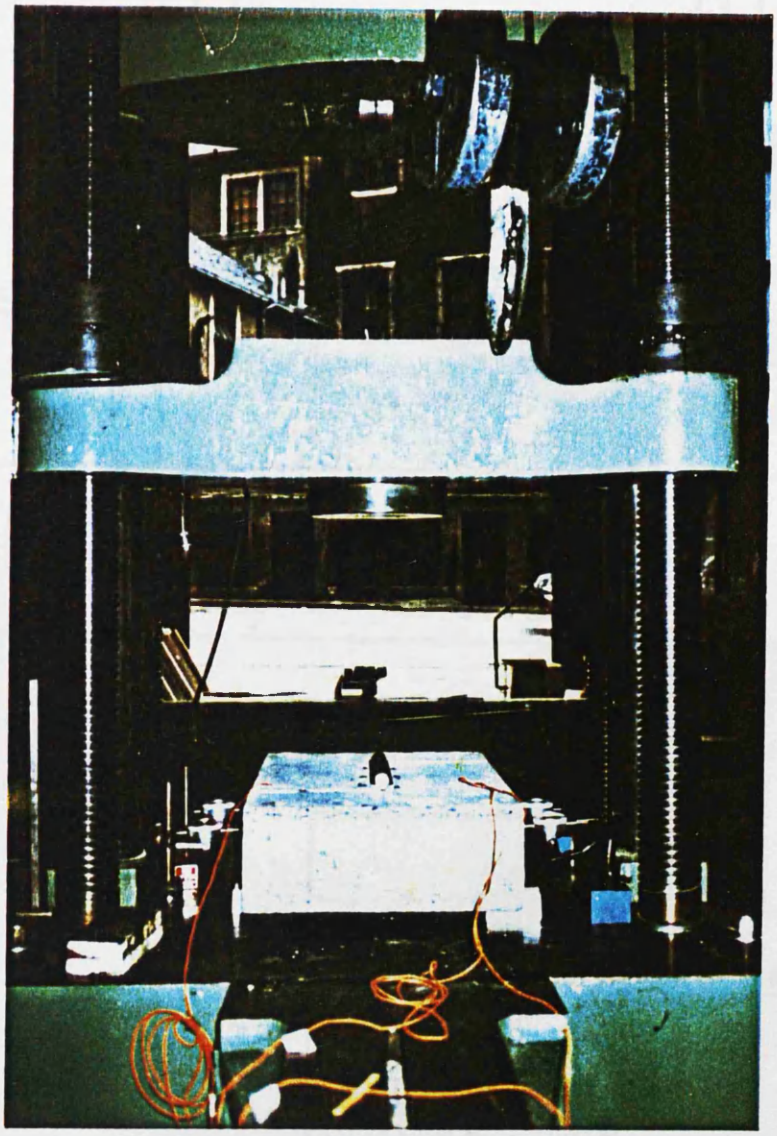

Figure (4.10) Arrangement for the precracking of specimen

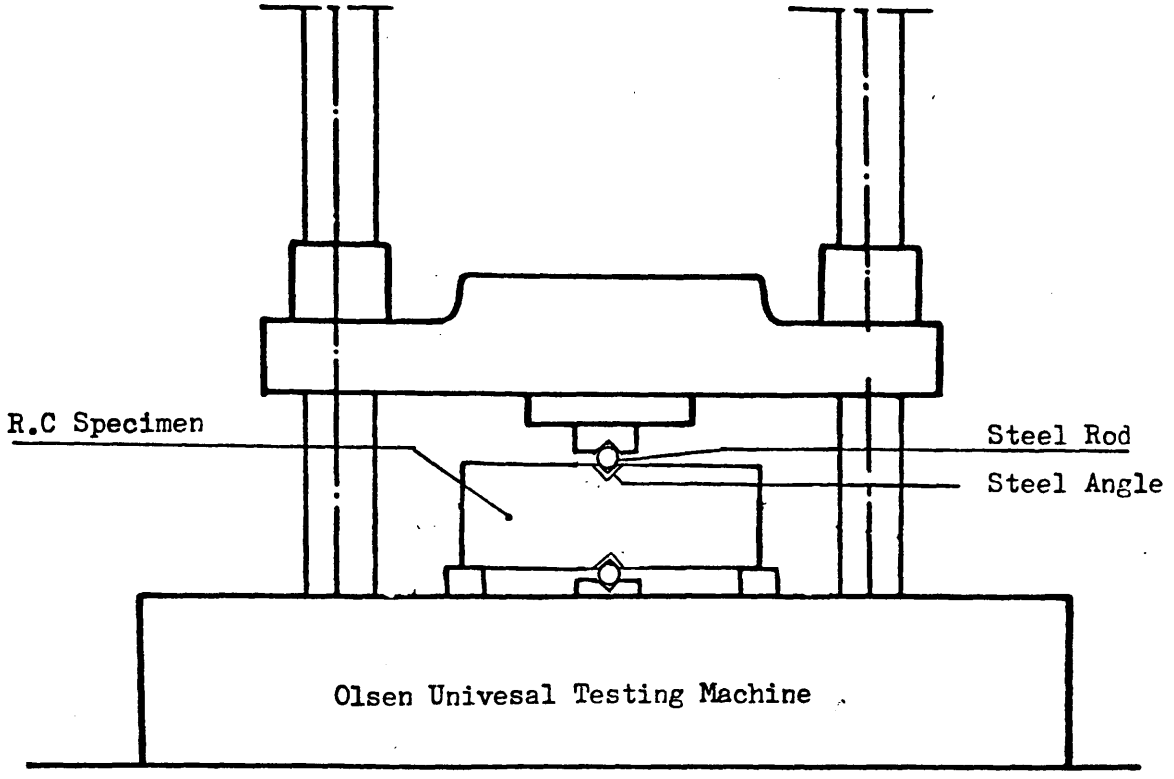

(a) ELEVATION

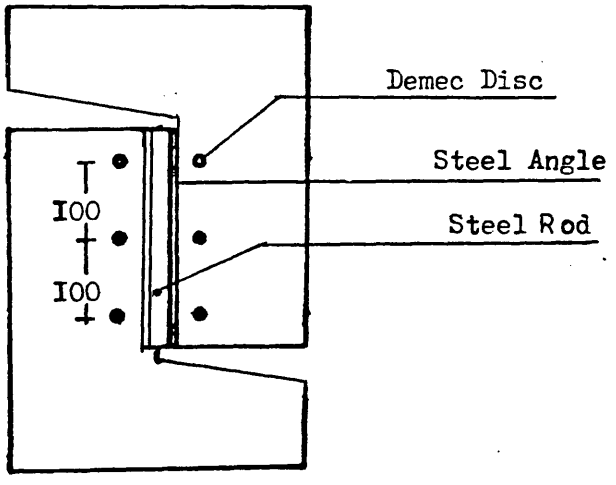

(b) PLAN

Figure (4.11) Initial cracking of specimen

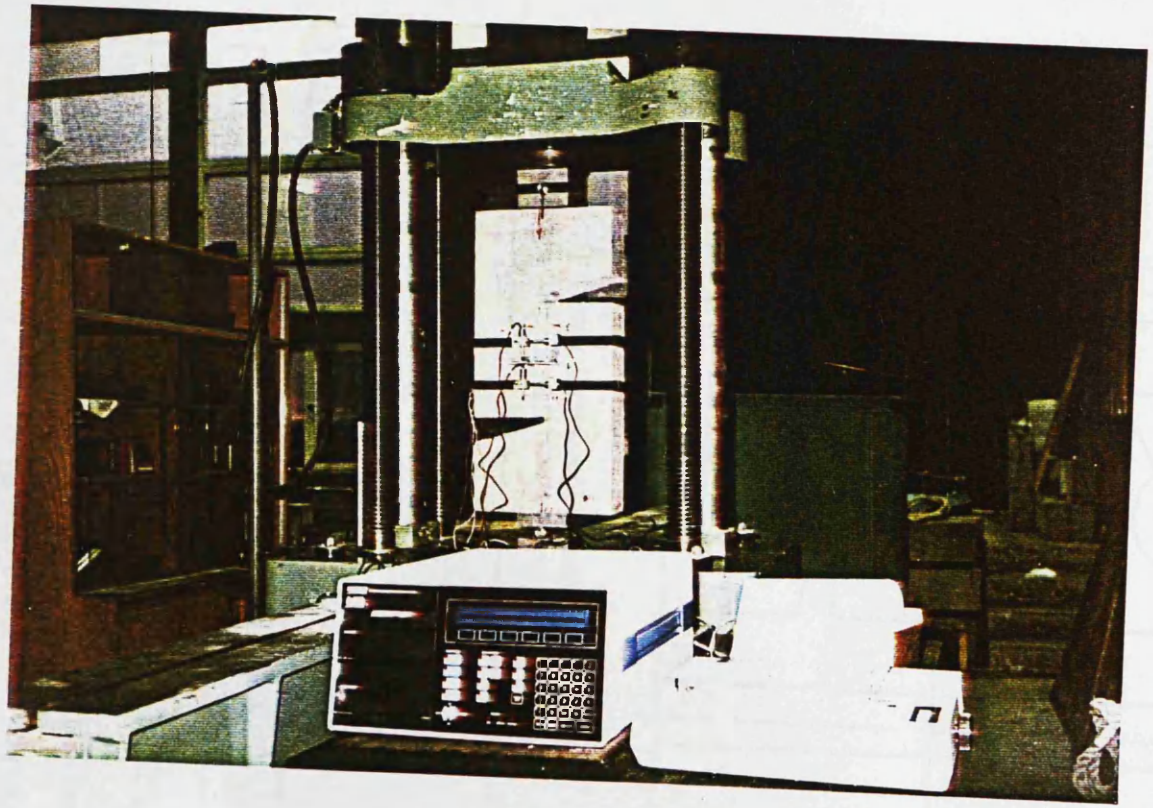

Figure (4.12) Arrangement of a typical specimen ready for testing

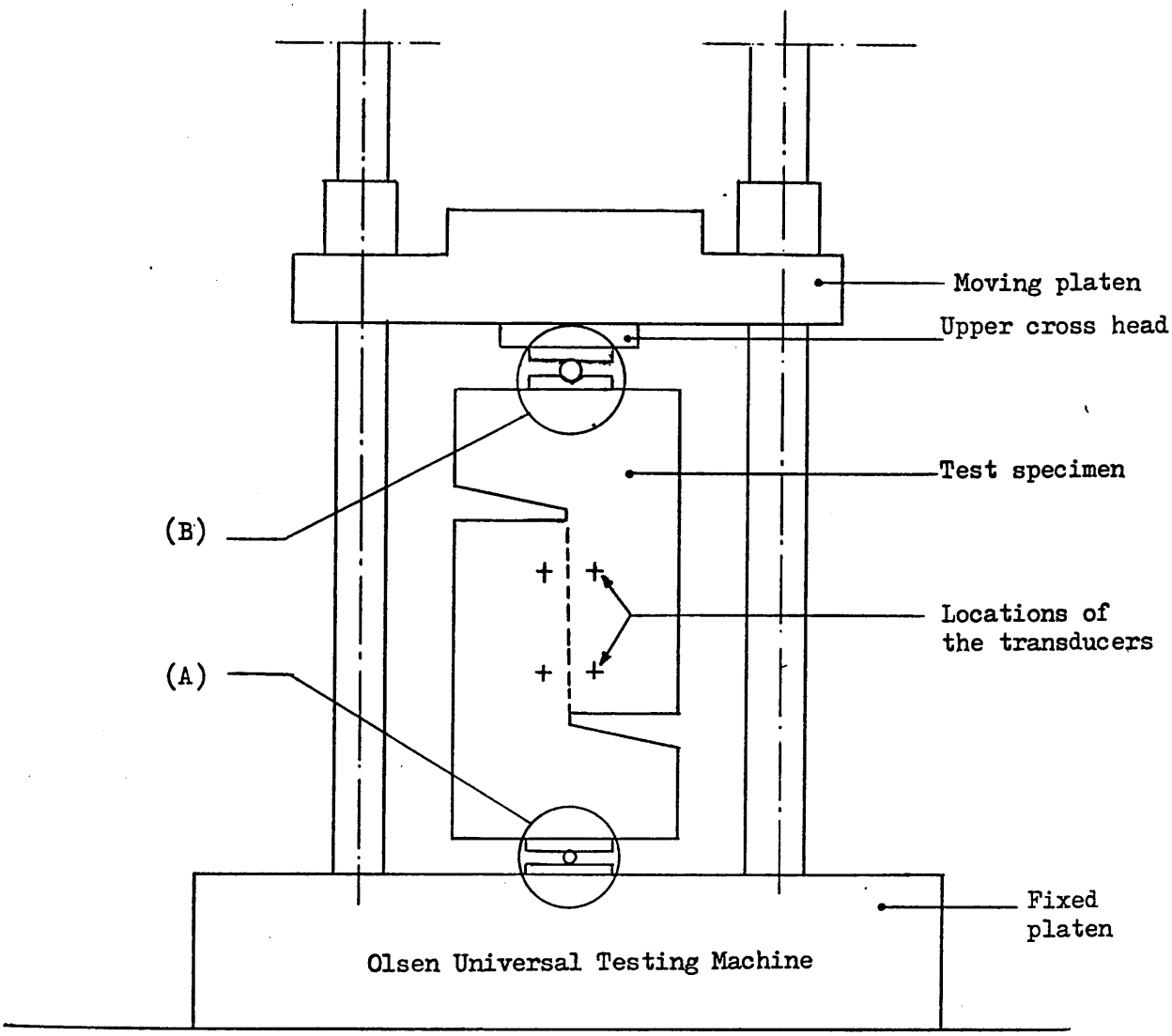

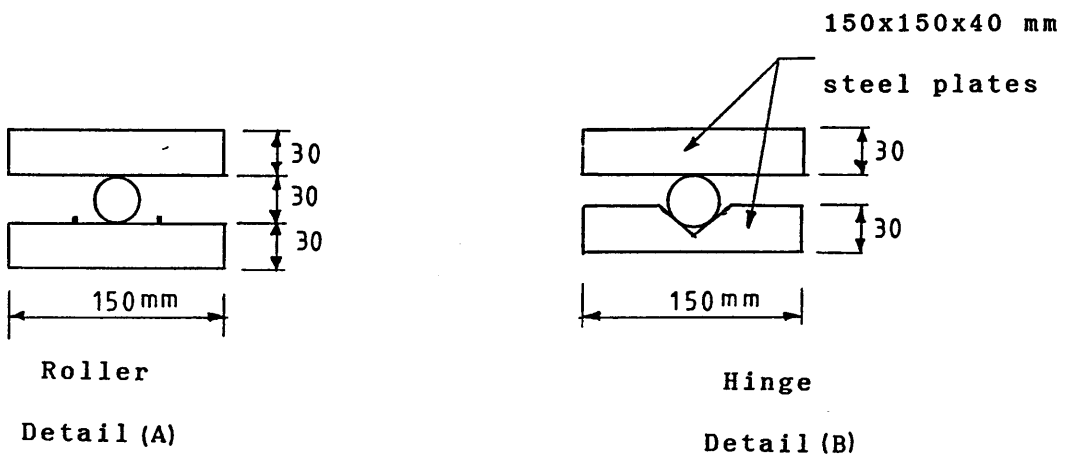

Figure (4.13) View of specimen with loading Arrangement

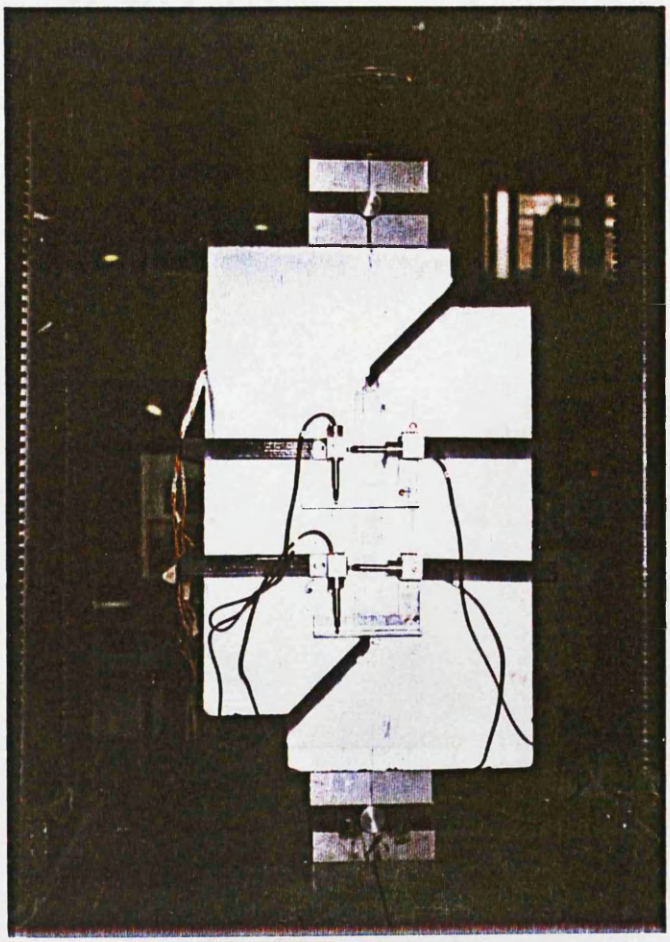

Figure (4.14) Arrangement of transducers

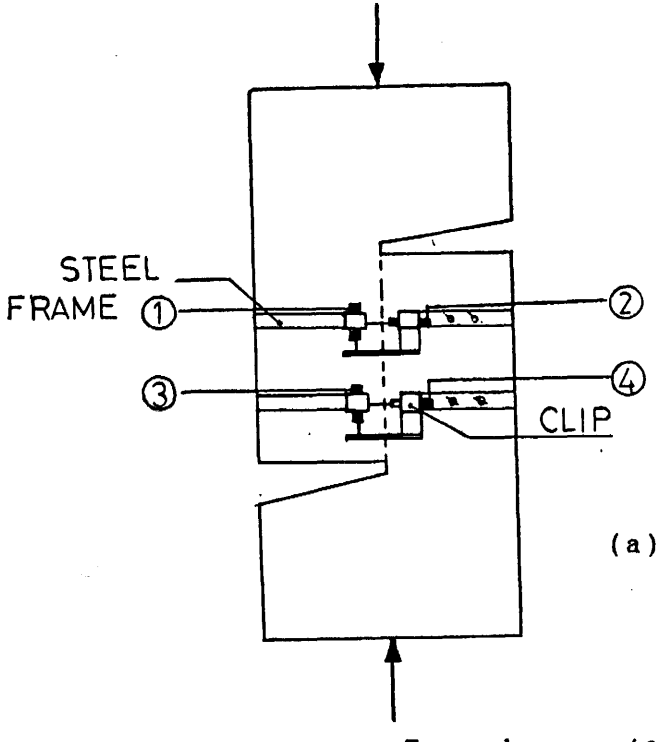

(a) Face (1)

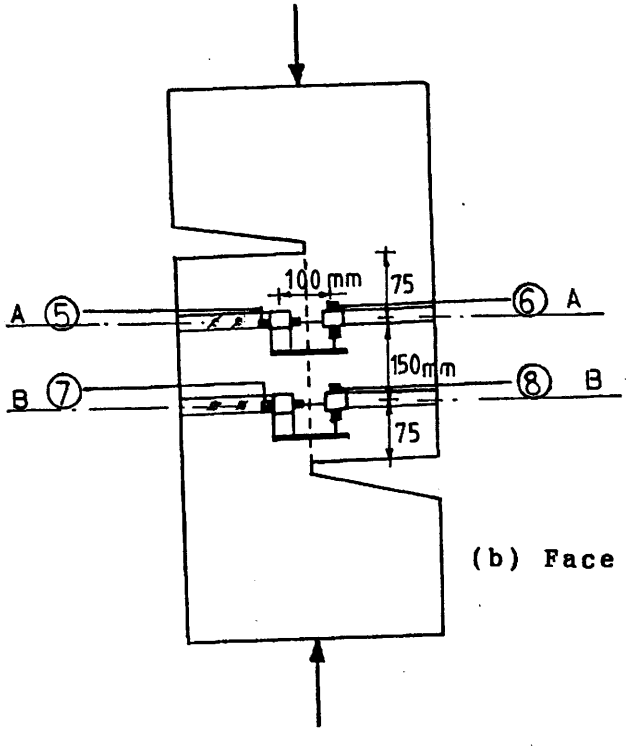

(b) Face (2)

Transducres (2) (4)
Transducers (5) (7) to measure crack width

Transducers (1) (3)
Transducers (6) (8) to measure shear displacement

Figure (4.15) Schematic representation of measuring arrangements

REFERENCES

(1) BS : 882 and 1201, 1965 "Specifications for aggregate from natural sources for concrete" London, British Standard Institute, 1965.

(2) BS 1881 : Part 5: 1970 "Method of testing concrete", pp. 12-13.

(3) DOE-TRRL supplementary report No. 254, DOE & DTP, 1977, "Recommended standard practices for structural testing of steel methods".

CHAPTER (5)

DOWEL TEST RESULTS

5.1 Introduction

The results of the dowel tests under both monotonic and repeated loadings, i.e series 2, are presented in this chapter. A fuller analysis of these results will be given in Chapter 7. Full details of the dowel test specimens and types of loading were given earlier in Table (3.1).

5.2 Monotonic Loading

5.2.1 General

The results of the specimens 2.1.1 - 2.1.4 of group (1) and 2.2.1 & 2.2.2 of group (2) are presented in this section. The results of group (1) will allow an assesement of :

(1) the effect of the amount of the dowel bars crossing the shear plane on the ultimate dowel strength, on the shear stiffness characteristics and on the basic mechanism of the dowel action,

(2) the effect of the types of loadings, and

(3) the contribution of dowel action to the total shear transfer across the crack.

Group (2) are used for providing additional information on the internal strain and stress distribution in the dowel bars and repeat two of the tests of group (1) which will allow the different mechanisms of shear transfer through dowel action , i.e. direct

shear, kinking and flexure of the bars, to be distingushed and hence lead to a better understanding of dowel action behaviour.
The general behaviour of the dowel specimens is described by the following relations :

(a) Shear load versus shear displacement.

(b) Shear load versus crack width.

(c) Crack width versus shear displacement.

(d) Shear load versus the strain in the dowel bar.

A summary of the principal test results, i.e the ulimate shear load, shear displacement and crack width at ultimate load, are given in Table (5.1). Both shear displacement and crack width are taken as the average values measured by the transducers positioned on the two sides of the specimen (refer to Chapter 4, Figure 4.15).

Figure (5.1) shows the relation of the applied shear load and the average shear displacement measured at two different levels (levels A and B defined in Figure (4.15). No significant difference between the shear displacement measured at the two predescribed levels was observed. Accordingly, it was considered appropriate to only use the average of the displacements measured at level "A".

5.2.2 Group (1)

Specimen 2.1.1

The shear load-shear displacement curve is shown in Figure 5.2.). From this figure a linear relationship was found up to 0.29 of the ultimate shear load (V_{du}).

Figure (5.3) shows the change in the crack width against the applied load. This increase in the crack width was not expected to exist because of the smooth surface of the shear plane. However, the increase was very small compared with the corresponding increase in the shear displacement. Also from Figure(5.3) it can be seen that the crack width increased more rapidly near to the failure load. This can also be noticed from the ratio of the crack width to the shear displacement shown in Figure (5.4).

No steel strains were recorded in this test because of the deficiency of the strain gauges.

Specimen 2.1.2

From the shear load versus shear displacement relationship shown in Figure (5.2b) a linear relation was observed up to 0.40 of the ultimate load. Beyond this load level the specimen exhibited significant nonlinear behaviour up to the failure.

Crack widening was also observed in this test as shown in Figure (5.3b). From this figure and Figure (5.4b) it can be seen that the widening of the crack was very small as was observed before in the previous test.

Eight strain gauges were used to measure the strains in the dowel bars crossing the shear plane. They were fixed to the top surface of the bar and their positions are shown in Figure (5.5). The relation between the shear load and the steel strains is shown in Figure (5.6). No readings were obtained from the strain gauges in positions 1, 1', 2, 2' and 4, for the other positions the strains could be measured up to 0.78 - 0.87 of the ultimate load. From

this figure high compressive strains can be observed at position 3, 3' and 4'. In general the trend of the shear load-steel strains curves was similar to that of the shear load -shear displacement.

Specimen 2.1.3

The different relations between the applied shear load, shear displacement and the crack width are shown in Figures (5.2c-5.4c). The specimen showed trends similar to the previous specimen. The linear behaviour was observed until 0.21 Vdu.

The locations of the steel strain measurement are shown in Figure (5.5). All strain gauges were fixed on the top surfaces of the dowel bars. The relations between the shear load and the strains in the dowel bars are presented in Figure (5.7). It can be seen from this figure that the strains measured at position 3, 4 and 4' were compressive and they exceeded the yield strain at the failure load. At positions 1 and 2 low tensile strains were recorded (about 10% of the yield strain). No strains were recorded at the other positions because the gauges were damaged during the specimen preparation.

Specimen 2.1.4

Behaviour similar to the previous specimens was generally observed (see Figures 5.2d, 5.3d and 5.4d). However, linear behaviour was found up to 0.18 of the ultimate load. In this test sixteen strain gauges were used to measure the strains in the dowel bars and they were fixed at different positions shown in Figure (5.5) on the top surface of the bars.

Figure (5.8) shows the relation between shear load and strains in the dowel bars measured at positions 1, 3, 5, 7, 5', 7' as typical results. As it was observed before in the previous tests, high compressive strains were measured at positions 3, 7, 7' and at positions 1, 5 , 5' low tensile strains were recorded.

5.2.3 Group (2)

Specimen 2.2.1

The curves of shear load against the shear displacement and the crack width, and the crack width versus shear displacement are shown in Figures (5.2)-(5.4). In general, these three curves showed similar trends to those of the identical specimen 2.1.2. However, failure load of this specimen was slightly greater than that of specimen 2.1.2 which would be attributed to the difference in the concrete strength.

A total number of 11 pairs of strain gauges were used in this test and they have been attached to the top and the bottom surfaces of the dowel bars as shown in Figure (5.9). Unfortunately, no readings were recorded for the strains at positions 1 and 11 because they broke down. The strains at positions 21 and 22 could be measured only up to 0.64 of the failure load.

An antisymmetrical strain distribution was found on either sides of the shear plane which was relatively consistent [see Figures (5.10) - (5.13)]. Having such relation, it was considered sufficient to study steel strains measured on only one side of the specimen and positions 16 ,15, 5, 6, 20, 12, 19, 13 were chosen.

The relation between the applied shear load and the strains measured at these positions are shown in Figures (5.14) and (5.15). From these figures it can be seen that the applied shear load resulted in tensile strain at the top surface of the dowel bar and compressive strain at the bottom surface. Higher strains were observed at the positions near to the shear plane.

The distribution of the strain along the dowel bar and over a distance five times the dowel bar diameter from the shear plane at different load levels (namely 0.4, 0.6 ,0.8 ,0.9 and 1.0 of the failure load) are presented in Figure (5.16). These strains could be resolved to direct and flexural strains by the following equation and assuming a linear distribution of flexural strain across the bar cross-section:

$$\epsilon_d = \frac{\epsilon_T + \epsilon_B}{2} \qquad (5.1a)$$

$$\epsilon_f = \frac{\epsilon_T - \epsilon_B}{2} \qquad (5.1b)$$

where ϵ_d = axial strain

ϵ_f = flexural strain at the surface of bar

ϵ_T, ϵ_B = measured strain at the top and bottom surfaces of a dowel bar at the same position and are shown in Figures (5.17) and (5.18). The relations between the flexural and direct strains, the distances measured from the shear plane as a function of the bar diameter and the applied shear load as percentage of the failure load are shown in Figures (5.19) and (5.20). The calculated flexural and direct stresses at failure load using the measured stress/strain curves are presented in Figure (5.21).

From these figures, it can be noticed that the applied shear load resulted in high flexural strains & stresses in the dowel bars specially at position near to the shear plane and the ratio of the maximum flexural to direct strain was 4.24. Also, it should be noted that the maximum flexural strain exceeded the yield strain by 168 % and the maximum direct strain was only 0.56 of the yield strain.

After completing the test, the specimen was cut at the shear plane by using an electrical saw and the crack pattern of the two faces of the shear area was traced by a black marker as shown in Figures (5.22 a,b). This crack pattern revealed high localized circumferencial tensile stresses around some dowel bars.

Specimen 2.2.2

This specimen is identical to specimen 2.1.4. The ultimate load was greater than that of specimen 2.1.4 which could be due to the difference in concrete strength.

Figures (5.2c - 5.5c) show the different relations between the shear load, shear displacement and crack width. Similar observations to those mentioned about the behaviour of specimen 2.1.4 were noticed in this test.

A total number of 11 pairs of strain gauges were used in this test. They were attached to the top and the bottom surfaces of the dowel bar as shown in Figure (5.9). No readings were obtained from the strain gauges placed at the shear plane because of their damage during the concrete casting. Another three strain gauges (namely numbers 2, 4 and 6) did not work properly during the test.

Similar to specimen 2.2.1, antysymmetrical distribution was found between the strain measuremnts at either side of the shear plane as shown in Figures (5.23) and (5.24).

The relation between the strains measured at positions 9',10',2',3', 13,14 ,6',7' and the applied shear load are shown in Figure (5.25). The distribution of the strain along the diameter of the dowel bar and over a distance nine times the bar diameter from the shear plane at different load levels is shown in Figure (5.26). Figures (5.27) and (5.28) show the same relation but for the flexural and direct strains.

The relations between these flexural and direct strains or stresses, and the distances measured from the shear plane as function of the bar diameter for different levels of applied shear load are shown in Figures (5.29) - (5.31). Trends similar to those stated for specimen 2.2.1 were obtained. The ratio of the maximum flexural to direct strain was 5.15 and the maximum flexural strain exceeded the proof strain by 124%. The maximum direct strain was only 0.43 of the proof strain.

The crack patterns on the two faces of the shear plane are shown in Figures (5.32 a,b). Continuous cracks at a distance equal to concrete cover are observed in this specimen which are different from the previous test, specimen 2.2.1 .

5.2.4 General Observations

(1) The crack at shear plane only slightly widened as the applied shear load increased, the ratio of crack width to shear displacement was about 10% on average.

(2) All specimens showed similar behaviour described by a linear response up to about an average 0.24 of the ultimate load followed by a nonlinear behaviour until failure.

(3) Failure of all specimens was due to yielding of dowel bars crossing the crack plane.

(4) A marked increase in the ultimate shear load was noted as a result of increasing the reinforcement ratio.

(5) The steel strain measurements of group (2) revealed two things: (a) an antisymmetrical relation between the strain/stress on either sides of the shear plane and (b) bending of the dowel bars crossing the shear plane.

5.3 Repeated Loading

5.3.1 General

The results of specimens 2.1.2A, 2.1.3A and 2.1.4A of group (1) tested under repeated shear load are described in this section. These specimens were identical to specimens 2.1.2, 2.1.3 and 2.1.4 which were tested under monotonic loading. The history of the repeated shear load applied to each specimen was previously described in Chapter (3).

The results of these tests were used for investigating the effect of the amount of the dowel bars crossing the shear plane and to compare this with monotonic loading behaviour.

The general behaviour of the specimens is described by relationships similar to those of the monotonic tests:

(a) shear load versus shear displacement (Figures 5.33 and 5.34)

(b) shear load versus crack width (Figures 5.35 and 5.36),

(c) crack width versus shear displacement (Figures 5.37 and 5.38), and

(d) shear load versus strains in dowel bars (Figures 5.40 to 5.42).

The positions of the steel strain gauges for specimen 2.1.3A and 2.1.4A are shown in Figure (5.39). A summary of principal results (namely shear failure load, shear displacement and crack width measured at failure) is presented in Table (5.1).

5.3.2 General Observations

(1) As was found in the monotonic tests, the change in the crack width against the applied shear load was much less than the equivalent shear displacement.

(2) The crack width to the shear displacement ratio measured at the maximum shear load for the cycle number 1, 2, 23 and 43 slightly decreased with increasing cycles.

(3) The specimens experienced large shear displacement at the first loading cycle. For subsequent cycles the response tended to stabilize in the sense that area enclosed by the hysteresis loops of load cycles decreased only very slightly. In fact there was an insignificant difference between the 23 & 43 cycles.

(4) The specimen response to the first cycle of loading was

characterized by an approximately linear shear stiffness as the shear load was increased. Response in subsequent cycles was characterized by a high shear stiffness at low load levels and a gradual decrease in the stiffness with increasing the load.

(5) Significant residual displacements occured when the applied load was released to zero on the first cycle. On subsequent cycles the residual displacements was subtantially less, becoming of approximately equal magnitude at high number of cycles.

(6) During unloading shear displacement decreased slightly at high load, but decreased rapidly as the load approached zero.

(7) The shear load -steel strain curves showed trends similar to those of the shear load -shear displacement curves. Compressive and tensile strains as high as three times the proof strain, were measured on the top and the bottom surfaces of the dowel bars at a distance three times the bar diameter from the shear plane. Lower tensile or compressive strains were recorded at the shear plane and on the top surface of the dowel bar.

(8) For the last cycle where the shear load was increased until failure, the specimens exhibited a nonlinear behaviour and failure was caused by yielding of the reinforcement .

Table (5.1): Test specimen details of series (2) (Dowel action).

Specimen No.	No. and size of stirrups	Reinforcement ratio %	Comp. concrete strength f_{cu} N/mm²	Yield stress of shear stirrup f_y N/mm²	Ultimate shear load (kN)	Ultimate shear stress (N/mm²)	Shear displacement at ultimate load (mm)	Crack width at ultimate load (mm)	Type of loading
Group (1)									
2.1.1	1Y8	0.22	46	535 N/mm²	31	0.69	3.58	0.268	M *
2.1.2	2Y8	0.45	48		51	1.14	3.28	0.201	M
2.1.2A	2Y8	0.45	48		33.4	0.74	1.216	0.173	R †
2.1.3	4Y8	0.89	47		94	2.09	2.86	0.425	M
2.1.3A	4Y8	0.89	47		75.6	1.68	1.939	0.868	R
2.1.4	6Y8	1.34	45		146	3.24	1.183	0.149	M
2.1.4A	6Y8	1.34	45		111.2	2.47	1.368	0.213	R
Group (2)									
2.2.1	2Y8	0.45	52	535 N/mm²	55	1.2	2.7	0.140	M
2.2.2	6Y8	1.34	60		162	3.60	1.310	0.213	M

* M : monotonic loading.

† R : repeated loading.

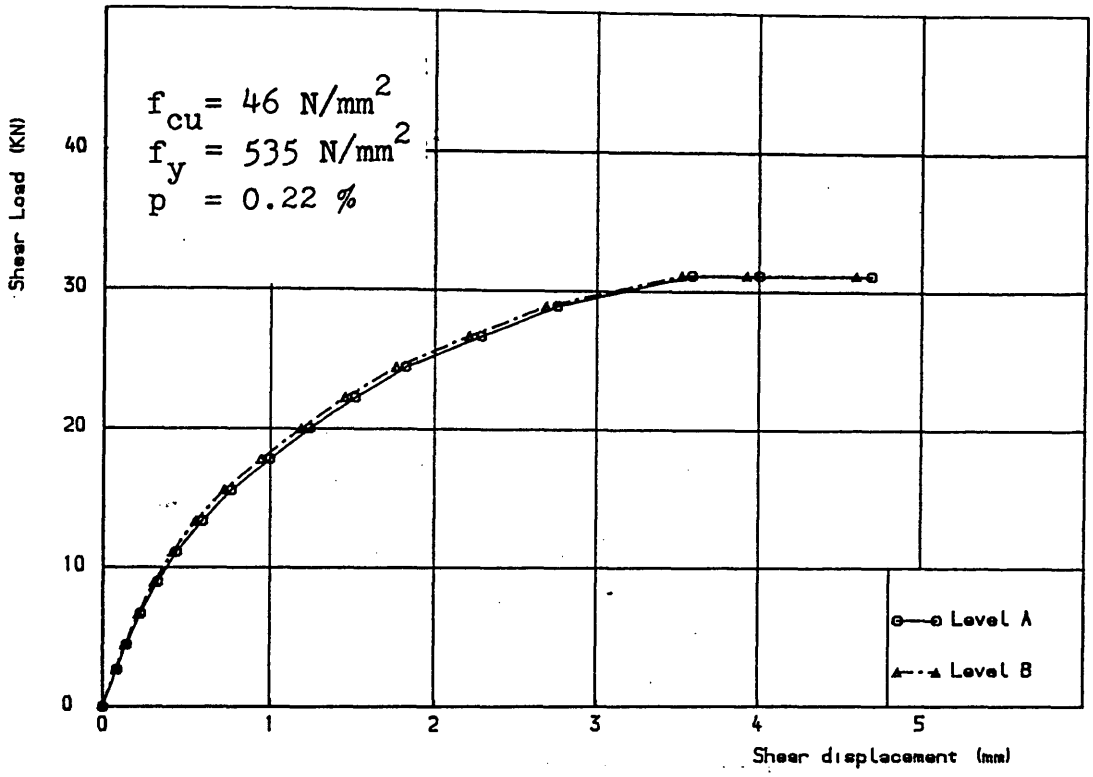

(a) Specimen 2.1.1

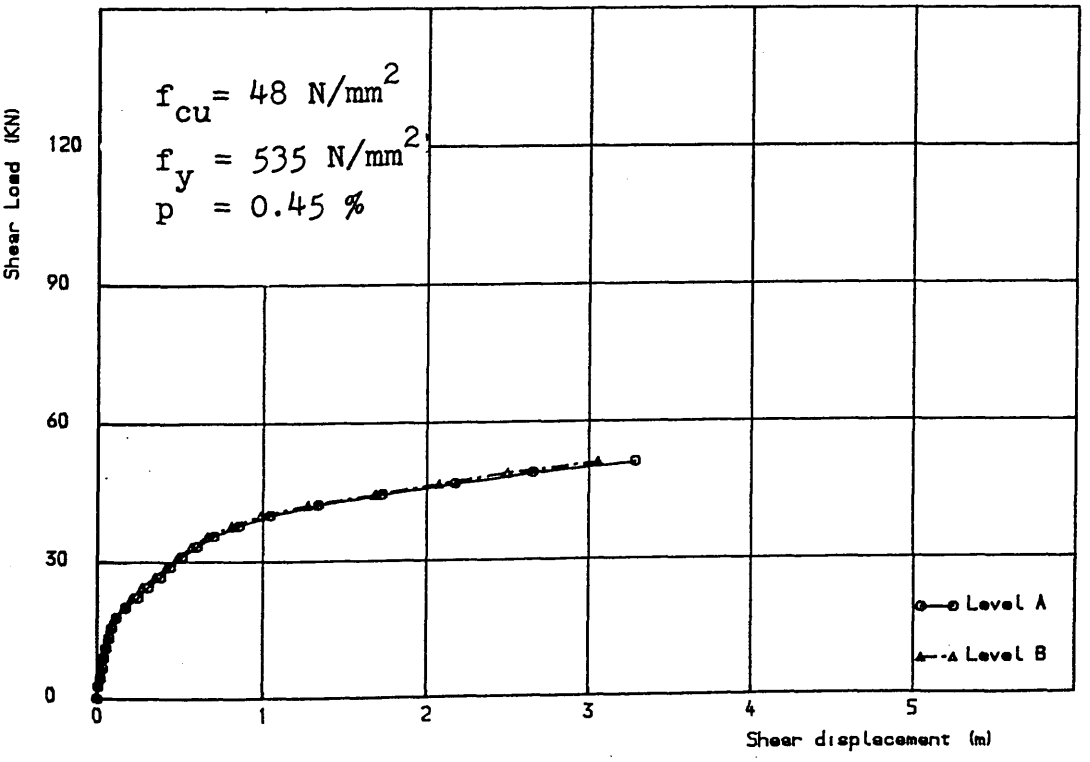

(b) Specimen 2.1.2

Figure(5.1) Comparison between the shear load vs. shear displacement measured at levels "A" & "B" for specimens of group (1)–series 2

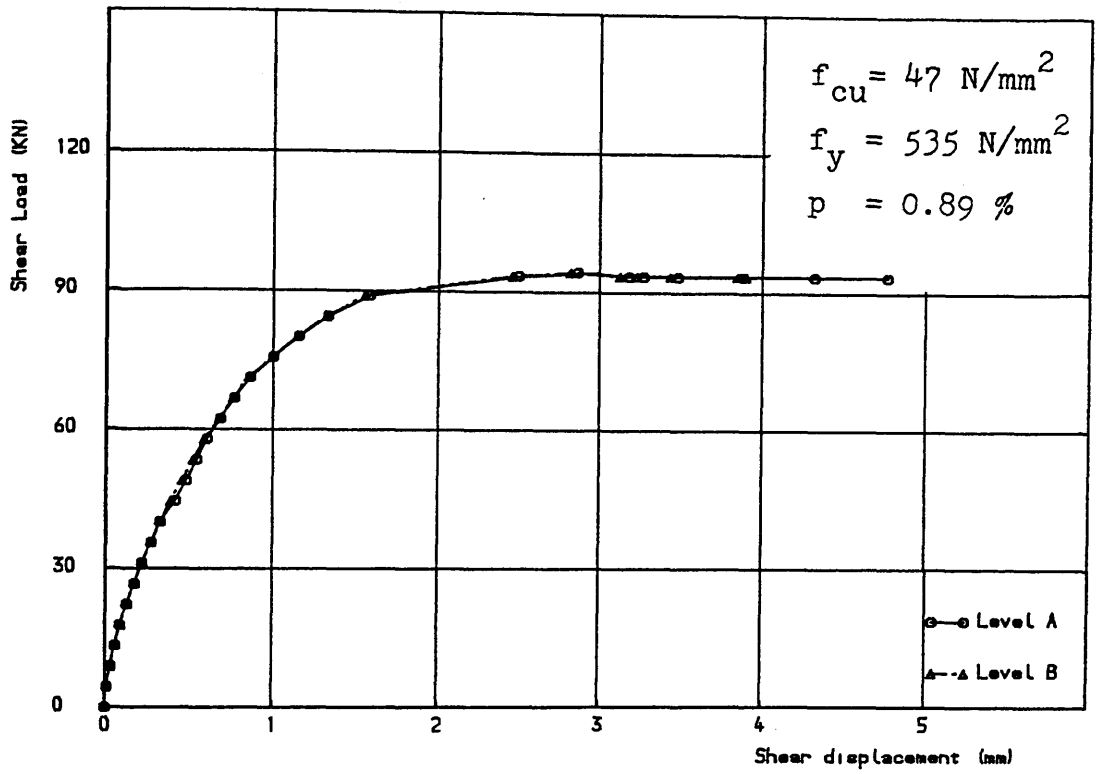

(c) Specimen 2.1.3

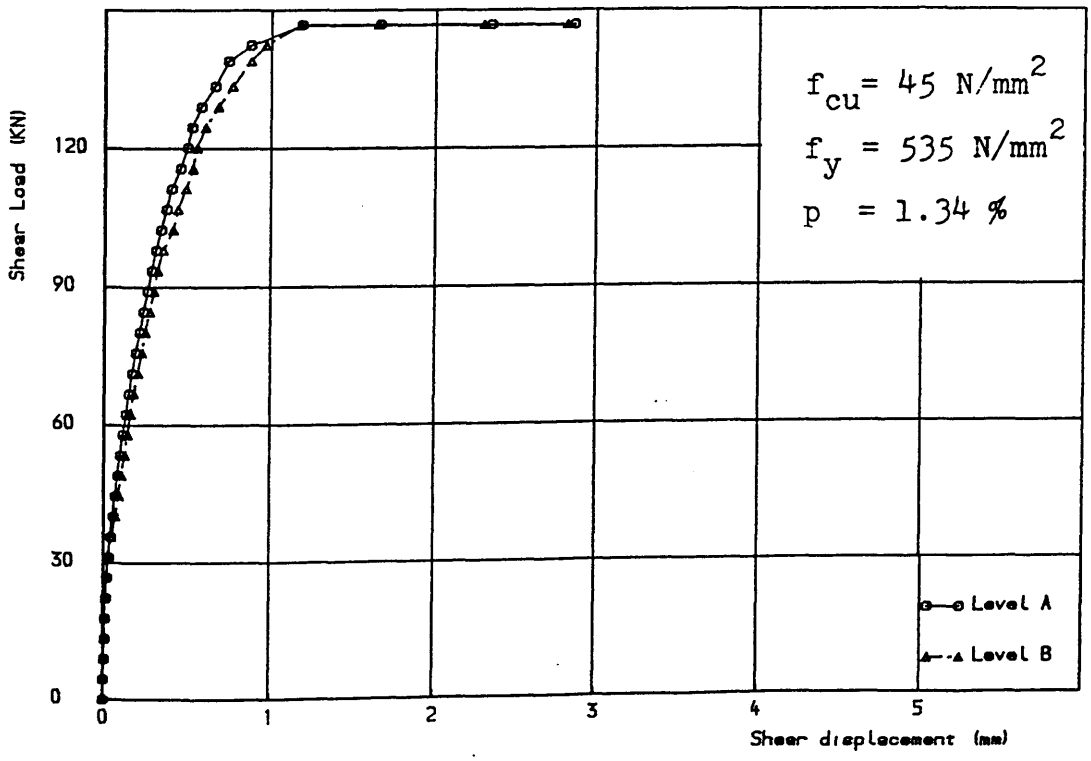

(d) Specimen 2.1.4

Figure(5.1) (Cont.) Comparison between the shear load vs. shear displacement measured at levels "A" & "B" for specimens of group (1)-series 2

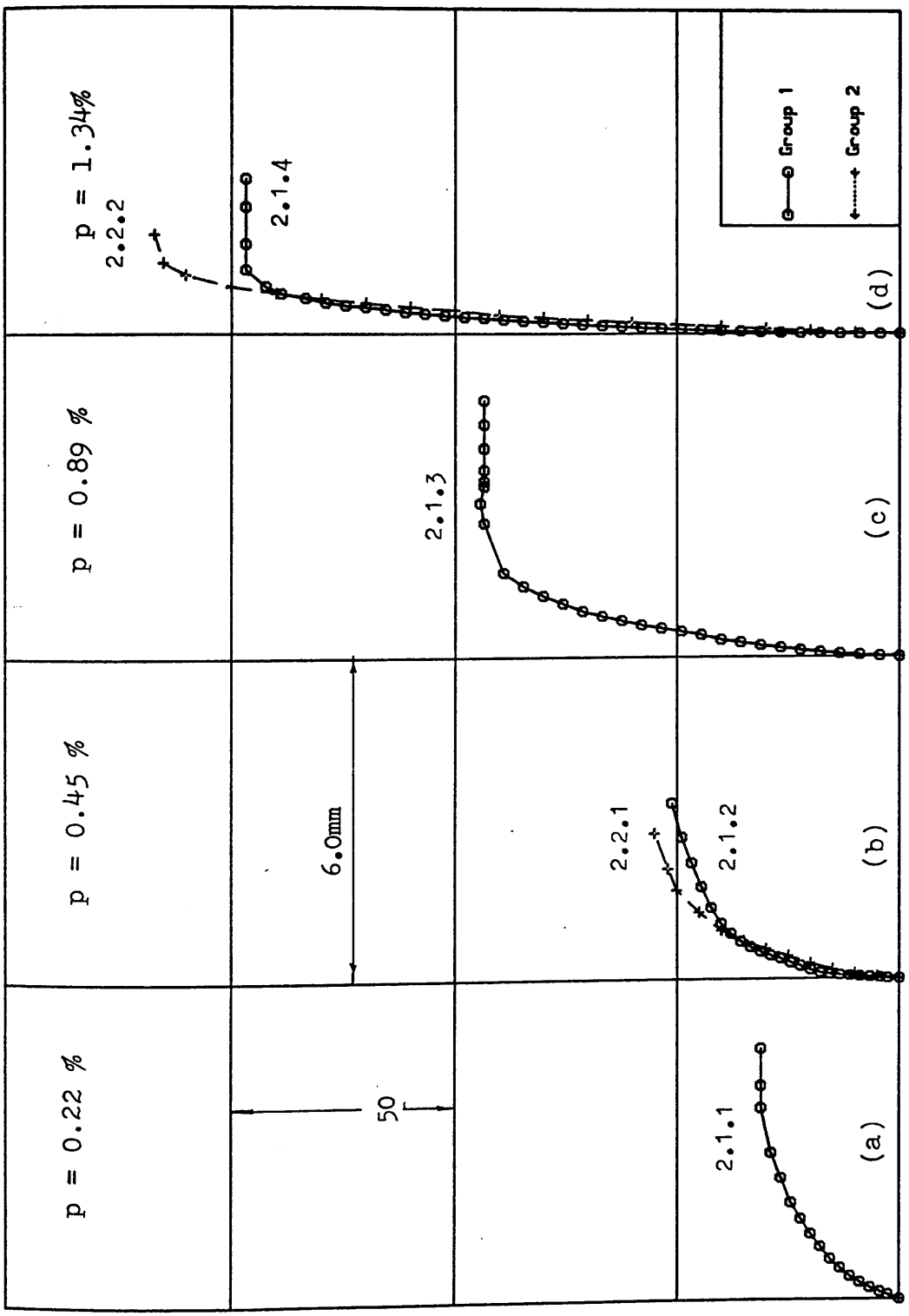

Figure(5.2) Shear load vs. shear displacement for series -2 (monotonic load)

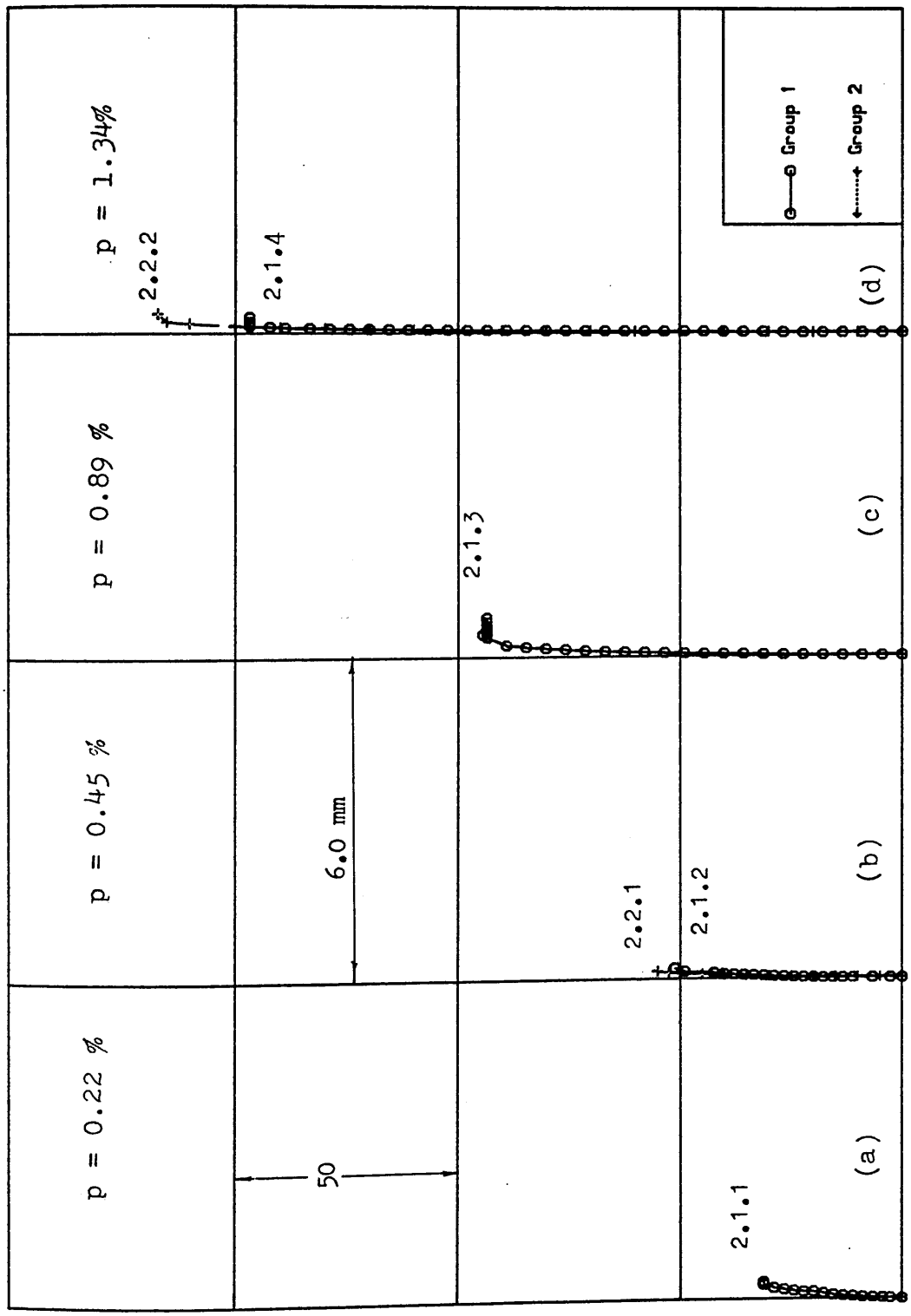

Figure(5.3) Shear load vs. crack width for series-2 (monotonic load)

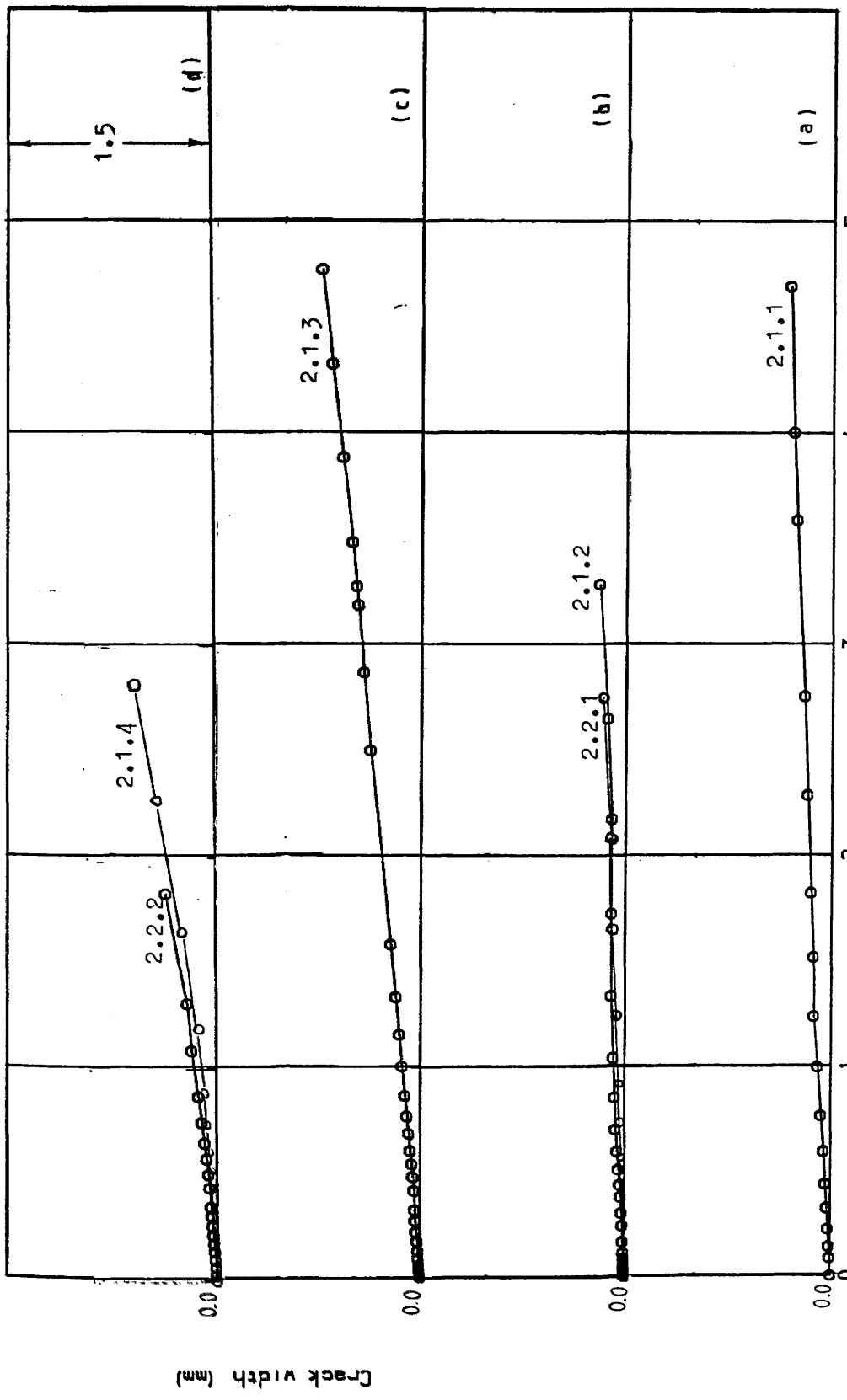

Figure(5.4) Crack width vs. shear displacement for series-2 (monotonic load)

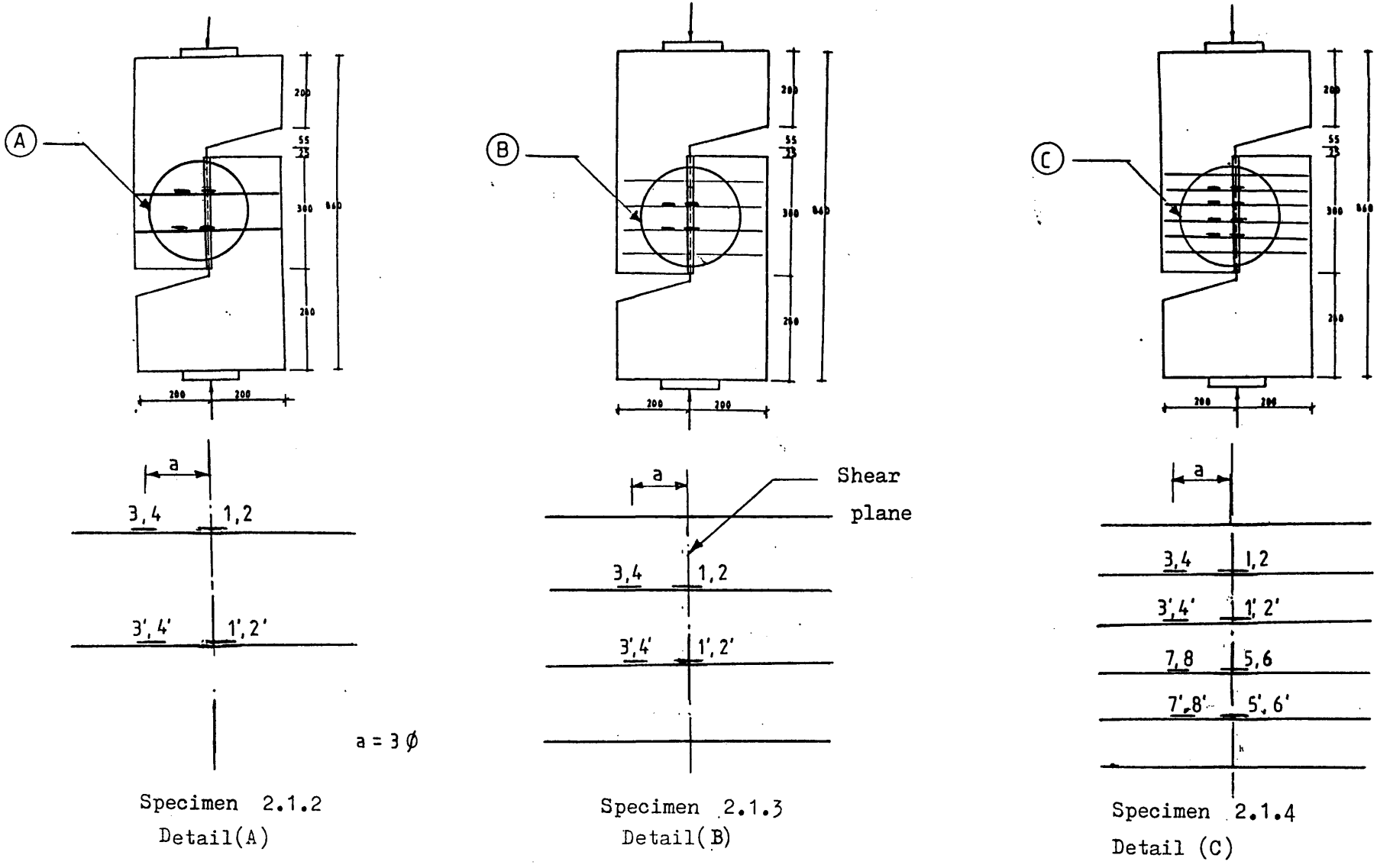

Specimen 2.1.2
Detail(A)

Specimen 2.1.3
Detail(B)

Specimen 2.1.4
Detail (C)

Figure(5.5) Position of steel strain gauges for group(1)–series 2 under monotonic load

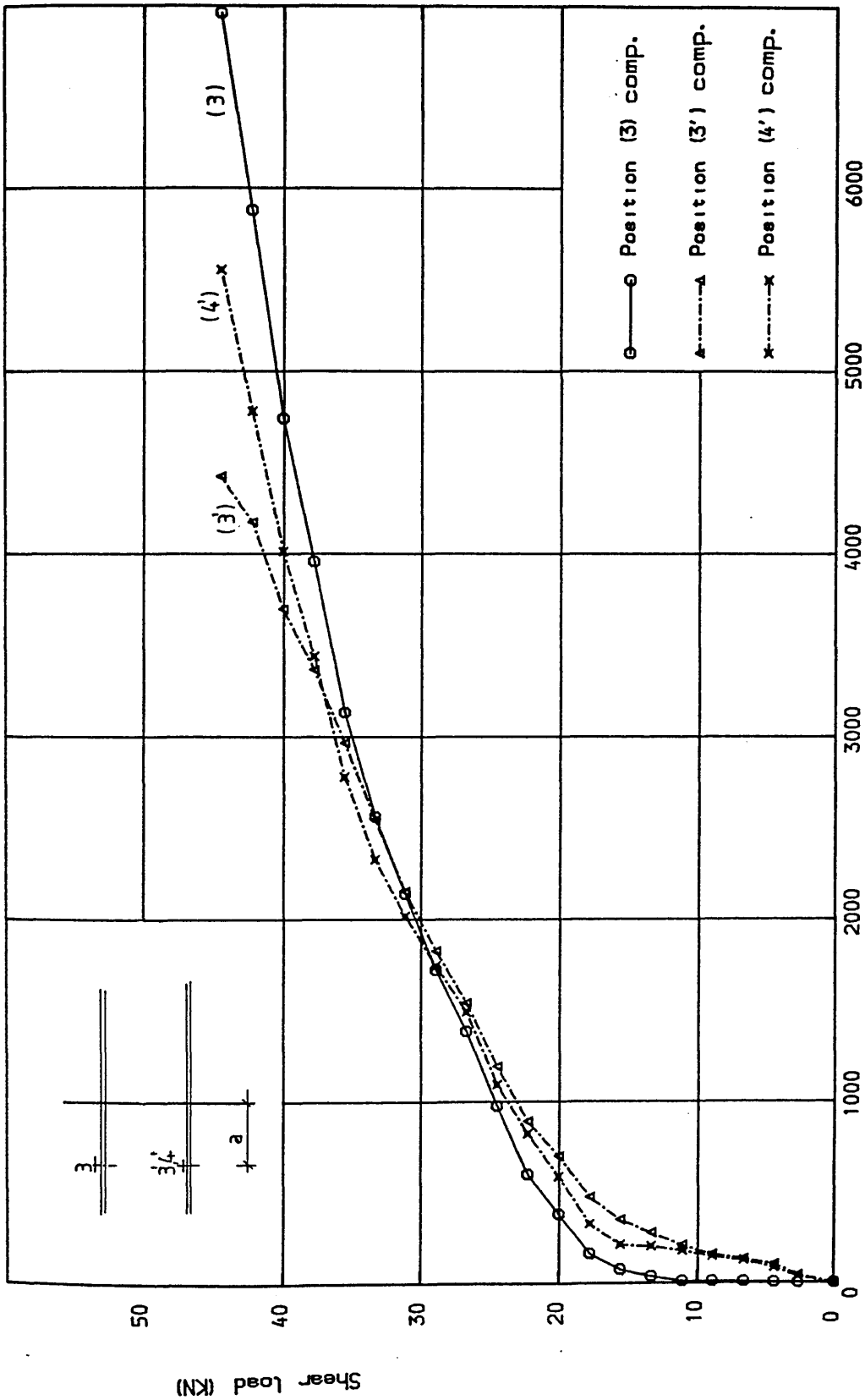

Figure (5.6) Shear load vs steel strain for specimen 2.1.2

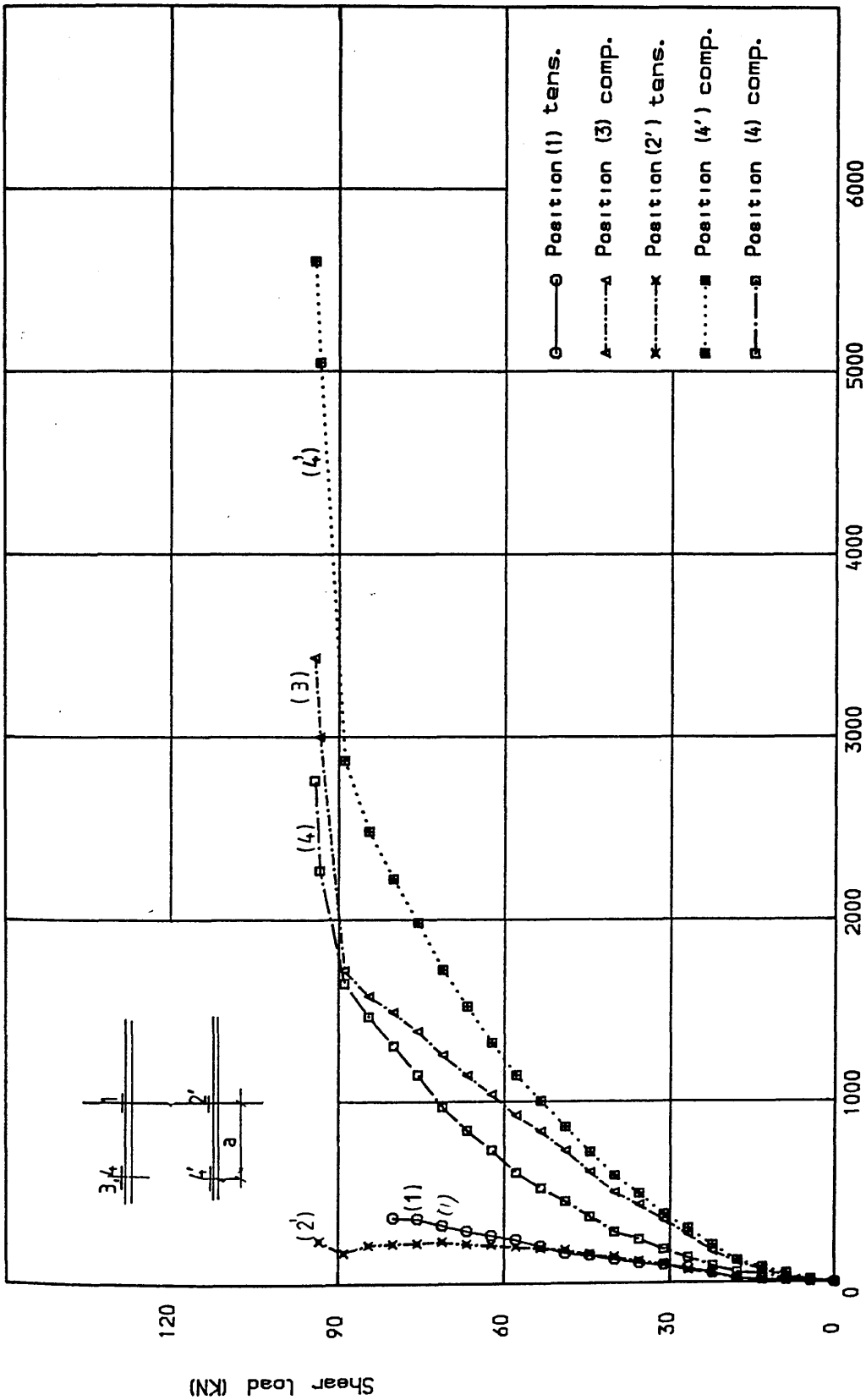

Figure (5.7) Shear load vs steel strain for specimen 2.1.3

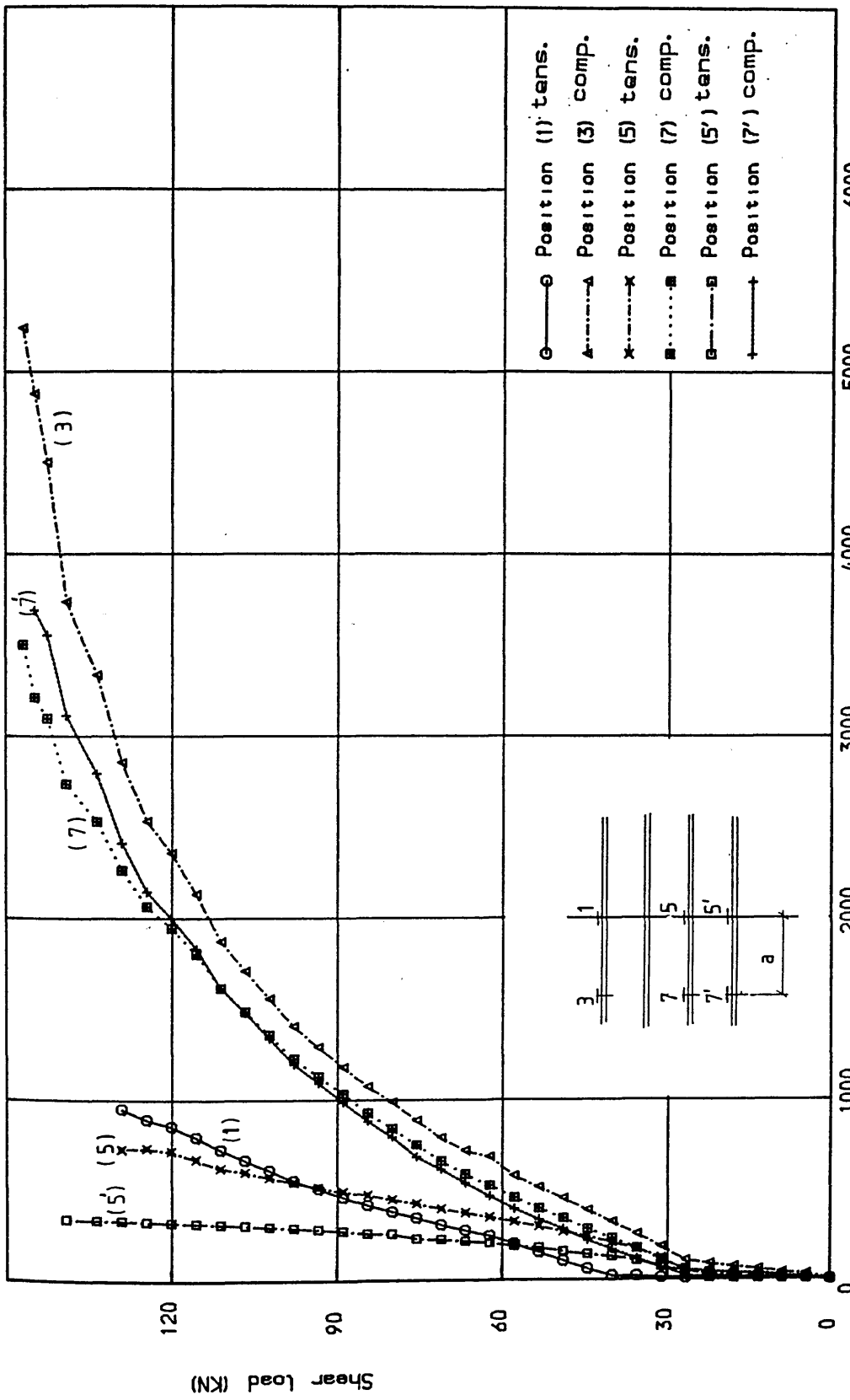

Figure (5,8) Shear load vs steel strain for specimen 2.1.4

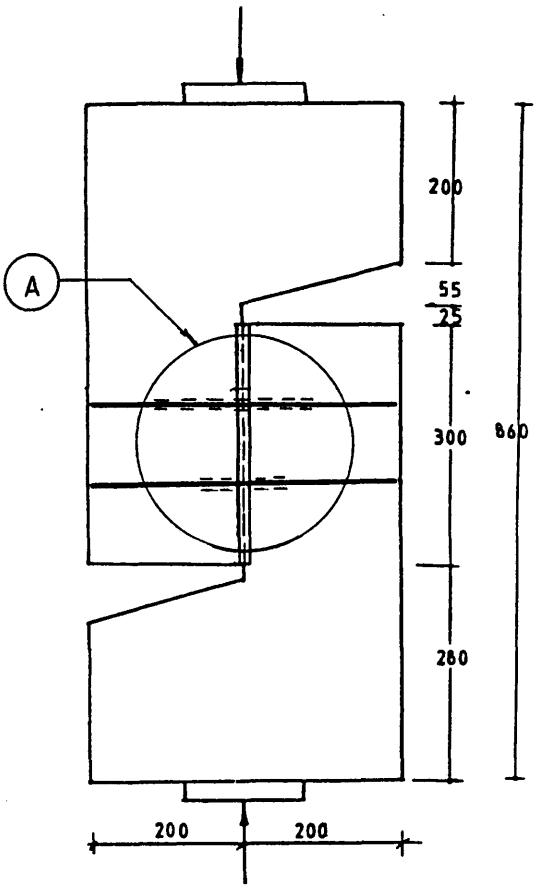

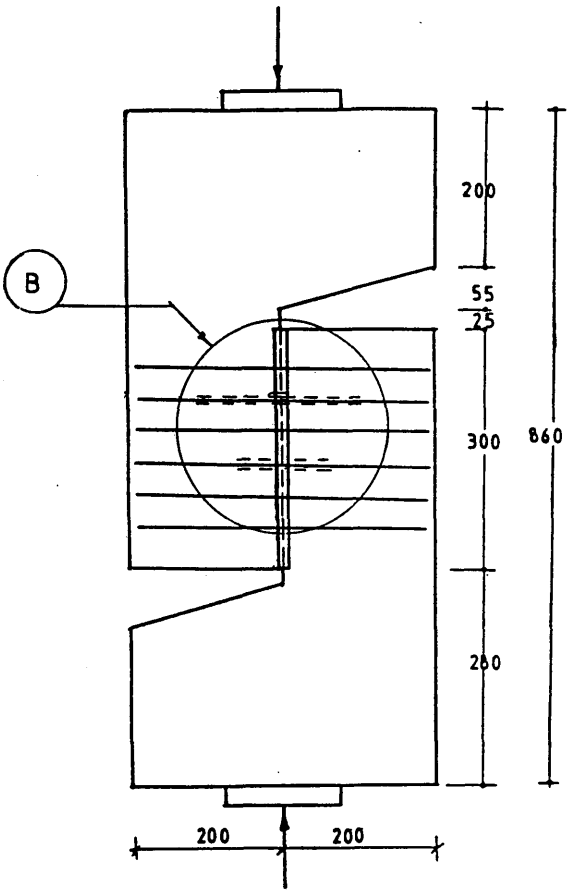

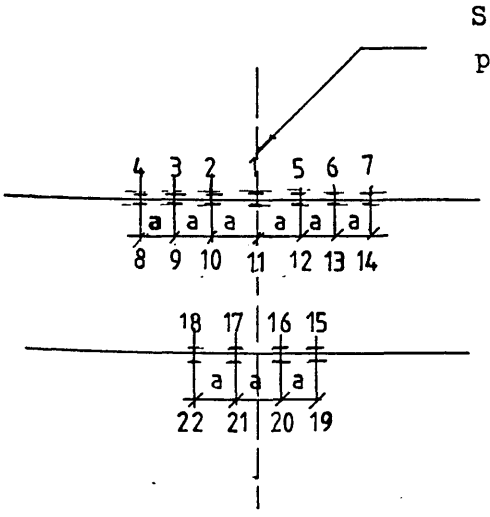

Specimen 2.2.1

Detail(A)

a= 3Ø

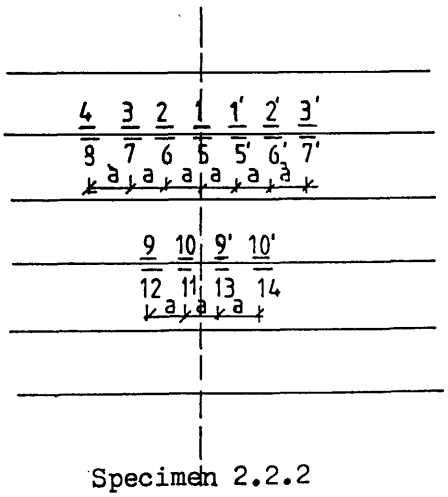

Specimen 2.2.2

Detail (B)

Figure(5.9) Position of steel strain gauges for group(2)– series 2

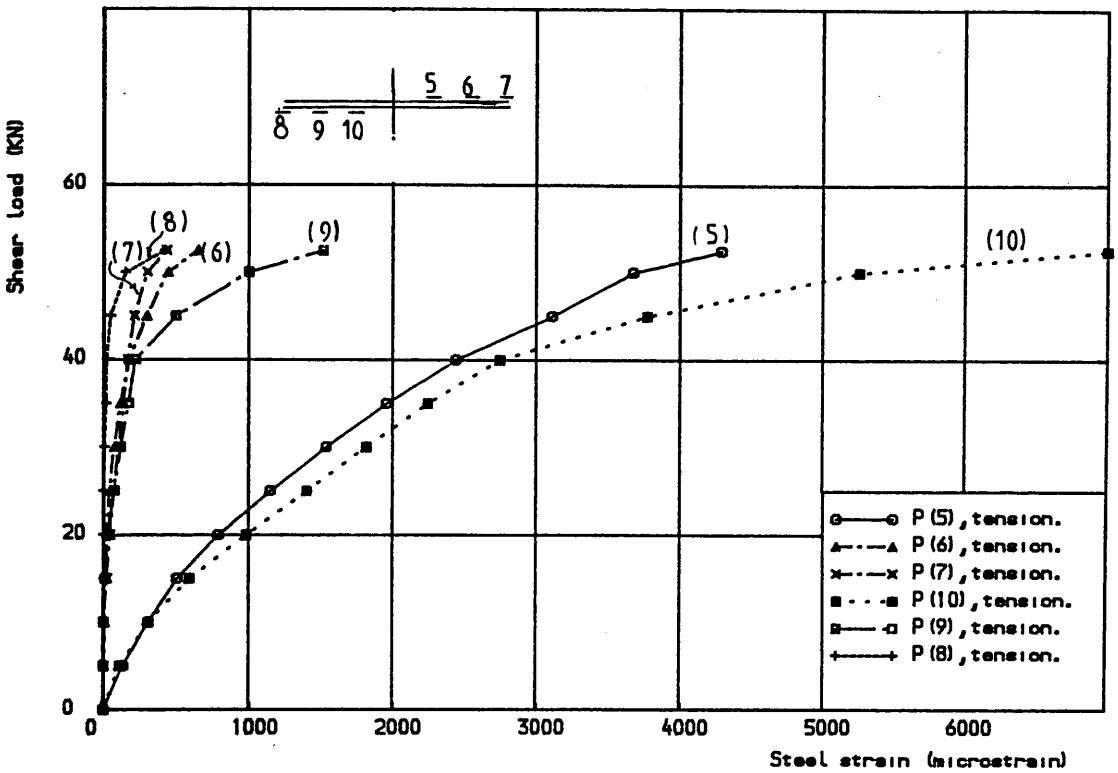

Figure (5.10) Shear load vs steel strain for specimen 2.2.1
(positions 5, 6, 7 - 10, 9, 8)

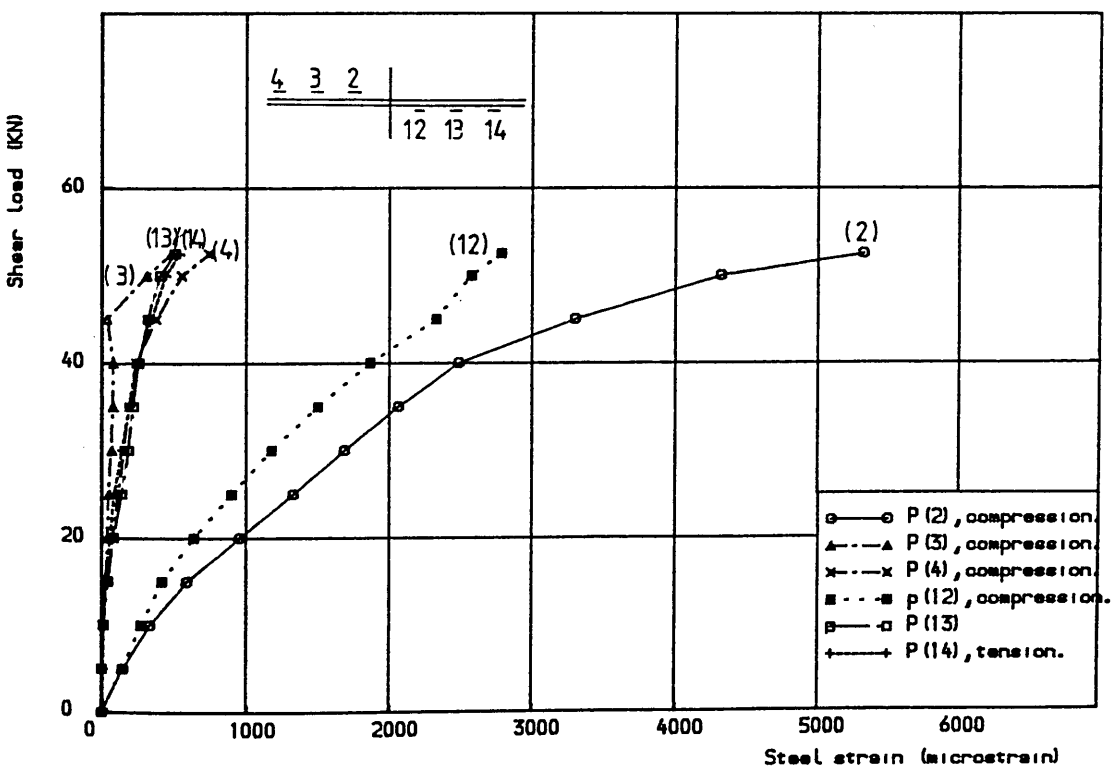

Figure (5.11) Shear load vs steel strain for specimen 2.2.1
(positions 2, 3, 4 - 12, 13, 14)

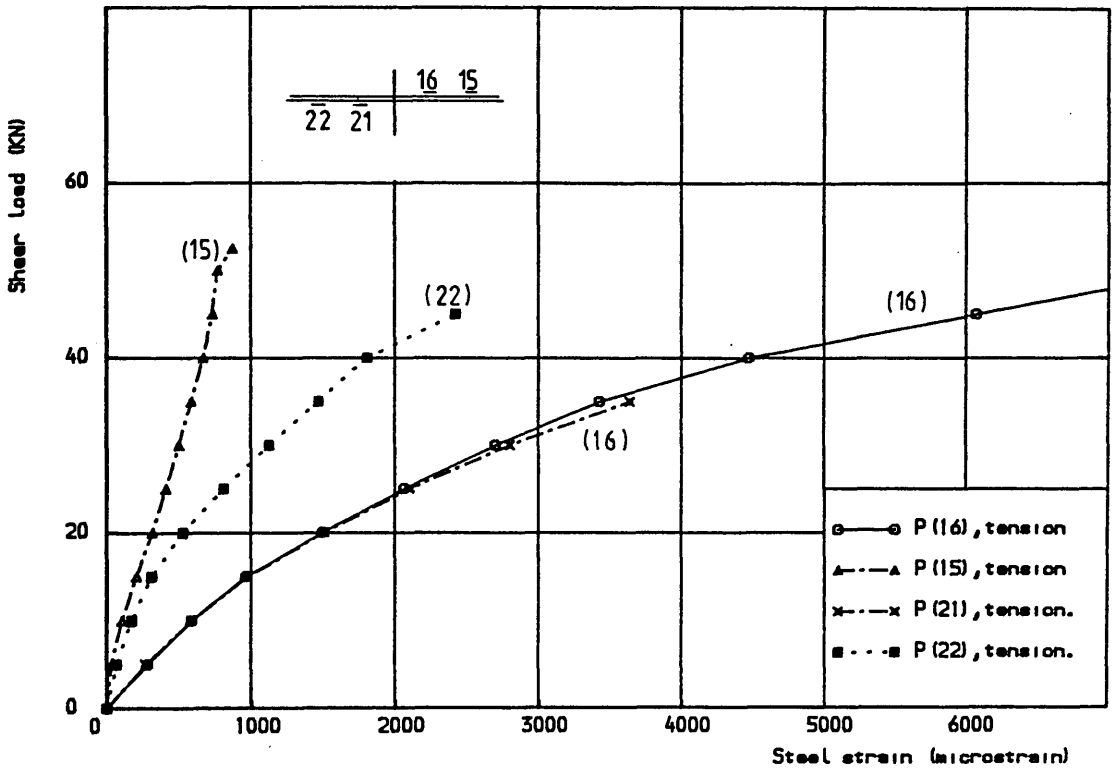

Figure (5.12) Shear load vs steel strain for specimen 2.2.1 (positions 16, 15 - 21, 22)

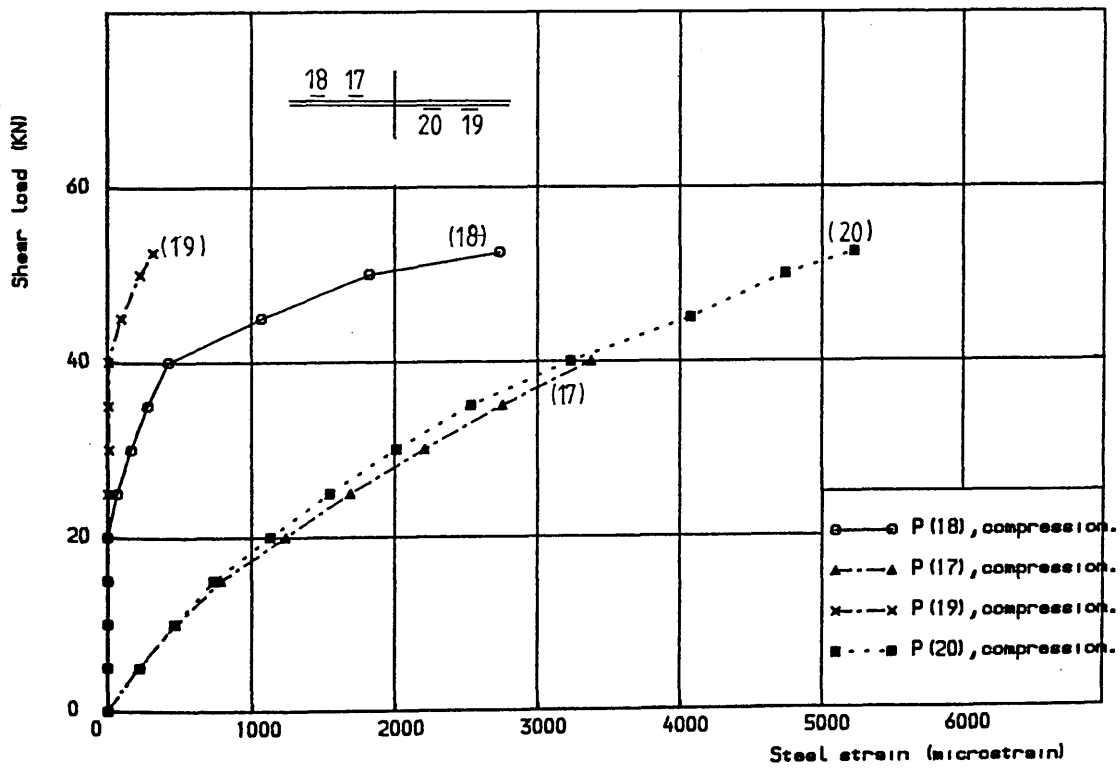

Figure (5.13) Shear load vs steel strain for specimen 2.2.1 (positions 18, 17 - 19, 20)

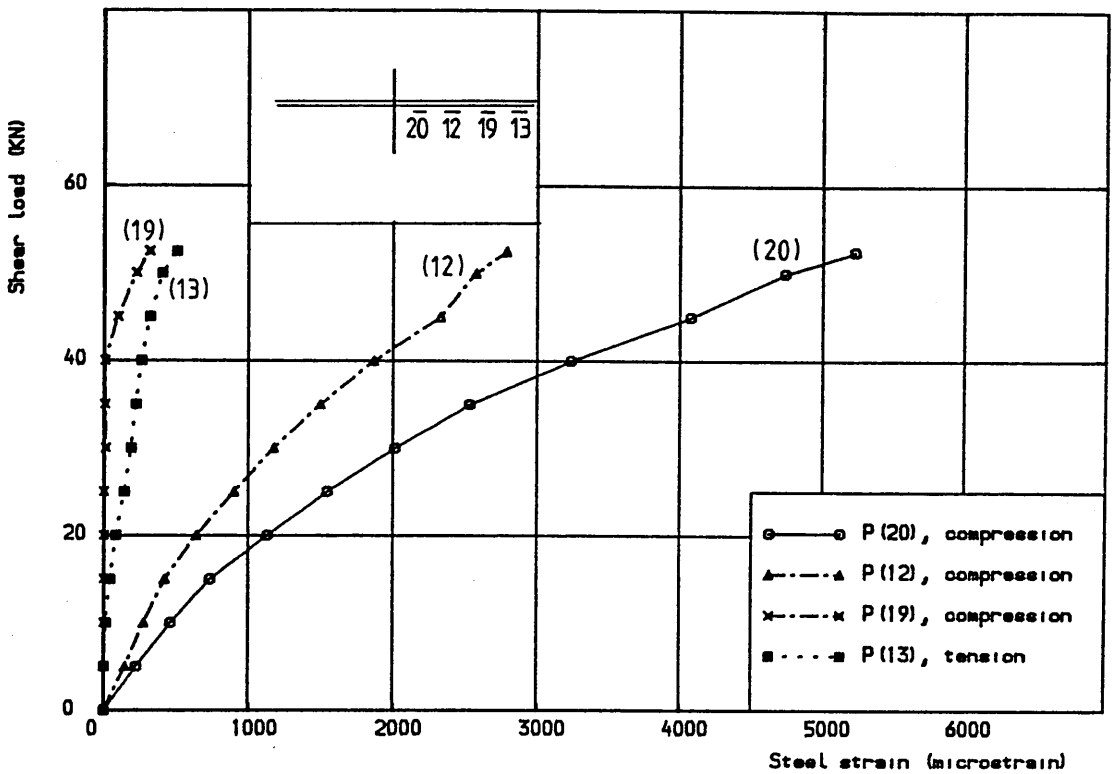

Figure (5.14) Shear load vs steel strain for specimen 2.2.1
(positions 20, 12, 19, 13)

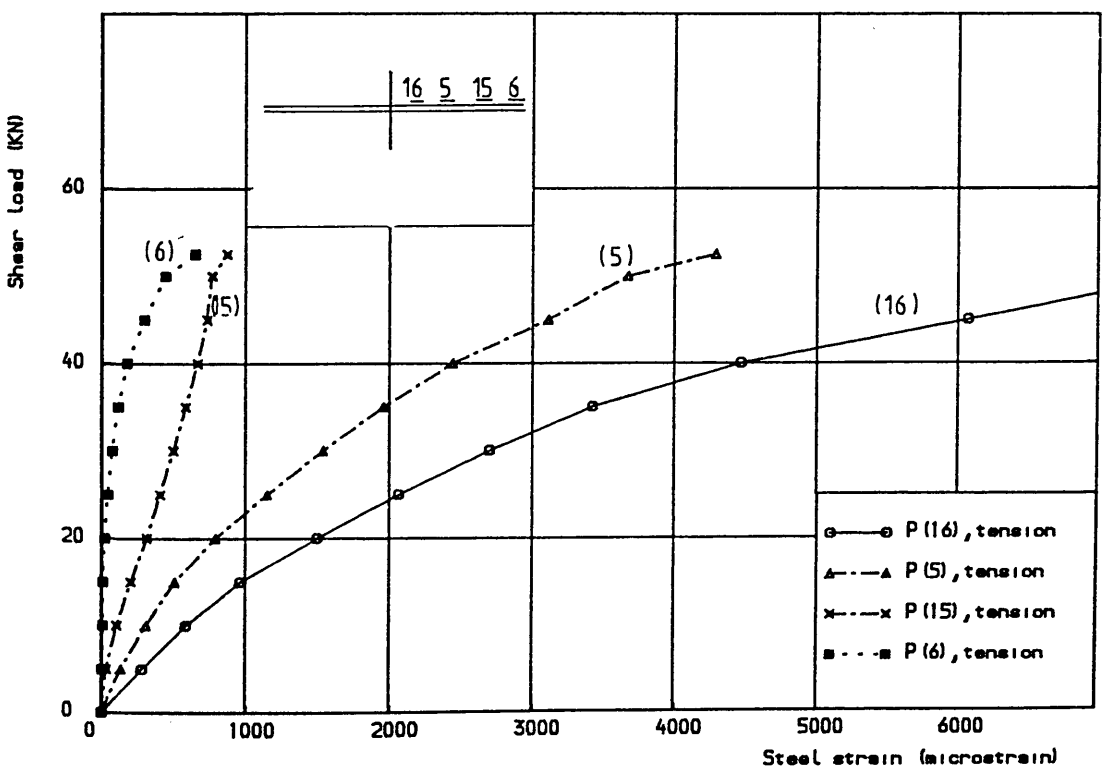

Figure (5.15) Shear load vs steel strain (microstrain)
(positions 16, 5, 15, 6)

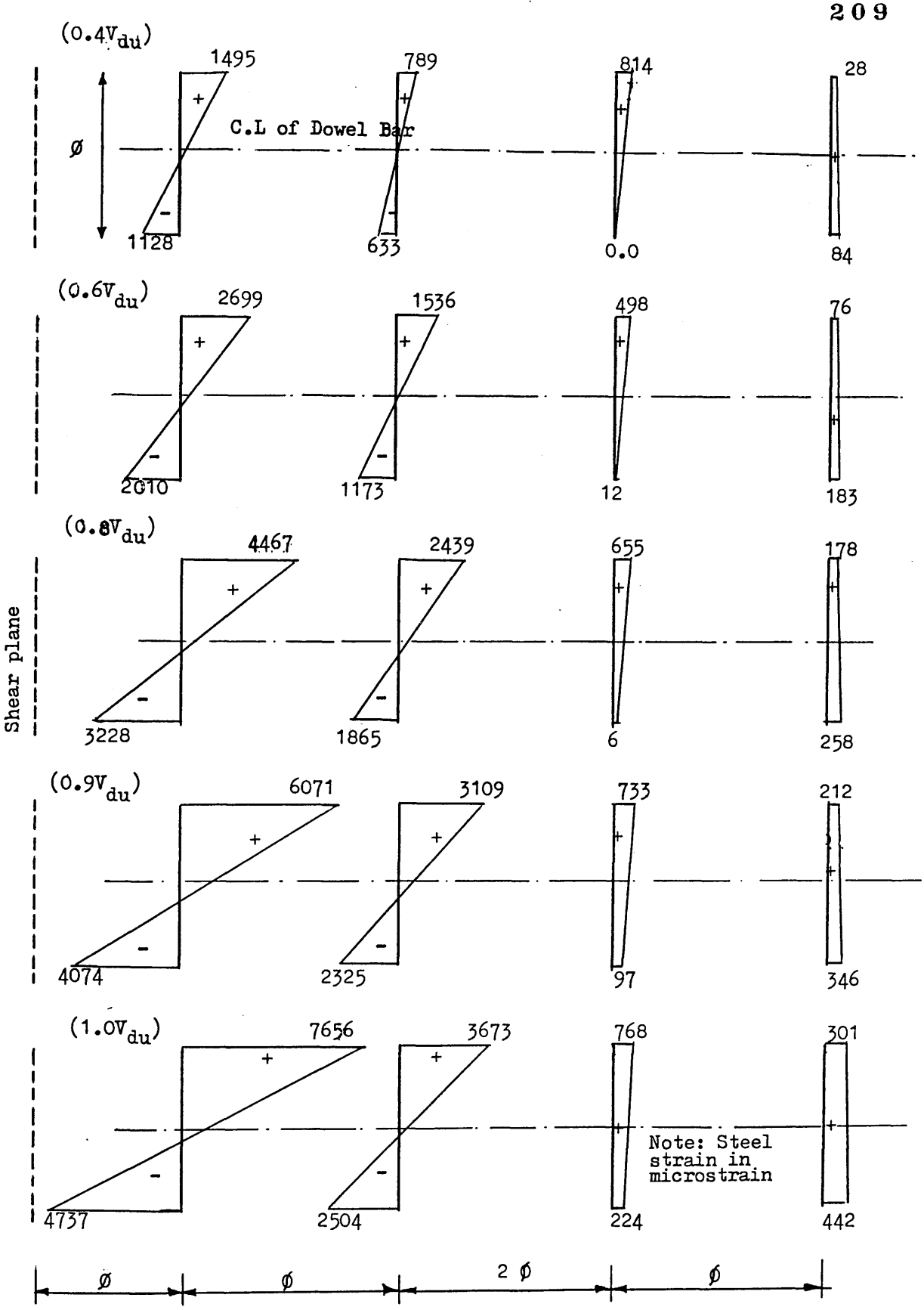

Figure(5.16) Strain distribution across a dowel bar along a distance 5Φ measured from the crack face at the centre line of specimen 2.2.1

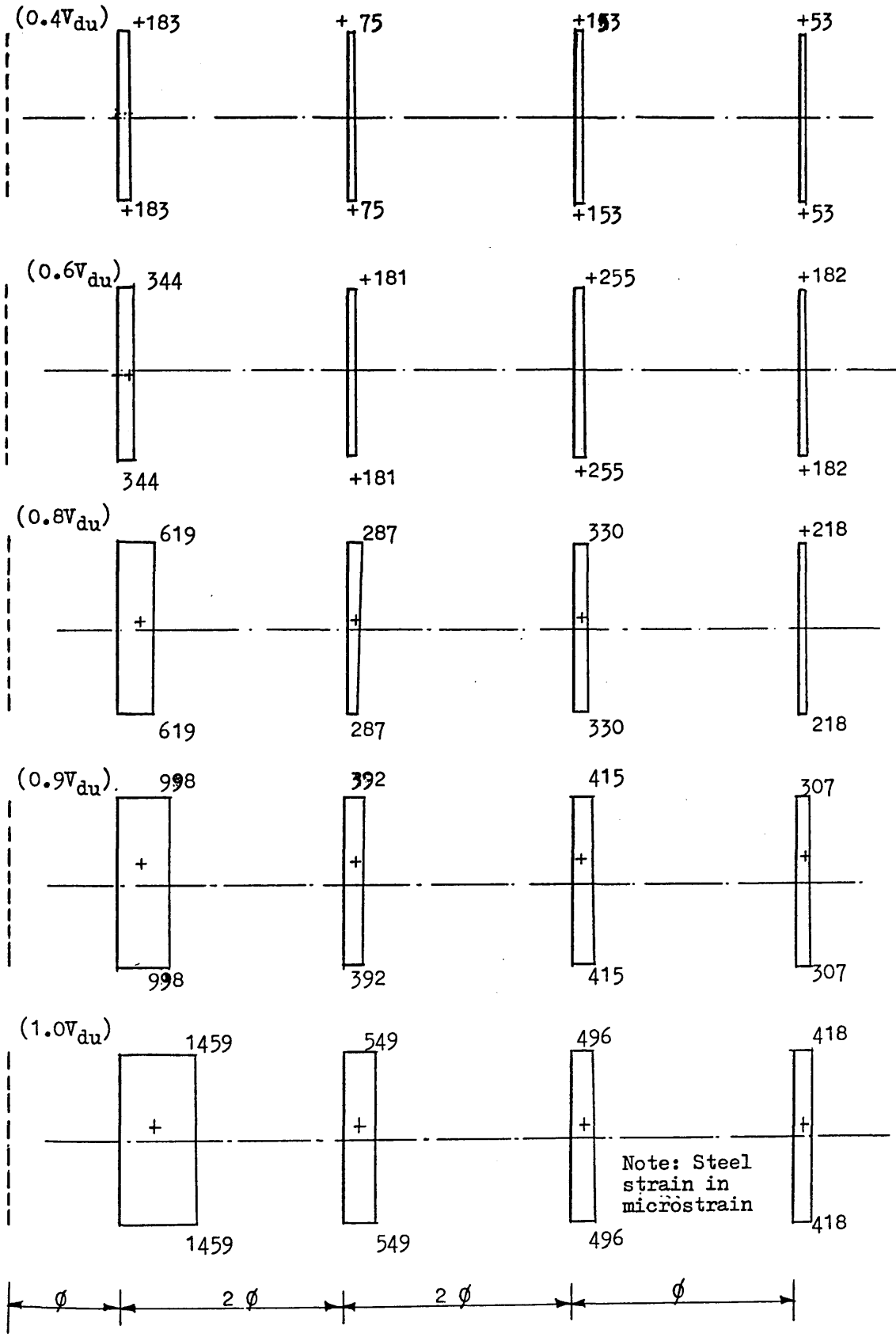

Figure(5.17) Distribution of resolved direct steel strain of specimen 2.2.1

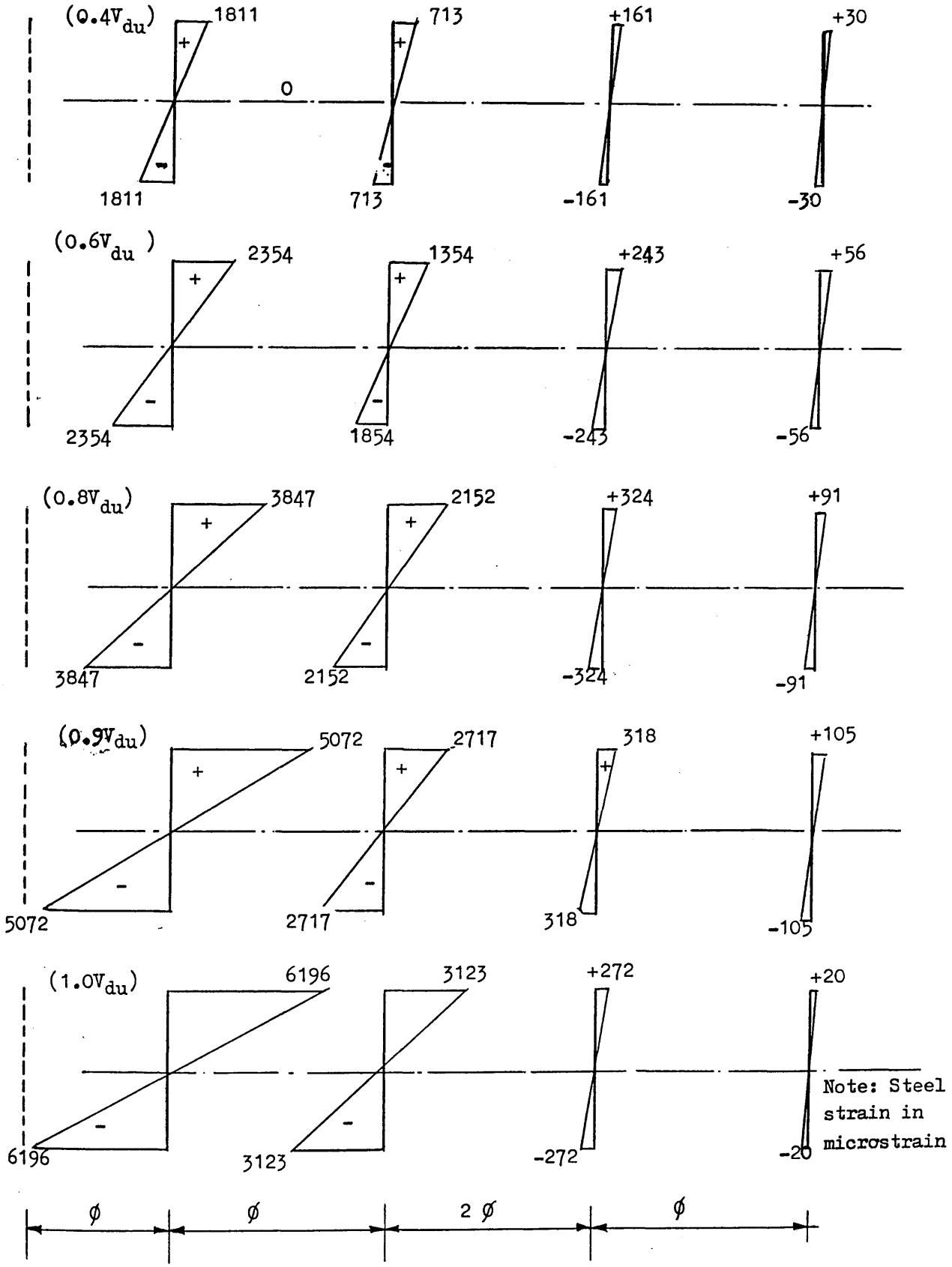

Figure(5.18) Distribution of the resolved flexural steel strain of specimen 2.2.1

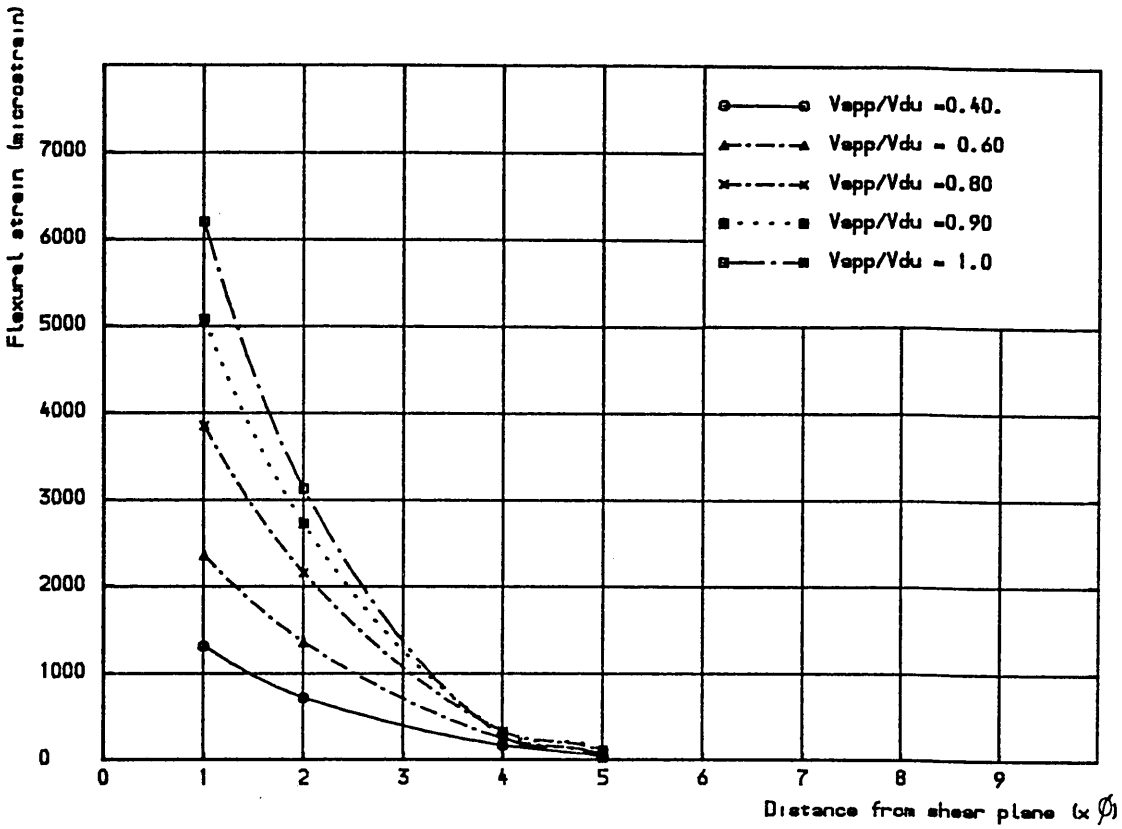

Figure (5.19) Distribution of flexural steel strain along a distance 5Ø for specimen 2.2.1

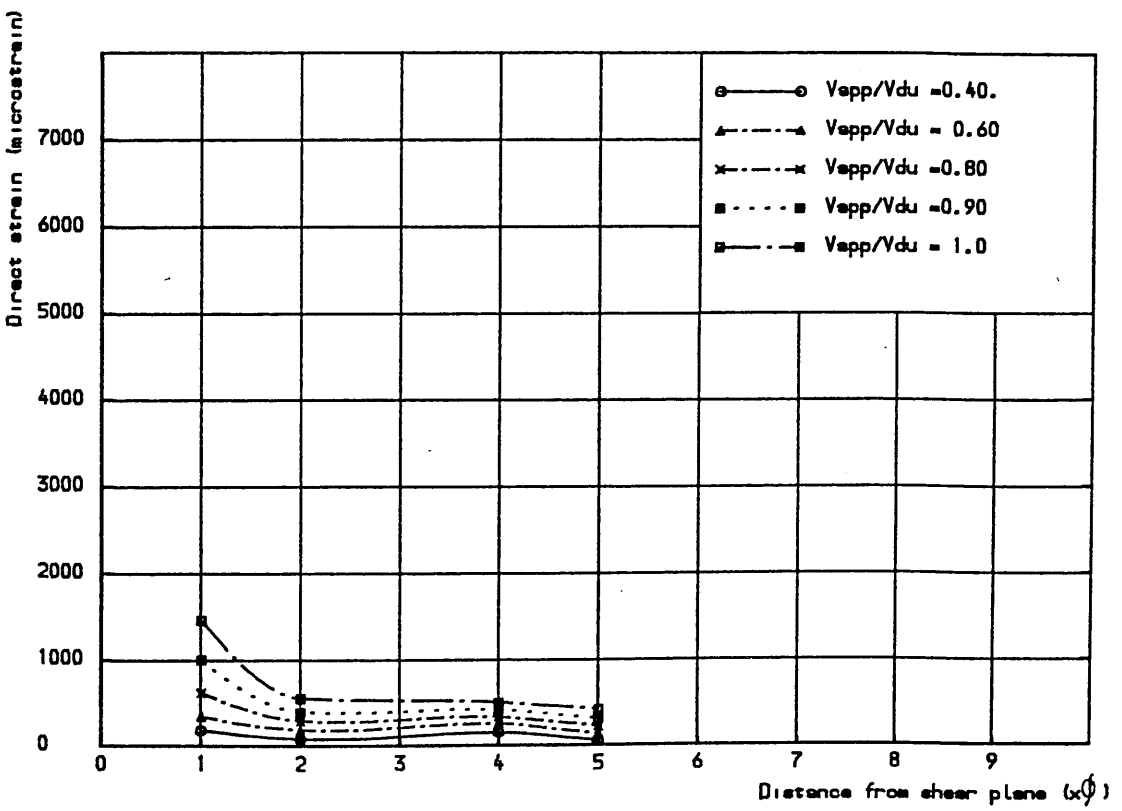

Figure (5.20) Distribution of direct steel strain along a distance 5 Ø for specimen 2.2.1

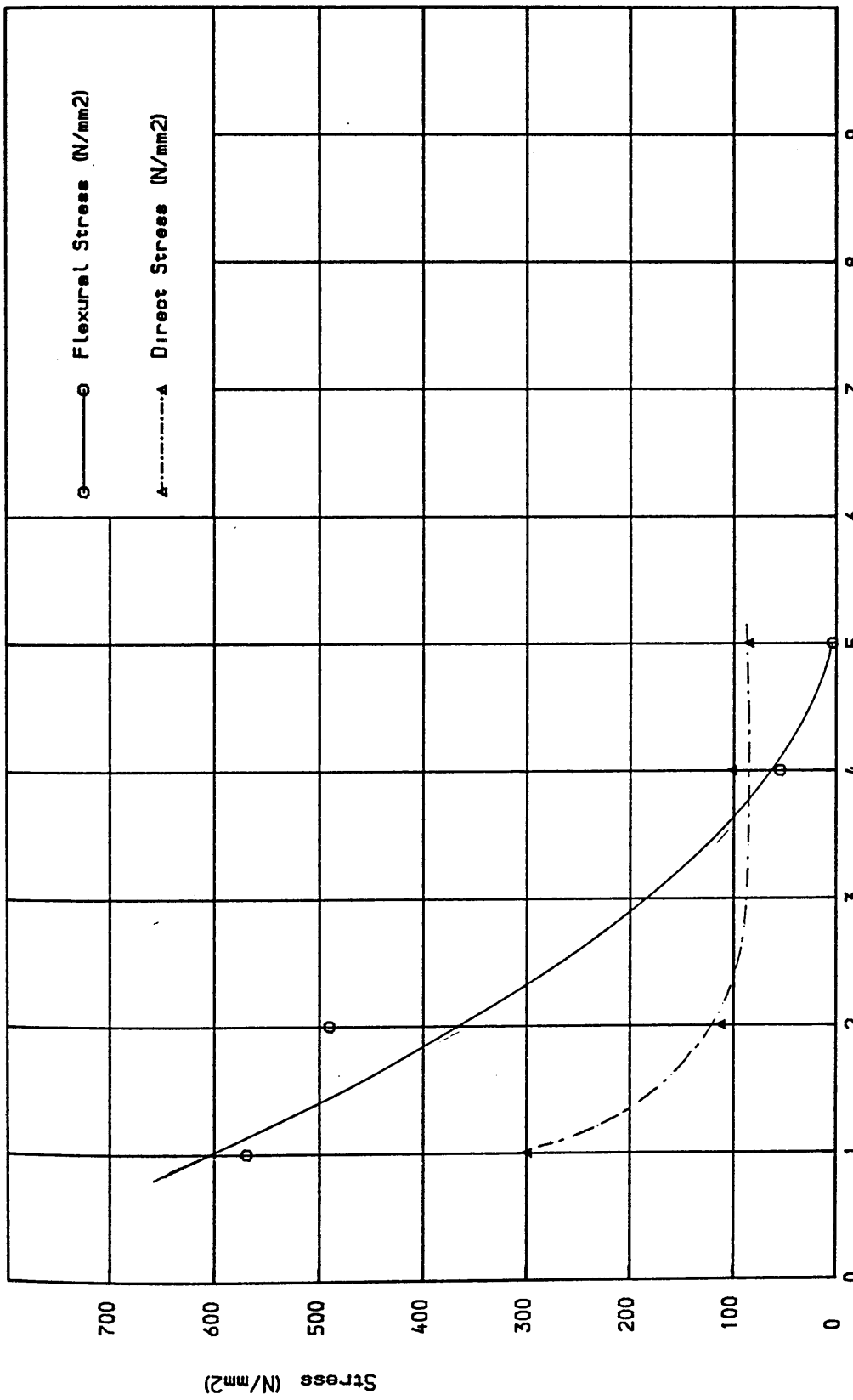

Figure (5.21) Distribution of flexural and direct stresses along a distance 5ϕ at ultimate load for specimen 2.2.1

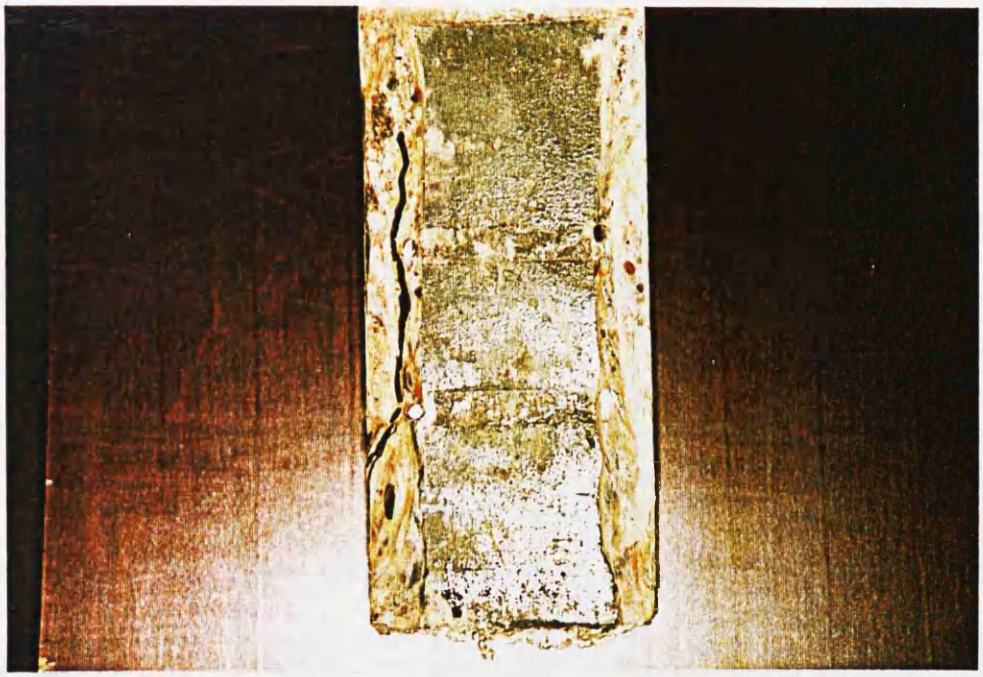

(a)

(b)

Figure(5.22) Crack pattern of the two faces of the shear plane, specimen 2.2.1

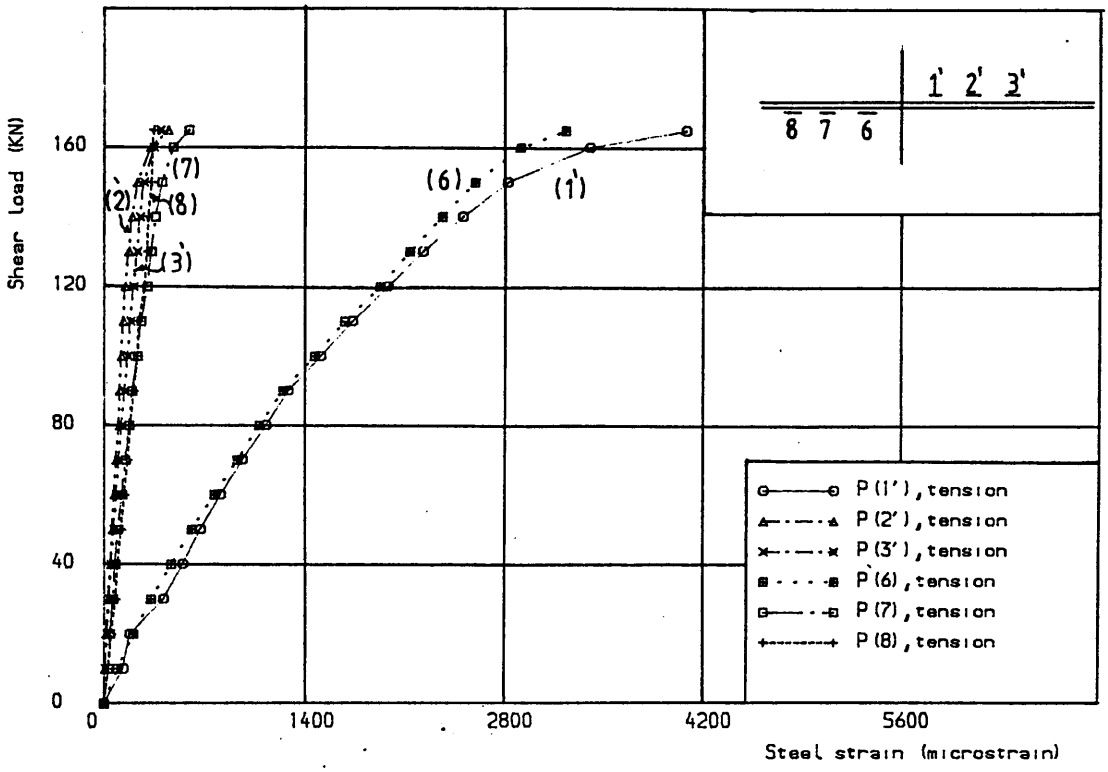

Figure (5.23) Shear load vs steel strain for specimen 2.2.2
(positions 1', 2', 3' - 6, 7, 8)

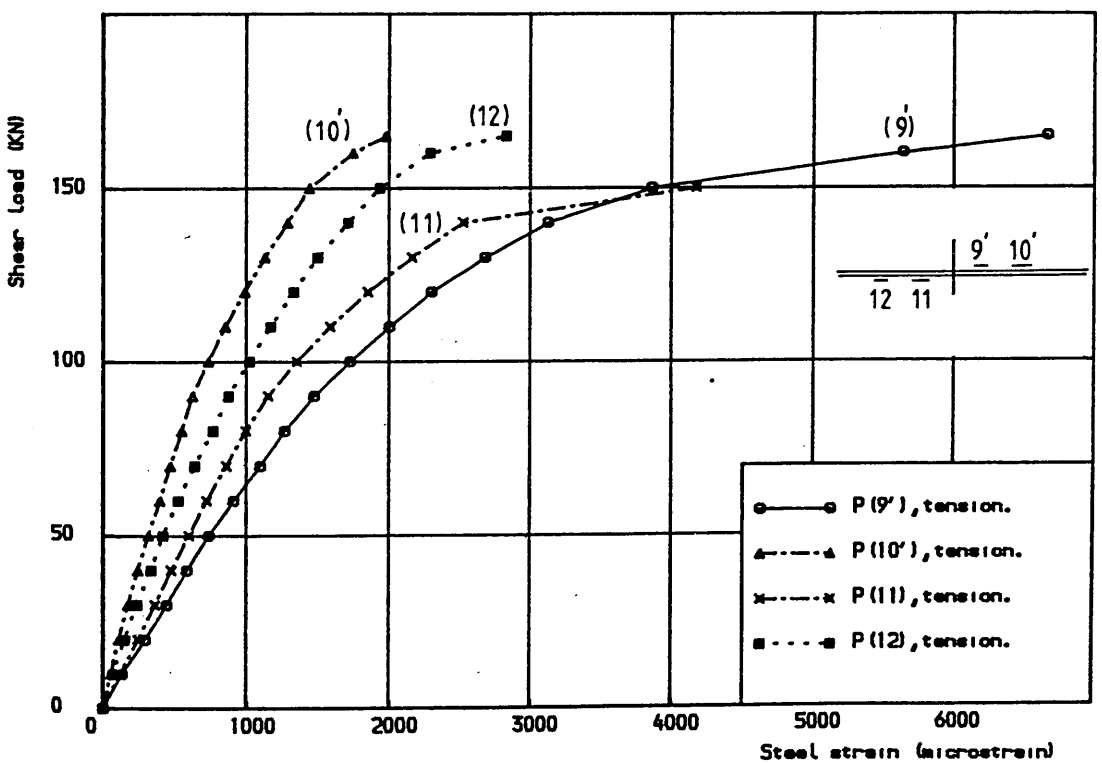

Figure (5.24) Shear load vs steel strain for specimen 2.2.2
(positions 9', 10' - 11', 12)

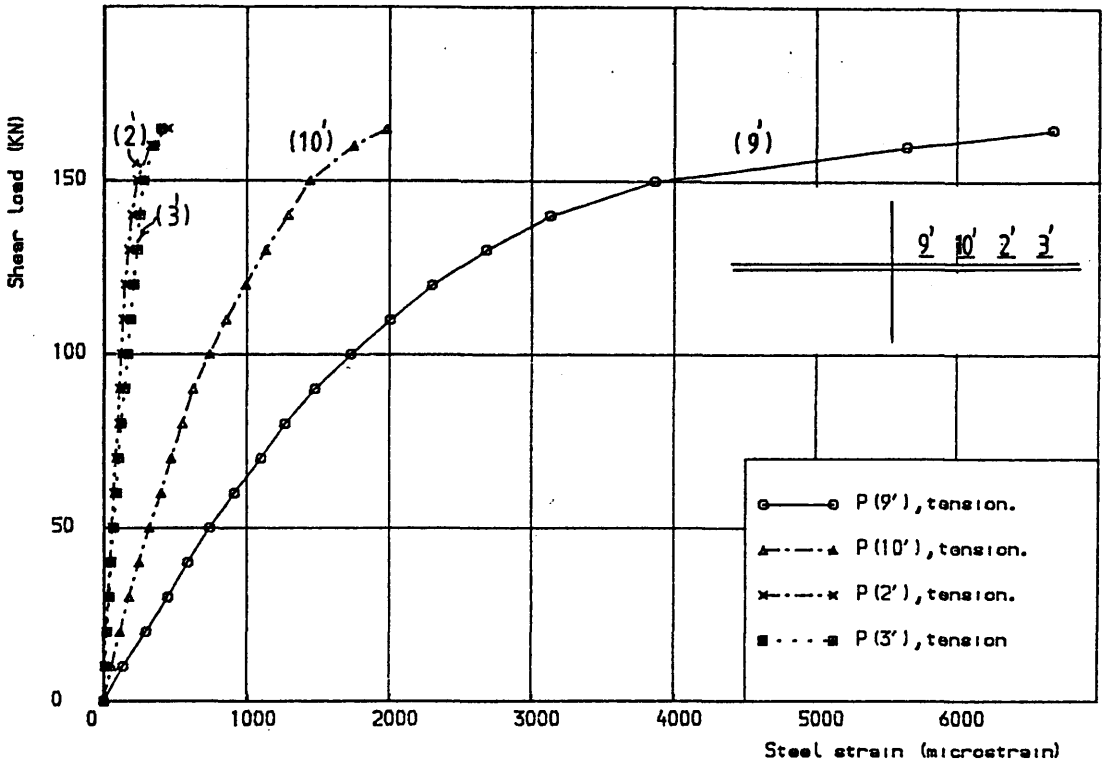

Figure (5.25 a) Shear load vs steel strain for specimen 2.2.2 (positions 9', 10', 2', 3')

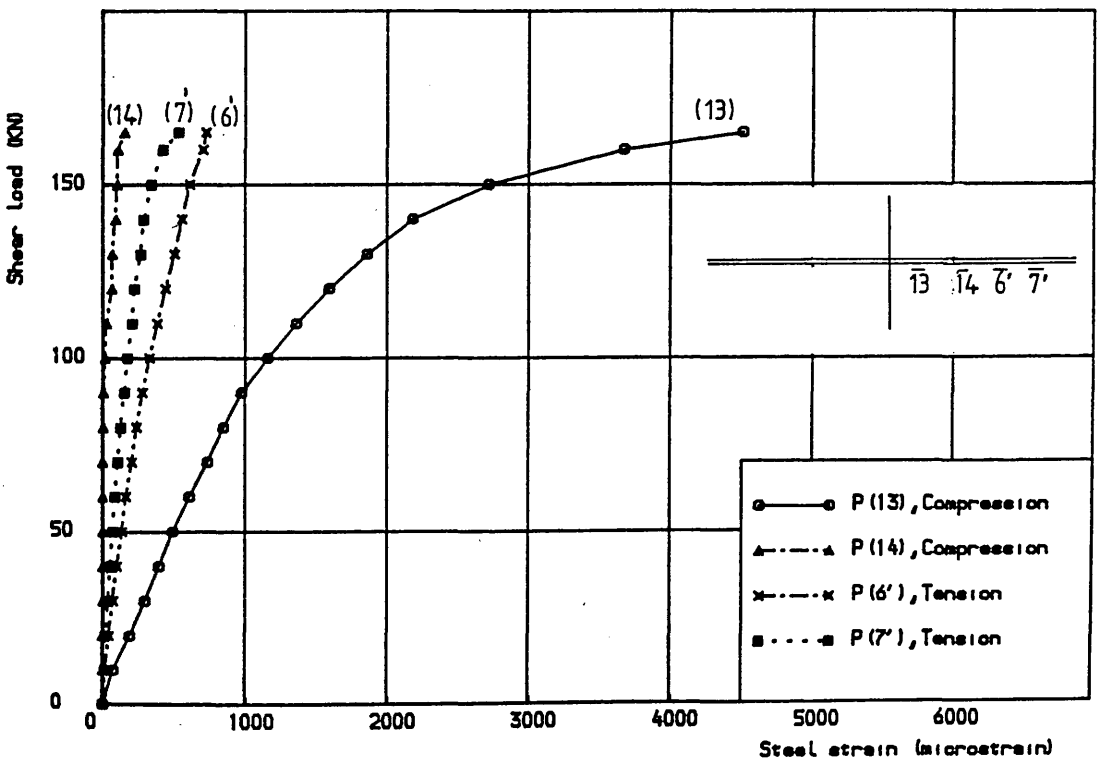

Figure (5.25 b) Shear load vs steel strain for specimen 2.2.2 (positions 13, 14 - 6', 7')

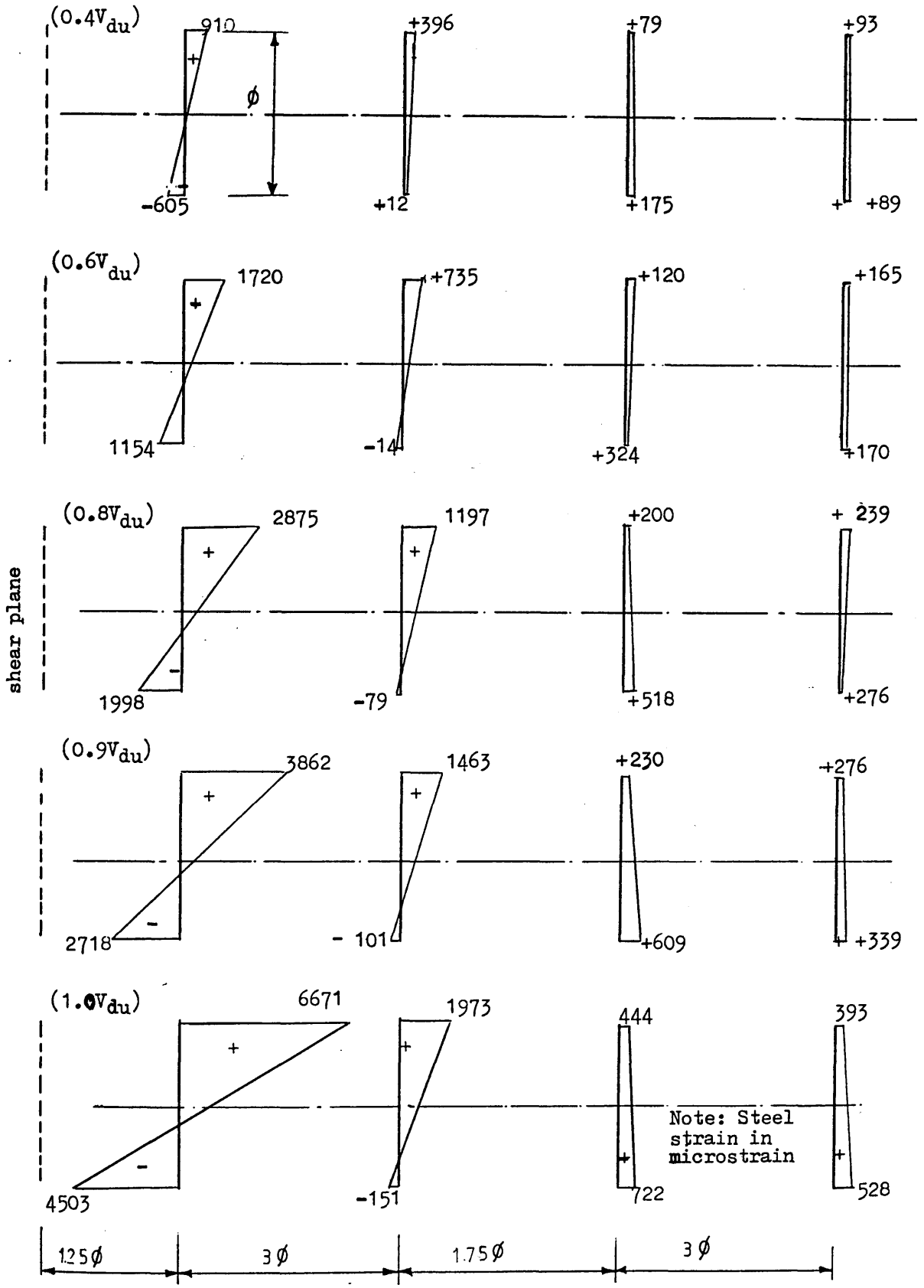

Figure(5.26) Strain distribution across a dowel bar and along a distance of 9Ø measured from the shear plane at the centre line of specm.2.2.1

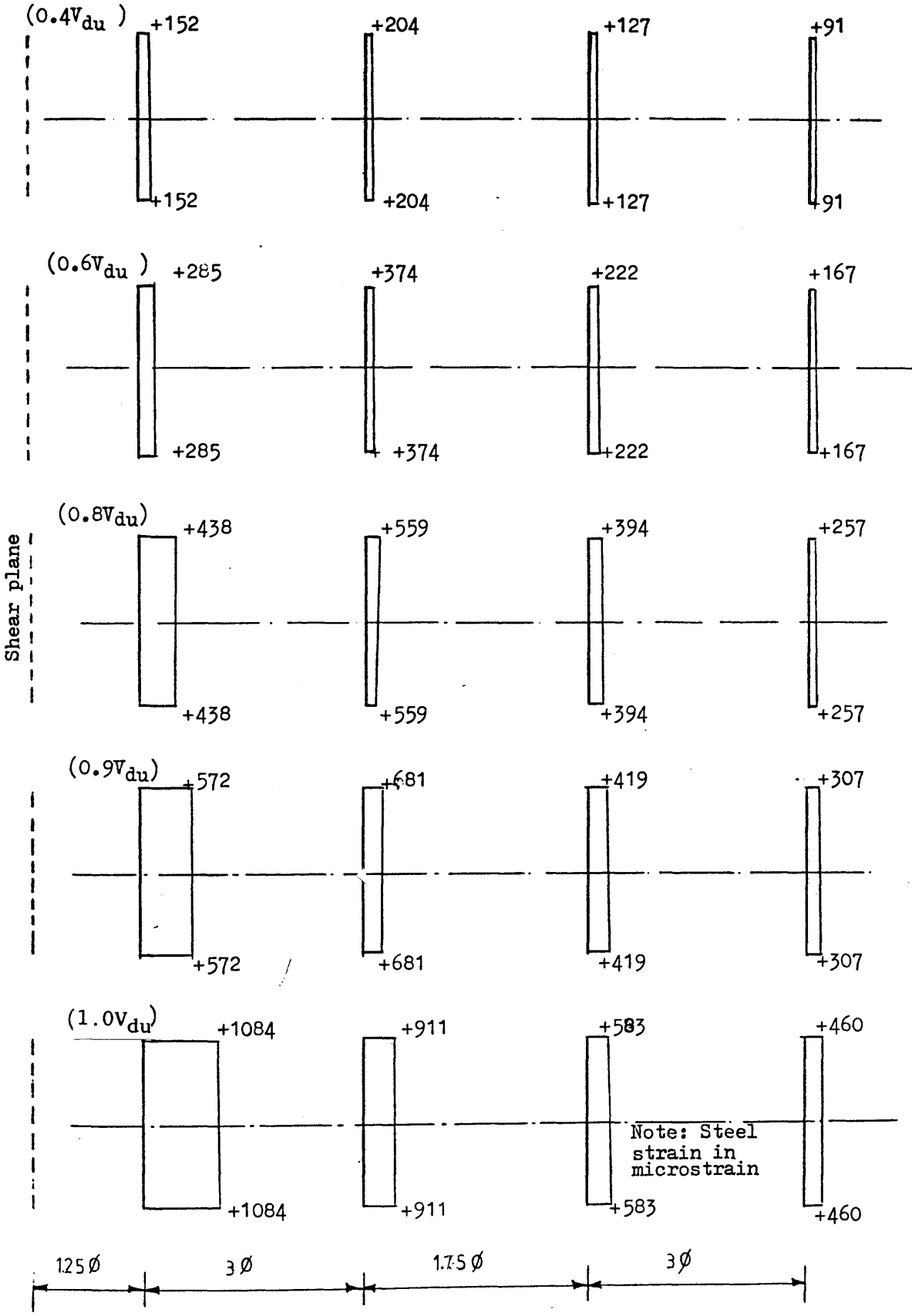

Figure(5.27) Distribution of resolved direct steel strain of specimen 2.2.2

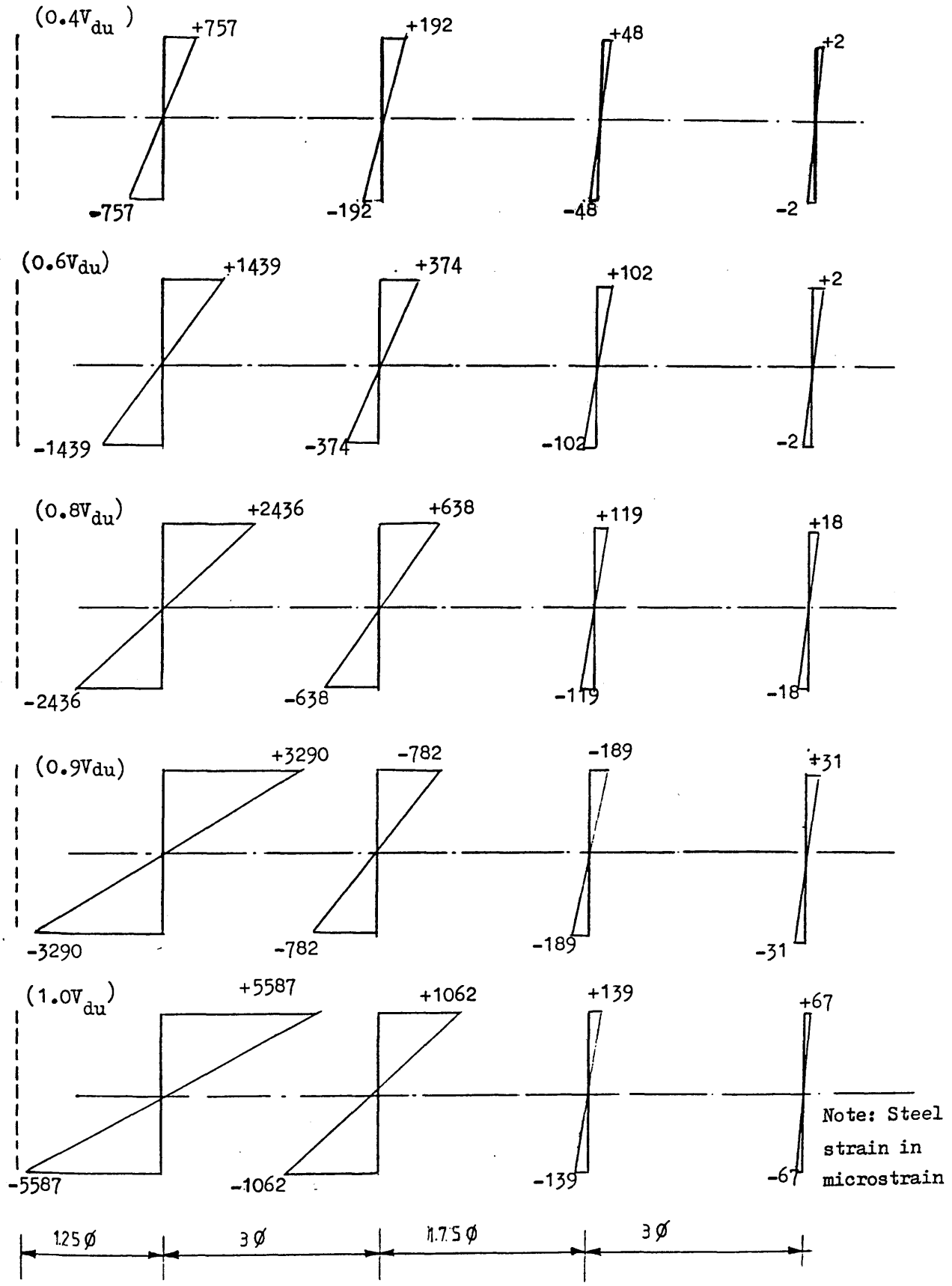

Figure(5.28) Distribution of the resolved flexural steel strain of specimen 2.2.2

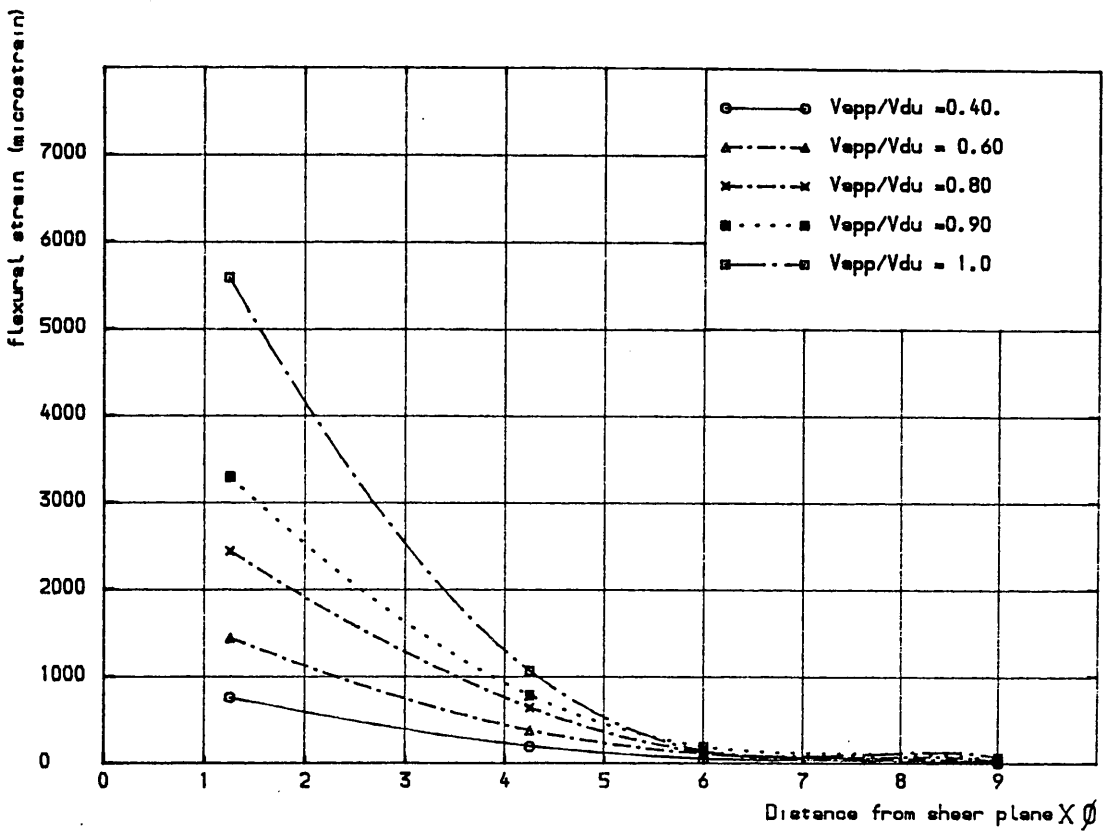

Figure(5.29) Distribution of flexural strain along a distance 9Φ from the shear plane for specimen 2.2.2

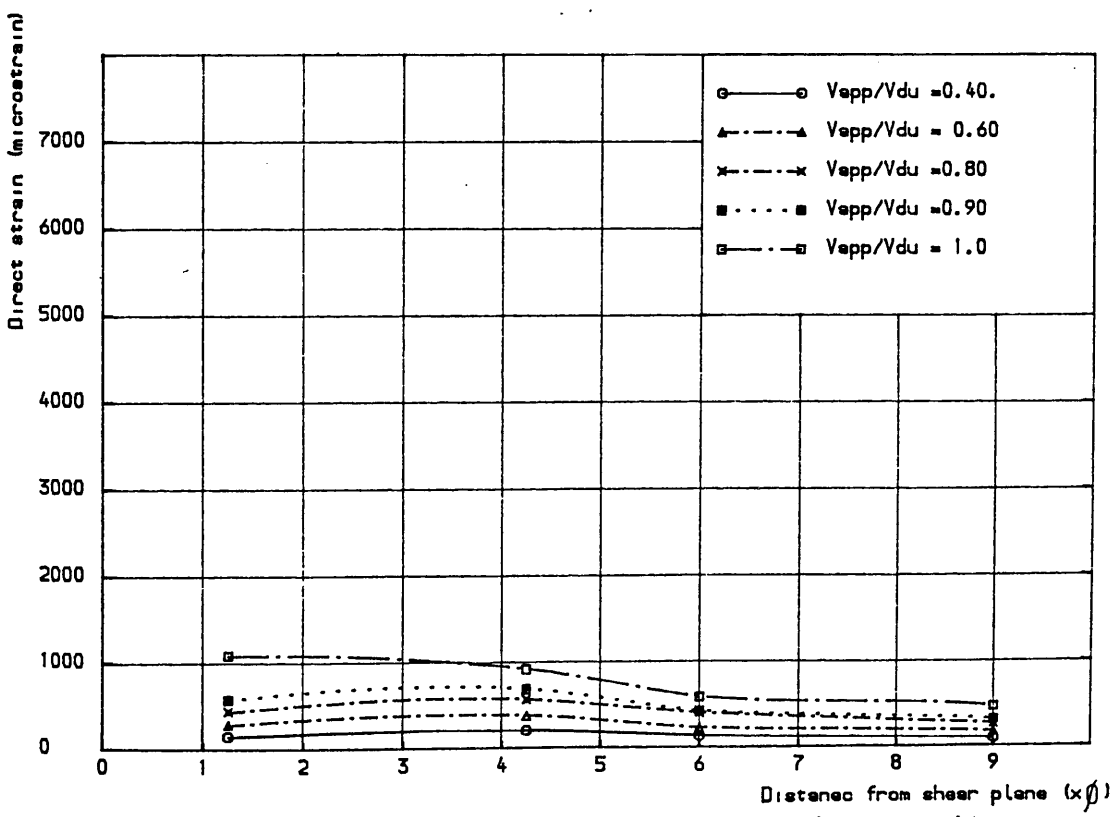

Figure(5.30) Distribution of direct strain along a distance 9Φ for specimen 2.2.2

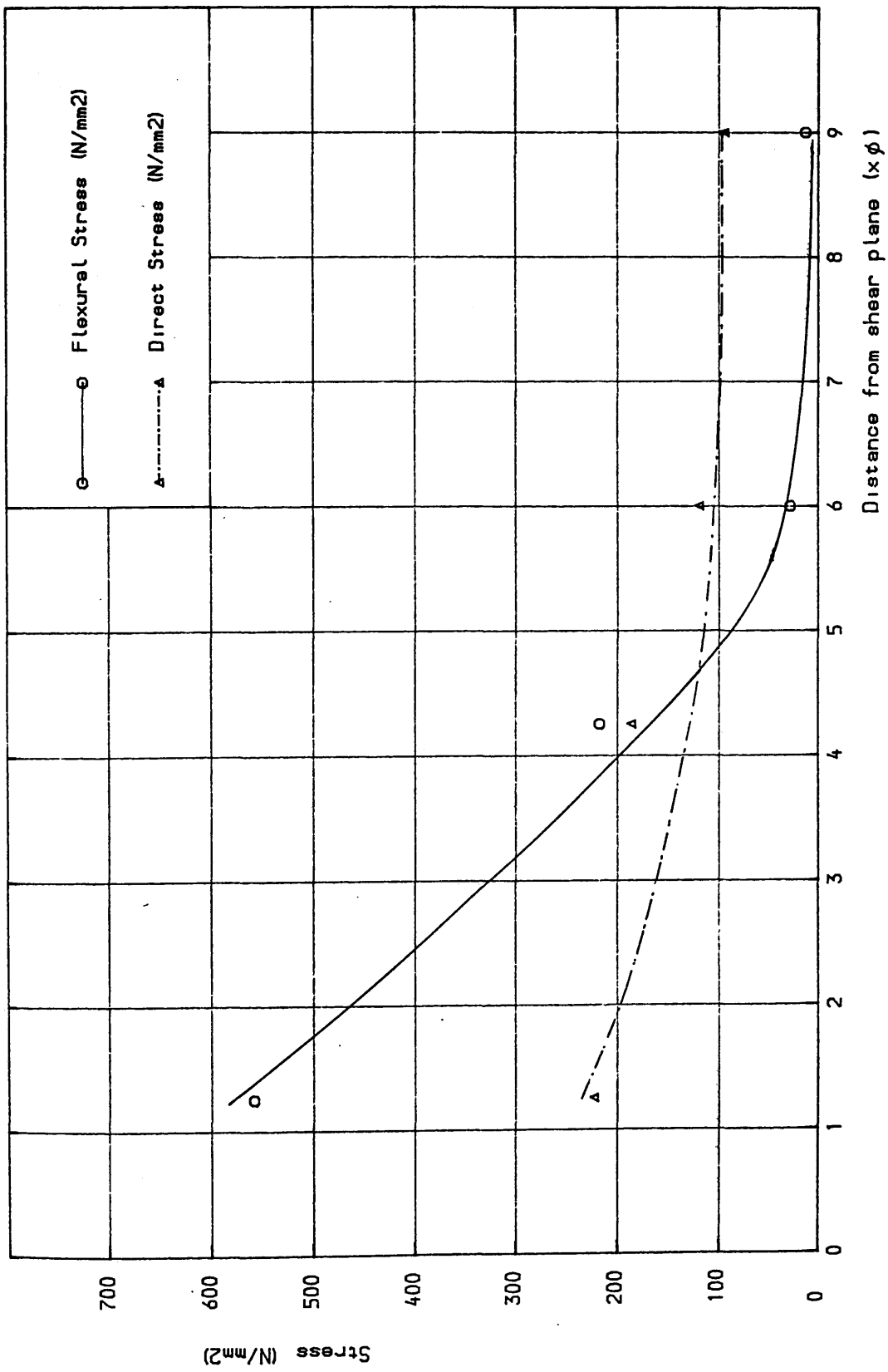

Figure (5.31) Distribution of flexural and direct steel stresses for specimen 2.2.2 at failure load

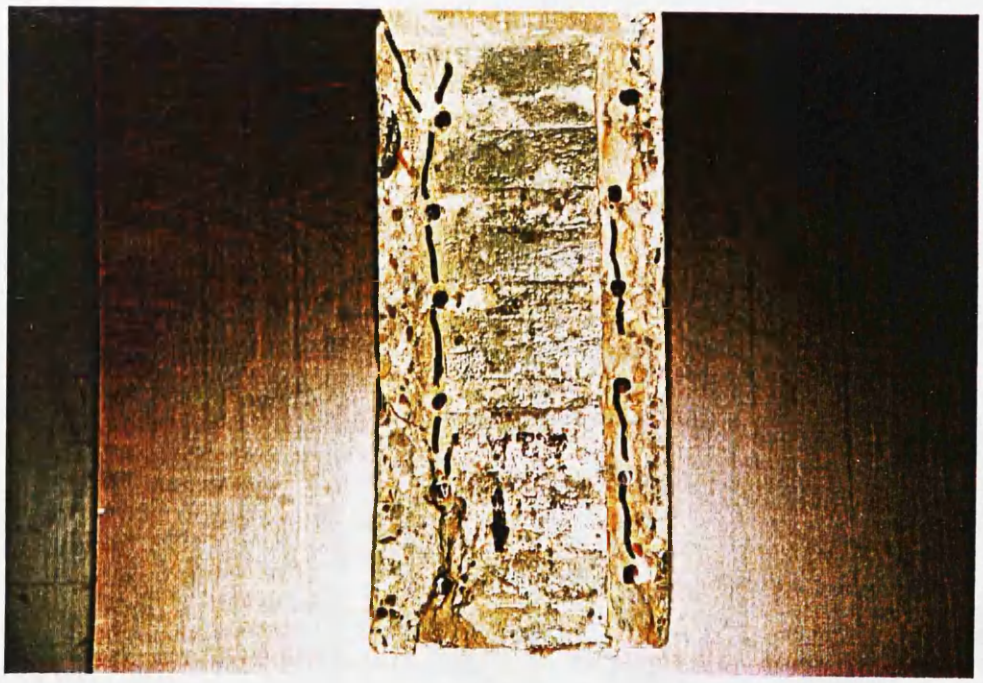

(a)

(b)

Figure(5.32) Crack pattern of the two faces of the shear plane, specimen 2.2.2

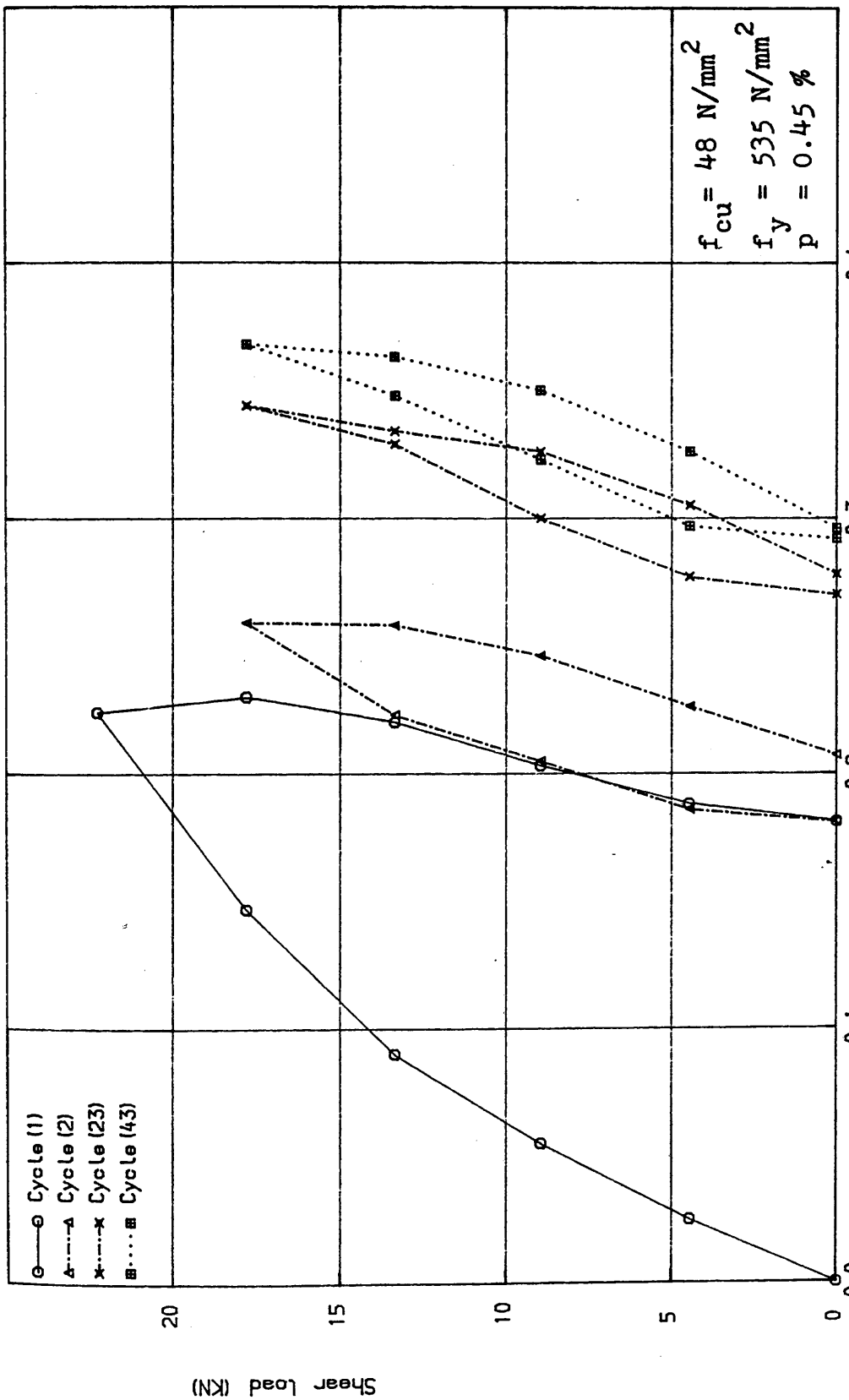

Figure (5.33 a) Shear load vs shear displacement for specimen 2.1.2A

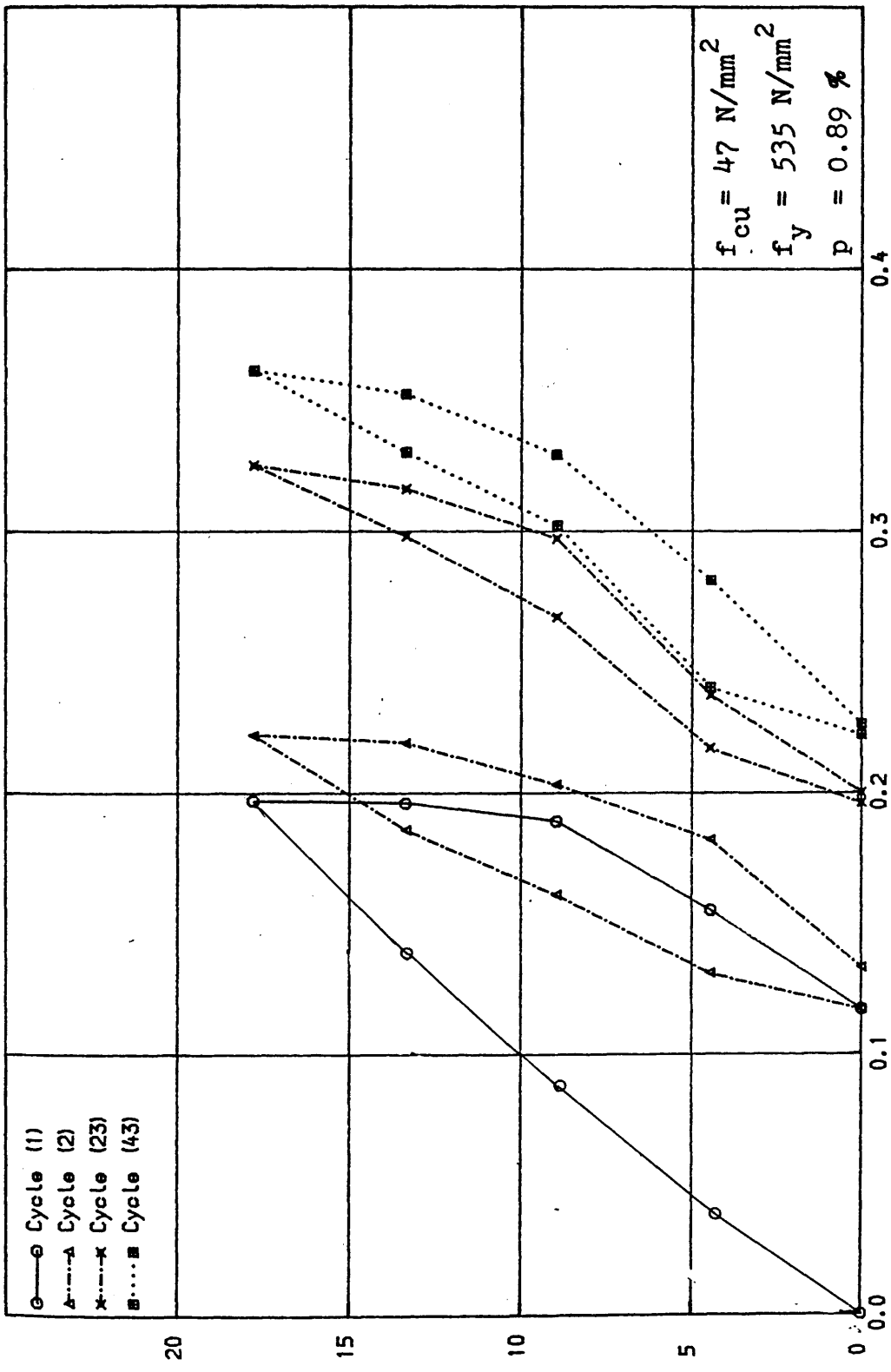

Figure (5.33 b) Shear load vs shear displacement for specimen 2.1.3A

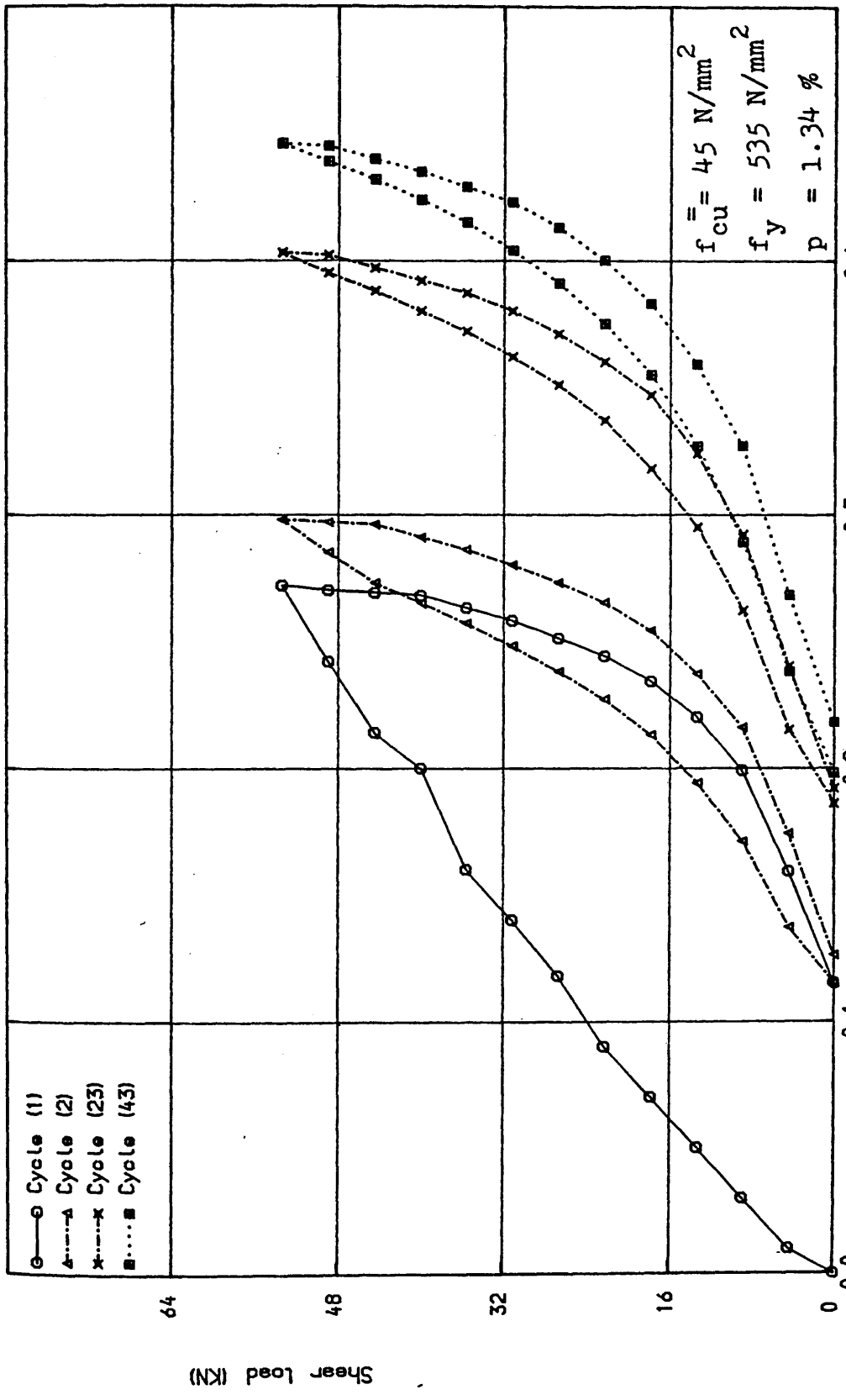

Figure (5.33 c) Shear load vs shear displacement for specimen 2.1.4A

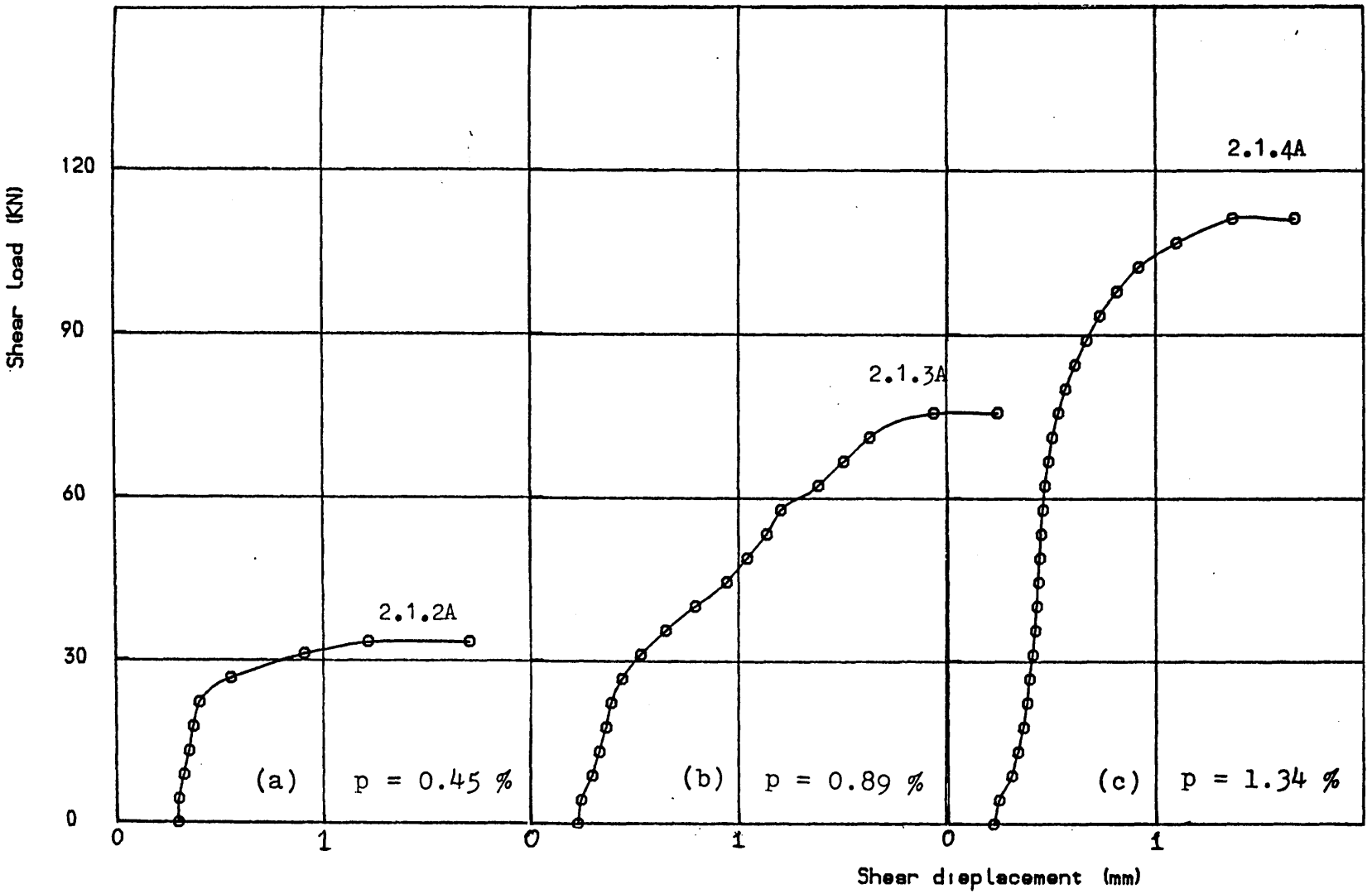

Figure (5.34) Shear load vs shear displacement for specimens of group 1 series 2 tested under repeated loading at (last cycle)

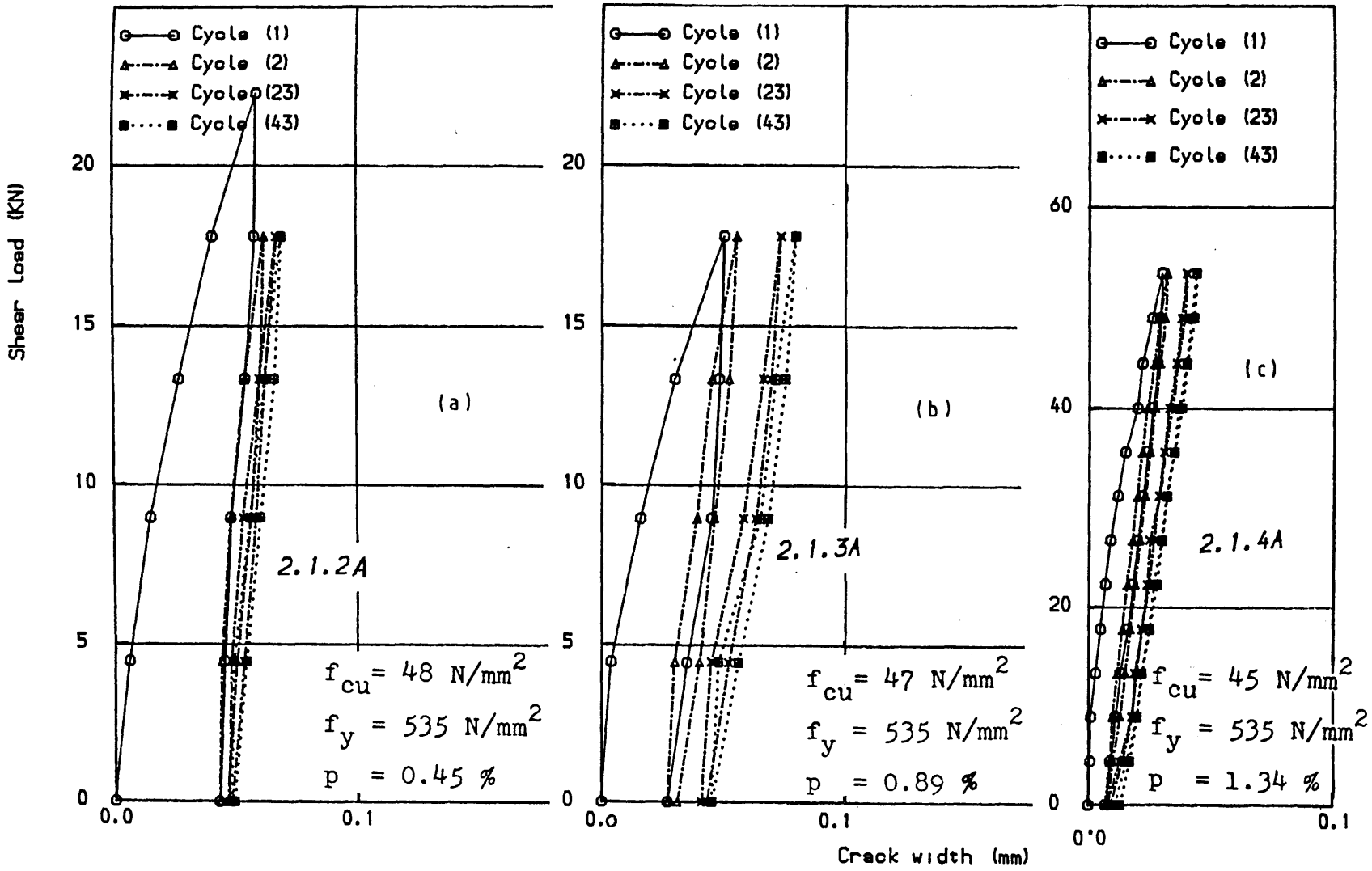

Figure (5.35) Shear load vs crack width for specimens of group 1, series 2 tested under repeated loading

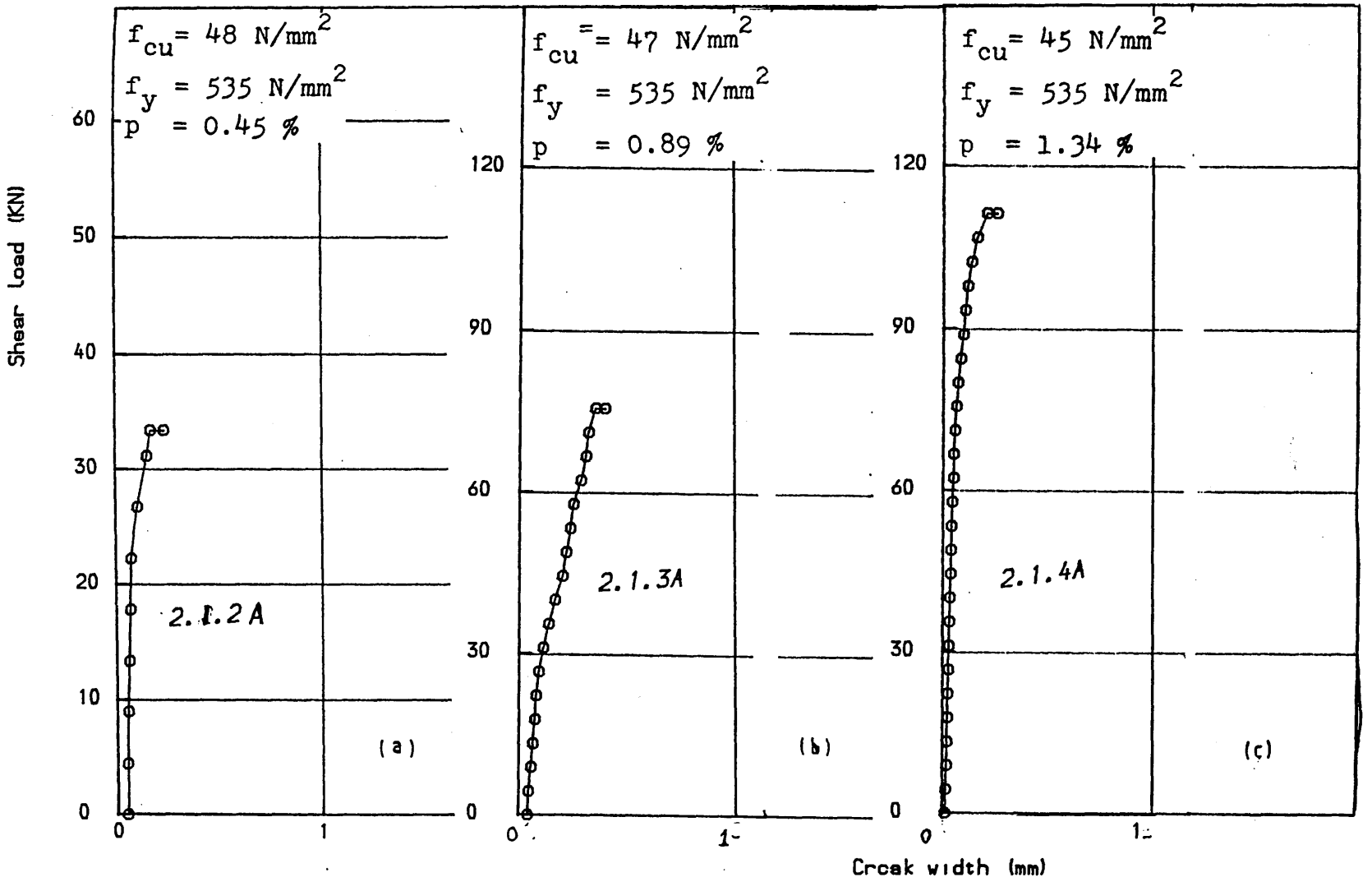

Figure (5.36) Shear load vs crack width for specimens of groups 1, series 2 tested under repeated loading (last cycle)

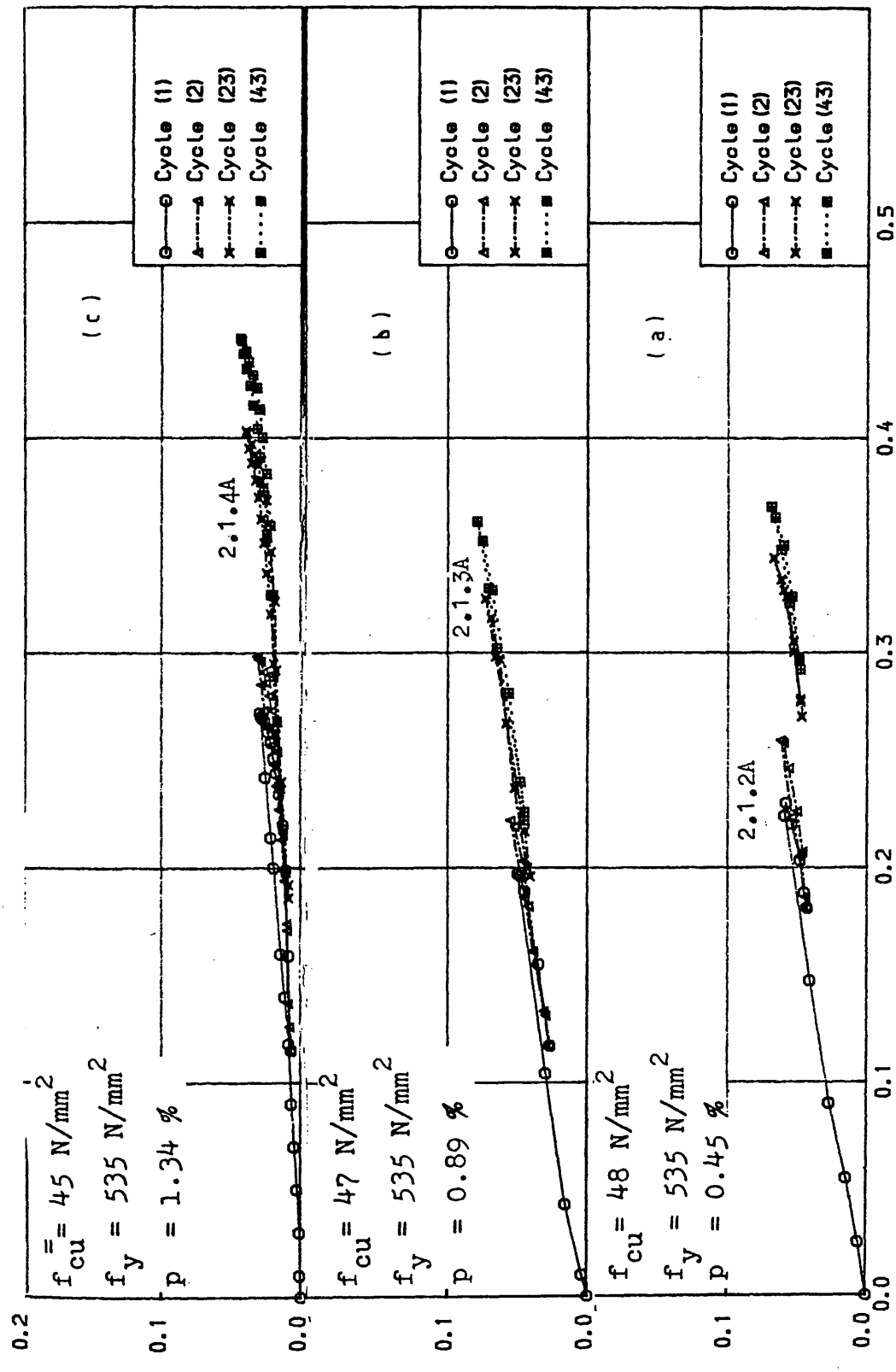

Figure (5.37) Crack width vs shear displacement for specimens of groups 1, series 2 tested under repeated loading (last cycle)

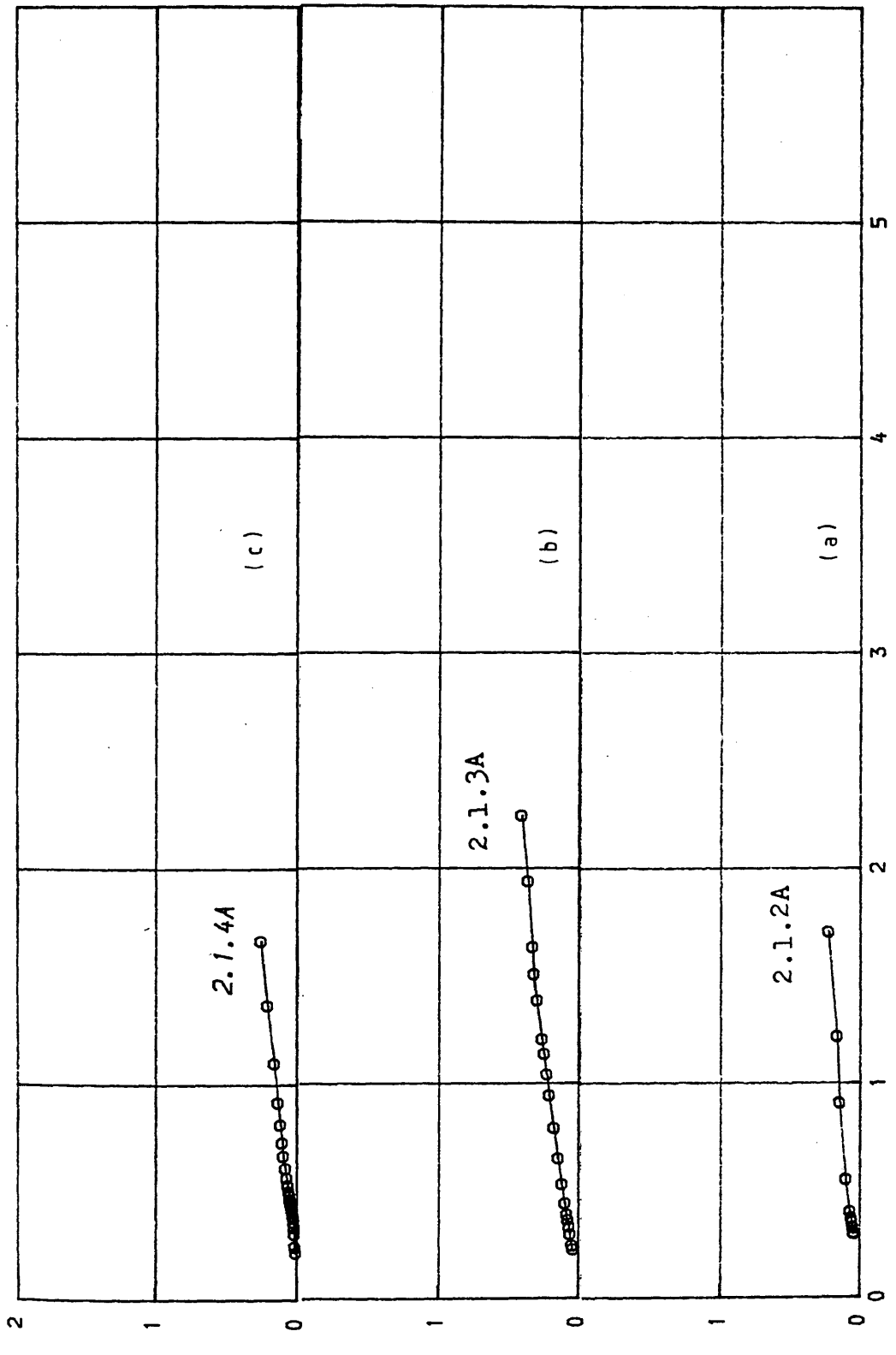

Figure (5.38) Crack width vs shear displacement for specimens of groups 1, series 2 tested under repeated loading (last cycle)

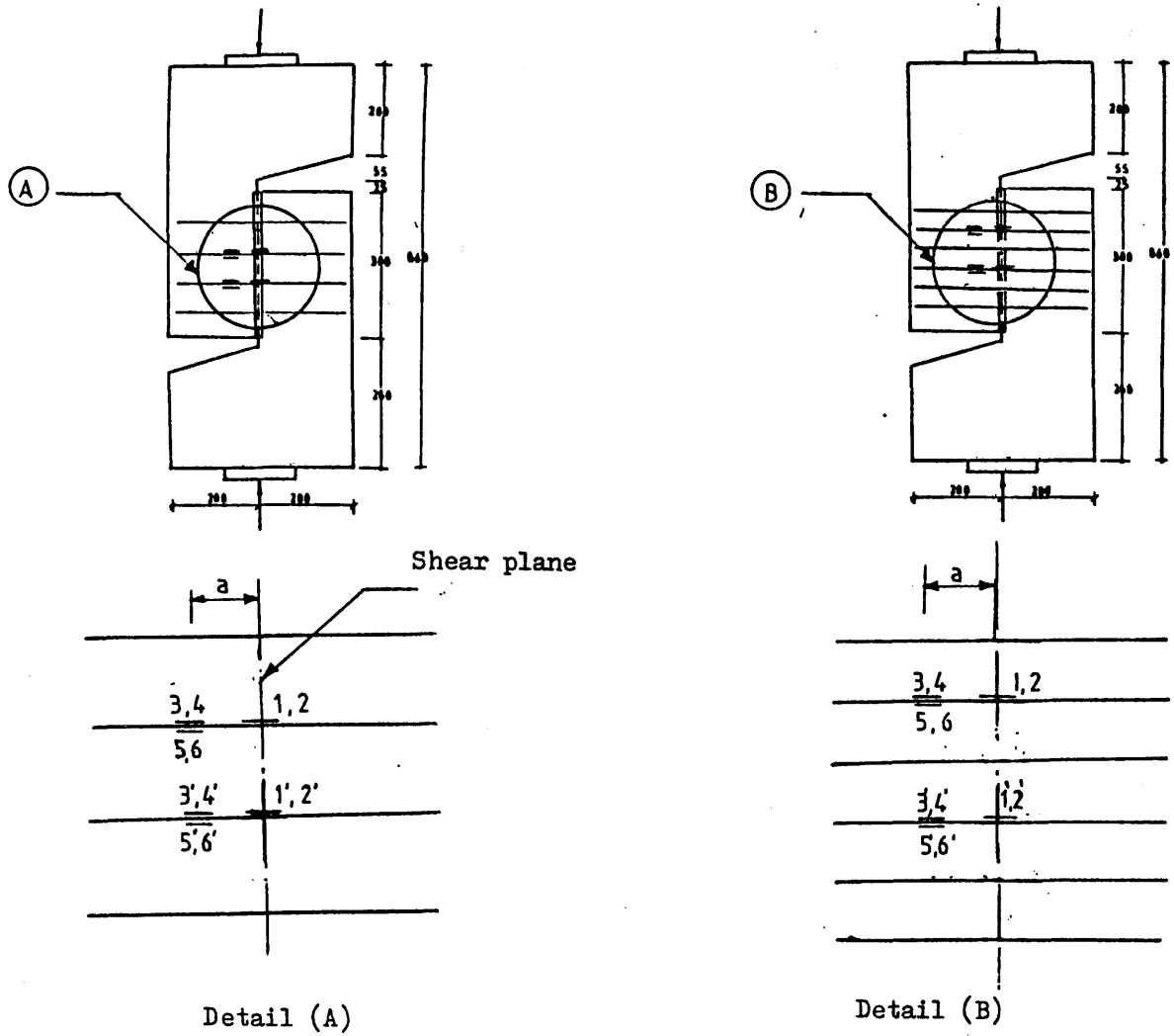

Figure (5.39) Position of strain gauges for group 1 of series 2 under repeated loading

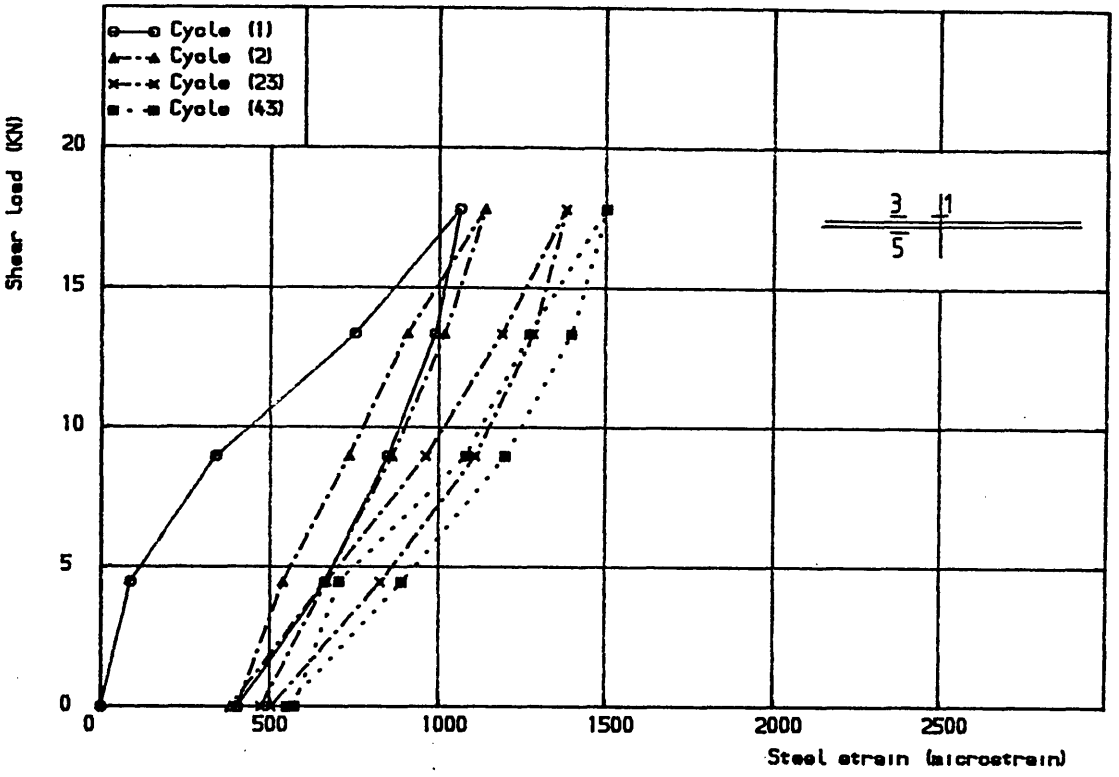

Figure (5.40 a) Shear load vs steel strain for specimen 2.1.3A at position (3)

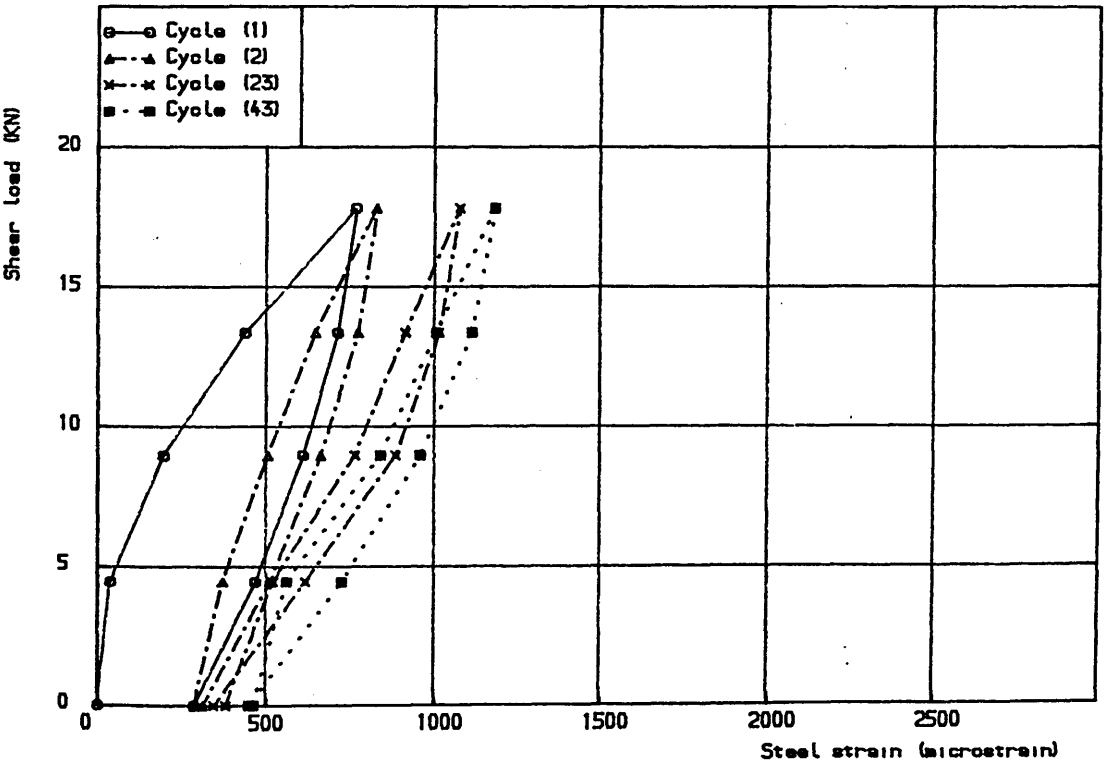

Figure (5.40 b) Shear load vs steel strain for specimen 2.1.3A at position (5)

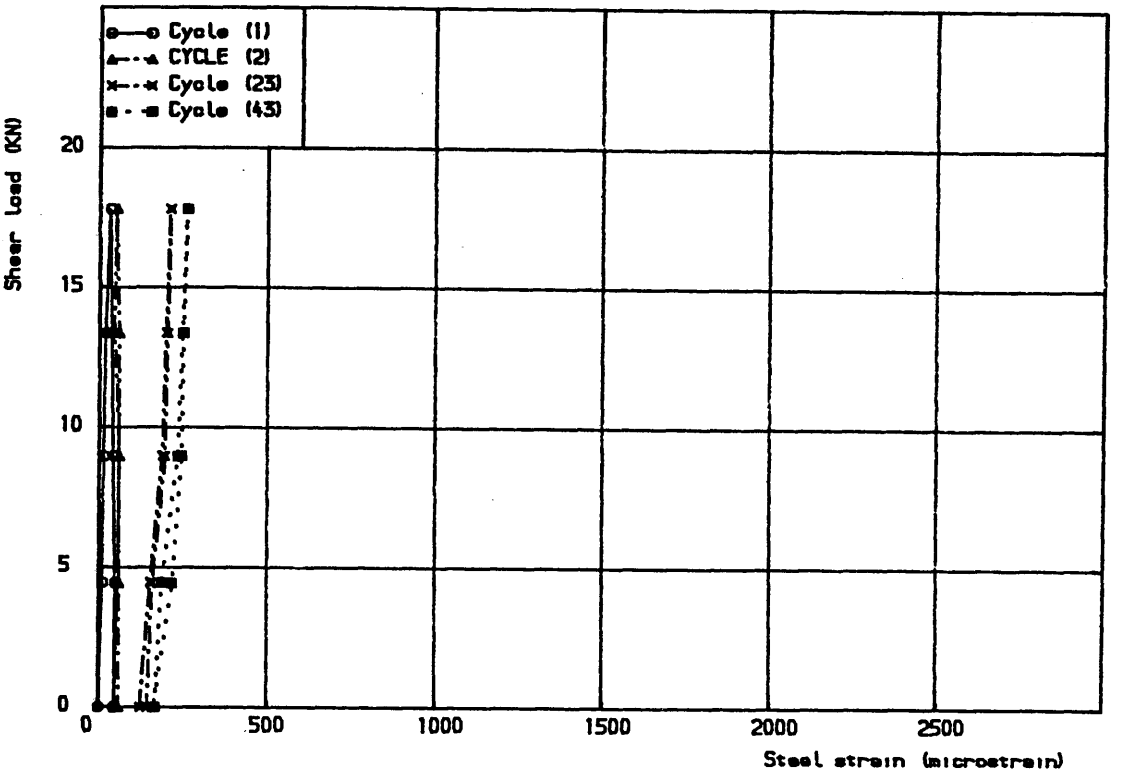

Figure (5.40 c) Shear load vs steel strain for specimen 2.1.3A at position (1)

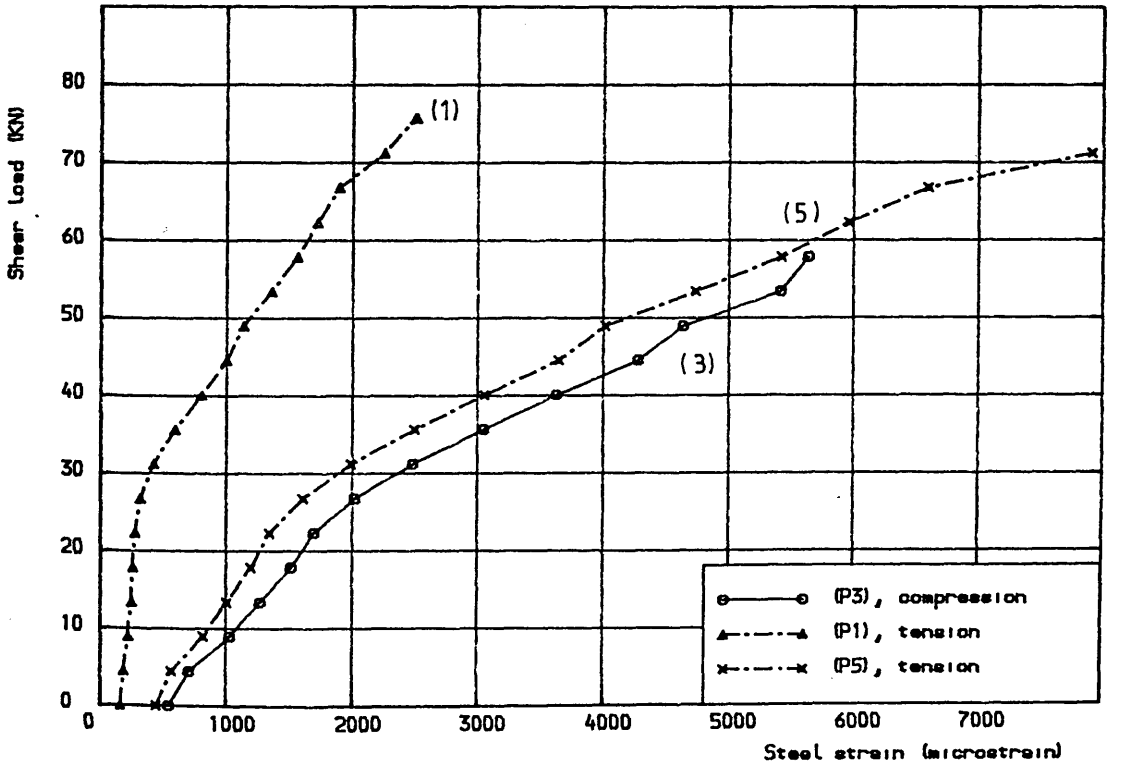

Figure (5.40 d) Shear load vs steel strain for specimen 2.1.3A, last cycle

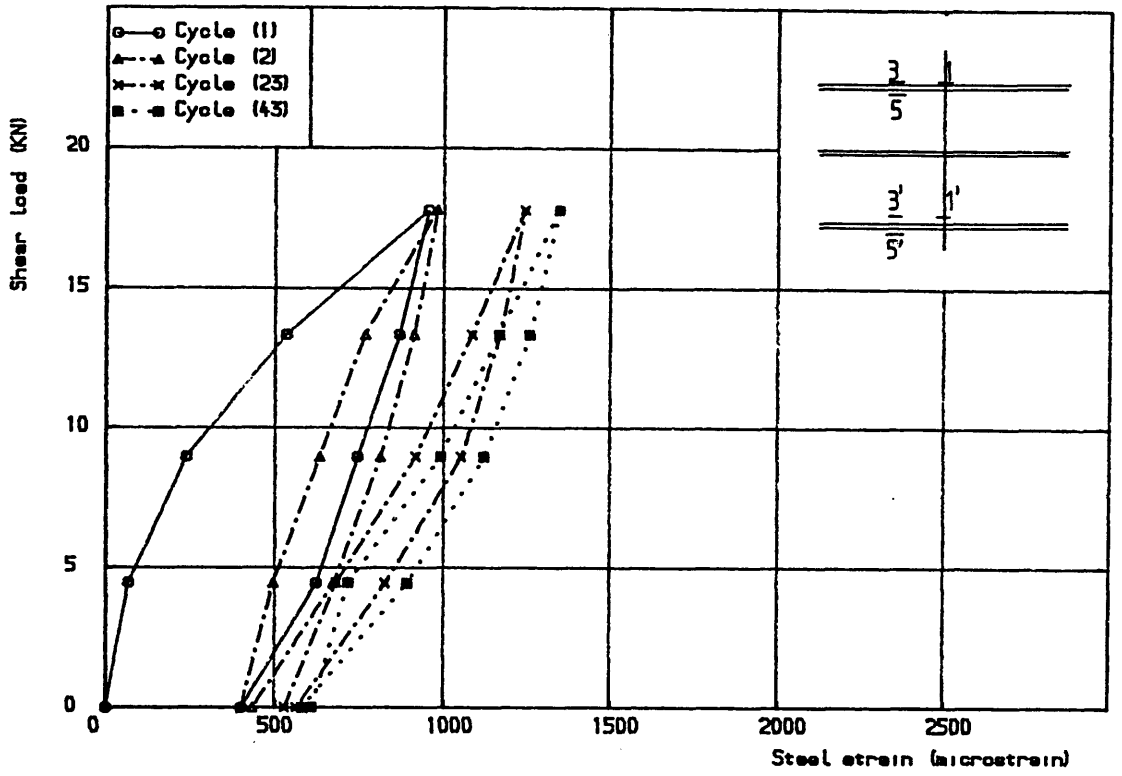

Figure (5.41 a) Shear load vs steel strain for specimen 2.1.3A at position (3')

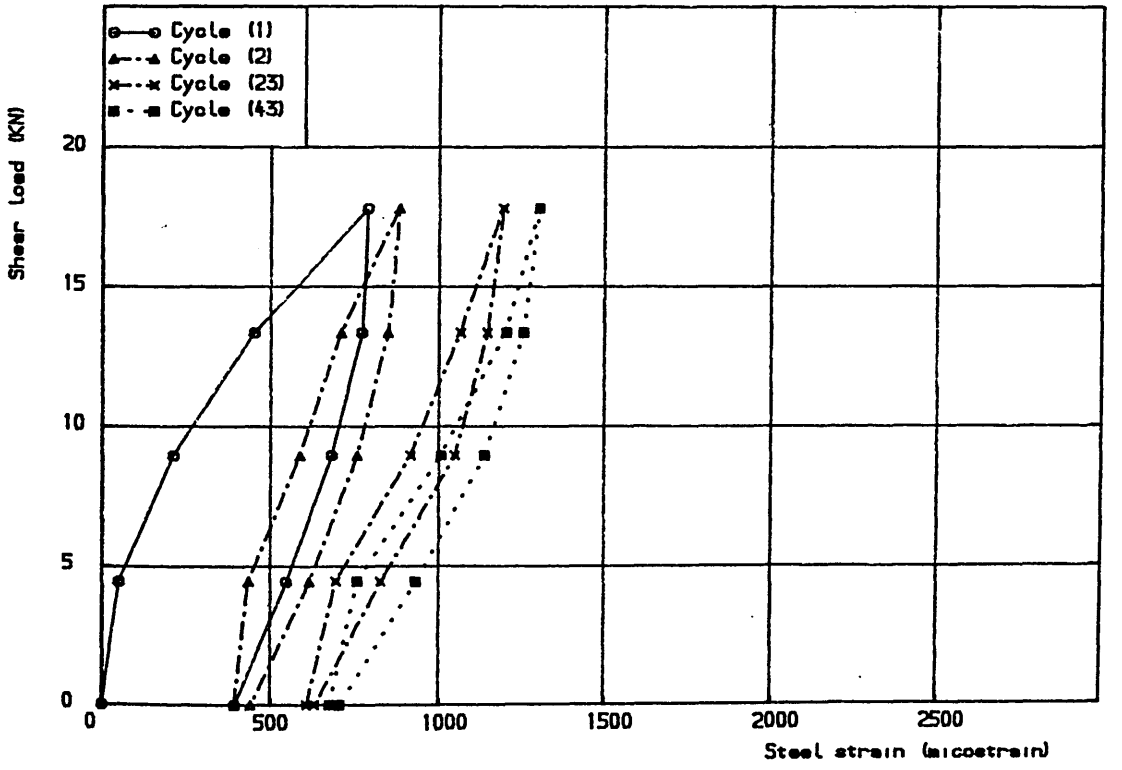

Figure (5.41 b) shear load vs steel strain for specimen 2.1.3A at position (5')

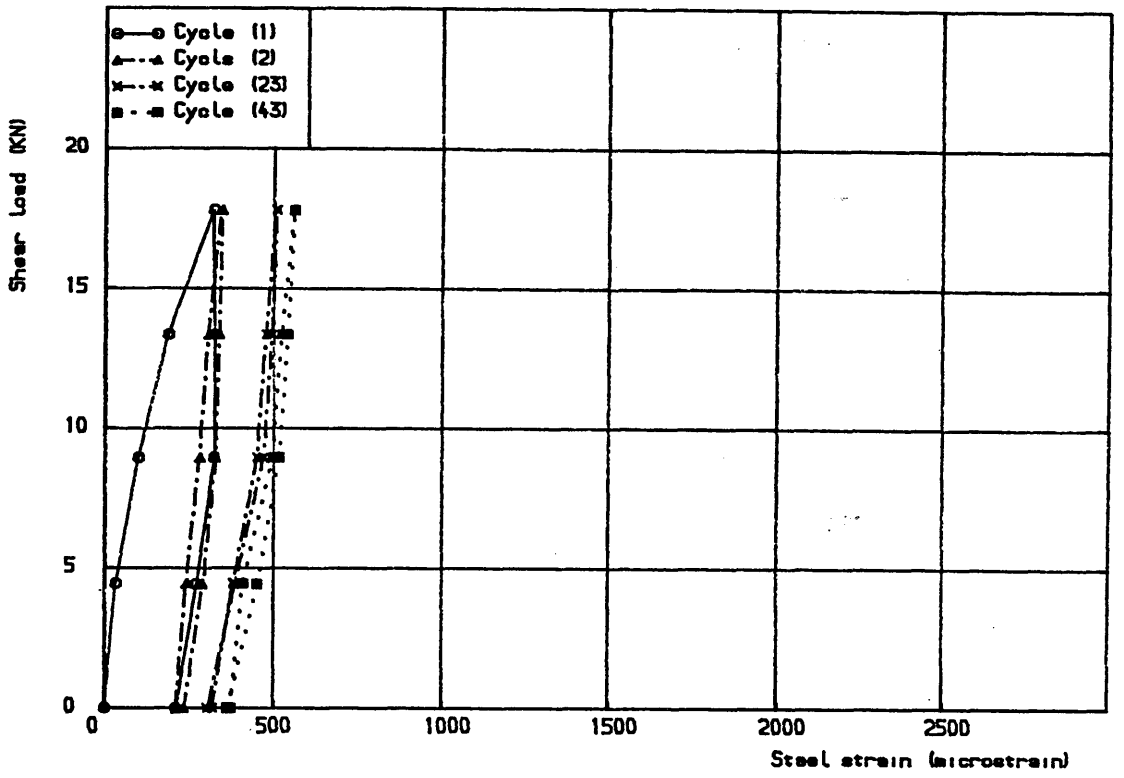

Figure (5.41 c) Shear load vs steel displacement for specimen 2.1.3A at position (1')

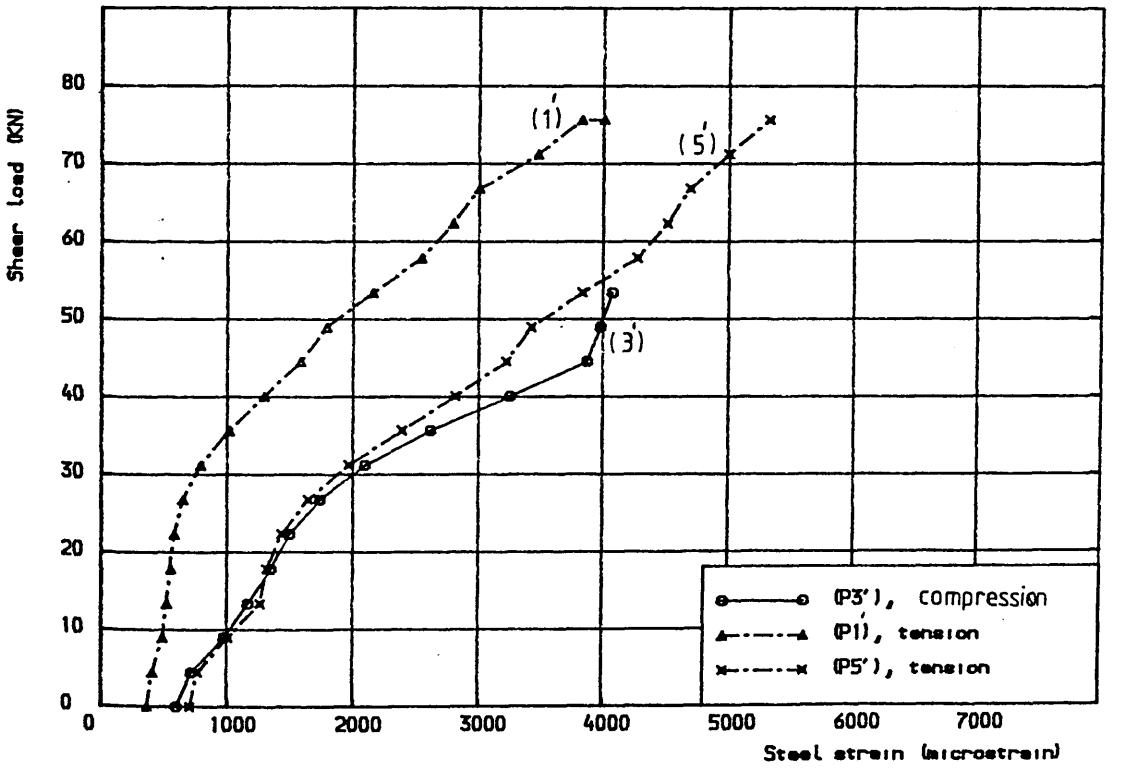

Figure (5.41 d) Shear load vs steel strain for specimen 2.1.3A, last cycle

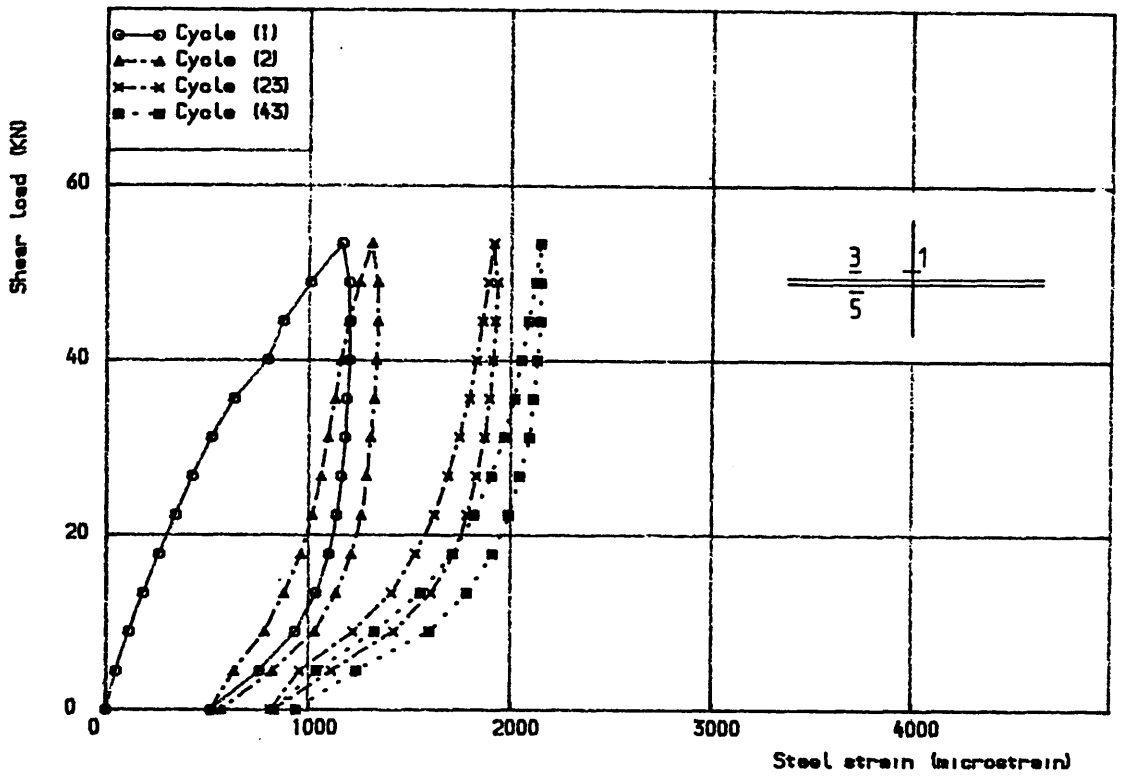

Figure (5.42 a) Shear load vs steel strain for specimen 2.1.4λ, (position 3)

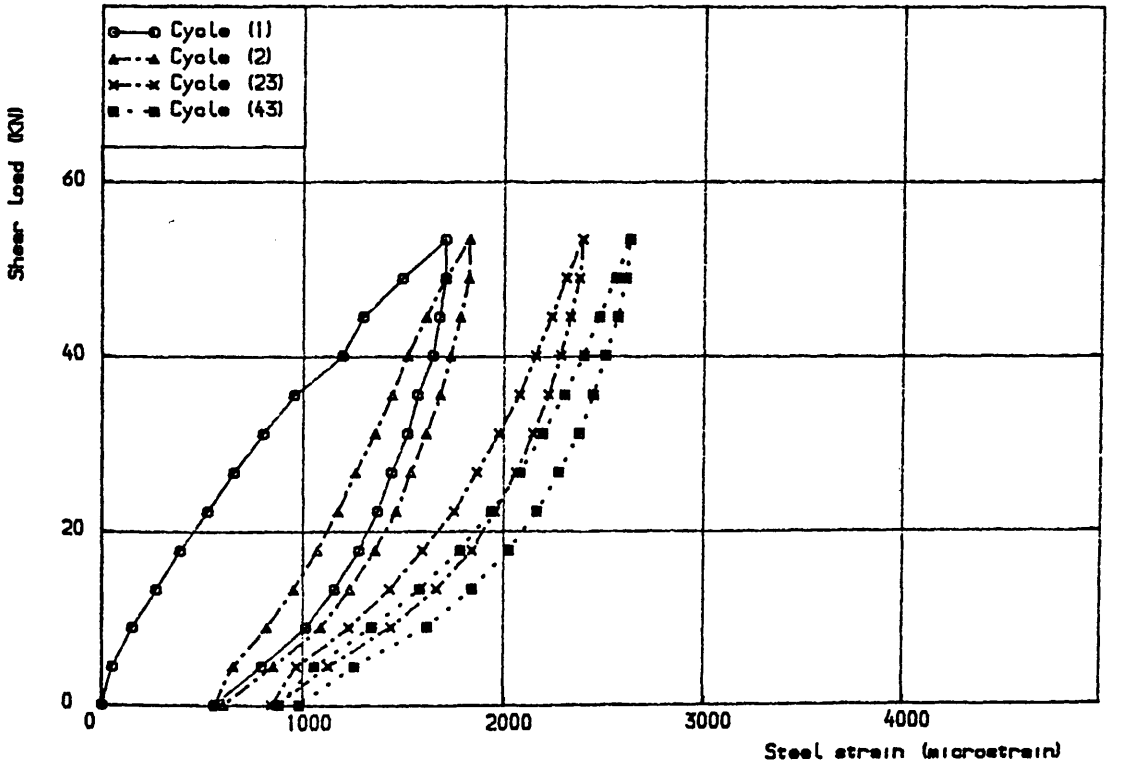

Figure (5.42 b) Shear load vs steel strain for specimen 2.1.4λ, (position 5)

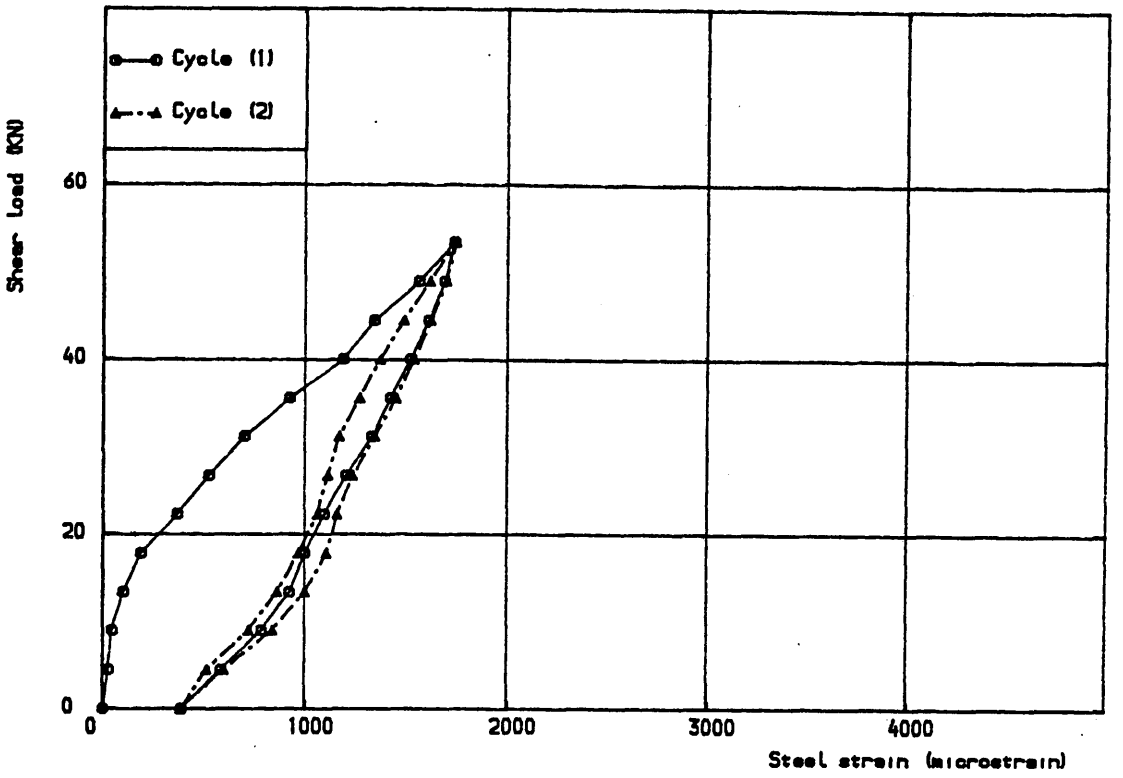

Figure (5.42 c) Shear load vs steel strain for specimen 2.1.4A (position 1)

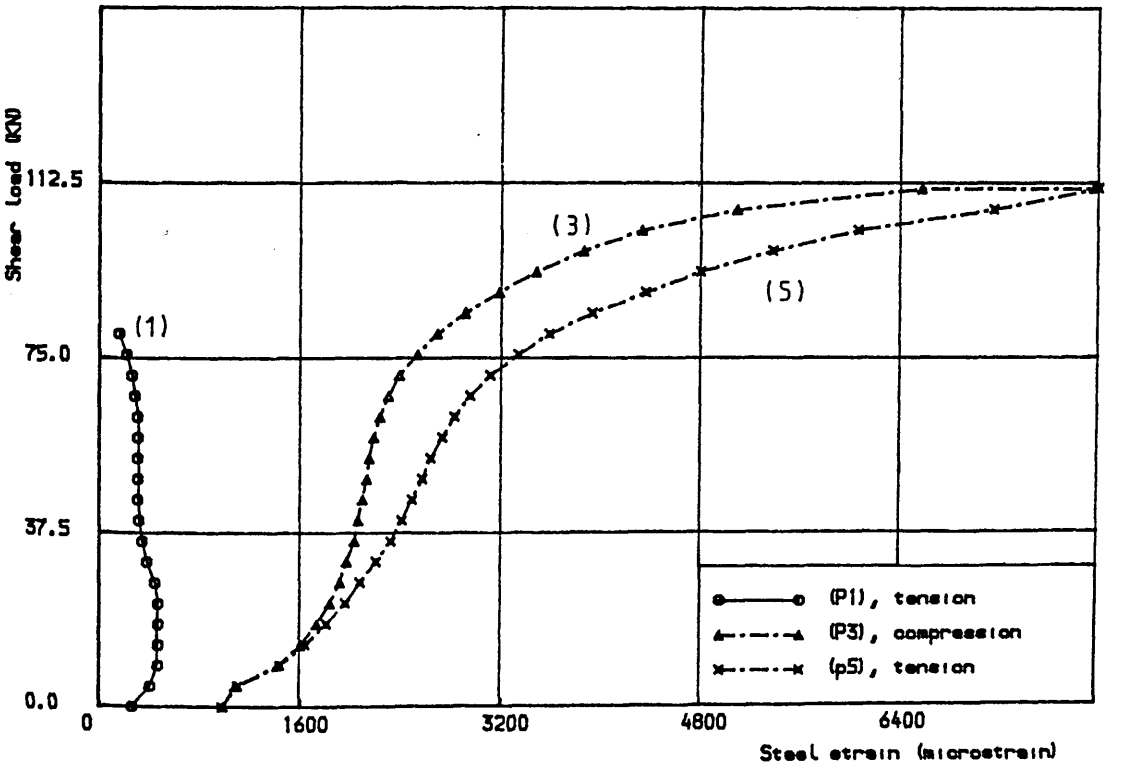

Figure (5.42 d) Shear load vs steel strain for specimen 2.1.4A, last cycle

CHAPTER (6)

COMBINED ACTION RESULTS

6.1 Introduction

This chapter presents the results of the shear transfer tests which combine the actions of interface shear transfer and dowel mechanisms under both monotonic and repeated loadings ,i.e. series 3. The analysis and discussion of these results are given in the next chapter.

6.2 Monotonic Loading

6.2.1 General

The results of specimens of groups (1), (2), (3) and (5), tested under monotonic loading, are described in this section. The purpose of these groups was to study the effect of the following variables:

(1) the reinforcement ratio of the bars crossing the crack plane (i.e. 0.28%, 0.56%, 1.12% and 1.68%)

(2) the initial crack width (0.125 mm and 0.40 mm),

(3) the type of transverse reinforcement (high tensile deformed bars and mild tensile plain bars of 8 mm diameter).

Group (5) repeated two of the tests of group (2) in order to provide additional information on the distribution of strains and stresses in the transverse reinforcement.

Similar to the dowel tests the overall behaviour of the specimens is described by the following relationships:

(a) Shear load versus shear displacement

(b) Shear load versus crack width

(c) Crack width versus shear displacement

(d) Shear load versus steel strain

A summary of the principal test results is given in Table (6.1), along with specimen details and include the ultimate shear load, shear displacement and crack width at failure.

6.2.2 Group (1)

The specimens of this group, numbers 3.1.1, 3.1.2, 3.1.3 and 3.1.4, had an average initial crack width of 0.125 mm and included high tensile deformed bars of 8 mm diameter with 0.20% proof stress of 535 N/mm^2. The concrete compressive strength varied from 45 N/mm^2 to 52 N/mm^2 with a target value of 45 N/mm^2. The reinfocement ratios were varied from 0.27% to 1.68%. The relationships mentioned above are shown in Figures (6.1) - (6.3) and (6.5). The positions of the strain gauges on the transverse reinforcement are shown in Figure (6.4).

The shear load versus shear displacement behaviour, Figure (6.1), was similar for all specimens. A linear relationship up to an average 0.7 of the ultimate shear load was noted followed by significant nonlinear behaviour.

The change in the crack width against the applied shear load showed trends similar to that of the shear load versus shear displacement

(see Figure 6.2).

The ratios of the crack width to shear displacement, Figure (6.3), show that up to an average 0.85 of the ultimate shear load all specimens had similar crack opening paths indicating that behaviour is independent of the reinforcement ratio up to this stage. This observation suggests that the major contribution to the applied shear load is due to interface shear transfer through the interlocking of the aggregate particles along the crack faces.

Beyond 0.85 of the ultimate shear load a small difference was observed between the crack opening paths of the specimens (see Figure 6.3), reflecting the degradation of the interface shear transfer mechanism and a greater contribution from dowel action. The shear load versus steel strain curves showed trends similar to those of the shear load versus shear displacement and crack width as can be seen from Figure (6.5). It should be noted that the average of the strains at the predescribed positions were taken. Tensile strains were recorded for all gauges.

6.2.3 Group (2)

The specimens of this group are 3.2.1, 3.2.2, 3.2.3 and 3.2.4 and were identical to the specimens 3.1.1, 3.1.2, 3.1.3 and 3.1.4 of group (1) except that the average initial crack width was 0.40 mm. The positions of the steel strain gauges were the same as group (1) as shown in Figure (6.4).

The main relationships between shear load, shear displacement, crack width and steel strains are shown in Figures (6.6) - (6.9). General trends of the shear load versus shear displacement and shear load

versus crack width curves, Figures (6.6) and (6.7), were similar to those of group (1). However, the range of linear behaviour was less in this case , being observed up to an average 0.57 of the ultimate shear load.

The ratio of the crack width to shear displacement for these specimens were less than those for the specimens of group (1). This may reflect the difference in the contribution of the interface shear transfer mechanism and dowel action compared with specimens of group (1).

6.2.4 Group (3)

This group comprises specimens 3.3.1, 3.3.2, 3.3.3, 3.3.4 which were identical to those of group (1), i.e. 3.1.1, 3.1.2, 3.1.3 and 3.1.4, except they were reinforced with 8mm diameter plain mild tensile steel bars instead.

Figures (6.10) and (6.11) show that all specimens exhibited similar trends. Linear behaviour was observed up to an average 0.64 of the ultimate shear load. From Figure (6.12) it can also be seen that the specimens had approximately the same crack opening path during the linear stage. As explained earlier, at this stage such similarity of the crack opening path reflects the dominance of the interface shear transfer and the independence of behaviour on the amount of the transverse reinforcement.

A change in the crack opening paths was observed in the nonlinear stage, showing an increased influence of the amount of the transverse reinforcement.

From Figure (6.13) the curves of the shear load versus average steel strain showed trends similar to those of the shear load against both shear displacement and crack width.

6.2.5 Group (5)

The specimens of this group ,i.e. 3.5.1 and 3.5.2, were identical to specimens 3.2.2 and 3.2.4 of group (2) respectively. However, the number and positions of the strain gauges used to measure the strains in the reinforcing bars were different [see Figure 6.17)].

Comparisons of the test results of each identical pairs gives some measure of the degree of scatter and indicates whether the current method of fixing the strain gauges had a major influence upon behaviour. Comparisons are shown in Figures (6.14) - (6.16) and (6.27) - (6.29). From these figures some degree of scatter was apparant specially for specimen 3.5.1 and 3.2.2. However the overall behaviour of specimens of group (5) are similar to those of group (2).

A major purpose of this group was to study the strain/stress distribution in the transverse reinforcement at and near the cracked section in order to obtain better understanding of the interaction between the interface shear transfer and dowel action mechanisms.

Specimen 3.5.1

19 pairs of strain gauges were attached to the top and bottom surfaces of the reinforcing bars crossing the crack plane (see Figure 6.17a). The selected strain measurements are presented in Figures

(6.18) and (6.19). From these figures a close antisymmetrical relationship can be observed between the strains measured on either side of the crack plane indicating a consistent data. Consequently only a typical distribution is considered here and for this purpose the strains measured on one side of the specimen at positions 13, 14, 15 and 18, 19, 20 were chosen.

The distribution of the strains along the cross section of reinforcing bar and over a distance 6.25 times the bar diameter from the crack plane and at different load levels,i.e 0.40 , 0.60 , 0.80 , 0.90 and 1.0 of the shear failure load, were presented in Figure (6.20). These strains were resolved into direct and flexural strains using equations (5.1a,b) and Figures (6.21) and (6.22) presents the resulting distributions.

The relations between the flexural and the direct strains, the distances measured from the crack plane as a function of the bar diameter and the applied shear load are illustrated in Figures (6.23) and (6.24). It can be seen that higher flexure and direct strains occurred at the positions near the crack plane . Also the flexural strains diminish at a higher rate compared with the direct strain as the distance from the crack plane increased. The flexural strains died out altogether at about 6.20 the bar diameter whereas the direct strain reduced to constant value. At the shear failure load the ratio of the maximum flexural to direct strain was 1.18. The ratios of both flexural and direct strains to the proof strain , i.e 0.002, were 1.67 and 1.41 respectively. The calculated flexural and direct stresses at the failure load were shown in Figure (6.25).

After the test was completed, the specimen was cut at the shear plane by using an electric saw and the two faces of the crack were investigated. Photographs were taken as shown in Figure (6.26). There was no evidence of any localized damage to the concrete adjacent to the reinforcing bars as was mentioned by Walraven[1]. However there were signs of crushing and sliding over the whole face.

Specimen 3.5.2

11 pairs of strain gauges were positioned on the top and bottom surfaces of the reinforcing bars as shown in Figure (6.17b). Unfortunately complete readings were not obtained from the strain gauges placed at the crack plane (i.e. positions 4 and 11) and also at position 3 due to being damaged during the loading process. The strains obtained at all other positions are shown Figures (6.30) to (6.33). Fairly close antisymmetrical distributions , similar to previous tests, were obtained about the crack plane. Accordingly typical strains at positions 5, 6, 7 and 12, 13, 14 were chosen to provide the required information about the strain and stress distributions as in the previous test.

The distribution of strain along the cross section of the reinforcing bar crossing the crack plane and over a distance 6.25 times the bar diameter from the crack plane are shown in Figure (6.34) measured at 0.4, 0.6 ,0.8, 0.9 and 1.0 of the ultimate load.

The decomposed flexural and direct strains using equations (5.1a,b) are presented in Figures (6.35) and (6.36). Also the relations of these strains with the distance measured from the crack plane as a function of the bar diameter at the different load levels are shown

in Figures (6.37) and (6.38). Behaviour similar to specimen 3.5.1 can be seen. However, at ultimate shear load the ratio of the maximum flexural to direct strain was 1.52. The ratio of both flexural and direct strains to the yield strain were 1.38 and 0.91 respectively. The distribution of the calculated stresses are shown in Figure (6.39). The specimen was also cut at the centre line after the test was completed. The two faces of the crack are shown in Figure (6.40). Splitting cracks at a distance approximately equal to the concrete cover, marked in black, were noticed. These patterns were different from the previous test. Again, no evidence of localised damage was observed.

6.2.6 General Observations

- In general all specimens exhibited similar behaviour.

- Behaviour was linear up to an average 0.70,0.57 and 0.69 of the ultimate load for specimens of groups (1),(2) and (3) respectively.

- At any load level ,the change in shear displacement was always greater than the change in the crack width .

- Greater ratios of crack width to shear displacement for specimens of groups (1) and (3), i.e. initial neck width 0.125 mm, were noticed compared with those of group (2), i.e. initial crack width 0.40 mm.

- The ultimate shear load increased with the increase of the reinforcement ratio .

- The testing of the identical specimens showed a small degree of scatter.

- The steel strain measurements of group (5) revealed four things : (a) an antisymmetrical distribution of the strain/stress about the precracked plane , (b) a noticable direct tensile strain/stress in the transverse reinforcement, (c) strains only increased markedly at later stages of loading and (d) yielding of reinforcement at the ultimate shear load.

6.3 Repeated Loading

6.3.1 General

In this section the results of shear transfer tests under repeated loading are presented. The history of loading of each specimen was described earlier in Chapter (3).

These tests were conducted to study the influence of the following variables on the ultimate shear strength and the behaviour of the shear transfer:

(1) The area of the reinforcement crossing the crack plane.
(2) The initial crack width (0.125 mm & 0.40 mm)
(3) Type of the reinforcement crossing the crack plane
(4) History of loading
(5) type of loading ,i.e monotonic and repeated loadings.

The general behaviour is described by relations similar to those of the monotonic loading which are :

(a) shear load versus shear displacement,
(b) shear load versus crack width,
(c) crack width versus shear displacement, and

(d) shear load versus steel strain in the reinforcing bars crossing the crack plane.

For each set of specimens the first three of the above relationships are presented first for load cycles 1, 2, 23 and 43 followed by the last load cycle in individual figures. The fourth relationship is always presented at the end and the average strain measured at positions shown in Figure(6.4) was used.

A summary of principal results giving the ultimate shear strength, shear displacement and the crack width measured at ultimate load is presented in Table (6.1).

6.3.2 Group (1)

The specimens of this group are 3.1.1A, 3.1.2A, 3.1.3A and 3.1.4A which are identical to specimens 3.1.1, 3.1.2, 3.1.3 and 3.1.4 tested under monotonic loading.

The main relations for this group are shown in the following figures:

(a) Shear load versus shear displacement (Figures 6.41, 6.43, 6.45, 6.47 and 6.53).

(b) Shear load versus crack width (Figures 6.42, 6.44, 6.46, 6.48 and 6.54).

(c) Crack width versus shear displacement (Figures 6.49 to 6.52 and 6.55).

(d) Shear load versus steel strain (Figures 6.56 to 6.60).

6.3.3 Group (2)

Specimens 3.2.1A, 3.2.2A, 3.2.3A and 3.2.4A are tested under repeated loading . They are paired with specimens 3.2.1, 3.2.2, 3.2.3 and 3.2.4 of the monotonic loading. The figures showing the various relationships are as follows:

(a) Shear load versus shear displacement (Figures 6.61, 6.63, 6.65, 6.67 and 6.73)

(b) Shear load versus crack width (Figures 6.62, 6.64, 6.66, 6.68 and 6.74)

(c) Crack width versus shear displacement (Figures 6.69 to 6.72 and 6.75)

(d) Shear load versus steel strain (Figures 6.76-6.78) .

Unfortunately no steel strains were obtained for specimens 3.2.1A and 3.2.4A due to the damage of the strain gauges during casting.

6.3.4 Group (3)

Specimens 3.3.1A, 3.3.2A, 3.3.3A and 3.3.4A were tested under repeated loading and paired with specimens 3.3.1, 3.3.2, 3.3.3 and 3.3.4 which are tested under monotonic loading.

The main relationships for this group are shown in the following figures:

(a) Shear load versus shear displacement (Figures 6.79, 6.81, 6.83, 6.85 and 6.91)

(b) Shear load versus crack width (Figures 6.80, 6.82, 6.84, 6.86 and 6.92)

(c) Crack width versus shear displacement (Figures 6.87 to 6.90 and 6.93)

(d) Shear load versus steel strain (Figures 6.94 to 6.98).

6.3.5 Group (4)

The main aim of this group was to study the effect of the load history on the ultimate shear strength where the maximum repeated loading was varied.

The specimens 3.4.1A and 3.4.2A of this group were subjected to a maximum repeated loading of 0.57 the ultimate shear load calculated by Mattock's equation (Equation 2.21) instead of 0.75 which was applied to the identical specimens 3.1.1A and 3.1.4A of group (1).

The ultimate shear load, shear displacement and crack width measured at ultimate load are listed in Table (6.1).

6.3.6 General Observations

- In general the shear load versus shear displacement, shear load versus crack width and shear load versus steel strain curves of cycle numbers 1 , 2 , 23 & 43 showed similar trends for all specimens .

- The change in the shear displacement was greater than the change in crack width . This difference was greater for specimens of group (2), i.e. initial crack width 0.40 mm, compared with specimens of groups (1)and (3), i.e. initial crack width 0.125 mm.

— The ratio of the crack width to shear displacement (including the residual displacements) measured at the maximum shear load for the cycle numbers 1, 2, 23 & 43 decreased with the increase of cycling numbers. The specimens of groups (1) and (3), i.e. initial crack width 0.125 mm had a higher ratio compared with specimens of group (2), i.e. initial crack width 0.40 mm.

— The specimens exhibited a large increase in both shear displacement and crack width at the first loading cycle. For the subsequent cycles at the same shear load the response tended to settle and the rate of the increase for both shear displacement and crack width decreased with cycling.

— The trend of the first cycle of the shear load — shear displacement & shear load — crack width curves was different compared with the second and the subsequent cycles. The specimen response to the first cycle was characterized by a gradual reduction in the shear stiffness as the applied shear load increased . Response to the subsequent cycles was characterized by higher shear stiffness at low load level and gradual decrease in the stiffness with the increase of the applied load .

— The area enclosed by the hysteresis loop decreased significantly after the first cycle. For subsequent cycles it was approximately equal .

— Residual displacements were found when the load was released to zero . The residual displacement of the first cycle was very large compared with the resdual of the subsequent cycles . For specimens with initial crack width of 0.40 mm, the residual of the shear

displacements measured for cycles 23 and 43 was much greater with the equivalent residual of the specimens with initial crack width 0.125 mm.

- During unloading and at higher load a little decrease in shear displacement and crack width was observed. As the load approached to zero load the displacements decreased rapidly.

— For the last load cycle where the applied load was increased monotonicaly to failure , the specimens behaved similar to the previous load cycle up to the maximum repeated load level. As the load increased the specimens showed nonlinear behaviour .

— The shear load versus steel strain exhibited similar behaviour to shear load versus shear displacement. The strains measured at all positions were tension . Failure occurred due to yielding of transvers reinforcement.

Table (6.1): Test specimens details of series (3) (combined action)

Specimen number	No. and size of stirrups	Reinf. Ratio ρ %	Yield stress of stirrups f_y	Concrete comp. stress f_{cu} N/mm²	Concrete tensile stress f_t N/mm²	Initial crack width mm	Type of loading	Ultimate shear load kN	Ultimate shear stress N/mm²	Ultimate shear displacement mm	Ultimate crack width mm
Group (1)											
3.1.1	1Y8	0.27		50	3.26	0.125	M *	169	4.69	0.443	0.370
3.1.1A	1Y8	0.27		50	3.26	0.120	R	125	3.47	0.596	0.309
3.1.2	2Y8	0.56		52	3.3	0.130	M	258	7.16	0.600	0.522
3.1.2A	2Y8	0.56	535	52	3.3	0.136	R †	196	5.44	0.829	0.493
3.1.3	4Y8	1.12	N/mm²	47	3.2	0.120	M	380	8.88	0.675	0.570
3.1.3A	4Y8	1.12		47	3.2	0.125	R *	285	7.9	0.641	0.360
3.1.4	6Y8	1.56		45	3.18	0.130	M	413	11.6	0.698	0.627
3.1.4A	6Y8	1.56		45	3.18	0.132	R	382	10.6	0.818	0.506
Group (2)											
3.2.1A	1Y8	0.27		53	2.97	0.39	R	111	3.08	1.122	0.336
3.2.1	1Y8	0.27		53	2.97	0.39	M	130	3.60	0.840	0.300
3.2.2	2Y8	0.56		60	3.0	0.39	M	187	5.22	1.04	0.529
3.2.2A	2Y8	0.56	535	60	3.0	0.41	R	169	4.69	1.256	0.452
3.2.3	4Y8	1.12	N/mm²	48	2.83	0.40	M	284	7.06	1.158	0.567
3.2.3A	4Y8	1.12		48	2.83	0.39	R	245	6.81	1.557	0.466
3.2.4	6Y8	1.56		50	3.1	0.36	M	365	10.41	1.180	0.566
3.2.4A	6Y8	1.56		50	3.1	0.40	R	347	9.64	1.654	0.471

* M : Monotonic case at loading

\+ R : Repeated case at loading

Table (6.1): (Cont'd.)

Specimen number	No. and size of shear stirrups	Reinf. Ratio ρ %	Yield stress of shear stirrups f_y	Comp. concrete strength f_{cu} N/mm²	Tensile stress of concrete f_t N/mm²	Initial crack width mm	Type of loading	Ultimate shear load kN	Ultimate shear stress N/mm²	Ultimate shear displacement (mm)	Ultimate crack width (mm)
Group (3)											
3.3.1	1Y8	0.27		55	3.4	0.125	M	151	4.19	0.443	0.570
3.3.1A	1Y8	0.27		55	3.4	0.125	R	120	3.3	0.625	0.585
3.3.2	2Y8	0.56		50	3.2	0.130	M	235	6.5	0.623	0.613
3.3.3A	2Y8	0.56	475	50	3.2	0.127	R	173	4.8	0.700	0.635
3.3.3	4Y8	1.12	N/mm²	49	5.1	0.125	M	293	8.13	0.606	0.600
3.3.3A	4Y8	1.12		49	3.1	0.126	R	262	7.27	0.834	0.763
3.3.4	6Y8	1.68		47	3.9	0.125	M	386	10.72	0.739	0.664
3.3.4A	6Y8	1.68		47	2.9	0.127	R	346	9.6	0.805	0.563
Group (4)											
3.4.1A	2Y8	0.56	535	46	2.7	0.125	R	204	5.67	0.920	0.646
3.4.2A	6Y8	1.68	N/mm²	45	2.9	0.125	R	392	10.89	0.868	0.738
Group (5)											
3.5.1	2Y8	0.56	535	50	3.1	0.40	M	183	5.08	1.27	0.61
3.5.2	6Y8	1.68	N/mm²	60	3.1	0.40	M	367	10.20	1.44	0.94

* M : Monotonic case at loading
† R : Repeated case at loading

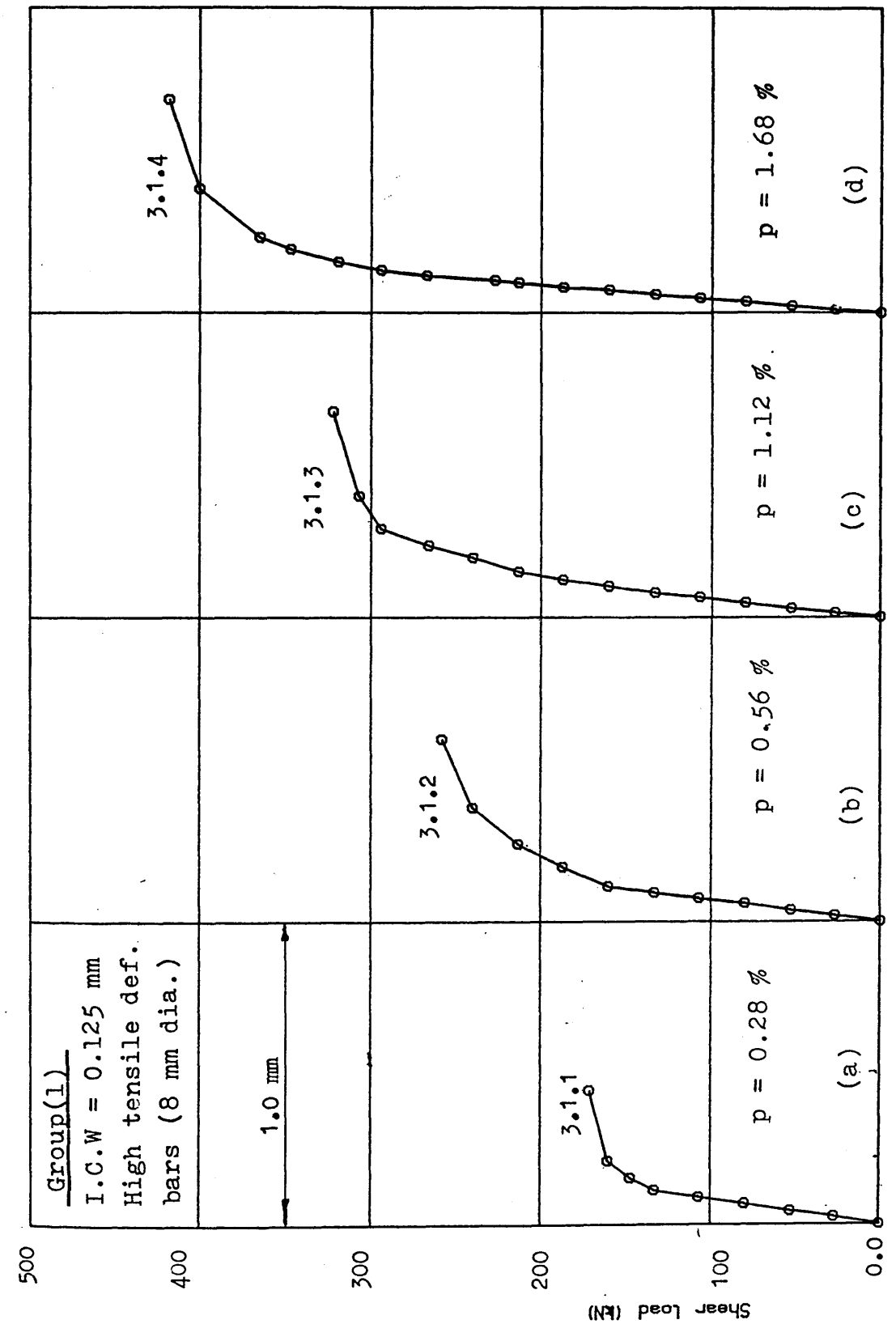

Figure(6.1) Shear load vs. shear displacement for group (1) – series 3 under monotonic load

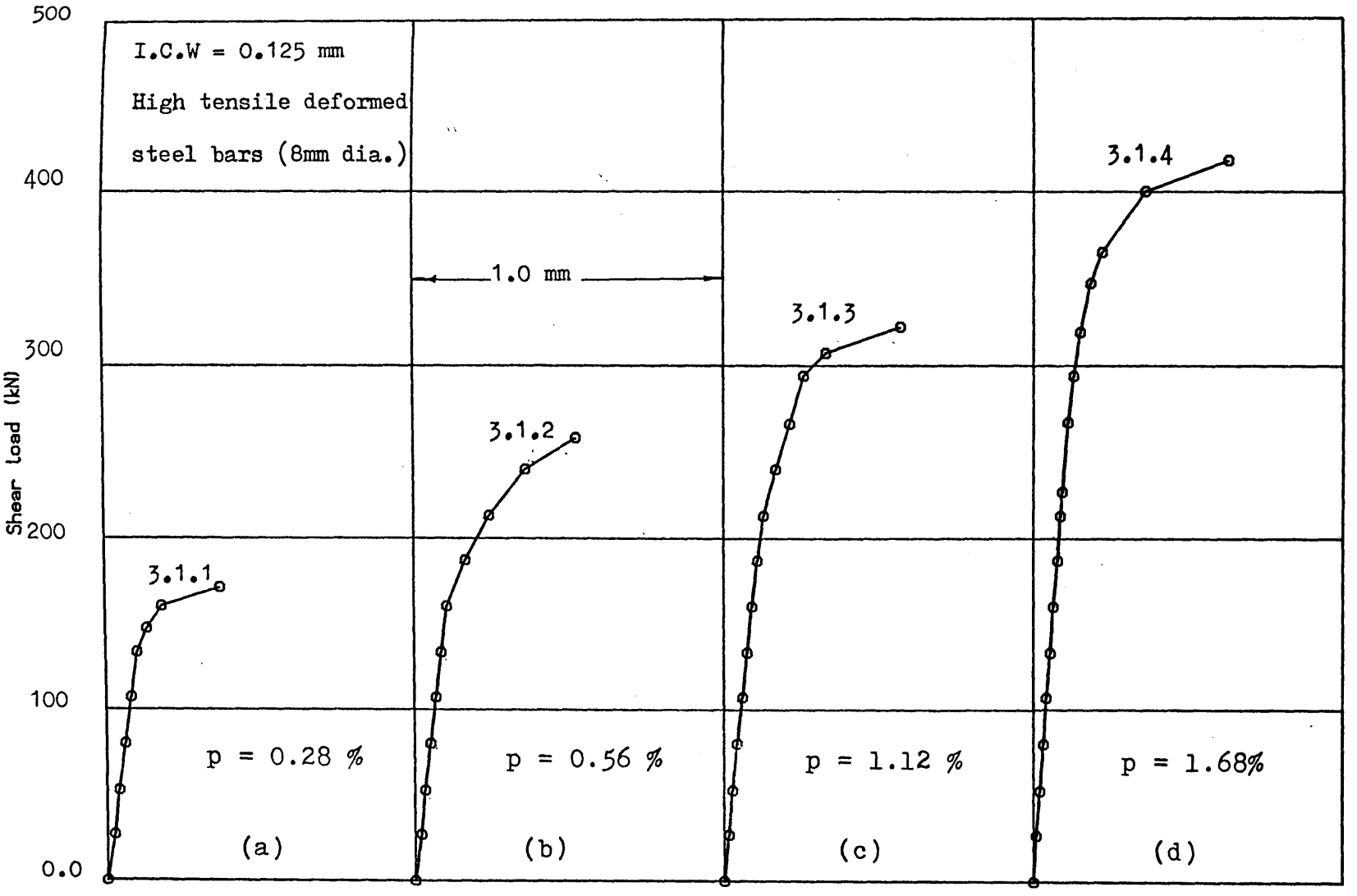

Figure(6.2) shear load vs. crack width for group (1) – series 3 under monotonic load

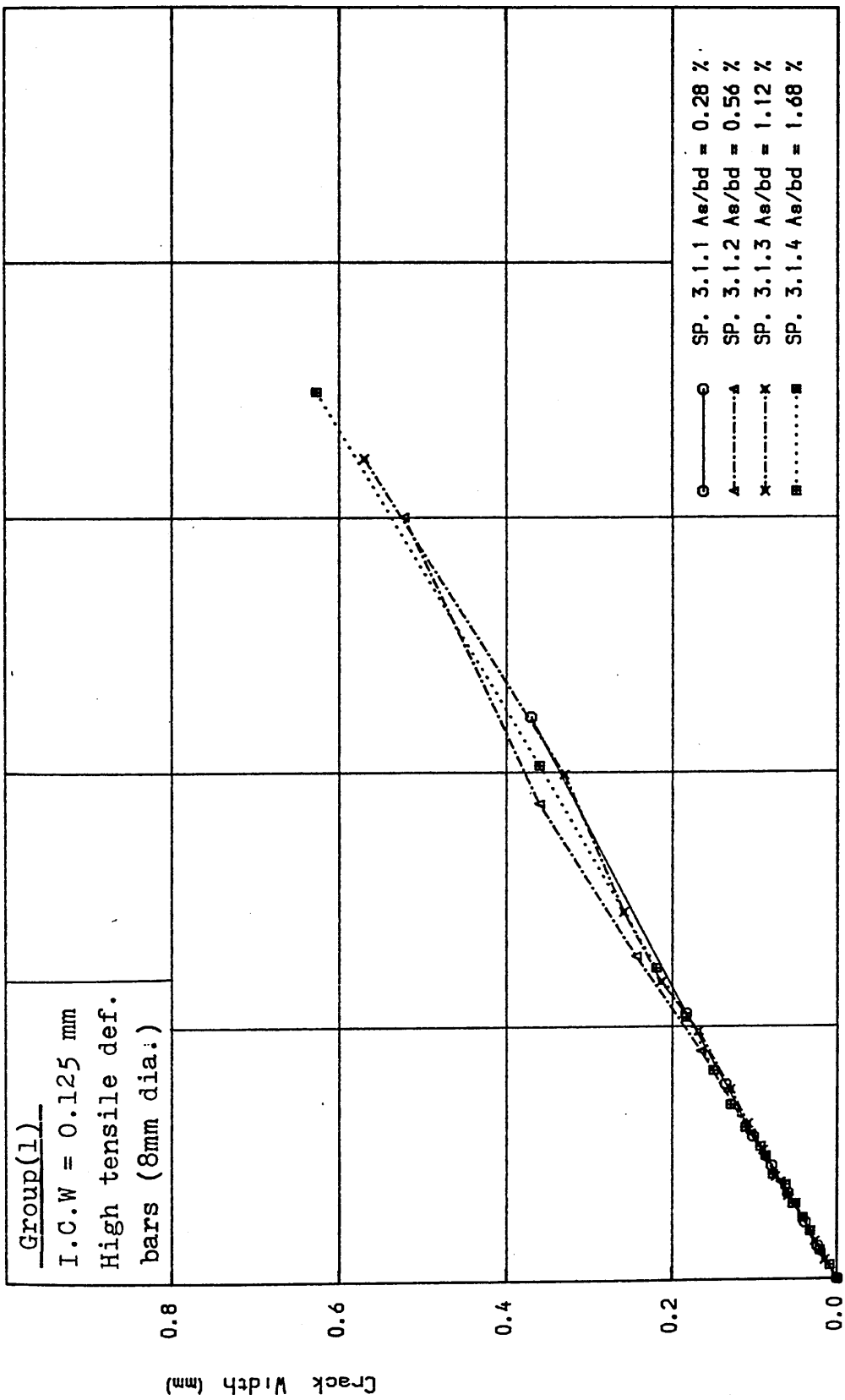

Figure(6.3) Crack width vs. shear displacement for group (1) – series 3 under monotonic load

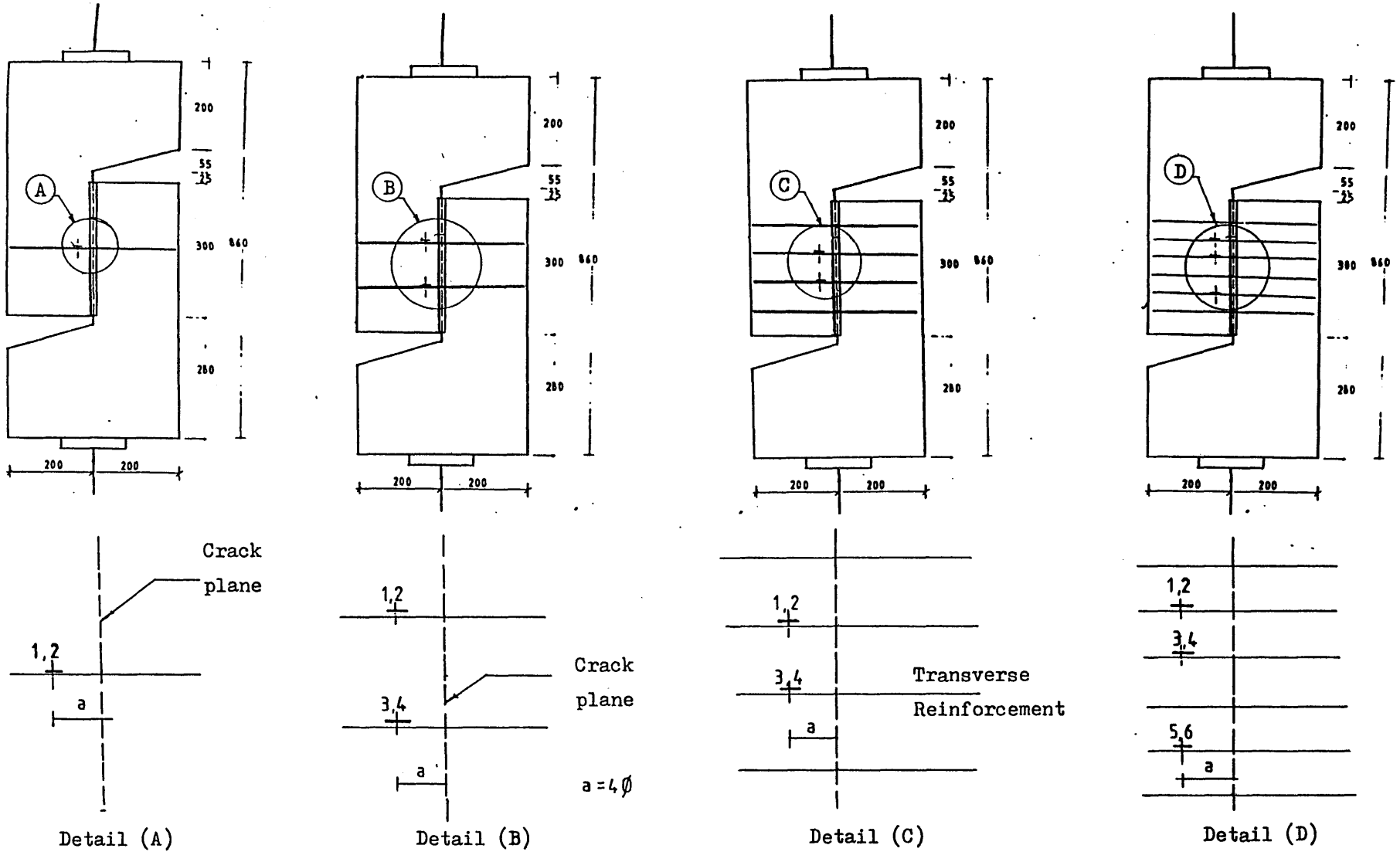

Figure(6.4) Positions of the strain gauges for groups (1),(2) and (3) of series-3 under monotonic and repeated loadings .

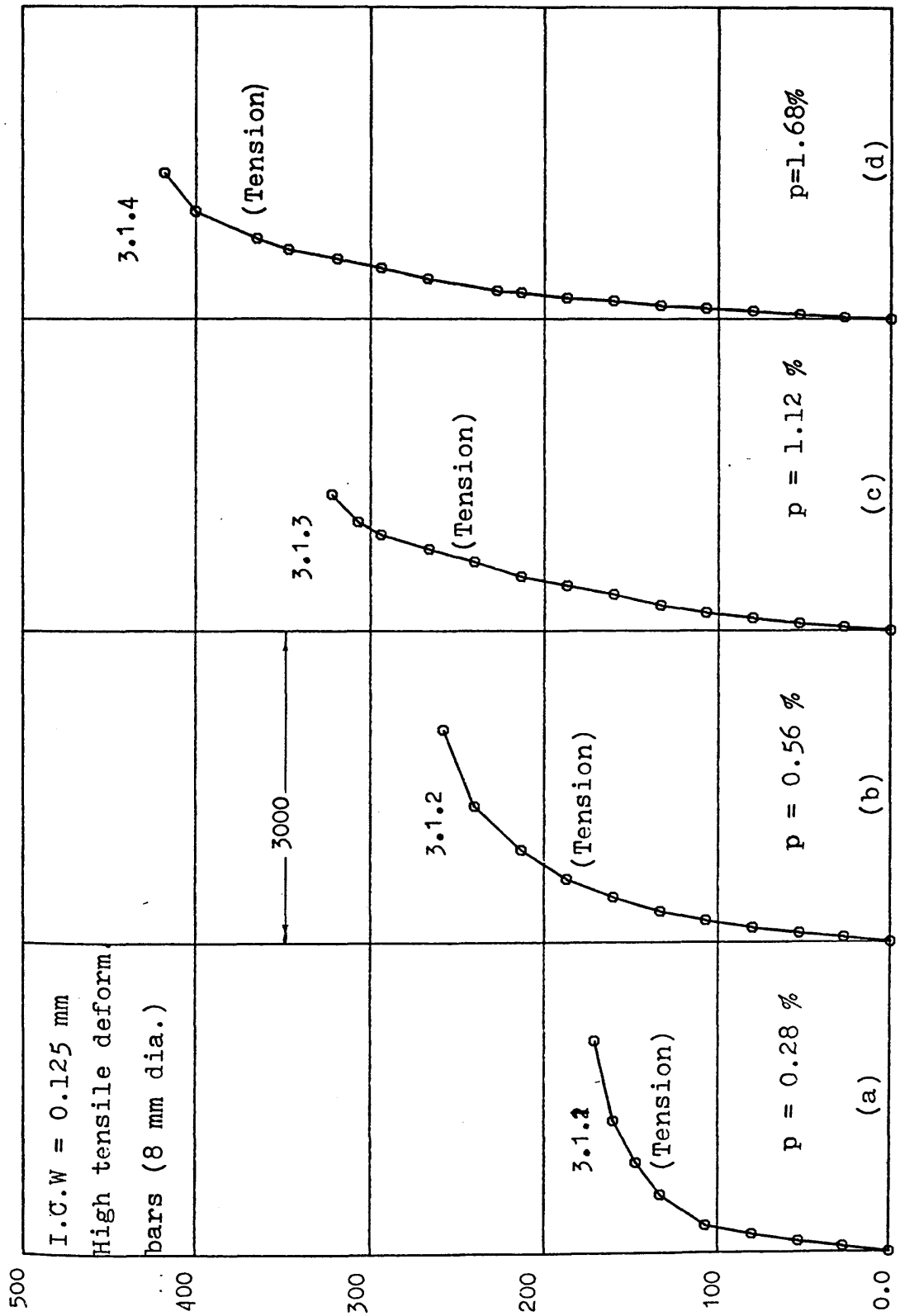

Figure(6.5) Shear load vs. steel strain for group (1) – series 3 under monotonic load

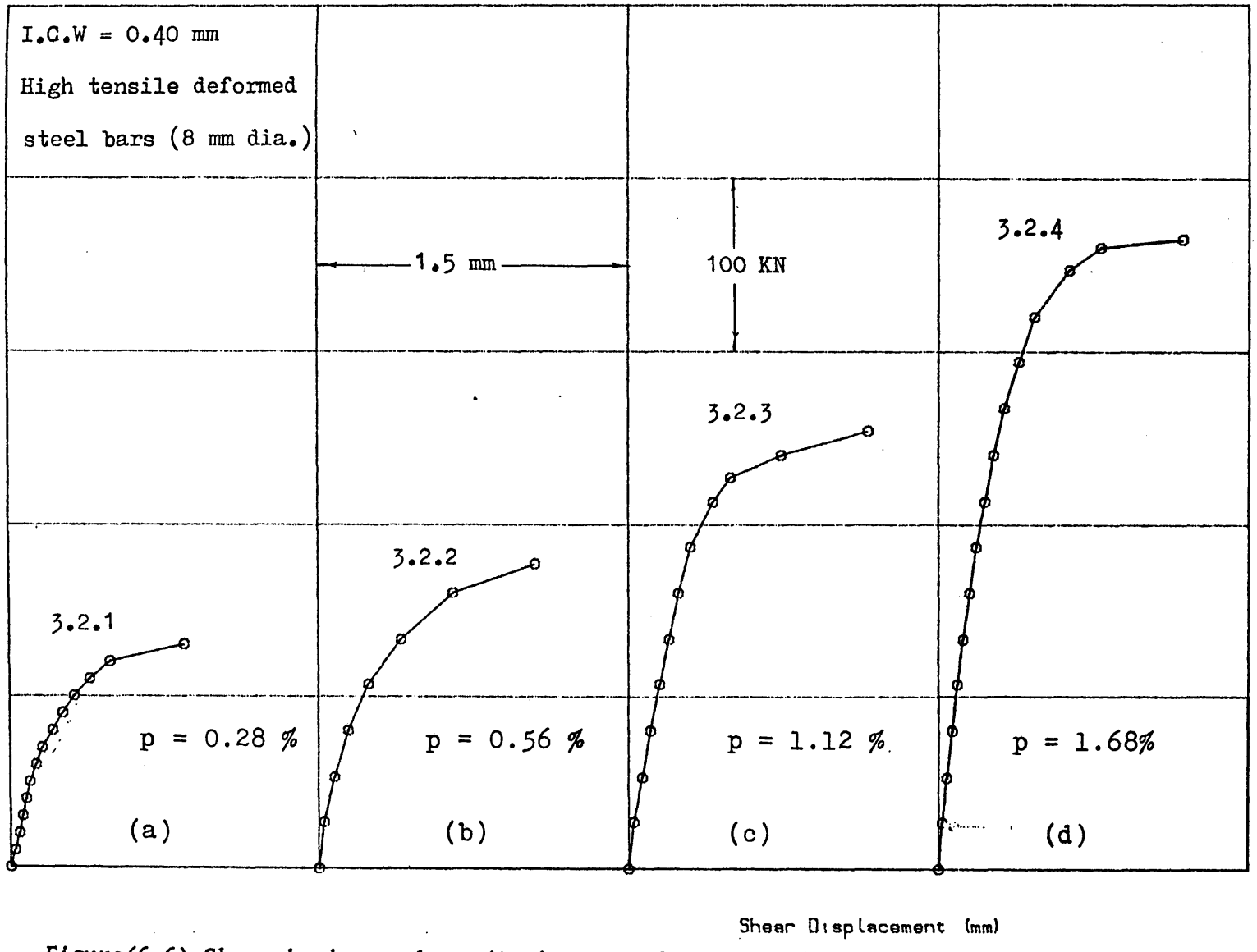

Figure(6.6) Shear load vs. shear displacement for group (2) – series 3 under monotonic load

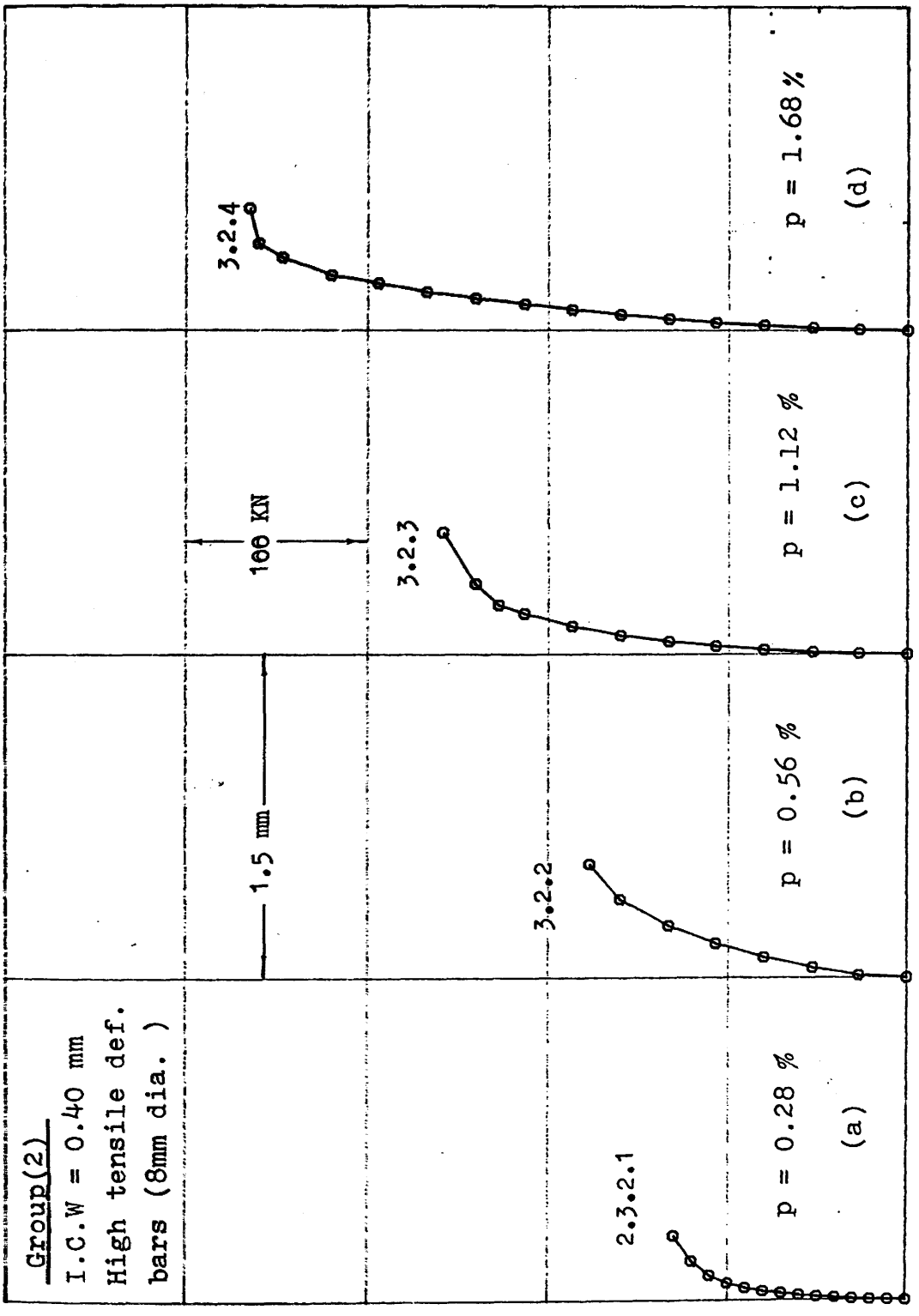

Figure(6.7) Shear load vs. crack width for group (2) – series 3 under monotoic load

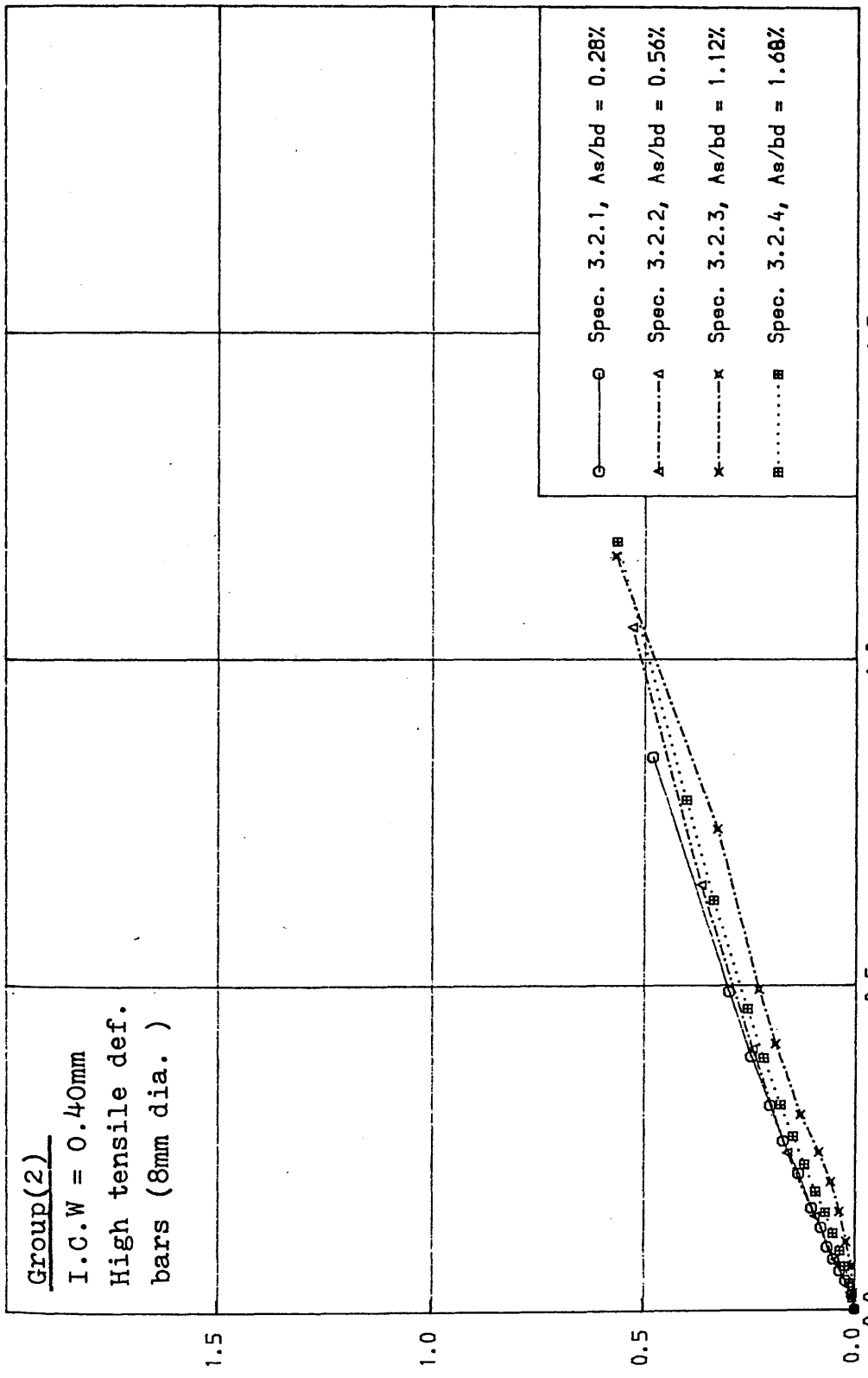

Figure(6.8) Crack width vs. shear displacement for group (2) – series 3 under montonic load

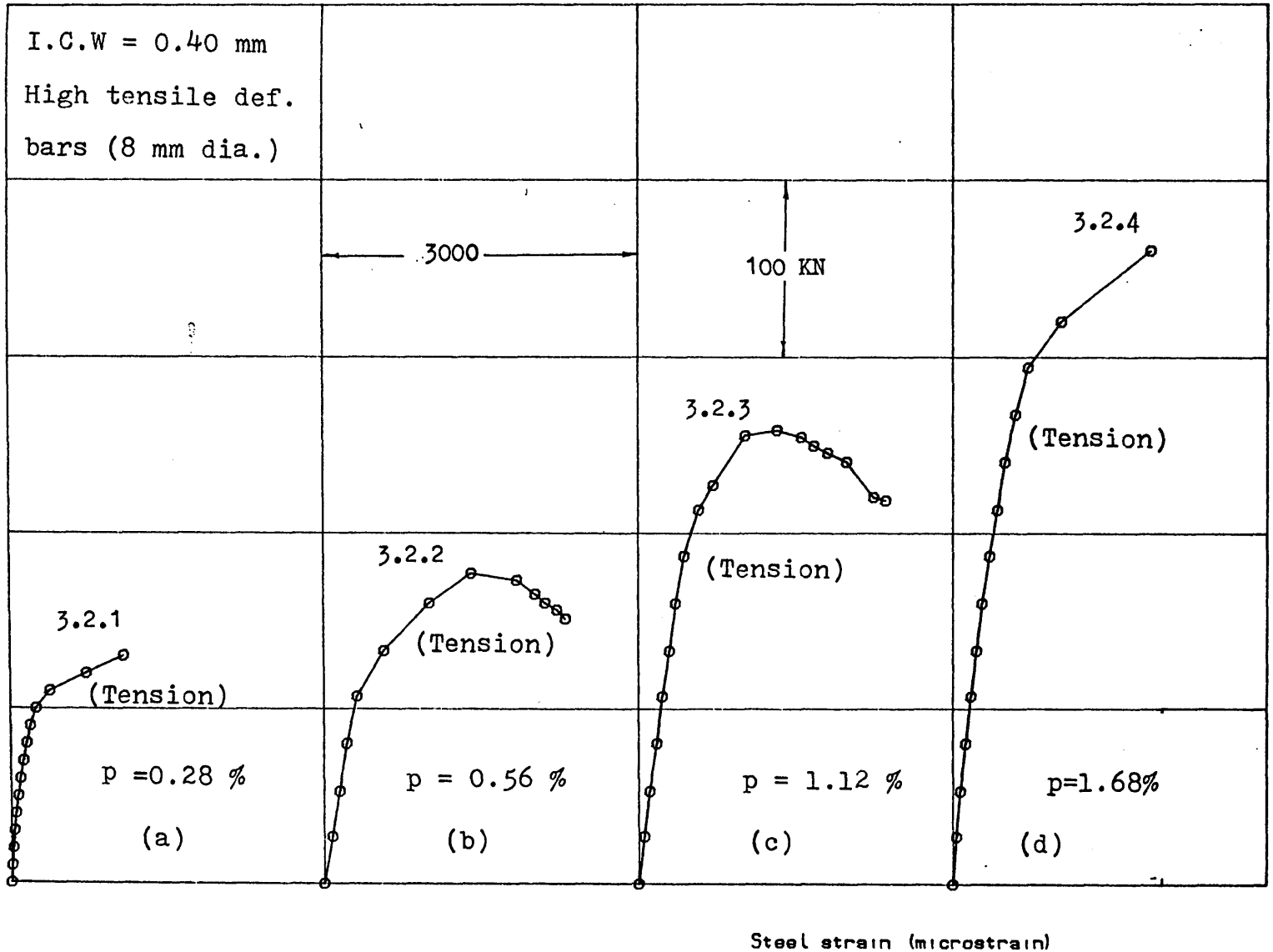

Figure(6.9) Shear load vs. steel strain for group (2) – series 3 under monotonic load

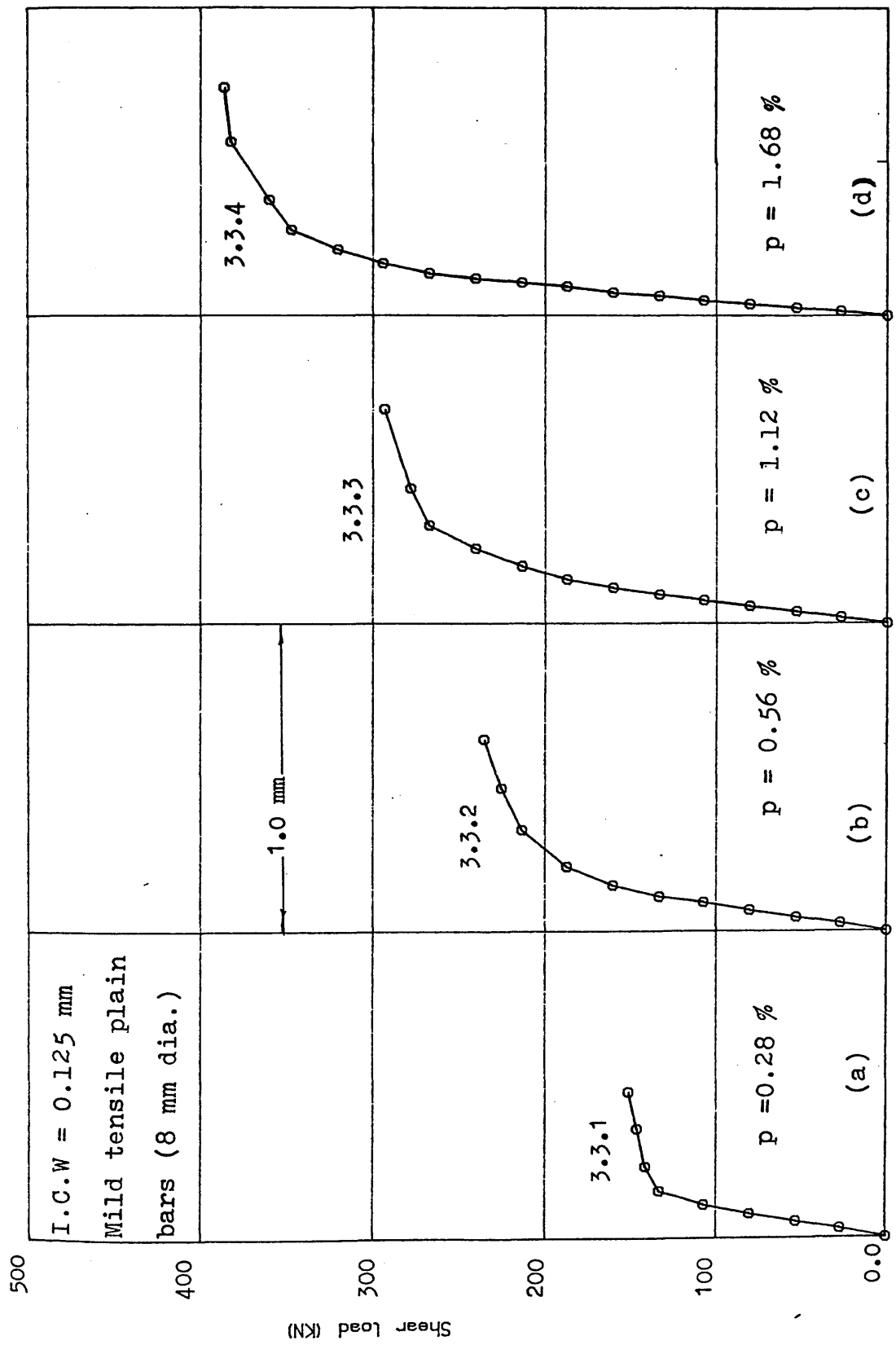

Figure(6.10) Shear load vs. shear displacement for group (3) - series 3 under monotonic load

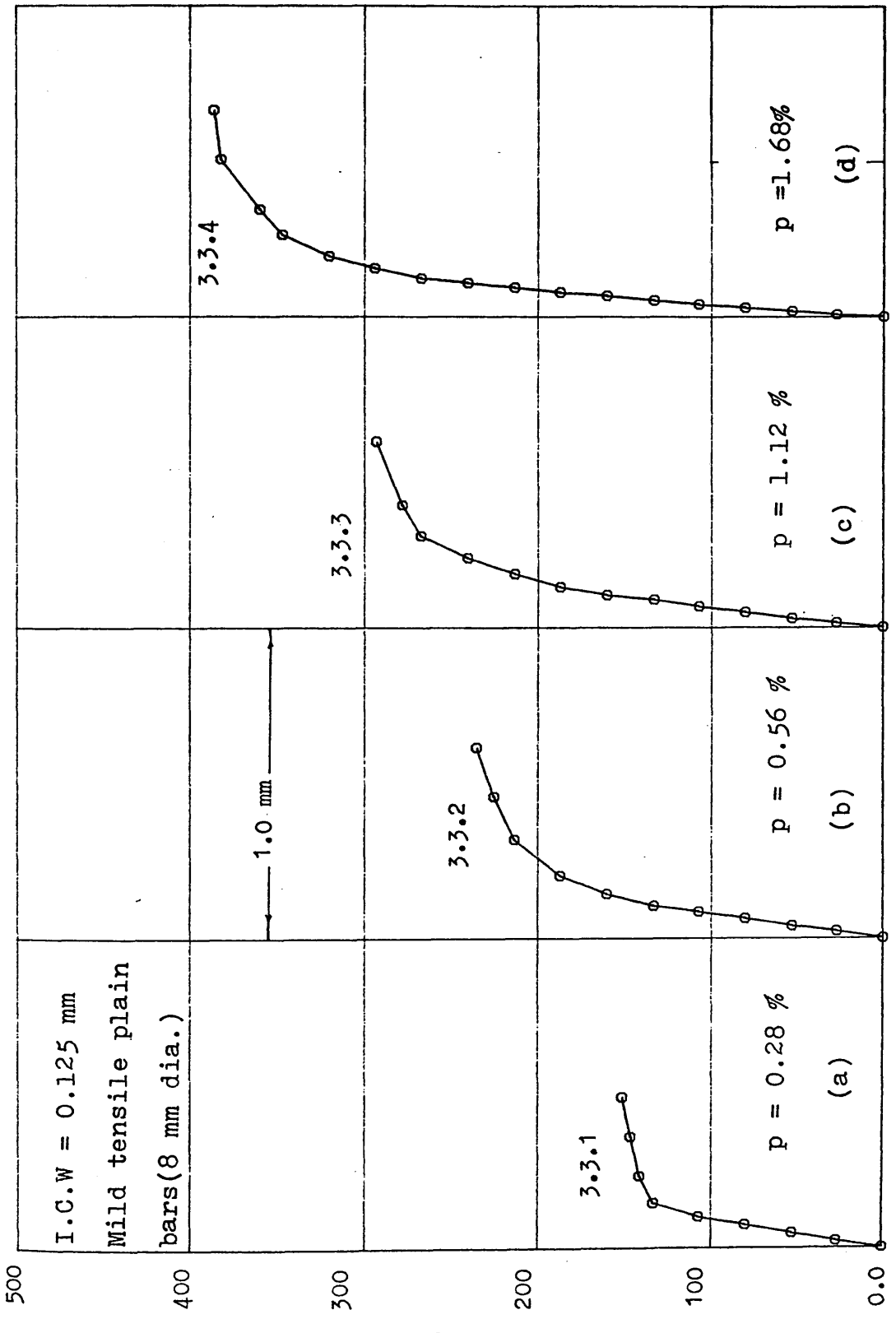

Figure(6.11) Shear load vs. crack width for group (3) – series 3 under monotonic load

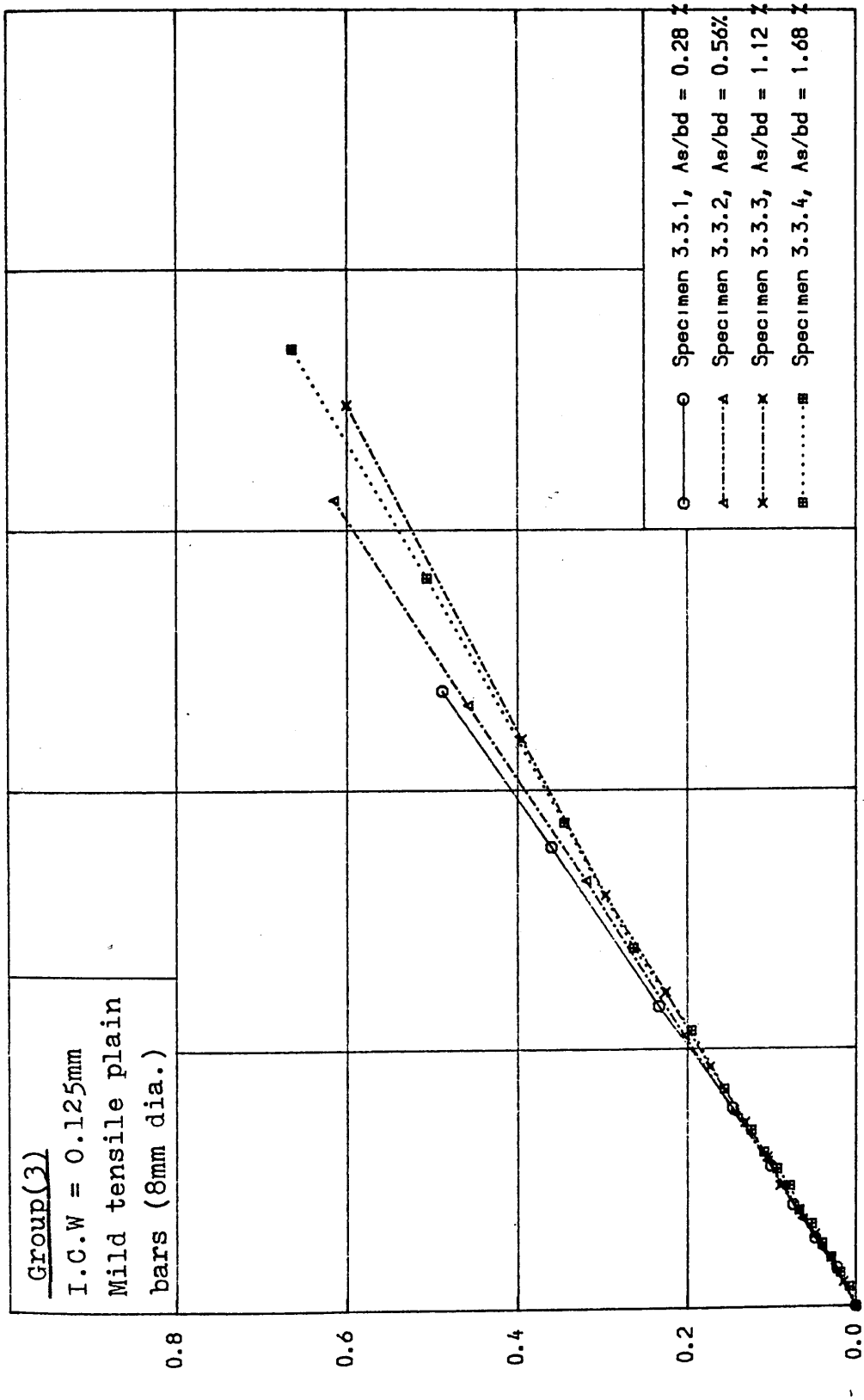

Figure(6.12) Crack width vs. shear displacement for group (3) – series 3 under monotonic load

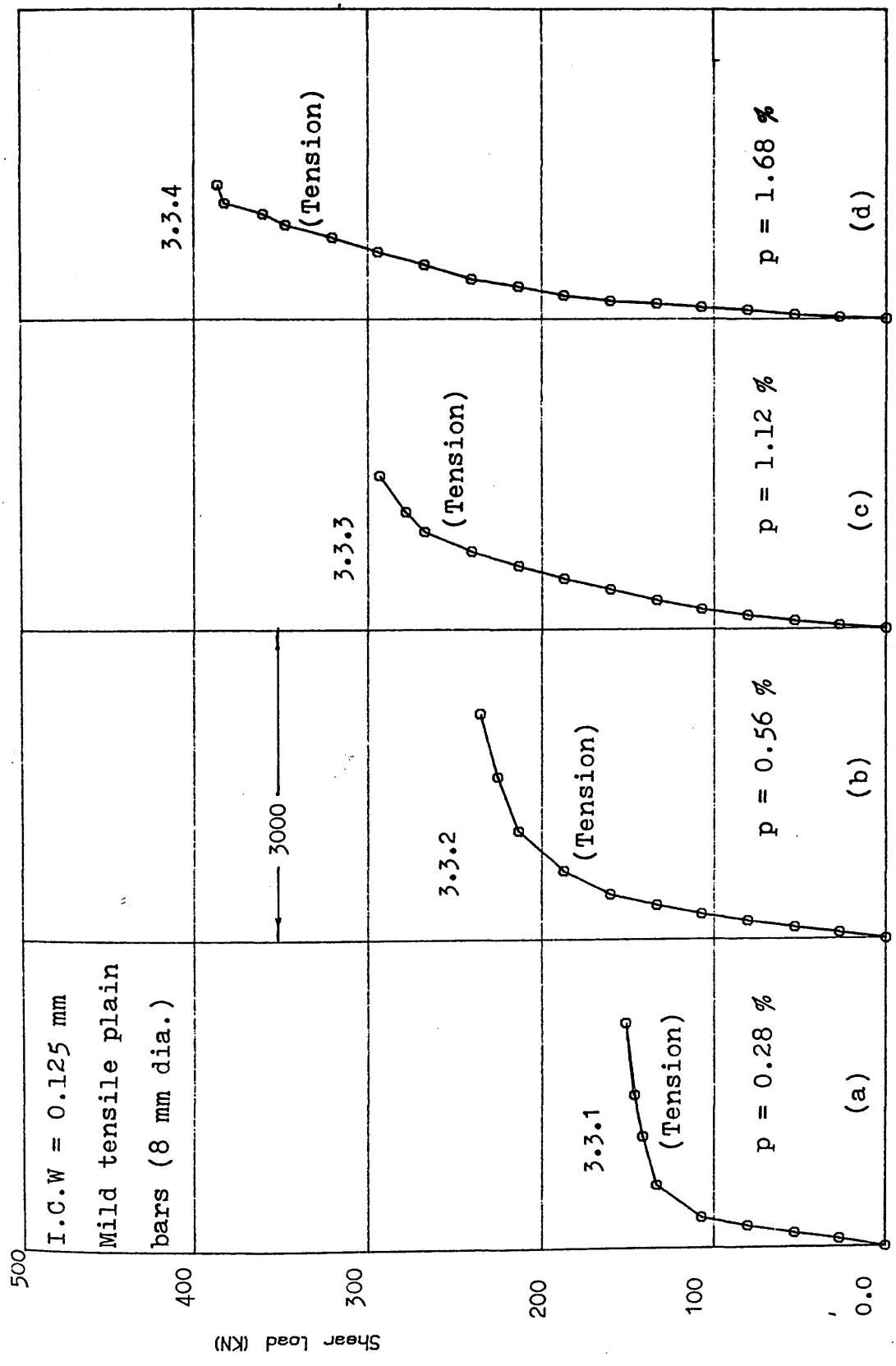

Figure(6.13) Shear load vs. steel strain for group (3) – series 3 under montonic load

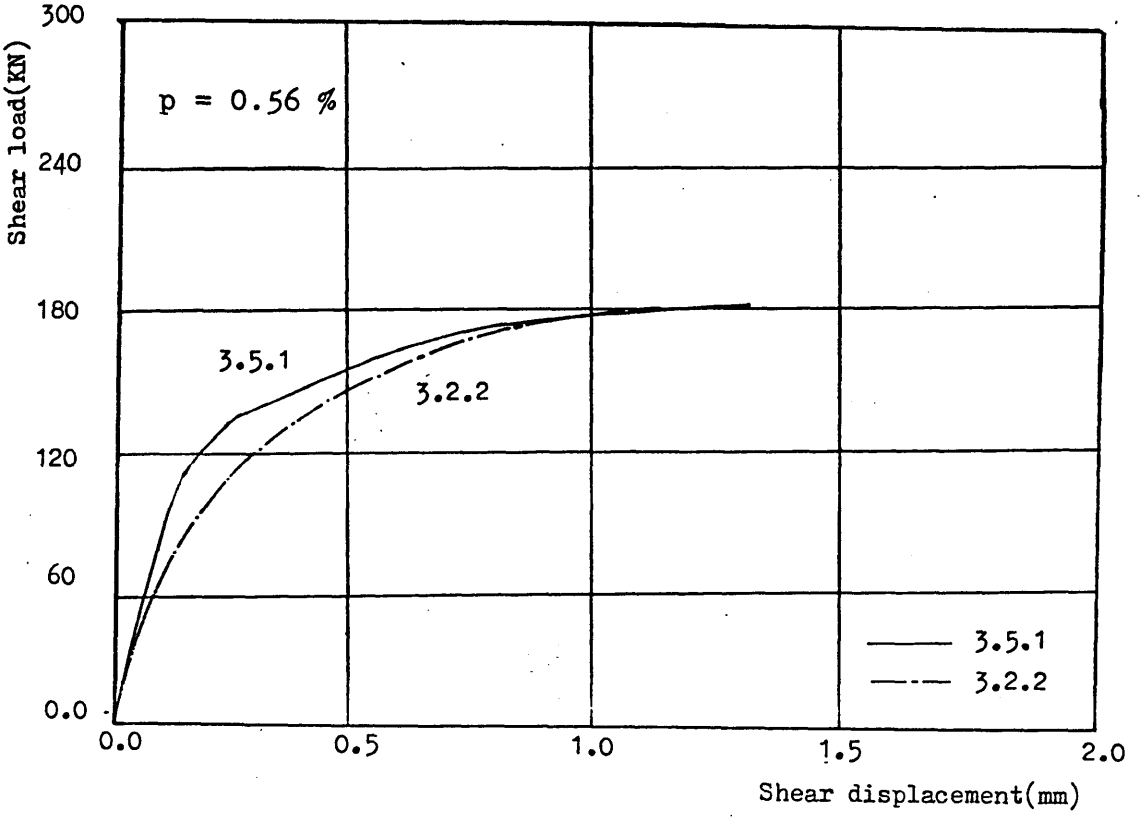

Figure (6.14) Comparison of shear load vs shear displacement for specimens 3.5.1 and 3.2.2 of series 3 (monotonic loading)

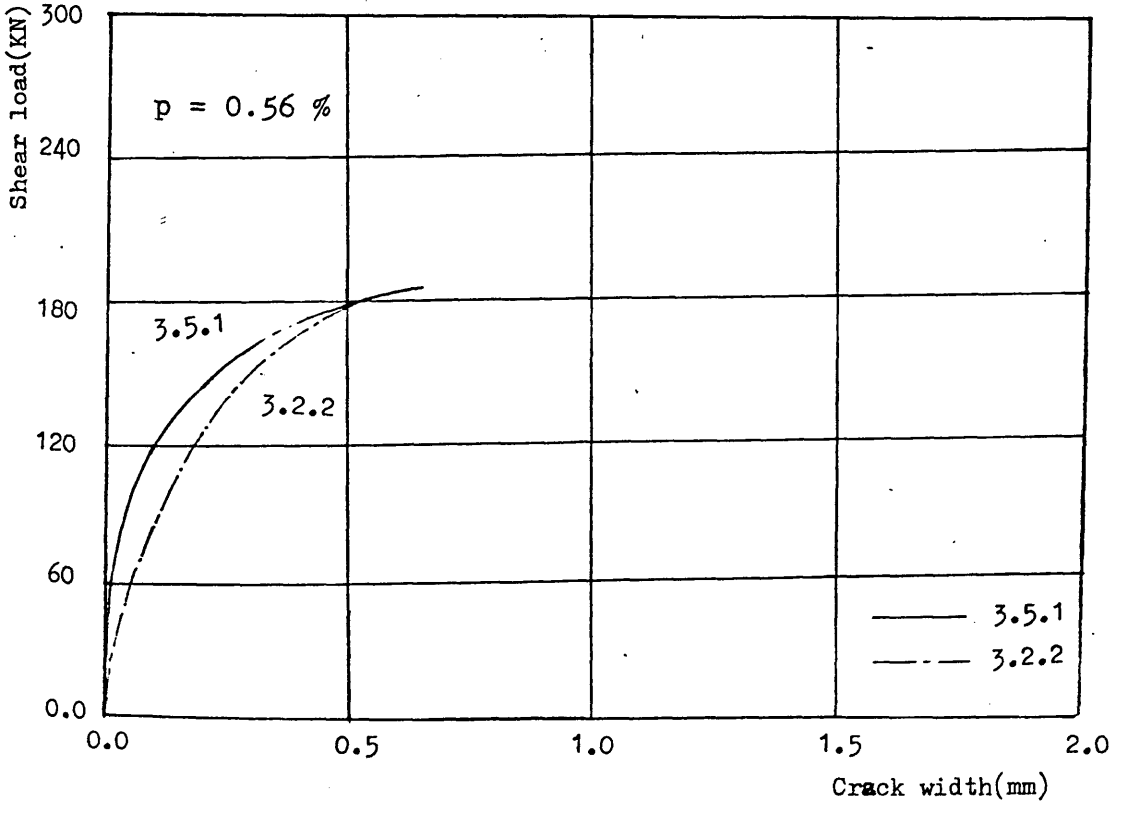

Figure (6.15) Comparison of shear load vs crack width relationships for specimens 3.5.1 and 3.2.2 of series 3 (monotonic loading)

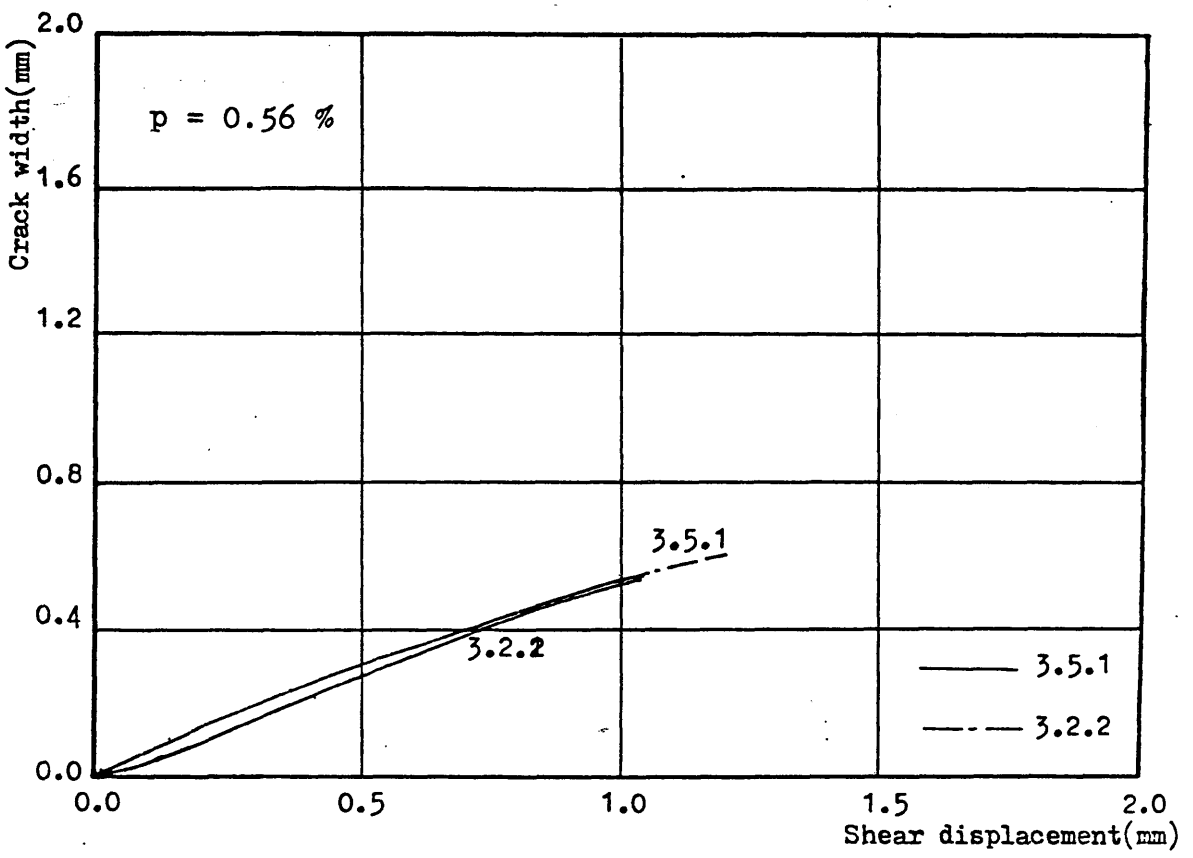

Figure(6.16) Crack width vs. shear displacement for specimens 3.5.1 and 3.2.2

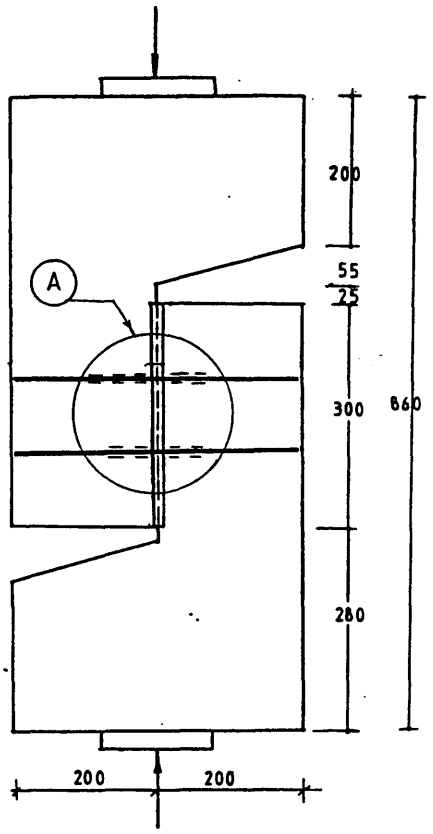

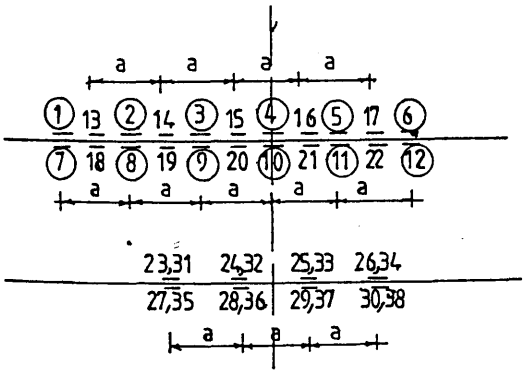

a = 2.5 ϕ

Specimen 3.5.1

Detail (A)

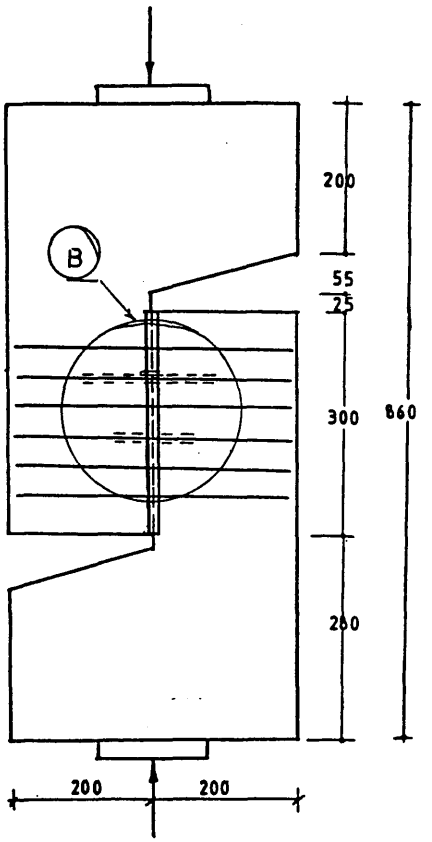

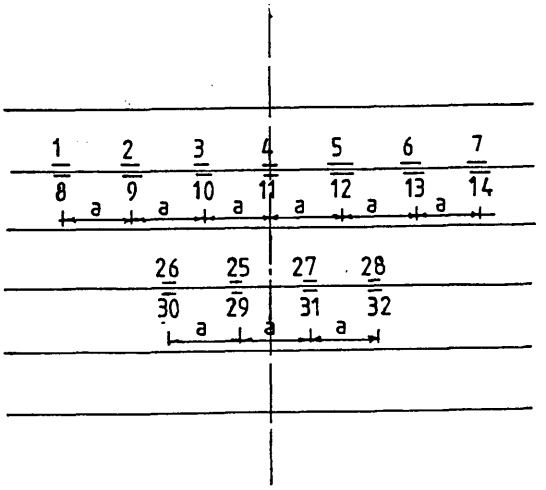

Specimen 3.5.2

Detail (B)

Figure(6.17) Positions of the steel strain gauges for group(5)

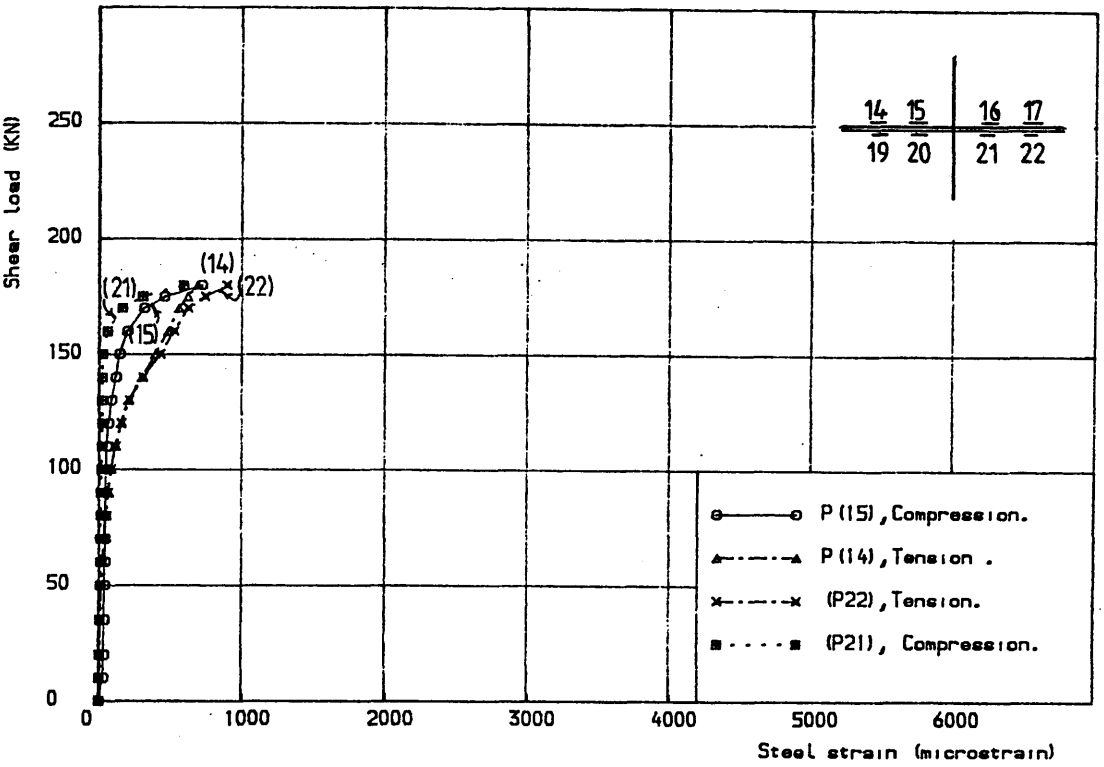

Figure (6.18 a) Shear load vs steel strain for specimen 3.5.1, (positions 14, 15 - 21, 22)

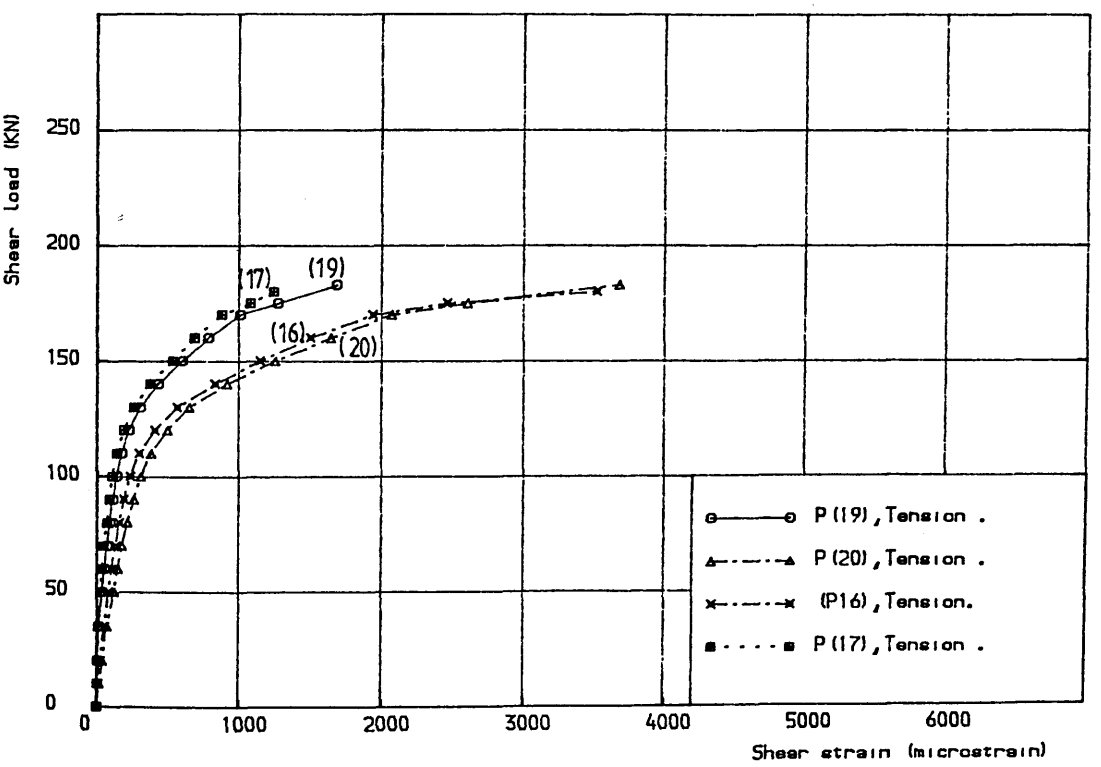

Figure (6.18 b) Shear load vs steel strain for specimen 3.5.1, (positions 14, 20 - 16, 17)

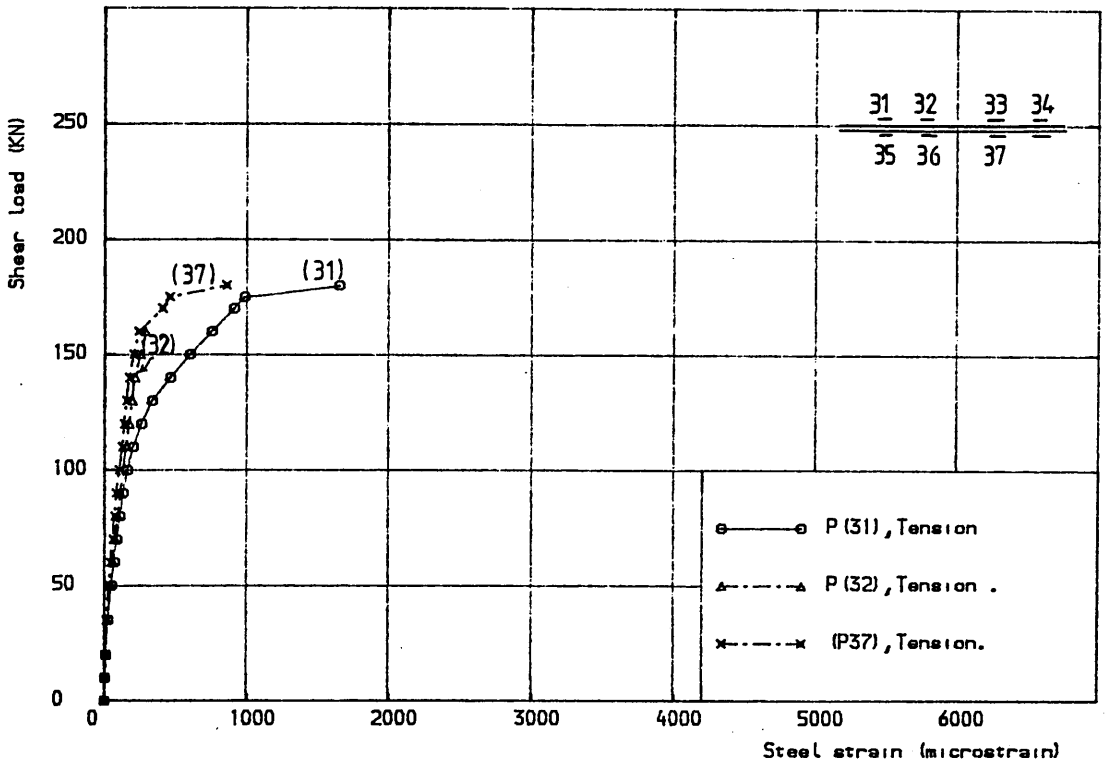

Figure (6.19 a) Shear load vs steel strain for specimen 3.5.1, positions 31, 32 - 37, 38

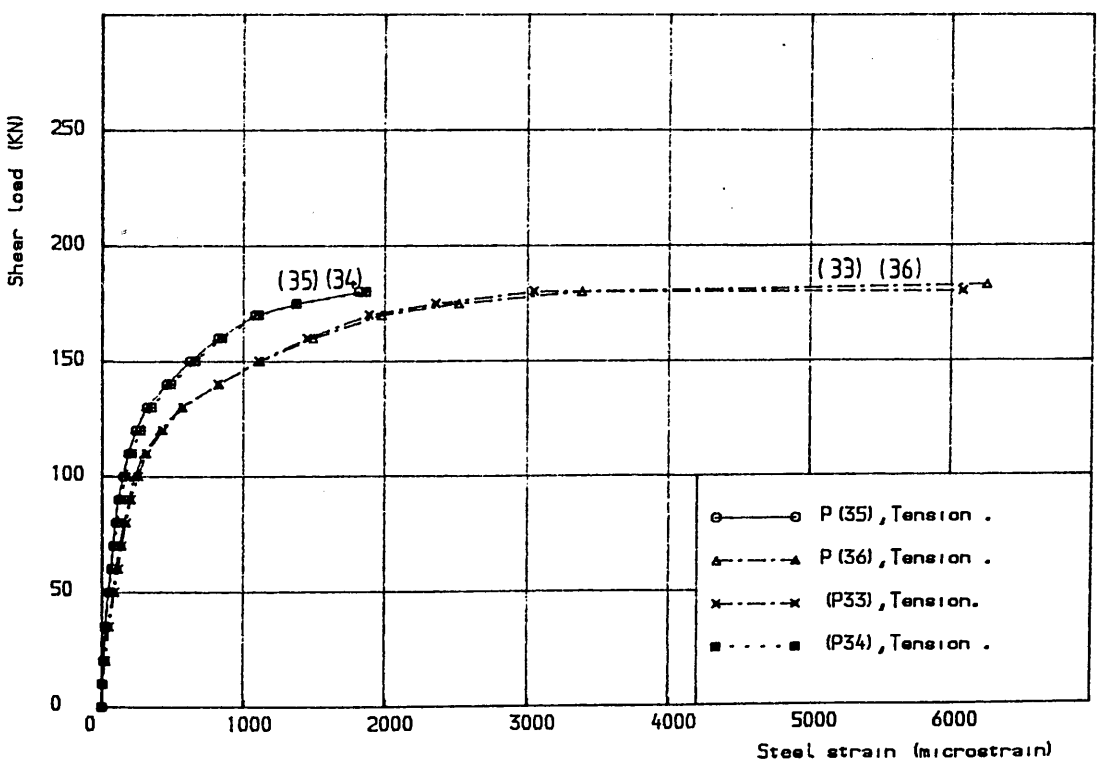

Figure (6.19 b) Shear load vs steel strain for specimen, positions 35, 36 - 33, 34

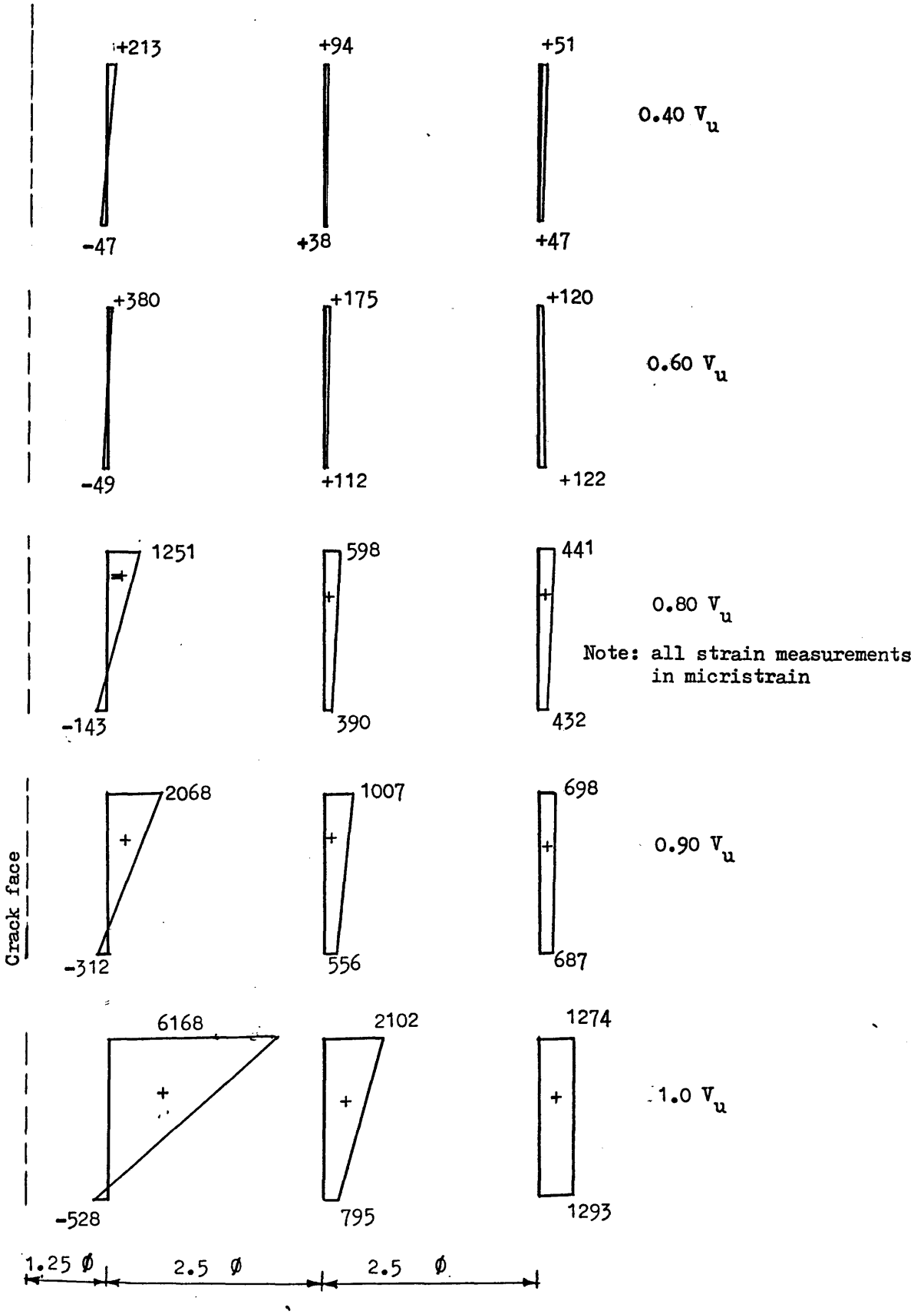

Figure (6.20) Strain Distribution across a transverse reinforcing bar and along a distance of 6.25Ø measured from the crack face, specimen 3.5.1

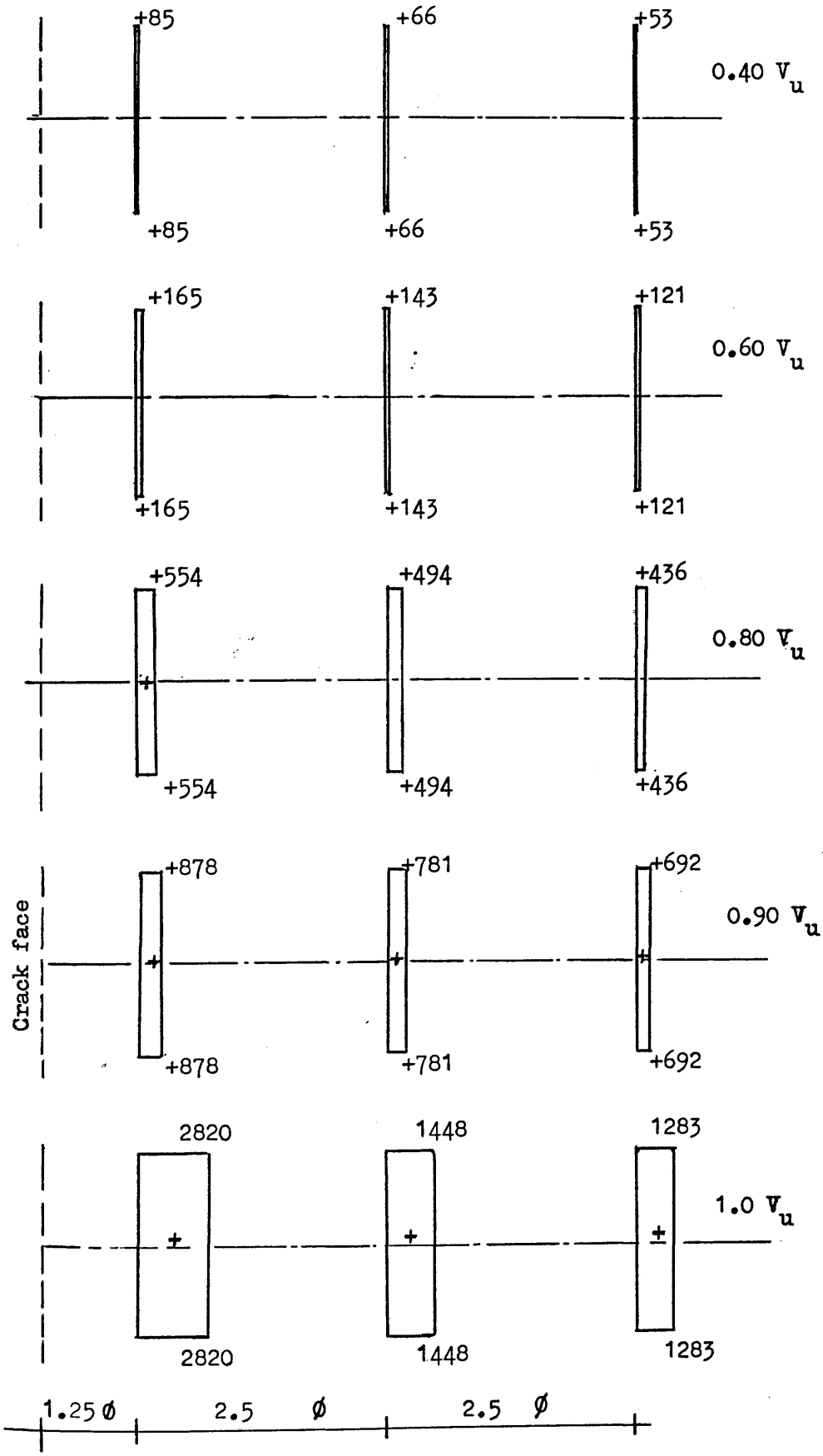

Figure (6.21) Distribution of the direct strain of specimen 3.5.1

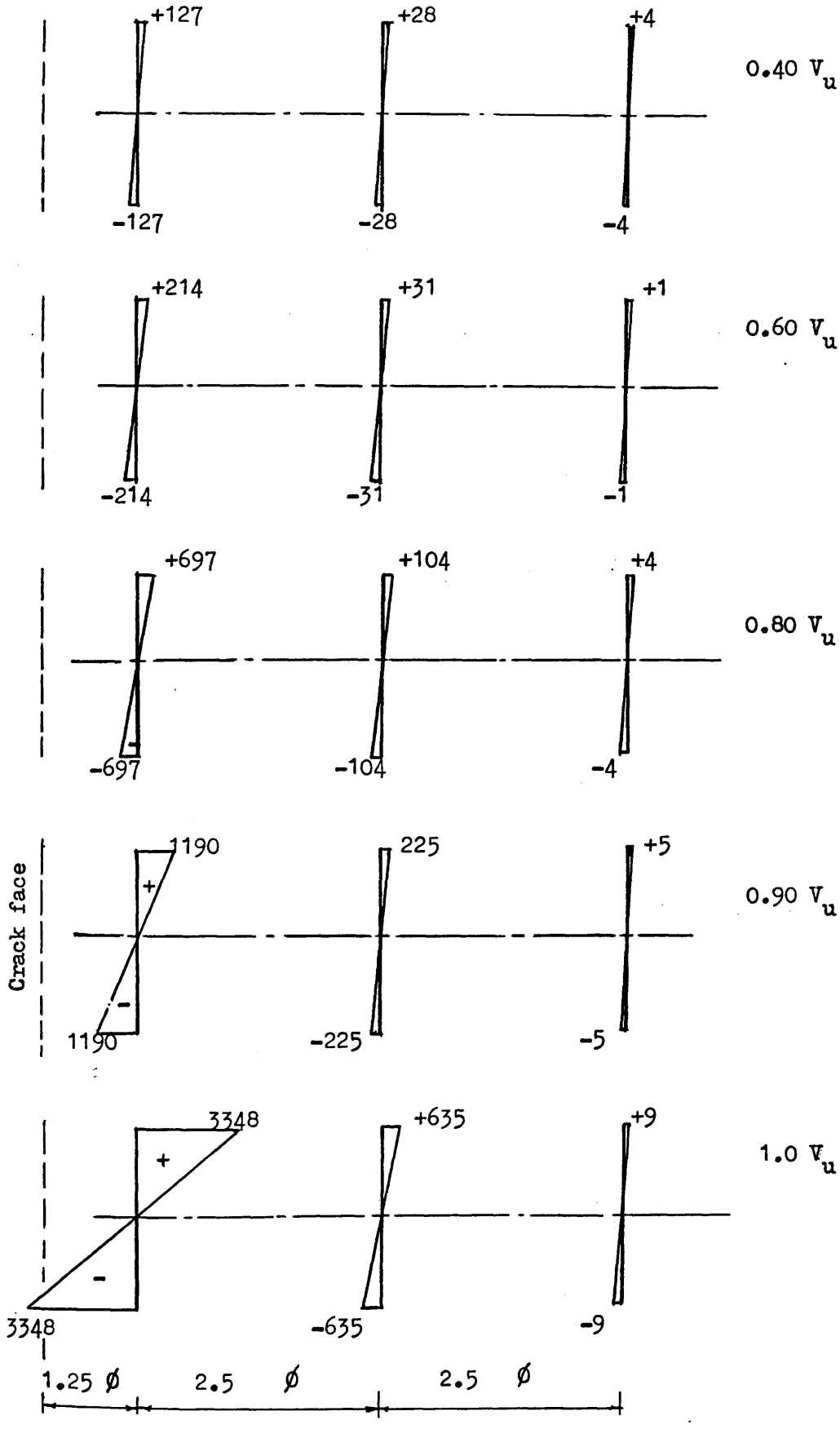

Figure (6.22) Distribution of the flexural strain of specimen 3.5.1

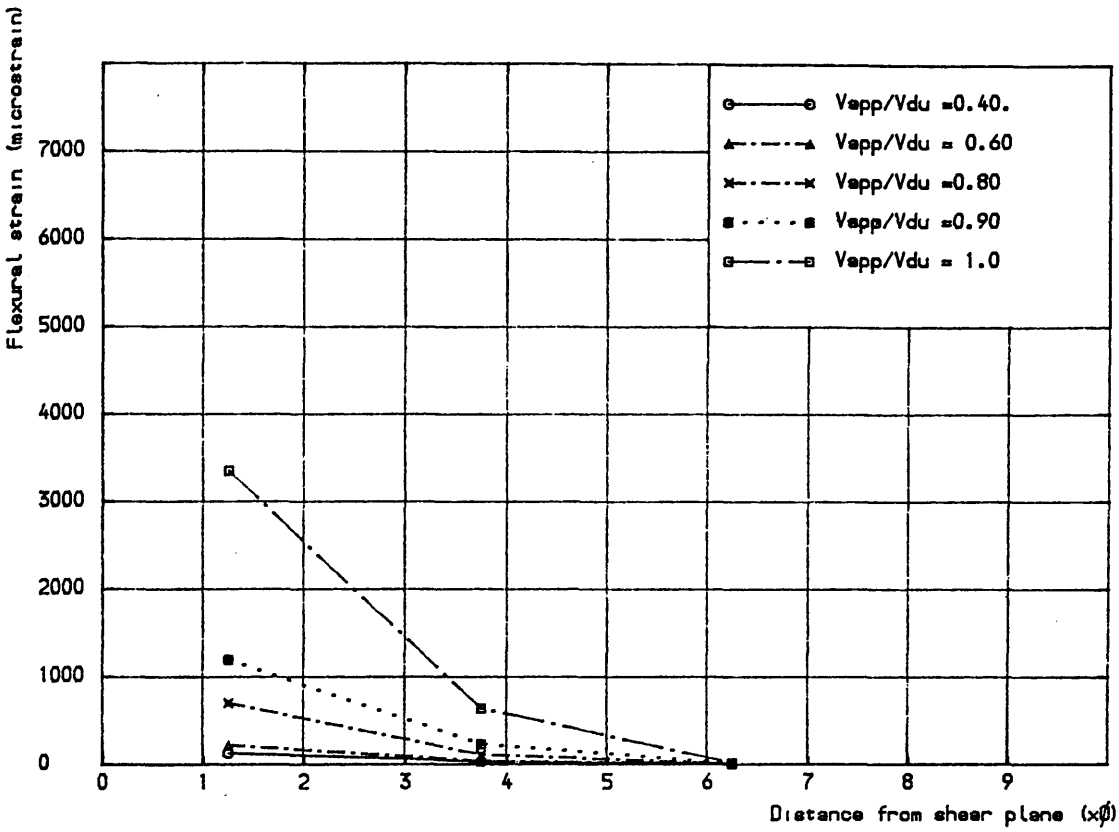

Figure (6.23) Distribution of flexural steel strain along a distance 6.25Ø from the crack plane (specimen 3.5.1)

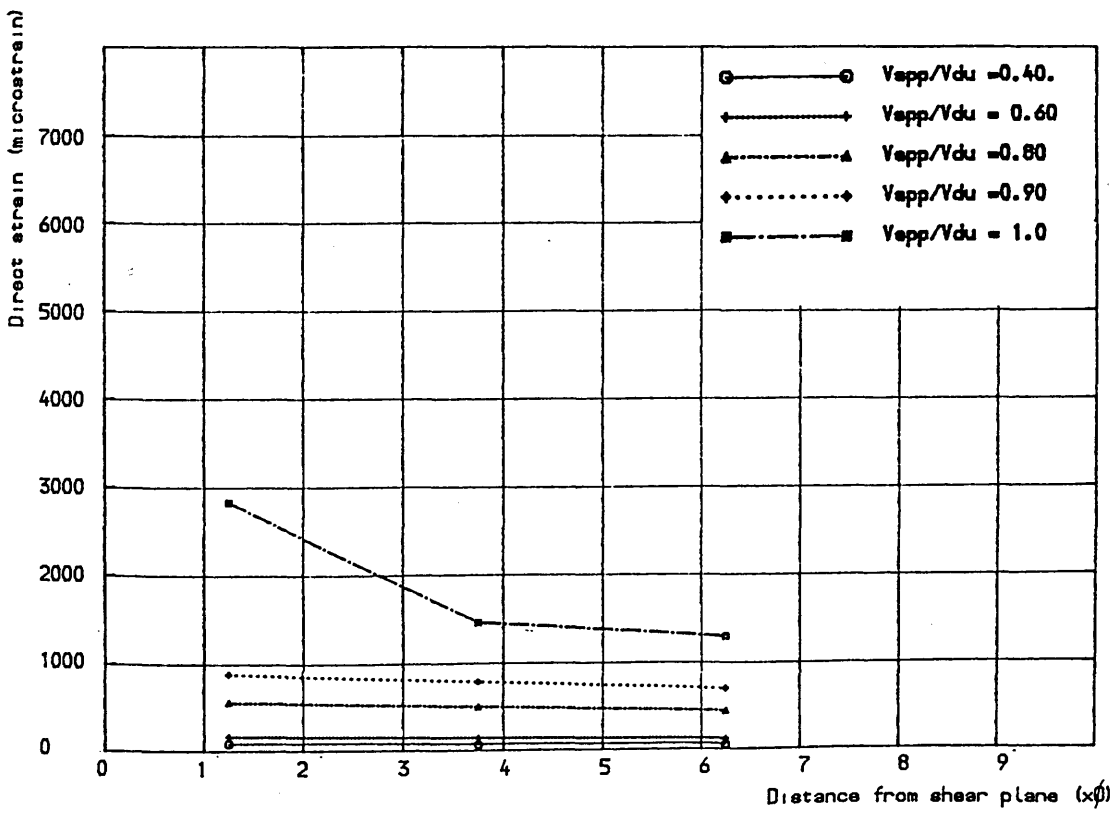

Figure (6.24) Distribution of direct steel strain along a distance 6.25Ø from the shear plane (specimen 3.5.1)

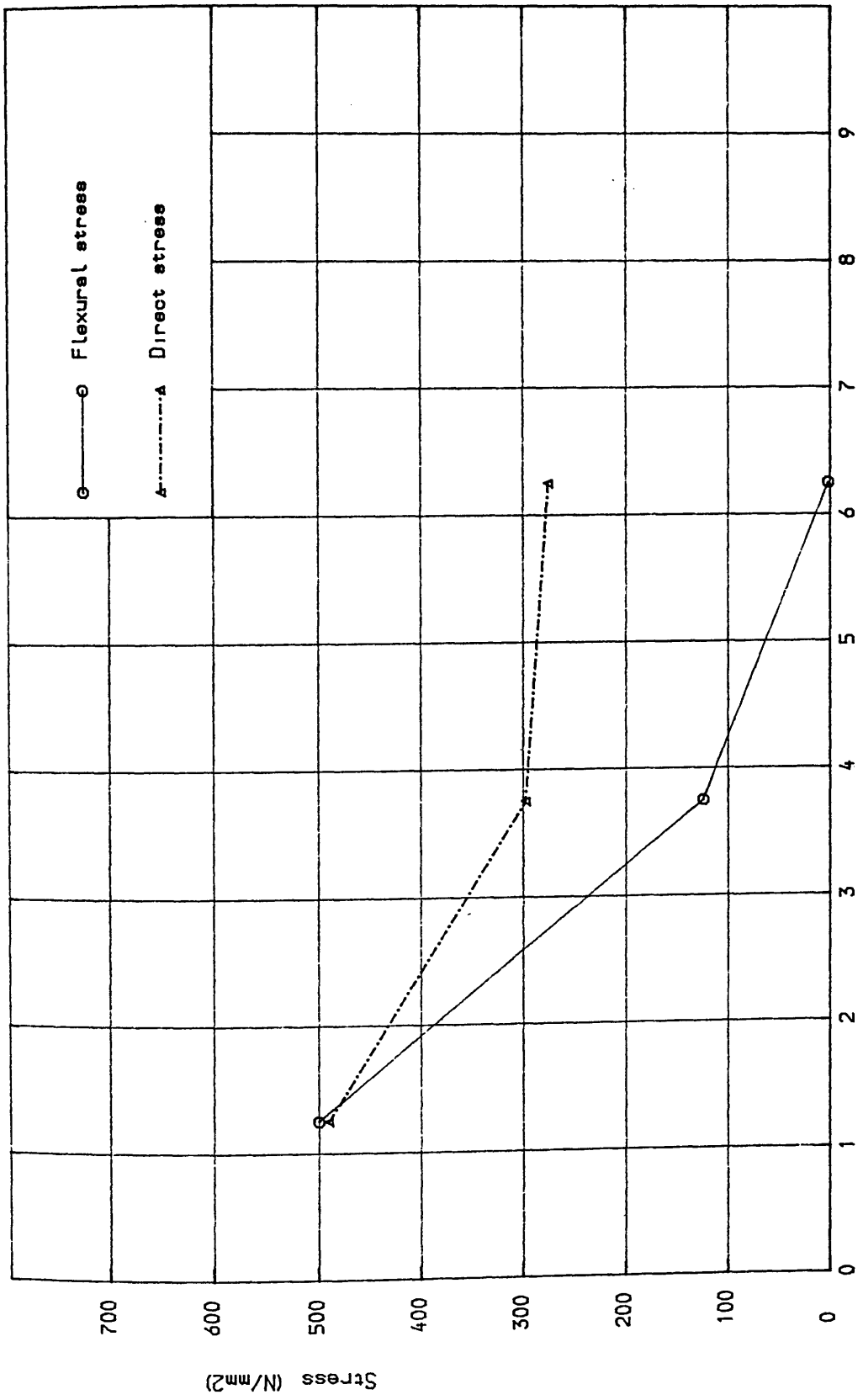

Figure (6.25) Distribution of flexural and direct stress along a distance 6.25ϕ from shear plane (specimen 3.5.1)

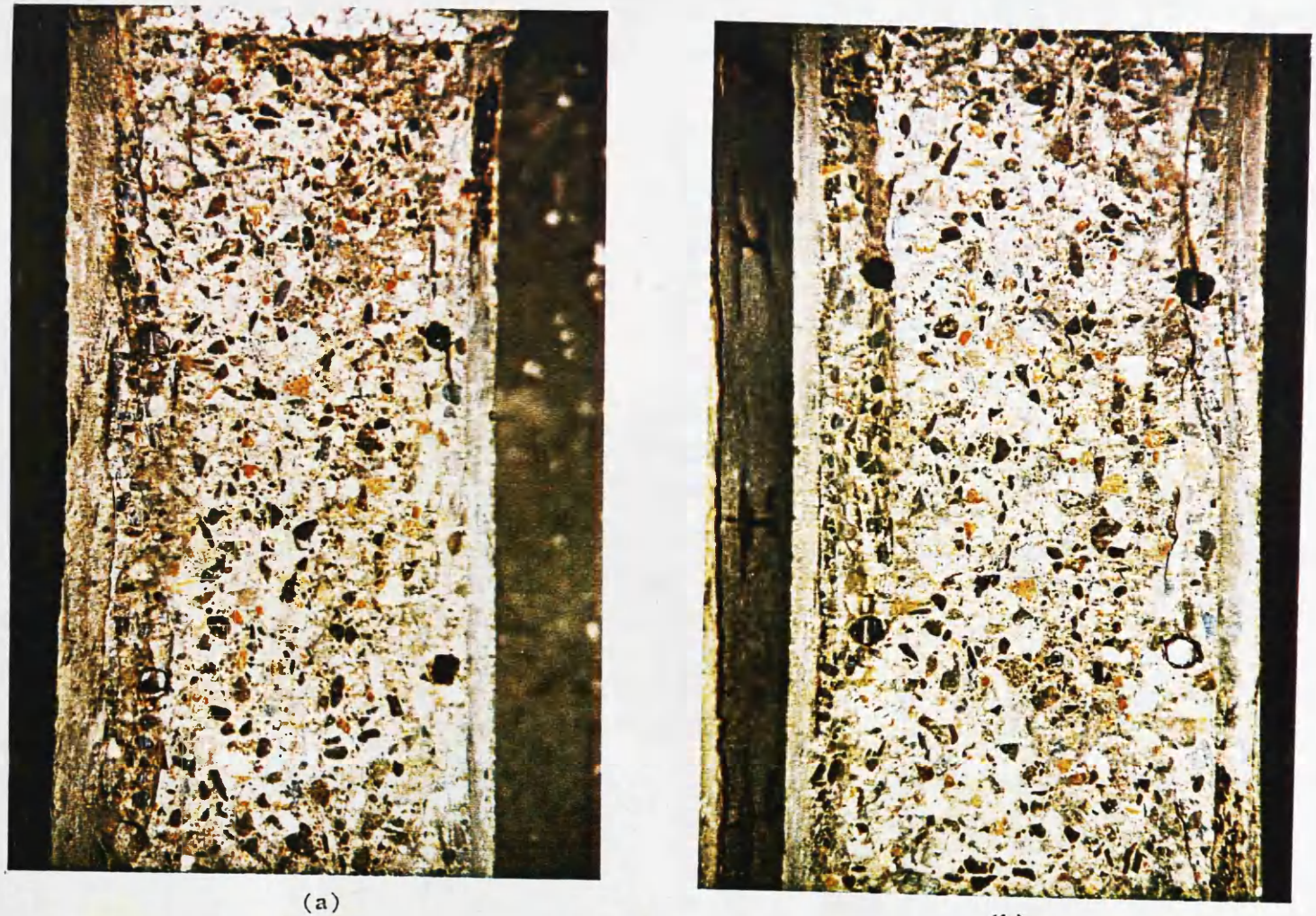

(a) (b)

Figure(6.26) Crack pattern of the two faces of the shear plane for specimen 3.5.1

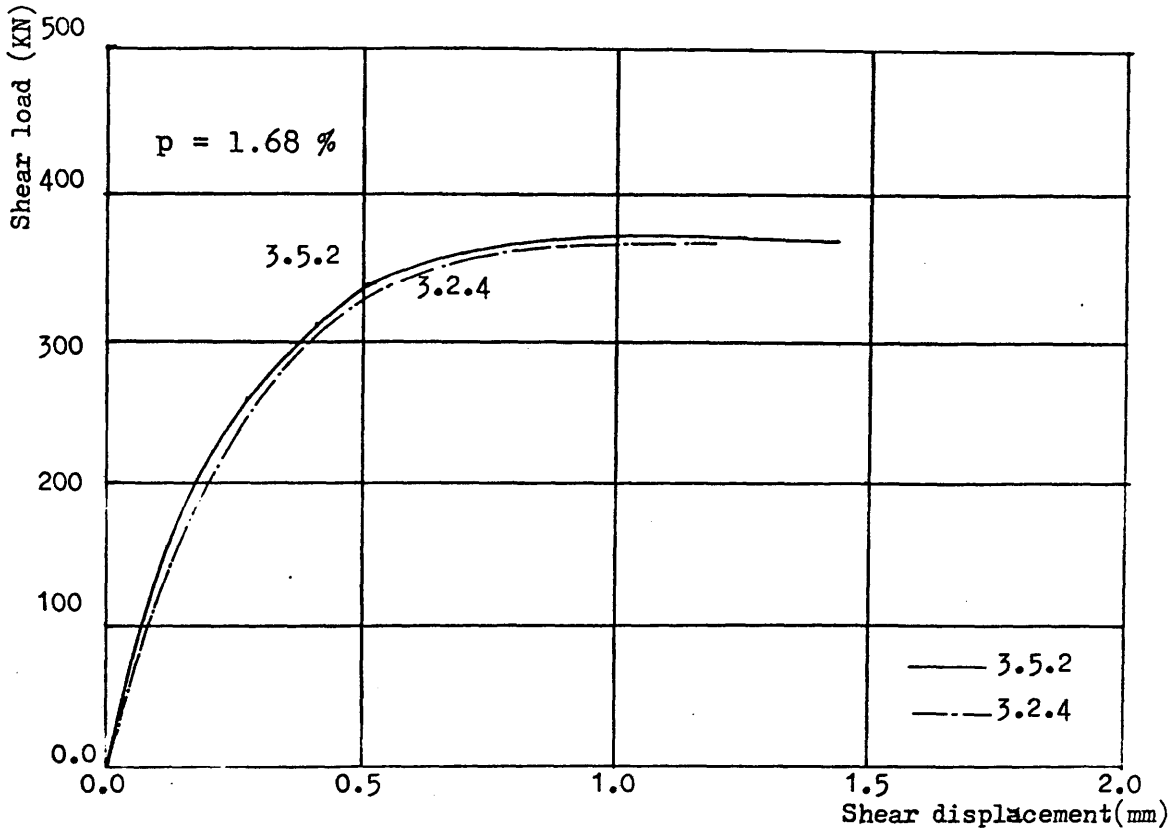

Figure(6.27) Shear load vs shear displacement for specimens 3.5.2 and 3.2.4 .

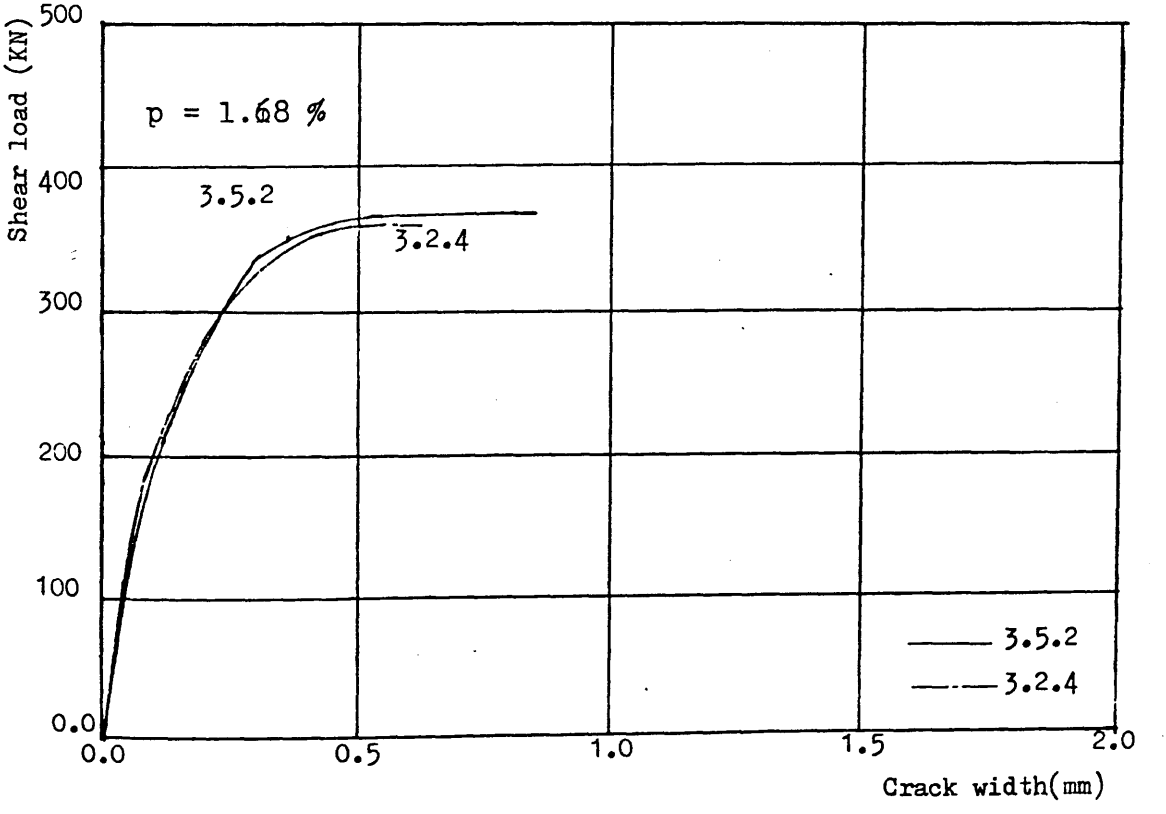

Figure(6.28) Shear load vs crack width for specimens 3.5.2 and 3.2.4

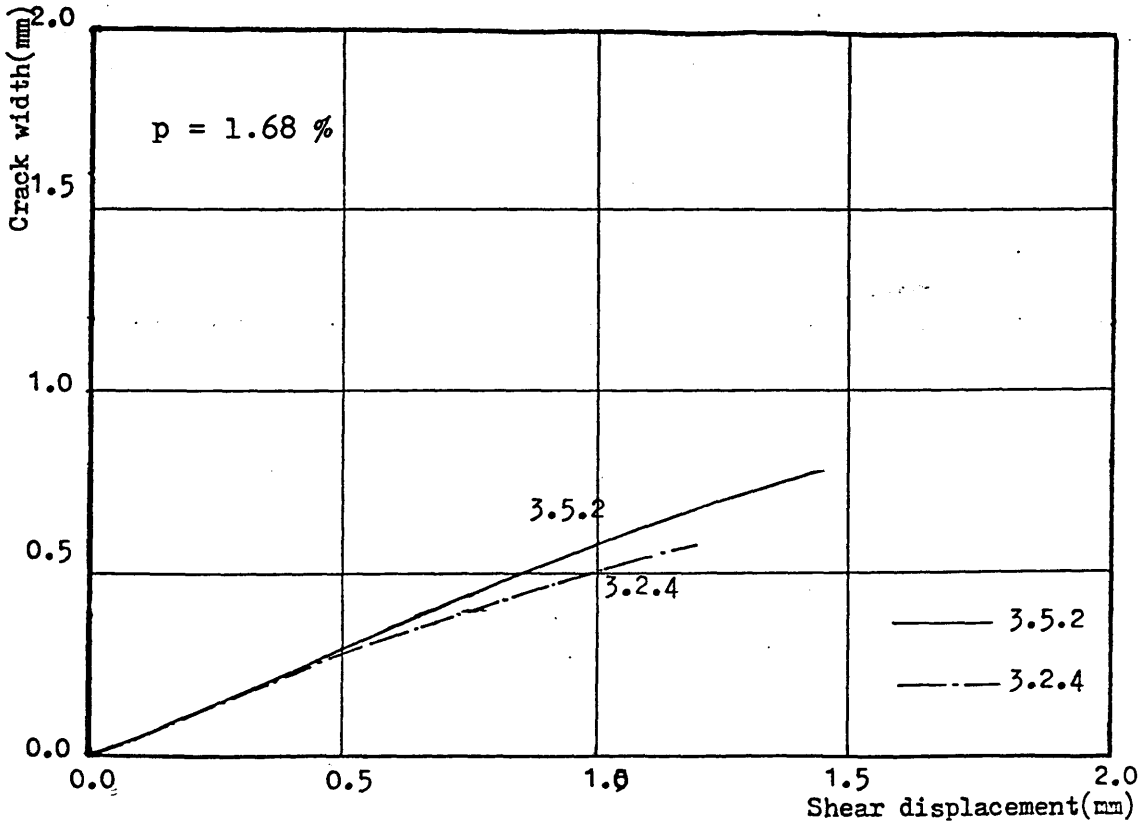

Figure(6.29) Crack width vs shear displacement for specimens 3.5.2 and 3.2.4

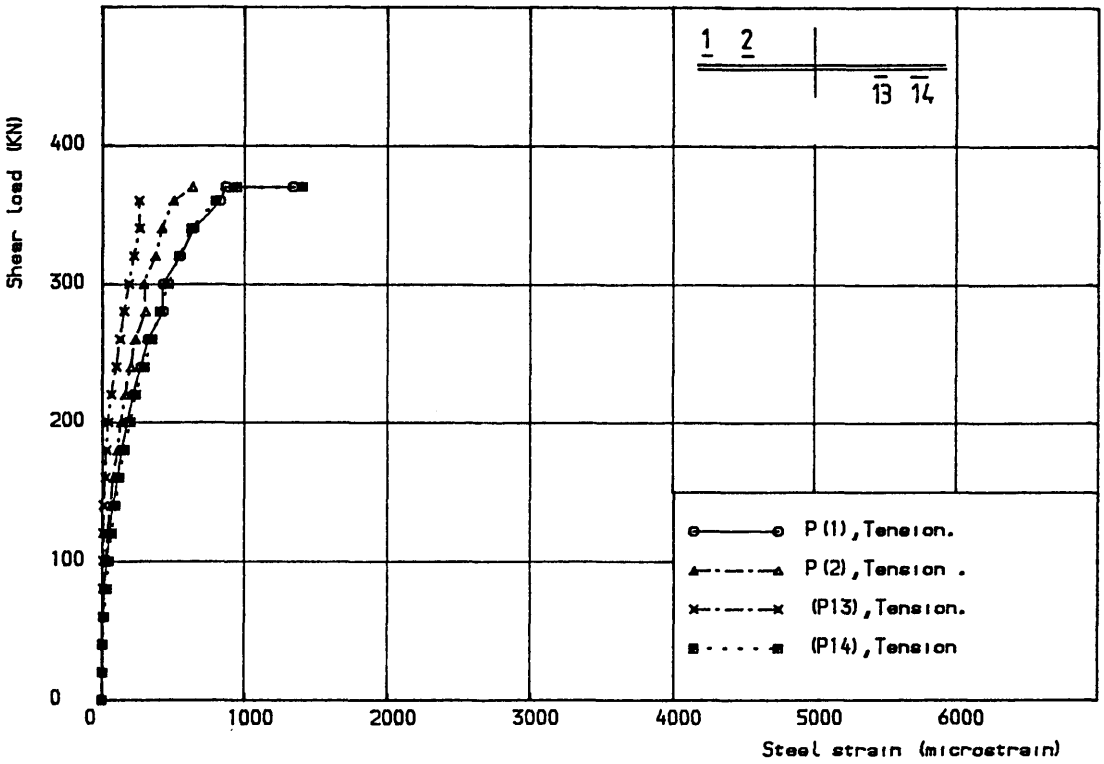

Figure (6.30) Shear load vs steel strain for specimen 3.5.2 (positions 1,2 - 13,14)

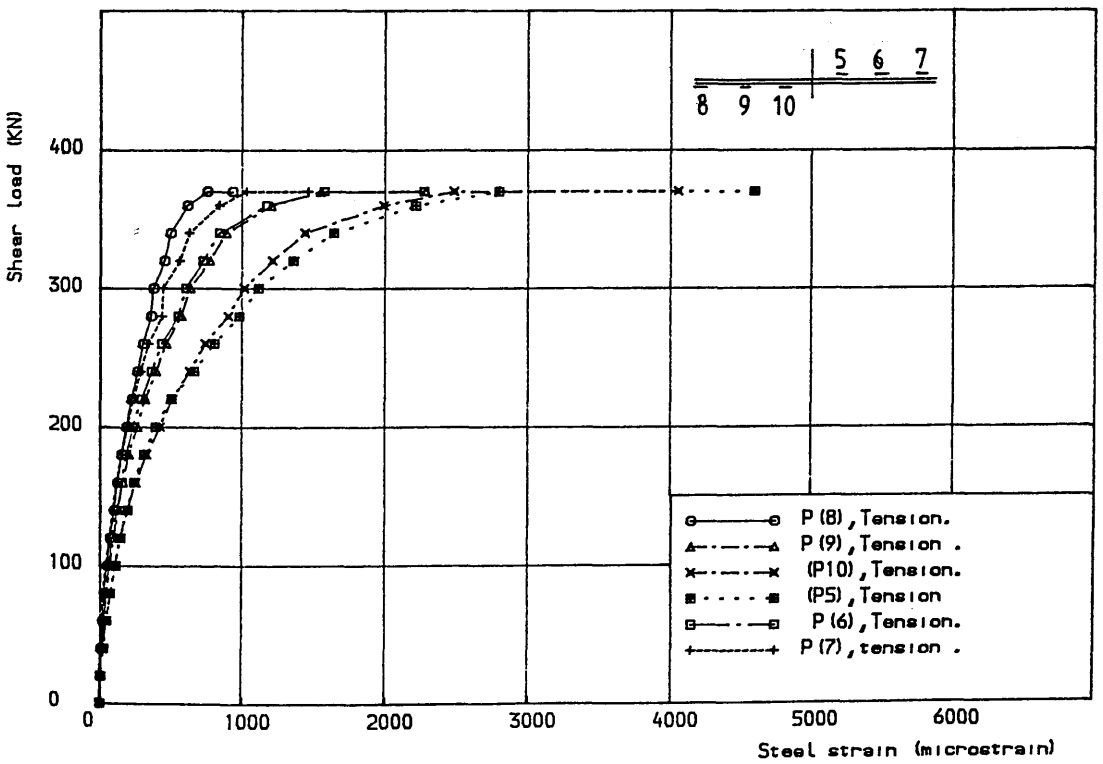

Figure (6.31) Shear load vs steel strain for specimen 3.5.2 (positions 5,6,7 - 8,9,10)

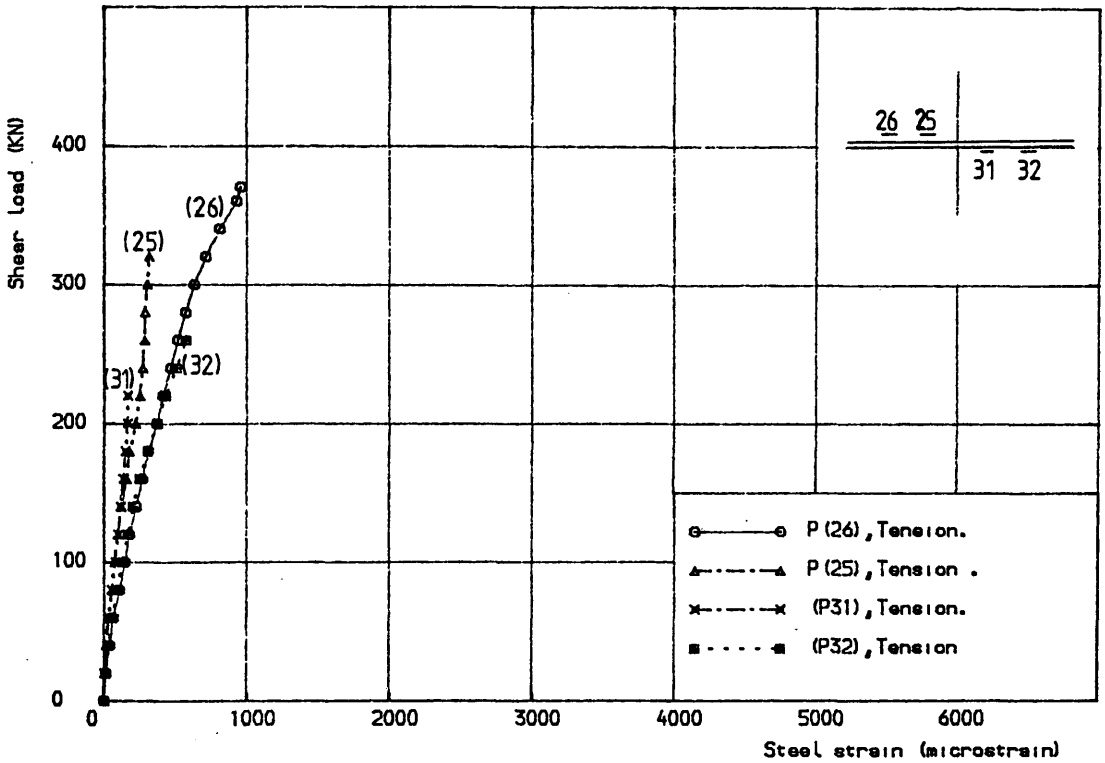

Figure (6.32) Shear load vs steel strain for specimen 3.5.2
(positions 25,26 - 31,32)

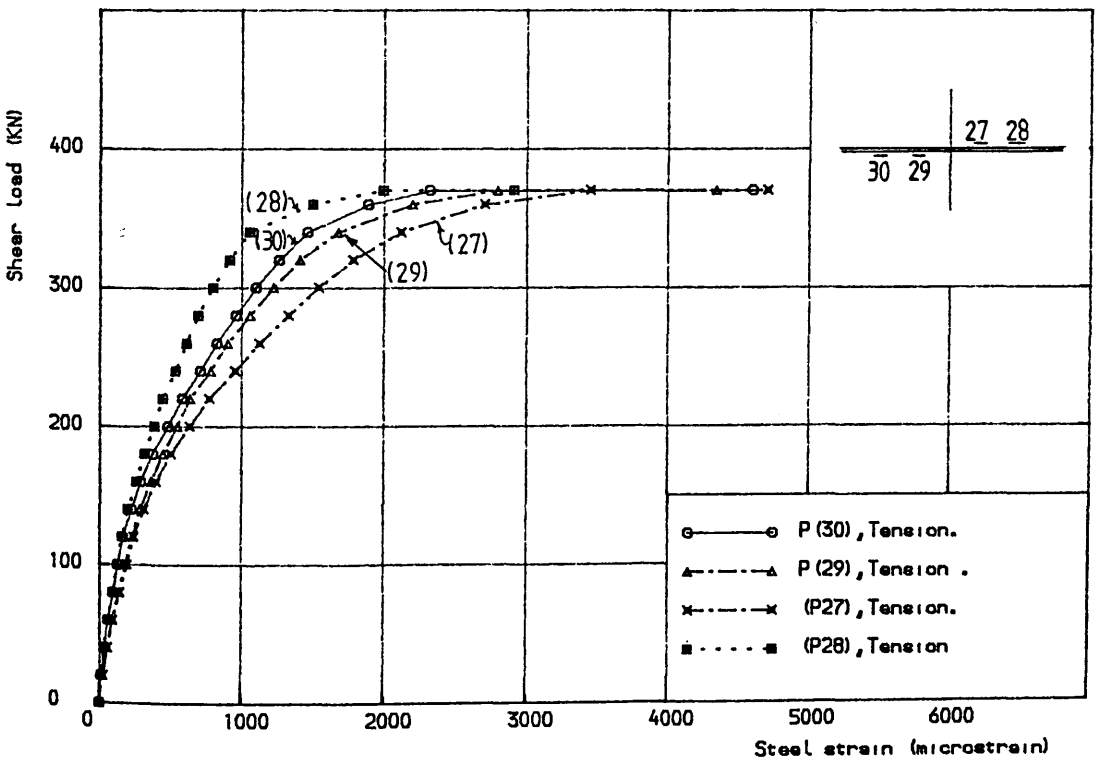

Figure (6.33) Shear load vs steel strain for specimen 3.5.2
(positions 29,30 - 27,28)

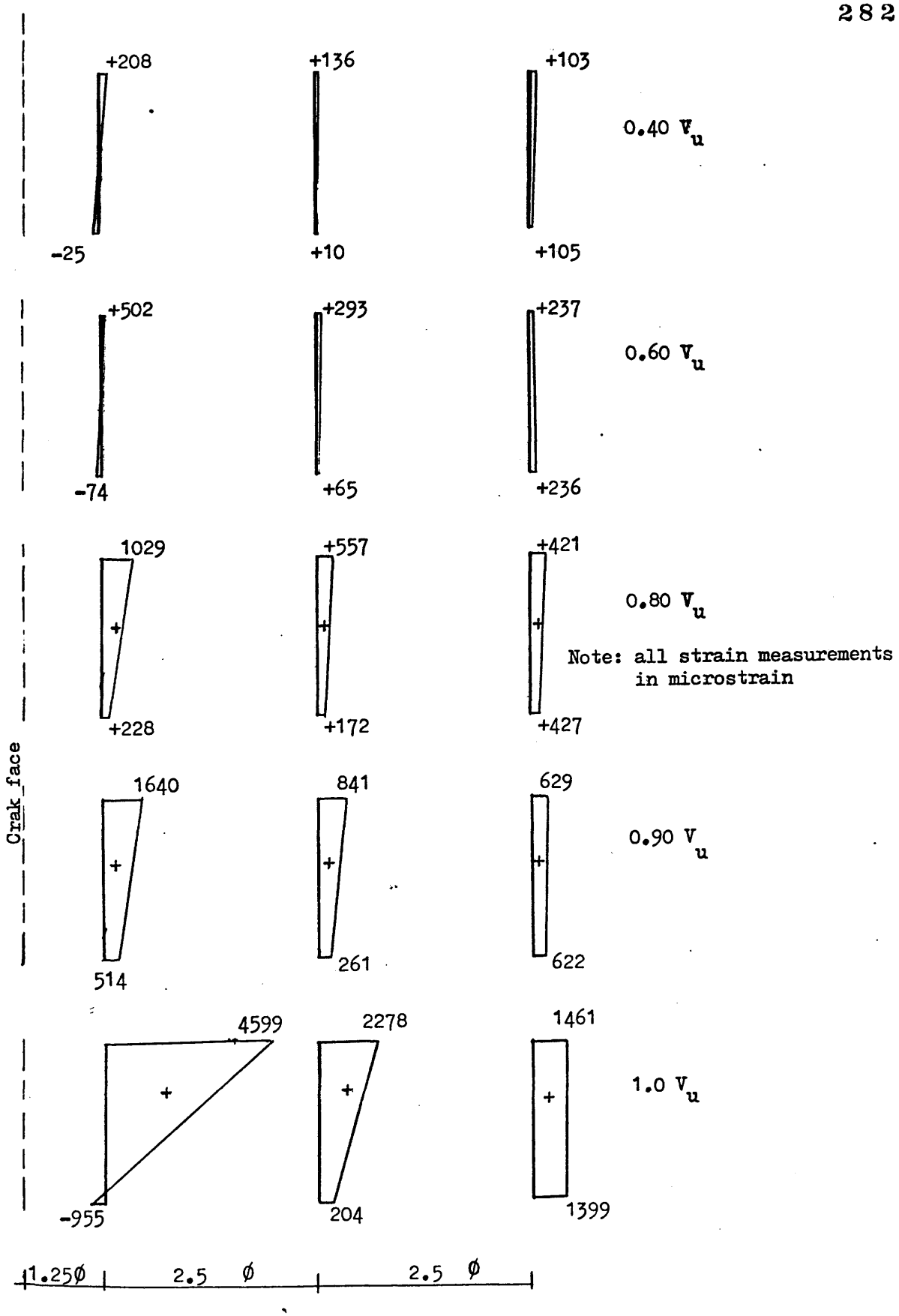

Figure (6.34) Strain distribution across a transverse reinforcing bar and along a distance of 6.25 Ø measured from the crack face specimen 3.5.2

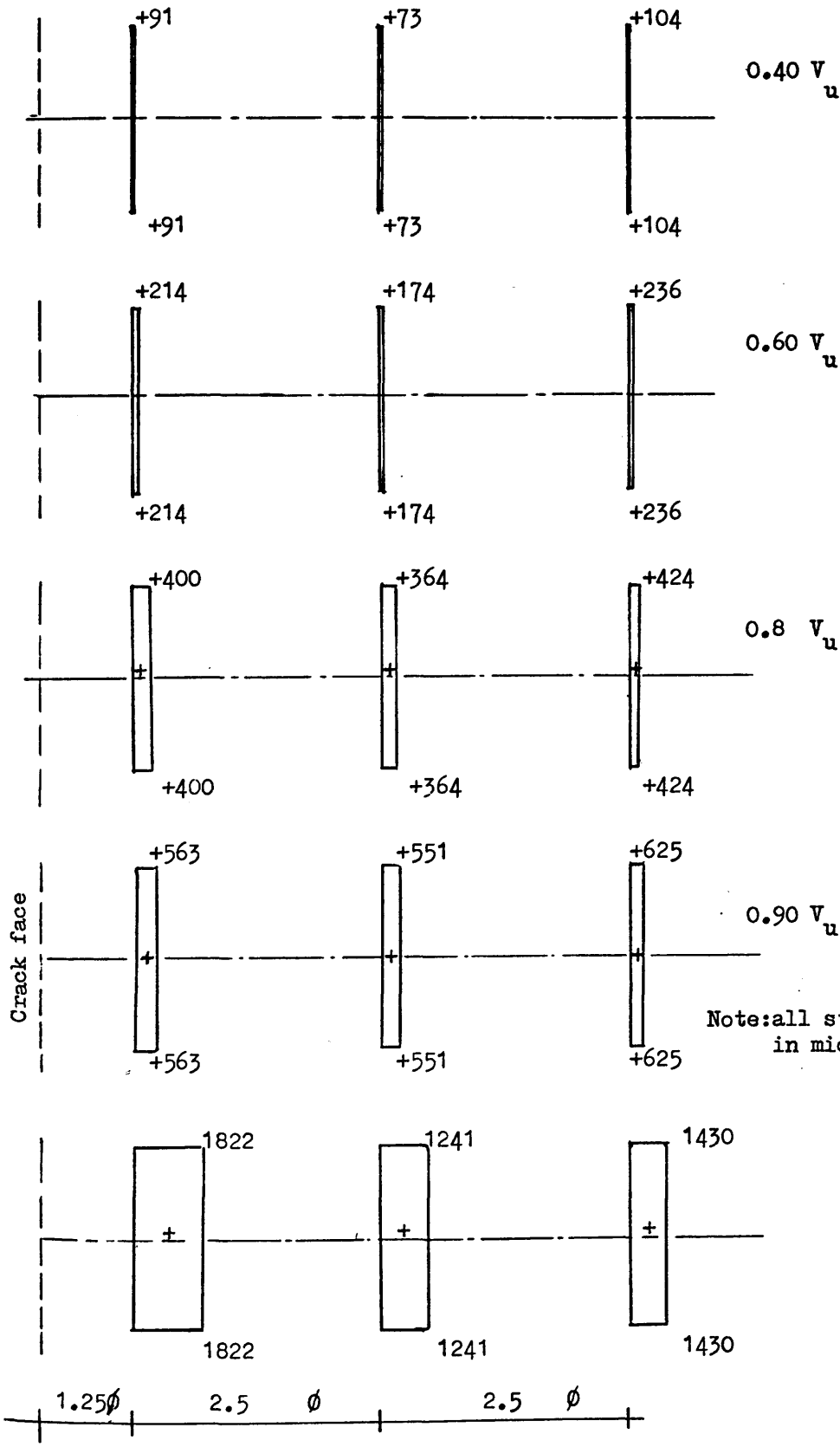

Figure (6.35) Distribution of the direct strain of specimen 3.5.2

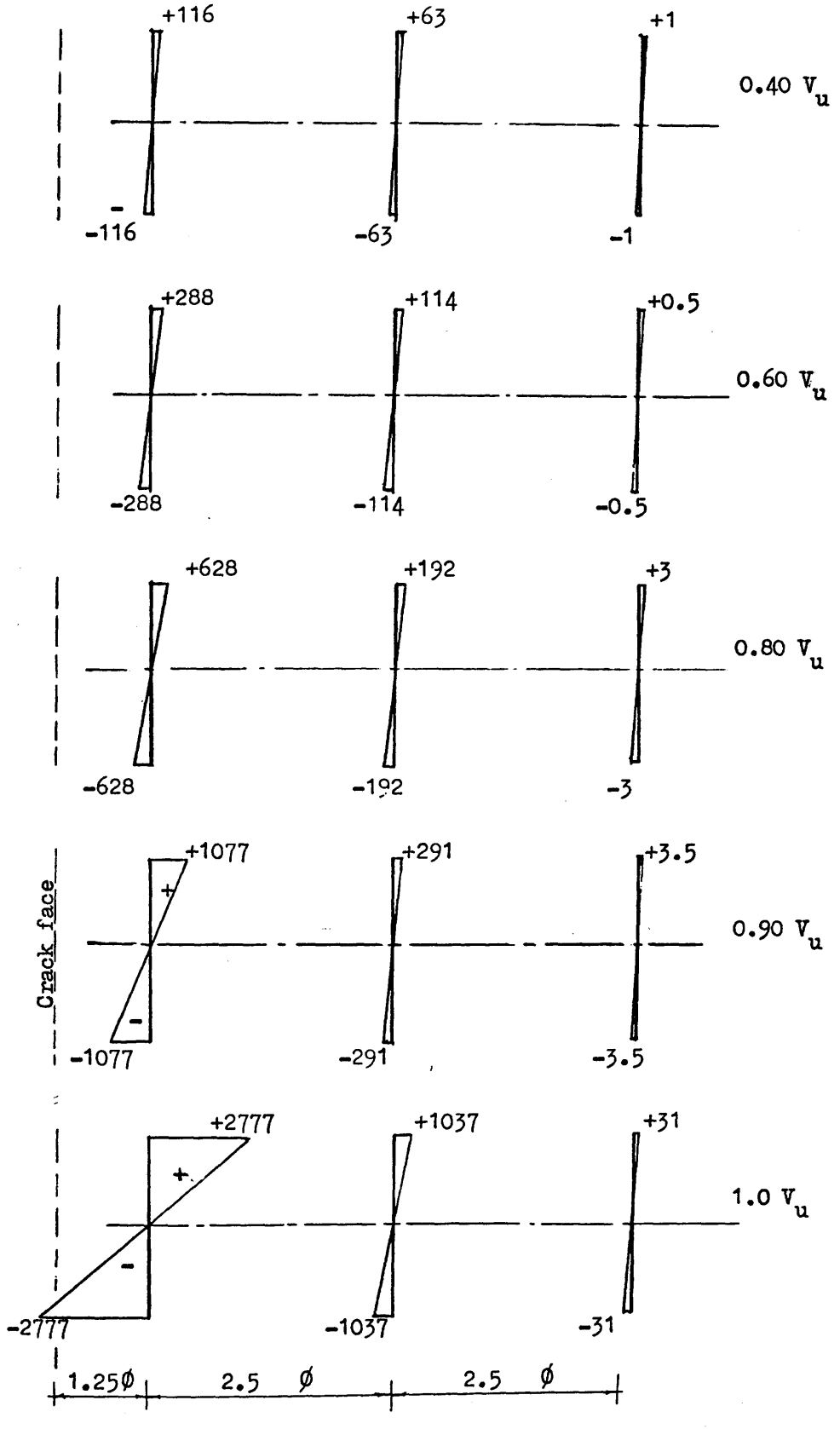

Figure (6.36) Distribution of the flexural strain of specimen 3.5.2

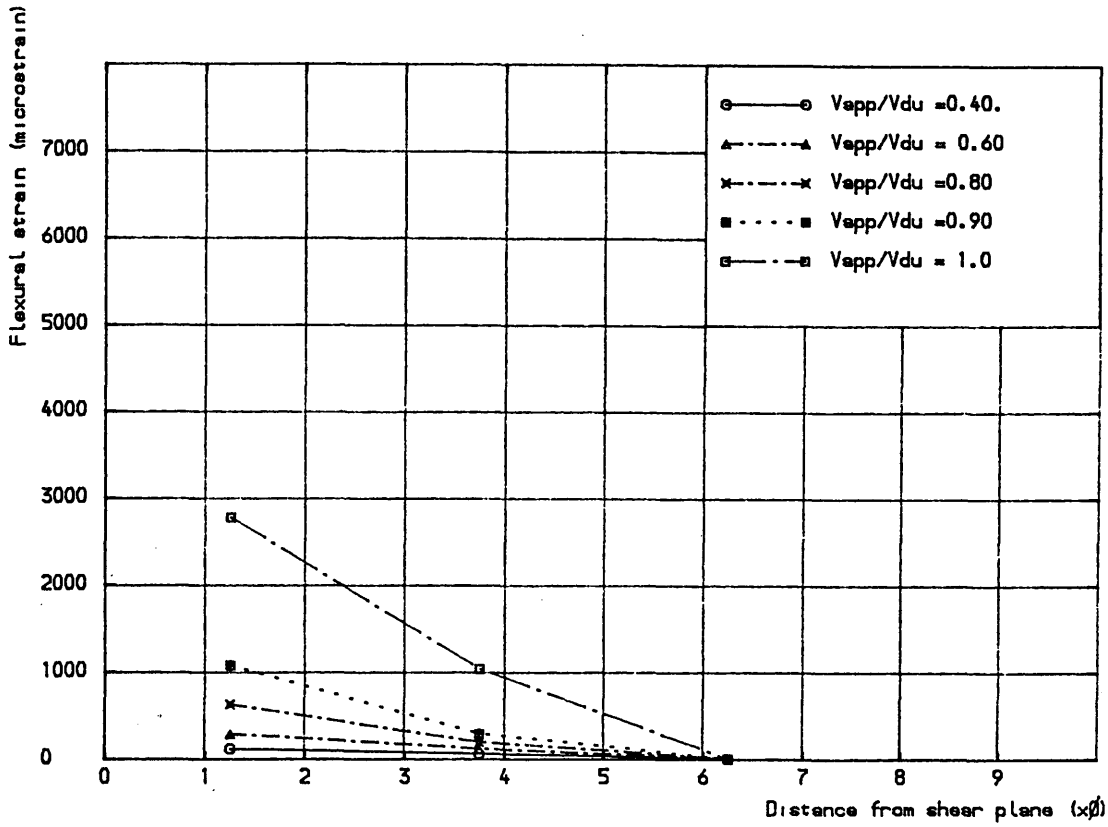

Figure(6.37) Distribution of the flexural steel strain along a distance 6.25Φ from the shear plane, spec. 3.5.2

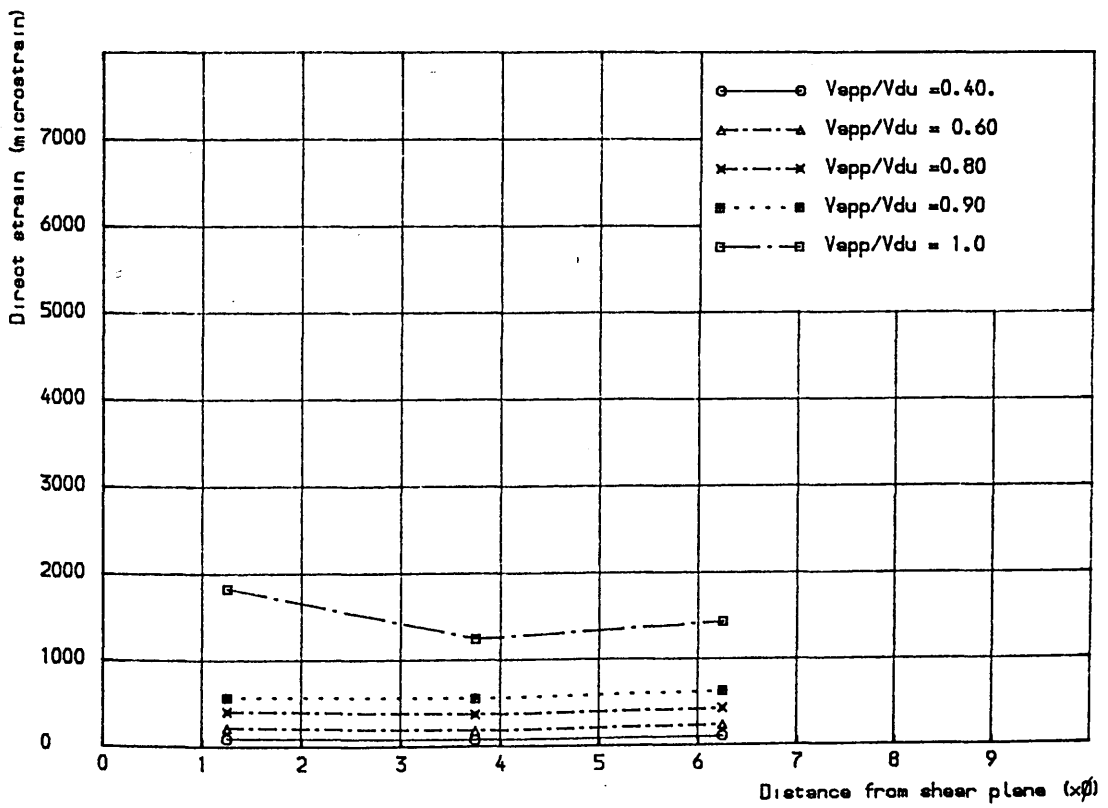

Figure(6.38) Distribution of the direct steel strain along a distance 6.25Φ from the shear plane, speciemen 3.5.2

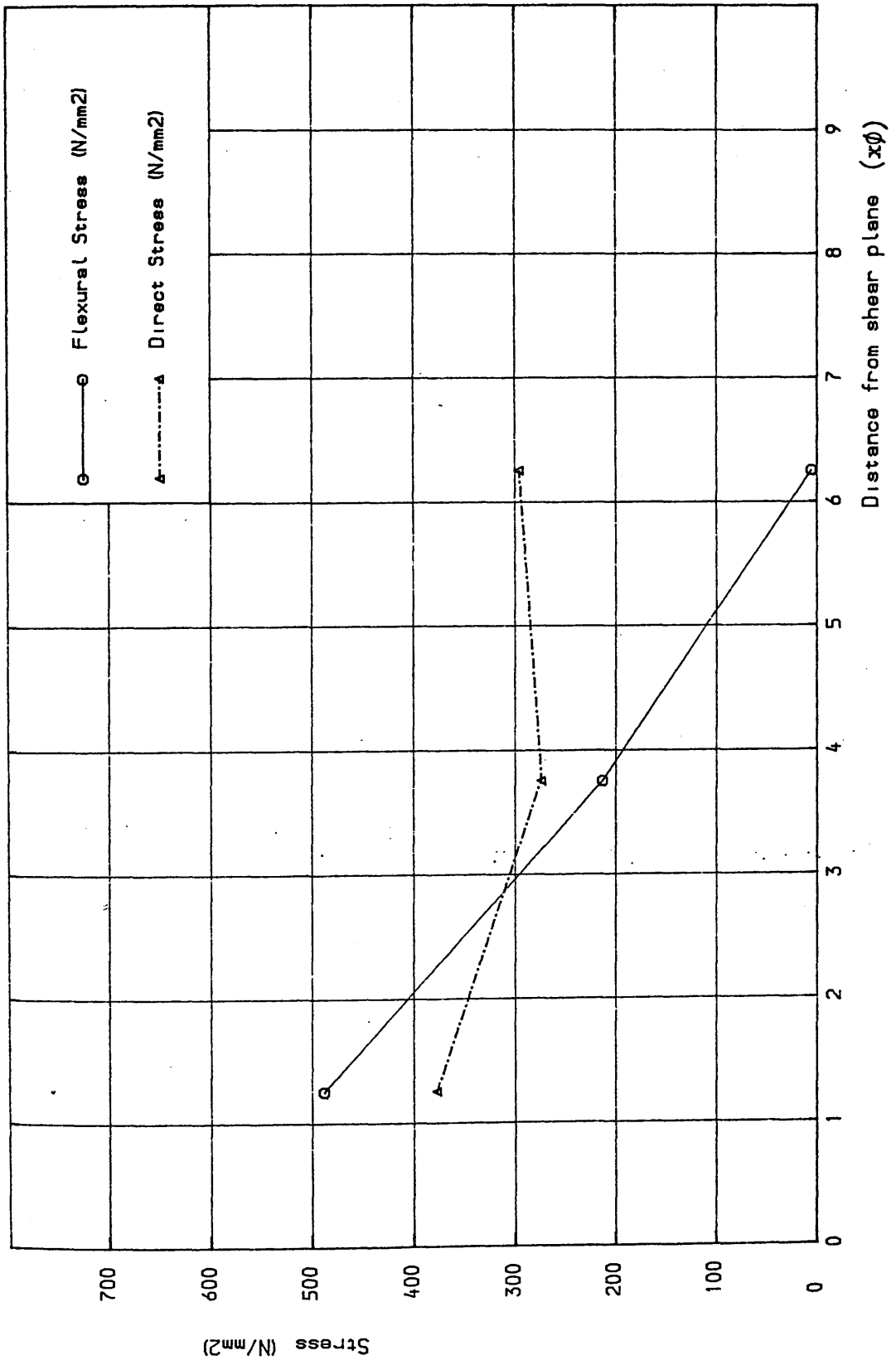

Figure (6.39) Distribution of flexural and direct stresses along a distance 6.25Ø from the shear plane, specimen 3.5.2

(a)

(b)

Figure(6.40) Crack pattern of the two faces of the shear plane for specimen 3.5.2

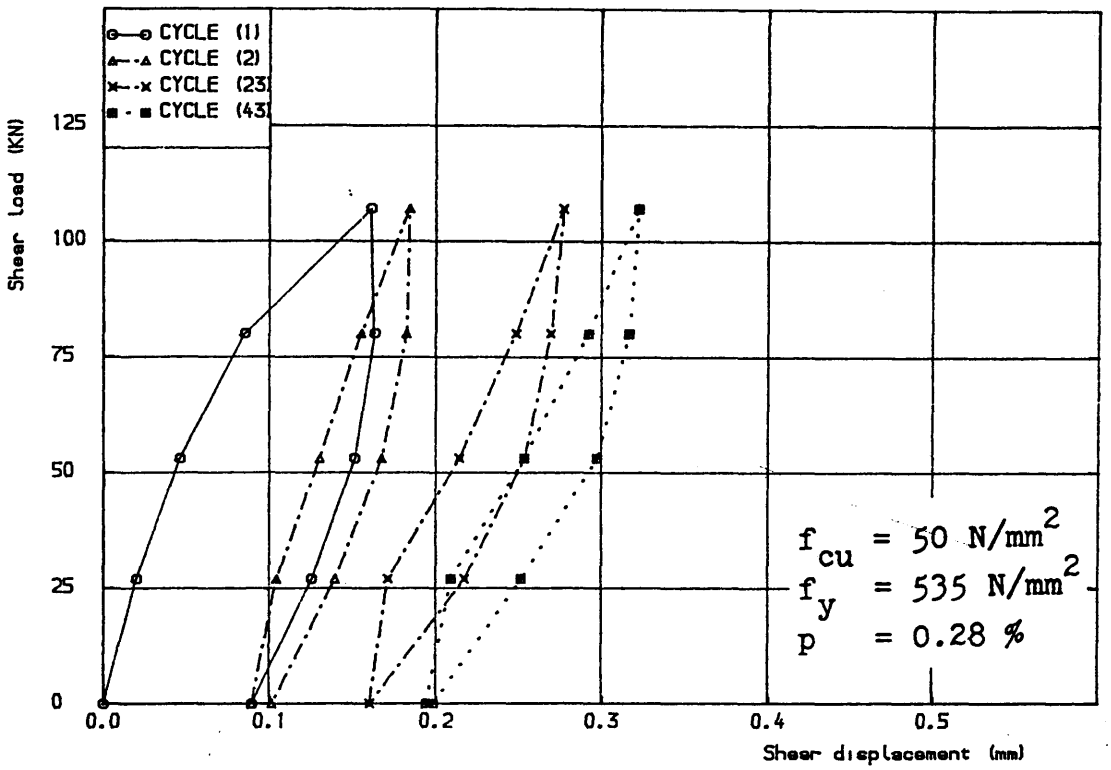

Figure (6.41) Shear load vs shear displacement, specimen 3.1.1A, load cycles 1, 2, 23 and 43

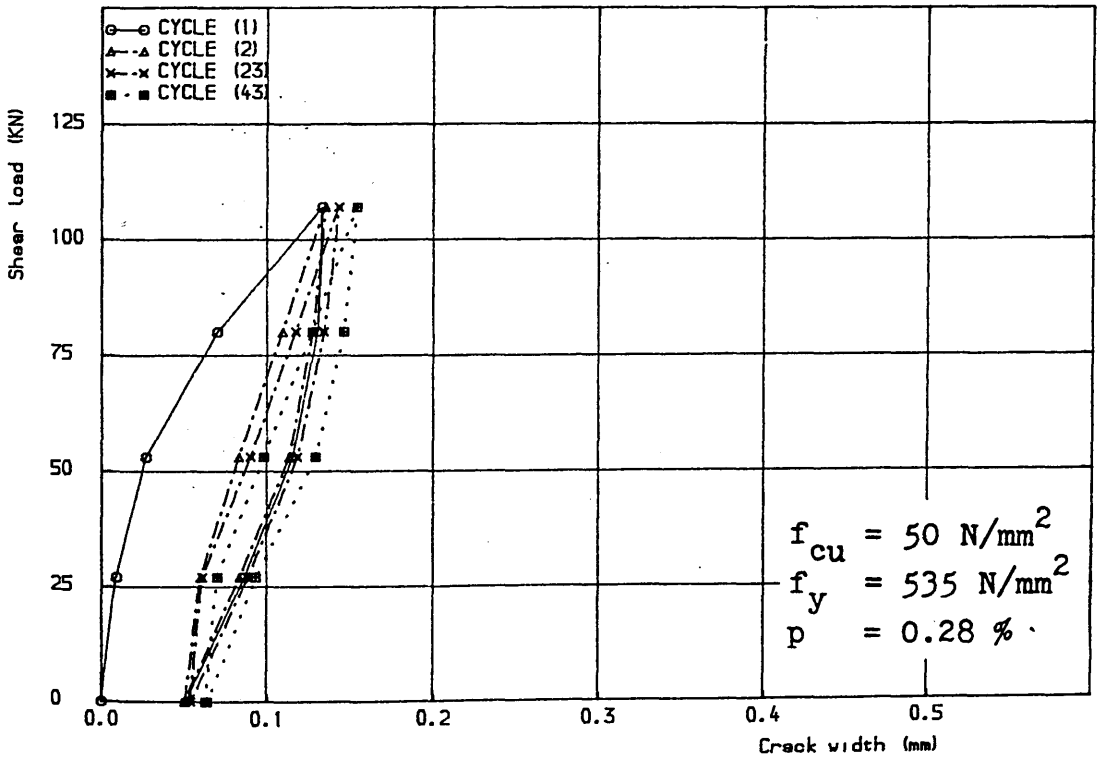

Figure (6.42) Shear load vs crack width, specimen 3.1.1A, load cycles 1, 2, 23 and 43

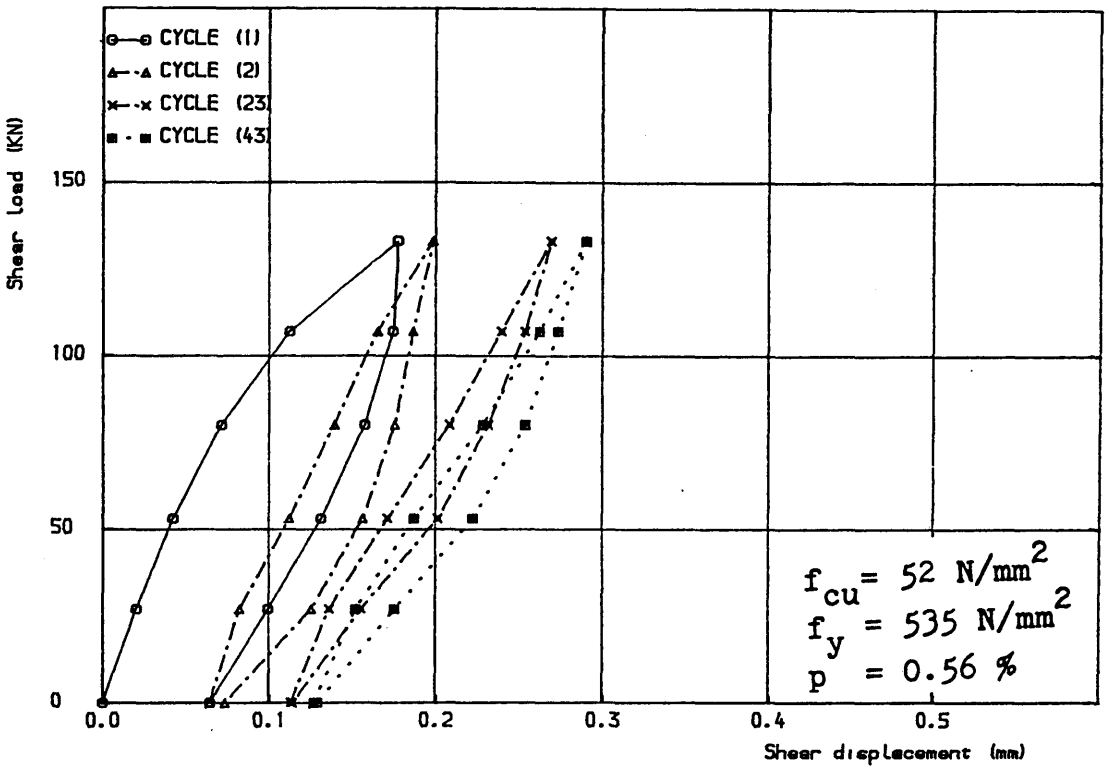

Figure (6.43) Shear load vs shear displacement, specimen 3.1.2A

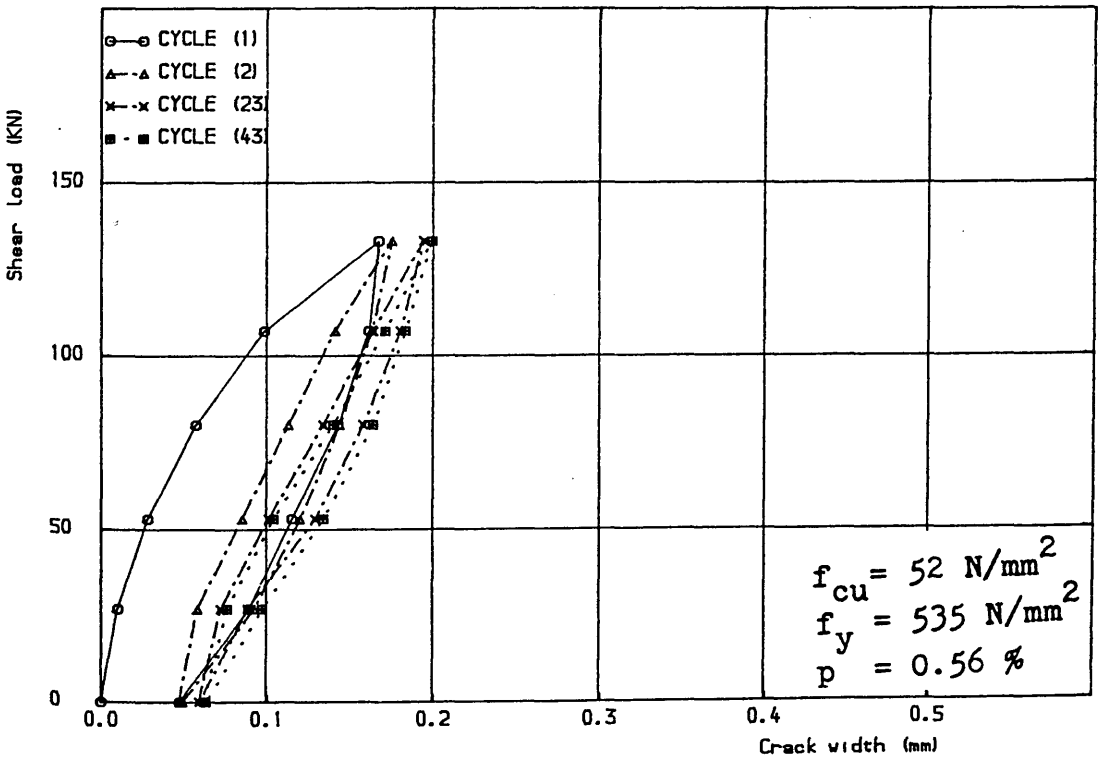

Figure (6.44) Shear load vs crack width, specimen 3.1.2A

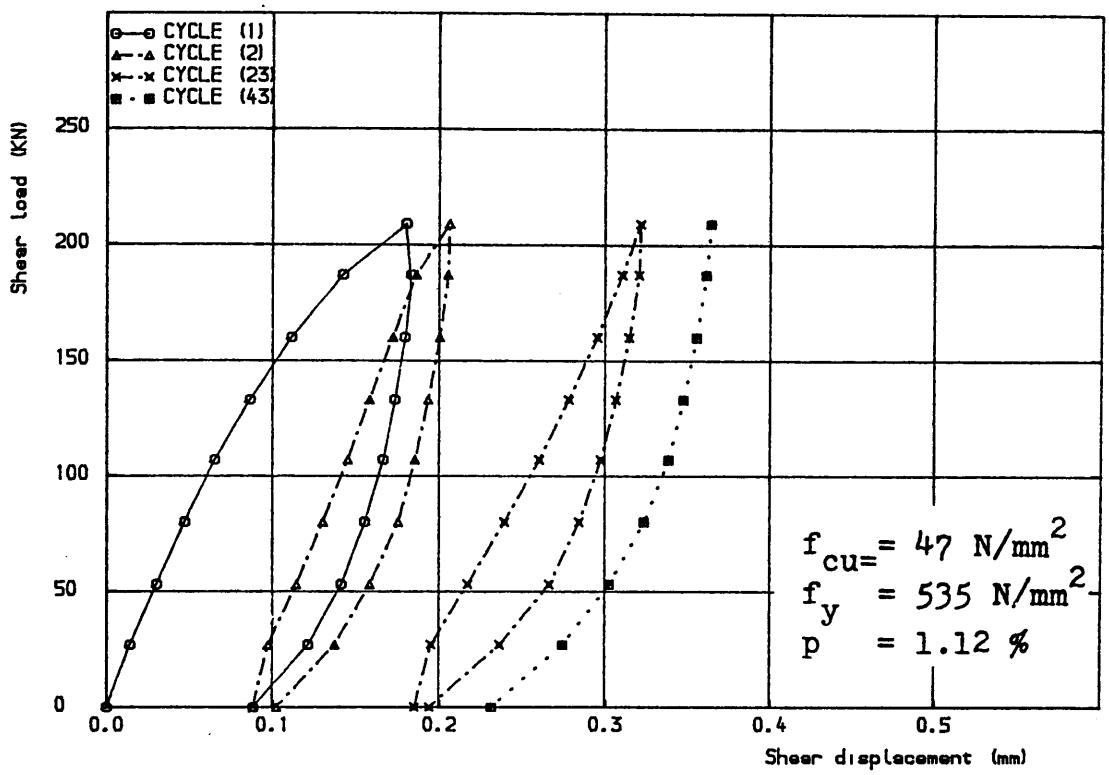

Figure (6.45) Shear load vs shear displacement, specimen 3.1.3A, load cycles 1, 2, 23 and 43

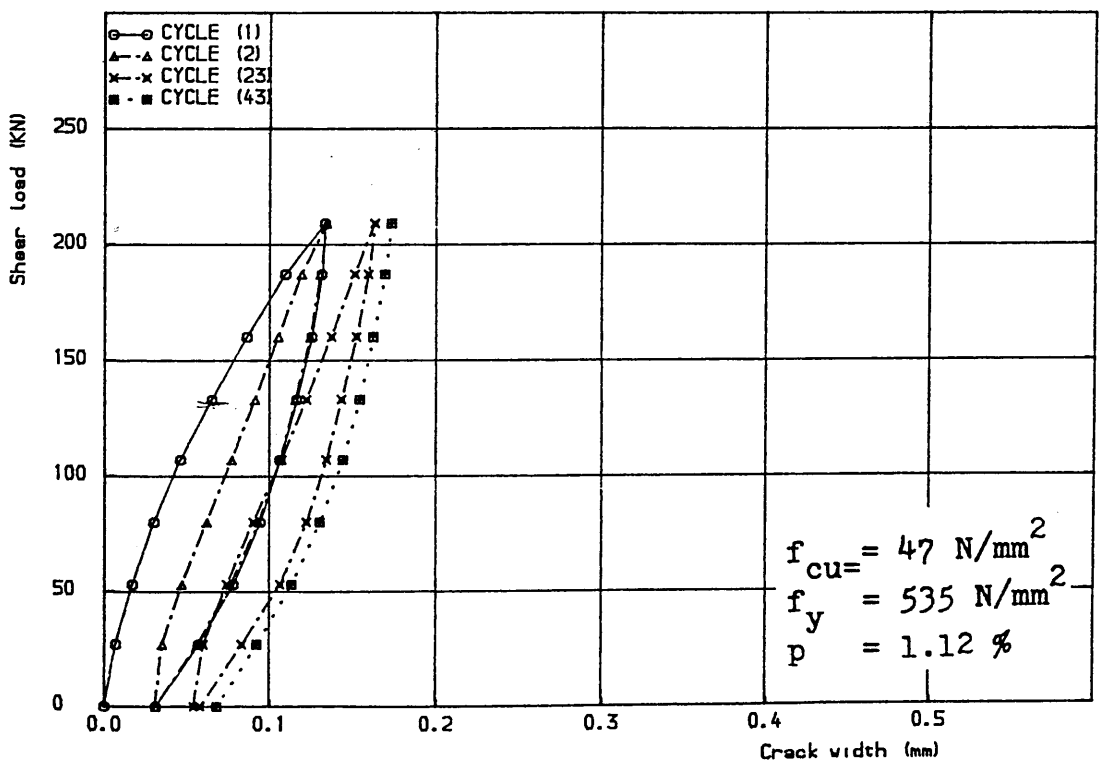

Figure (6.46) Shear load vs crack width, specimen 3.1.3A, load cycles 1, 2, 23 and 43

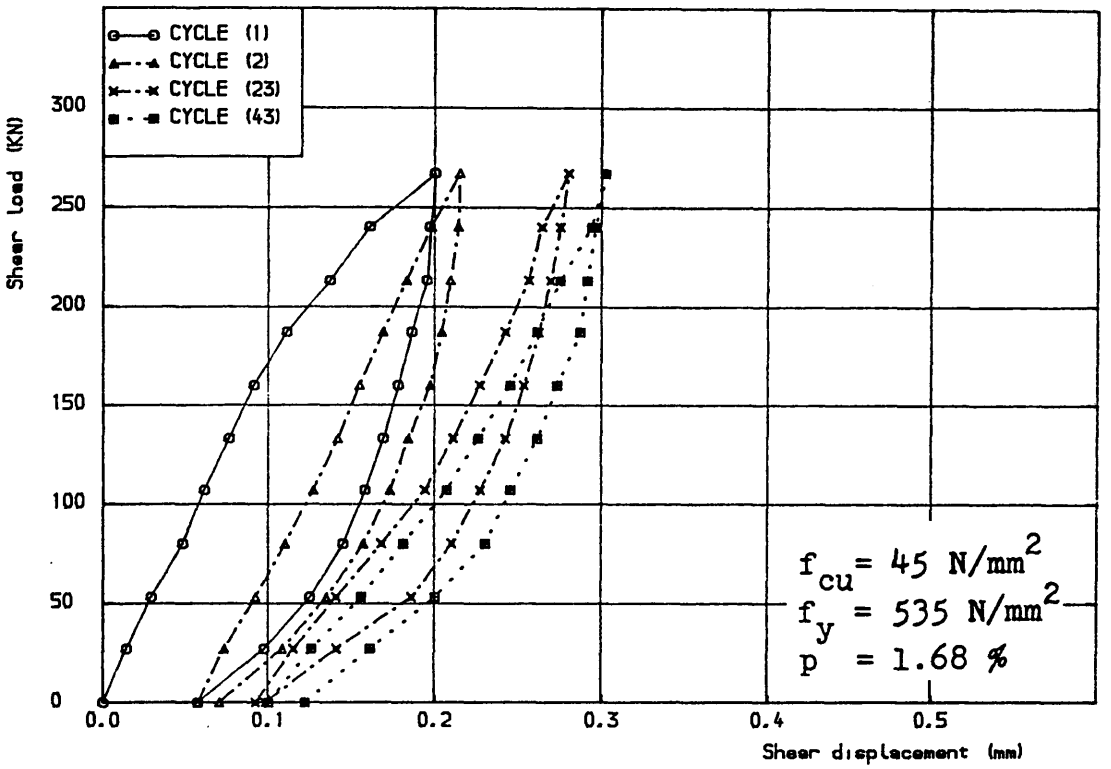

Figure (6.47) Shear load vs shear displacement, specimen 3.1.4A, load cycles 1, 2, 23 and 43

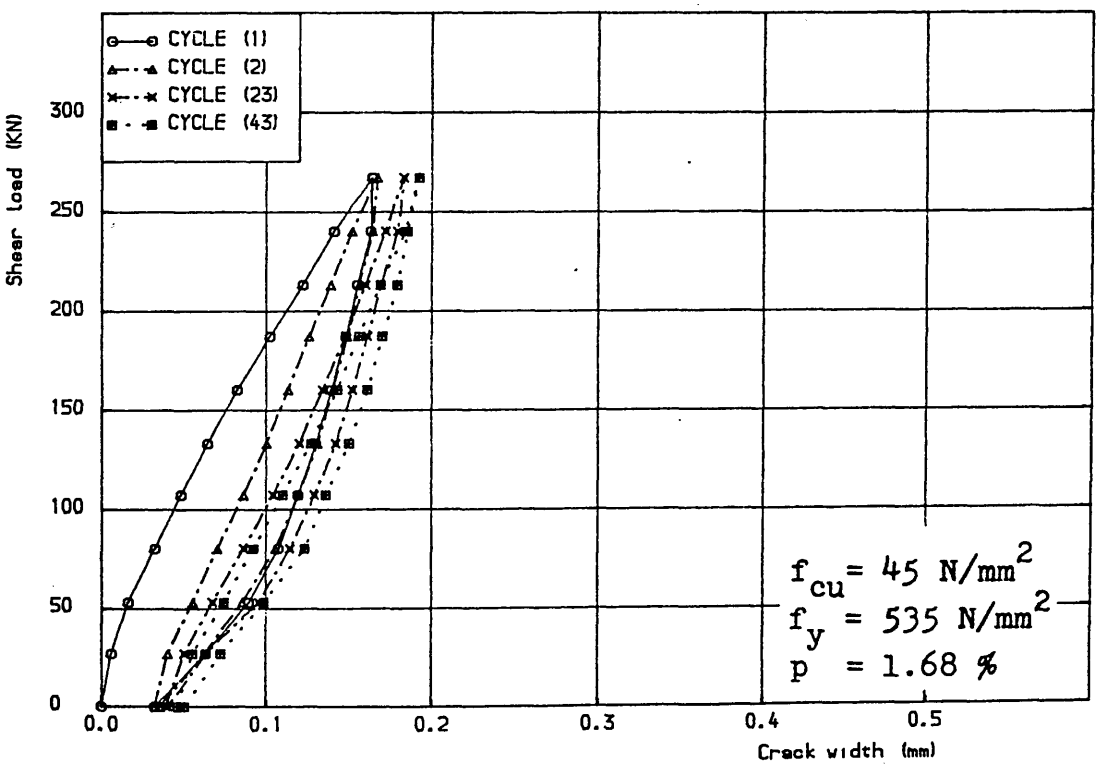

Figure (6.48) Shear load vs crack width, specimen 1.1.4A, load cycles 1, 2, 23 and 43

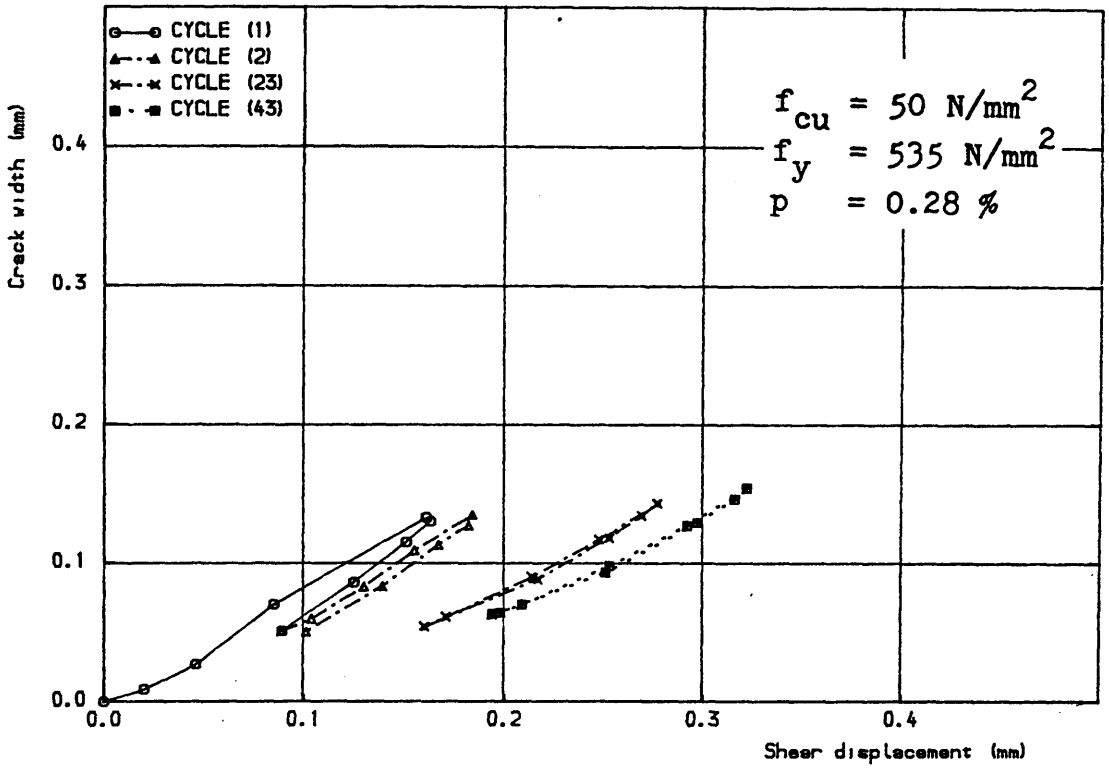

Figure (6.49) Crack width vs shear displacement, specimen 3.1.1A, load cycles 1, 2, 23 and 43

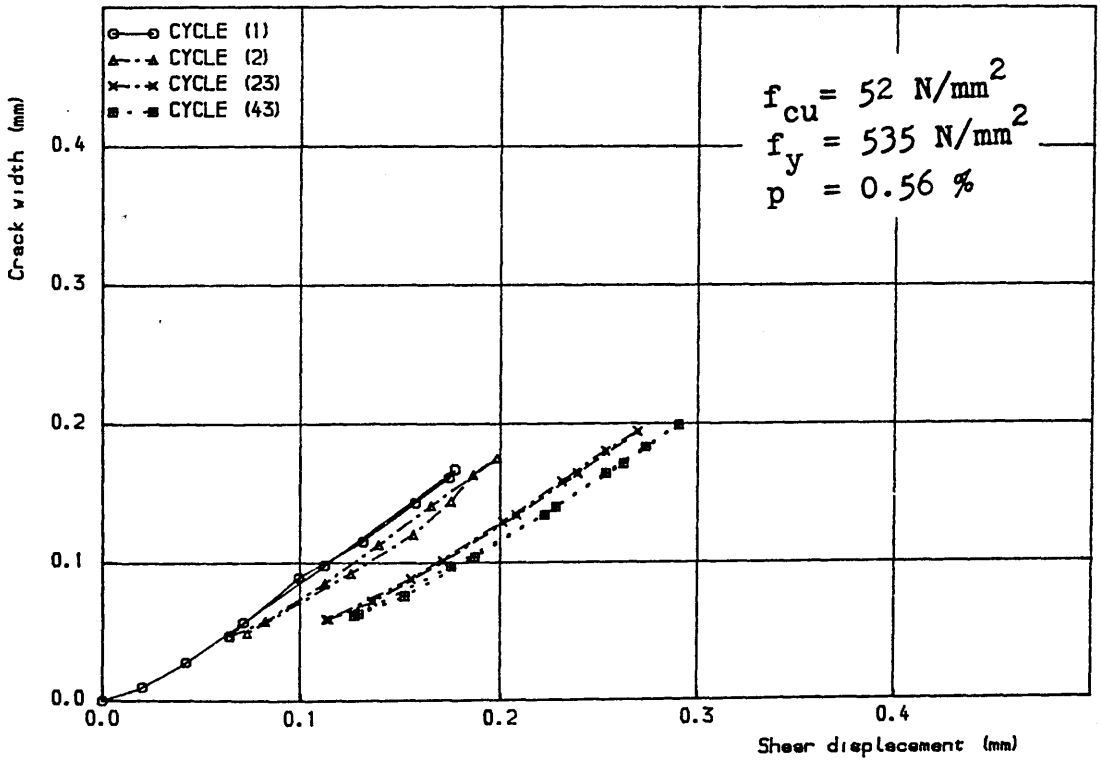

Figure (6.50) Crack width vs shear displacement, specimen 3.1.2A, load cycles 1, 2, 23 and 43

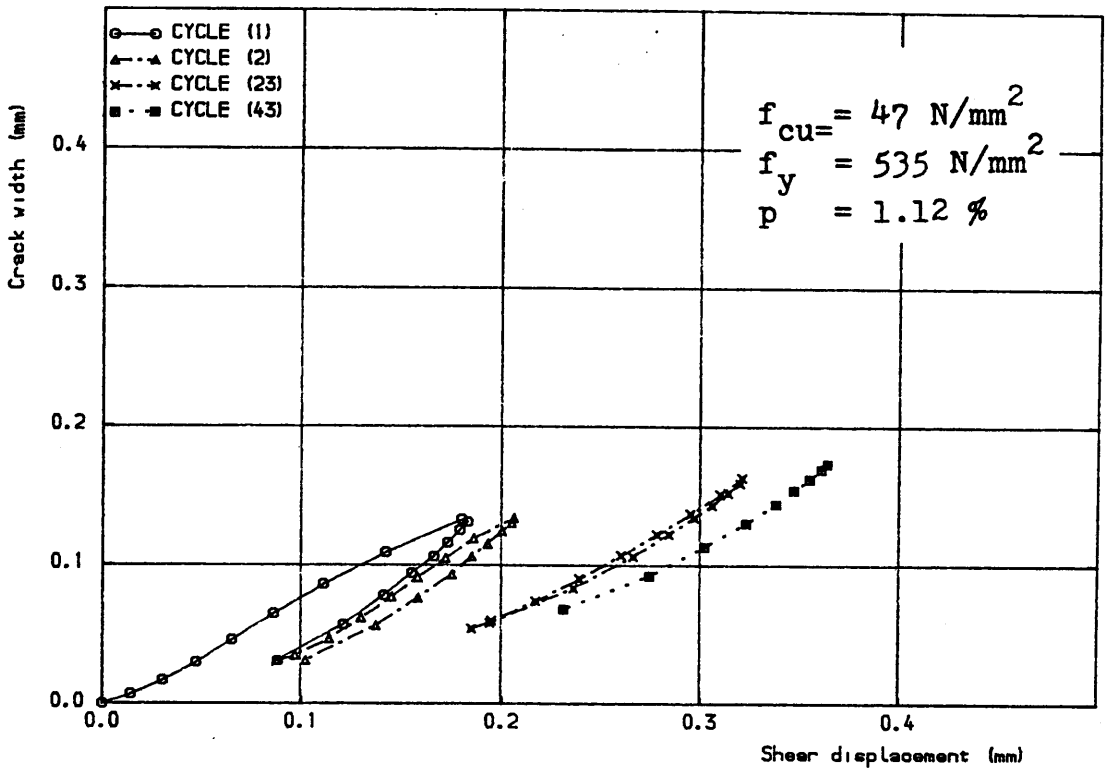

Figure (6.51) Crack width vs shear displacement, specimen 3.1.3A, load cycles 1,2,23 and 43

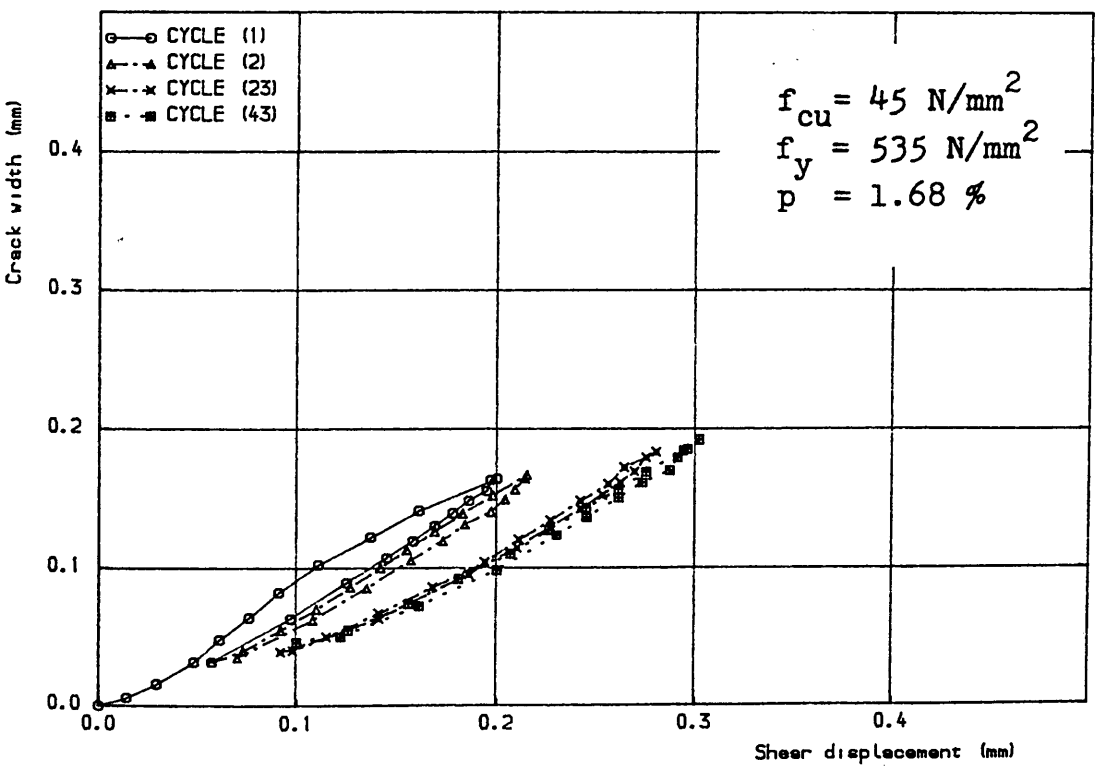

Figure (6.52) Crack width vs shear displacement, specimen 3.1.4A, load cycles 1,2,23 and 43

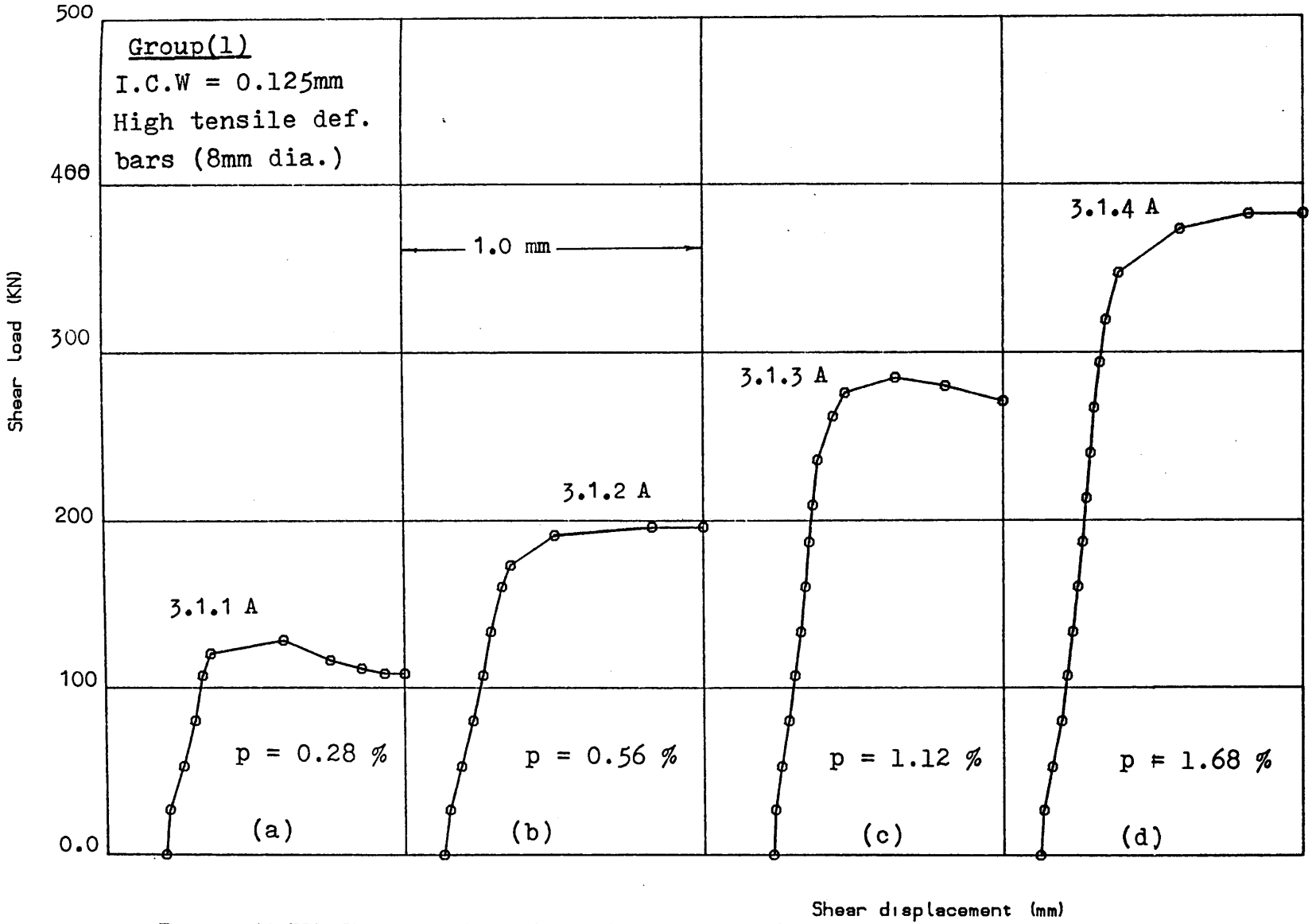

Figure (6.53) Shear load vs shear displacement for specimens of group 1 tested under repeated loading, last cycle

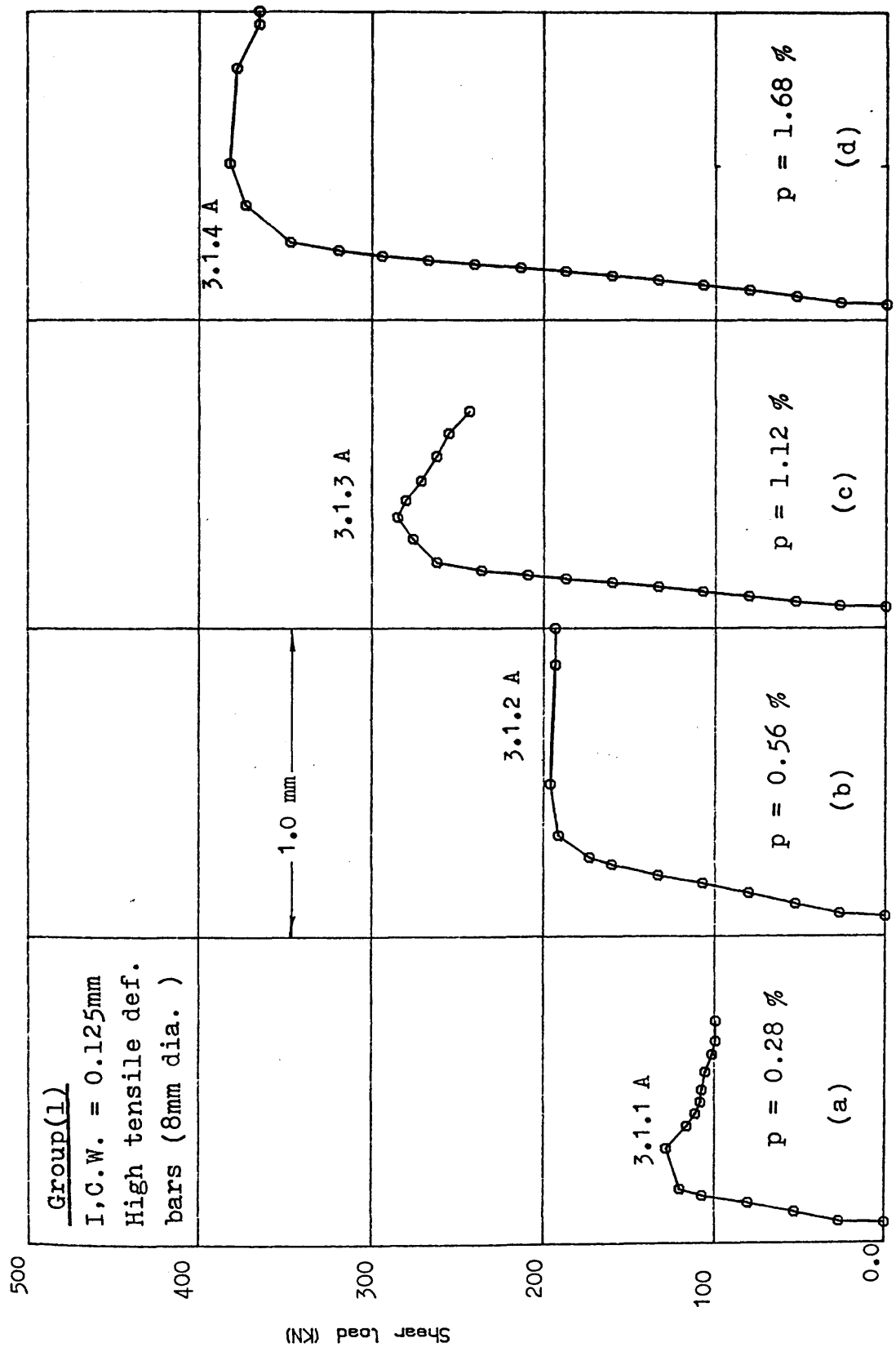

Figure (6.54) Shear load vs crack width for specimens of group I tested under repeated loading (last cycle)

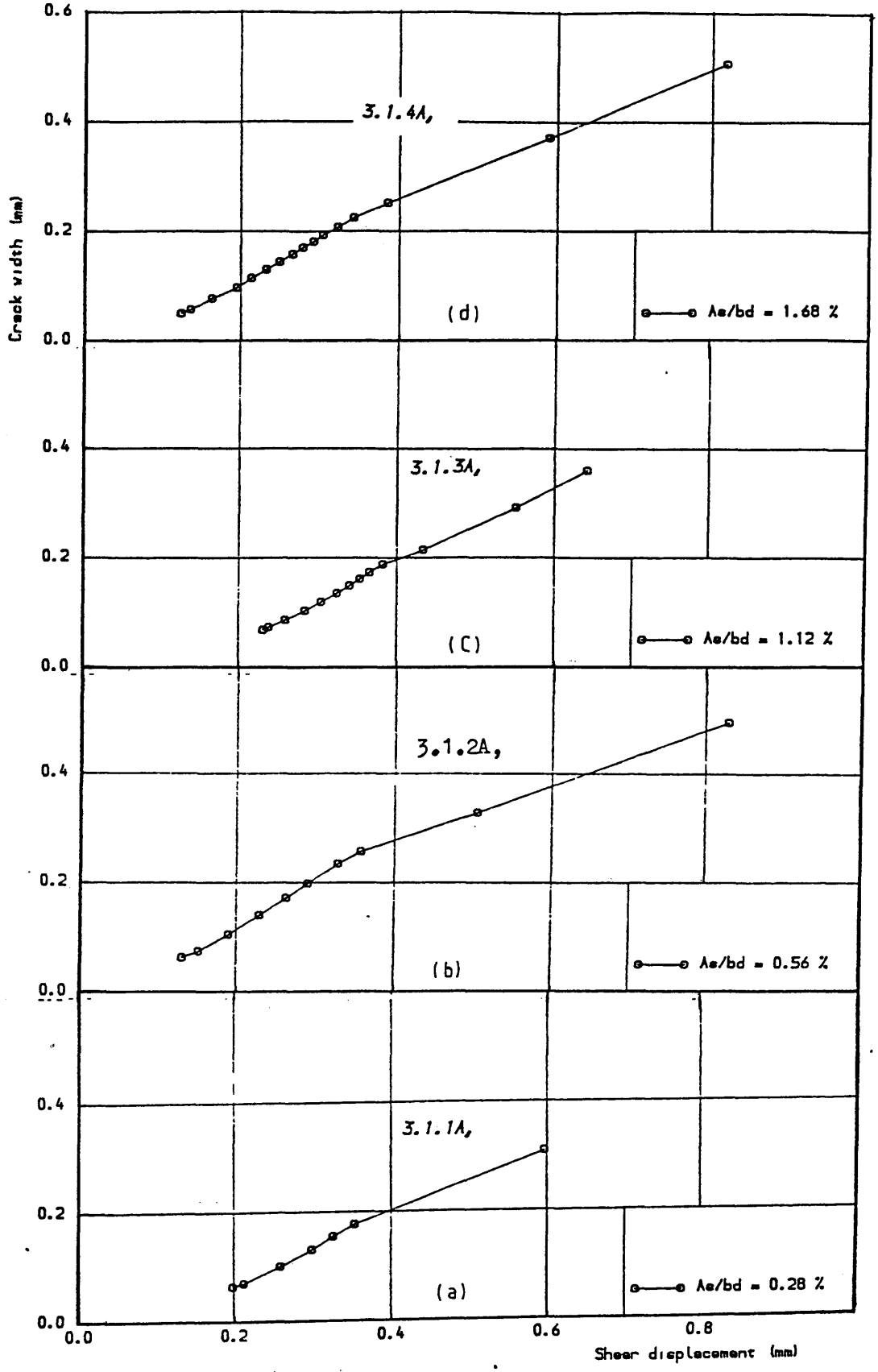

Figure(6.55) Crack width vs shear displacement for group(1) series-3 under repeated loading , last cycle .

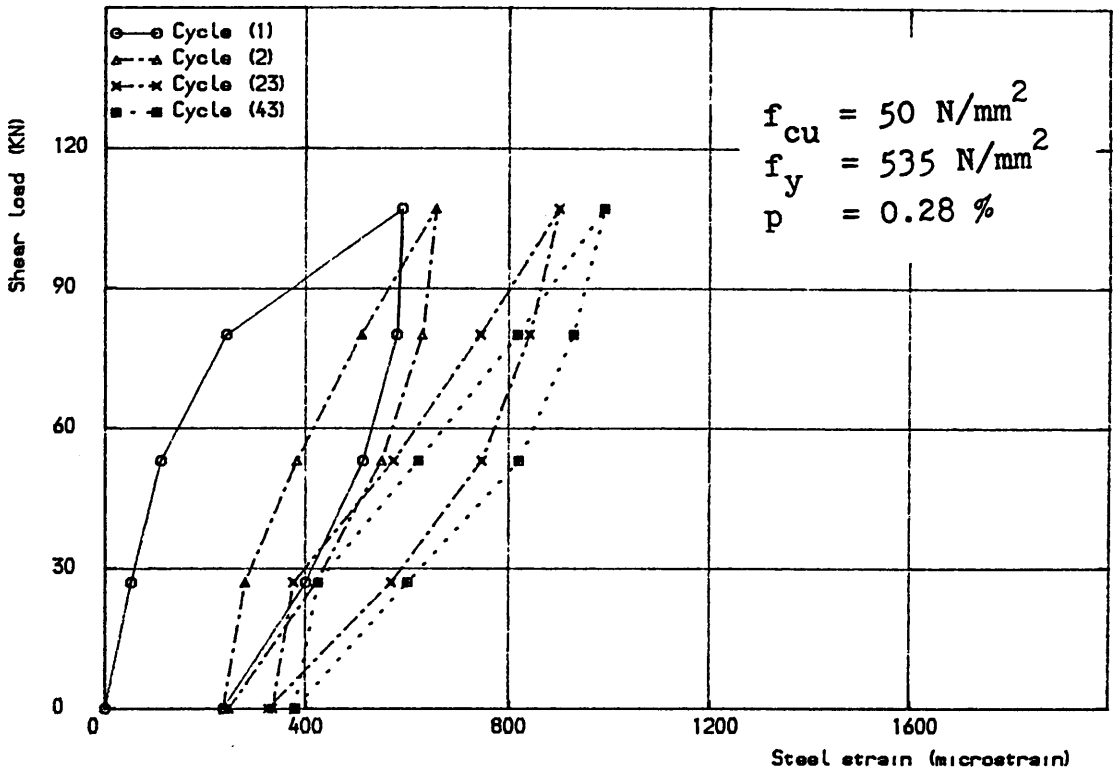

Figure (6.56) Shear load vs steel strain, specimen 3.1.1A, load cycles 1, 2, 23 and 43

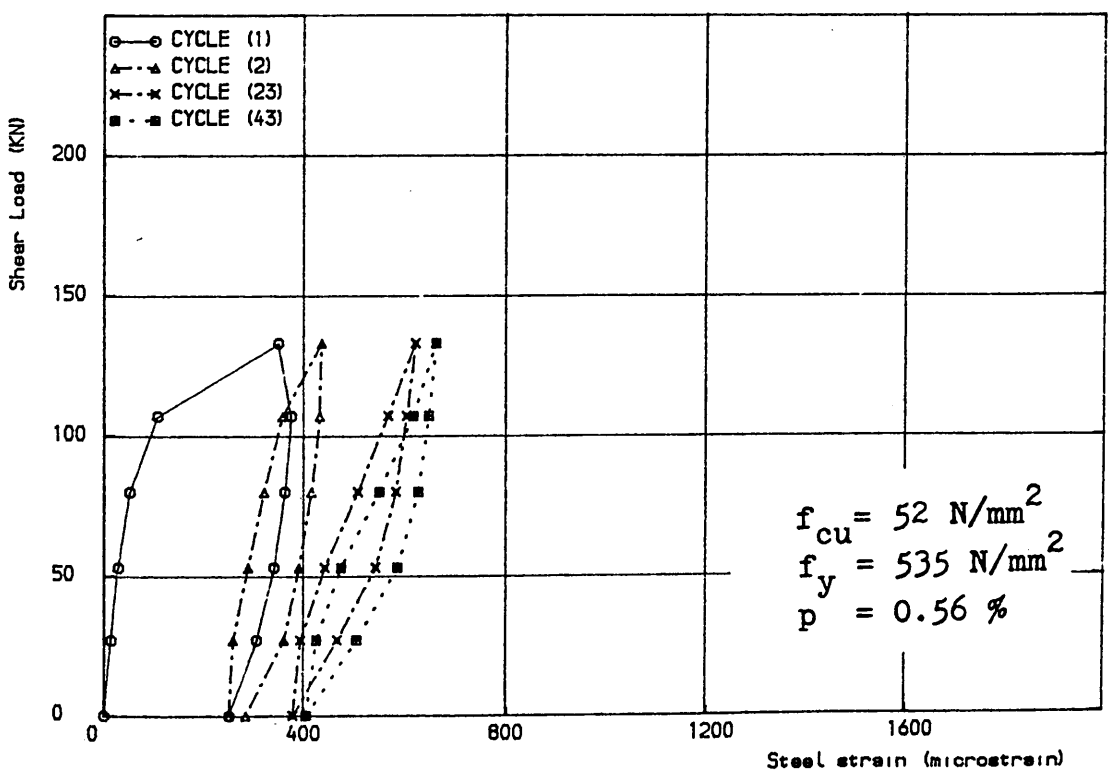

Figure (6.57) Shear load vs steel strain, specimen 3.1.2A load cycles 1, 2, 23 and 43

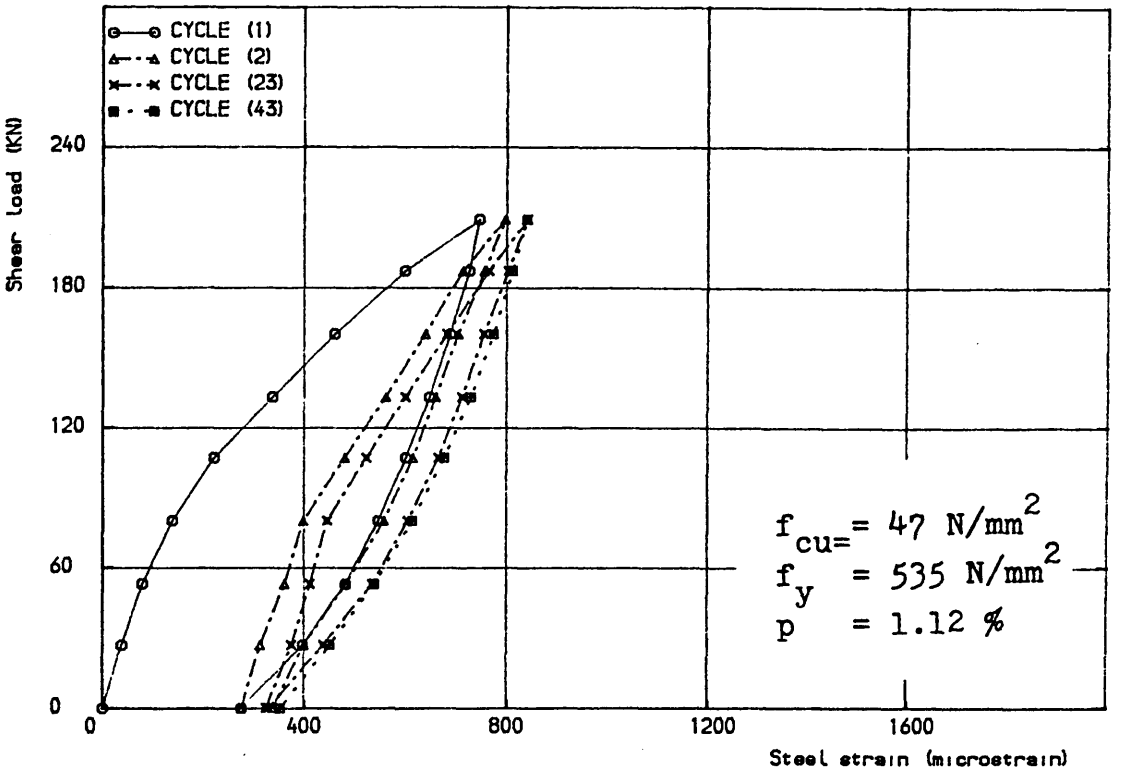

Figure (5.58) Shear load vs steel strain, specimen 3.1.3A, load cycles 1, 2, 23 and 43

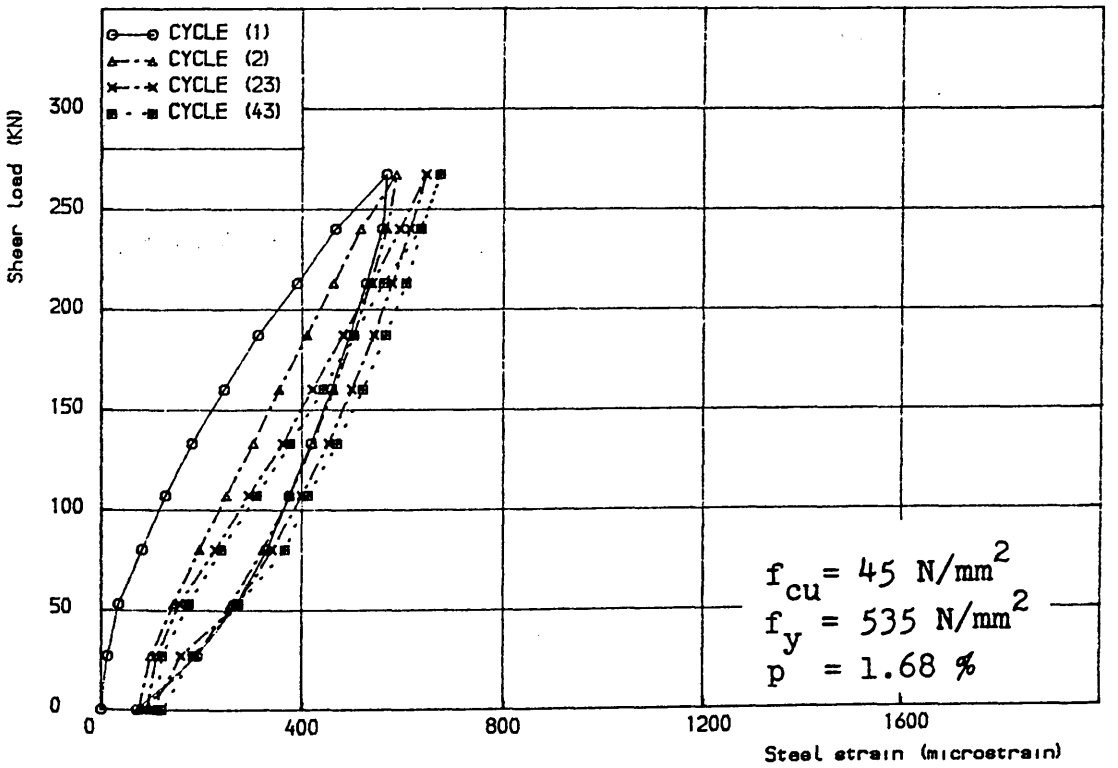

Figure (6.59) Shear load vs steel strain, specimen 3.1.4A, load cycles 1, 2, 23 and 43

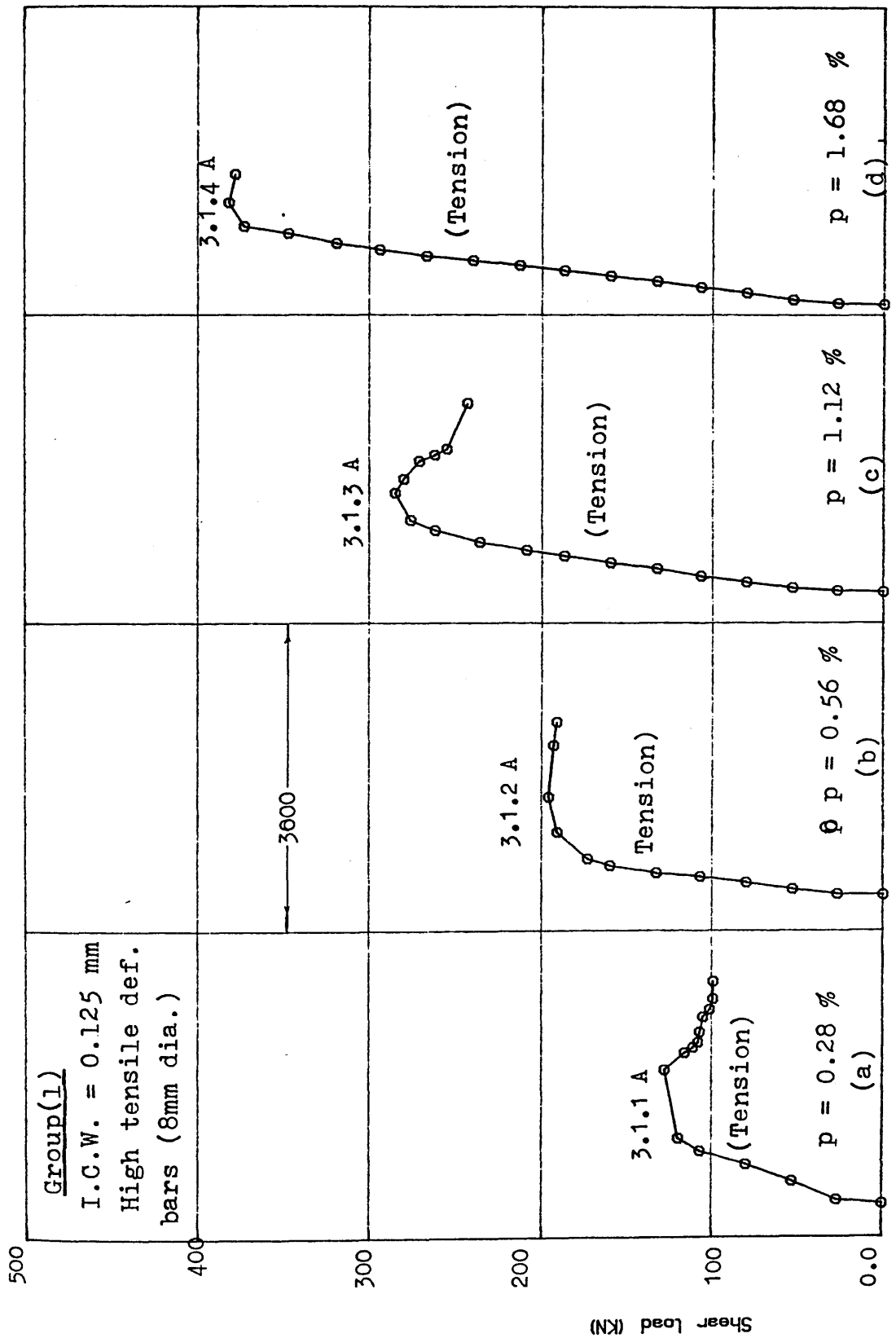

Figure (6.60) Shear load vs steel strain for specimens of group 1, series 3 tested under repeated loading, last cycle

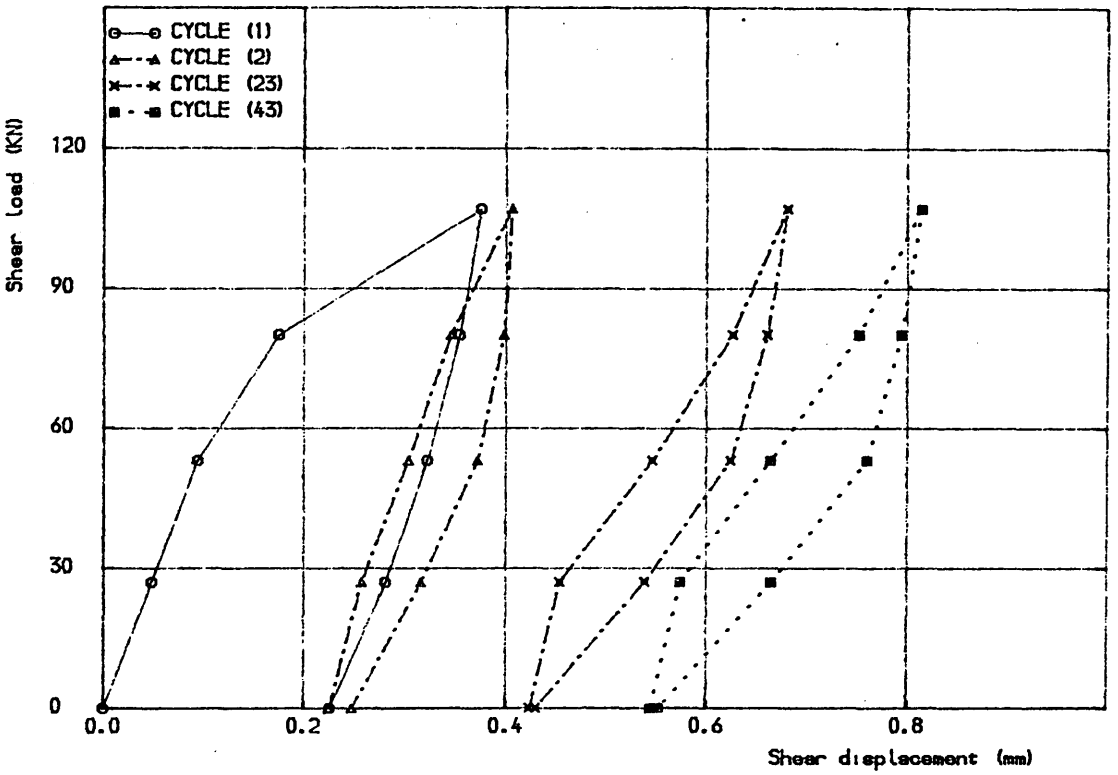

Figure (6.61) Shear load vs shear displacement, specimen 3.2.1A, load cycles 1, 2, 23 and 43

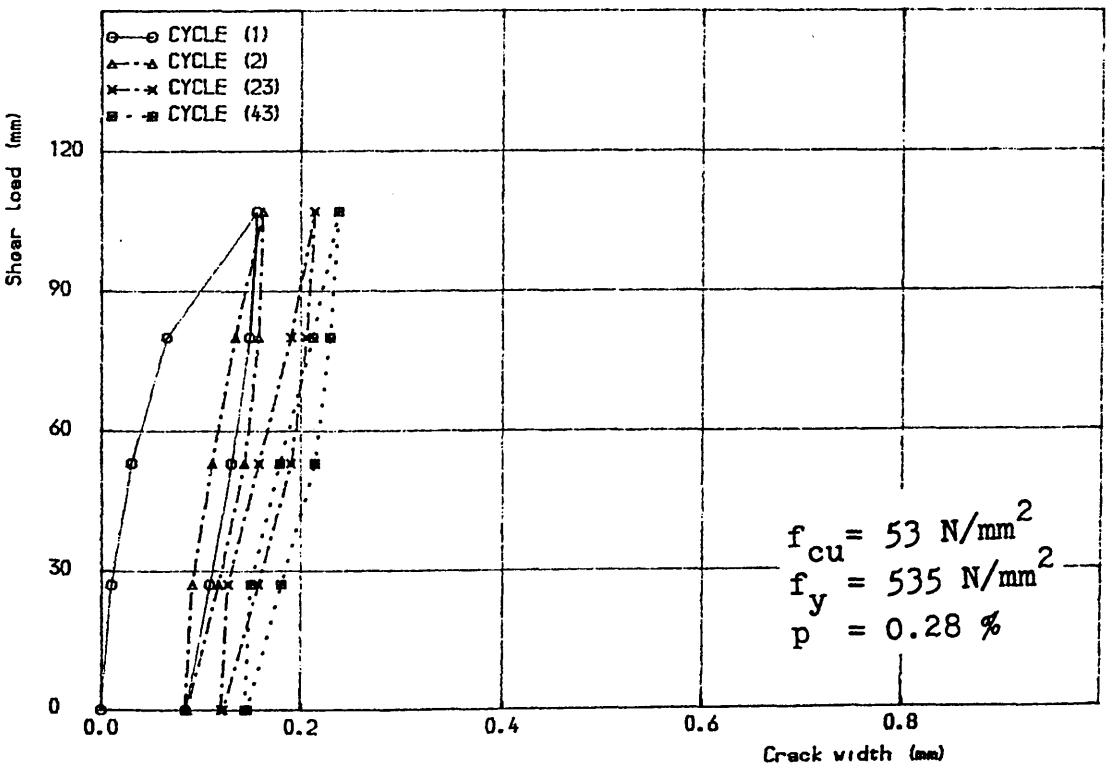

Figure (6.62) Shear load vs crack width, specimen 3.2.1A load cycles 1, 2, 23 and 43

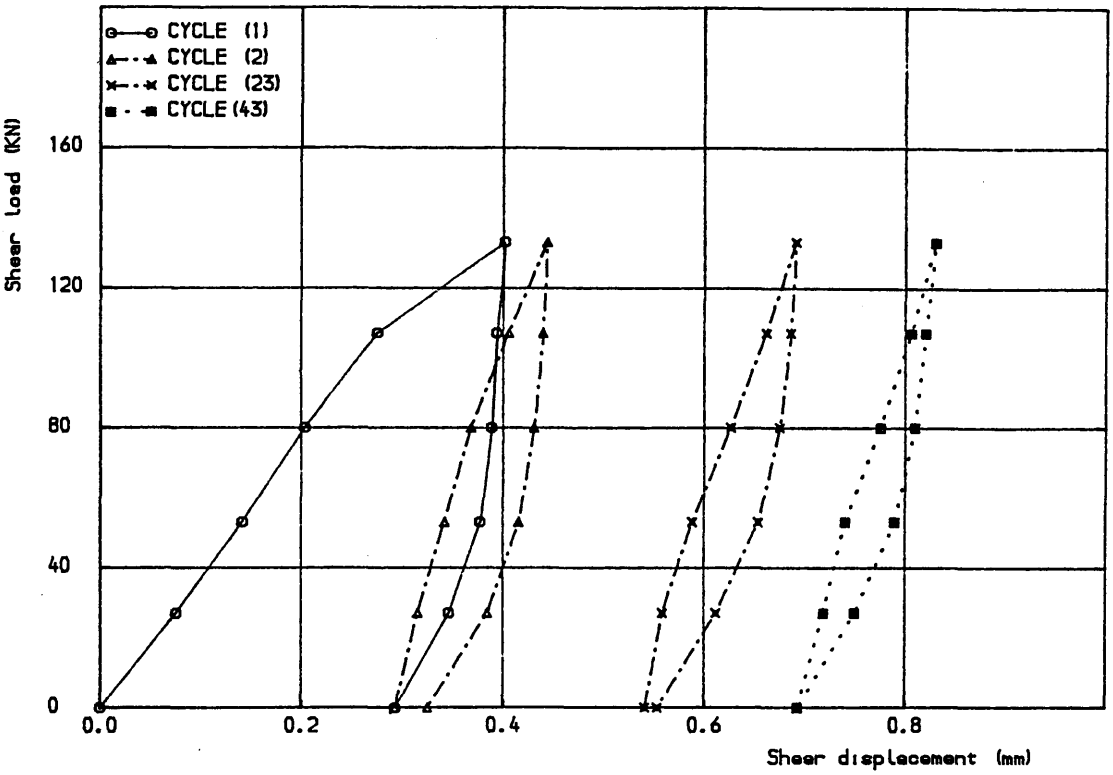

Figure (6.63) Shear load vs shear displacement, specimen 3.2.2λ, load cycles 1, 2, 23 and 43

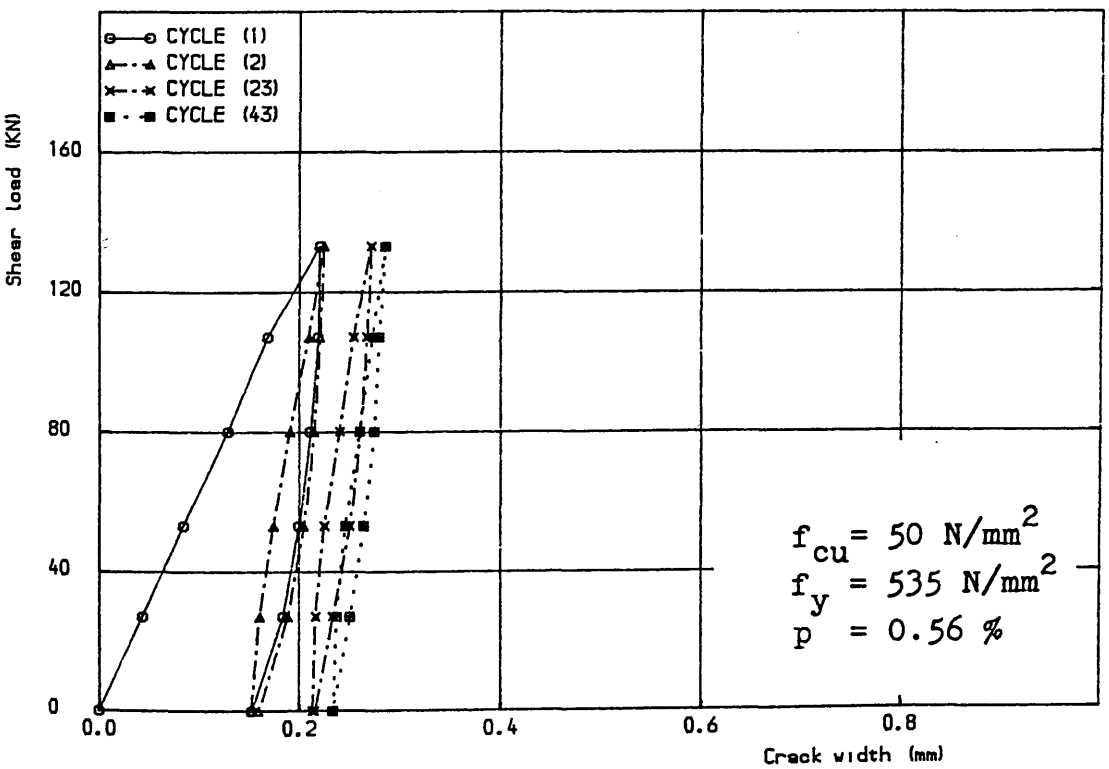

Figure (6.64) Shear load vs crack width, specimen 3.2.2λ, load cycles 1, 2, 23 and 43

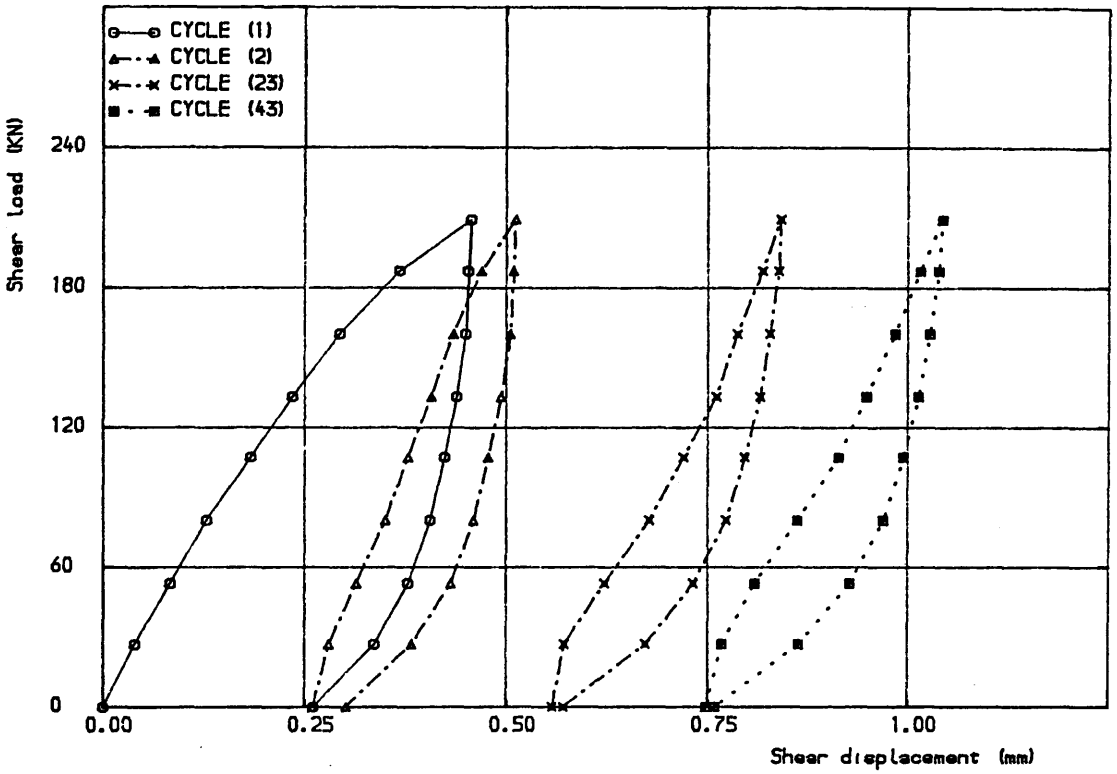

Figure (6.65) Shear load vs Shear displacement, specimen 3.2.3A, load cycles 1, 2, 23 and 43

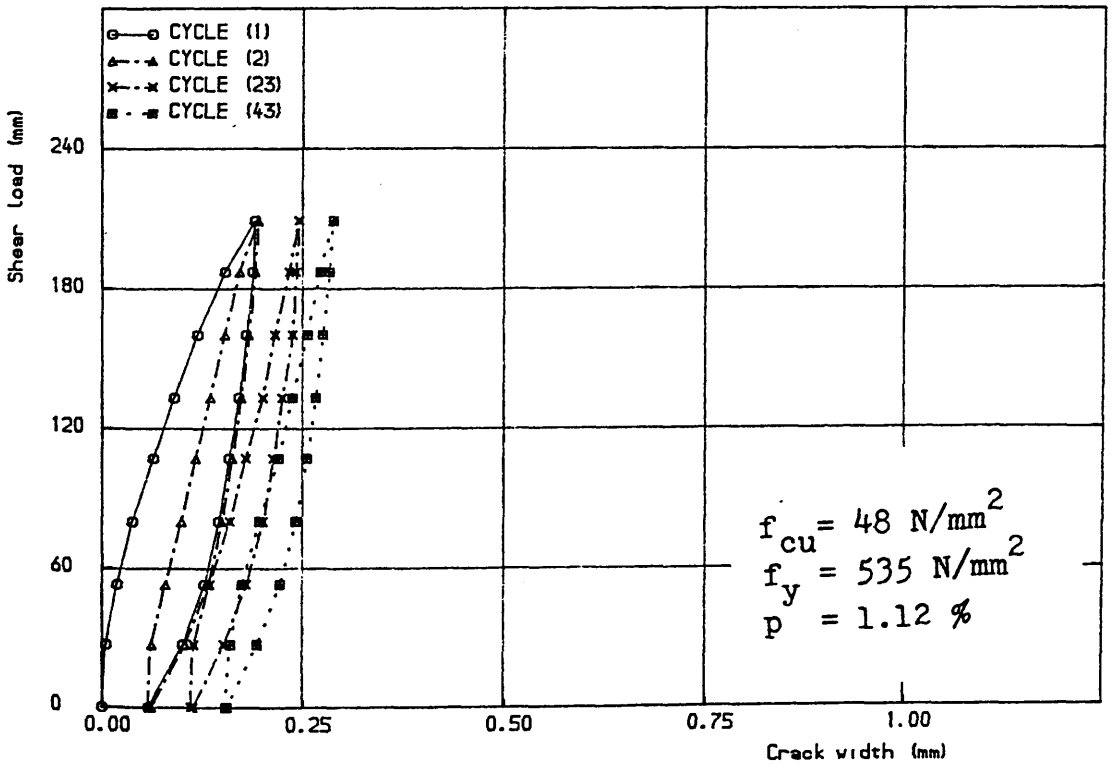

Figure (6.66) Shear load vs crack width, specimen 3.2.3A, load cycles 1, 2, 23 and 43

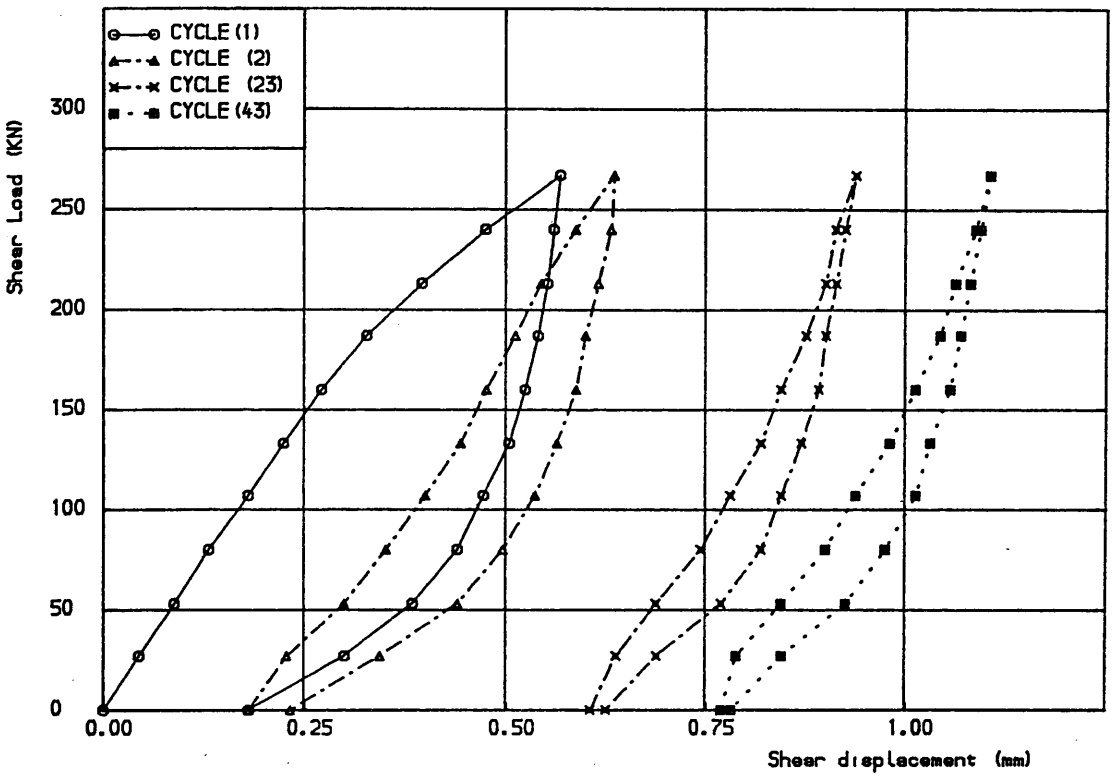

Figure (6.67) Shear load vs shear displacement, specimen3.2.4A, load cycles 1, 2, 23 and 43

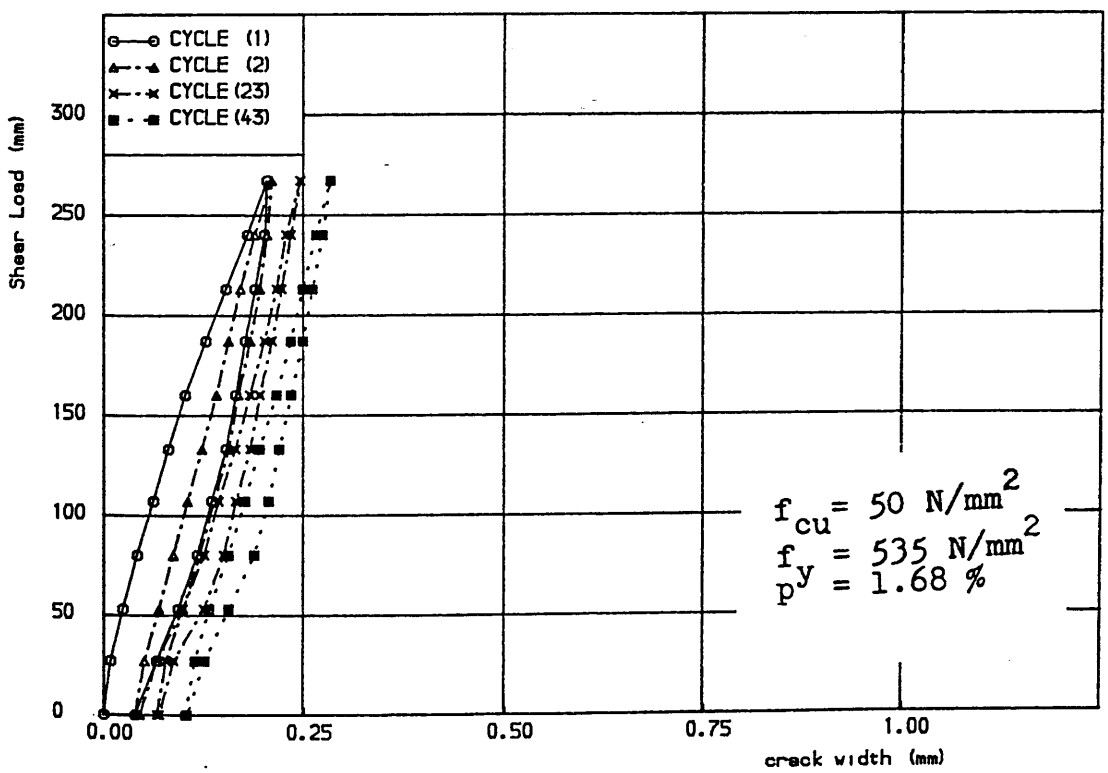

Figure (6.68) Shear load vs crack width, specimen 3.2.4A, load cycles 1, 2, 23 and 43

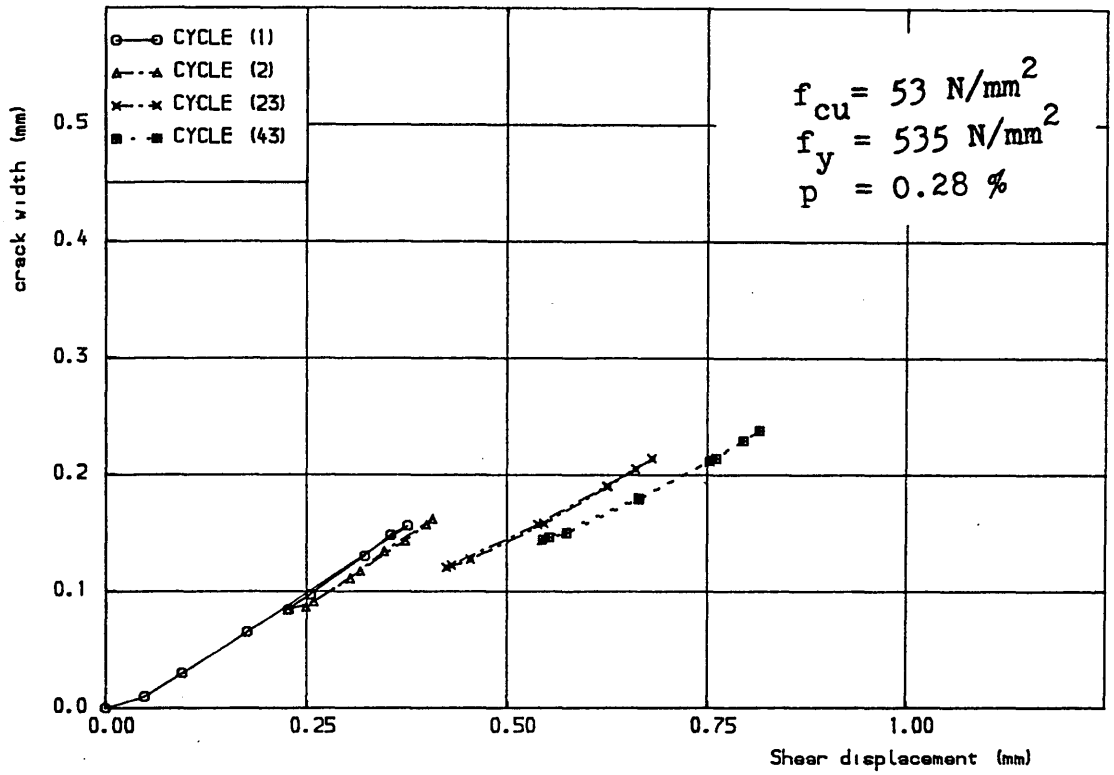

Figure(6.69) *crack width vs shear displacement, specimen 3.2.1A, load cycles 1, 2, 23 and 43*

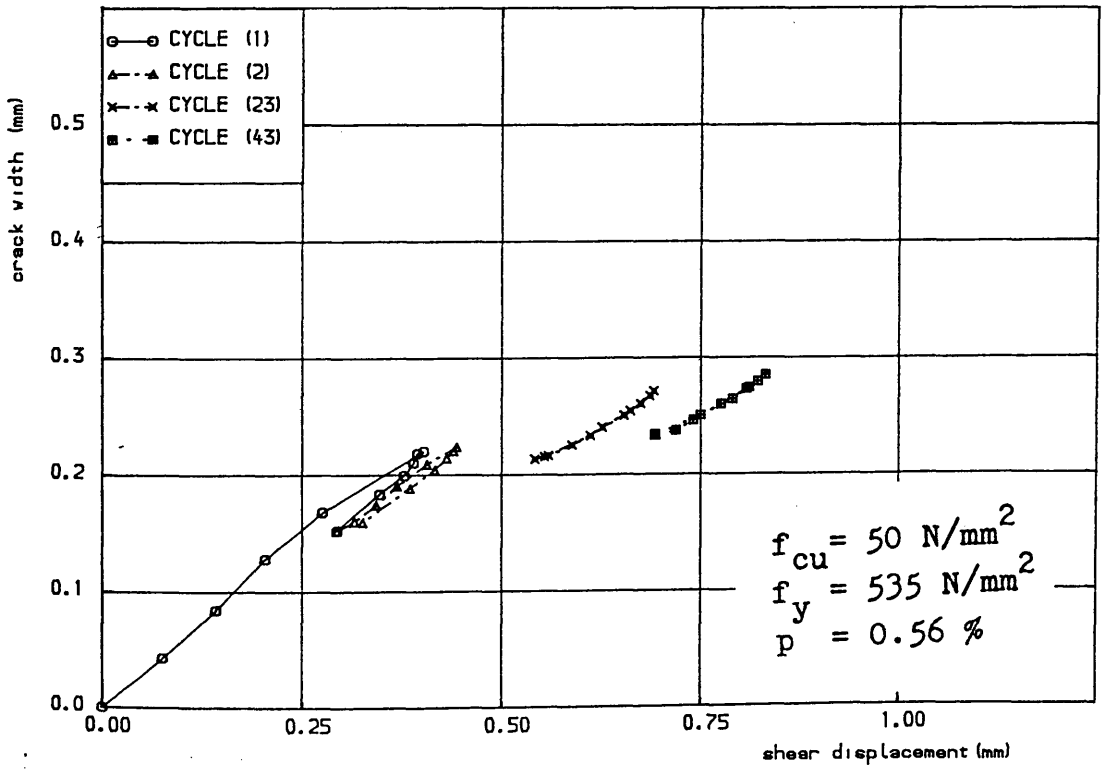

Figure(6.70) *Crack width vs shear displacement, specimen 3.2.2A load cycles 1, 2, 23 and 43*

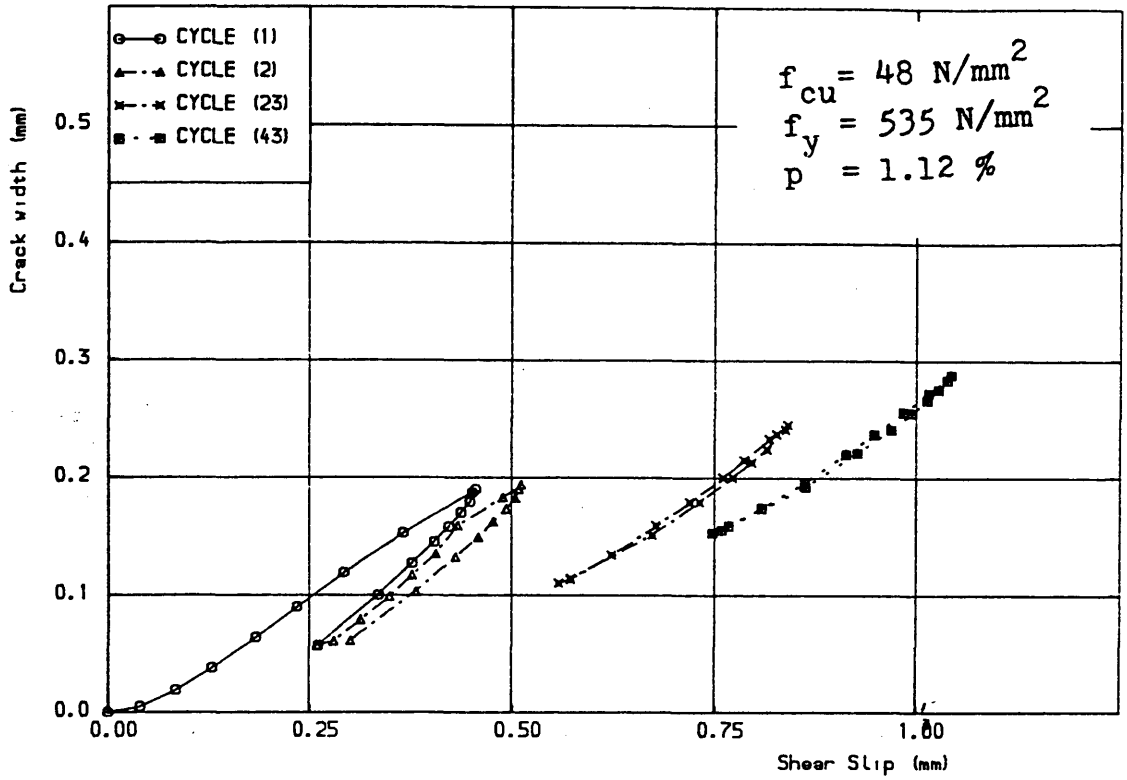

Figure(6.71) *crack width vs shear displacement, specimen 3.2.3A, load cycles 1, 2, 23 and 43*

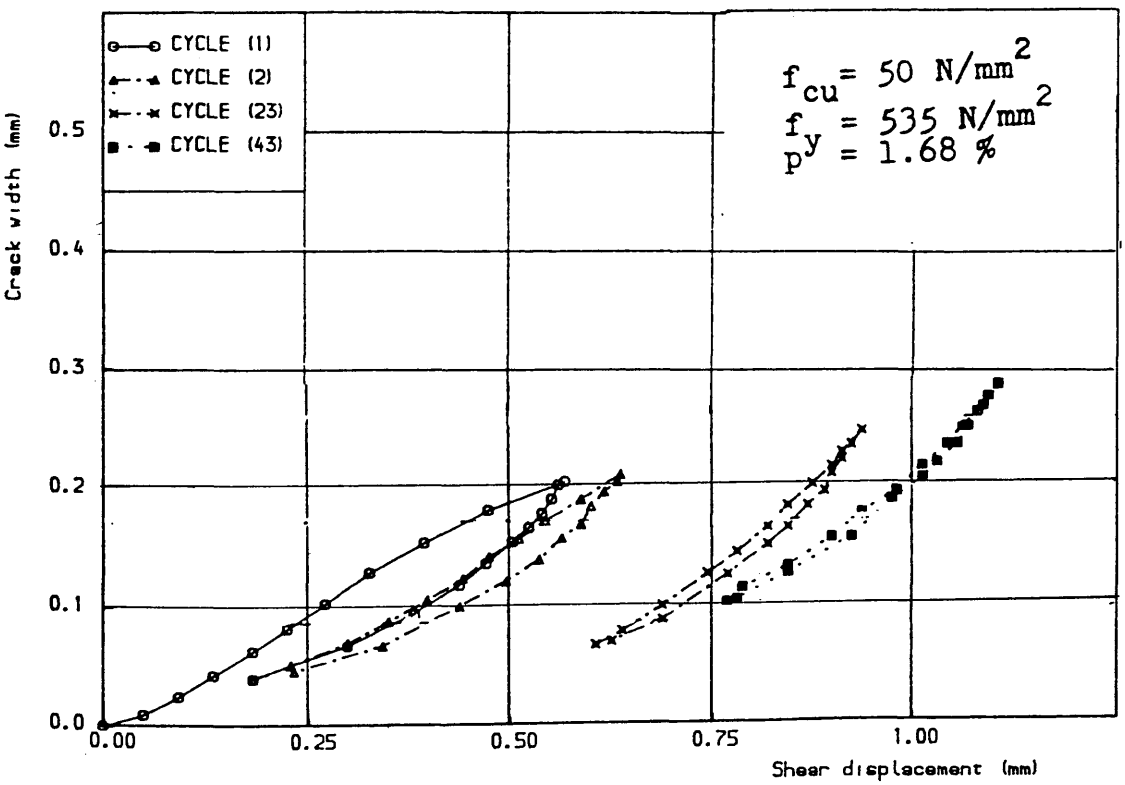

Figure(6.72) *Crack width vs shear displacement, specimen 3.2.4A, load cycles 1, 2, 23 and 43*

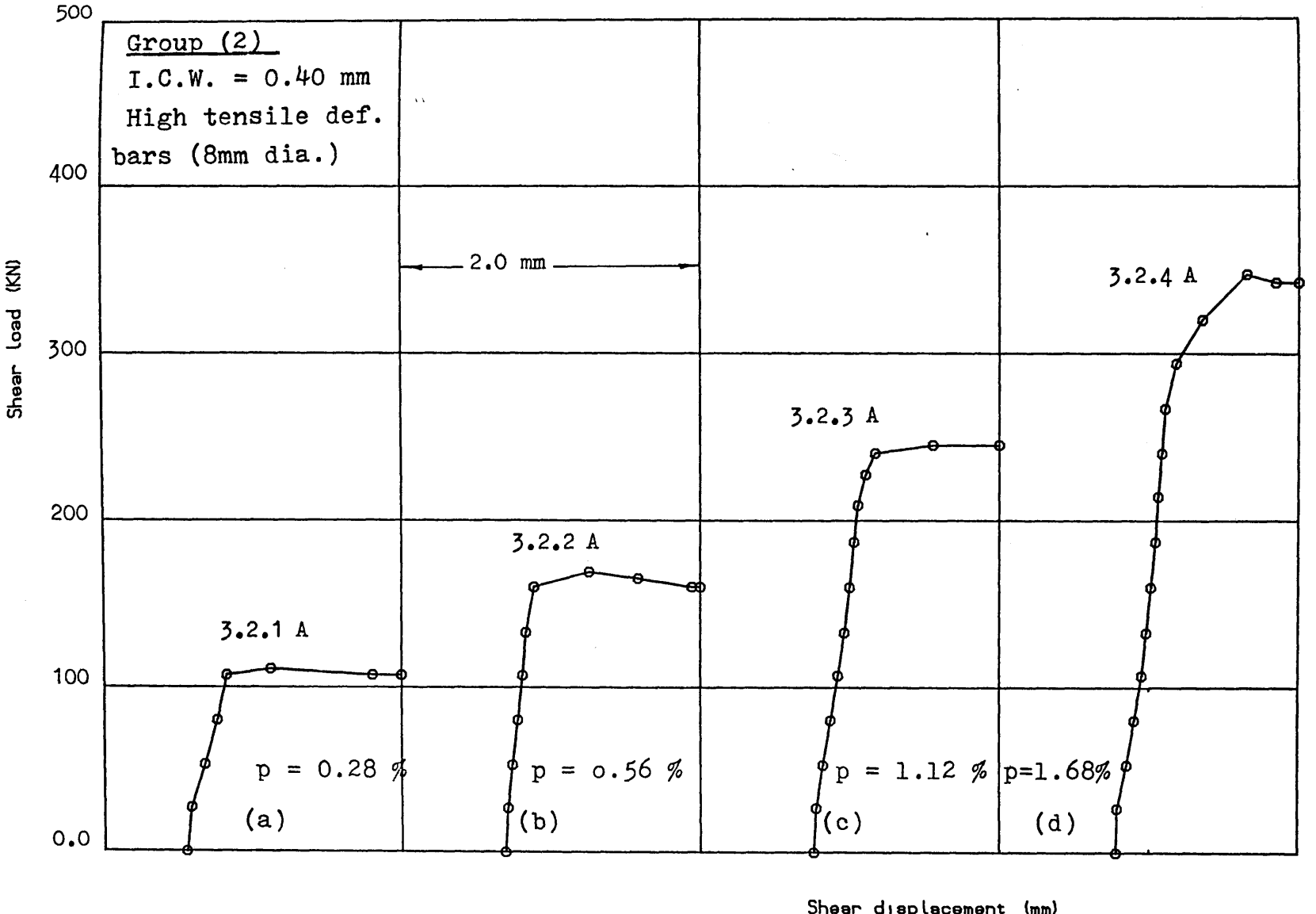

Figure(6.73) *Shear load vs shear displacement for group 2 series 3 tested under repeated loading (last cycle)*

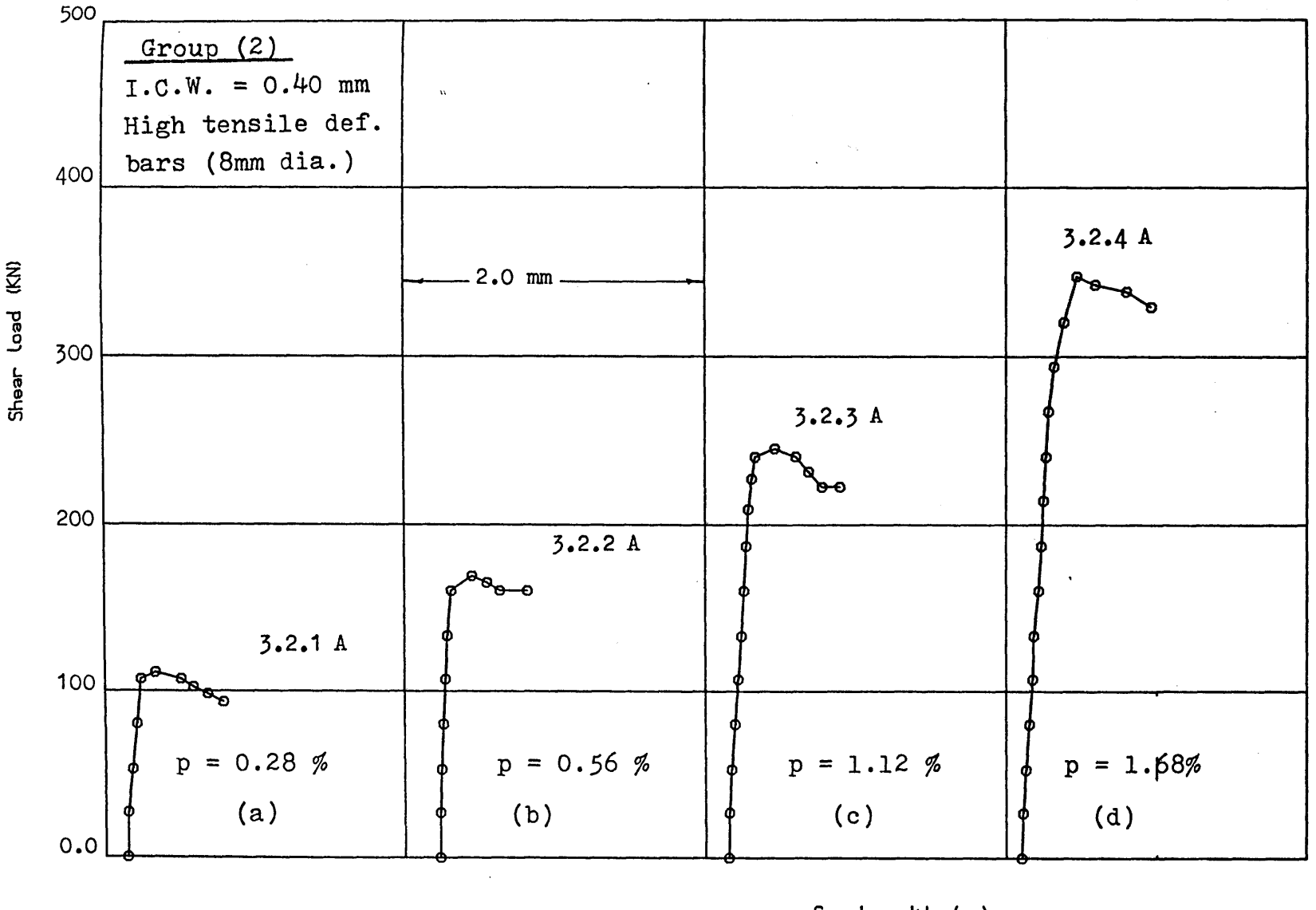

Figure(6.74) *Shear load vs crack width for specimens of group 2 series 3 tested under repeated loading, last cycle*

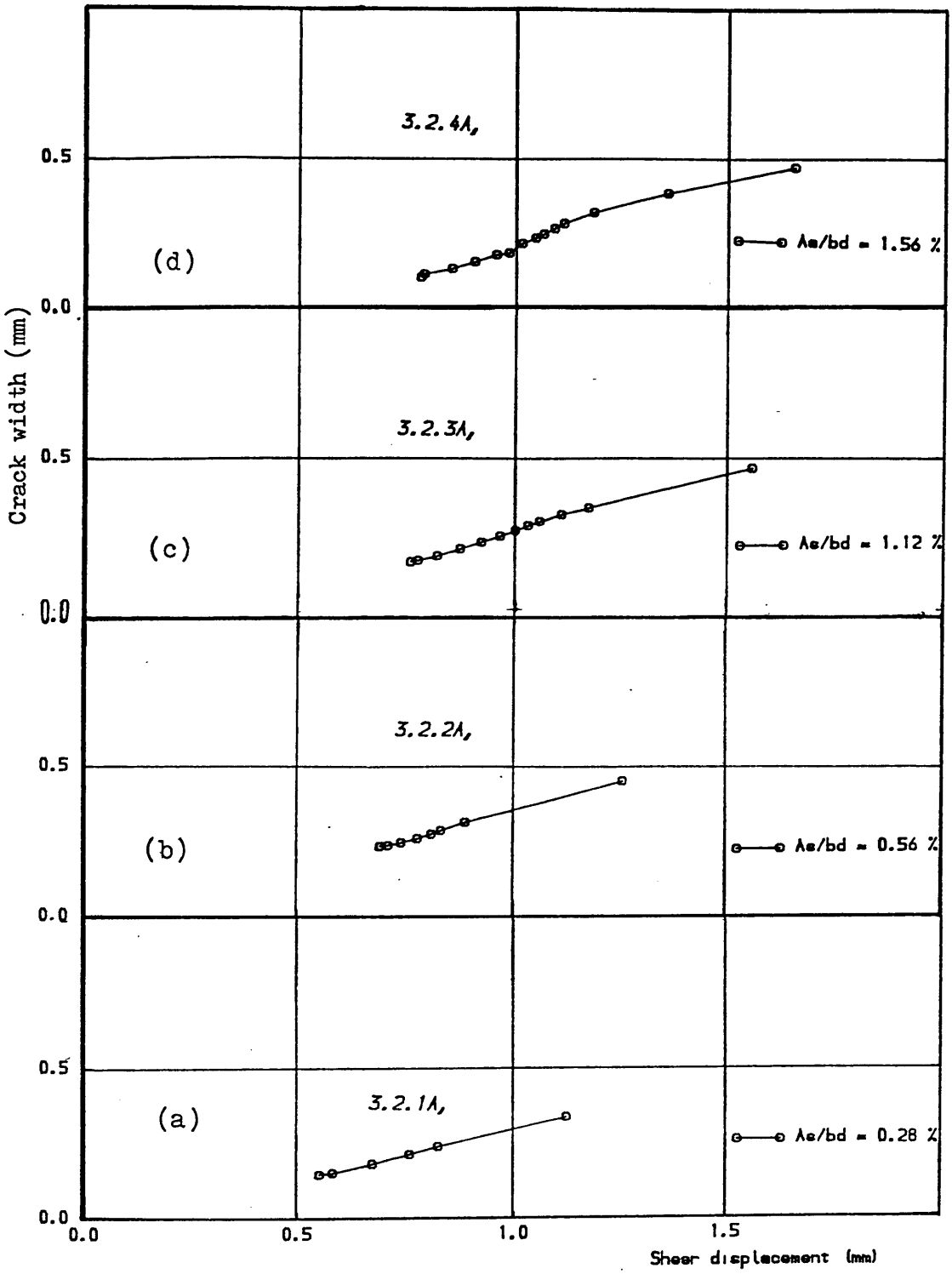

Figure(6.75) Crack width vs shear displacement for specimens of group(2) series-3 tested under repeated loading,last cycle .

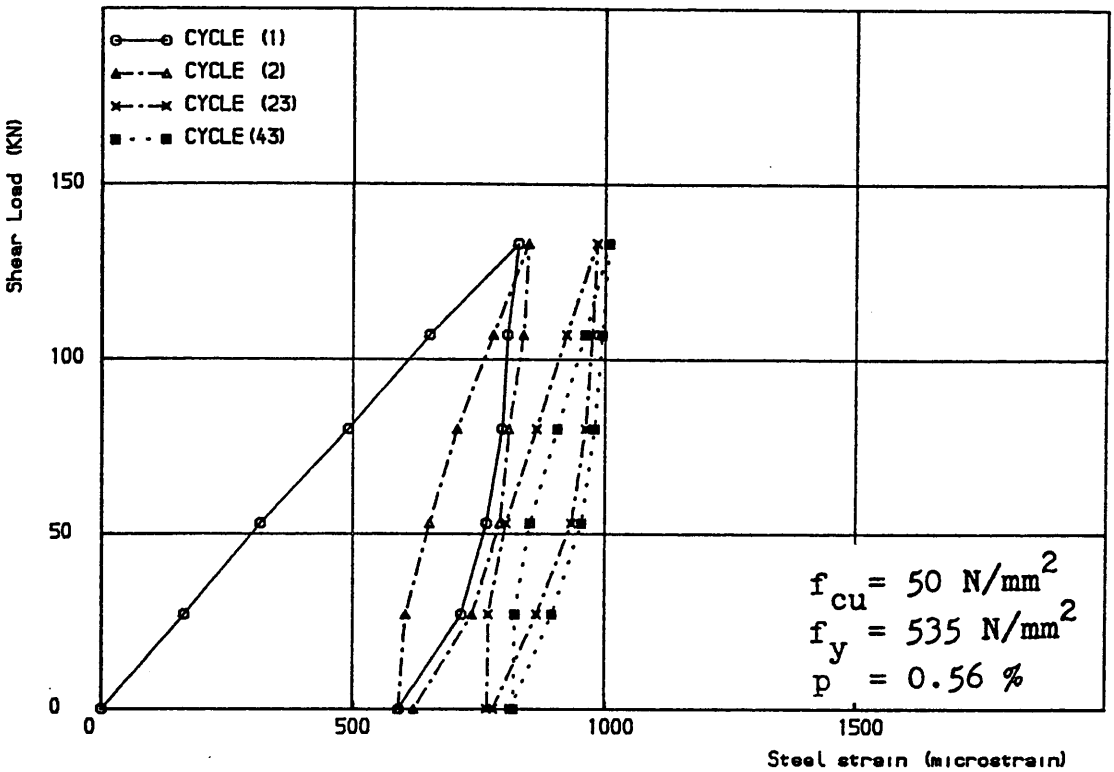

Figure (6.76) Shear load vs steel strain, specimen 3.2.2A, load cycles 1, 2, 23 and 43

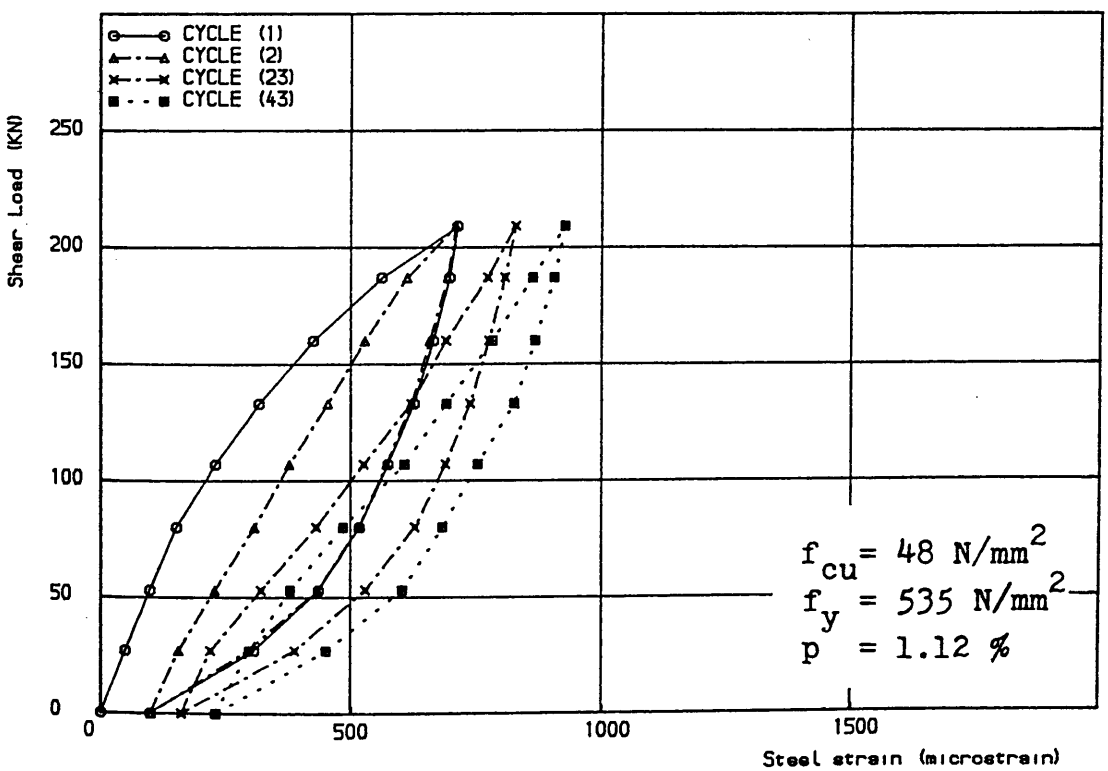

Figure (6.77) Shear load vs steel strain, specimen 3.2.3A, load cycles 1, 2, 23 and 43

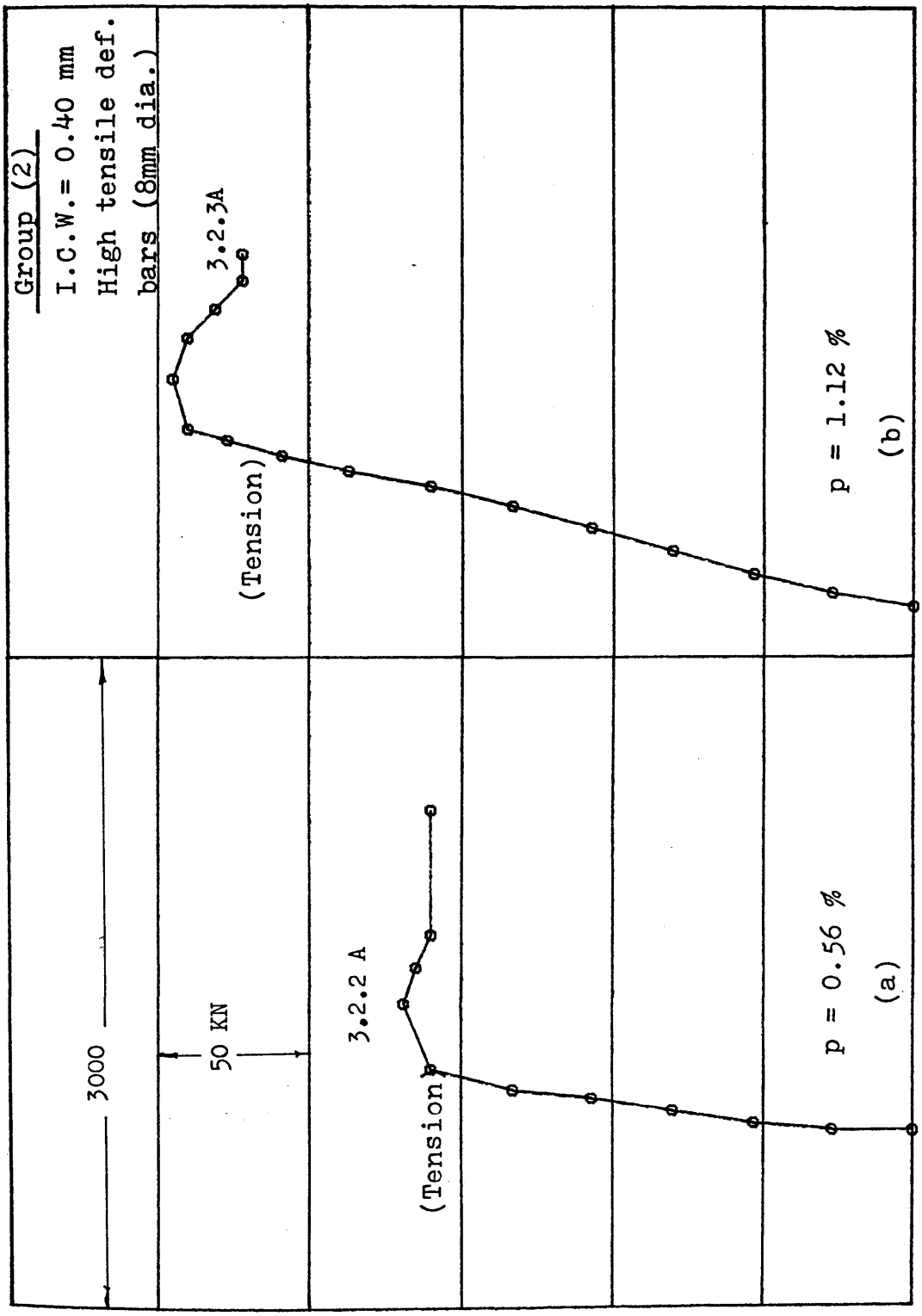

Figure (6.78) Shear load vs steel strain for specimens 3.2.2A and 3.2.3A, last cycle

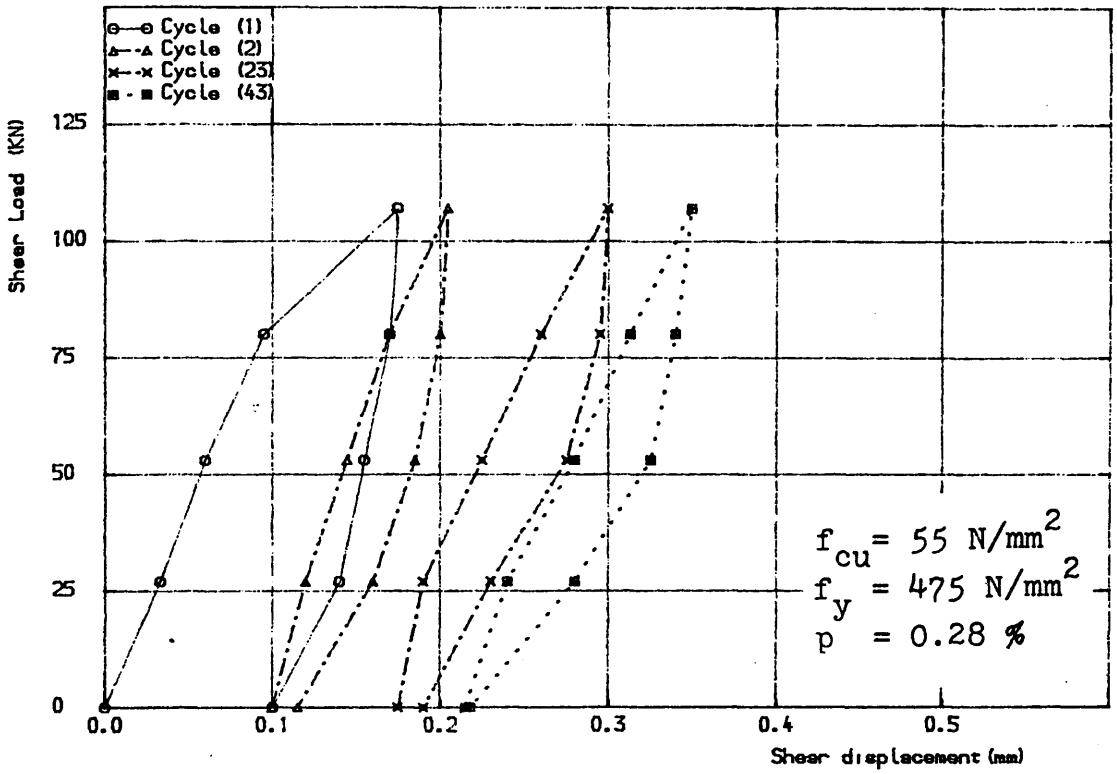

Figure (6.79) Shear load vs shear displacement, specimen 3.3.1A load cycles 1, 2, 23 and 43

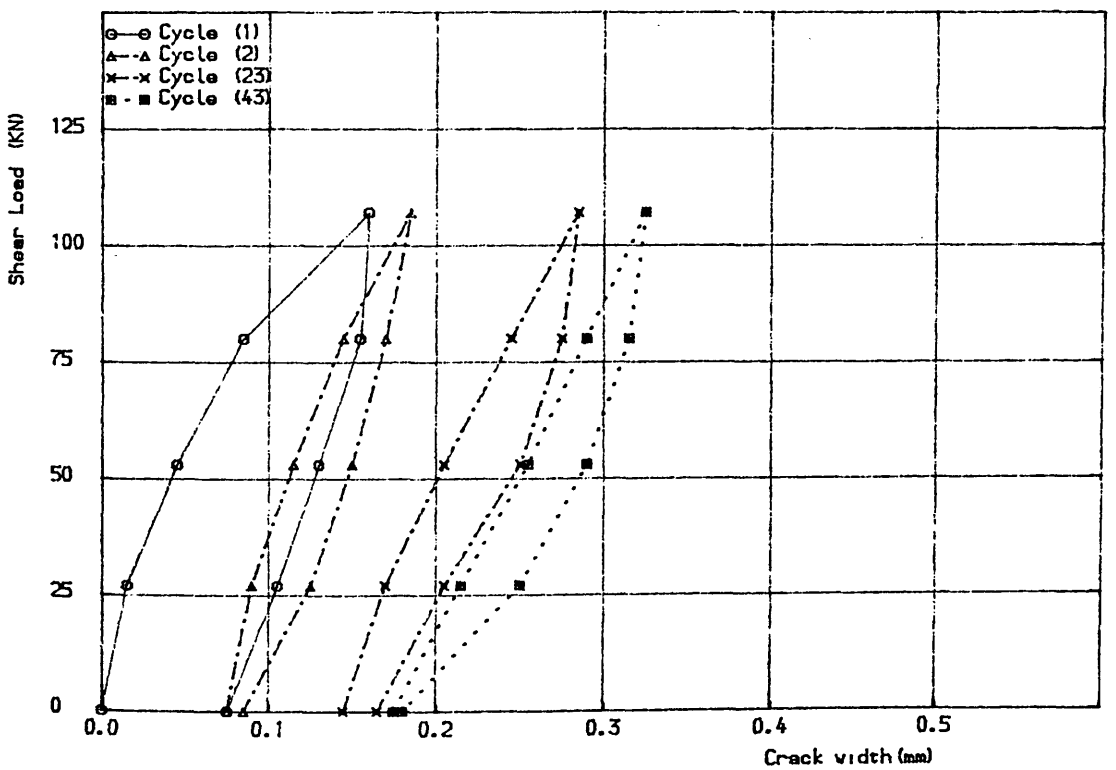

Figure (6.80) Shear load vs crack width, specimen 3.3.1A, load cycles 1, 2, 23 and 43

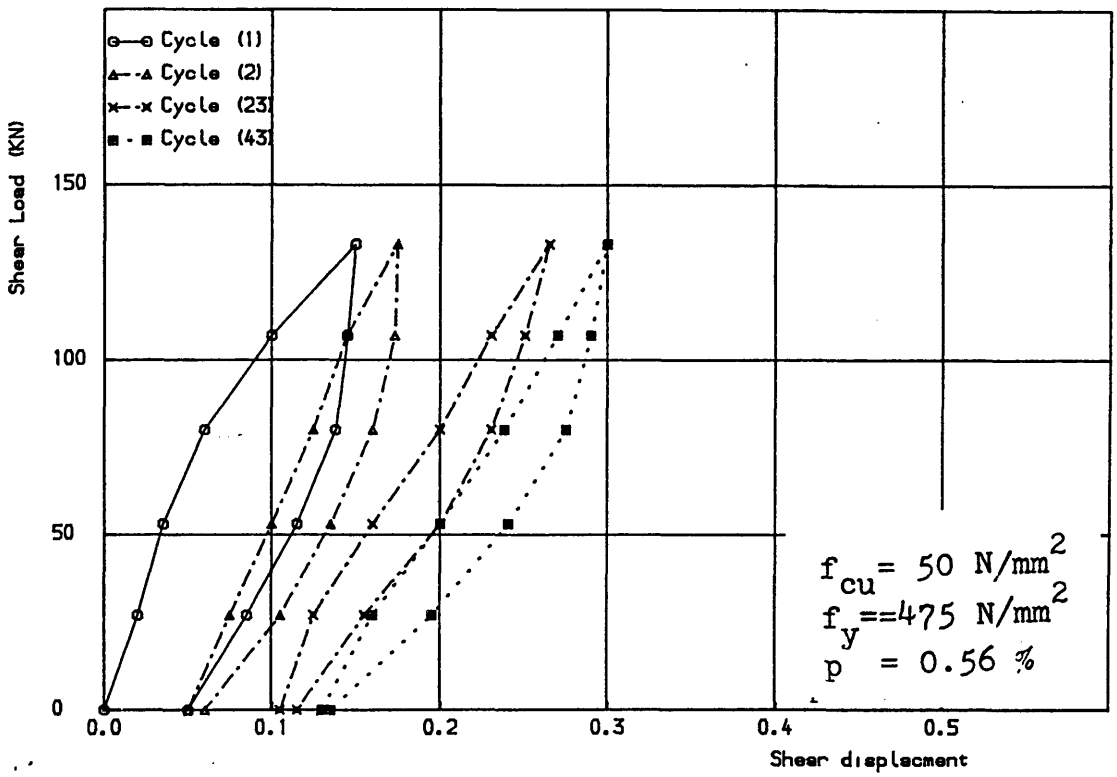

Figure (6.81) Shear load vs shear displacement, specimen 3.3.2A, load cycles 1, 2, 23 and 43

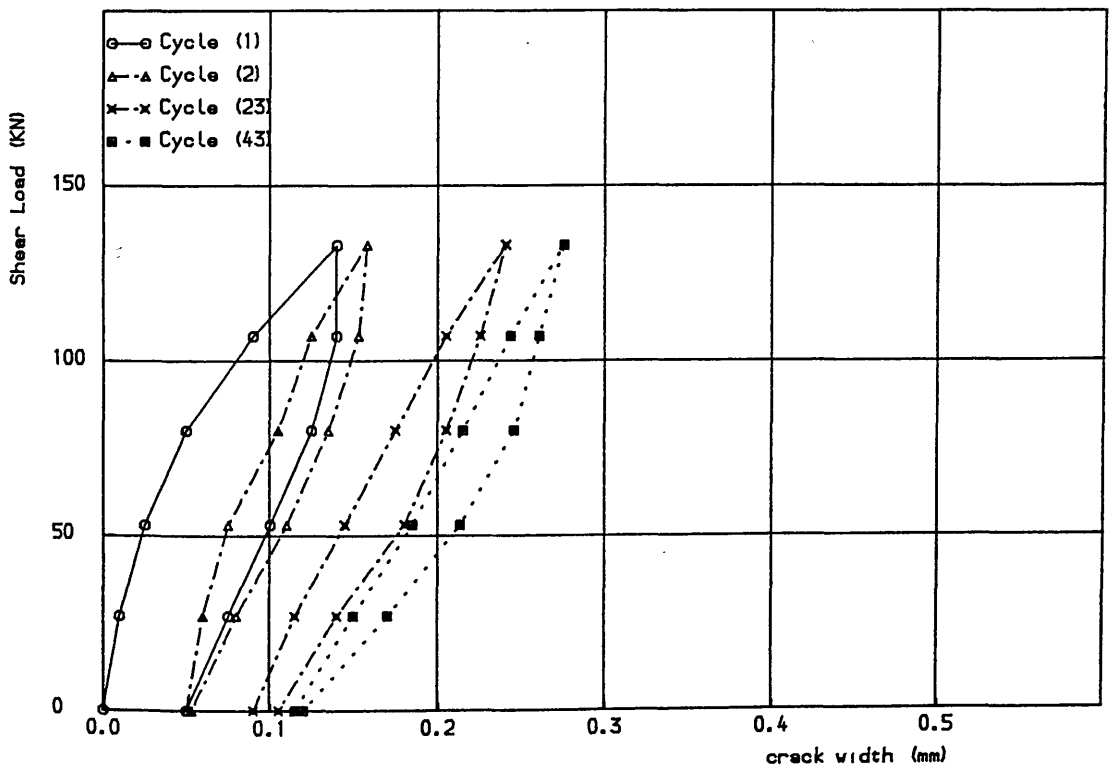

Figure (6.82) Shear load vs crack width, specimen 3.3.2A, load cycles 1, 2, 23 and 43

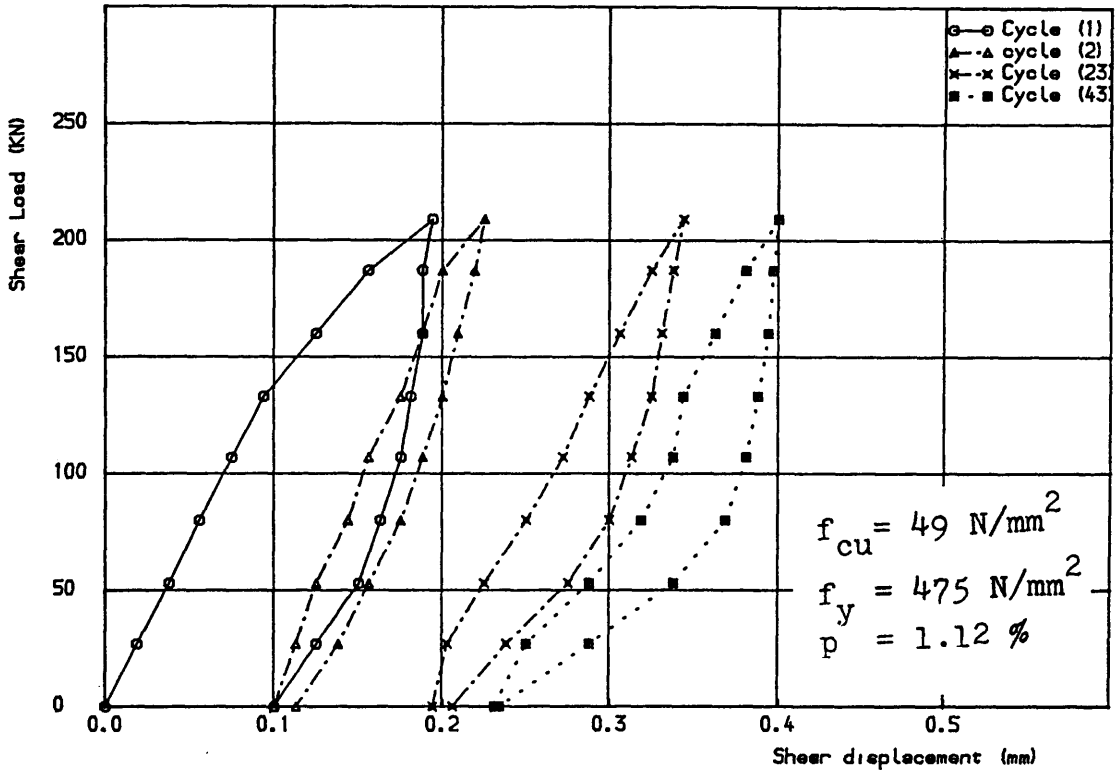

Figure (6.83) Shear load vs shear displacemnt, specimen 3.3.3A, load cycles 1, 2, 23 and 43

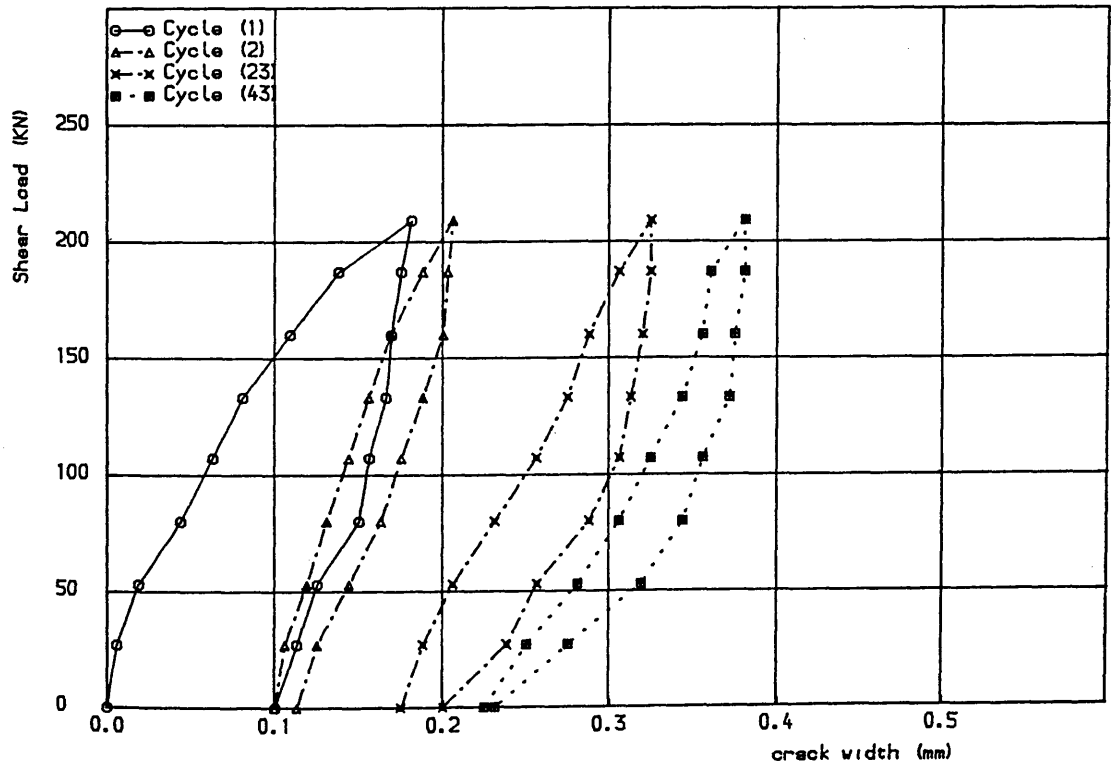

***Figure (6.82) Shear load** vs crack width , specimen 3.3.3A, load cycles 1, 2, 23 and 43*

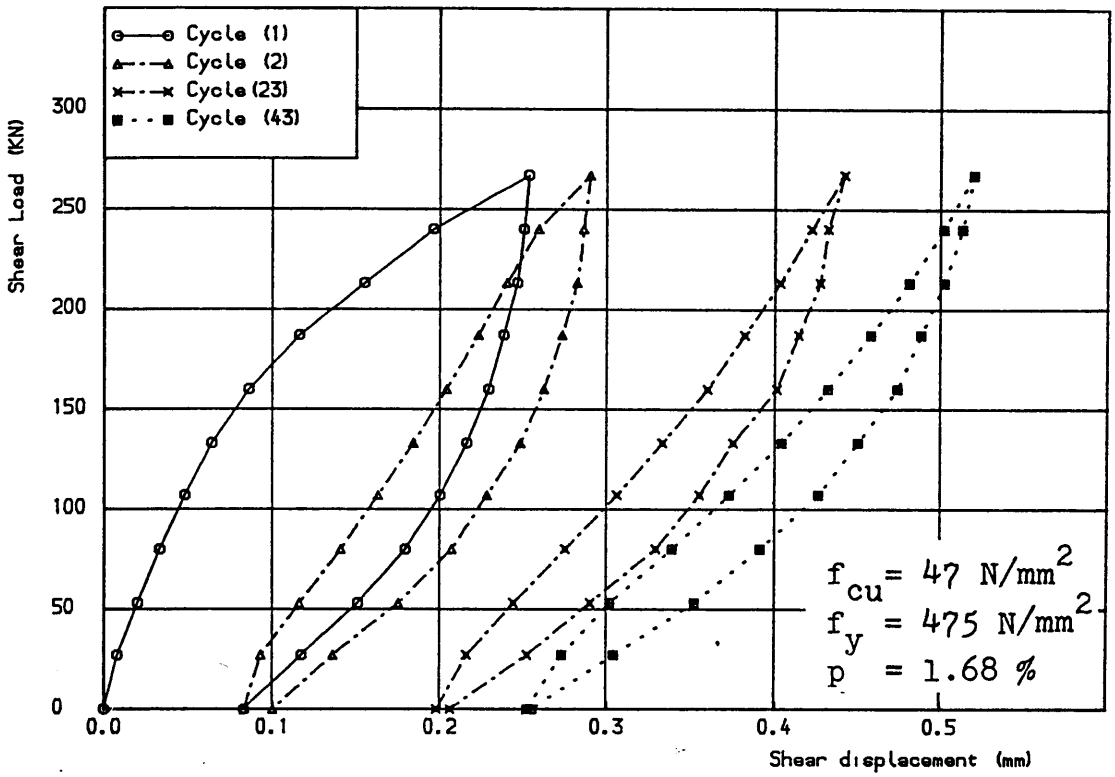

Figure (6.85) Shear load vs shear displacement, specimen 3.3.4A, load cycles 1, 2, 23 and 43

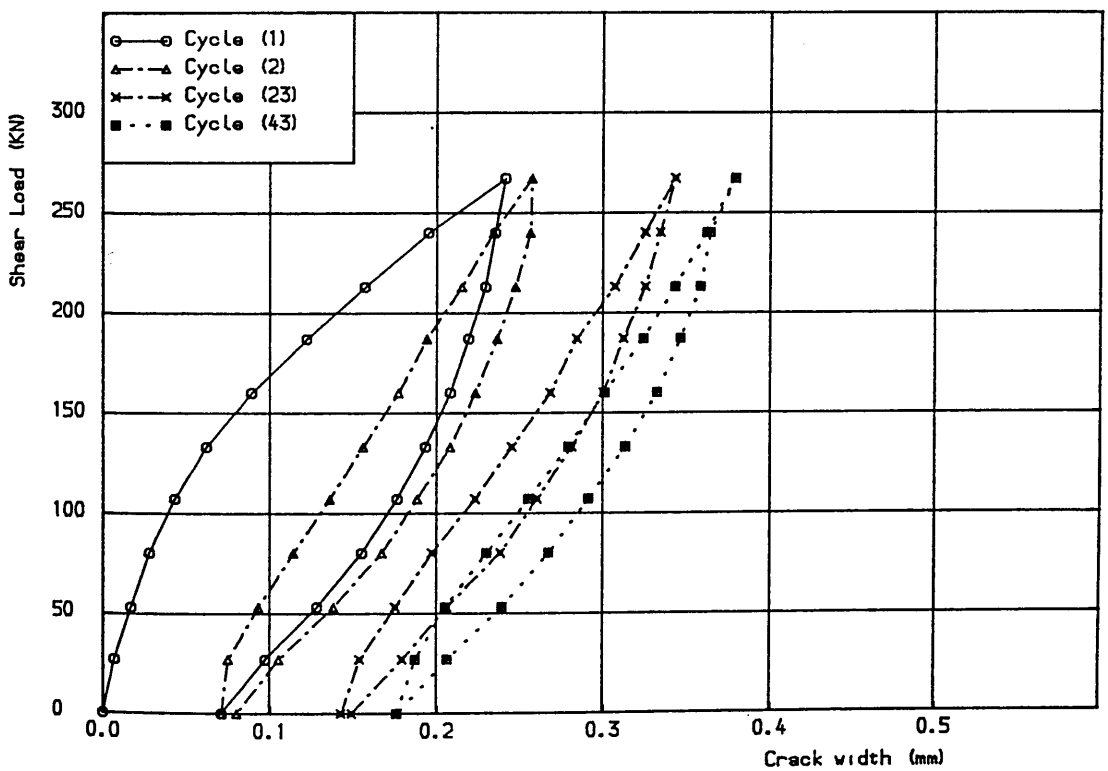

Figure (6.86) Shear load vs crack width, specimen 3.3.4A, load cycles 1, 2, 23 and 43

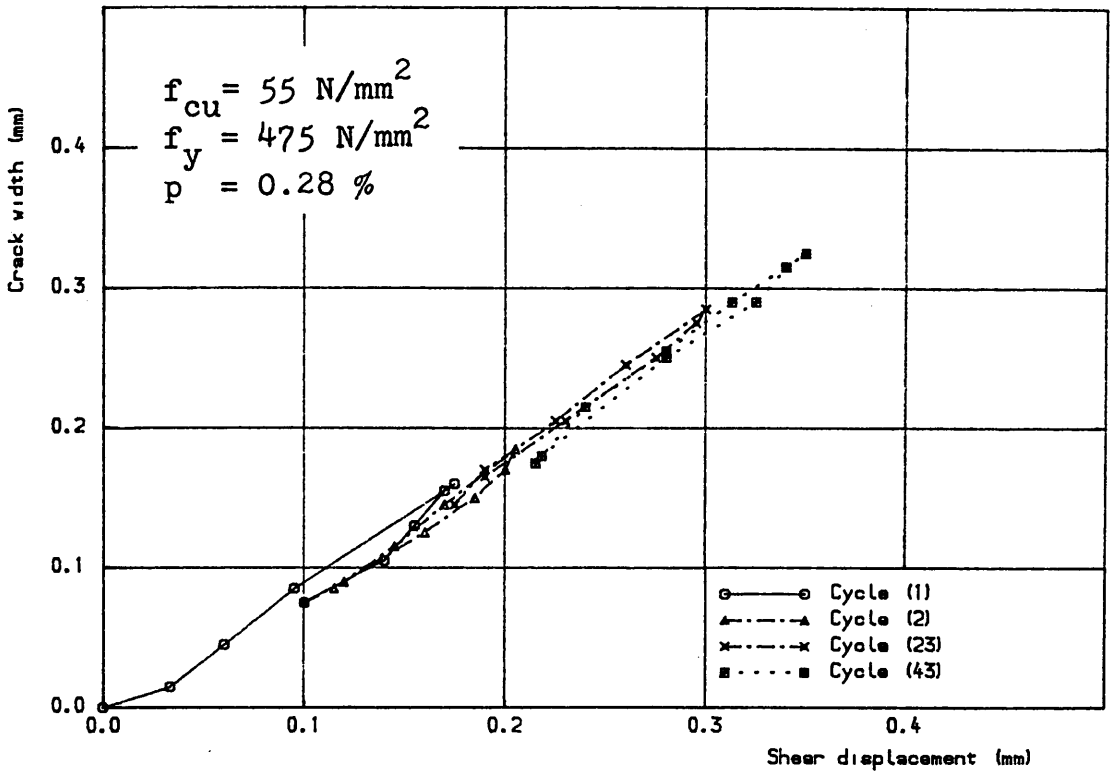

Figure(6.87) *Crack width vs shear displacement, specimen 3.3.1A, load cycles 1, 2, 23 and 43*

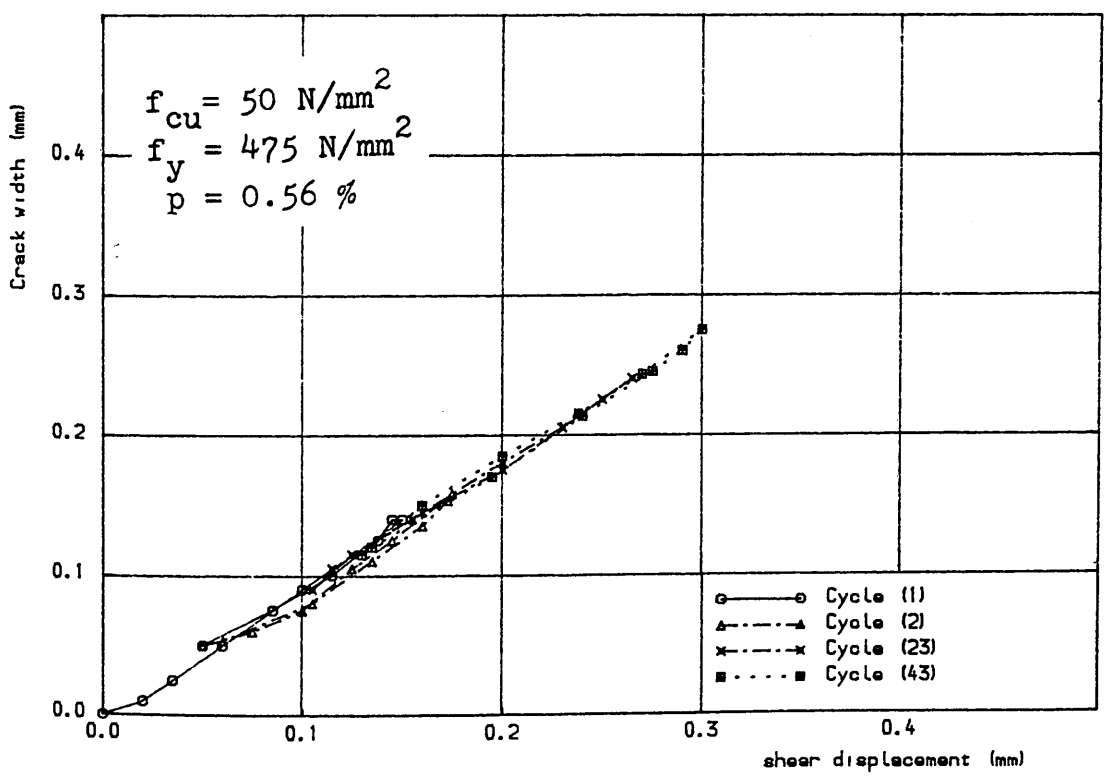

Figure(6.88) *Crack width vs shear displacement, specimen 3.3.2, load cycles 1, 2, 23 and 43*

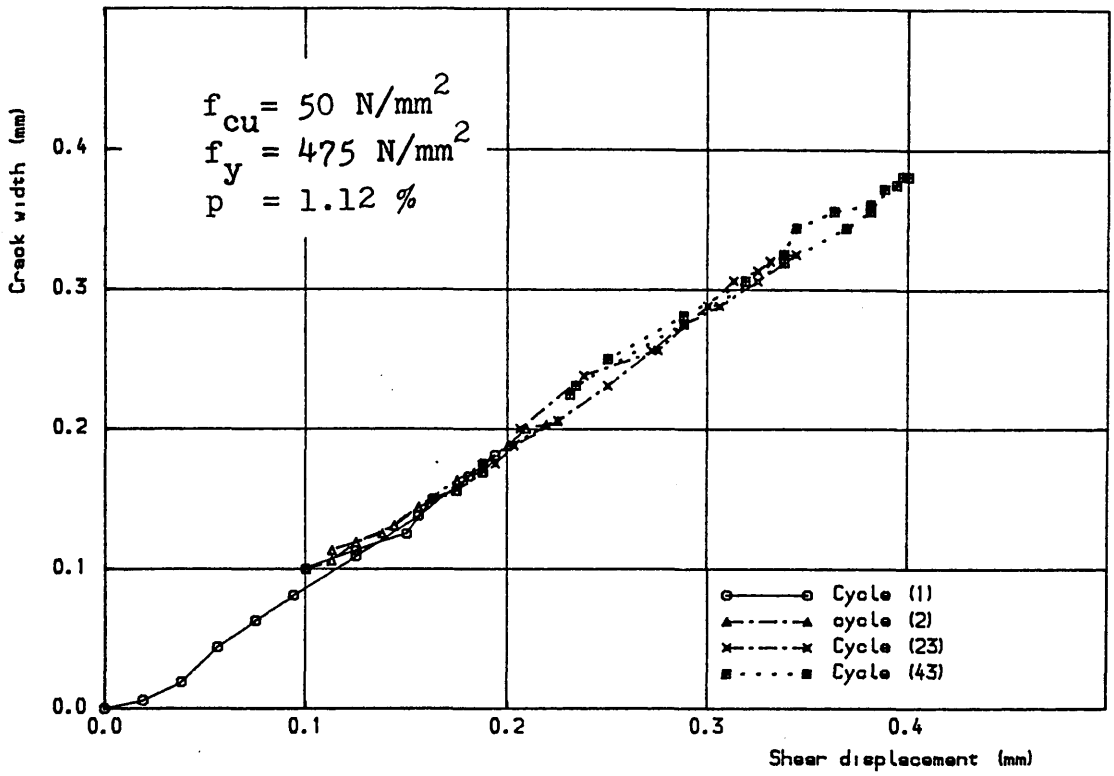

Figure(6.89) *Crack width vs shear displacement, specimen 3.3.3A, load cycles 1, 2, 23 and 43*

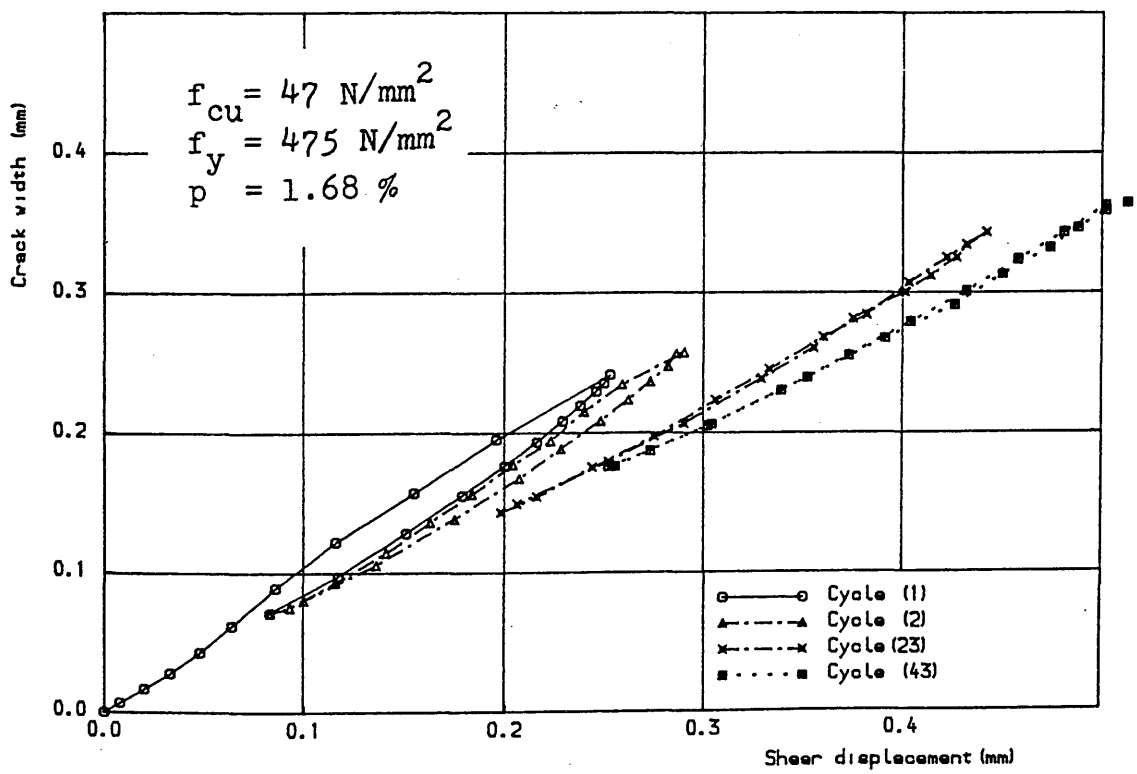

Figure(6.90) *Crack width vs shear displacement, specimen 3.3.4A, last cycle*

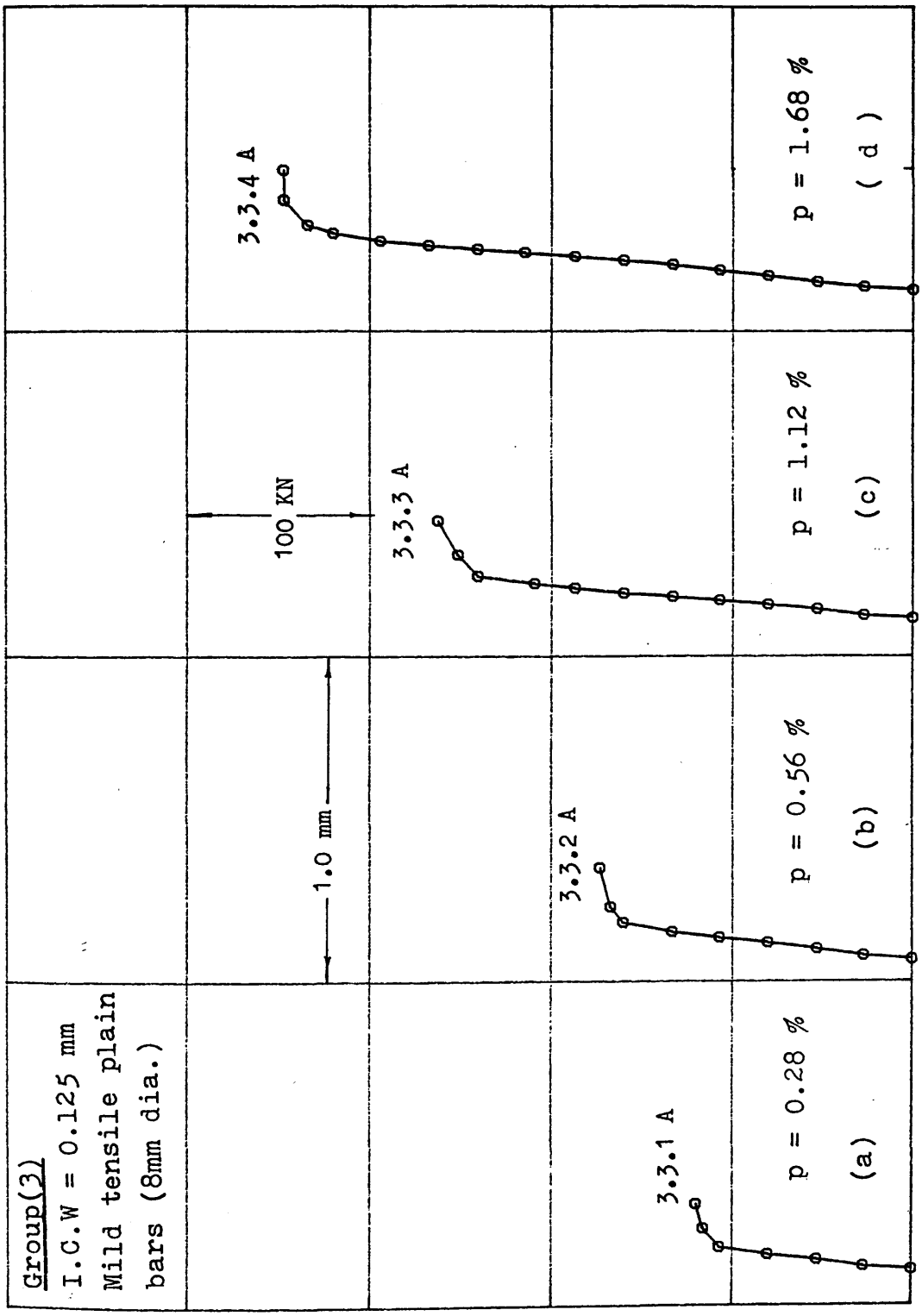

Figure(6.91) *Shear load vs shear displacement for specimens of group 3, series 3 tested under repeated loading (last cycle)*

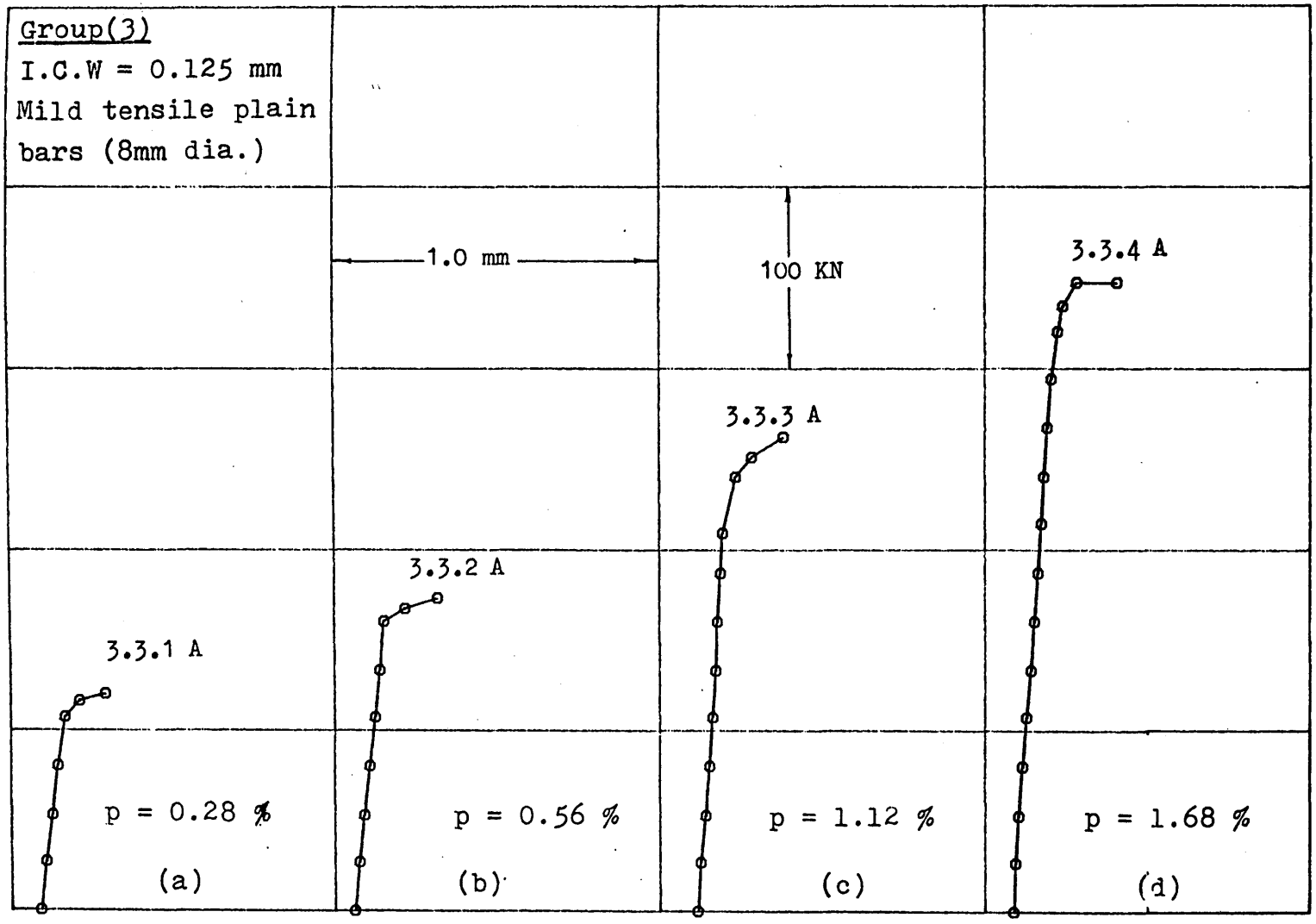

Figure(6.92) *Shear load vs crack width for specimens of group 3, series 3 tested under repeated loading (last cycle)*

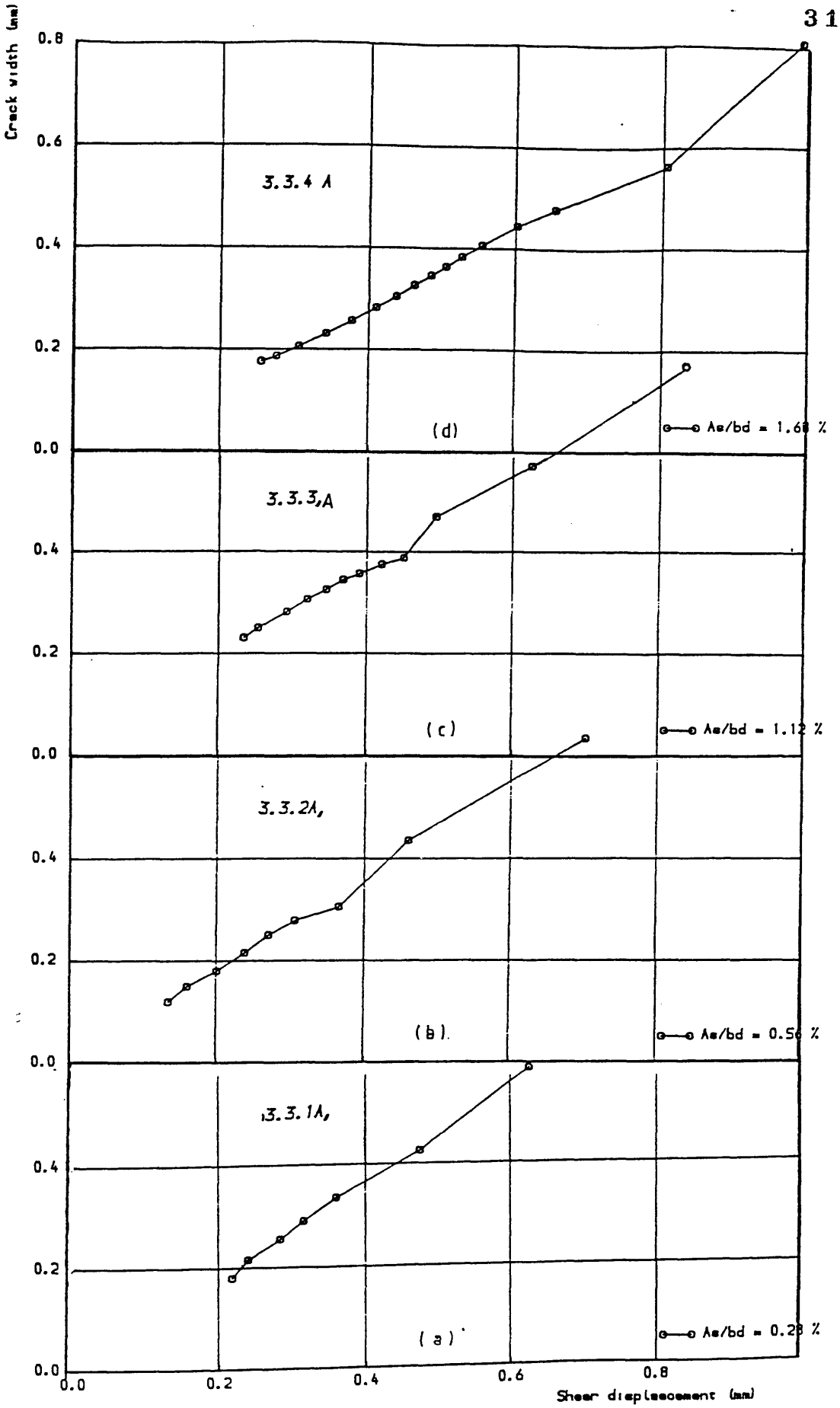

Figure(6.93) Crack width vs shear displacement for group(3) series-3 under repeated loading , last cycle.

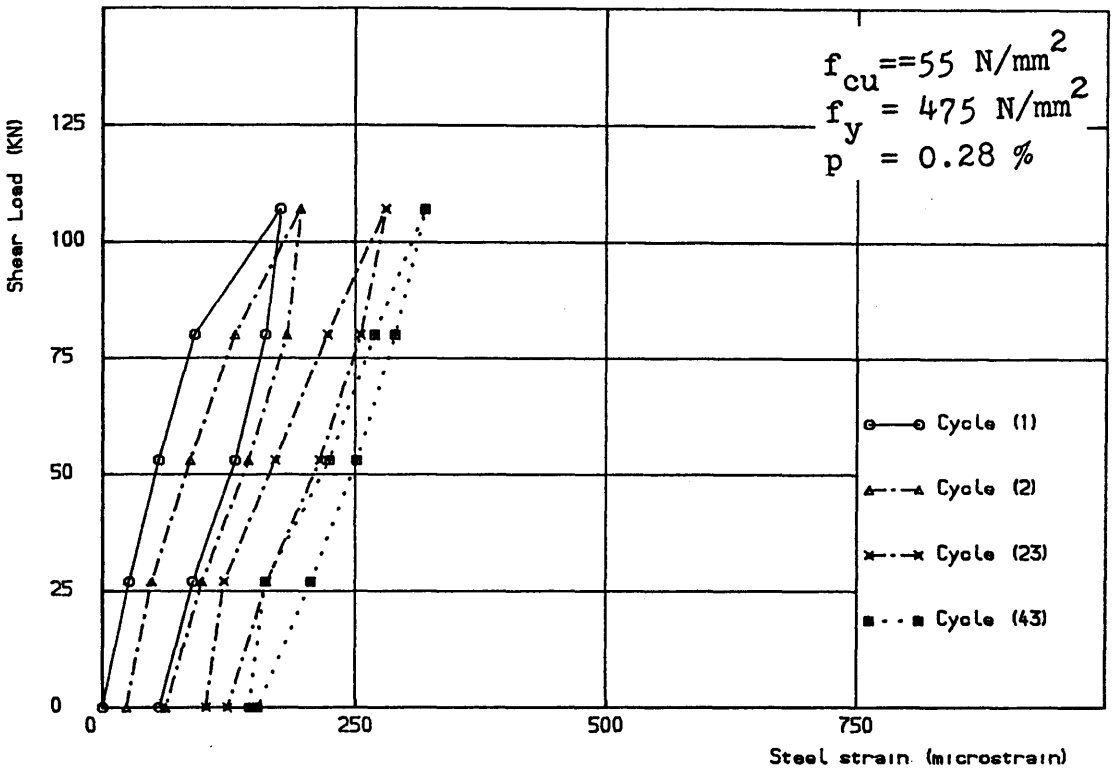

Figure(6.94) *Shear load vs steel strain for specimen 3.3.1A, load cycles 1,2,23,43*

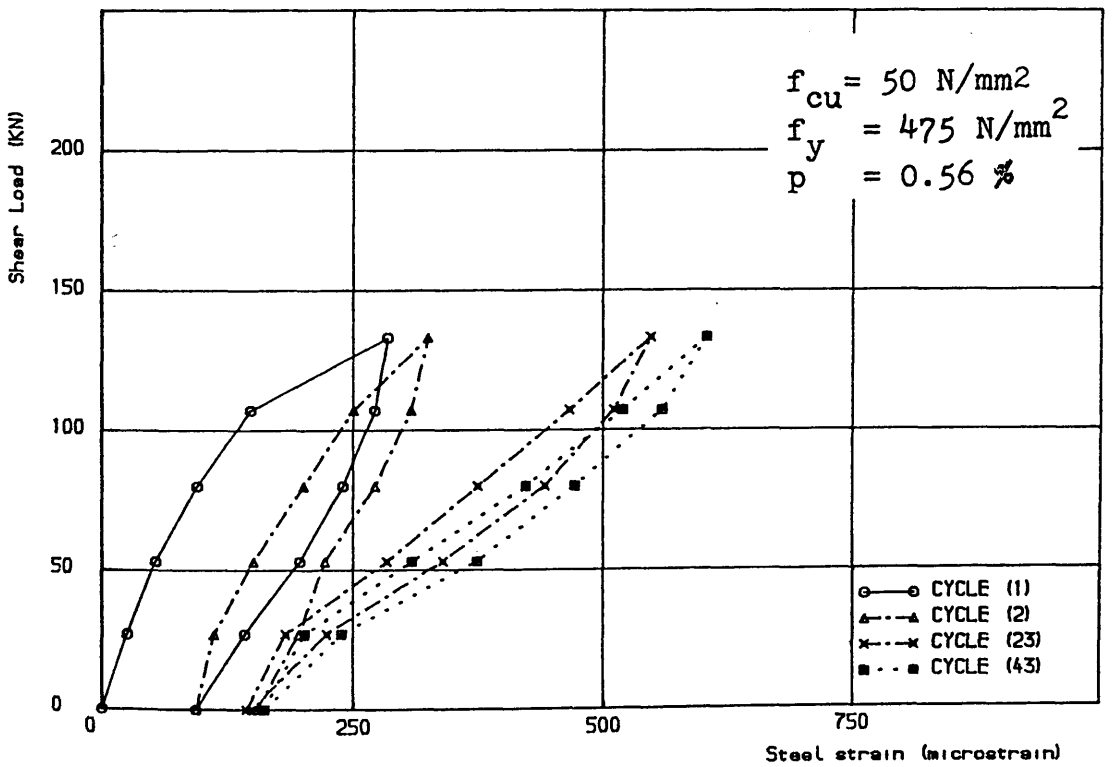

Figure(6.95) *Shear load vs steel strain for specimen 3.3.2A, load cycles 1,2,23 and 43*

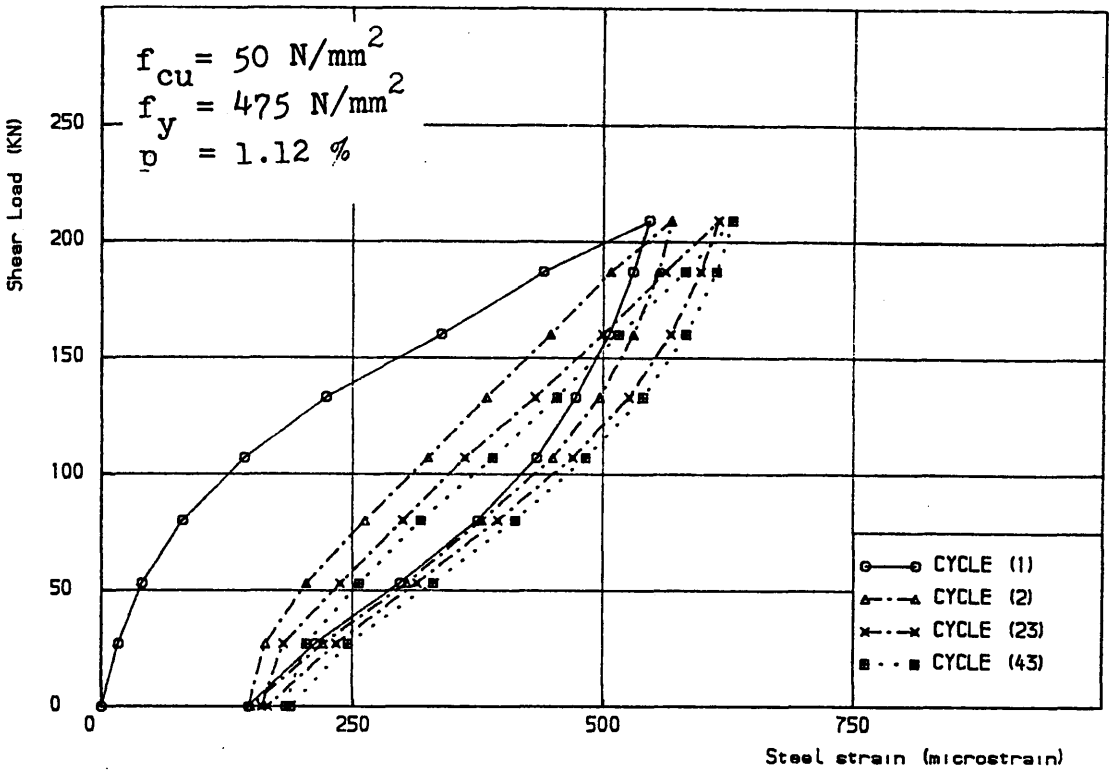

Figure(6.96) *Shear load vs steel strain for specimen 3.3.3 A, load cycles 1, 2, 23 and 43*

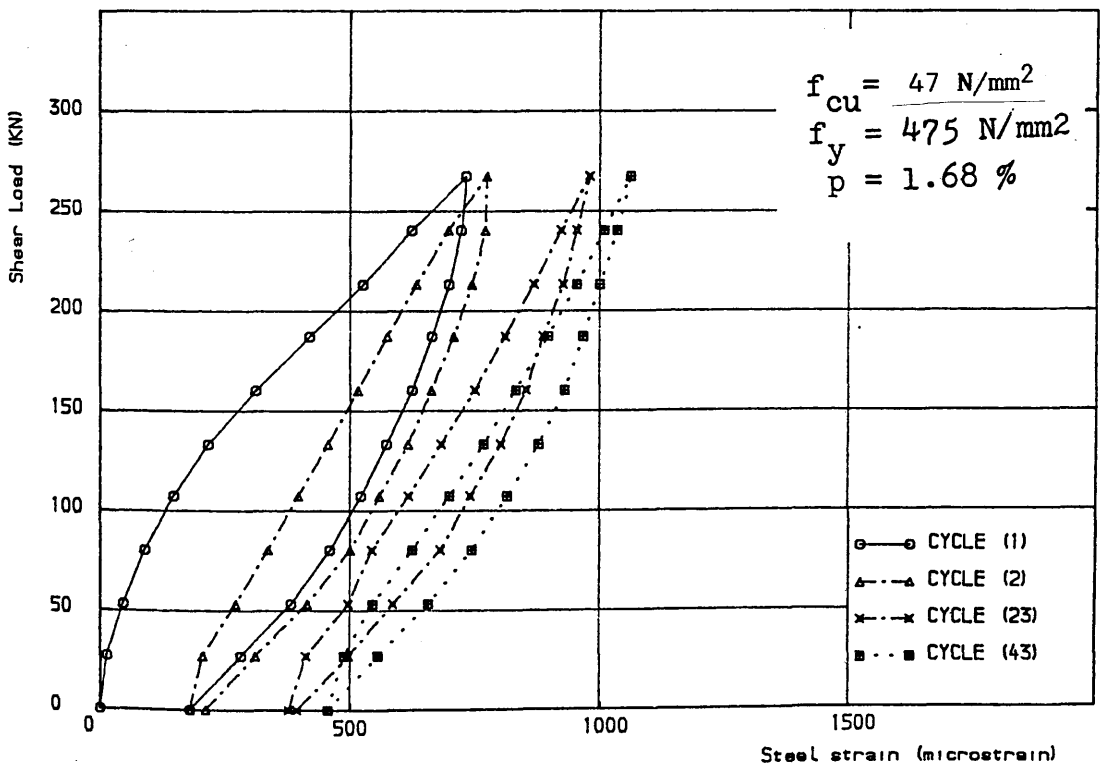

Figure(6.97) *Shear load vs steel strain for specimen 3.3.4A, load cycles 1, 2, 23 and 43*

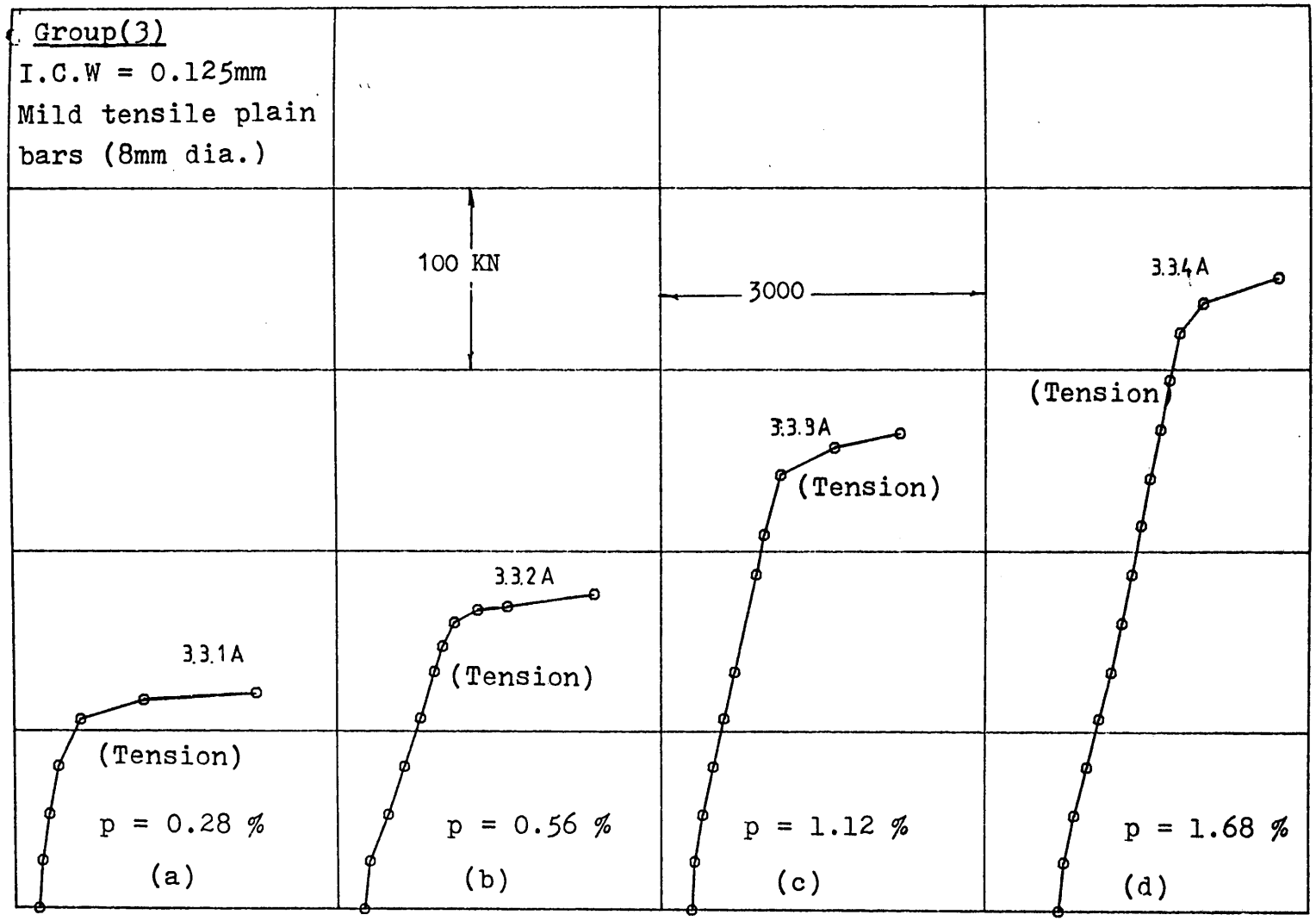

Figure(6.98) *Shear load vs steel strain for specimens of group (3) under repeated loading, last cycle*

REFERENCES

(1) Walraven, J.C. "Experimental on shear transfer in cracks in concrete". Part 2: Analysis of test results, Report 5-79-10. Steven Laboratory, Delft University of Technology.

CHAPTER (7)

DISCUSSION AND ANALYSIS OF TEST RESULTS

7.1 Introduction

This chapter discusses and analyses the experimental results presented in chapters (5) and (6) respectively. It is divided into four main sections: the first two sections deal with dowel action under monotonic and repeated loading whereas the other two sections deal with the combined action.

Although the monotonic tests were carried out to act as a comparator for the repeated tests they were also analysed in their own right to test and improve current theories, and to form the basis of a unified theory covering all cases.

7.2 Dowel action under monotonic loading

7.2.1 General behaviour

Generally dowel action behaviour under monotonic loading was nonlinear with the shear stiffness diminishing as the applied shear load increased. This nonlinear response can be attributed to two causes:

(a) crushing or splitting of concrete underneath and around the dowel bars due to the high localized bearing stress.

(b) the axial and flexural loading on the reinforcement can cause plastic stresses in the reinforcement and hence a reduction of the dowel bar stiffness:

As all dowel specimens were made with smooth preformed cracks, insignificant crack widening during shear load was expected. However, some widening occurred which might be attributed to the damage to the concrete around the dowel bar. This would reduce the effectiveness of the tensile anchorage of the dowel bar within the concrete and could explain why crack widening occurred, even though there was no overriding of the crack faces. Kinking of the dowel bars at high shear load may also cause such crack widening due to stretching of the bars.

The increase in the ultimate shear stress due to the increase of the reinforcement ratio is evident from Figure (7.1). An increase in reinforcement ratio from 0.22% to 1.34% resulted in an increase of 337% in the ultimate shear load. It can also be seen that there is a close linear relationship between the ultimate shear load and the reinforcement ratio.

7.2.2 Dowel action mechanisms

Specimens 2.2.1 and 2.2.2 were tested to investigate in more detail the various dowel action mechanism:

Pauley et al[1] has suggested three separate mechanisms by which dowel bars resist shear load, i.e. direct shear, kinking and flexure. The majority of previous investigation agreed that direct shear is not an important mode of deformation. Kinking of reinforcement has been a subject of some debate [2],[3],[4],[5],[6],[7] as explained in chapter (2), although there was no argument that kinking did occur at large shear displacement across the crack. Flexural action of the dowel bars has been recognized[8] as the most important mechanism, occurring with significant deformation of the concrete around, and

especially beneath, the bars.

This behaviour has been modelled[9],[12],[13],[14] by considering the dowel bar as a beam on elastic foundation. However, the high stress concentrations in the concrete supporting the bar result in nonlinear deformations so that only the initial dowel stiffness can be predicted by this model. The softening of the concrete supporting a dowel bar results in a redistribution of the reactions, so that the maximum bending moment in the bar moves away from the crack location and it may be assumed that failure would occur when the bar reaches its ultimate bending capacity.

An attempt was made to investigate these different mechanisms using the results of specimens 2.2.1 and 2.2.2. The distribution of the average flexure and axial tensile strains and stresses were shown in Figures (5.17) to (5.21) and (5.26) to (5.31). Although insufficient measurements were obtained at the shear plane due to the damage of the strain gauges, the general distributions of the strains show that the dominant mechanism with no doubt is the flexure of the dowel bars. However, axial tensile strains were also induced in the dowel bars which are a good indication of the partial kinking of the reinforcement, especially at high applied shear load, where axial strains were relatively increased, especially at positions near the shear plane indicating the enhancement of kinking mode. The large increase of shear displacement is also an evidence of such an hypothesis. Thus, it can be concluded that the principal mechanism of dowel action is the flexure mode of the dowel bars, but at high shear load the kinking mechanism also participates in resisting the shear force.

7.2.3 Calculation of ultimate shear load

From the previous discussion on dowel action mechanisms it is possible to derive an equation to predict the ultimate shear load resisted by dowel action.

Assuming that flexural action is the dominant mechanism, failure will occur when the bar reaches its ultimate bending moment. The plastic moment M_p can be obtained from an analysis of the section, giving

$$M_p = 1/6\ f_y\ \phi^3 \qquad (7.1)$$

where

f_y is the yield stress of the reinforcing bar

ϕ is the diameter of the bar

A study of the internal equilibrium required to produce this moment gives the ultimate dowel force V_{du} as

$$V_{du} = n.\frac{2M_p}{L} \qquad (7.2)$$

where L is the length between the plastic hinges on each side of the shear plane.

n is the number of bars crossing the crack plane, assuming that all bars are the same material and diameter and behave identically.

From equations (7.1) and (7.2)

$$V_{du} = \frac{nf_y\phi^3}{3L} \qquad (7.3)$$

The position of plastic hinge depends on many parameters including the concrete strength, the bond between concrete and reinforcing bar,

type of bar, the bar diameter and the spacing between bars. However, it seems that the most important parameter is the bar diameter because this has a strong influence on the bond strength and the mode of concrete failure[15], i.e. splitting or crushing of the concrete, the condition which must affect the location of the plastic hinge. Thus assuming that the span length between the plastic hinges is a linear function of the bar diameter

$$\text{i.e. } L = c\Phi \qquad (7.4)$$

where c is coefficient which can be determined from the test data and which depends on the other properties such as concrete strength and bar spacing and type of reinforcement. From the test data a value of c = 0.88 gave acceptable fit to the data.

Then from equations (7.3) and (7.4)

$$V_{du} = 0.378.n.\Phi^2 f_y \qquad (7.5)$$

An empirical equation was also obtained using linear regression analysis of the test results shown in Figure (7.1), leading to

$$V_{du} = (c_1 + c_2\, \rho f_y).\ A_c.f_{cu}^{1/2} \qquad (7.6)$$

where

f_y is yield stress of the dowel bars (N/mm^2)

f_{cu} is the concrete compressive stress (N/mm^2)

ρ is the reinforcement ratio of the dowel bars crossing the shear plane

A_c is the area of shear plane (mm^2)

C_1, C_2 are constants computed from the analysis of test data and equal to 0.016 and 0.065 respectively.

This expression fits test results with correlation coefficient 0.998 as shown in Figure (7.1).

The ultimate shear force given by equations (7.5) and (7.6) and the experimental shear load are compared in Table (7.1a) and show a close prediction. Therefore, it can be deduced that the concrete strength has insignificant effect on the ultimate dowel force. This deduction is consistent with previous investigations [10]. Comparison is also made with equations of Millard and Johnson [10] and Walraven [11] to test their applicability (see Table 7.1a). It can be seen that the proposed equations showed a reasonable agreement with other investigations which indicates their general validity.

7.2.4 Beam on elastic foundation theory

As discussed in Chapter (2) this theory has been used by several research workers[12],[13],[14] to describe the load-displacement response of dowel action.
This theory is compared with the experimental results in Figure (7.2) using equation (2.14) i.e.

$$V_d = 0.166 \Delta G_f^{0.75} \Phi^{1.75} E_s^{0.25}$$

G_f = 730 N/mm^2 is used which is similar to that value used by Millard/Johnson[10] and Walraven [11]. Figure (7.2) shows that the initial shear stiffness of the specimens were reasonably predicted by this theory but there was a poor correlation after the onset of concrete crushing. Therefore, this theory is only adequate in the initial stages which is not unexpected since it is based on linear-elasticity.

7.2.5 Nonlinear dowel action theories

Walraven [11] formulated a semi-empirical expression (equation 2.16) to predict the behaviour of dowel action throughout the whole loading range. This expression,

$$V_d = 10(w+0.20)^{-1}\Delta^{0.36}\phi^{1.75}f_{cu}^{0.38}$$

assumes that both shear displacement and axial tension in the dowel bars causes a reduction in the foundation modulus because of the damage to the concrete. The numerical constants were obtained by a curve fit to the data of Paulay et al.[1] and White and Gergely[15]. This expression is compared with the results of the present investigation in Figure (7.2). It can be seen that although ultimate shear strength and displacements at ultimate load were predicted reasonably well, the stiffness was grossly underestimated between the onset of nonlinear behaviour and ultimate load. The correlation becomes increasingly poorer with increasing reinforcement ratio. This disparity is not too surprising since the modification of beam on elastic foundation theory was empiricably derived from just a few test results rather than resulting from a complete understanding of the internal mechanism involved.

However, Walraven's equation included the effect of artificially additional axial forces in the dowel bars in reducing the dowel stiffness. This situation did not exist in the present tests and could explain the difference. Nevertheless, if Walraven's equation is generally applicable it ought to be able to predict the present results.

The equation (2.17) proposed by Millard and Johnson[10], mainly derived from the work of Rumussen[16] and Dulaska[17], is given by

$$V_d = V_{du}\left[1 - \exp\frac{k_i\Delta}{V_{du}}\right]$$

This is also compared with the present test results in Figure (7.2). In general this equation gives a better prediction of the overall behaviour compared with Walraven's equation, particularly for lower reinforcement ratios. This tends to indicate that an exponential function, as assumed by Millard and Johnson, is a better assumption for representing the overall shear load-displacement relationship.

From the above, it can be deduced that the general validity of the available models to describe the nonlinear behaviour of the dowel action still requires further improvement.

7.2.6 Proposed idealization of shear load-shear displacement relationship

In this section a purely empirical approach is used to predict the overall behaviour of dowel action.

From the test results the shear load-shear displacement curve can be subdivided into four ranges, the initial linear stage and three successive nonlinear stages. The nonlinear stages can also be approximated by linear relationships for simplicity. Thus, the overall shear load-shear displacement curve is idealized by the quadrilinear curve shown in Figure (7.3) . The range for each stage of the idealized curve, i.e. points a,b,c and d, is demarked by values of shear load and shear displacement as proportions of the ultimate shear load and shear displacement. These values were taken as the average of the experimental values.

The ultimate shear load can be calculated using either equations (7.5) or (7.6). Based on a regression analysis of test results (see Figure 7.4) the ultimate shear displacement is given by

$$\Delta_u = 4.015 - 0.366\ \rho f_y \qquad (7.7)$$

where

Δ_u is ultimate shear displacement (mm)

ρ is the reinforcement ratio of dowel bars

f_y is the yield stress of dowel bars (N/mm^2).

The different stages shown in Figure (7.4) are then described by the following expressions:

stage (1) $$V_d = [3.207\ (\Delta/\Delta_u)]V_{du} \qquad (7.8a)$$

$$0 \leq V \leq 0.247,\ \Delta \leq 0.077\Delta u$$

stage (2) $$Vd = [0.098 + 1.9\ (\Delta/\Delta_u)]V_{du} \qquad (7.8b)$$

$$0.843V_{du} \leq V_d \leq 0.247V_{du},\ 0.387\Delta_u \leq \Delta \leq 0.077\Delta_u$$

stage (3) $$V_d = [0.74 + 0.256\ (\Delta/\Delta_u)]V_{du} \qquad (7.8c)$$

$$V_{du} \leq V_d \leq 0.843V_{du},\ \Delta_u \leq \Delta \leq 0.387\Delta_u$$

The calculated shear load-shear displacement relationship based on this idealization showed reasonable agreement with the experimental results as shown in Figure (7.5). In fact, it was difficult to test this method against the data of other researchers, to generalize its use, because the available results were not clear enough to plot the shear load-shear displacement curves.

7.2.7 Conclusions

Based on the previous discussion and analysis of the dowel action test results under monotonic loading the following conclusions can be summarized:

1. A nonlinear behaviour of dowel action was found similar to previous investigations[1],[10],[11],[17].

2. The principal mechanism of dowel action is the flexural mode of the dowel bars which is consistent with the findings obtained by Paulay et al[1], Dulaska[17] and Millard[10]. At higher shear load, i.e. 0.80 of the ultimate shear load, and up to failure, Kinking mechanism also participates in resisting shear force.

3. Beam on elastic foundation model is only adequate to predict the initial linear stage of dowel action behaviour.

4. Equation (2.17) proposed by Millard/Johnson[10] showed that an exponential function is a better assumption to represent the dowel load-displacement relationship. However, the available nonlinear models [10],[11] did not show good correlation with the present results and still require further improvement.

5. An alternative model was proposed by the author to predict the dowel load-displacement relationship which is based on the idealization of this relationship as a quadrilinear curve as described in section 7.2.6.

6. The increase in the reinforcement ratio crossing the shear plane from 0.22% to 1.34% resulted in an increase of 337% in ultimate

dowel force. Also a close linear relationship was found between the ultimate dowel force and reinforcement parameter pfy.

7. The ultimate dowel force is reasonably predicted by the suggested semi-empirical and empirical equations (7.5) and (7.6).

7.3 Dowel action under repeated loading

7.3.1 General behaviour

There was marked difference in the behaviour between the first and the subsequent cycles as shown in Figures (5.33a), (5.33b) and (5.33c). The changing behaviour can be summarized as follows:

1). First cycle: when specimen was loaded to the required shear load, a large displacement was induced compared to those of the subsequent cycles. The relationship between shear load and shear displacement can be approximated by a linear relationship. The unloading branch was nonlinear. At zero shear load, a large displacement existed.

2) Second cycle: the specimens 2.1.2A and 2.1.3A showed slightly different behaviour from specimen 2.1.4A. The incremental shear displacement measured at maximum repeated shear load was less than the displacement of the first cycle and the secant stiffness at this load was higher than the first cycle by approximately 50%. The loading branch of the shear load-shear displacement relationship exhibited nonlinear behaviour.

As the applied load was released, shear displacement initially

decreased at a low rate, but at low shear load the shear displacement decreased rapidly indicating a softer response. At zero shear load the residual of shear displacement was approximately 15% - 18% of the residual measured at the first cycle.

3) Subsequent cycles: the behaviour tends to stabilize. This could be judged by evaluating the damping factor β which was defined by Jacobson[18] as

$$\beta = \frac{1}{2\pi} \cdot \frac{\text{Area within hystersis loop}}{\text{Area under "skeleton curve"}}$$

$$= \frac{1}{2\pi} \cdot \frac{A_h}{A_1} \qquad (7.9)$$

where A_h and A_1 are shown in Figure (7.6).

From the shear load-shear displacement curves it can be seen that A_h and A_1 of cycles 23 and 43 are approximately equal. Accordingly, the calculated damping factors for these cycles numbers would be almost equal reflecting a very small amount of energy dissipation. By this stage, the specimens exhibited nonlinear behaviour both in the loading and unloading ranges.

When the shear load was released, the specimen responded similarly to the second cycle. However, the pinched trend to shear load-shear displacement was more noticeable compared to the second cycle especially for specimen 2.1.4A. The incremental residual shear displacement at zero load was very small.

4) Last cycle: the shear load was applied until failure occurred. A specimen exhibited similar behaviour to the previous cycle up

to the level of the repeated load as expected. As the load exceeded this level by an average 50% a softer behaviour existed and the trend became similar to that of the monotonic load although failing at a much lower load, as can be seen from Figure (7.7a).

This general behaviour shall be discussed in the next section.

7.3.2 Mechanism of dowel action

For the first cycle up to the repeated shear load the behaviour is obviously similar to monotonic loading. At this load level most of the shear force is resisted by the dowel bars due to the deterioration of concrete conditions around these bars. This can be deduced by referring to the high strains measured in the dowel bars (see Figures 5.40a, b and 5.41 a,b and 5.42 a,b).

The nonlinear behaviour during unloading can be attributed to the restoring force in the dowel bars and the fractured concrete around the dowel bars which prevents the dowel bars from returning back to their original positions causing residual shear displacement at zero load.

For subsequent cycles, at low applied shear load the reinforcement offers little resistance in the case of specimens 2.1.2a and 2.1.3a which indicates that the concrete surrounding the dowel bars has not yet started to degradate. But in case of specimen 2.1.4a, i.e. higher reinforcement ratio 1.34%, a different response occurred at same stage of loading where dowel bars resisted most of shearing force (see Figure 5.42 a,b), indicating some degradation of the concrete around the dowel bars. This difference in behaviour may be

attributed to the effect of the reinforcement ratio on the condition of the concrete supporting the dowel bars.

For low reinforcement ratios a larger amount of concrete would support the dowel bars compared with the case of high reinforcement ratio. This can be confirmed by referring to Figures (5.22) and (5.32) where the crack pattern of the shear planes of specimens reinforced with two and six stirrups across the shear plane were investigated. As the applied shear load increased again up to the maximum repeated load, a softer response was observed for specimens 2.1.2a and 2.1.3a indicating less resistance from the concrete surrounding the dowel bars which resulted in an increase of the strain in the reinforcement. For specimen 2.1.4a under the application of the shear load, the concrete in the neighbourhood of the shear plane does not provide adequate support to the dowel bars. Thus the bars curvature increase until contact is made between the reinforcement and concrete. At this stage the stiffness of the dowel increases considerably (see Figure 5.33).

The dowel stiffness of different stages during the unloading procedure showed a softer behaviour if they are compared with equivalent ones of first cycle. This softer behaviour during loading and unloading stages as the number of load cycle increases was expected due to the distress of the concrete conditions and the increase in the strain of dowel bars.

Based on the previous analysis and the behaviour of monotonic loading, the behaviour of the last cycle can be explained.

From the above, it can be seen that the dominant modes of dowel

action changes according to the magnitude of the dowel load applied to the reinforcement. For very small dowel forces, it can be assumed that the dowel bar transfer the forces across the crack by the shear resistance of the reinforcement. At this stage the bar only spans a distance approximately equal to the initial crack width. As the dowel forces increase, the bearing stresses induced by the dowel on the concrete deteriorate the initially cracked concrete around the bar, and consequently, the unsupported length of the dowel increases. At this point, the dowel forces are transferred across the crack primarily by bending deformations of the reinforcement. As the load increases, the unsupported length of the dowel decreases as the bars curve around the concrete and consequently dowel stiffness increases. However, both dowel stiffness and unsupported length are parameters which are difficult to estimate approximately and depend on the state of stresses in concrete surrounding the dowel bar, on the level of axial and dowel stresses sustained by reinforcement and the bar diameter.

7.3.3 Effect of reinforcement ratio

The influence of the reinforcement ratio is investigated in two ways:

(1) by fixing the repeated load as an absolute value for a certain number of load cycles.

(2) by fixing the repeated applied load as a ratio of the ultimate load obtained from the monotonic test.

The first condition is obtained by comparing the behaviour of specimen 2.1.2a (ρ = 0.45%) with 2.1.3a (ρ = 0.89%) where both were subjected to a repeated shear load of 18 kN.

From Figures (5.33a and 5.33b), it can be seen that the reinforcement has little effect on the overall behaviour but has a significant influence on the ultimate shear strength [see Figure 5.34)]. The increase of reinforcement ratio from 0.45% to 0.89% resulted in increase of 126% in the ultimate shear load.

The second condition is obtained by comparing specimens 2.1.2a and 2.1.4a where ratio of 0.35 of the ultimate monotonic load was used. A significant difference was found in the overall behaviour of these two specimens, as can be seen from Figures (5.33a) and (5.33c). This reflects the effect of spacing between dowel bars on the concrete condition surrounding the dowel bars as previously explained in Section 7.3.2. The effect of the reinforcement ratio on the ultimate shear strength can be seen by comparing the ratios of the ultimate shear load to the maximum repeated loading. These ratios were 1.72 and 2.10 for reinforcement ratios 0.45% and 1.34%. Thus the repeated loading has less effect on the ultimate shear load for specimens with higher reinforcement ratio.

7.3.4 Effect of type of loading

The difference in behaviour between monotonic and repeated loading is shown in Figures (7.7) and (7.8). It can be seen that repeated loading resulted in a significant reduction in the ultimate shear load. The ratios of the experimental ultimate shear force for both types of loadings are given in Table (7.2) where it can be seen that the ultimate shear load under repeated load is approximately 0.60-0.80 of that under monotonic loading.

From a linear regression analysis of these results an equation to predict the ultimate shear load is given by

$$V_{du} = [-0.021 + 0.055\ \rho f_y]A_c.f_{cu}^{0.5} \qquad (7.10)$$

where

V_{du} is ultimate shear load resisted by dowel action under repeated loading (N)

f_y is the yield stress of dowel bars (N/mm²)

f_{cu} is the cube compressive stress of concrete (N/mm²)

A_c is the area of shear plane (mm²)

as shown in Figure (7.8).

A general equation to predict the ultimate shear force resisted by dowel action which includes the effect of type of loadings, number of cycles, concrete strength, reinforcement ratio and type of reinforcement was derived from equations (7.6) and (7.10) and based on the following assumptions:

(1) The ultimate dowel force increases linearly with the increase of the reinforcement parameter ρf_y.

(2) The ultimate dowel force decreases linearly with the increase of number of load cycles

(3) The maximum repeated loading is ≤ 0.35 the ultimate dowel load under monotonic loading.

This equation is given by

$$\frac{V_{du}}{A_c\sqrt{f_{cu}}} = \underbrace{\left[0.016+0.065\rho f_y\right]}_{\text{"first term"}} - \underbrace{\left[8.60\text{x}10^{-4}N[1+0.27\rho f_y]\right]}_{\text{"second term"}} \qquad (7.11)$$

where

V_{du} = ultimate shear load resisted by dowel action (N)

f_y = yield stress of dowel bars (N/mm²)

f_{cu} = cube compressive stress of concrete (N/mm²)

A_c = area of shear plane (mm²)

N = number of cycles before increasing load to failure.

The first term in this equation represents the effect of monotonic loading whereas the second term represents the effect of repeated loading.

A comparison between the calculated ultimate shear strength resisted by dowel action under both monotonic and repeated loads using Equation (7.11) and experimental results is given in Tables (7.1b,c) which shows good prediction.

A comparison of shear load-shear displacement curves for monotonic and repeated loadings shows that under this history of loading it seems that initial stiffness for specimens with lower reinforcement ratio was not significantly affected (see Figure 7.7a) whereas with high reinforcement ratio a noticable effect was observed, i.e. the monotonic test specimen exhibited a stiffer response. A sudden decrease in tangent stiffnesses at higher stage of loading for repeated loading specimens was also observed compared with these of the monotonic loading.

Figure (7.7b) shows that crack widening due to repeated loading was larger than that measured in the monotonic tests. Thus the previous assumption, made about the cause of the crack widening, in spite of the smoothness of the crack surfaces, due to the damage of the concrete around the dowel bar which reduces the effectiveness of the tensile anchorage bars, is more realistic.

7.3.5 Conclusions

From the earlier discussion on the test results of dowel action under repeated loading the following conclusions can be drawn:

1. The dominant modes of dowel action changes according to the magnitude of the applied shear load, number of load cycles and the condition of concrete surrounding the dowel bars.

2. The repeated load has less effect on the ultimate dowel force for specimens with higher reinforcement ratio but at the same time it has significant influence on the overall behaviour. This was found when specimens with reinforcement ratios 0.45% and 1.34% were subjected to maximum repeated load of 0.35 the ultimate monotonic shear load for 43 cycles before the load was increased to failure.

3. According to the history of repeated load used in this study the ultimate dowel force was approximately 0.60-0.80 of that under monotonic loading.

4. The ultimate dowel force which was found to increase in a linear relationship as the reinforcement ratio increased can be calculated by Equation (7.10).

5. A general equation, i.e. Equation (7.11) was derived to predict the ultimate dowel force under both monotonic and repeated loads.

7.4 Shear transfer by combined action under monotonic loading

7.4.1 General Behaviour

The main characteristics of behaviour by combined action can be summarized as follows:

- Behaviour is dinstinctly nonlinear.
- There is a greater tendency for crack widening which is caused by interface shear transfer mechanism.
- Failure occurred due to yielding of the transverse reinforcement as indicated by steel strain measurements.
- Spacing between transverse reinforcement affects the crack pattern along the plane area. With a narrow spacing splitting cracks were observed as shown in Figure (6.40).

7.4.2 Mechanism of shear transfer

It is well established that shear is transferred across cracked reinforced concrete sections by a combination of dowel action and interface shear transfer mechanisms. Although several hypothesis have been proposed to explain the behaviour of each mechanism individually, in practical situation shear transfer is a more complex phenomenon due to the interaction between these different mechanisms.

Several previous studies[19],[20],[21],[22] described the behaviour of shear transfer only in terms of the relationship between the applied shear load and the measured shear displacement and crack width. Another important parameter, the stress in the reinforcing bars crossing the crack, was not included. This was due to the experimental difficulties of measuring the strain in an embedded reinforcing bar when it is simultaneously pulled by normal forces and transversely pressed by dowel action. Consequently, the data obtained were not sufficient to completely define the transmission of the internal forces. The tests of group (5)-series 3 were mainly conducted in an attempt to complete this lack of information.

The relative contribution of dowel action and shear transfer by combined action can be assessed by comparing the two identical pairs of dowel specimens from group (2)-series 2 and the corresponding combined action specimens of group (5)-series 3. This comparison reflects the effect of the roughness of the crack surfaces on the internal stresses in the reinforcing bars crossing the cracked section.

It was clear from Table (7.3) that interface shear transfer mechanism resulted in a noticeable reduction in the ratio of flexural to direct strain in the transverse reinforcing bars. This reduction can be attributed to an increase in direct strains or to the decrease in the flexural strains or to both of them. Table (7.3) attempts to clarify this question by comparing the ratios of both flexural and direct strains to the yield strain, i.e. ϵ_f/ϵ_y and ϵ_d/ϵ_y, for each pair of specimens. It can be seen that ϵ_d/ϵ_y ratio of the combined action compared with dowel action increases by 96% and 69% while the ϵ_f/ϵ_y decreased by 46% and 49%. Thus, it was evident that interface shear transfer causes tensile stress in the shear transverse reinforcement which restrains the crack from widening. This in turn was accompanied by a reduction in the flexure capacity of the reinforcing bar crossing the crack plane which is the principal mechanism of dowel action as deduced previously from the dowel action tests.

From the above, the activation of interface shear transfer and dowel action can be further assessed by analysing the tensile and flexural strains in the transverse reinforcement.

The relations of the applied shear load against the strains measured on the top and at the bottom surfaces of the reinforcing bar crossing the crack plane and at different distances from the crack plane for specimens of group (5)-series 3 are presented in Figures (7.9) and (7.10). At initial stages the interface shear transfer is the dominant mechanism which is confirmed by the small increase in shear displacement due to the interlocking of the protrusions along the crack surfaces. Also from the steel strain close to the crack plane, i.e. at distance 1.25 times the bar diameter, the difference in the strain on the top and bottom surfaces indicates little bending, i.e. dowel action [see Figures (7.9) and (7.10a)].

With a further increase in the applied shear load, behaviour becomes nonlinear and a greater increase in the shear displacement occurs. This reflects the deterioration of the interface shear transfer mechanism and development of the dowel action. This was also evident from the increase in the flexural strains.

At stages near to the failure load, the dominance of dowel action became obvious from the considerable increase in flexural strains in the reinforcement and from the large increase in shear displacement. This reflects the deterioration of the interface shear transfer mechanism due to the shearing off of the asperities along the crack surfaces which causes less contact between the opposite faces of the crack and a greater tendency for the crack to slip.

These different stages are summarized and schematically shown in Figure (7.11). The limits of different stages shown in this figure can be determined from the transition zones of shear load versus shear displacement curves.

7.4.3 Idealization of the shear load-shear displacement relationship

Previous studies [22],[24] predicted the behaviour of shear transfer across a cracked section by using the elasto-plastic dowel action model and two phase model. The difficulty of using such methods is that the initial tensile stiffness of the reinforcement normal to the crack plane should be known. Moreover, in this method the interaction between the interface shear transfer and dowel action is not considered.

An empirical approach is used here to predict shear transfer behaviour. It is based on the idealization of the shear load-shear displacement relationship using a linear regression analysis of the test results and on the understanding of the internal mechanisms of the phenomenon.

As mentioned before, the experimental shear load-shear displacement curves for all specimens showed similar trends. This trend is initially characterized by a linear relationship and then followed by nonlinear relation up to the shear failure load. This nonlinear part can be simplified to a bilinear curve. Thus the overall response can be idealized by the trilinear curve abcd shown in Figures (7.11) and (7.12). The coordinates of these points are taken as a proportion of the ultimate shear load and the ultimate shear displacement, i.e. shear displacement measured at ultimate shear load. The coefficient γ, β shown in Figure (7.12) were determined by analysing the test results and their proposed values are given in Table (7.4a). It can be seen that the type of transverse reinforcement has less effect on these coefficients compared to an effect of initial crack width. Accordingly, the coefficients, γ,β can be calculated as a function of initial crack

width as shown in Table (7.4b)

The ultimate shear load can be calculated by equation (7.14) which is explained later [Section 7.4.7]. The ultimate shear displacement can be predicted as a function of the reinforcement parameter ρf_y. Both linear and power regression were used to find the relation between the measured shear displacement and the reinforcement parameter ρf_y. The power regression gave a better fit with coefficients 0.958, 0.969 and 0.959.

Thus, the following expression is suggested for the ultimate shear displacement Δ_u:

$$\Delta_u = c_1(\rho f_y)^{c_2} \qquad (7.12)$$

where

ρ is the ratio of transverse reinforcement

f_y is yield stress of transverse reinforcement (N/mm^2)

c_1, c_2 are coefficients which depend on the initial crack width rather than type of transverse reinforcement and are given by:

$$c_1 = 0.254 + 1.41\ w_o \qquad (7.12a)$$

$$c_2 = 0.294 - 0.287\ w_o \qquad (7.12b)$$

where w_o is the initial crack width (mm).

Comparison between experimental and calculated ultimate shear displacements is shown in Figure (7.13).

The linear stages a-b, b-c and c-d can be described by the general linear expression

$$V = [a + b\,(\Delta/\Delta_u)]V_u \qquad (7.13)$$

where the values of a and b are given in Table (7.5).

Comparison between the idealized shear load-shear displacement curves and the test results is shown in Figures (7.14), (7.15) and 7.16). From these figures it can be seen that the method of idealization shows fairly good agreement with test results.

The proposed method of idealizing the shear load-shear displacement relationship is also compared with experimental results of the investigation carried out by Mattock[21] and Walraven[22] [see Figures (7.17) and (7.18)]. It can be seen that the proposed method showed a reasonable agreement with the test results of Mattock and Walraven especially for the first two stages. However, the difference between the predicted and the experimental results is acceptable since these curves [21],[22] represents average measurements.

From the above, it seems that the proposed equations give a reasonable prediction for the overall behaviour of shear transfer by combined action.

7.4.4 Effect of the transverse reinforcement ratio

The reinforcement ratio ranged between 0.28%-1.68% and its influence on the shear transfer was investigated for three different conditions:

(a) A cracked section of initial crack width 0.125 mm and shear transverse reinforcement of high tensile deformed bars of 8 mm diameter. [Group (1)].

(b) A cracked section of initial crack width 0.40 mm with shear transverse reinforcement similar to that of group (1). [Group (2)].

(c) A cracked section of initial crack width 0.125 mm with shear transverse reinforcement of mild tensile plain bars of 8 mm diameter. [Group (3)].

From Figures (7.19 & 7.20) and (7.21 & 7.22) it can be seen that the reinforcement ratio has less effect at initial stages, although a greater effect was found on specimens with larger initial crack width [see Figures (7.23) & (7.24)].

As the applied shear load reaches the nonlinear stage the reinforcement ratio has a greater effect. This can be seen from Table (7.6) which compares the secant stiffnesses for specimens with minimum and maximum reinforcement ratios at three different shear displacements (0.05 mm, 0.20 mm and 0.40 mm). These values are arbitrarly chosen to cover the initial, intermediate and latest stages for any shear tests.

However, this influence can be attributed to the different roles of interface shear transfer mechanism and dowel action at different load levels. At low shear load the applied force is mainly resisted by the interface shear transfer mechanism due to the interlocking of the asperties along the crack surfaces. At higher shear load dowel action, which is mainly a function of the reinforcement ratio, will be activated, causing a noticeable difference in the behaviour between specimens with different reinforcement ratio.

Also, it appears that the crack widening path is only slightly affected by the amount of shear reinforcement for an initial crack width 0.125 mm [see Figures (6.3) and (6.12)] especially at the initial stage. For larger initial crack width of 0.40 mm a greater influence was observed [see Figure (6.8)]. This may be due to the difference in the initial bond condition between concrete and the transverse reinforcement, caused by the precracking operation, or to the difference in the contact area between the crack surfaces, i.e. the greater initial crack width the lesser area of contact and aggregate interlocking.

The increase in reinforcement ratio from 0.28% to 1.68% for condition (b), i.e. initial crack width of 0.40 mm resulted in a greater increase in the ultimate shear strength (180%), compared to these of conditions (a) and (c), i.e. initial crack width of 0.125 mm (144% and 155%) which implies the effectiveness of dowel action in the case of large initial crack widths [see Figure 7.25]. Thus it can be deduced that with smaller initial crack widths, the transverse reinforcement ratio would have less effect on the overall behaviour and the ultimate shear load.

7.4.5 Effect of initial crack width

The influence of the initial crack width can be obtained by comparing the results of groups (1), ω_o = 0.125 mm, and group (2), ω_o = 0.40 mm, shown in Figures (7.26) to (7.28) where it can be seen that its influence was considerable at all ratios, i.e. 0.28%, 0.56%, 1.12% and 1.68%. To quantify this effect, a comparison is made between the secant shear stiffnesses for each equivalent pair of specimens at shear displacements 0.05 mm, 0.20 mm, 0.40 mm and 0.60 mm as shown in Table (7.7).

The influence of initial crack width decreased with the increase of the shear transverse reinforcement. Also, for each reinforcement ratio, the increase in the shear stiffness due to the reduction in the initial crack width increased up to certain stage, i.e. at shear displacement 0.20 mm, which is in fact the beginning of the nonlinear trend. Beyond this stage and up to ultimate load, this increase in shear stiffness diminished. This can be explained as follows: at the initial stage most of shear forces are resisted by interface shear transfer mechanism as was assumed previously. With larger initial crack width the contribution of interface shear transfer should also be less. At a shear displacement of 0.20 mm, with small initial crack width, the interface shear transfer mechanism is still active while for specimens with large initial crack width this would have deteriorated. Therefore, the difference between the shear stiffnesses becomes greater compared with the initial stage.

Beyond this stage, i.e. shear displacement 0.20 mm, the dowel action would resist the majority of shear forces. Thus, the initial crack width at this stage would have less influence on the shear transfer behaviour as indicated by the reduction in the difference between the shear stiffness for specimens with different initial crack widths measured at shear displacements greater than 0.20 mm. This confirms the consistency of the suggested hypothesis.

Figure (7.28) shows that a great initial crack width resulted in a smaller growth in crack width. This can be explained by pronounce of sliding action over overriding action due to less contact and interlocking of the asperities along the two faces of the crack. This difference is shown in Figure (7.29) where the average inclination of the crack opening paths is shown for groups (1), (2)

and (3)-series 3 tested under monotonic loading. An increase in initial crack width from 0.125 to 0.40 mm resulted in a decrease in crack widening by approximately 37%.

The significant influence of the initial crack width on the ultimate shear transfer strength can be seen from Figure (7.25) and Table (7.8). The average reduction in the ultimate shear transfer strength due to the increase in initial crack width, i.e. from 0.40 mm to 0.125 mm, is approximately 21%.

7.4.6 Effect of type of shear transverse reinforcement

This section discusses the influence of mild tensile plain bars on shear transfer properties compared to high tensile deformed steel bars. The results of group (1), high tensile deformed bars, and (3), mild tensile plain bars, shown in Figures (7.30) to (7.32), are used for this purpose. Both had initial crack widths of 0.125 mm.

To quantify the effect of reinforcement type, a comparison between shear stiffnesses for each pair of specimens of group (1) and (3) measured at shear displacements 0.05 mm, 0.20 mm, 0.40 mm and 0.6 mm is given in Table (7.9).

The difference between shear stiffnesses with high tensile deformed bars and those with mild tensile plain bars increases as the shear load increases. The difference at initial stages is about an average of 4% whilst at later stages it increased to 11%. This follows from the fact that although bond is less effective for mild steel it does not play a prominent role in the initial stages because interface

shear transfer is the dominant mechanism. However the reduced bond has a greater effect on dowel action which is more dominant at the later stages. This can also be seen from Table (7.9) where the difference between the shear stiffnesses decreased with increasing transverse reinforcement ratio which showed previously a greater damage to the surrounding concrete due to the lesser spacing between the transverse reinforcing bars.

Figure (7.32) shows that specimens reinforced with mild steel exhibited only a slightly larger growth of crack width compared to high tensile deformed bars but was more prominent for lower ratios of transverse reinforcement. The average angles of inclination of the crack opening path with the shear plane for groups (1) and (3) were 41^{o} and 43^{o} respectively as shown in Figure (7.29). This reflects the slight effect of the bond condition between the transverse reinforcement and the surrounding concrete on the shear transfer mechanism.

From Figure (7.25) and Table (7.10), it can be seen that high tensile deformed bars produced a greater ultimate shear load compared to mild steel bars. Also the difference between the ultimate shear strength of the two types of reinforcement diminish very slightly with the increase of transverse reinforcement ratio with an average of 9% of the whole range. This reflects the greater damage to the bond in case of the deformed bars due to wedging action [25] which does not exist in the case of the plain bars. This in turn would reduce the normal restraint and dowel stiffnesses, i.e. interface shear transfer and dowel actions, which can lead to such smaller difference between the ultimate shear load of the two types of reinforcement at high

reinforcement ratio.

From the above it can be concluded that the bond condition had less effect on interface shear transfer mechanism compared to that on dowel action.

7.4.7 Calculation of ultimate shear transfer strength

The earlier analysis of the influence of the investigated parameters on the ultimate shear transfer strength showed the lesser effect of the transverse reinforcement type and the greater effect of initial crack width. Also, for the range of reinforcement ratios used here a linear relationship showed good fit to test results. Based on these findings and assuming that the ultimate shear strength decreases linearly with increase of intial crack width, an equation was derived to calculate the ultimate shear transfer load which is given by

$$\frac{V_u}{A_c\sqrt{f_{cu}}} = \left[0.552+0.141\rho f_y\right] - \left[0.549w_o[1+0.08\rho f_y]\right] \qquad (7.14)$$

where

V_u = ultimate shear transfer strength by combined action (N)

A_c = Area of shear plane (mm^2)

f_{cu} = cube compressive stress of concrete (N/mm^2)

ρ = ratio of transverse reinforcement

f_y = yield stress of transverse reinforcement (N/mm^2)

w_o = initial crack width (mm)

A comparison between the present test results and the predicted

ultimate shear transfer strength by Equation (7.14) showed good agreement as shown in Figure (7.25) and Table (7.11a).

Equation (7.14) was also used to predict the experimental results of other researchers such as Walraven [23] and Mattock [21], who used different initial crack widths, concrete strengths and transverse reinforcement. This is shown in Table (7.11b). It can be seen that Equation (7.14) exhibited a very good agreement with these test results and illustrates its wider applicability.

7.4.8. The relative contribution of interface shear transfer mechanism and dowel action.

The relative contributions of interface shear transfer mechanism and dowel action are assessed by comparing the calculated ultimate shear strengths for both dowel action and combined shear transfer using equations (7.6) and (7.14) as shown in Figures (7.33 a,b,c). It should be noted, however, that the contribution of interface shear transfer mechanism could be slightly overestimated because it might include the interaction between the two mechanisms which is not possible to measured alone. From these figures the following conclusions can be drawn:

- The contribution of dowel action and interface shear transfer mechanism to the total shear transfer across a crack is significantly influenced by the initial crack width and the transverse reinforcement ratio whereas the type of transverse reinforcement showed a negligible effect.

- The increase in initial crack width from 0.125 mm to 0.40 mm resulted in an average increase of 8% in the contribution of dowel action and consequently a reduction of interface shear transfer mechanism by the same percentage.

- The increase in reinforcement ratio from 0.45% to 1.68% resulted in an average increase of 16% and 10% to the contribution of dowel action in case of initial crack widths 0.125 mm and 0.40 mm.

7.4.9 Conclusions

1. A hypothesis is proposed to describe the mechanism of shear transfer across a cracked reinforced concrete section by the combined mechanism of dowel action and interface shear transfer which can be summarized as follows:
   at initial stage up to approximately 0.65 of the ultimate shear load (V_u) the majority of shear force is resisted by interface shear transfer mechanism. With further increase in applied shear load and up to $\approx 0.90\ V_u$ interface shear transfer deteriorates and dowel action develops. At the final stages to failure dowel action dominates and interface shear transfer mechanism breaks down.

2. The overall behaviour can be predicted by a new proposed method of idealizing the shear load-shear displacement relationship as described in section 7.4.3. This method showed a reasonable agreement with available test results[21],[22].

3. The transverse reinforcement ratio has less effect on shear stiffness at initial stages with smaller initial crack widths.

During the nonlinear stages the reinforcement ratio has in general a greater effect. Also with smaller initial crack widths, the transverse reinforcement ratio has lesseffect on the ultimate shear load.

4. The influence of initial crack width decreased with the increase of the transverse reinforcement. The average reduction in the ultimate shear transfer strength due to the increase in initial crack width from 0.40 mm to 0.125 mm is approximately 21%.

5. Bond conditions between transverse reinforcing bars and the surrounding concrete has a smaller effect on interface shear transfer mechanism compared to that on dowel action alone.

6. The transverse reinforcement of mild tensile plain bars does not show a significant influence on ultimate shear strength compared with high tensile deformed bars. An average reduction of 9% in ultimate shear strength was found as a result of using mild plain bars instead of high tensile deformed bars.

6. The derived imperical equation (7.14) to calculate the ultimate shear transfer strength showed very good agreement with test results of this present study and those of other investigations [23],[21]. This equation includes reinforcement ratio, type of transverse reinforcement, initial crack width and concrete strength.

7. In general the contribution of dowel action and interface shear transfer mechanism to the total shear transfer is much influenced

by initial crack width and the transverse reinforcement ratio compared to the type of transverse reinforcement, which showed a negligible effect. The contribution of dowel action and interface shear transfer mechanism ranges between 35-20% and 65-80% respectively depending on initial crack width, transverse reinforcement ratio and type of transverse reinforcement.

7.5 Shear transfer by combined action under repeated load

7.5.1 General behaviour and internal mechanisms of shear transfer

In this section the combined actions of interface shear transfer and dowel under repeated load will be analysed and compared to the equivalent monotonic loadings.

The analysis in section 7.4.2 of shear transfer under monotonic load showed that most of the applied shear force is resisted by interface shear transfer mechanism up to approximately 0.65 of the ultimate shear transfer strength. In the repeated shear load tests, the maximum applied repeated shear load was within this range. Therefore the interface shear transfer mechanism is expected to play an important role, especially at the first load cycle. Also it might be expected that dowel action would play a different role compared to monotonic loading.

It was generally observed that in all tests, the change in shear displacement was greater than the change in crack width at all cycles. This can be explained if it is assumed that the change in shear displacement and crack width is dependent upon,

(1) the roughness of the crack surfaces which is made of two components : local and general roughness.

(2) the normal restraint force provided by the transverse reinforcing bars and which relies on the bond between the concrete and the transverse reinforcement.

Due to the stronger effect of the normal restraint forces compared with the aggregate interlocking, the tendency of the crack surfaces to slip rather than widen would be greater as the shear load is applied.

This explanation was confirmed when the mild steel plain bars were used, the weaker bond between the concrete and plain bars reduce the normal restraint force and the ratio of the crack width to shear displacement increased indicating a greater tendency for the crack to widen compared with using high tensile deformed bars [see Figures (6.49-6.52) & (6.87-6.90)]. When interface shear transfer was reduced by increasing the initial crack width there was also a greater tendency for the two surfaces of the crack to slip rather than widen [see Figures (6.49-6.52) & (6.69-6.72)].

It was also generally observed from shear load-shear displacement relationships that the specimens response to the first load cycle was different to the second and subsequent cycles. On first loading, behaviour is the same as monotonically loaded specimens, with most of the shear resistance being provided by the direct bearing of asperities across the faces of the crack. The relationship in this stage is approximately linear [see Figure (7.34a)].

Initial unloading behaviour exhibited a high degree of resistance due to the restoring force in the transverse reinforcement and to the locking effect of the rubble which exists in the crack plane. As the shear load decreased and approached zero, the shear load displacement decreased more rapidly and a softer response was observed. This is attributed to the small resistance of the transverse reinforcing bars within the unbonded zone between the reinforcing bars and the surrounding concrete. The unloading behaviour can be idealized to trilinear curve [see Figure (7.34a)]. At zero shear load some residual shear displacement remain, corresponding to whatever frictional force continues to act between the crack faces.

Behaviour on subsequent cycles is somewhat different. With each cycle of load, the crack surfaces in contact are abraided and become smoother. Consequently the interface shear transfer would diminish and dowel action become more important. The shear load-shear displacement relationship for the subsequent loading cycles is nonlinear and the trend can also be idealized to a trilinear curve as shown in Figure (7.34b).

The higher shear stiffness during the first stage at low shear load can be explained by the restoring force in the shear transverse reinforcement. As the shear load increases the behaviour shows a softer response due to less frictional resistance between the two crack surfaces and also due to the low dowel stiffness because of the cracked concrete which supports the transverse reinforcing bars [stage 2, Figure (7.34b)]. During stage 3 at higher load, the shear stiffness increases mainly due to the increase in the dowel stiffness as the shear reinforcing bars come into contact with firm concrete

layers. The unloading behaviour for the subsequent cycles is similar to that of the first load cycle for similar reasons.

In the last cycle where shear was increased monotonically to failure, the shear load-shear displacement relationship can be idealized by the quadrilinear curve shown in Figure (7.34c). The first three stages are similar to those of previous load cycles. As the applied load exceeded the maximum repeated shear force, the shear stiffness does not change but at a higher load near to the failure there is a sudden decrease in the shear stiffness leading to stage 4. This is caused by complete break down of any interface shear transfer remaining and the rapid deterioration of the dowel action as a result of the combined axial tensile and flexural stresses in the transverse reinforcing bars.

Thus, it can be deduced that interface shear transfer is dominant mechanism in the first load cycle. At second cycle interface shear transfer is diminished considerably and dowel action becomes more effective and should not be neglected especially as the number of load cycles increase.

7.5.2 Effect of transverse reinforcement ratio

The effect of transverse reinforcement ratio was studied for the three cases of initial crack widths of 0.125 mm and 0.40 mm with high tensile deformed bars and mild steel plain bars with a crack width of 0.125 mm. In general for each condition no significant effect was observed on the overall behaviour for the first 43 load cycles. There was, however, an increase in the shear secant stiffness

measured at the selected loading cycles, i.e.numbers 1,2,23 and 43, as the transverse reinforcement ratio was increased up to ρ = 1.12% but there was little change between ρ = 1.12% and ρ 1.68% [see Tables (7.12) and (7.13)].

For the last cycle to failure the reinforcement ratio had a more noticeable effect on the main relationships as shown in Figures (7.35) to (7.37) and (7.38) to (7.40). It can be seen that the increase in reinforcement ratio from 0.28% to 1.68% resulted in an increase in the ultimate shear strength 205%, 212% and 188% on average for specimens of groups (1),(2) and (3) respectively.

Similar to section 7.3.3 two ways of studying the effect of the reinforcement ratio were examined:

(1) by fixing the applied repeated load as a ratio of the ultimate shear strength of the monotonic load as for groups (1),(2) and (3).

(2) by fixing the repeated loads as an absolute value to be applied on specimens with different reinforcement ratios as for each pairs of specimens 3.1.1A & 3.4.1A and 3.1.3A & 3.4.2A where each pair was subjected to maximum repeated shear loads of 107 kN and 200 kN respectively.

A comparison of the test results is shown in Table (7.14). From this table it can be deduced that the increase in reinforcement ratio from 0.28% to 0.56% and from 1.12% to 1.68% resulted in increase in the ultimate shear strength by 63% and 37% compared with 57% and 34% when the first way was used. This tends to indicate that reinforcement

ratio does not have significant effect on the shear transfer if the applied repeated load is changed within the range of the initial linear stage.

7.5.3 Effect of initial crack width

The influence of initial crack width can be observed in Figure (7.41) and Table (7.12). The primary effects on general behaviour of decreasing the initial crack from 0.40 mm to 0.125 mm was to increase the shear stiffness. The secant shear stiffnesses measured at the selected load cycles 1,2, 23 and 43 for specimens with initial crack width 0.125 mm were on average 3,2.25, 1.98 and 1.93 times those measured for crack width 0.40 mm. It can be noticed that these ratios show a certain trend, i.e. greater ratios at the first two cycles followed by lesser and approximately constant ratio. This trend is consistent with the hypothesis mentioned earlier about the effectiveness of interface shear transfer at the initial stage up to the maximum repeated loading and the dominant effect of dowel action as the number of load cycles increase.

The reduction in the initial crack width also resulted in an increase of the crack opening path [see Figure (7.42) and Table (7.15)]. This increase was on average 78%, 75%, 77% and 81% for the numbers of load cycles mentioned previously. This slight difference in the increase of the crack width to shear displacement ratio measured at the various cycles tend to indicate the insignificant effect of initial crack width on the interaction of interface shear transfer and dowel action.

The effect of initial crack width on the last cycle can be seen from the comparison shown in Figures (7.35) to (7.37). The increase of the initial crack width resulted in an increase in the residual shear displacement and crack width and reduction in shear stiffnesses, both tangent and secant stiffnesses. This increase in the residual shear displacement and crack width was on average 316% and 156% respectively. This shows that the bearing and crushing mode dominates the behaviour for small initial crack width, i.e. w_o = 0.125 mm, whereas sliding and overriding action predominates with large initial crack width, w_o = 0.40 mm, which agrees with the local and global roughness model (27) explained earlier in chapter (2).

Also, the increase in initial crack width caused an average reduction of 12.5% in the ultimate shear strength [see Table (7.16) and Figure (7.43)]

7.5.4 Effect of transverse reinforcement type

From Table (7.13) and Figure (7.44), it can be seen the secant shear stiffnesses measured at the load cycles 1,2,23 and 43 for specimens with high tensile deformed bars were on average 1.22, 1.20, 1.21 and 1.28 times those with mild plain bars. It can be noticed that these ratios were much less than those obtained due to the increase in crack width. Therefore it can be deduced that the bond between the transverse reinforcement and surrounding concrete has an inferior effect compared to the initial crack width. This deduction is also consistent with the local and global roughness model[27] and the hypothesis described earlier in section 7.5.1. The local and global roughness model assumes that the bearing mode dominates the behaviour

when the initial crack width is less than 0.25 mm, local concrete crushing occurs and there is little overriding. The resistance in this mode is less dependent on the amount of the normal restraint. However, a little overriding was confirmed from Figure (7.45) and Table (7.17), which compares the crack opening path. It can be seen that mild plain bars cause little increase in crack widening for the load cycles, 1,2,23 and 43, i.e. 12.7%, 11%, 7%, 5.6% on average. Such decrease in the ratios of crack width to shear displacement for the two type of transverse reinforcement as load cycles increases confirms the explanation mentioned earlier in section 7.4.6 about the greater degraduation of bond condition in the case of using deformed bars due to wedging action.

The influence of the reinforcement type on the ultimate shear transfer strength can be observed from Figure (7.46) and Table (7.18). An average reduction of 10% in the ultimate shear load was found as a result of using mild plain steel bars instead of high tensile deformed bars. From such small difference of 2.5% between the effect of the type of transverse reinforcement and the initial crack width on the ultimate shear transfer strength, it can be concluded that the difference of the mode of shear transfer behaviour would not affect significantly the ultimate shear transfer strength.

7.5.5 Effect of the level of repeated shear load

The effect of the repeated load level on the ultimate shear transfer was investigated by comparing the test results of specimens 3.1.2A and 3.1.4A of group (1) with specimens 3.4.1A and 3.4.2A of group (4), which are identical. Those of the first group were subjected to

maximum repeated shear loads of 139 kN and 267 kN which are approximately equal to 0.75 the calculated ultimate shear strength under monotonic load (V_u). For the second group, a maximum repeated shear loads of 0.57 V_u, 107 kN and 200 kN, were used.
Comparisons are given in Table (7.19). A 25% reduction in the maximum repeated shear load resulted in only 4% and 2% increase in the ultimate shear strength for reinforcement ratios of 0.56% and 1.68%. Hence it can be deduced that within a certain range of the repeated shear load level the ultimate shear transfer strength would be affected insignificantly. This finding, however, needs further investigation.

7.5.6 Effect of repeated shear loading

The difference in behaviour between the last cycle of repeated loading and the monotonic shear load will illustrate the cumulative effect of cyclic the load.

The repeated shear load resulted in an increase in the shear displacement [see Figures (7.47) and (7.53)]. This reflects the reduction of roughness of the crack surfaces by grinding the asperities and thus reducing the effectiveness of the interface shear transfer. However, for wider
initial cracks the repeated load had a less effect compared with small initial crack width. Figure (7.50) shows little difference between shear load versus shear displacement under both monotonic and repeated loading. The reason is that with large initial crack width the contact areas between the two surfaces of the crack is already small and the grinding effect would not cause much change to the

intial conditions of these contact area. This is confirmed by a comparison of shear load versus crack width shown in Figure (7.48), (7.51) and (7.54) where less change in crack width under repeated can be seen. Nevertheless, it seems that repeated loading has a lesser effect as the reinforcement ratios increase where shear forces at this stage, i.e. last load cycle, is mainly transferred by dowel action. Figures (7.49), (7.52) and (7.55) show that direction of the crack movement to the shear plane was less in the case of repeated shear loads. This again can be attributed to the difference in the smoothness of the crack surfaces between the two cases of loadings which will allow the crack surfaces to slip instead of widen.

Figures (7.56) to (7.58) compare the ultimate shear strengths of the monotonic and the repeated shear loads. It can be seen that the ultimate strength was less under repeated loading. The ratios of the ultimate shear transfer strengths under both types of loadings are given in Table (7.20). Generally it is found that the effect of repeated shear load decreases as transverse reinforcement ratio increases. Also, with large initial crack width the influence of the repeated load was less compared with the case of small initial crack width. The average reduction in the ultimate shear transfer strength as a result of applying the repeated load is 18% and 8% for cracked section with small and large initial crack widths respectively. This is consistent with the previous explanation that interface shear transfer in the case of large initial crack widths would not have a greater contribution for repeated loading compared with monotonic load due to the less contact area across the crack surfaces, so that the grinding effect would have little effect. At the same time dowel action is not expected to be highly influenced in such case.

7.5.7 Calculation of ultimate shear transfer strength under repeated load

The earlier analysis showed that type of transverse reinforcement had less effect on the ultimate shear transfer strength compared to the initial crack width. Based on this information and assuming the increase of the ultimate shear strength due to the increase in reinforcement ratio is linear the following equation was derived to calculate the ultimate shear transfer strength which includes the initial crack width, type of transverse reinforcement, reinforcement ratio and concrete strength:

$$V_{UR} = [0.254 + (0.164-0.10w_o)\rho f_y].f_{cu}^{0.5}.A_c \qquad (7.15)$$

where

V_{UR} is ultimate shear transfer strength (N)

ρ is shear transverse reinforcement ratio

A_c is area of the crack plane (mm^2)

f_y is yield stress of transverse reinforcement (N/mm^2)

f_{cu} is cube compressive stress of concrete (N/mm^2)

w_o is initial crack width (mm)

A comparison between the experimental and calculated ultimate shear transfer strengths by equation (7.15) is shown in Figure (7.59) and also given Table (7.21) which showed good agreement with test results.

A general equation to predict the ultimate shear transfer strength was also derived from Equations (7.14) and (7.15) which combined both monotonic and repeated loading and includes the number of load cycles beside the other parameters mentioned previously and is given by:

$$\frac{V_{UR}}{A_c\sqrt{f_{cu}}} \quad \left[(0.552-0.549w_o)+(0.141-0.044w_o)\rho f_y\right]-N\left[(0.0127w_o-6.93x10^{-3})\right.$$
$$\left. + (5.3x10^{-4}-1.30x10^{-3}w_o)\rho f_y\right] \qquad 7.16$$

where N is the number of load cycles before the load increases to failure. The maximum repeated load however should not exceed 0.75 the ultimate shear strength under monotonic loading.

This equation would lead to similar results for equations (7.14) and (7.15) if it is used in cases of monotonic or repeated loads. Therefore, there was no need to compare the experimental results and the calculated values using this equation.

It was recommended by Mattock [26] that shear transfer under cyclically reversing load can be taken as 0.80 of the shear transfer strength under monotonic loading. From this present study, it was found that shear transfer strength under repeated load can be taken as 0.7-0.9, depending on the initial crack width and type of transverse reinforcement. Taking into consideration the difference between the history of loadings used in this present and Mattock's studies it seems that this range, i.e. 0.7-0.9 is fairly consistent with Mattock's finding.

7.5.8 The Contribution of interface shear transfer mechanism and dowel action

The contribution of interface shear transfer and dowel action mechanisms under repeated shear load can be assessed by comparing the experimental results of dowel action tests with those of shear tests by combined actions.

To make a direct comparison with difference in the shear plane area and the concrete strength of each companion pairs of specimens were measured by considering the ultimate shear stress divided by the square root of the concrete strength.

Table (7.22) suggests that the contributions of the two mechanisms is not greatly influenced by the amount of transverse reinforcement and the initial crack width. For small initial crack width the interface shear transfer mechanism and dowel action resisted 86-79% and 14-21% of the ultimate shear load. With a large initial crack width the contribution of interface shear transfer mechanism was slightly decreased to 84-73% while the dowel action increased to 16-27%.

7.5.9 Conclusions

From the previous analysis of combined action test results under repeated loading the following conclusions can be drawn:

1. The general behaviour can be summarized as follows:
   the behaviour at the first load cycle is different compared with the second and subsequent cycles. For the first load cycle, the behaviour can be approximated by a linear trend. Response to the subsequent cycles is characterized by higher shear stiffness at low load level and a gradual decrease with increase of the applied load and the response tends to stabilize. Initial unloading behaviour exhibited a high degree of resistence and as the load decreased and approached zero the shear stiffness decreased more rapidly and a softer response was observed. At

zero shear load some residul displacements remain. In the last load cycle the behaviour was similar to the previous load cycle up to the maximum repeated load. As the applied load exceeded this level the shear stiffness does not change but at a higher load near to failure there was a sudden decrease in shear stiffness.

2. A hypothesis was proposed to describe the internal mechanisms at shear transfer by combined action as explained in section 7.5.1 and summarized and schematically presented in Figure (7.34).

3. The transverse reinforcement ratio has no significant effect on the overall behaviour for the first 43 load cycles. There was, however, an increase in shear secant stiffness measured at load cycles 1,2,23 and 43 as the transverse reinforcement ratio was increased to ρ = 1.12% but there was little change between ρ = 1.12 and 1.68%. For the last load cycle, the reinforcement ratio had more effect on the main relationship.

4. The increase in the reinforcement ratio, i.e. from 0.28 to 1.68% showed lesser effect on the ultimate shear strength with small initial crack width (205% and 188%) compared with large initial crack width (212%).

5. The reinforcement ratio seems not to have a significant effect on the ultimate shear transfer strength if the applied repeated load is varied within the range of the initial linear stage, i.e. $\leq 0.75\ V_u$, and under 43 cycles as used in this study.

6. The primary effect of decreasing initial crack width on the general shear transfer behaviour was to increase the shear secant stiffnesses measured at maximum repeated load.

7. The initial crack width affects the mode of interface shear transfer mechanism. With small initial crack width (w_o), i.e. w_o=0.125mm it seems that bearing and crushing modes dominate the behaviour wherea with larg initial crack width, i.e. w_o=0.40mm sliding and overiding predominate. This conclusion shows a consistency with the local and global roughness model[27].

8. The increase in initial crack width from 0.125mm to 0.40mm results in an average reduction of 12.5% in the ultimate shear transfer strength.

9. The use of mild tensile plain bars instead of high tensile deformed bars as transverse reinforcement does not result in a significant effect on the overall behaviour and ultimate shear transfer strength. The secant shear stiffnesses measured at maximum repeated load for the 43 cycles of specimens with high tensile deformed bars were on average 1.23 times those with mild plain bars. Also an average reduction of 10% in the ultimate shear transfer strength was found as a result of using mild tensile plain bars.

10. A general equation (7.16) is suggested to predict the ultimate shear transfer strength which includes the effect of type of loading, initial crack width, reinforcement ratio, transverse reinforcement type, and concrete strength. At present time this

equation is limited with maximum repeated load less than 0.75 the ultimate shear transfer strength under monotonic loading.

11. The ultimate shear transfer strength under repeated load can be taken as 0.7-0.9 of ultimate shear strength under monotonic load depending on the initial crack width and reinforcement ratio.

12. The relative contribution of interface shear transfer mechanism and dowel action to the total shear transfer is not greatly influenced by initial crack width. For a small initial crack width of 0.125mm the interface shear transfer mechanism and dowel action resisted 86-79% and 14-21% of the total shear transfer depending on reinforcement ratio. With a larger initial crack width of 0.40mm interface shear transfer decreased slightly to 84-73% while dowel action increased to 16-22%.

7.6 Comparison between shear transfer under repeated and reversing cyclic load.

In this present work reversing cyclic loads were not used. However, from the available information on this type of load (previously presented in chapter 2) a comparison of shear transfer by dowel action alone and combined action under repeated and reversible cyclic load[27] is shown in Figures (7.60) to (7.62). The following conclusions can be drawn:

(1) There is a similarity between the general behaviour under both types of loading.

(a) The change in shear displacement is greater than the change in crack width.

(b) Specimens exhibit large increase in displacements at the first load cycle and for subsequent cycles the response tends to stabilize and the rate of increase decreases with increasing number of load cycles [see Figure (7.60)].

(c) The trend of the shear load versus shear displacement at the first load cycle was different compared with the subsequent cycles. In general at the first load cycle an approximate linear relationship is observed. For subsequent cycles the trend become nonlinear which is characterized by a low shear stiffness at low shear load and gradual increase as shear load increases [see Figures (7.61) and (7.62)].

(d) Residual displacements existed when the shear load was released to zero. The residual displacements of the first cycle was large compared with those of the subsequent cycles.

(e) The area enclosed by hysteresis loop decreases after the first load cycle. As the cycles numbers increase this area was approximately equal indicating less energy dissipation.

(f) During unloading at higher load a small decrease in shear displacement occurs and as the load approached to zero the displacement decreases rapidly [see Figures (7.61) and (7.62)].

(2) As mentioned earlier the ultimate shear transfer strength under reversible cyclic load according to Mattock [26] was found to be

0.80 of the ultimate shear strength under monotonic load. For the repeated load this ratio was ranged between 0.70 to 0.90 and depends on the initial crack width and type of transverse reinforcement.

(3) Jimenez et al[27] quoted 65%-80% of the total applied shear load can be resisted by interface shear transfer mechanism and 20-32% by dowel action. According to the present study the contribution of interface shear transfer mechanism and dowel action under repeated load is evaluated asy 73-84% and 16-27% which are close to those percentages suggested by Jimenez et al.

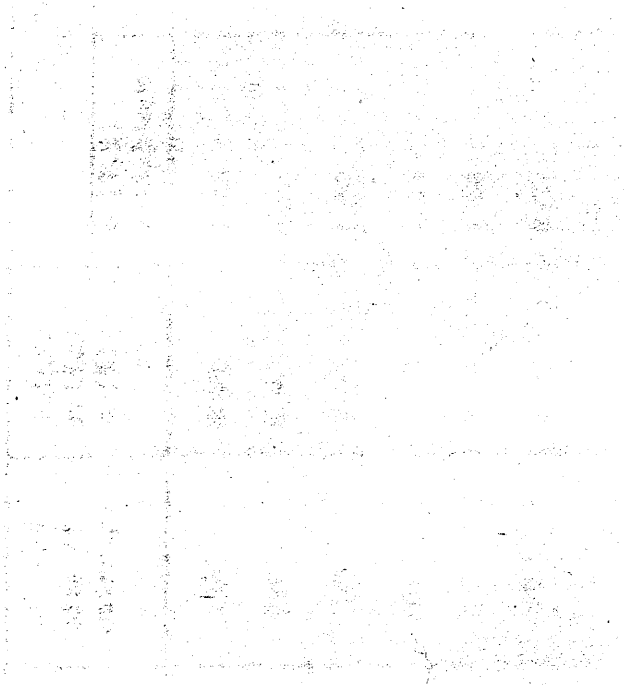

Table (7.1) Ratio of the calculated to the experimental ultimate shear load resisted by dowel action under monotonic load.

Spec. No.	No. and size of stirrups	Reinf. ratio ρ (%)	$V_{dU}(cal.)/V_{dU}^{(exp)}$				$V_{dU}(exp)$ (kN)
			Eq.(7.5) plast.hinge	Eq. (7.6) Empirical	Eq. (2.17) Millard/Johnson	Eq.(2.16) Walraven	
2.1.1	1Y8	0.22	0.83	0.91	0.85	0.83	31
2.1.2	2Y8	0.45	1.01	1.05	1.05	0.98	51
2.2.1	2Y8	0.45	0.94	0.98	1.00	0.95	55
2.1.3	4Y8	0.89	1.10	1.06	1.12	1.02	94
2.1.4	6Y8	1.34	1.06	0.99	1.08	0.71	146
2.2.2	6Y8	1.34	0.93	0.98	1.07	0.77	165

Table (7.1b) Comparison between experimental ultimate shear transfer stress by dowel action under monotonic loading and calculated values using Equation (7.11)

Specimen No.	No. and size of stirrups	Reinforcement ratio ρ (%)	Exp. Ultimate shear strength v_{du} (exp.) (N/mm^2)	Cal. Ultimate shear strength V_{du}(cal.) (N/mm^2)	$\frac{V_{du}\ (cal.)}{V_{du}\ (exp.)}$
2.1.1	1Y8	0.22	0.68	0.57	0.84
2.1.2	2Y8	0.45	1.13	1.07	0.94
2.2.1	2Y8	0.45	1.22	1.12	0.92
2.1.3	4Y8	0.89	2.08	1.99	0.96
2.1.4	6Y8	1.34	3.24	2.88	0.89
2.2.2	6Y8	1.34	3.66	3.32	0.91
					Ave. = 0.91

Table (7.1C) Comparison between experimental ultimate shear transfer stress by dowel action under repeated loading and the predicted values by using Equation (7.11)

Specimen No.	No. and size of stirrups	Reinforcement ratio ρ (%)	Exp. Ultimate shear strength V_{dUR} (exp.) (N/mm^2)	Cal. Ultimate shear strength V_{dUR} (cal.) (N/mm^2)	$\frac{V_{dUR}\ (cal.)}{V_{dUR}\ (exp.)}$
2.1.2A	2Y8	0.45	0.75	0.67	0.90
2.1.3A	4Y8	0.89	1.68	1.45	0.86
2.1.4A	6Y8	1.34	2.47	2.21	0.89
					Ave. = 0.88

Table (7.2) Comparison between the experimental ultimate shear load resisted by dowel action under monotonic and repeated load.

Reinforcement ratio ρ (%)	Ratio of applied rep. Load to ult. monotonic Load	V_{duR}^{*}	V_{du}^{+}	$\frac{V_{duR}}{V_{du}}$
0.45	0.35	33.36	51	0.65
0.89	0.19	75.6	94	0.80
1.34	0.36	111.20	146	0.77

* Experimental ultimate shear load of dowel action under repeated load.

\+ Experimental ultimate shear load of dowel action under monotonic load.

Table (7.3): Comparison between strain measured in the reinforcement crossing the shear plane of dowel action and combined action test specimens under monotonic loading.

Specimen No.	Shear * transverse reinforcement	$\frac{\varepsilon_f}{\varepsilon_d}$	$\frac{\varepsilon_f}{\varepsilon_y}$	$\frac{\varepsilon_d}{\varepsilon_y}$	Type of shear tests
3.5.1	2Y8	1.18	1.67	1.41	combined action
2.2.1	2Y8	4.24	3.09	0.72	dowel action
3.5.2	6Y8	1.52	1.38	0.91	combined action
2.2.2	6Y8	5.15	2.7	0.54	dowel action

* Number and size of stirrups crossing the crack plane.

ε_f = flexural strain in shear transverse reinforcement.

ε_d = direct strain in shear transverse reinforcement.

Table (7.4a): Values of coefficients γ, β.

No. of group	γ_1	γ_2	β_1	β_2
1	0.22	0.48	0.70	0.93
2	0.17	0.45	0.57	0.87
3	0.21	0.42	0.69	0.91

Note:

Group (1) : high tensile deformed bars and initial crack width 0.125 mm

Group (2) : high tensile deformed bars and initial crack width 0.40 mm

Group (3) : mild tensile plain bars and initial crack width 0.125 mm

Table (7.4b) Calculation of coefficients γ, β

Coefficient γ	Coefficient β
$\gamma_1 = 0.235-0.163\omega_o$	$\beta_1 = 0.75-0.454\omega_o$
$\gamma_2 = 0.485-0.163\omega_o$	$\beta_2 = 0.942-0.181\omega_o$

Table (7.5) Values of a and b of Equation (7.13)

Stage No.	Limits	a	b
(1)	$\sigma \uparrow \frac{\Delta}{\Delta_u} \uparrow \gamma_1$, $0 \uparrow \frac{V}{V_u} \uparrow \beta_1$	$a_1 = 0$	$b_1 = \frac{\beta_1}{\gamma_1}$
(2)	$\gamma_1 \uparrow \frac{\Delta}{\Delta_u} \uparrow \gamma_2$, $\beta \uparrow \frac{V}{V_u} \uparrow \beta_2$	$a_2 = \beta_1 - b_2 \gamma_1$	$b_2 = \frac{\beta_2 - \beta_1}{\gamma_2 \quad \gamma_1}$
(3)	$\gamma_2 \uparrow \frac{\Delta}{\Delta_u} \uparrow 1.0$, $\beta_2 \uparrow \frac{V}{V_u} \uparrow 1.0$	$a_3 = \beta_2 - b_3 \gamma_2$	$b_3 = \frac{1-\beta_2}{1-\gamma_2}$

Table (7.6): Effect of shear transverse reinforcement ratio on shear stiffness under monotonic loading.

Conditions	Initial shear stiffness at Δ = 0.05mm		$\frac{K_1}{K_2}$	Secant shear stiffness at Δ = 0.20 mm		$\frac{K_1''}{K_2'}$	Secant shear stiffness at Δ = 0.40		$\frac{K_1''}{K_2''}$
	K_1*	K_2 †		K_1' *	K_2'†		K_1'' *	K_2'' †	
(a) ω_o = 0.125, high tensile deformed steel	61.11	31.7	1.92	46.62	22.07	2.11	26.78	12.02	2.22
(b) ω_o = 0.40 mm, high tensile deformed steel	35.55	12.85	2.76	27.27	9.91	2.75	19.09	7.69	2.48
(c) ω_o = 0.125 mm, plain mild steel	61.11	29.76	2.05	44.13	19.58	2.25	25.79	10.41	2.47

* K_1 , K_1', K_1'' Shear stiffnesses of specimens with maximum reinforcement ratio (ρ = 1.68%)

† K_2 , K_2', K_2'' Shear stiffnesses of specimens with maximum reinforcement ratio (ρ = 0.28%)

Table (7.7): Effect of initial crack width on shear stiffness under monotonic laoding.

Reinforcement Ratio	Initial shear stiffness at Δ = 0.05mm		$\frac{K_1}{K_2}$	Secant shear stiffness at Δ = 0.20mm		$\frac{K_1}{K_2}$	Secant Shear stiffness at Δ = 0.40mm		$\frac{K_1}{K_2}$	Secant shear stiffness at Δ = 0.60mm		$\frac{K_1}{K_2}$
ρ (%)	K_1*	K_2 †		K_1	K_2		K_1	K_2		K_1	K_2	
0.28	31.7	12.85	2.47	22.07	9.91	2.22	12.02	7.69	1.56	-	-	-
0.56	36.67	19.83	1.85	27.77	13.14	2.11	17.36	9.42	1.84	12.23	7.27	1.68
1.12	41.66	23.77	1.75	33.24	17.84	1.86	21.70	14.63	1.48	15.21	11.24	1.35
1.68	61.11	35.55	1.70	46.22	27.27	1.70	26.78	19.09	1.40	19.67	15.53	1.26

* K_1 Shear stiffness of specimens with ω_o = 0.125 mm of group (1) - series 3

* K_2 Shear stiffness of specimens with ω_o = 0.40 mm of group (2) - series 3

Table (7.8) Effect of initial crack width on the ultimate shear strength.

Reinforcement ratio $\rho\%$	Ultimate shear load (kN)		$\frac{V_{U2}}{V_{U1}}$
	V_{U1} (ω_o = 0.125mm)	V_{U2} (ω_o = 0.40mm)	
0.28	169	120	0.78
0.56	258	187	0.72
1.12	320	254	0.79
1.68	413	365	0.88

Table (7.9): Effect of types of shear transverse reinforcement on the shear stiffness under monotonic loading.

Reinforcement Ratio ρ(%)	Initial shear stiffness at Δ = 0.05 mm		$\frac{K_1}{K_3}$	Secant shear stiffness at Δ = 0.20mm		$\frac{K_1}{K_3}$	Secant shear stiffness at Δ = 0.40 mm		$\frac{K_1}{K_3}$	Secant shear stiffness at Δ = 0.60mm		$\frac{K_1}{K_3}$
	K_1*	K_3†		K_1	K_3		K_1	K_3		K_1	K_3	
0.28	31.7	29.76	1.06	22.07	19.58	1.127	12.02	10.41	1.15	-	-	-
0.56	36.67	35.70	1.02	27.77	26.04	1.07	17.36	15.62	1.11	12.23	10.91	1.12
1.12	41.66	41.66	1.0	33.24	31.25	1.06	21.70	19.34	1.12	15.21	13.51	1.125
1.68	61.11	61.11	1.0	46.67	44.13	1.05	26.78	25.79	1.03	19.67	18.02	1.09

* K_1 : Shear stiffness of specimens - with shear transverse reinforcement of high tensile deformed bars - of group (1) - series 3.

* K_3 : Shear stiffness of specimens - with shear transverse reinforcement of mild plain steel bars - of group (3) - series 3.

Table (7.10) Influence of types of shear transverse reinforcement on the ultimate shear strength under monotonic loading.

Reinforcement ratio ρ %	Ultimate shear load (kN)		$\frac{V_{U3}}{V_{U1}}$
	*V_{U1}	+ V_{U3}	
0.28	169	151	0.89
0.56	258	235	0.91
1.12	320	293	0.92
1.68	413	386	0.93

* V_{U1} Ultimate shear strength for specimens reinforced with high tensile deformed bars of Group (1) Series 3.

+ V_{U3} Ultimate shear strength for specimens reinforced with mild plain steel bars of Group (3) Series 3.

Table (7.11) Comparison between experimental and calculated ultimate shear stress under monotonic load according to Equation (7.14)

Specimen No.	Reinforcement ratio ρ %	Experimental ultimate shear stress v_u(exp.) (N/mm^2)	Calculated ultimate shear stress v_u(cal.) (N/mm^2)	$\frac{v_u(cal.)}{v_u(exp.)}$
Group (1)				
3.1.1	0.28	4.69	4.80	1.02
3.1.2	0.56	7.16	6.40	0.89
3.1.3	1.12	8.88	8.82	0.99
3.1.4	1.68	11.6	11.38	0.98
				Ave.=0.97
Group (2)				
3.2.1	0.25	5.6	3.62	1.00
3.2.2	0.56	5.22	5.01	0.96
3.2.3	1.12	7.06	7.42	1.05
3.2.4	1.68	10.41	10.20	0.97
				Ave.=0.995
Group (3)				
3.3.1	0.28	4.19	4.67	1.11
3.3.2	0.56	6.50	5.91	0.91
3.3.3	1.12	8.13	8.11	0.99
3.3.4	1.68	10.72	10.65	0.99
				Ave.=1.0

Table (7.11b) Comparison between the experimental results[23],[21] and the predicted ultimate shear transfer strength by combined action under monotonic load using Equation (7.14)

Reinf. parameter fy (N/mm^2)	Initial crack width w_o (mm)	Reinf. yield stress fy (N/mm^2)	Concrete comp. stress f_{cu} (N/mm^2)	Exp. ult. shear stress v_u(exp.) (N/mm^2)	Cal. ult. shear stress v_u(cal.) (N/mm^2)	$\frac{V_u(cal.)}{V_u(exp.)}$
Walraven's test results[23]						
2.43	0.05	460	56.1	6.72	6.44	0.96
4.86	0.02			10.83	9.14	0.84
7.29	0.03			12.56	11.63	0.93
9.72	0.02			14.19	14.24	1.003
						Ave. = 0.93
2.43	0.01	460	19.9	4.65	3.96	0.85
4.86	0.01			6.04	5.49	0.90
7.29	0.01			6.55	7.00	1.06
						Ave. = 0.95
2.43	0.01	460	38.2	6.83	6.40	0.93
4.86	0.01			8.69	7.60	0.88
7.29	0.01			9.65	9.60	0.99
9.72	0.01			9.94	11.70	1.17
						Ave. = 0.95
Matlock's test results[21]						
1.54	0.23	413	34.47	3.17	3.6	1.13
3.19	0.23			5.38	4.9	0.91
4.757	0.23			6.62	5.88	0.88
6.17	0.23			7.93	7.20	0.91
7.72	0.23			8.10	8.3	1.02
9.10	0.23			8.28	9.3	1.12
						Ave. =0.995

Table (7.12): Effect of initial crack width on secant shear stiffnesses measured at load cycles 1, 2, 23 and 43

Specimen number	Reinforcement ratio ρ (%)	Initial crack width ω_o (mm)	Secant shear stiffness (N/mm^3)			
			Cycle (1)	Cycle (2)	Cycle (23)	Cycle (43)
3.1.1A	0.28	0.125	21.56	36.54	29.6	27
3.2.1A	0.28	0.40	8.02	17.11	12.03	11.40
3.1.2A	0.56	0.125	38.8	40.59	34.87	33.4
3.2.2A	0.56	0.40	11.69	31	31	32
3.1.3A	1.12	0.125	44.88	66.9	58	59.4
3.2.3A	1.12	0.40	14.91	27.2	24	22.9
3.1.4A	1.68	0.125	54	67	57.29	52.5
3.2.4A	1.68	0.40	16.97	21.14	29.04	28.6

Table (7.13): Effect of transverse reinforcement type on shear secant stiffnessesses measured at load cycles 1, 2, 23 and 43.

Specimen number	Reinforcement ratio ρ %	Type of shear trans. reinf.	Shear secant stiffness (N/mm^3)			
			Cycle (1)	Cycle (2)	Cycle (23)	Cycle (43)
3.1.1A	0.28	D *	21.56	36.54	29.6	27
3.3.1A	0.28	M †	18.85	31.42	27.5	24
3.1.2A	0.56	D	38.8	40.59	34.87	33.4
3.3.2A	0.56	M	32	38.4	30	28.23
3.1.3A	1.12	D	43.88	66.9	58	59.4
3.3.3A	1.12	M	37.47	58.16	48.46	43.01
3.1.4A	1.68	D	53	67	57.29	52.5
3.3.4A	1.68	M	38	46.37	39.34	35.8

* High tensile deformed bars

† Mild plain bars

Table (7.14): Comparison between test results of specimens 3.1.1.A, 3.4.1 and 3.1.3A, 3.4.2A.

Specimen number	Reinforcement ratio ρ (%)	Reinforcement yield stress f_y (N/mm²)	Concrete compressive stress f_{cu} (N/mm²)	Initial crack width ω_o (mm)	Maximum repeated Load (KN)	Ultimate shear load Vu (KN)	Ultimate shear stress v_u (N/mm²)	Ultimate shear displacement Δ_u (mm)	Ultimate crack width ω_u (mm)
3.1.1A	0.28	535	50	0.120	107	125	3.47	0.596	0.309
3.4.1A	0.56	535	46	0.125		204	5.67	0.920	0.646
3.1.3A	1.12	535	47	0.125	200	285	7.9	0.641	0.360
3.4.2A	1.68	535	45	0.125		392	10.89	0.868	0.738

Table (7.15): Effect of initial crack width on crack width to shear displacement ratio measured at load cycles 1, 2, 23 and 43.

Specimen number	Reinforcement ratio ρ (%)	Initial crack width ω_o (mm)	Crack width/shear displacement			
			Cycle (1)	Cycle (2)	Cycle (23)	Cycle (43)
3.1.1A	0.28	0.125	0.82	0.88	0.76	0.71
3.2.1A	0.28	0.40	0.42	0.43	0.37	0.35
3.1.2A	0.56	0.125	0.90	0.95	0.86	0.84
3.2.2A	0.56	0.40	0.55	0.48	0.39	0.35
3.1.3A	1.12	0.125	0.74	0.87	0.71	0.71
3.2.3A	1.12	0.40	0.42	0.55	0.48	0.46
3.1.4	1.68	0.125	0.82	0.85	0.76	0.72
3.1.4A	1.68	0.40	0.56	0.58	0.54	0.55

Table (7.16) Comparison of ultimate shear load for specimens of groups (1) & (2) - Series tested under repeated loading.

Reinforcement ratio ρ %	Ultimate shear load V_U (kN)		$\frac{V_{UR2}}{V_{UR1}}$
	*V_{UR1}	+V_{UR2}	
0.28	125	111	0.88
0.56	196	169	0.86
1.12	285	245	0.86
1.68	382	347	0.90
			Ave. 0.875

* Ultimate shear load for specimens of group (1) - Series 3 tested under repeated load ($\omega_o \simeq 0.125$ mm).

+ Ultimate shear load for specimens of group (2) - Series 3 tested under repeated load ($\omega_o \simeq 0.40$ mm).

Table (7.17): Effect of transverse reinforcement type on crack width/shear displacement ratio measured at load cycles 1, 2, 23 and 43.

Specimen number	Reinforcement ratio ρ (%)	Type of shear trans. reinf.	Crack width/shear displacement			
			Cycle (1)	Cycle (2)	Cycle (23)	Cycle (43)
3.1.1A	0.28	D *	0.82	0.88	0.76	0.71
3.3.1A	0.28	M †	0.91	1.04	1.16	1.11
3.1.2A	0.56	D	0.92	0.95	0.86	0.84
3.3.2A	0.56	M	0.93	0.86	0.93	0.94
3.1.3A	1.12	D	0.74	0.87	0.71	0.71
3.3.3A	1.12	M	0.93	0.7	1.0	0.92
3.1.4A	1.68	D	0.82	0.85	0.76	0.72
3.3.4A	1.68	M	0.45	0.89	0.81	0.75

* High tensile deformed bars

† Mild plain bars

Table (7.18) : Effect of transverse reinforcement type on ultimate shear transfer strength by combined action under repeated load.

Reinforcement ratio (%)	Ultimate shear load V_{DR} (kN)		$\frac{V_{UR3}}{V_{UR1}}$
	*V_{UR1}	+V_{UR3}	
0.28	125	120	0.96
0.56	196	173	0.88
1.12	285	262	0.92
1.68	382	346	0.90

Ave. = 0.915

* Ultimate shear load for specimens of group (1) Series 3 tested under repeated load.

+ Ultimate shear load for specimens of group (3) - Series 3 tested under repeated load.

Table (7.19): Effect of the level of repeated shear load.

Specimen number	Reinforcement ratio ρ %	Reinforcement yield stress f_y (N/mm²)	Concrete compressive stress f_{cu} (N/mm²)	Initial crack width ω_o (mm)	Ratio of max. applied repeated load to ult. monotonic shear load	Ultimate shear load V_u (kN)	Ultimate shear stress ment v_u (N/mm²)	Ultimate shear displacement Δ_u (mm)	Ultimate crack width ω_u (mm)
3.1.2A	0.56	535	50	0.120	0.75	196	5.44	0.829	0.495
3.4.1A	0.56	535	46	0.125		204	5.67	0.920	0.646
3.1.4A	1.68	535	45	0.130	0.57	382	10.6	0.818	0.506
3.4.2A	1.68	535	45	0.125		392	10.89	0.868	0.738

Table (7.20) Comparison between the experimental ultimate shear loads of specimens of Seres 3 tested under monotonic and repeated load.

Reinforcement ratio ρ %	Experimental ultimate shear Load (kN)		$\frac{V_{UR}}{V_U}$
	V_U	V_{UR}	
Group (1), $\omega_o \simeq$ 0.125 mm, shear transverse reinf. of high tensile deformed bars			
0.28	169	125	0.73
0.56	258	196	0.75
1.12	320	285	0.89
1.68	414	382	0.92
			Ave.=0.82
Group (2), $\omega_o \simeq$ 0.40 mm, shear transverse reinf. of high tensile deformed bars			
0.28	130	111	0.85
0.56	187	169	0.90
1.12	254	245	0.96
1.68	365	347	0.95
			Ave.=0.92
Group (3), $\omega_o \simeq$ 125 mm, shear transverse reinf. of mild plain bars			
0.28	151	120	0.79
0.56	235	173	0.74
1.12	293	262	0.89
1.68	386	346	0.89
			Ave.=0.82

Table (7.21) Comparison between experimental and calculated ultimate shear load under repeated load.

Specimen number	Reinforcement ratio ρ %	Experimental stress v_{UR} (N/mm^2)	Calculated ult.shear stress v_{UR} (N/mm^2)	$\frac{v_{UR(cal)}}{v_{UR(exp)}}$
Group (1) - Series 3				
3.1.1 A	0.28	3.47	3.39	0.976
3.1.2 A	0.56	5.44	5.19	0.954
3.1.3 A	1.12	7.9	8.22	1.04
3.1.4 A	1.68	10.6	11.3	1.06
				Ave. = 1.007
Group (2) - Series 3				
3.2.1 A	0.28	3.08	3.04	0.98
3.2.2 A	0.56	4.69	4.67	0.995
3.2.3 A	1.12	6.81	6.78	0.995
3.2.4 A	1.68	9.64	9.62	0.998
				Ave. = 0.992
Group (3) - Series 3				
3.3.1 A	0.28	3.3	3.3	1.0
3.3.2 A	0.56	4.8	4.5	0.987
3.3.3 A	1.12	7.27	7.14	0.986
3.3.4 A	1.68	9.6	9.6	1.0
				Ave. = 0.980

Table (7.22): Ratio of shear transfer by dowel action to shear transfer by combined action under repeated load at last cycle.

Nos. and size of stirrups crossing shear plane	$A = (\frac{v_{duR}}{\sqrt{f_\omega}})$	$B = (\frac{{}^{\dagger}v_{uR1}}{\sqrt{f_{cu}}})$	$C = (\frac{{}^{*}v_{uR2}}{\sqrt{f_{cu}}})$	A/B	A/C
2Y8	0.107	0.75	0.66	0.14	0.16
4Y8	1.15	1.15	0.98	0.21	0.25
6Y8	1.72	1.72	1.36	0.21	0.27

${}^{\dagger}v_{uR1}$: ultimate shear transfer stress by combined action across cracked section with ω_o 0.125 mm

${}^{*}v_{uR2}$: ultimate shear transfer stress by combined action across cracked section with ω_o 0.40 mm

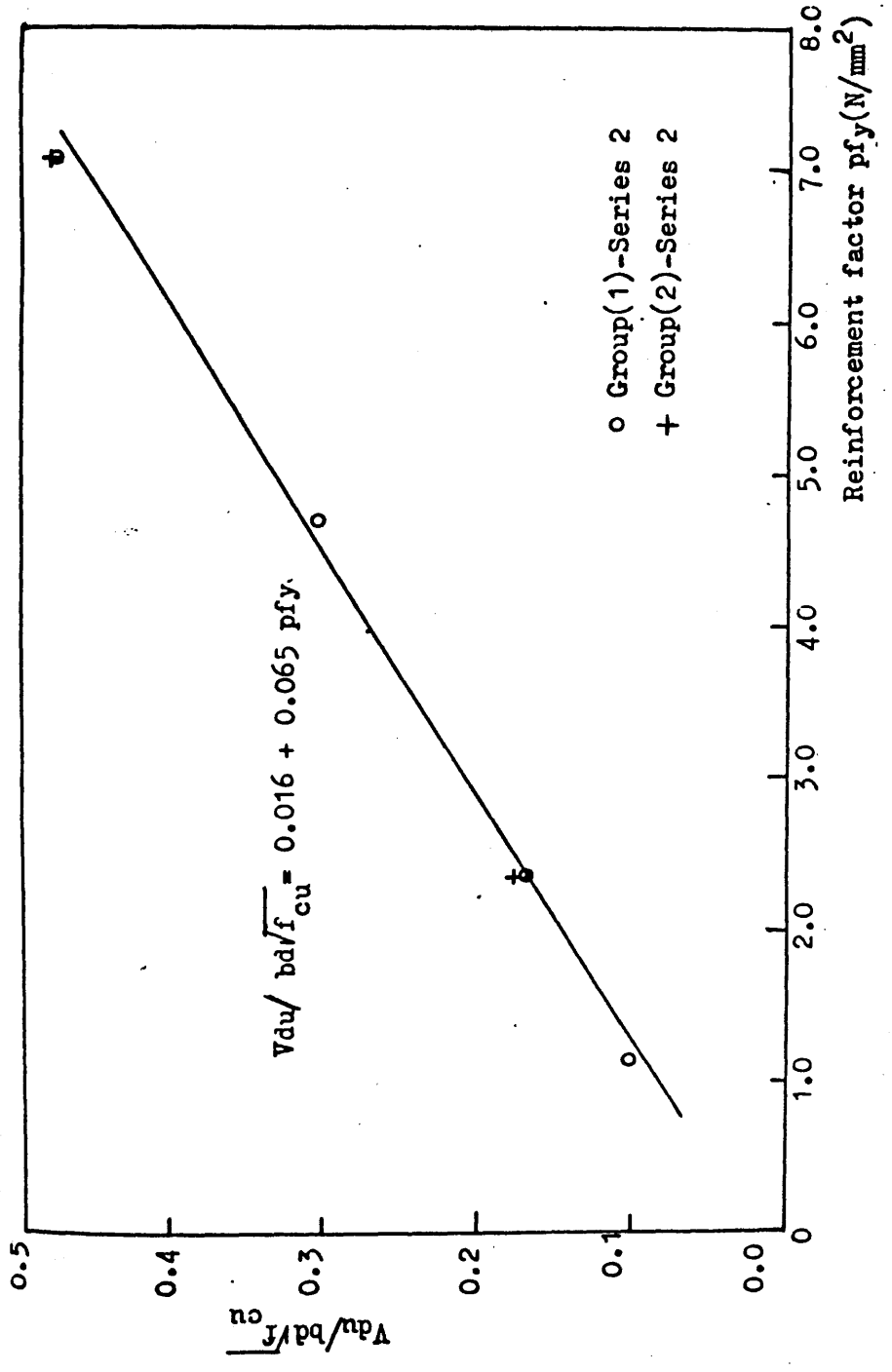

Figure(7.1) Ultimate shear strength vs. reinforcement factor ρf_y for dowel action specimens of groups (1)&(2)-series 2 under monotonic loading.

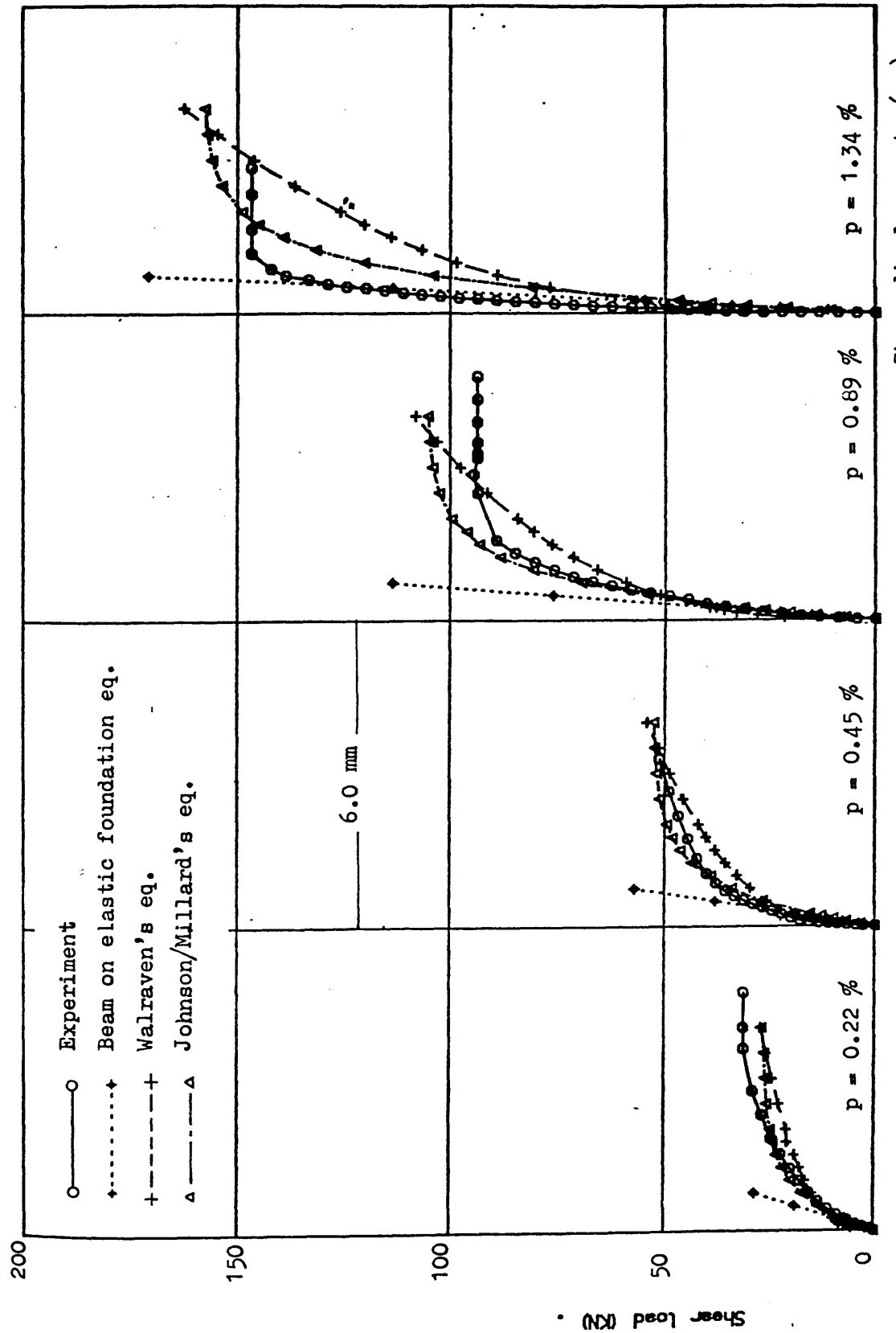

Figure(7.2) Comparison between the experimental and calculated shear load vs. shear displ. according to the available models.

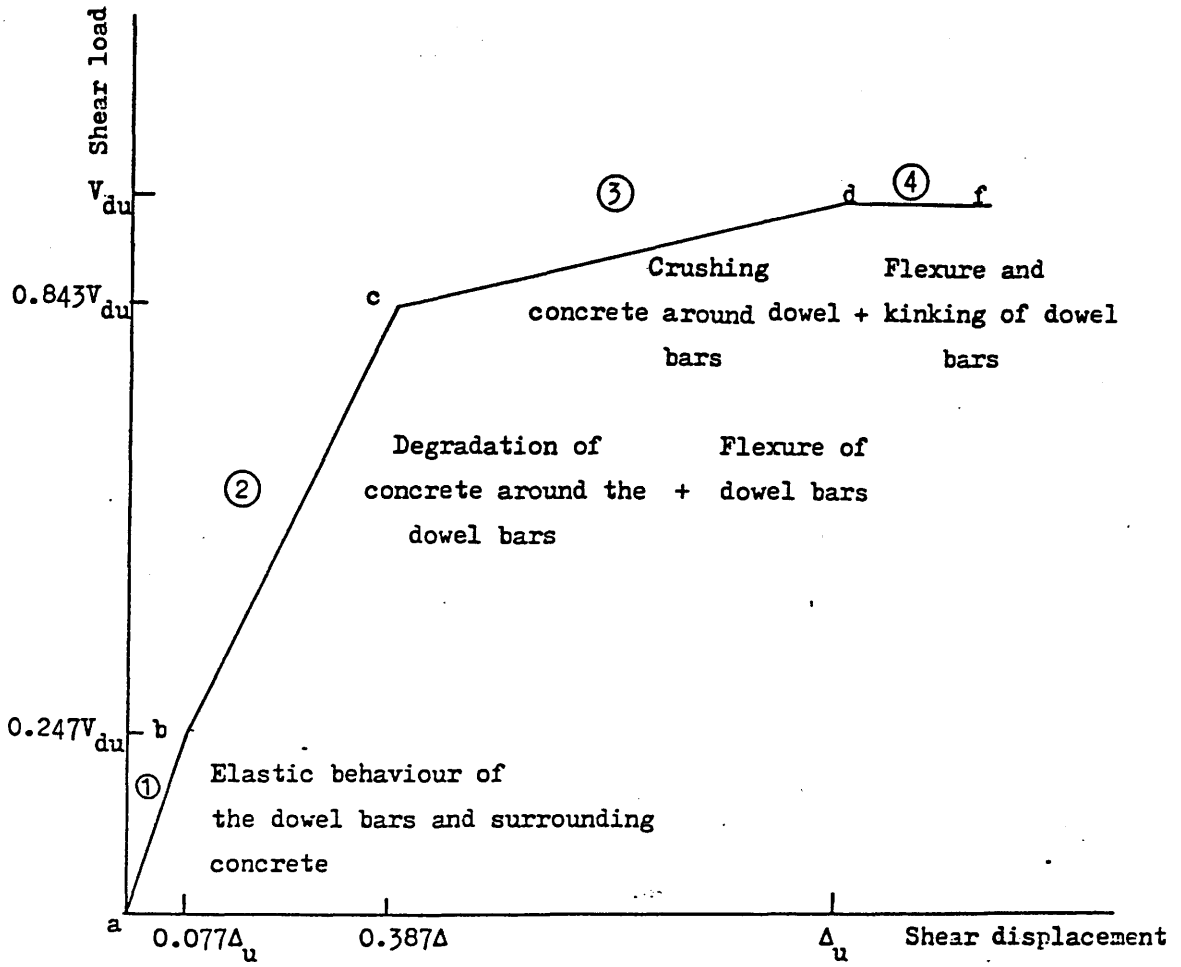

Figure(7.3) Schematic presentation for the idealized shear load vs. shear displacement of the dowel action under monotonic load .

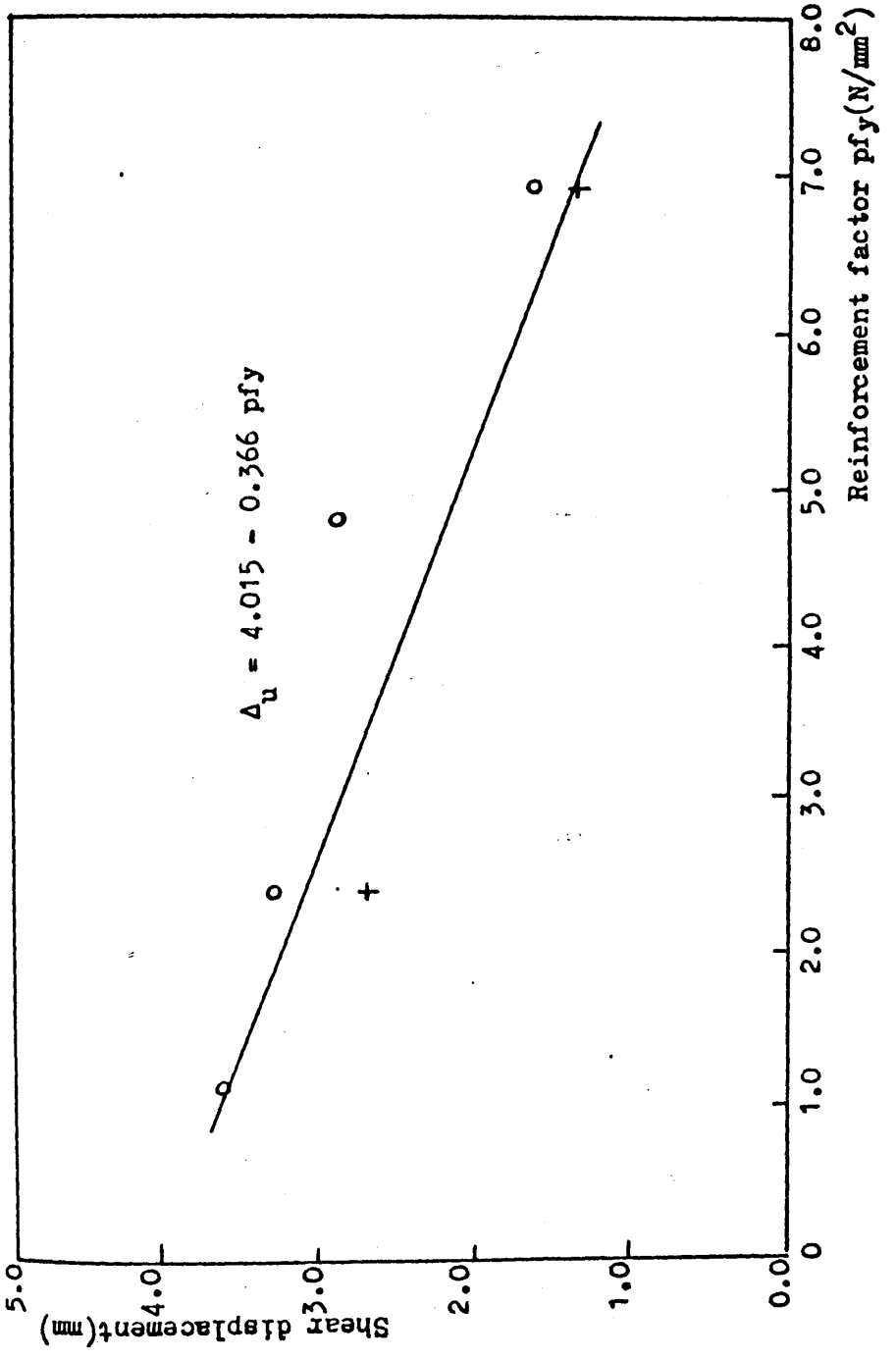

Figure(7.4) Ultimate shear displacement vs. reinforcement factor ρf_y for dowel action specimens of groups (1)&(2)-series 2 tested under monotonic load

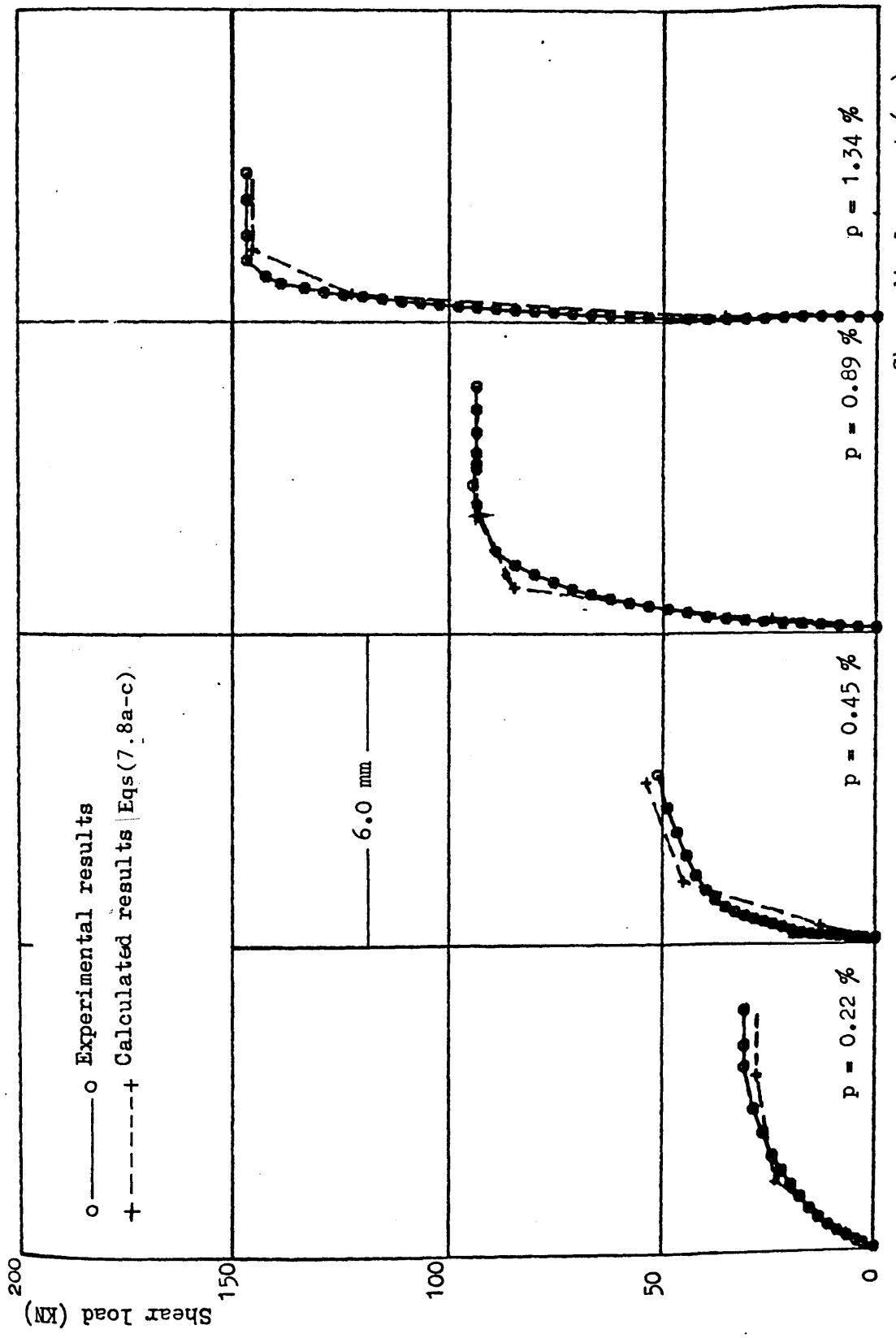

Figure(7.5) Comparison between the experimental and calculated shear load vs. shear displ. for dowel action specimens under monotonic load, group(1)-series 2

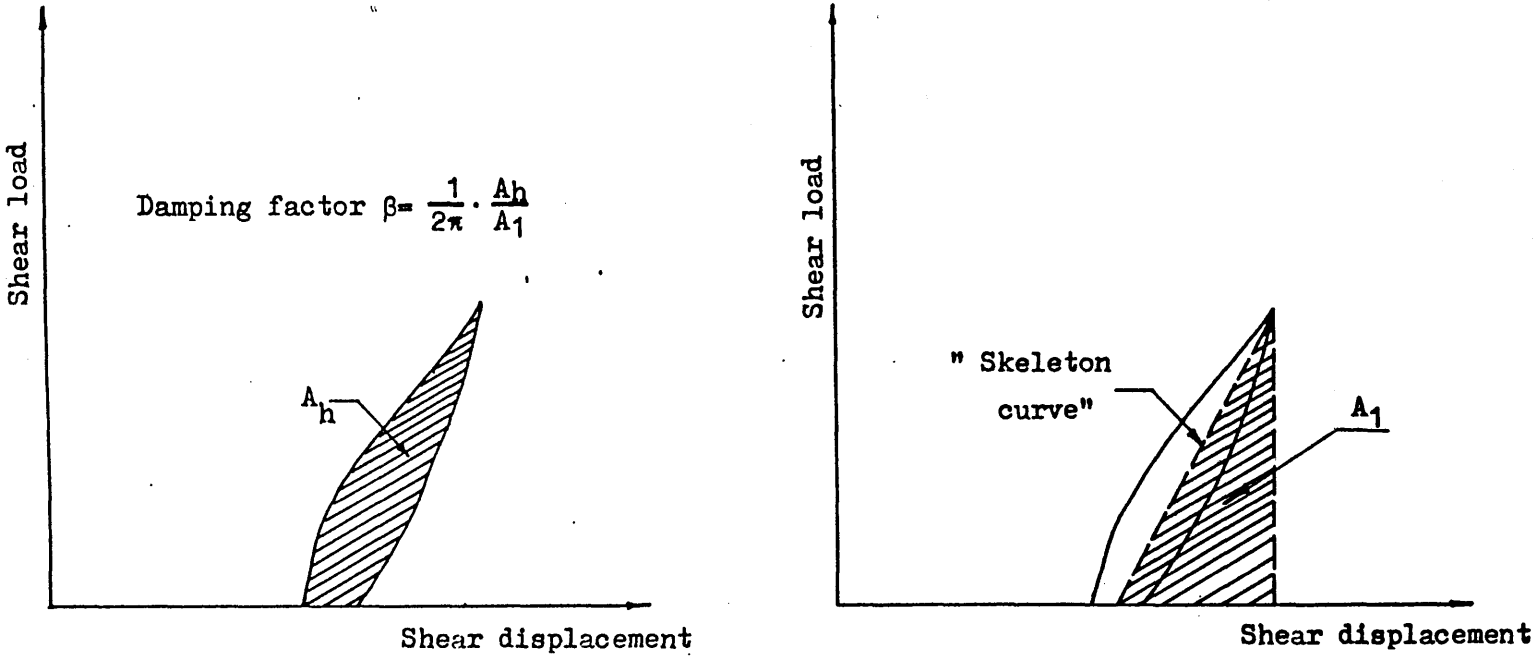

Figure(7.6) Schematic diagram to show the definition of A_h and A_1 for certain cycle number

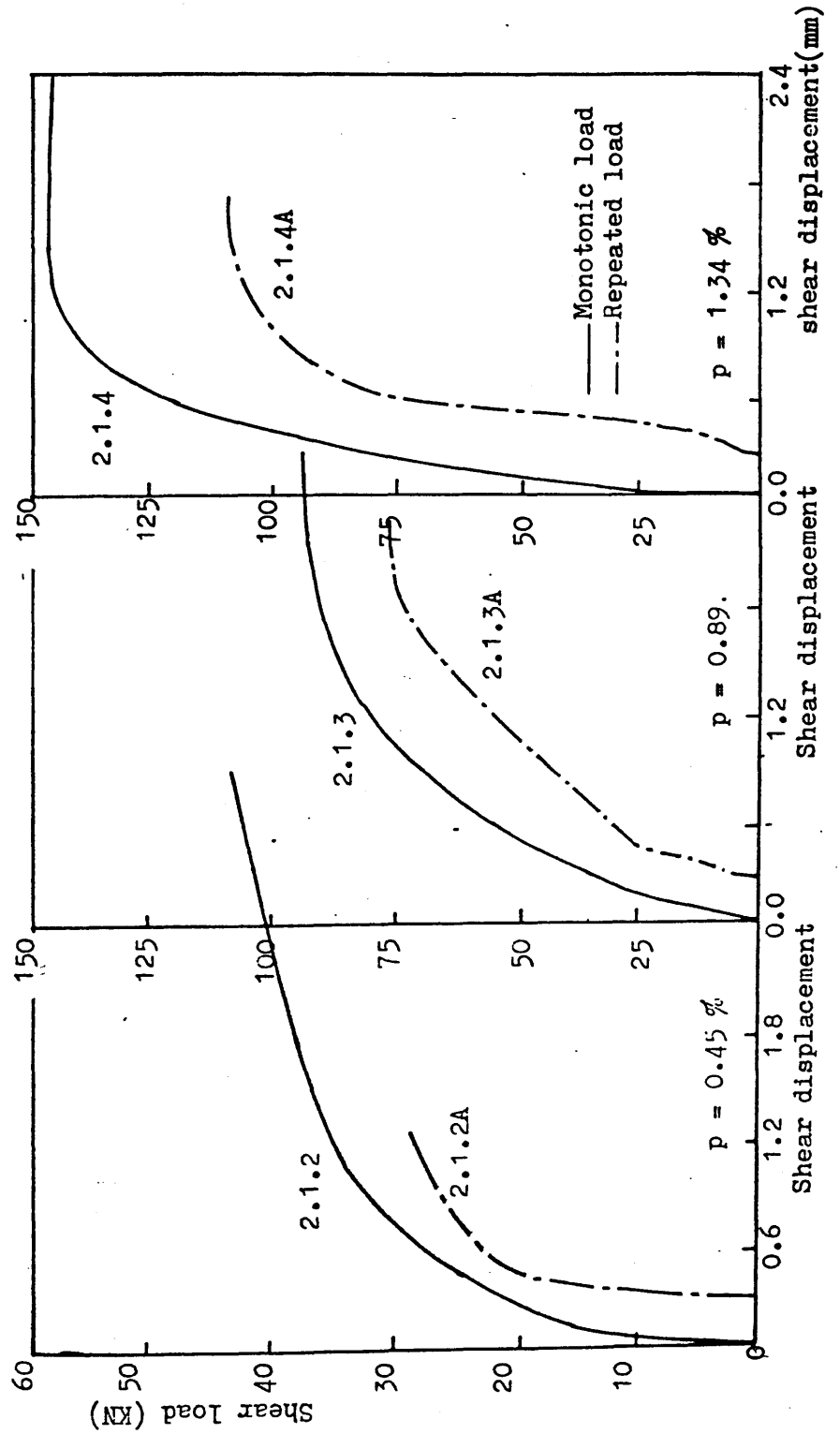

Figure(7.7a) Comparison between shear load vs. shear displacement for dowel action specimens of group(1)-series 2 tested under monotonic and repeated load (last cycle)
load cycle)

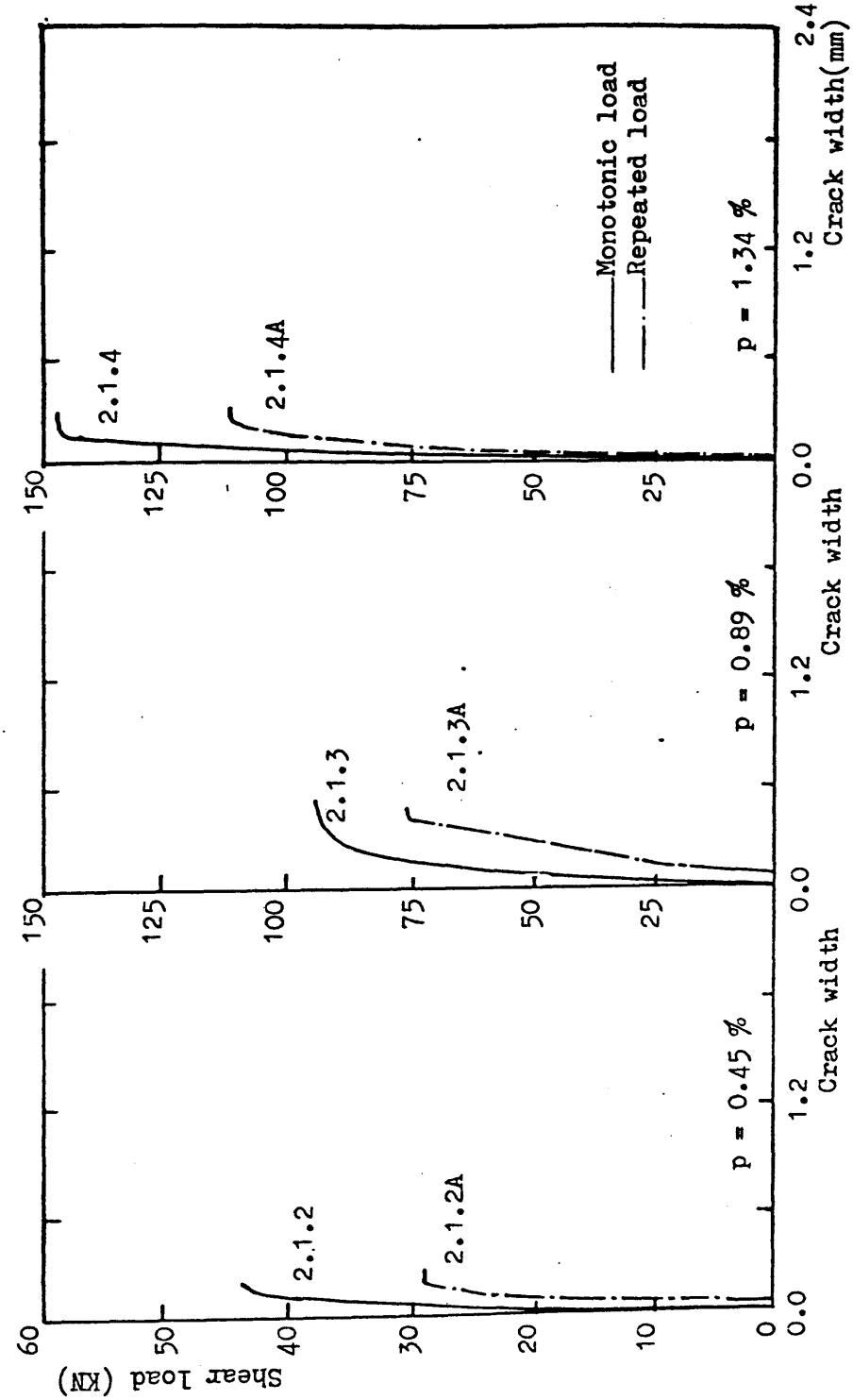

Figure(7.7b) Comparison between shear load vs. crack width for dowel action specimens of group(1)-series 2 tested under monotonic and repeated load (last cycle)

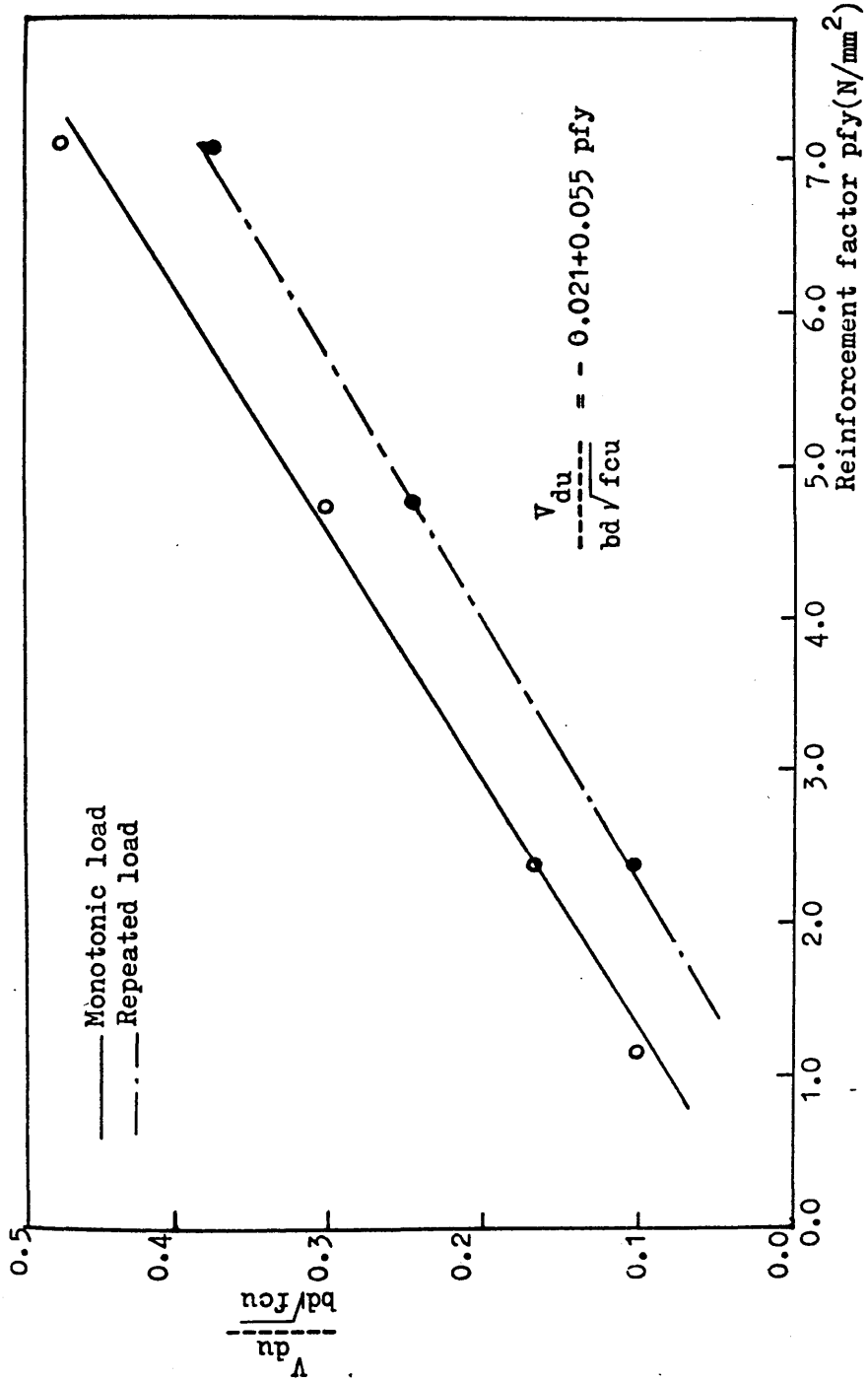

Figure(7.8) Comparison between ultimate shear load for dowel action specimens of group(1)-series 2 tested under monotonic and repeated load

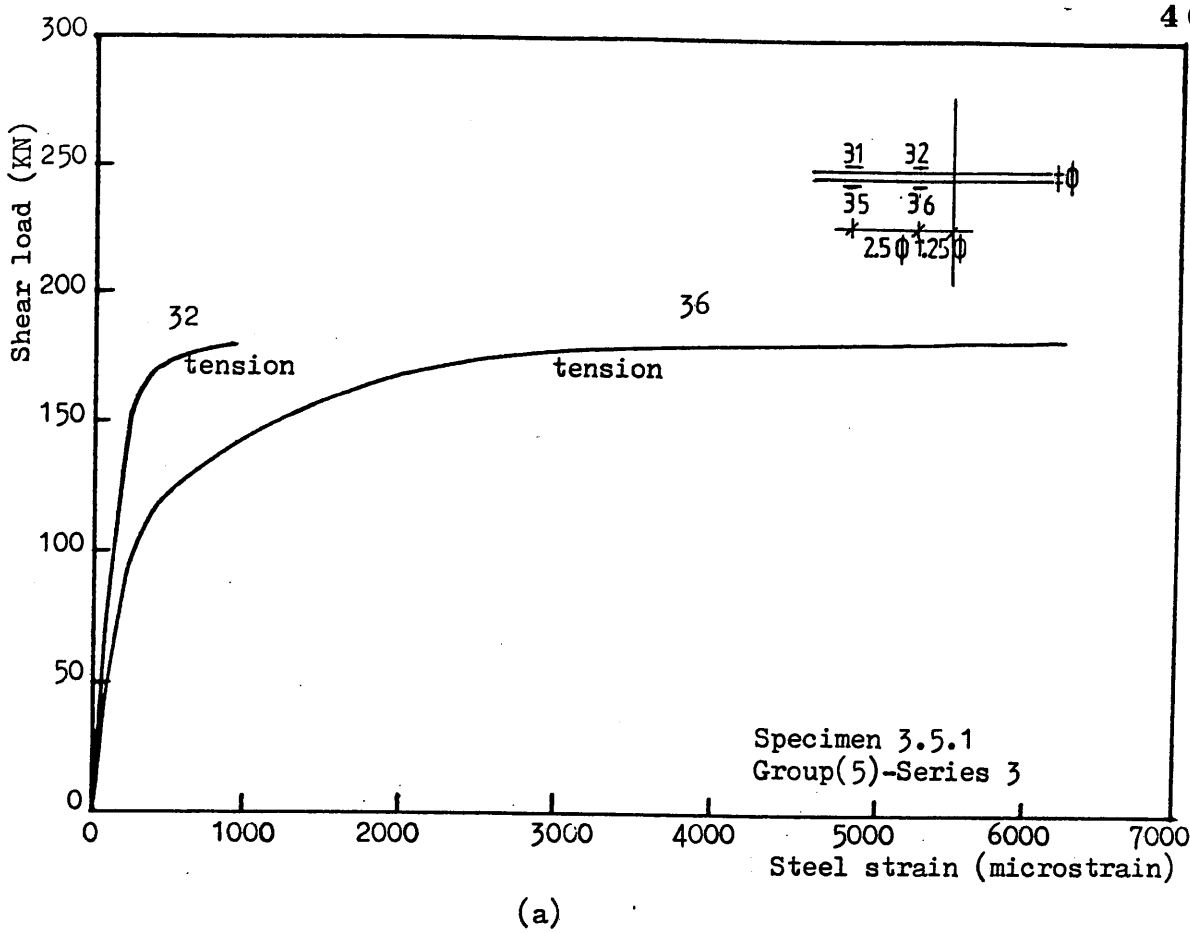

(a)

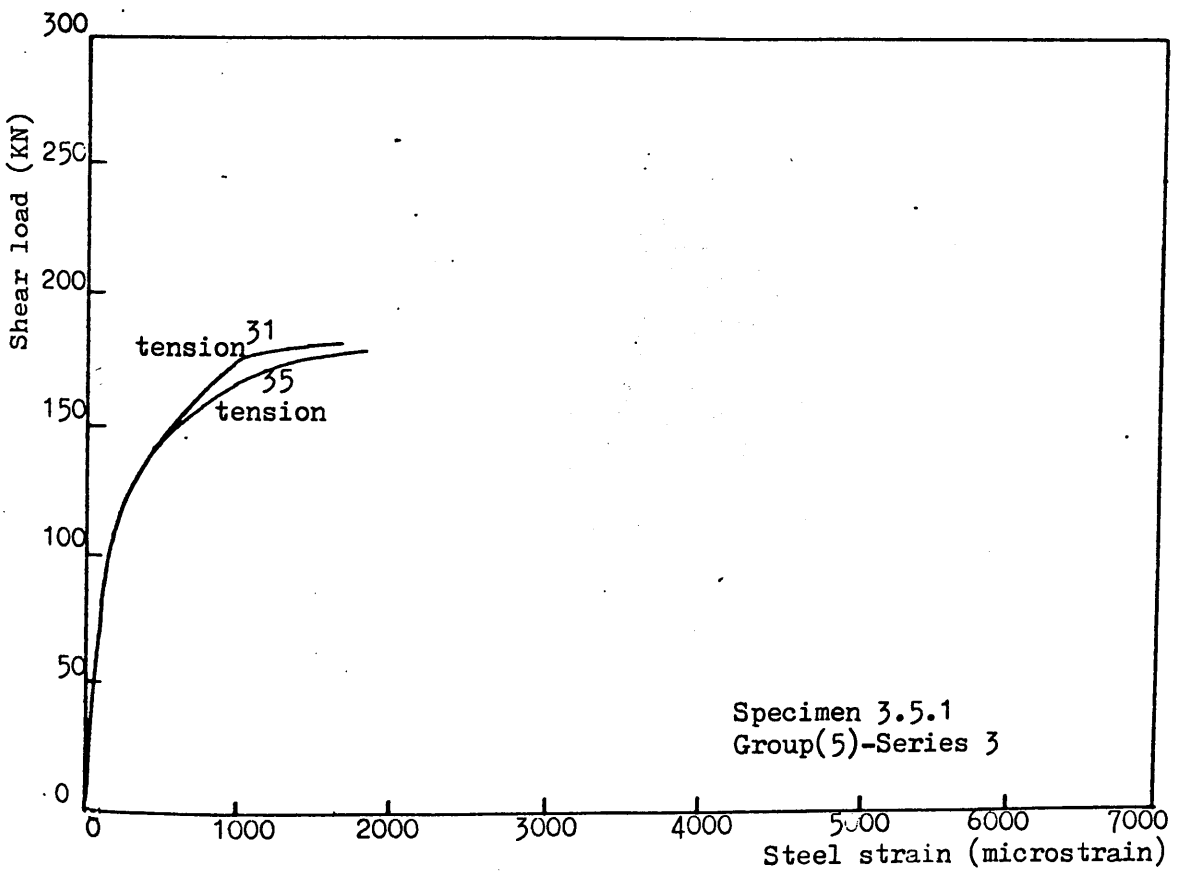

Figure(7.9) Shear load vs. steel strain for combined action specimen 3.5.1 with w_o= 0.40 mm and ρ = 0.56 %

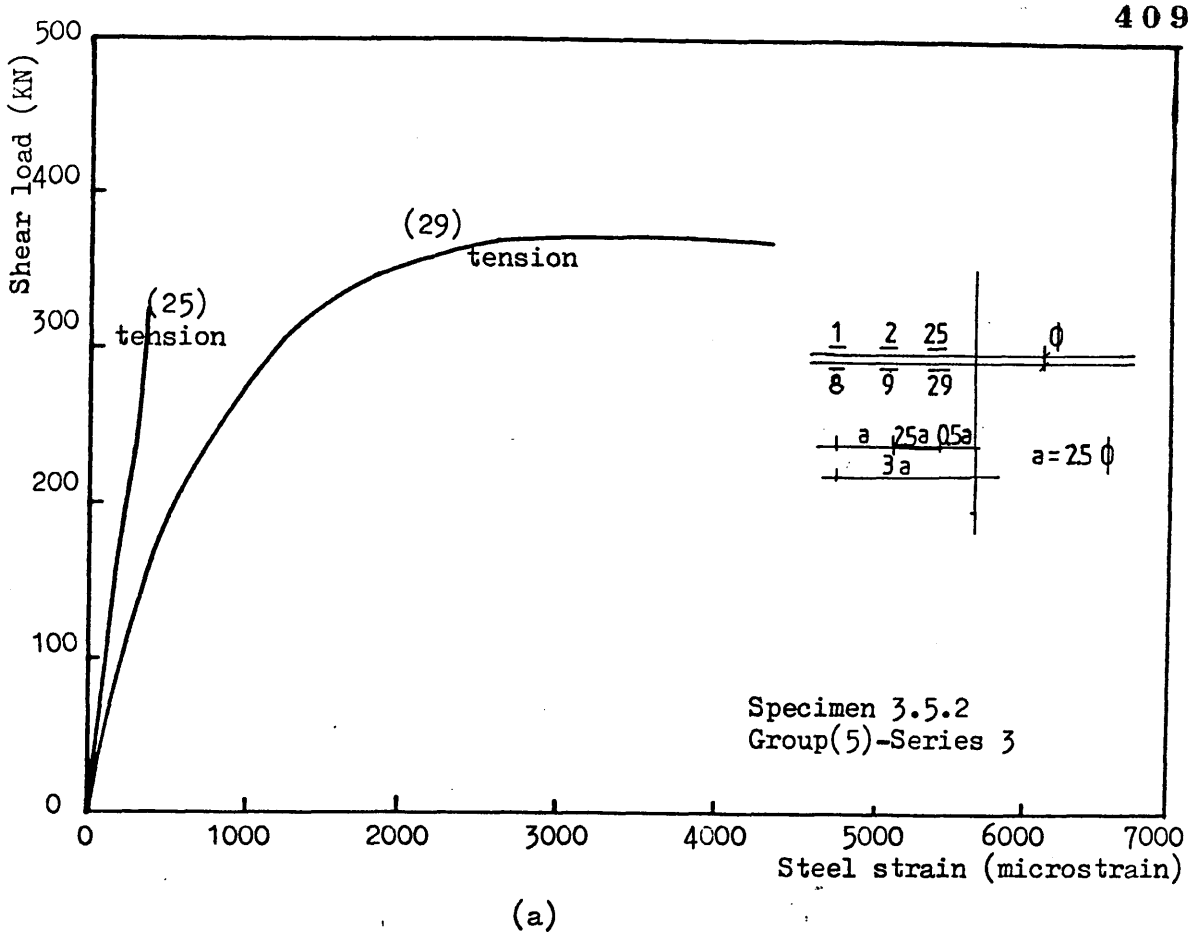

(a)

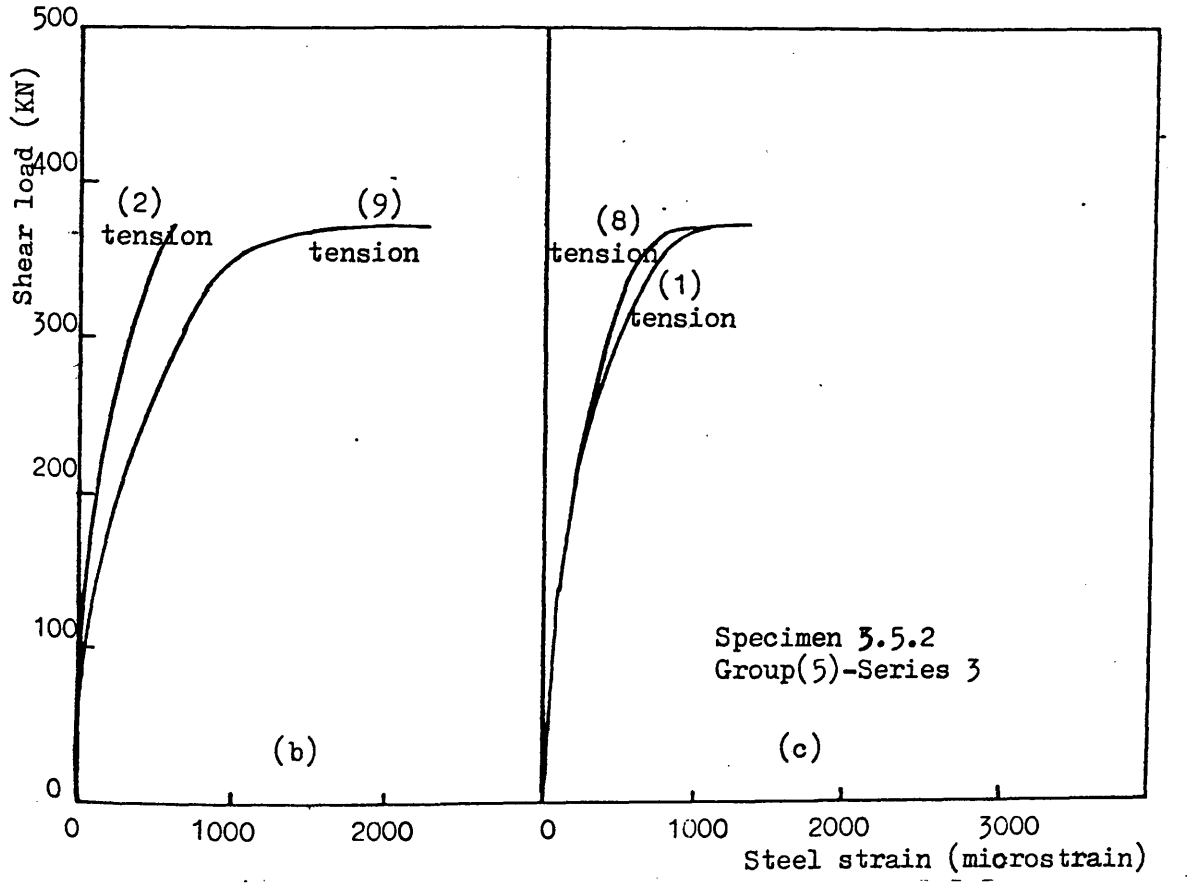

Figure(7.10) Shear load vs. steel strain for combined action specimen 3.5.2 with w_o= 0.40 mm and ρ = 1.68 %

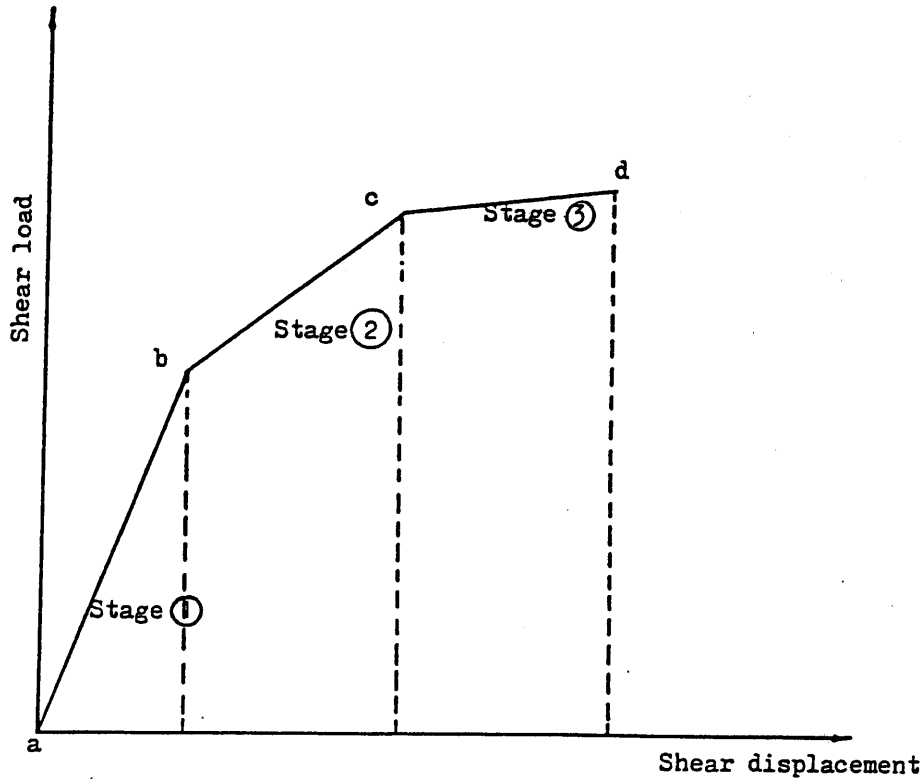

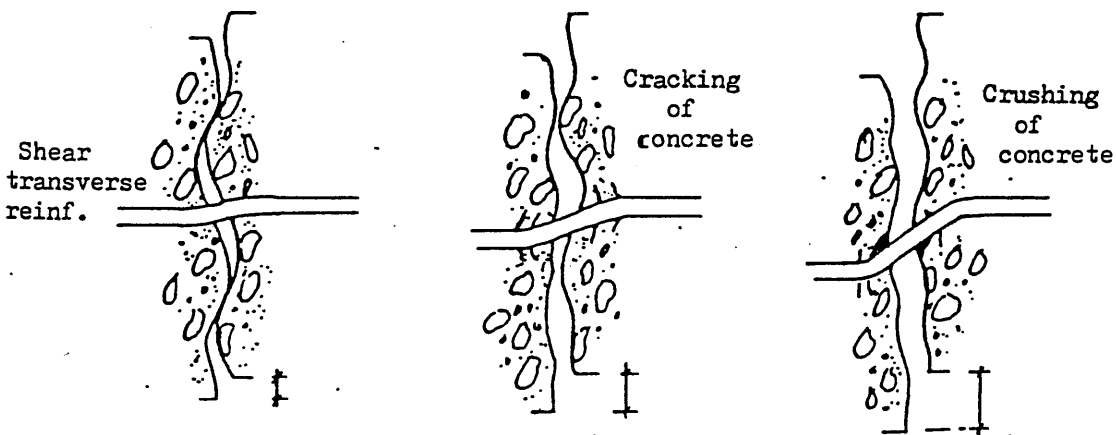

Stage 1 (a-b)
Majority of shear force resisted by interface shear transfer mechanism

Stage 2 (b-c)
Developement of dowel action mechanism and deterioration of inter-face shear transfer mechanism

Stage 3 (c-d)
Majority of shear force resisted by dowel action and break down of inter-face shear transfer mechanism

Figure(7.11) Schematic presentation of shear transfer mechanism by combined action under monotonic load

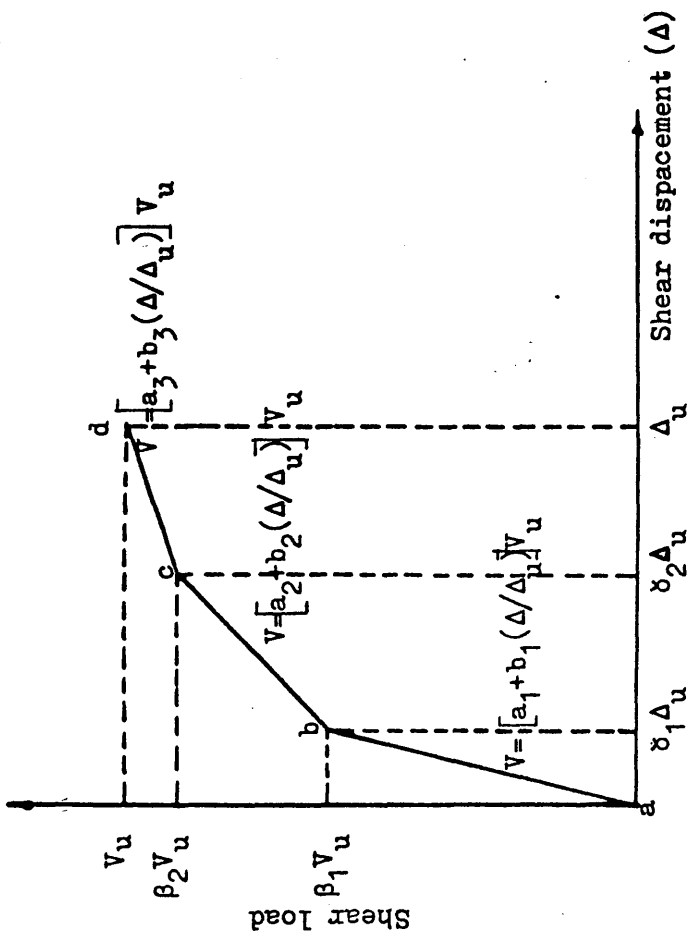

Figure(7.12) Idealization of the shear load vs. shear displacement under monotonic load.

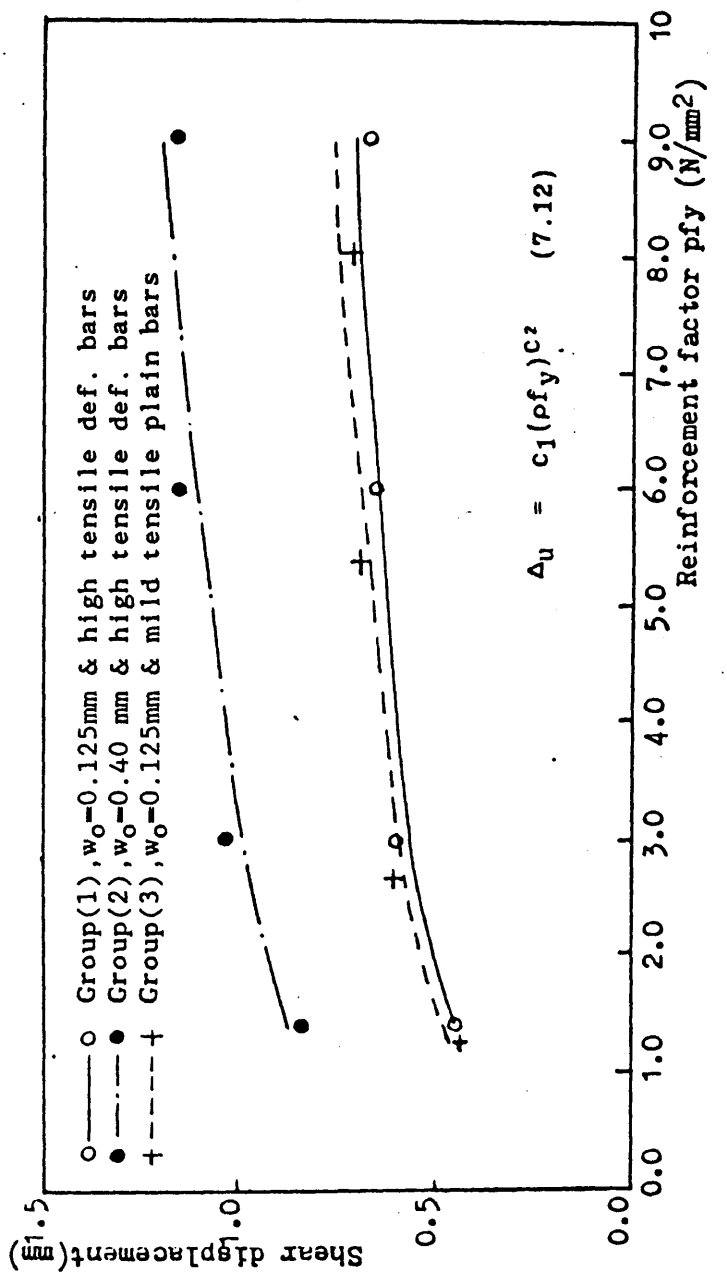

Figure(7.13) Comparison between experimental and calculated ultimate shear displacement for combined action specimens of groups (1),(2)&(3)-series 3 tested under mon. load.

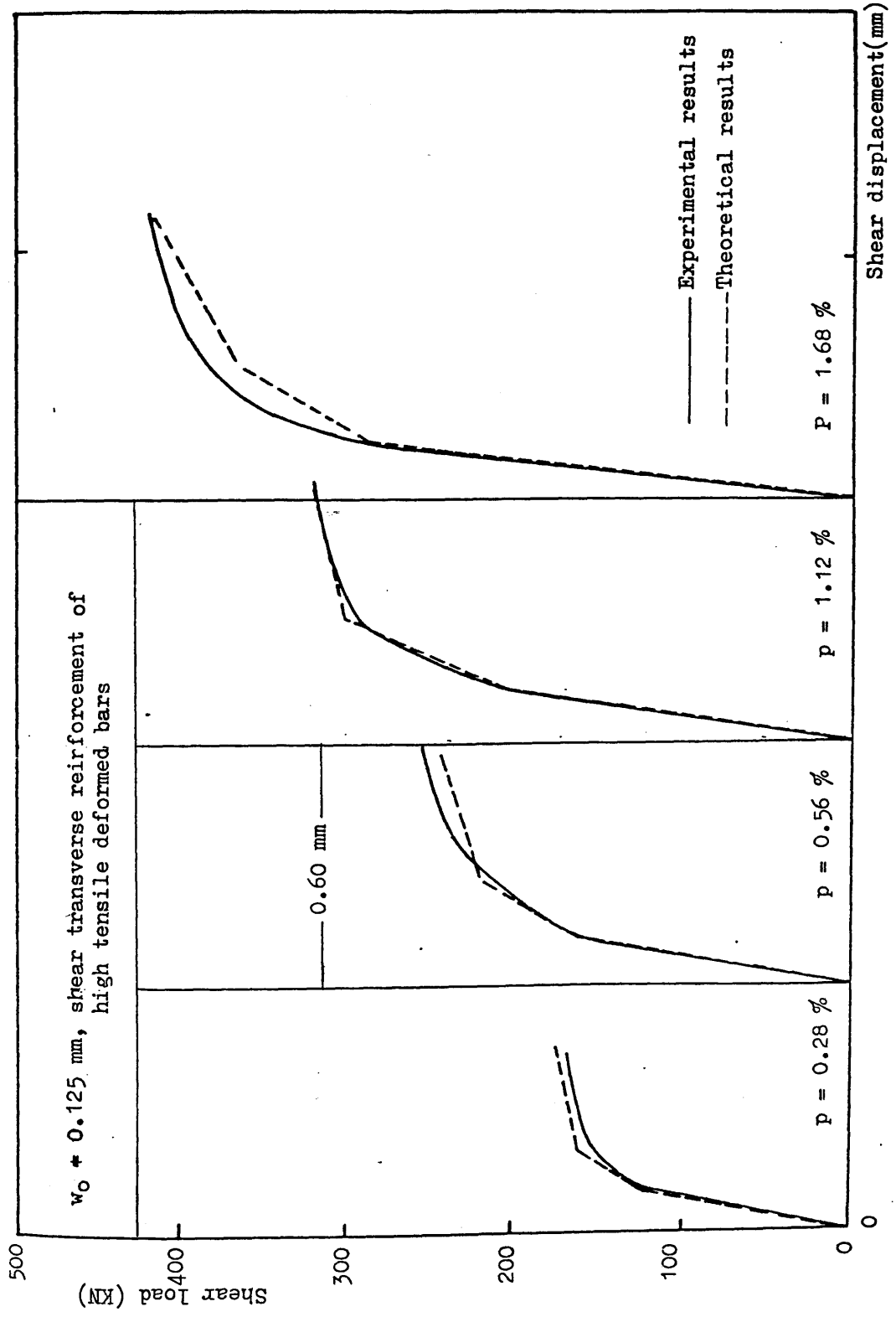

Figure(7.14) Comparison between the experimental and theoretical shear load vs. shear displ. for combined action specimens with w_o=0.125mm and high tensile deformed bars tested under monotonic load, group(1)-series 3

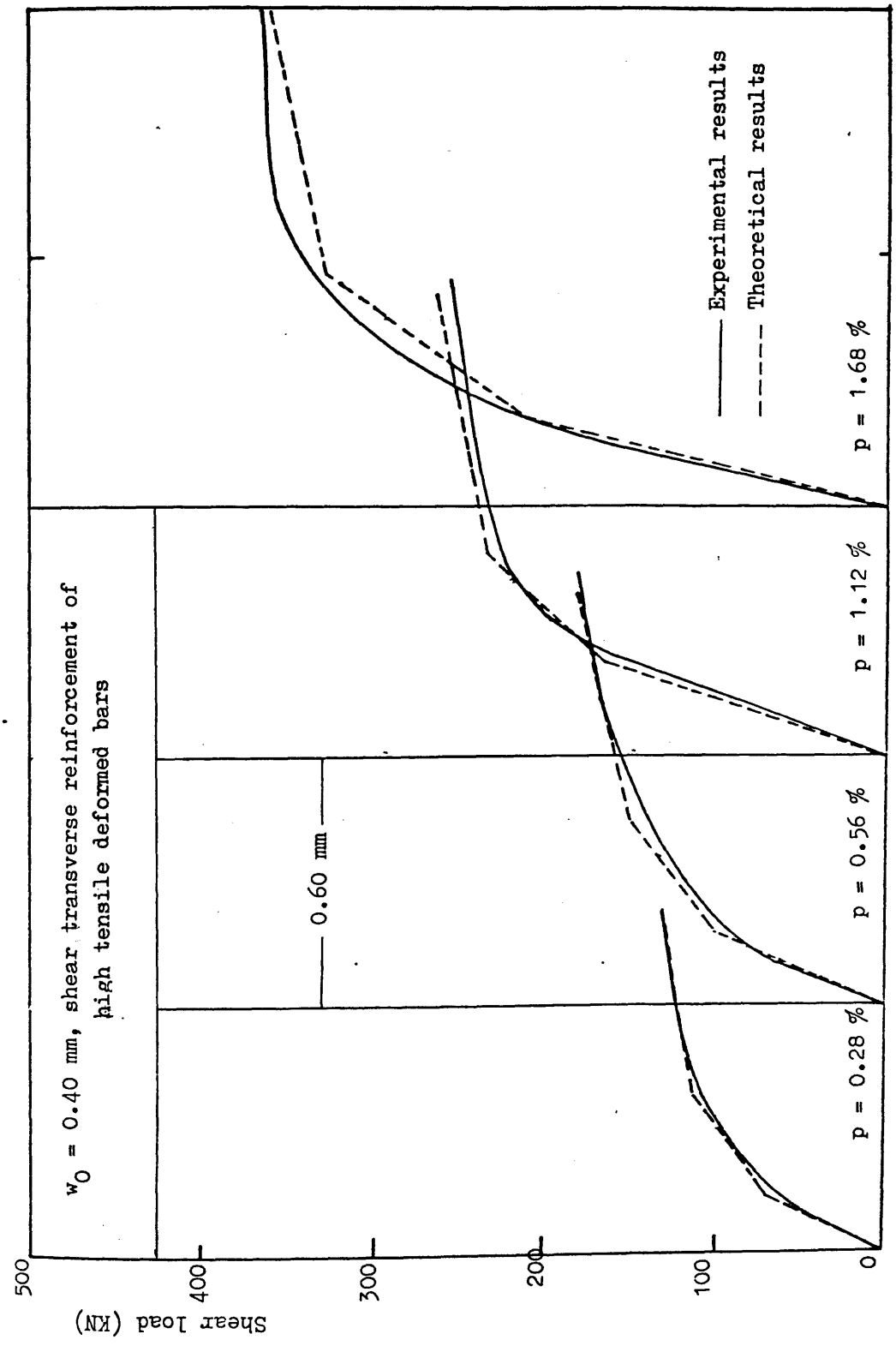

Figure(7.15) Comparison between the experimental and calculated shear load vs. shear displ. for combined action specimens with w_o=0.40mm and high tensile deformed bars tested under monotonic load, group(2)-series 3

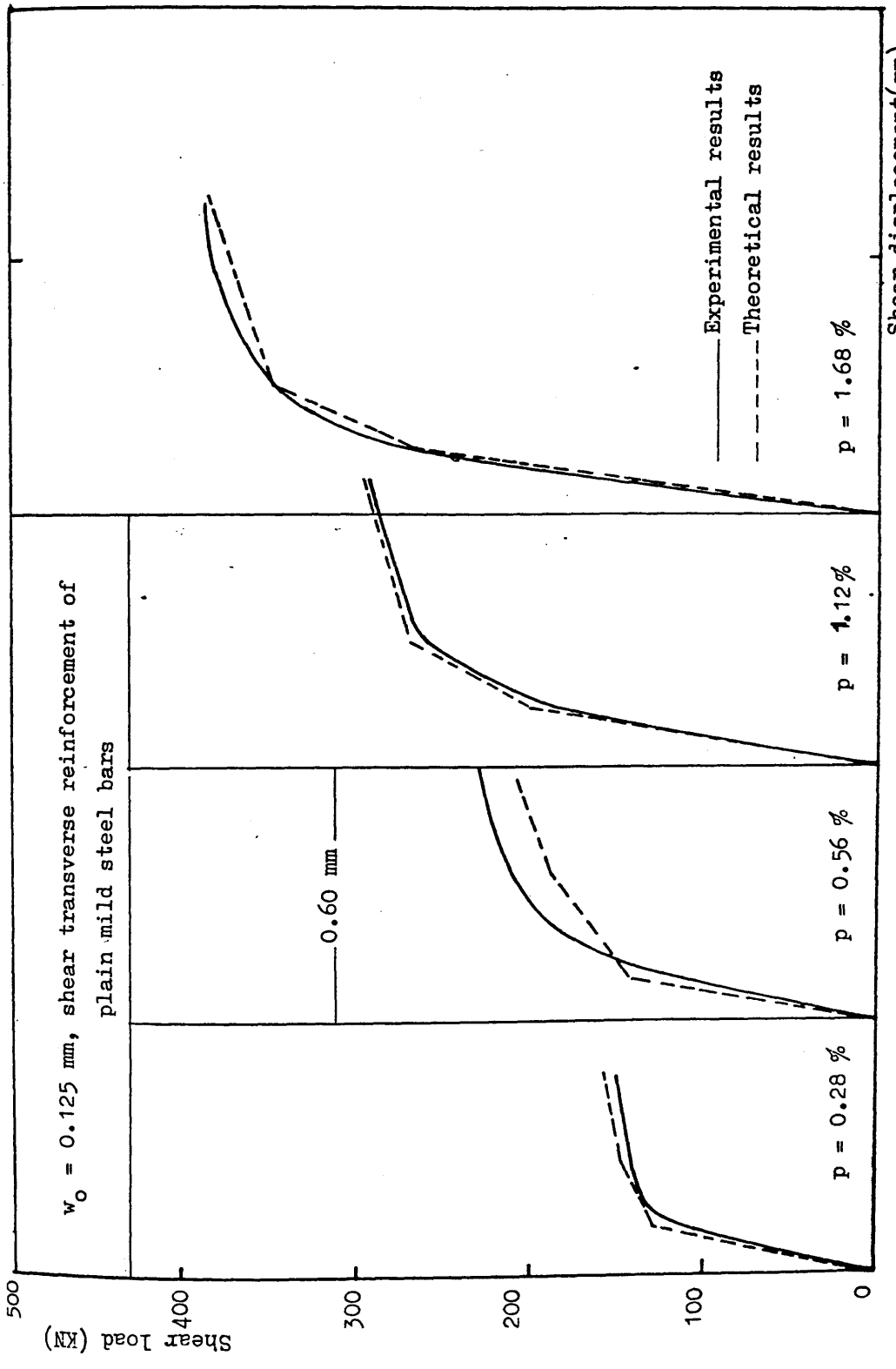

Figure(7.16) Comparison between the experimental and theoretical shear load vs. shear displ. for combined action specimens with w_o=0.125mm and mild tensile plain bars tested under monotonic load, group(3)-series 3

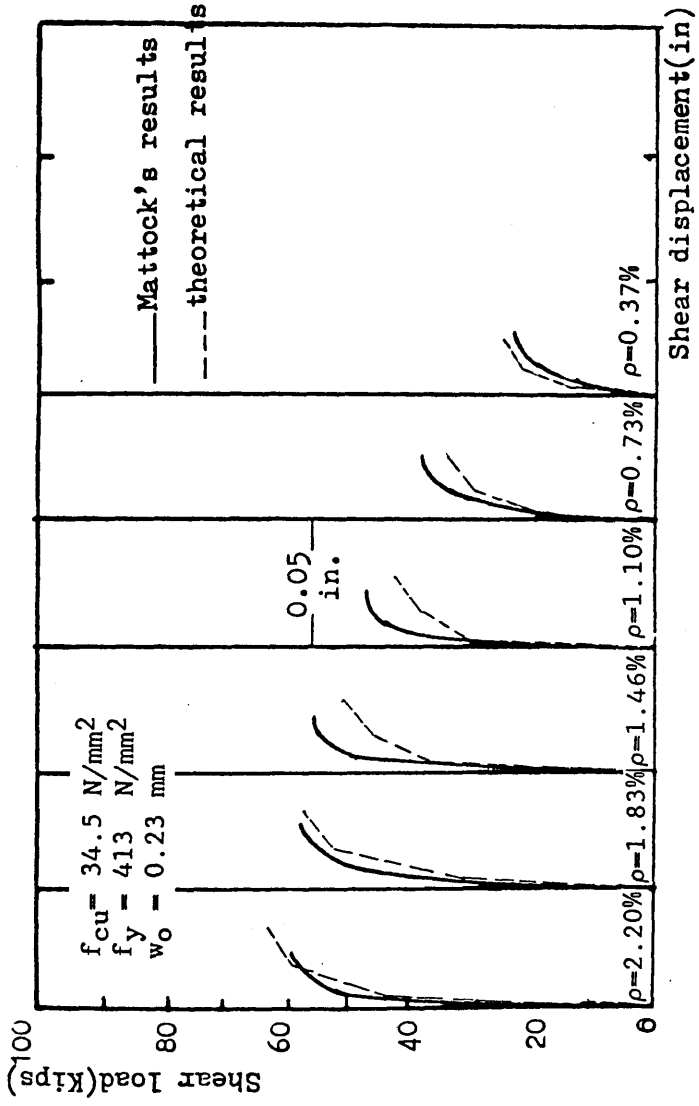

Figure(7.17) Comparison between Mattock's test results(21)and the calculated shear load vs. shear displacement according to the proposed method of idealization.

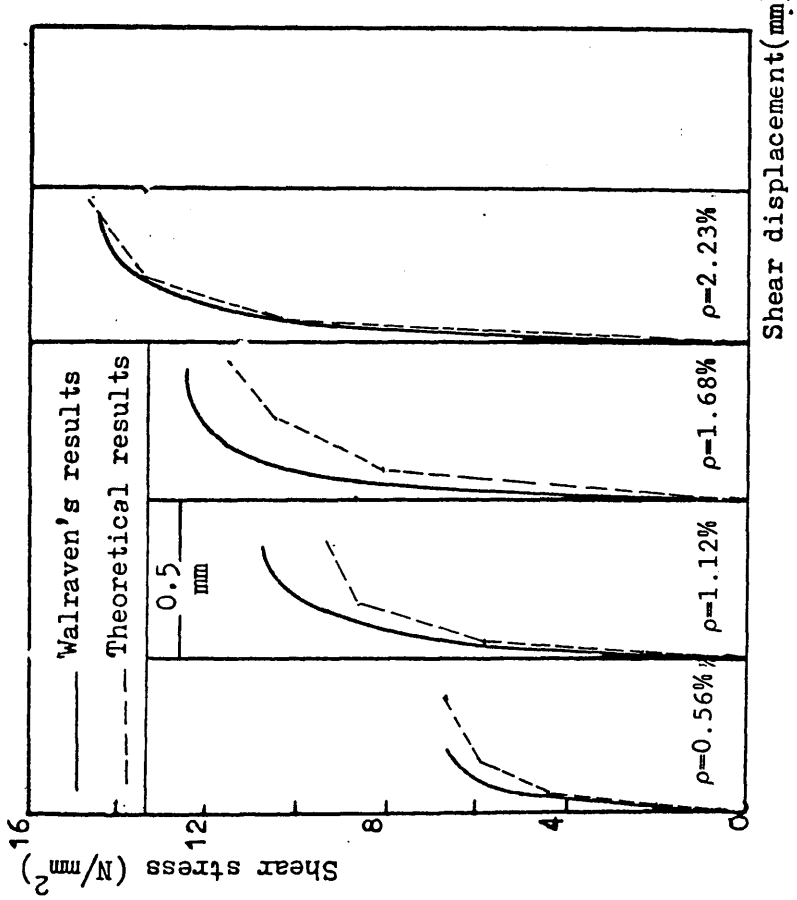

Figure(7.18) Comparison between Walraven's test results(22)and the calculated shear load vs. shear displacement according to the proposed method of idealization

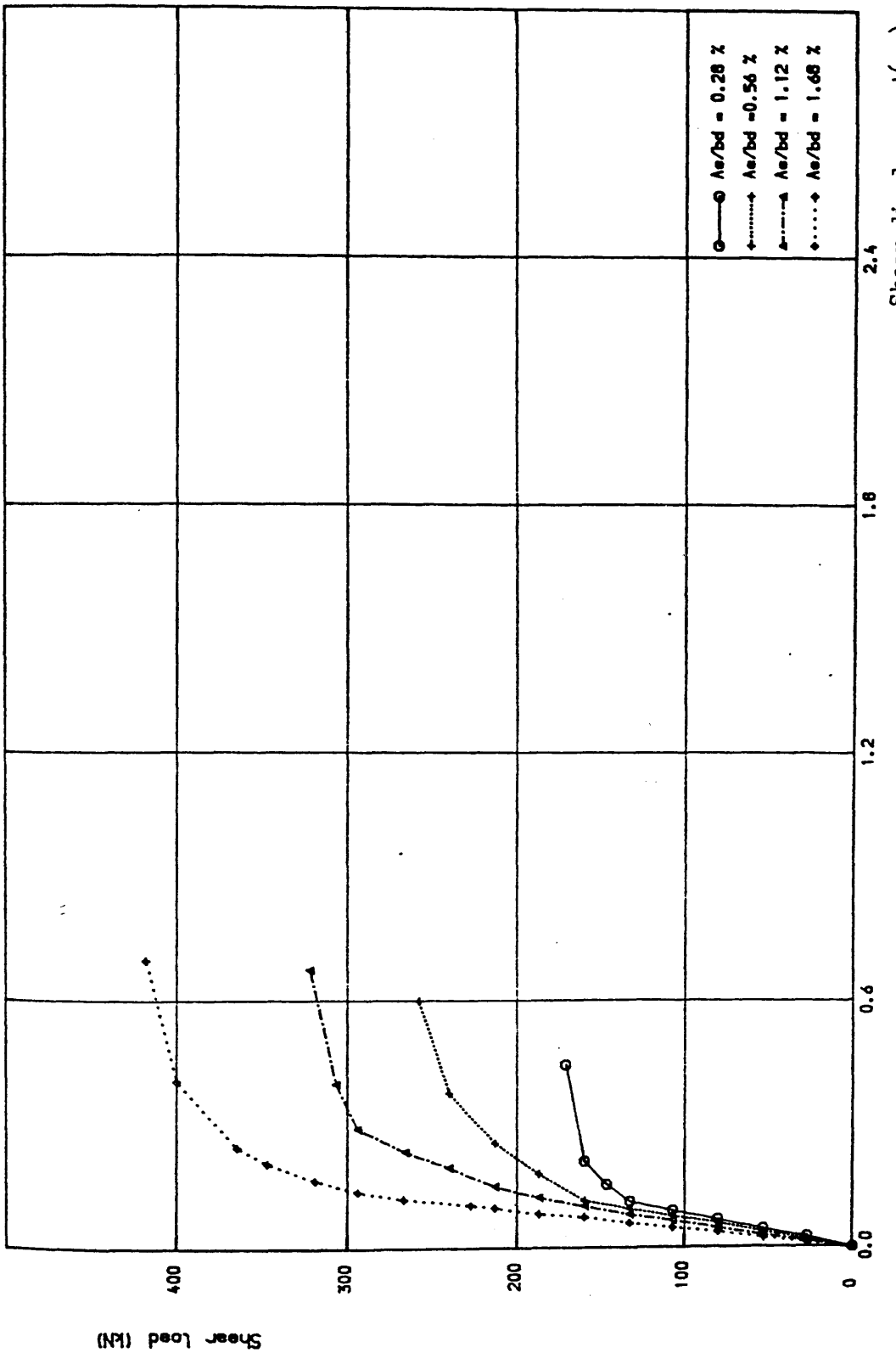

Figure(7.19) Effect of transverse reinforcement ratio on shear load vs. shear displacement for combined action specimens with w_o=0.125mm and high tensile deformed bars under monotonic load, group(1)—series 3.

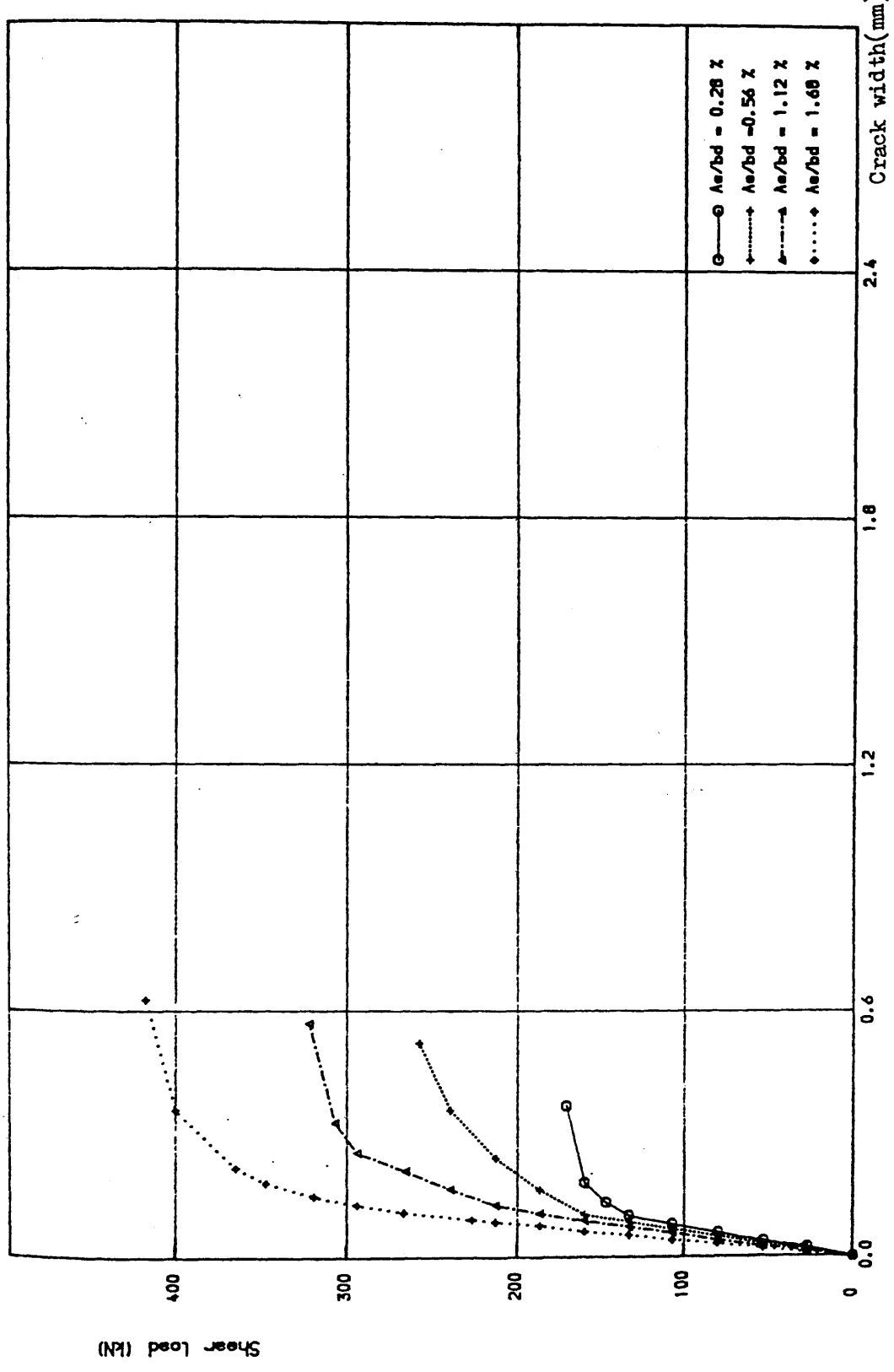

Figure(7.20) Effect of transverse reinnforcement ratio on shear load vs. crack width for combined action specimens with w_o=0.125mm and high tensile deformed bars under monotonic load, group(1)-series 3.

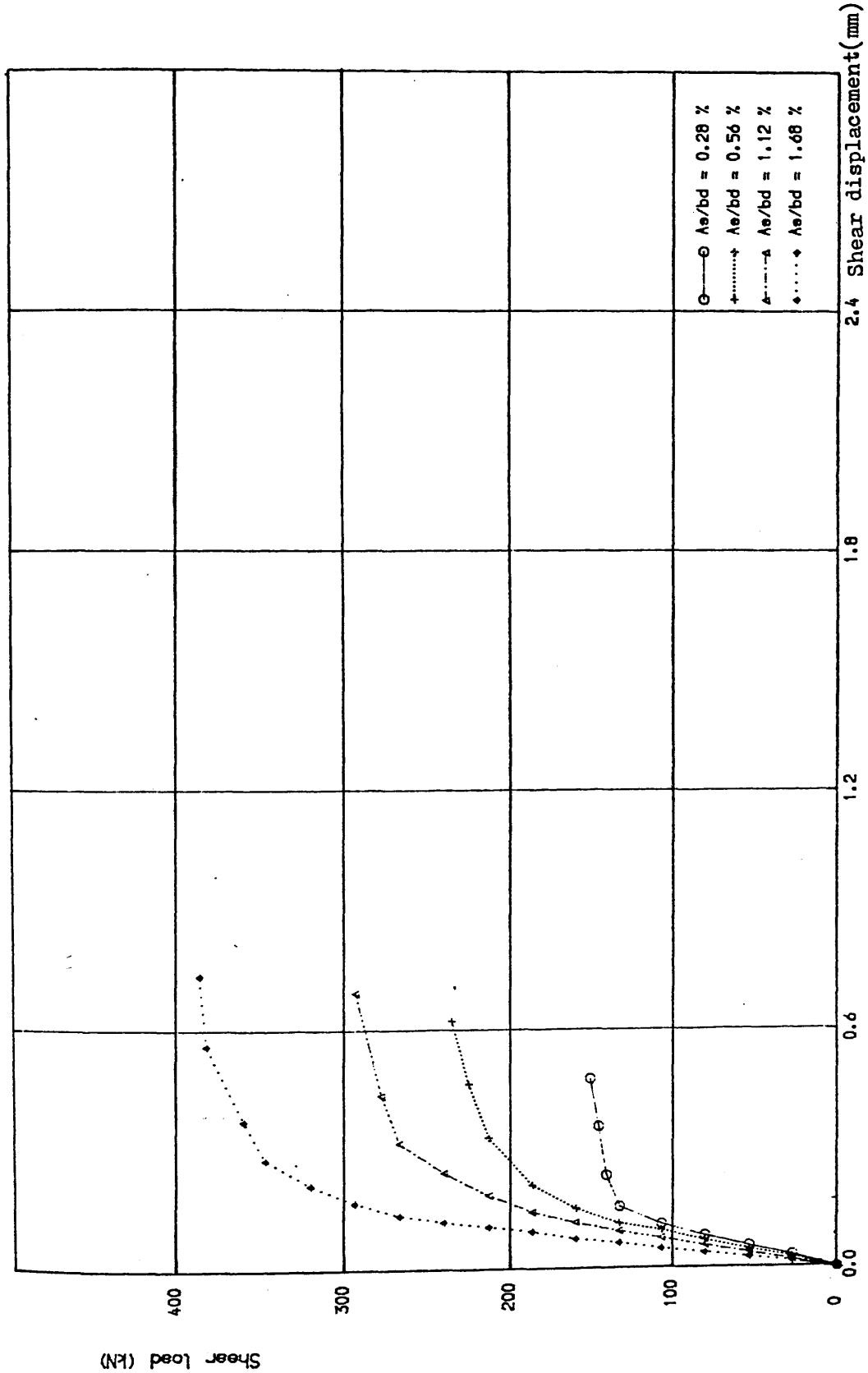

Figure(7.21) Effect of transverse reinforcement ratio on shear load vs. shear displacement for combined action specimens with w_o=0.125mm and mild tensile plain bars under monotonic load, group(3)—series 3.

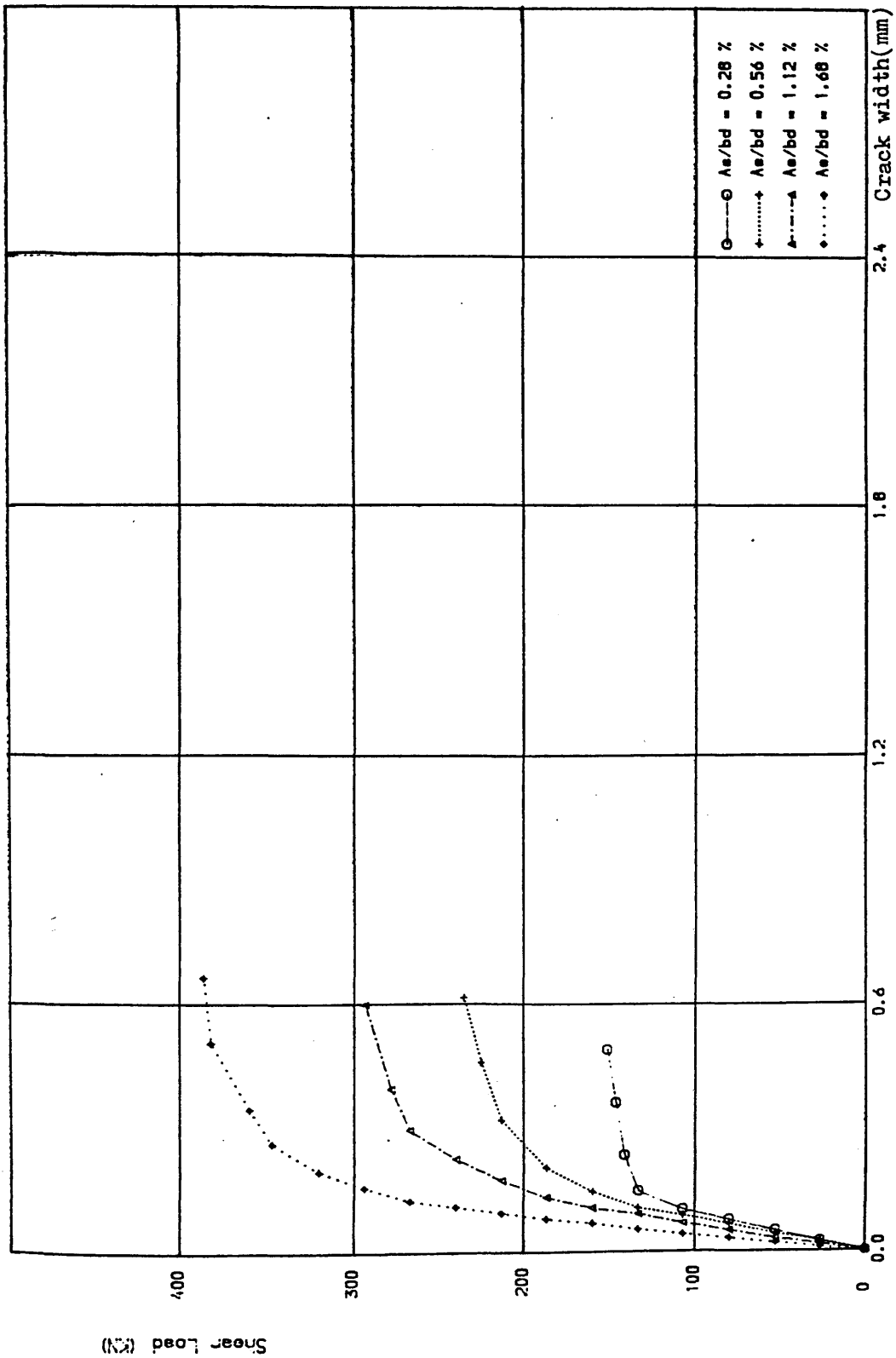

Figure(7.22) Effect of transverse reinforcement ratio on shear load vs. crack width for combined action specimens with w_o=0.125mm and mild tensile plain bars under monotonic load, group(3)-series 3.

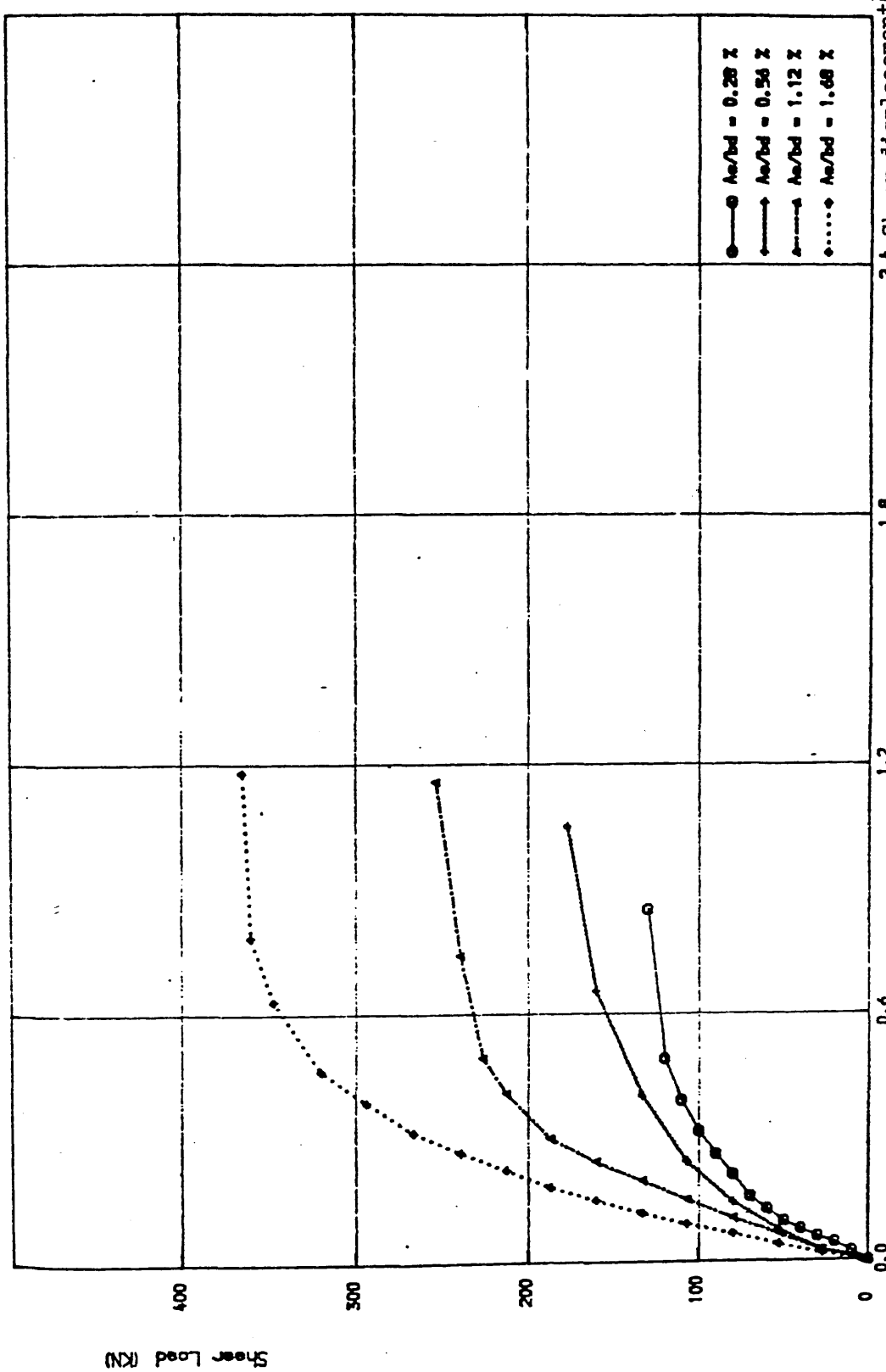

Figure(7.23) Effect of transverse reinforcement ratio on shear load vs. shear displacement for combined action specimens with w_o=0.40mm and high tensile deformed bars under monotonic load, group(2)-series 3

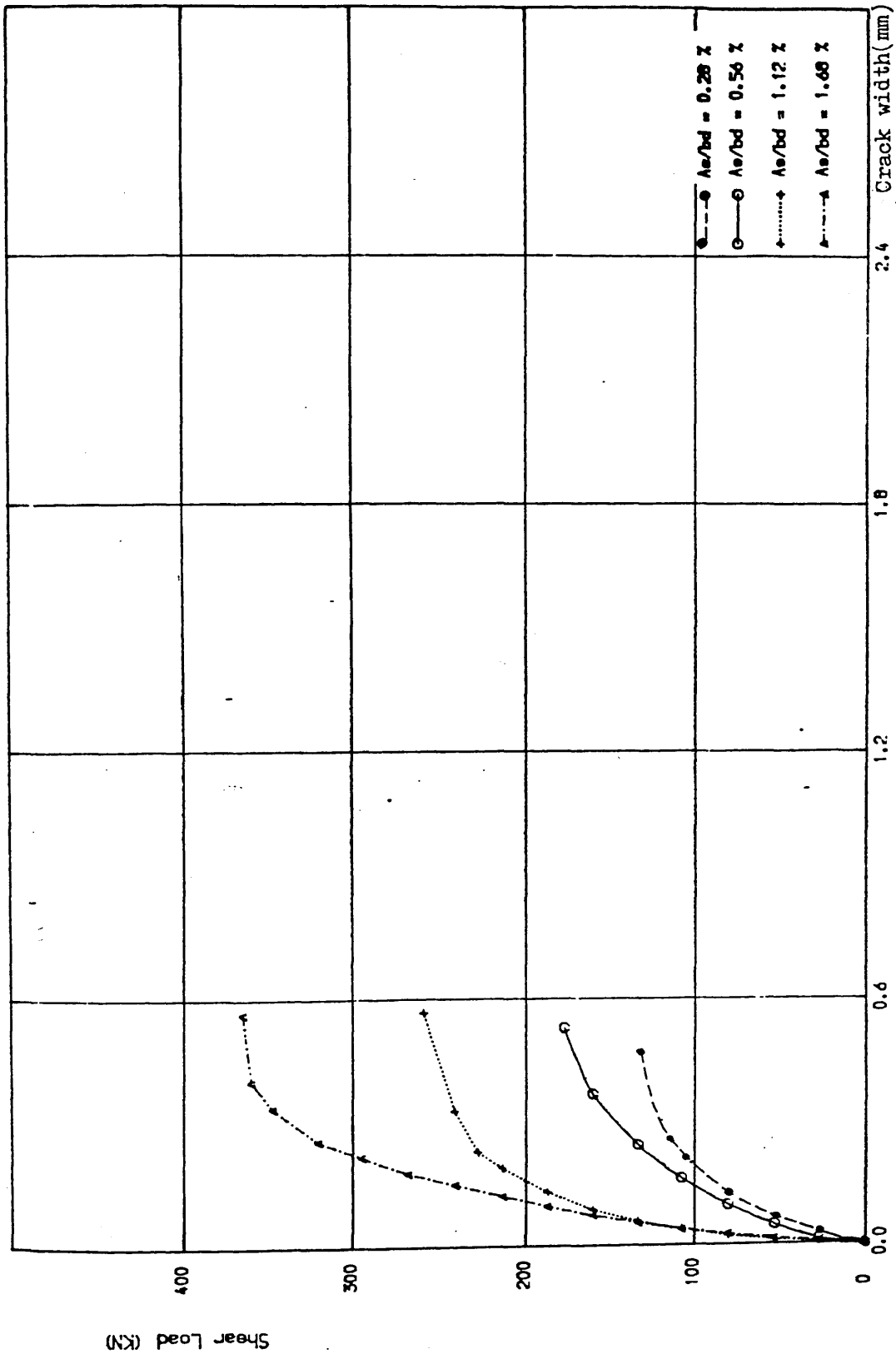

Figure(7.24) Effect of transverse reinforcement ratio on shear load vs. crack width for combined action specimens with w_o=0.40mm and high tensile deformed bars under monotonic load, group(2)-series 3.

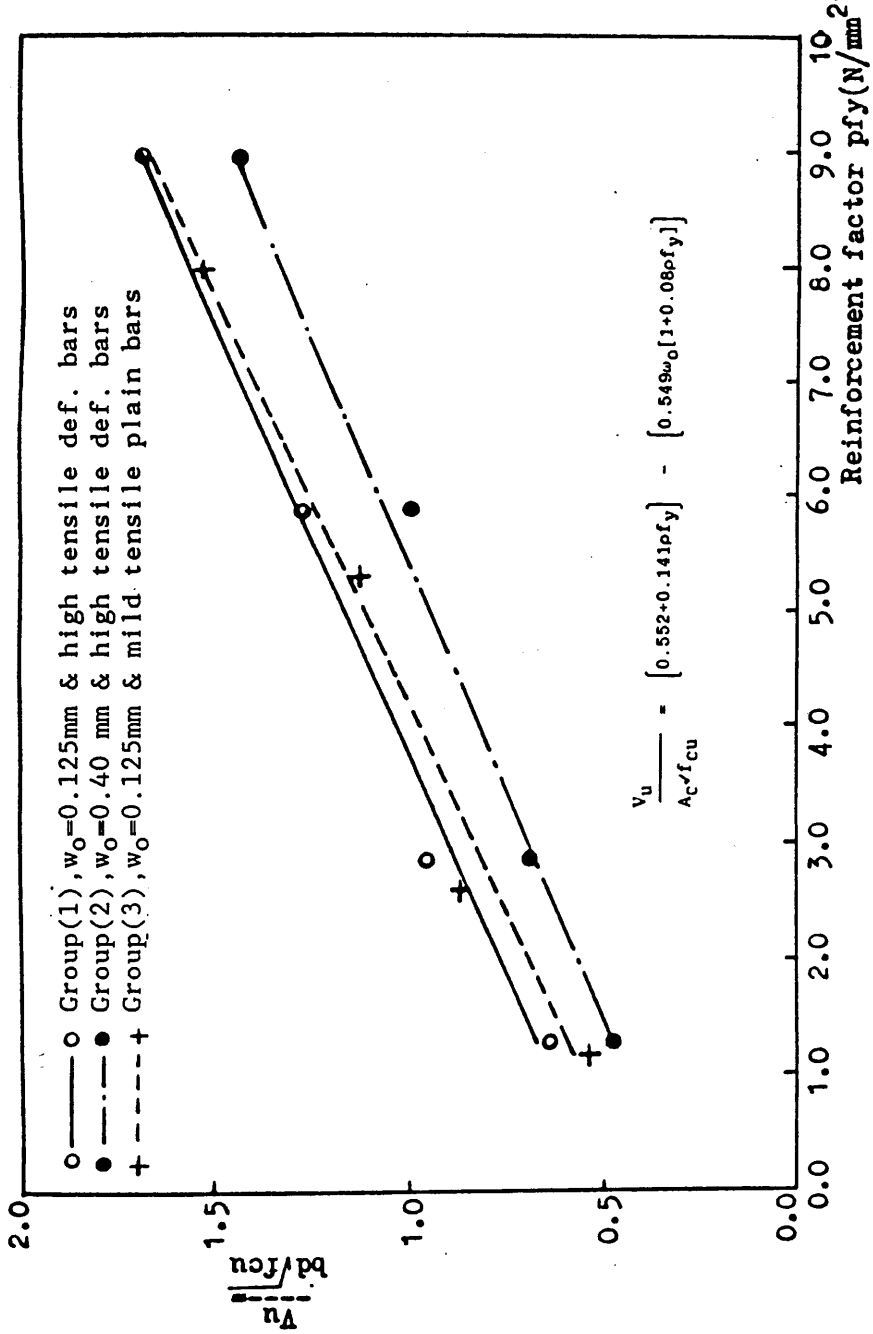

Figure(7.25) Comparison between experimental and calculated ultimate shear strength for combined action specimens under monotonic load, groups (1),(2)&(3)-series 3

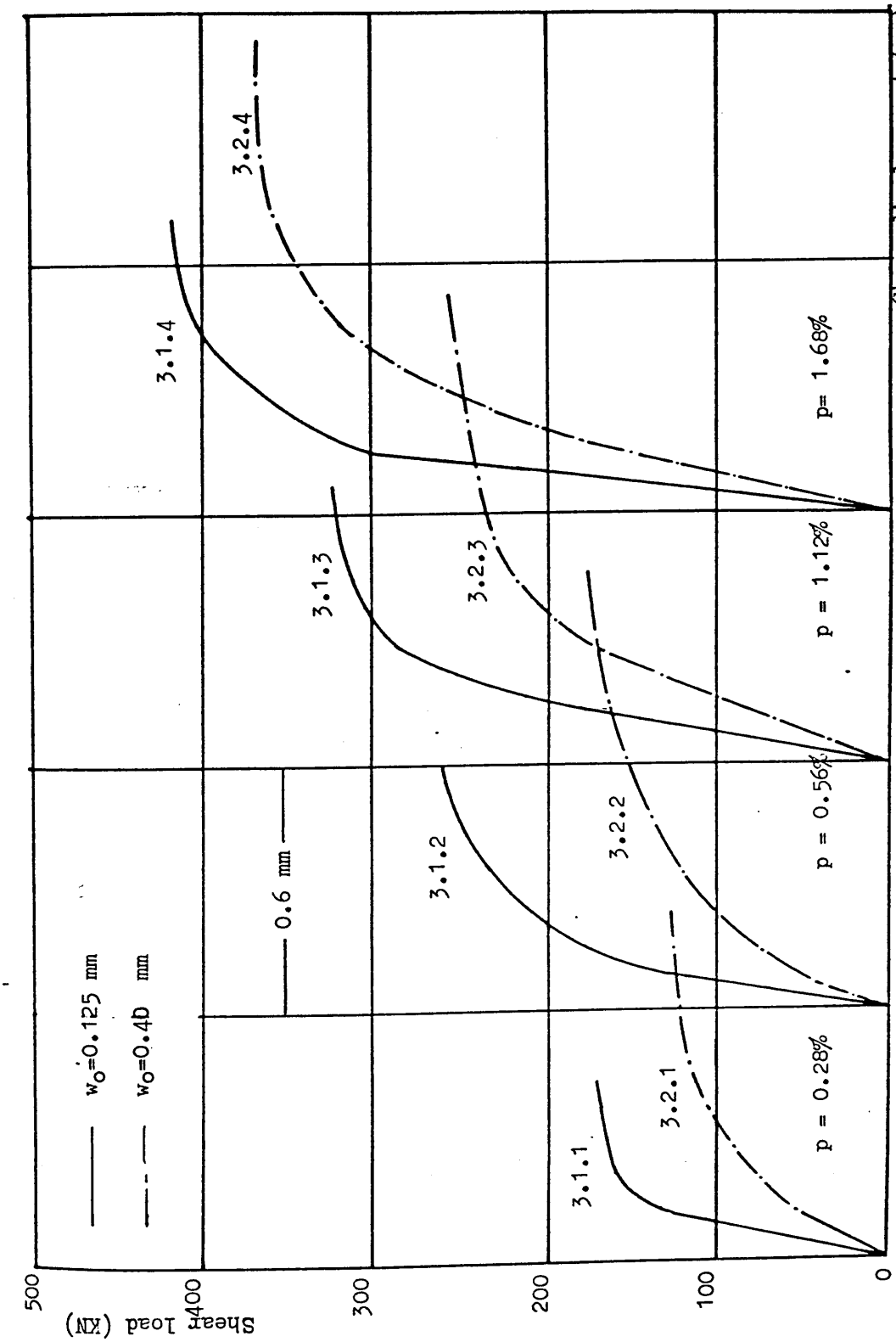

Figure(7.26) Effect of initial crack width on shear load vs. shear displacement for combined action specimens under monotonic load.

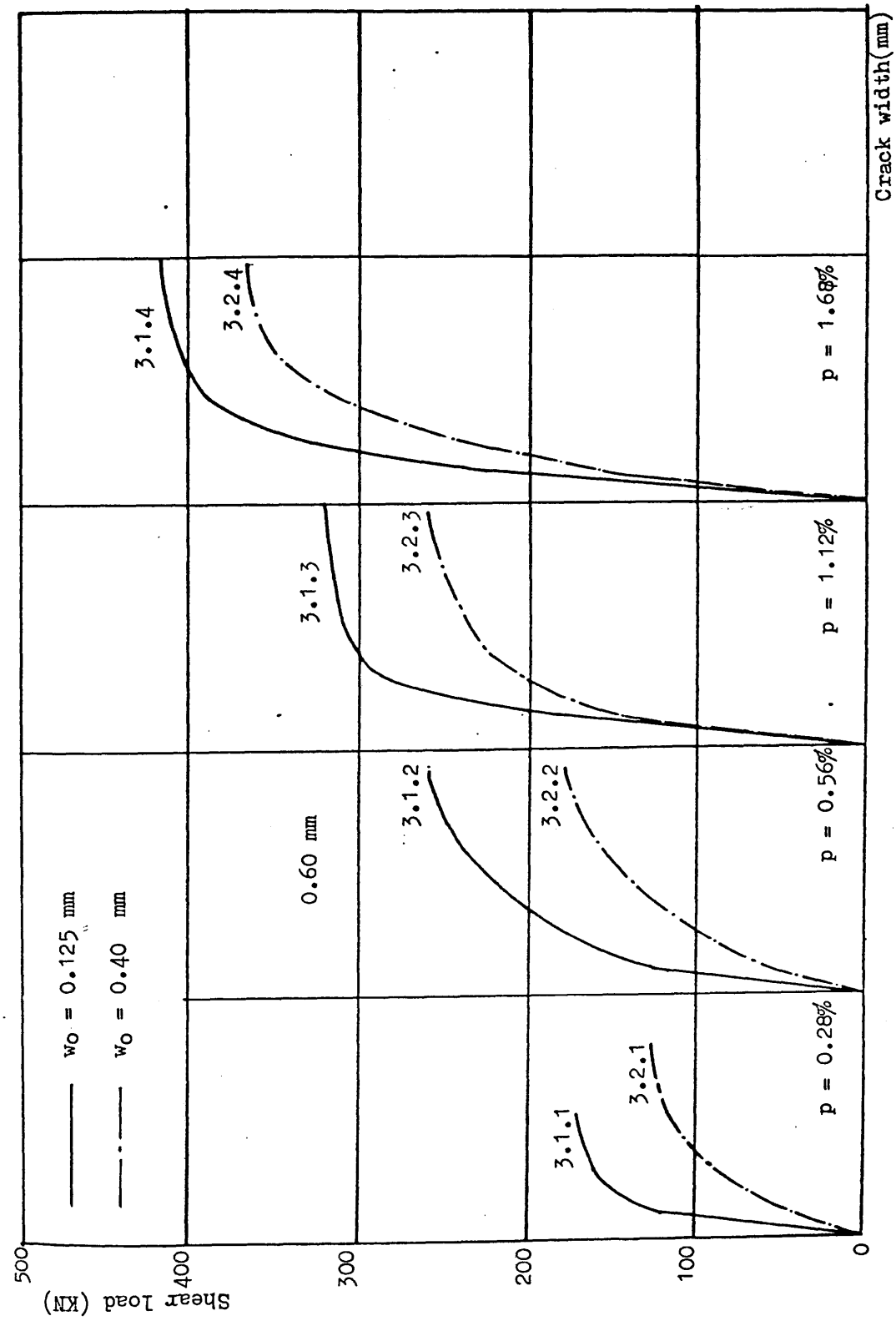

Figure(7.27) Effect of initial crack width on shear load vs. crack width for combined action specimens under monotonic load.

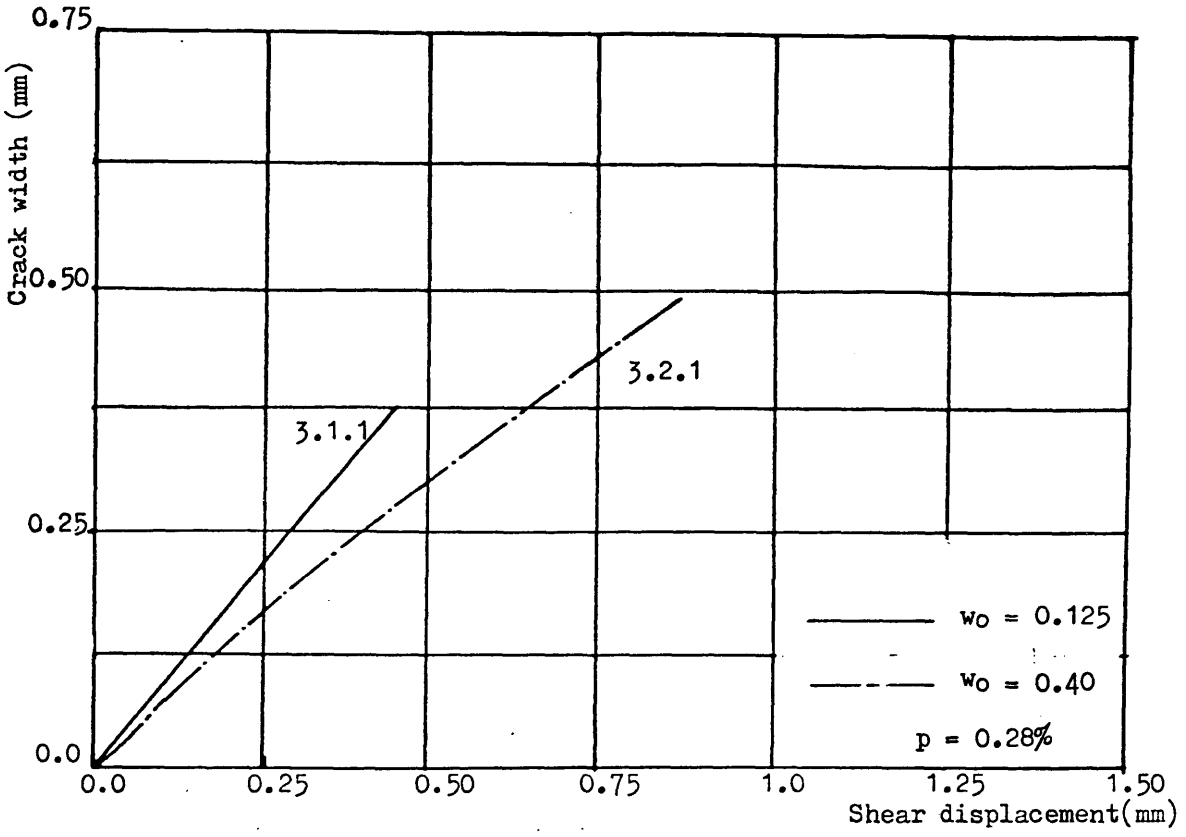

(a)

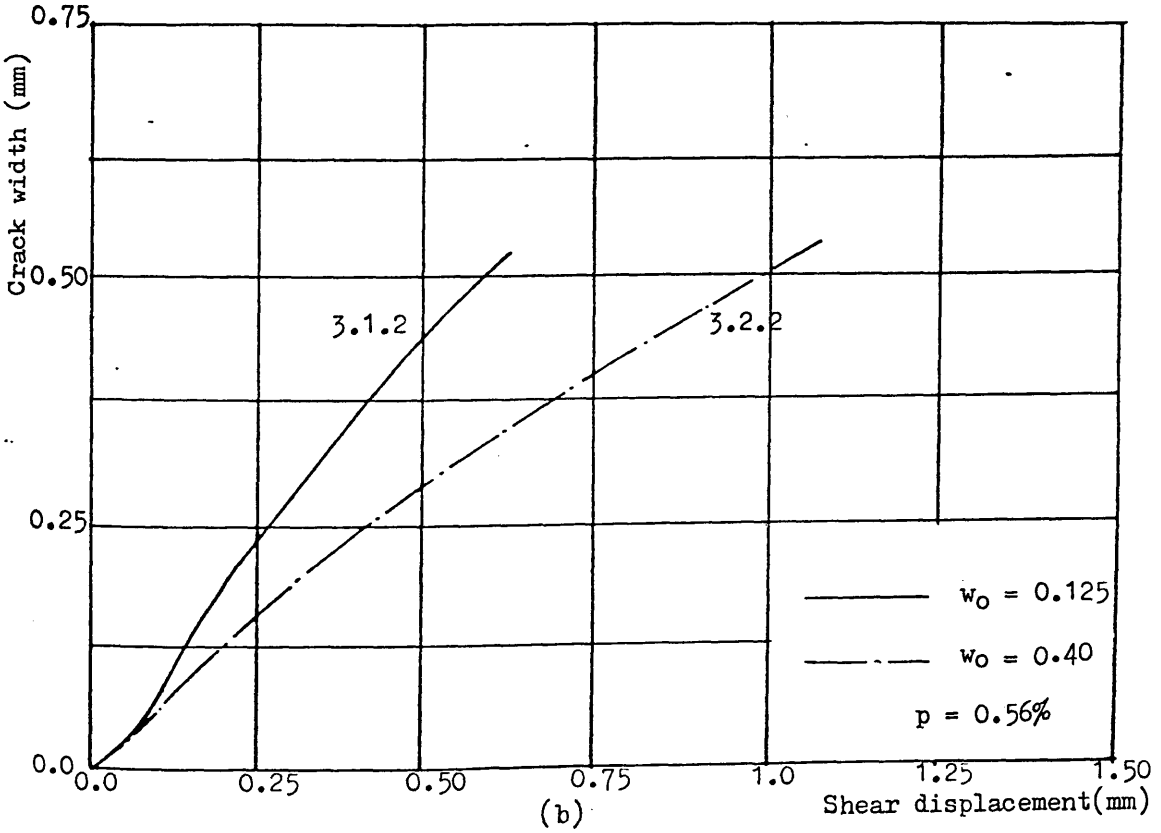

(b)

Figure(7.28) Effect of initial crack width on crack opening path for combined action specimens under monotonic load

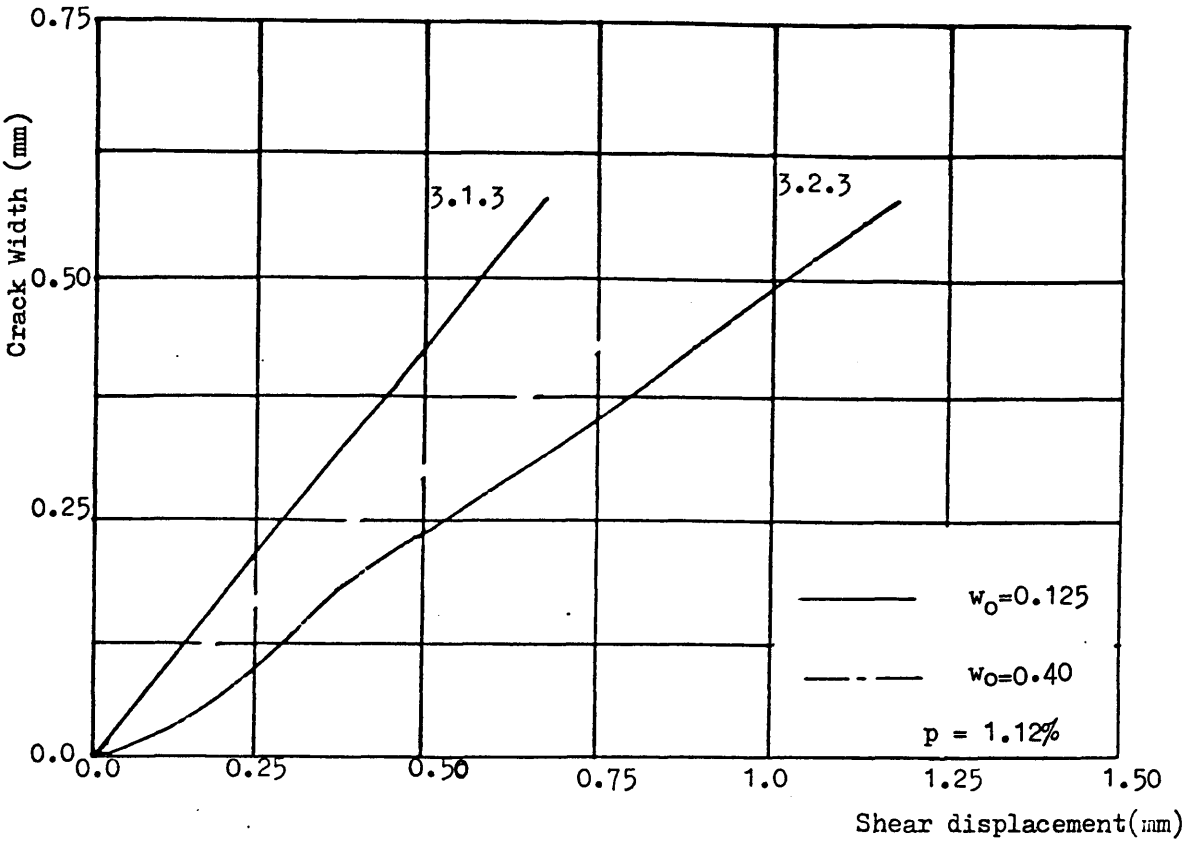

(c)

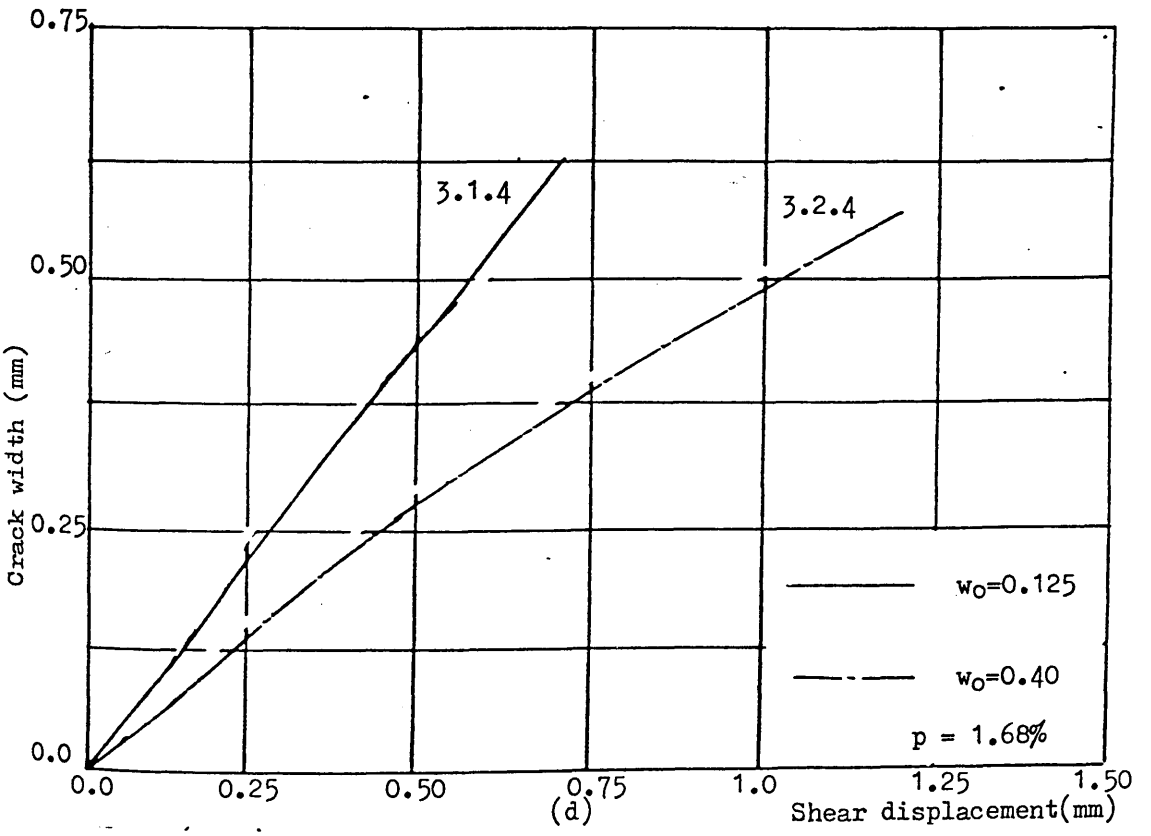

(d)

Figure(7.28 cont.)Effect of initial crack width on crack opening path for combined action specimens under monotonic load

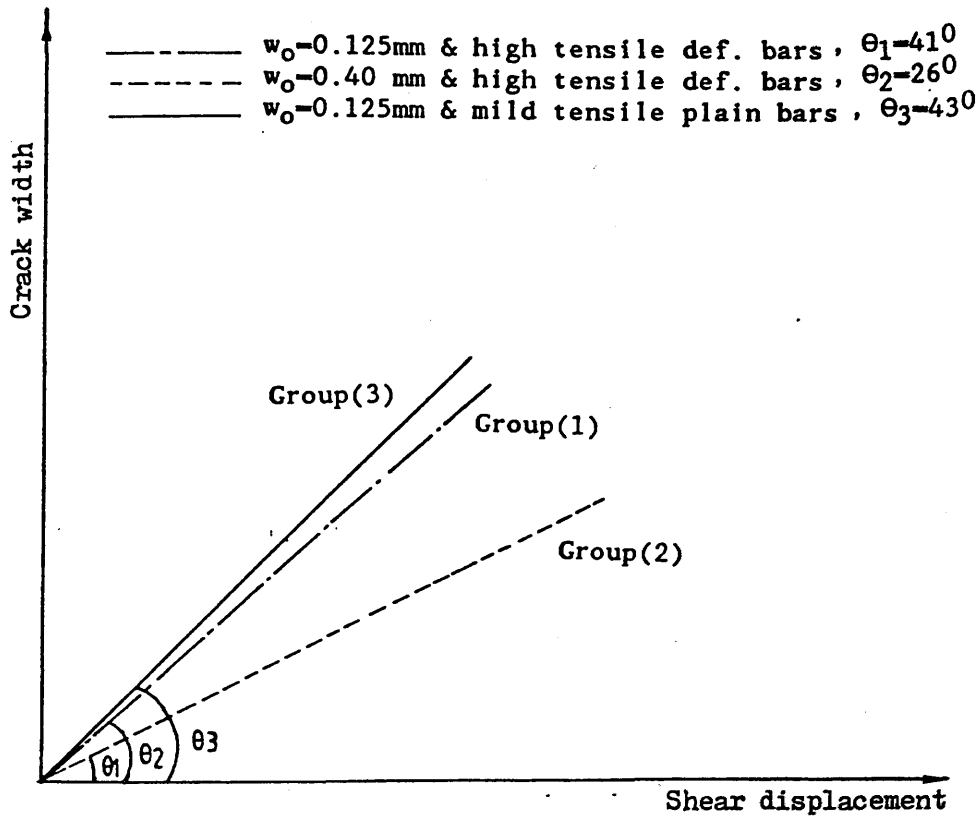

Figure(7.29) The average of inclination of the crack opening path with shear plane for combined action specimems under monotonic load (series 3)

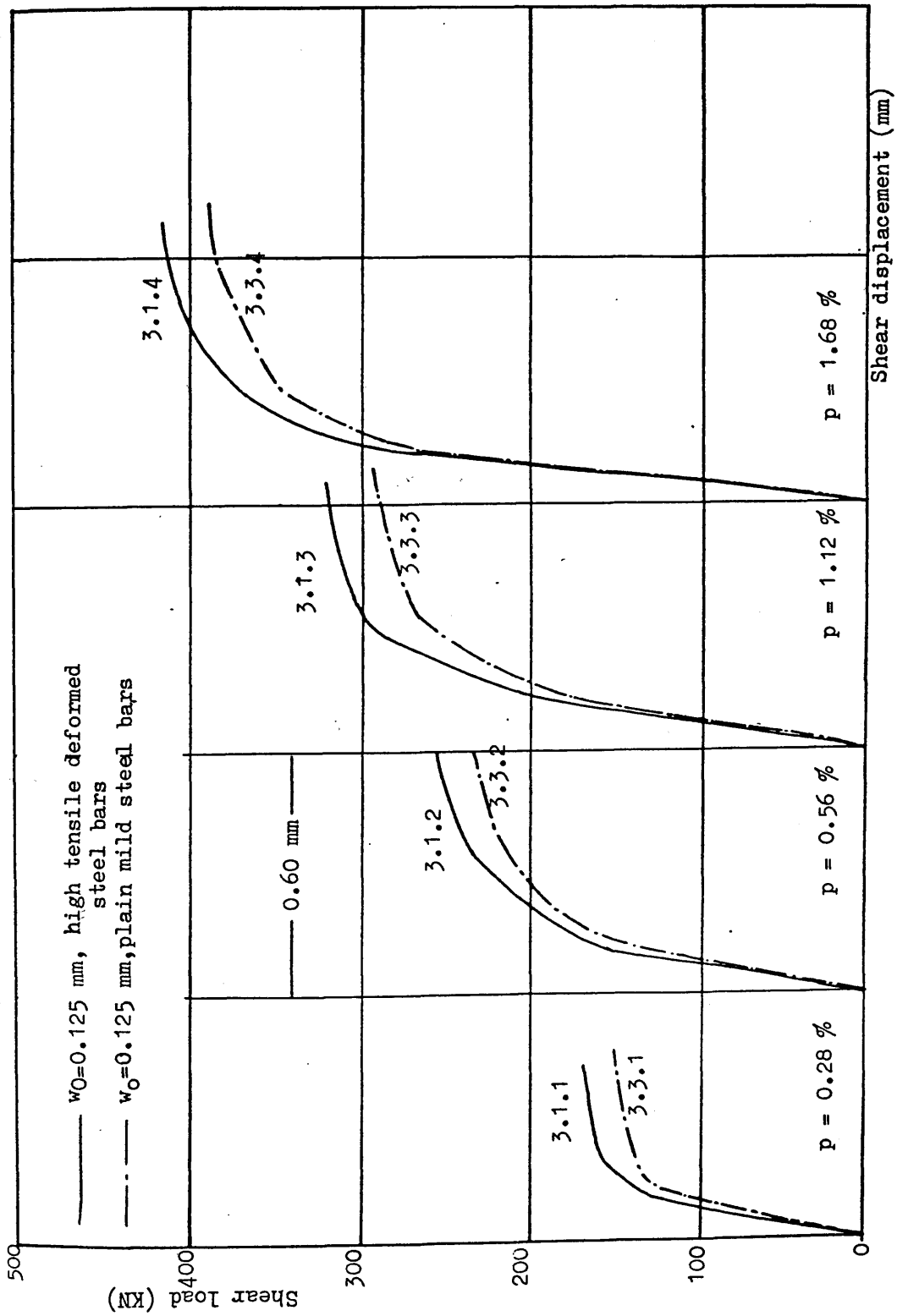

Figure(7.30) Effect of transverse reinforcement type on shear load vs. shear displacement for combined action specimens under monotonic load

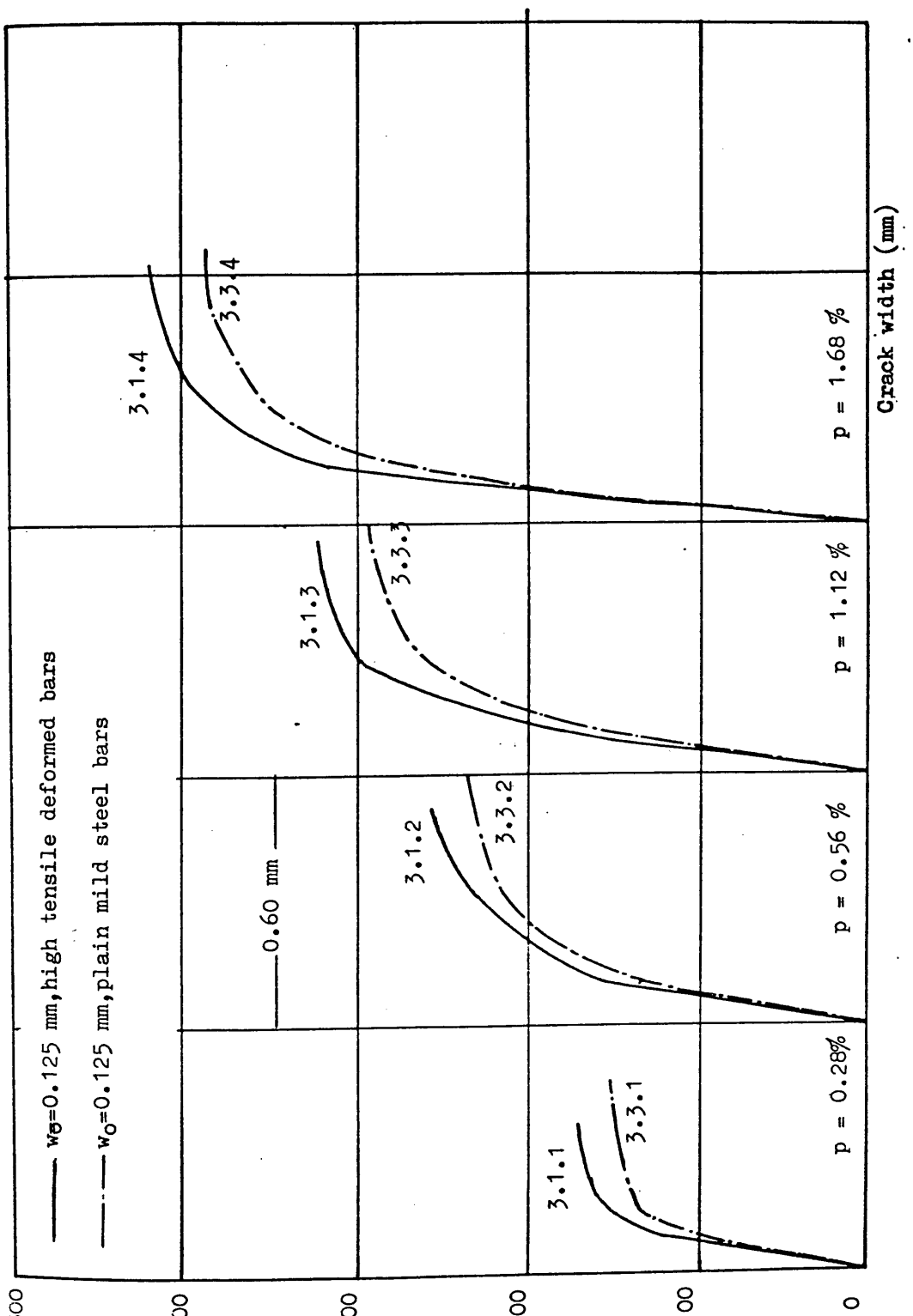

Figure(7.31) Effect of transverse reinforcement type on shear load vs. crack width for combined action specimens under monotonic load

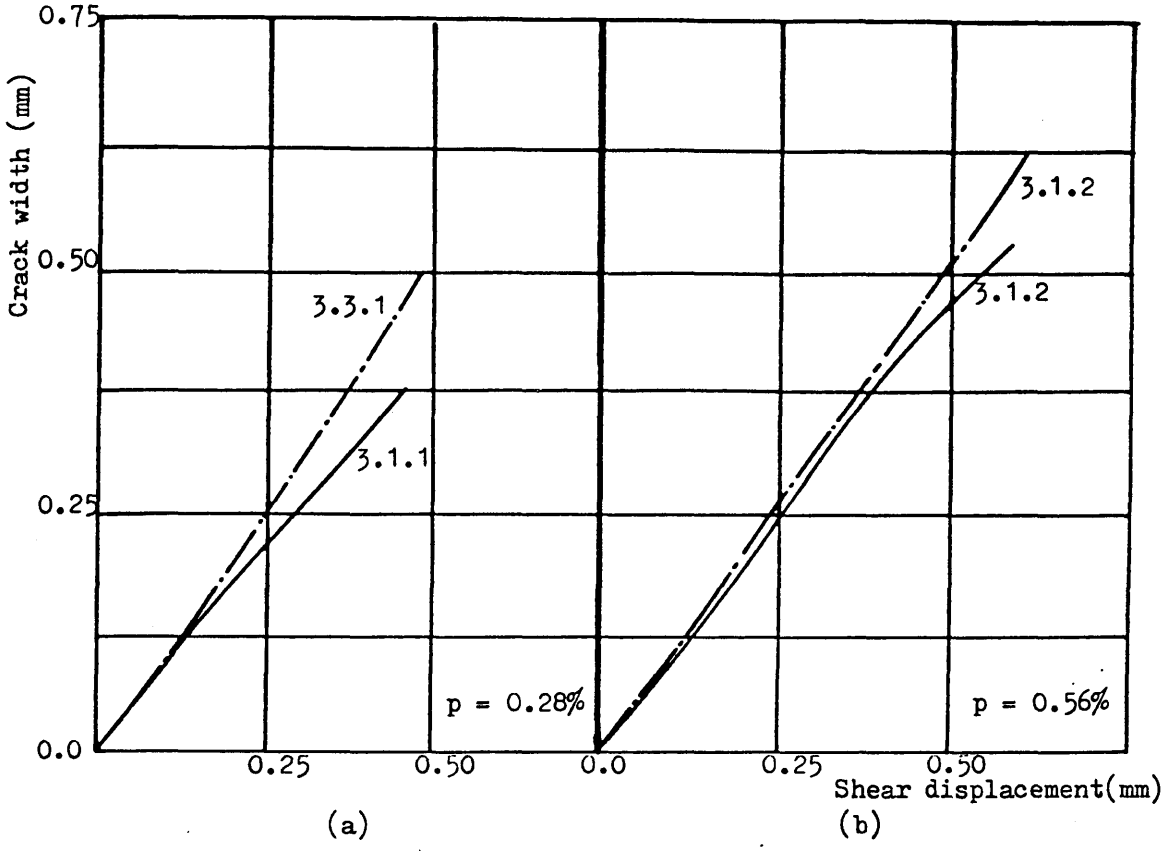

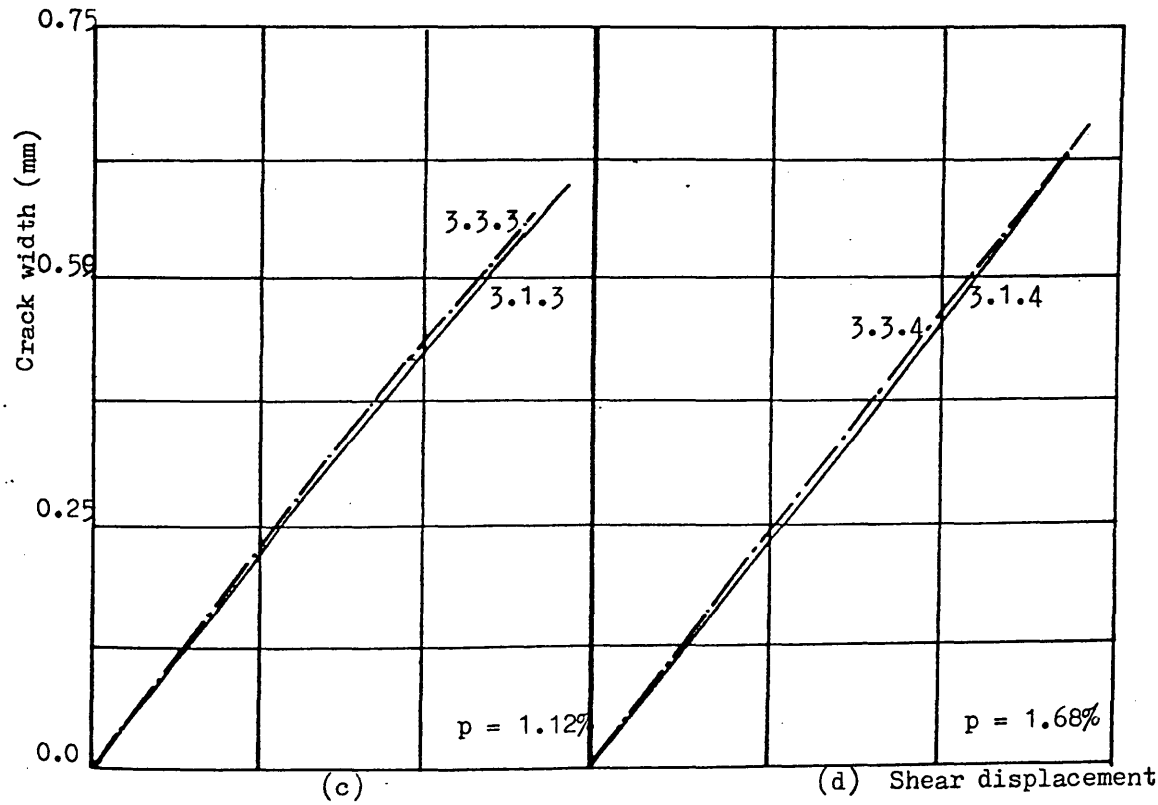

Figure(7.32) Effect of transverse reinforcement type on crack opening path for combined action specimens under monotonic load.

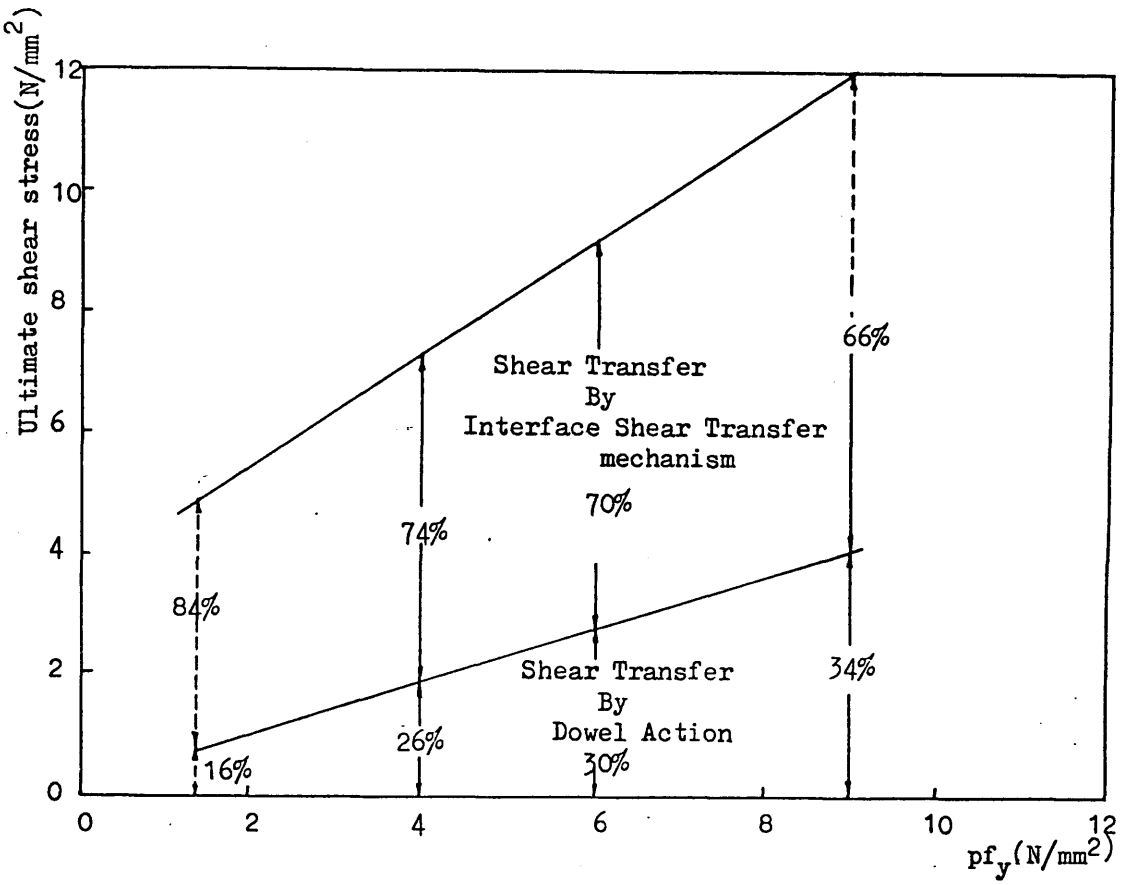

Figure(7.33a) Contribution of the interface shear transfer mechanism and the dowel action for specimens with w_o=0.125mm and transverse reinforcement of high tensile deformed bars under monotonic load.

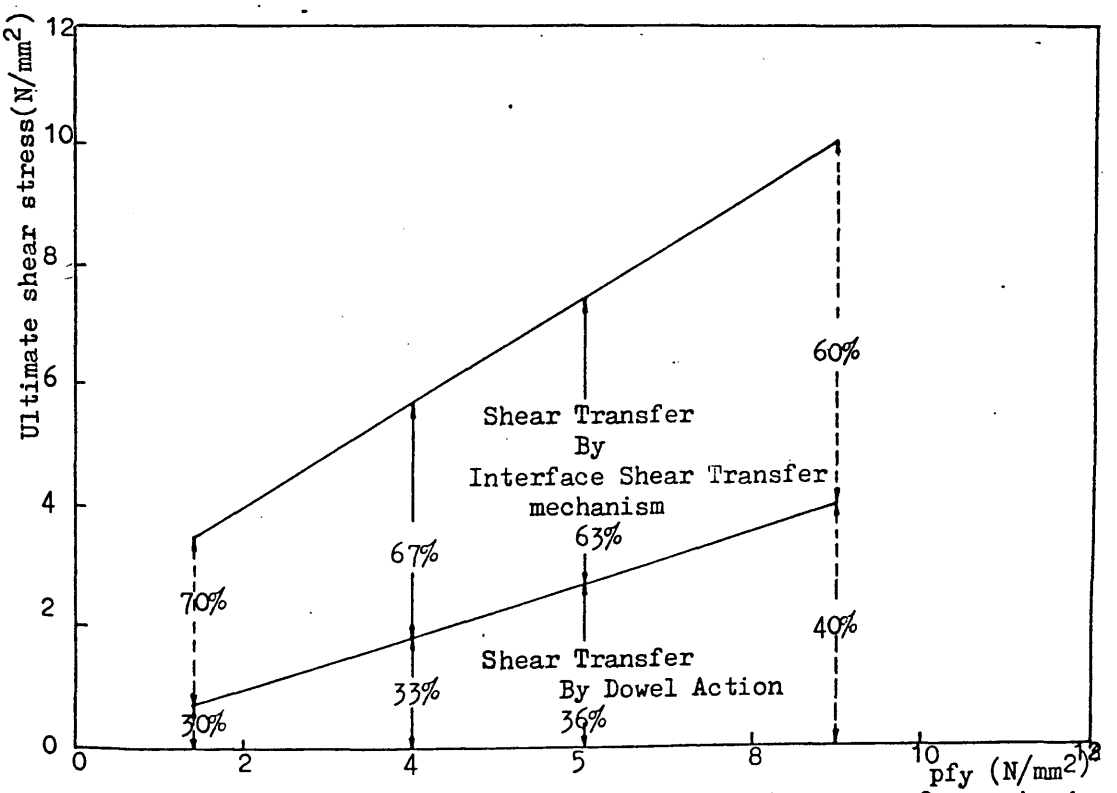

Figure(7.33b) Contribution of the interface shear transfer mechanism and the dowel action for specimens with w_o=0.40mm and transverse reinforcement of high tensile deformed bars under monotonic load.

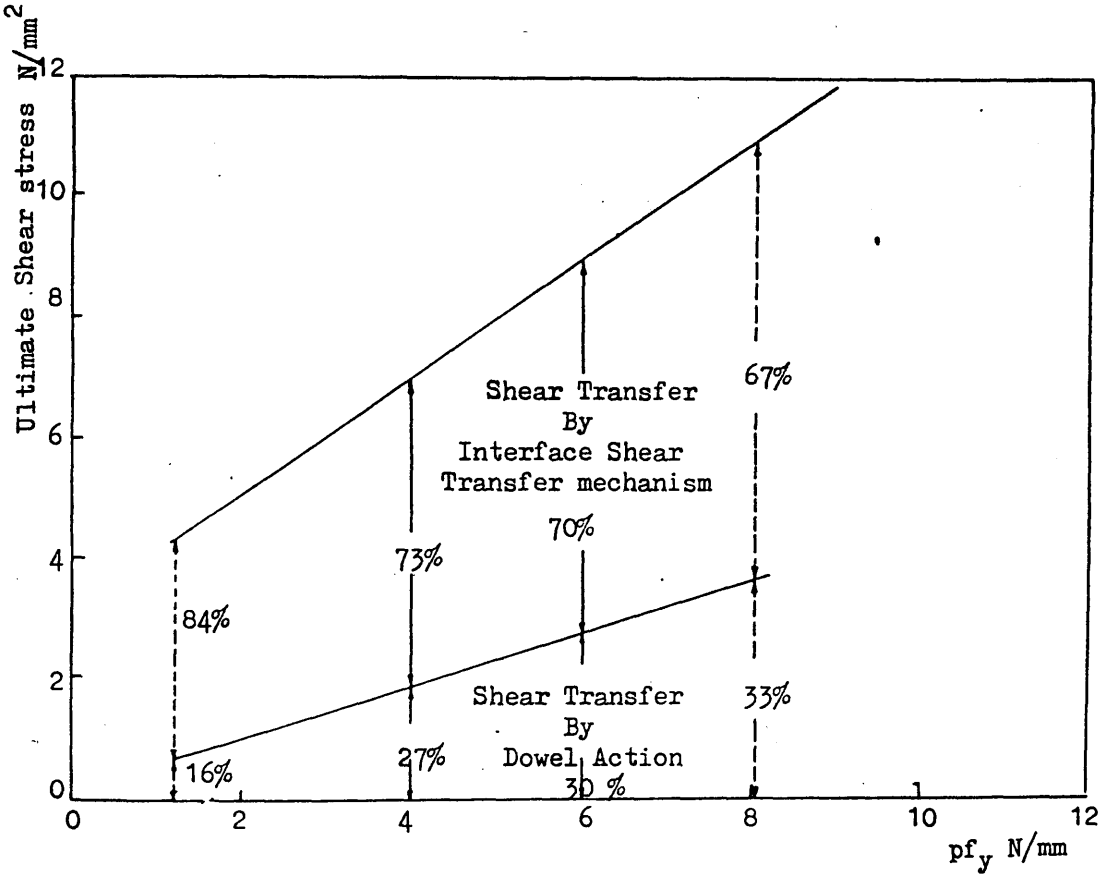

Figure(7.33c) Contribution of the interface shear transfer mechanism and the dowel action for specimens with w_o=0.125mm and transverse reinforcement of mild tensile plain bars under monotonic load.

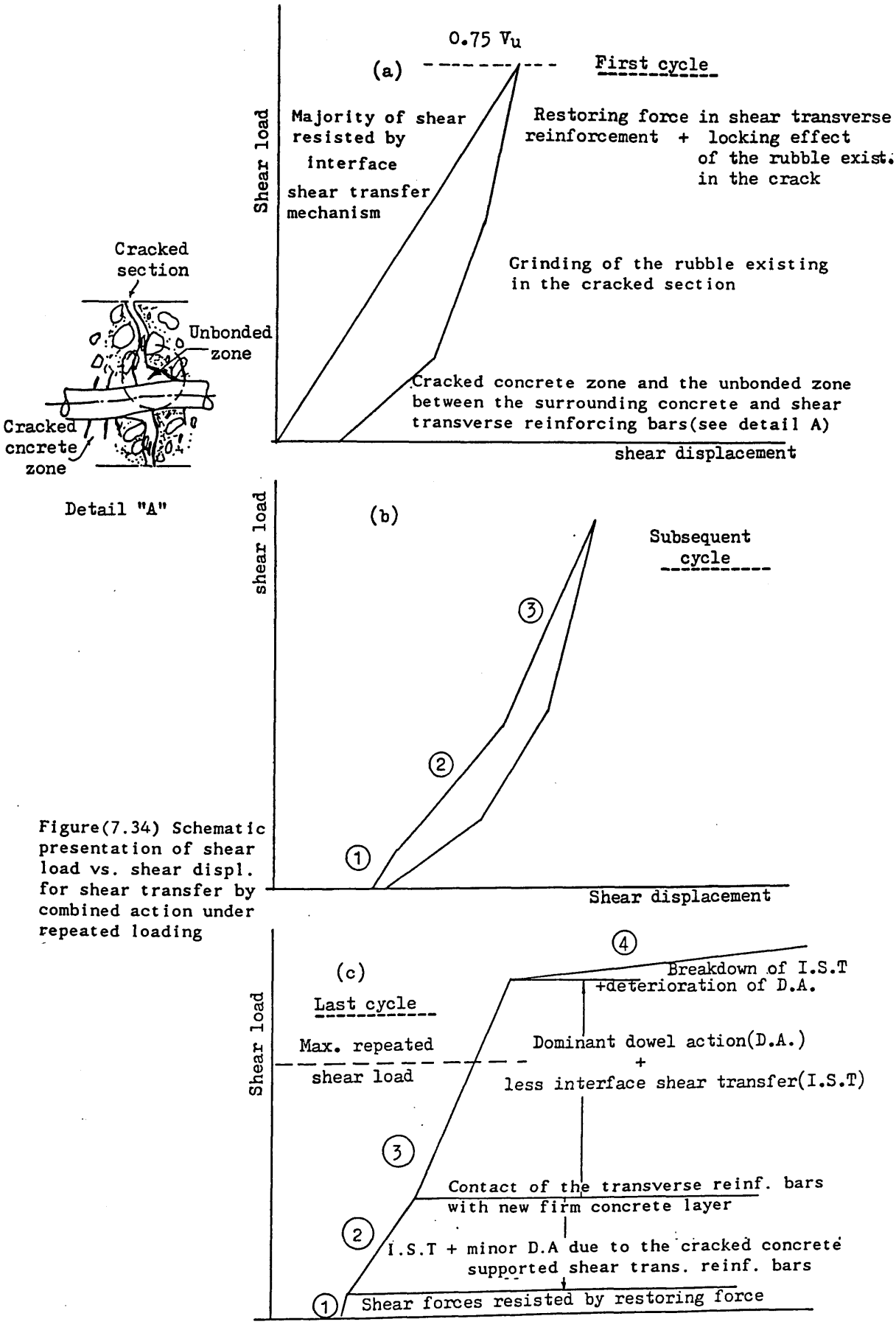

Figure(7.34) Schematic presentation of shear load vs. shear displ. for shear transfer by combined action under repeated loading

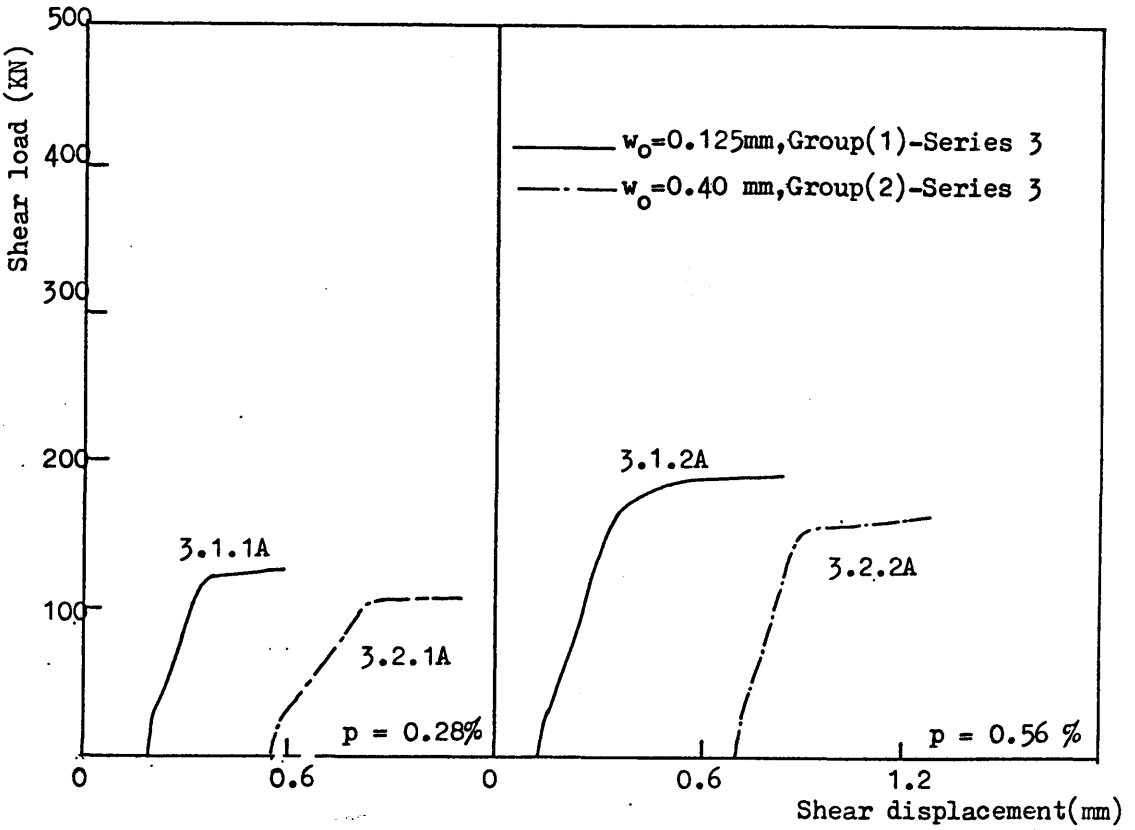

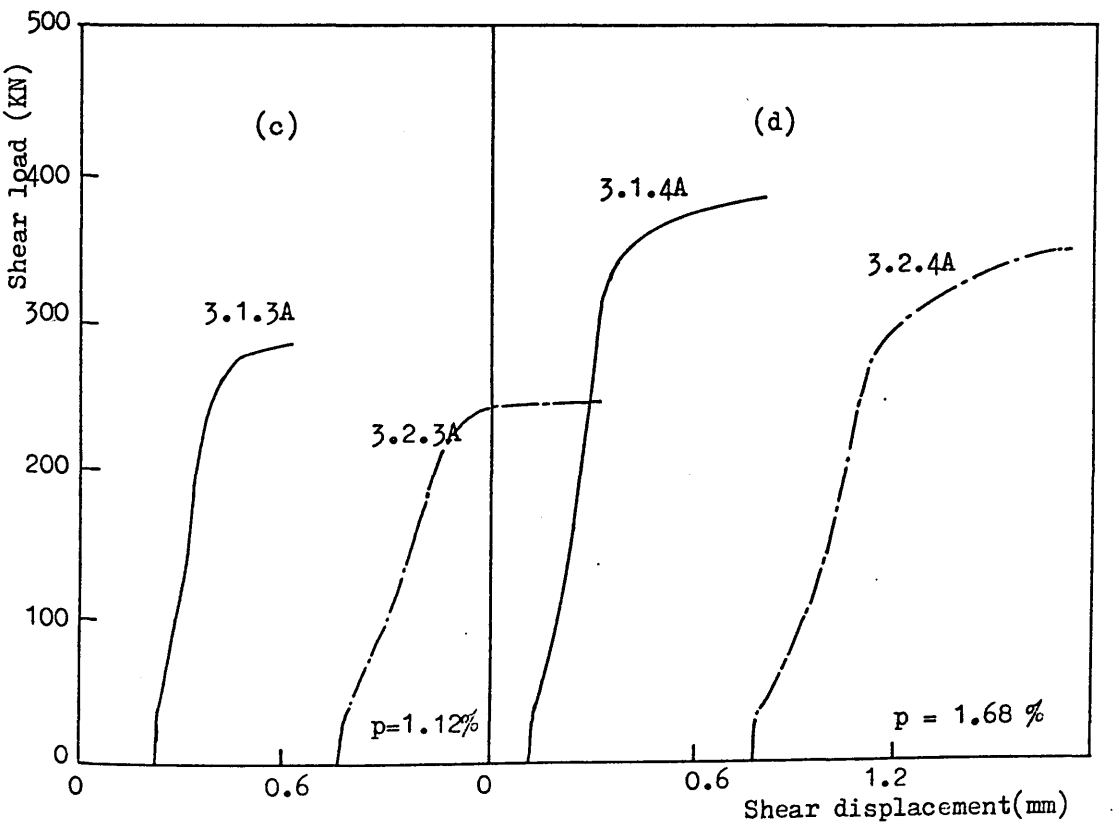

Figure(7.35) Effect of initial crack width on shear load vs. shear displacement for combined action specimens under repeated load(last cycle)

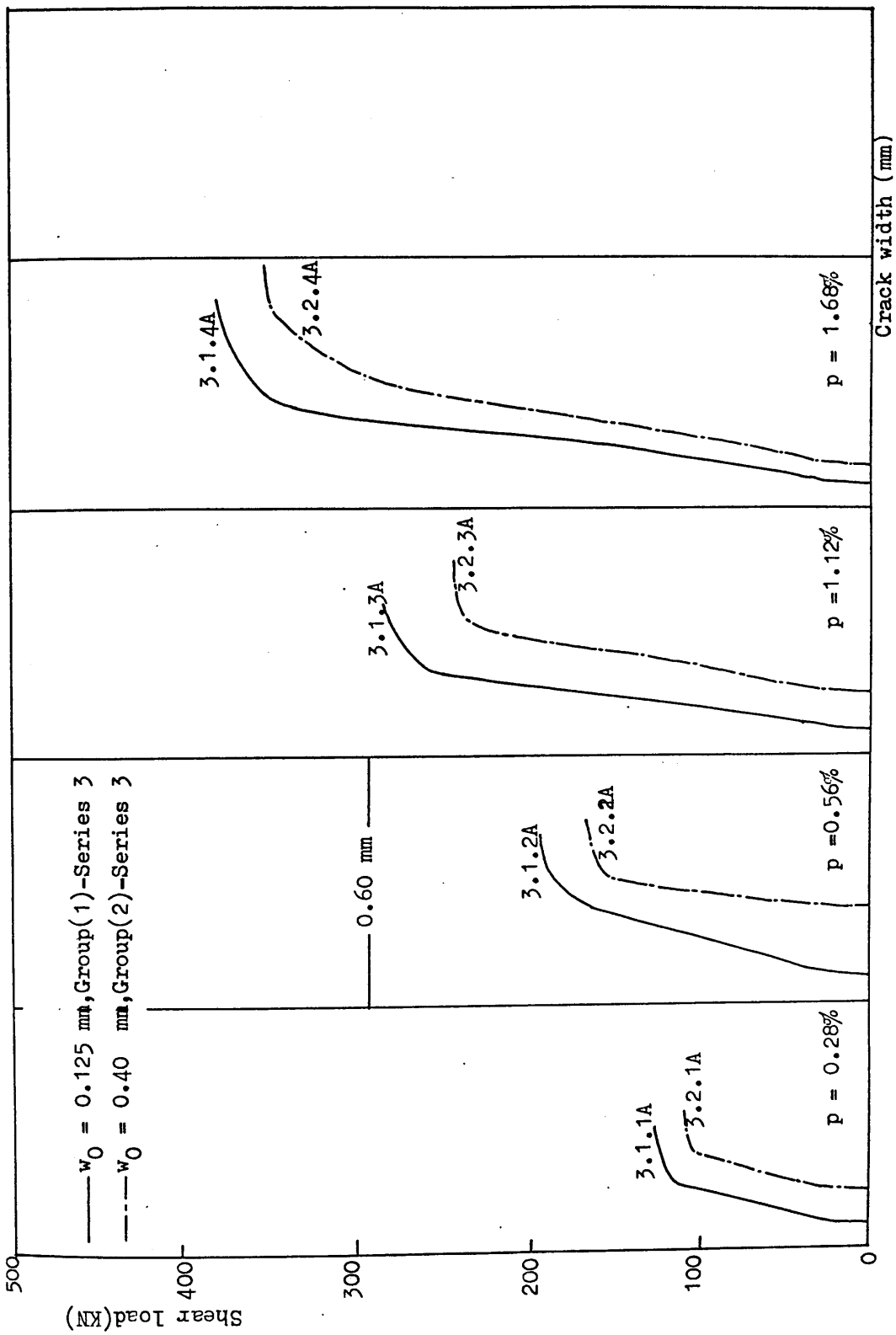

Figure(7.36) Effect of initial crack width on shear load vs. crack width for combined action specimens under repeated load (last cycle)

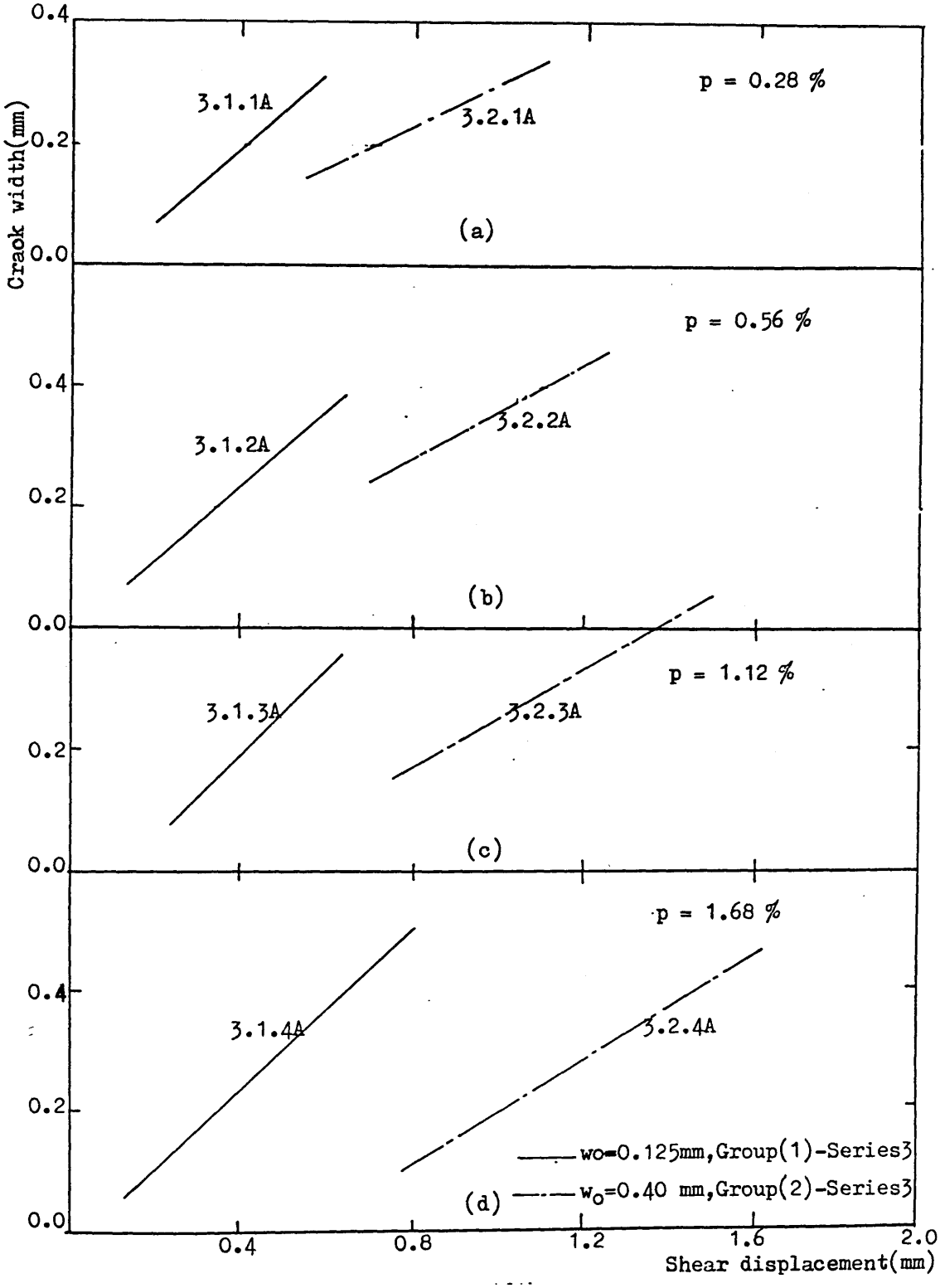

Figure(7.37) Effect of initial crack width on crack width vs. shear displacement for combined action specimens under repeated load (last cycle)

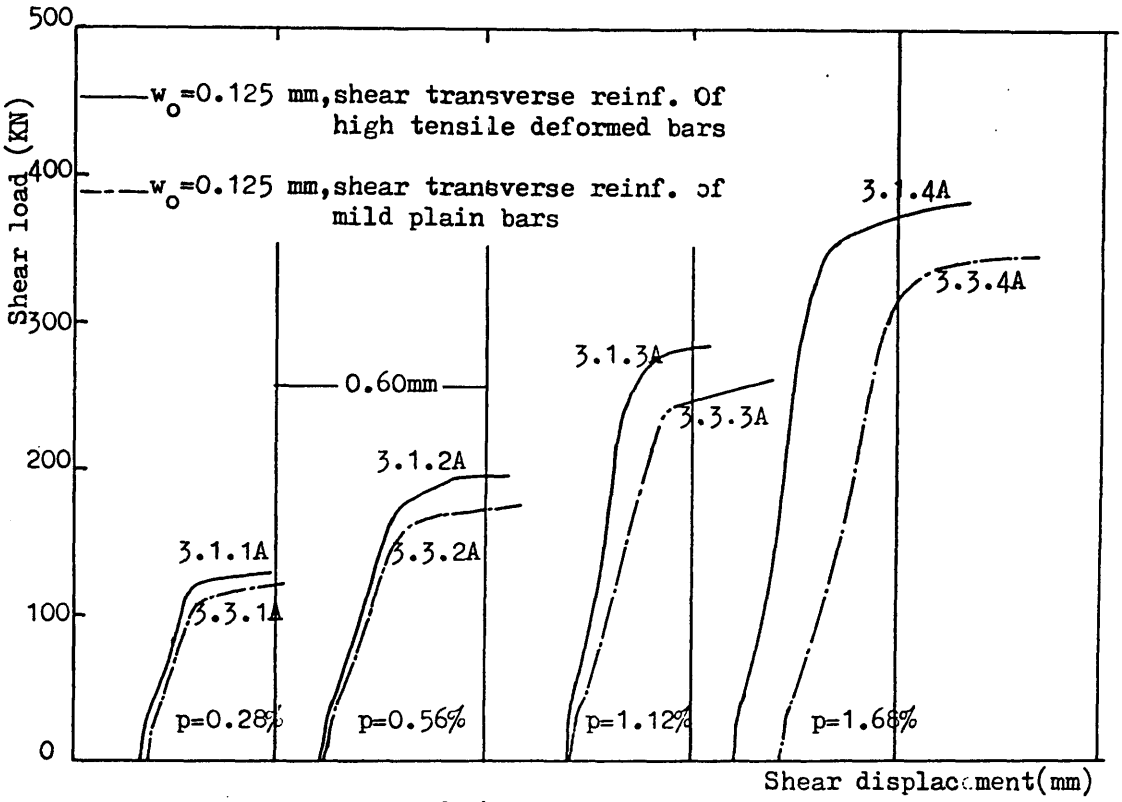

Figure(7.38) Effect of transverse reinforcement type on shear load vs. shear displaecment for combined action specimens under repeated load (last cycle)

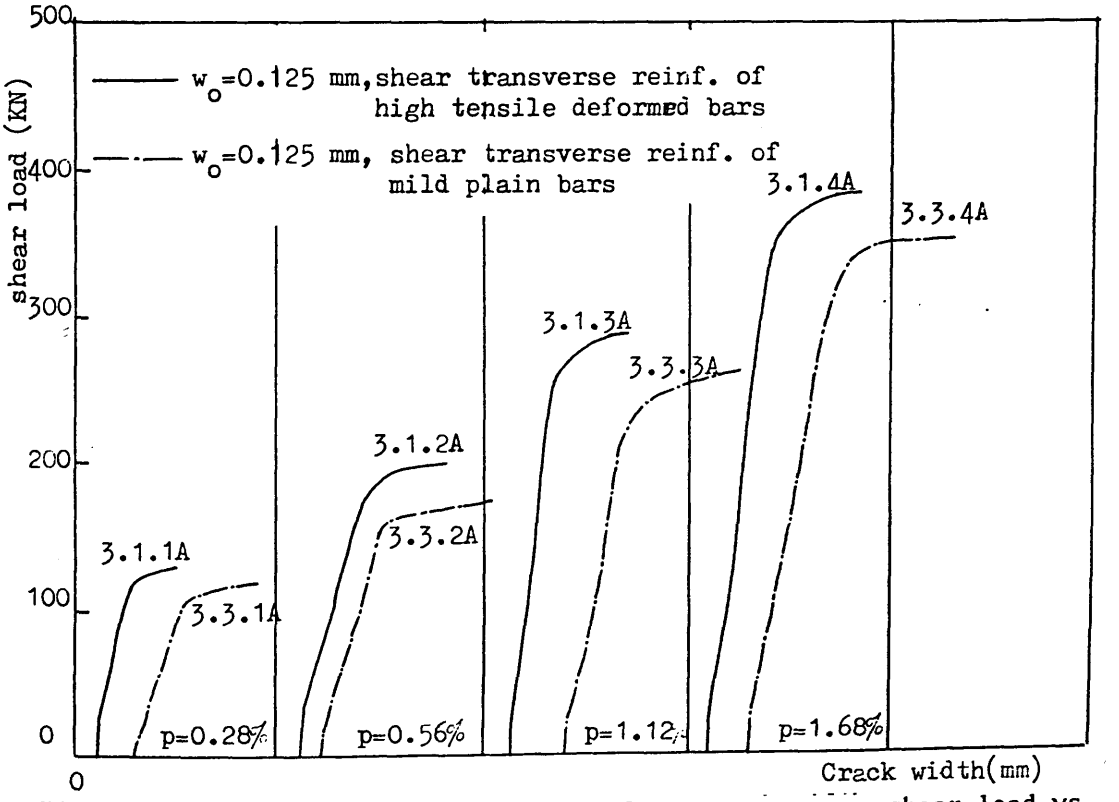

Figure(7.39) Effect of transverse reinforcement type on shear load vs. crack width for combined action specimens under repeated load (last cycle)

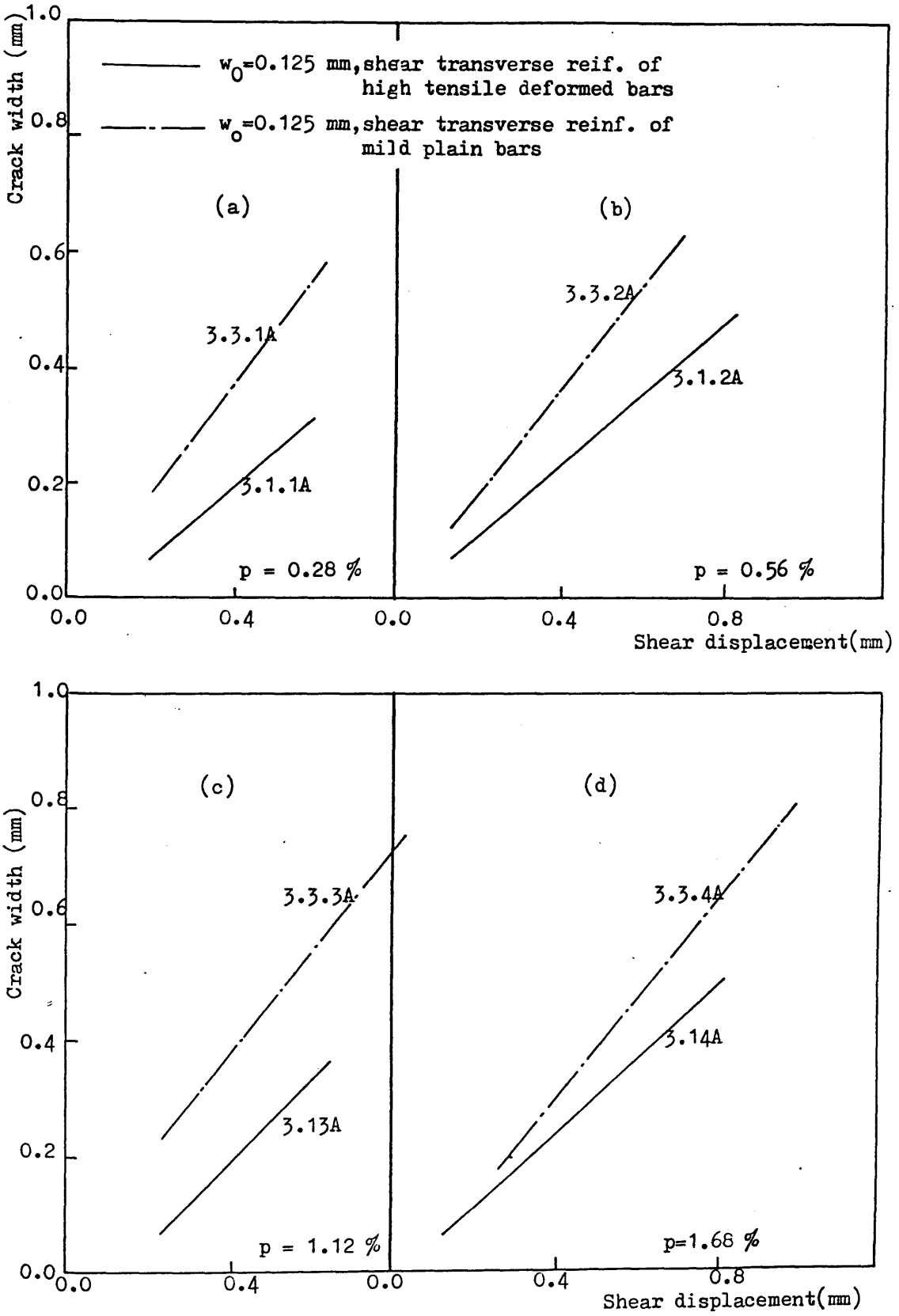

Figure(7.40) Effect of transverse reinforcement type on crack width vs. shear displacement for combined action specimens under repeated load (last cycle)

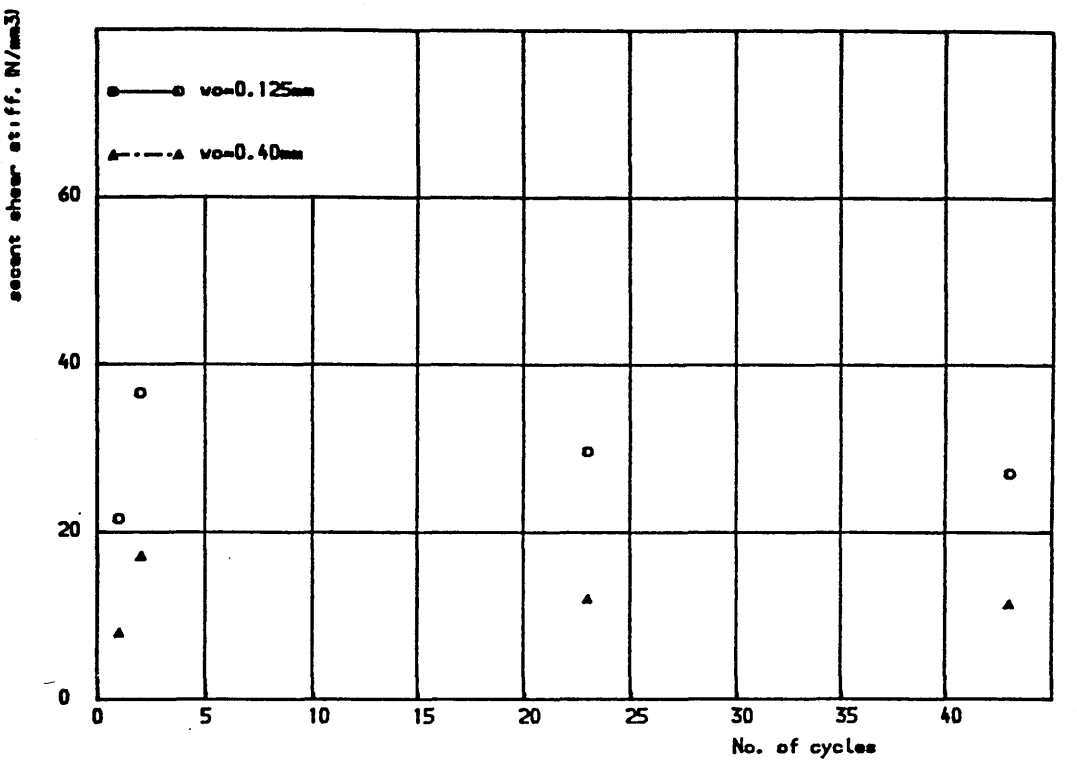

(a) Shear transverse reinforcement ratio 0.28 %

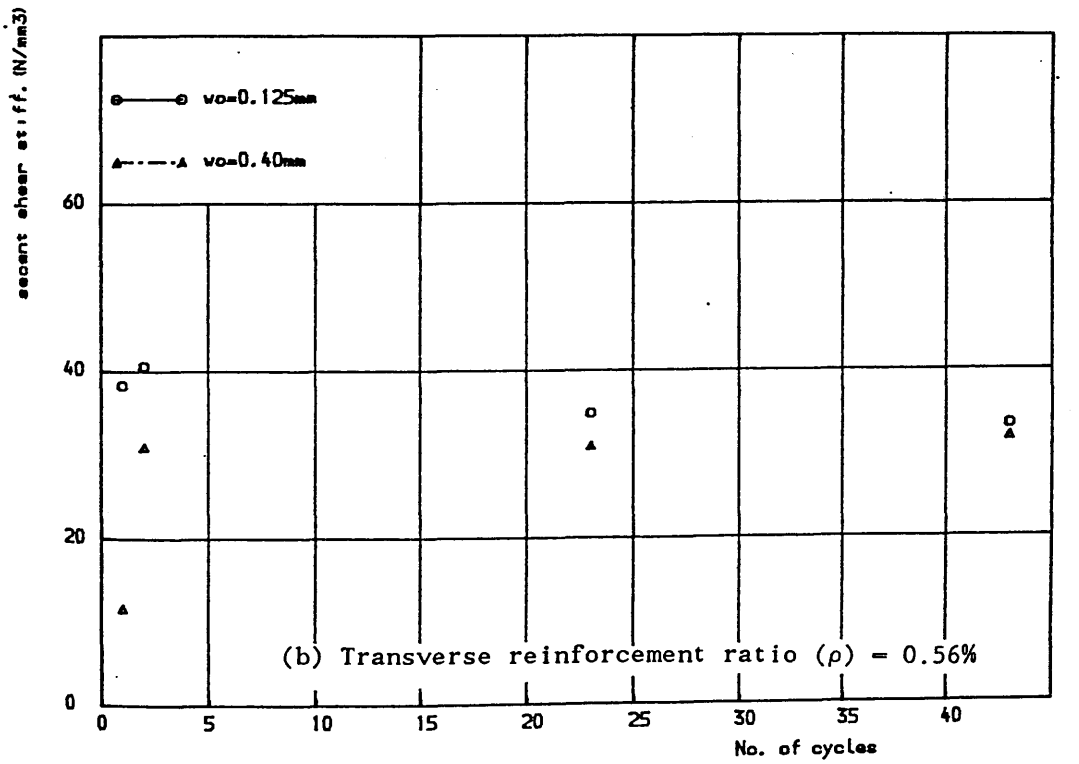

(b) Transverse reinforcement ratio (ρ) = 0.56%

Figure(7.41) Effect of initial crack width on secant shear stiffness vs. number of load cycles for combined action specimens

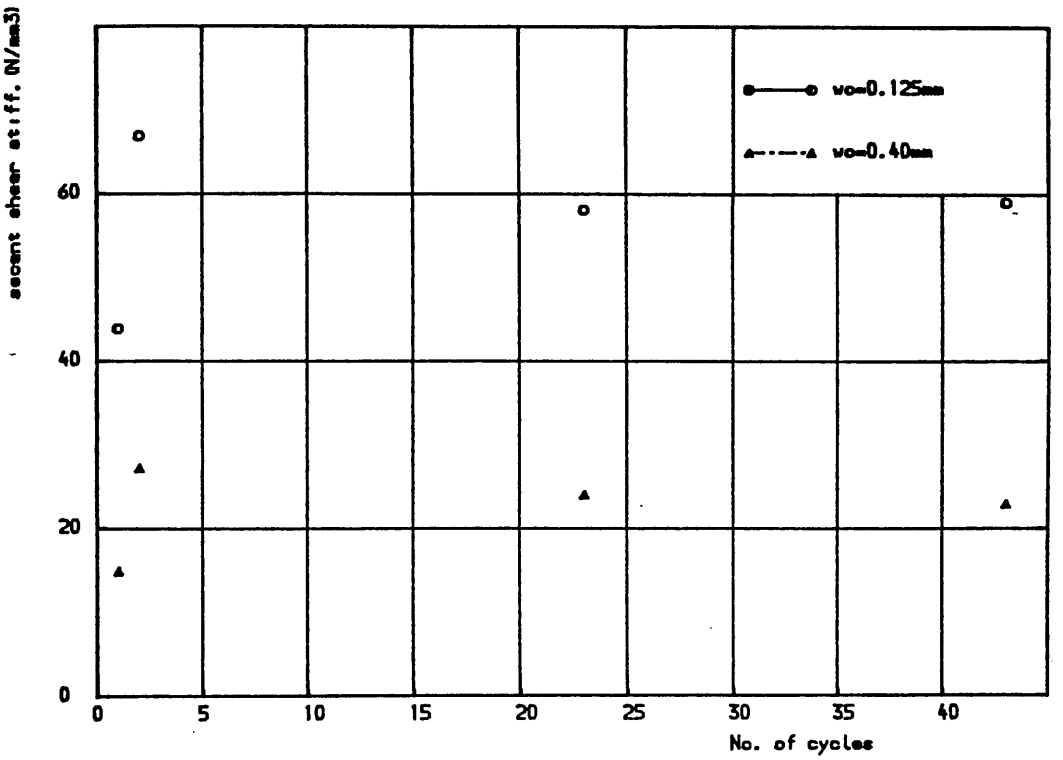

(c) Shear transverse reinforcement ratio 1.12 %

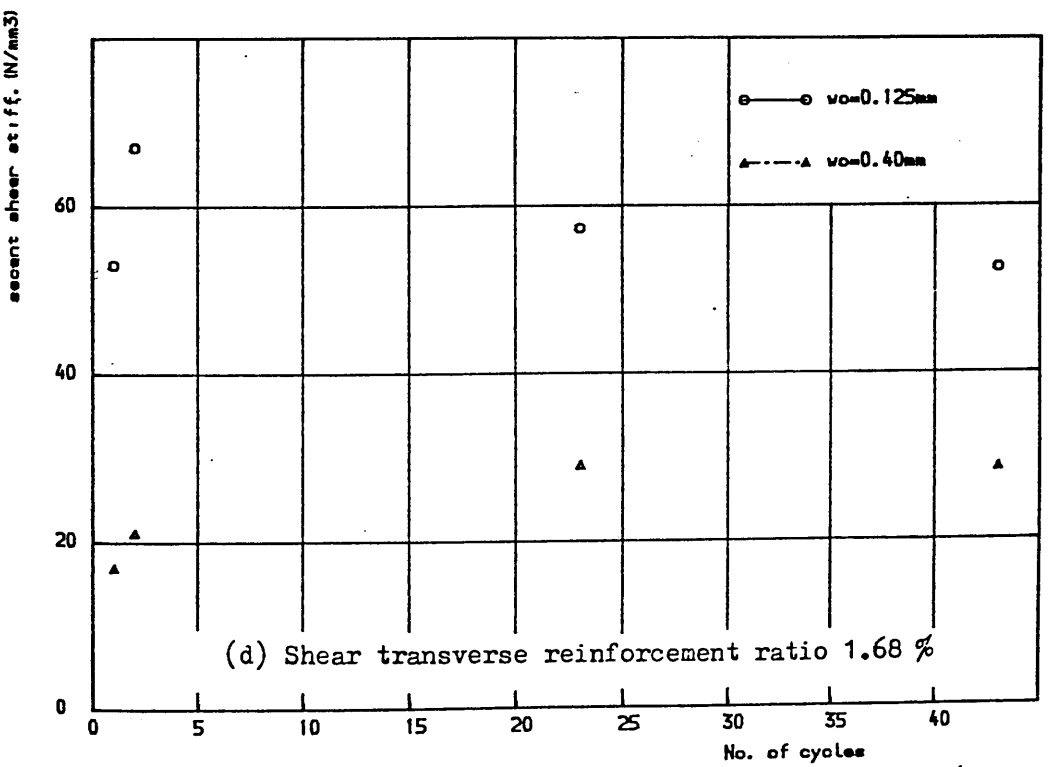

(d) Shear transverse reinforcement ratio 1.68 %

Figure(7.41)Cont. Effect of initial crack width on secant shear stiffness vs. number of load cycles for combined action specimens

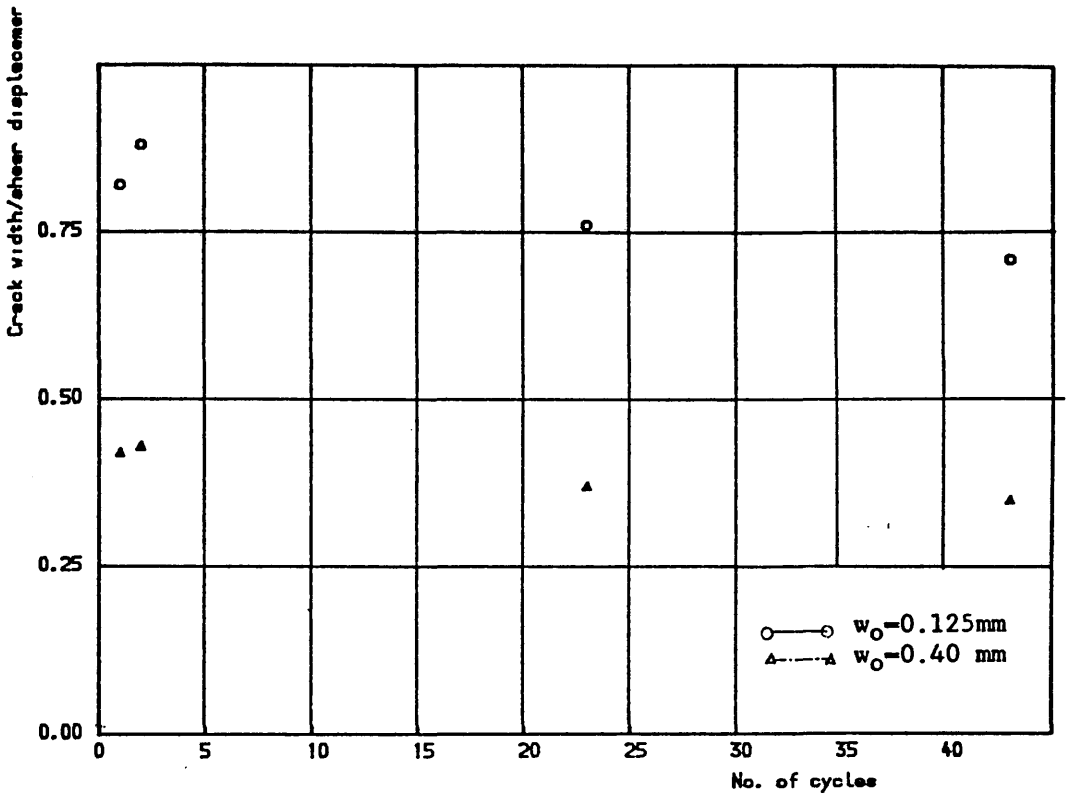

(a) Shear transverse reinforcement ratio 0.28 %

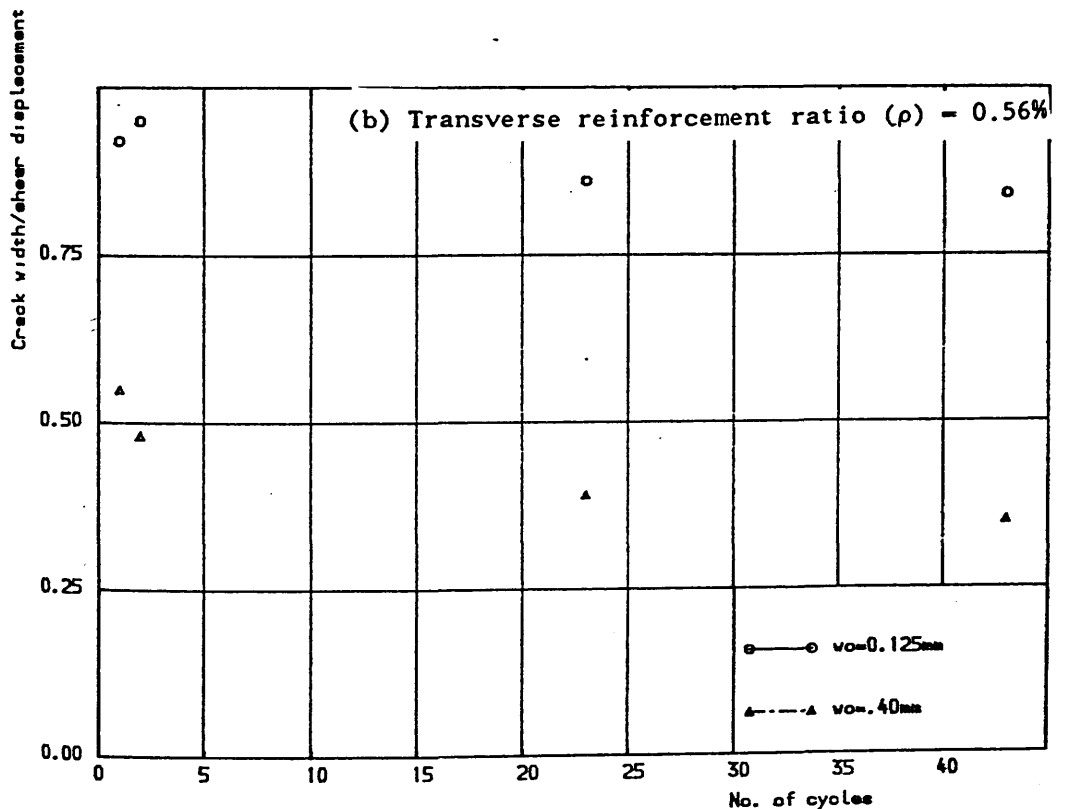

Figure(7.42) Effect of initial crack width on crack width / shear displacement ratio vs. number of load cycles for combined action specimens.

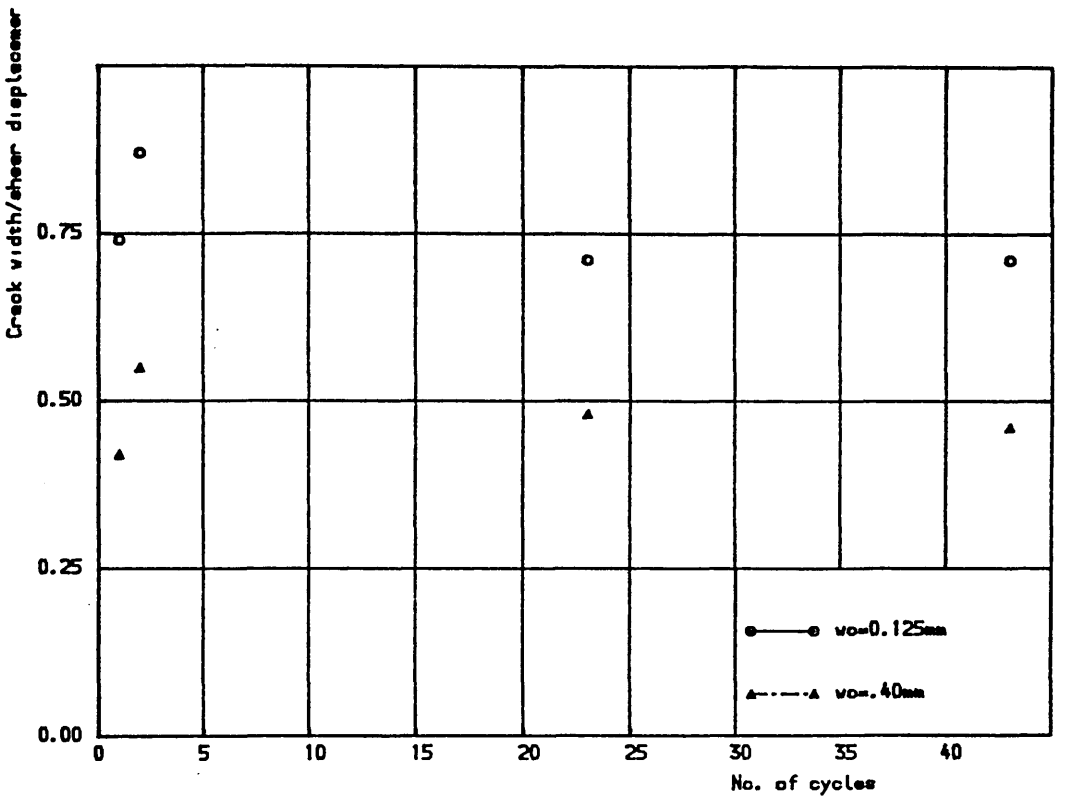

(c) Shear transverse reinforcement ratio 0.1.12 %

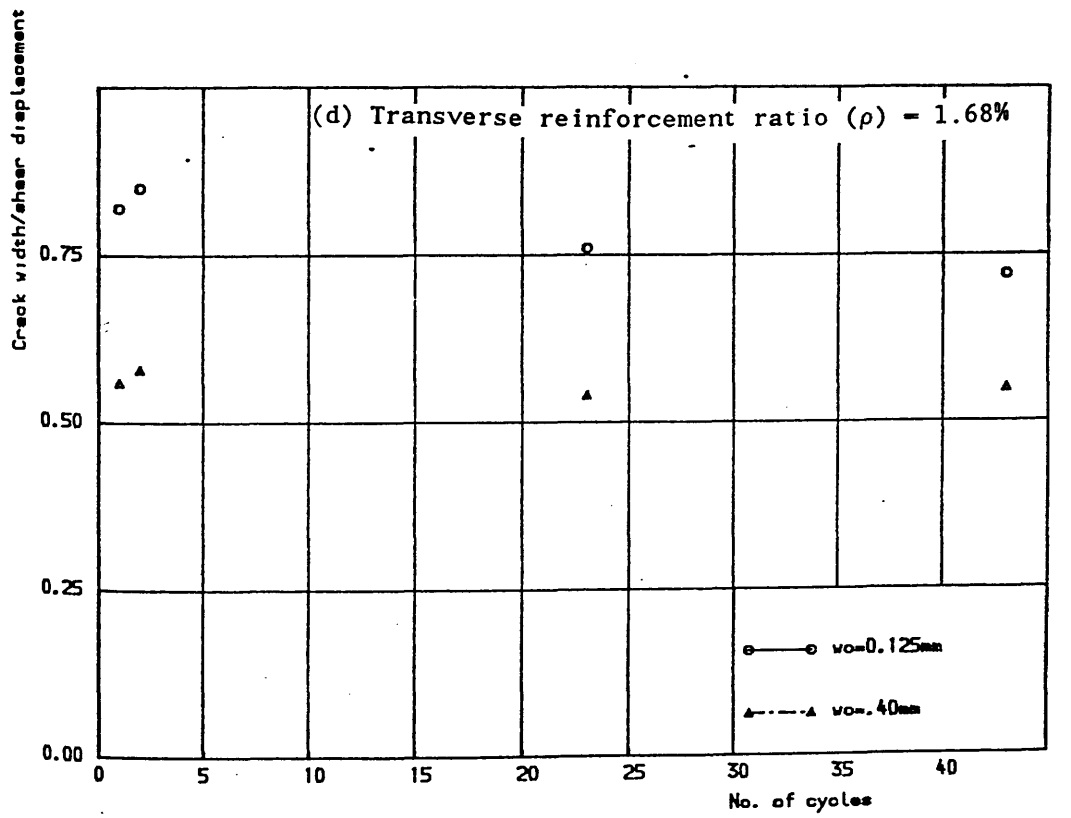

Figure(7.42) Cont. Effect of initial crack width on crack width /shear displacement vs. number of load cycles for comined action specimens

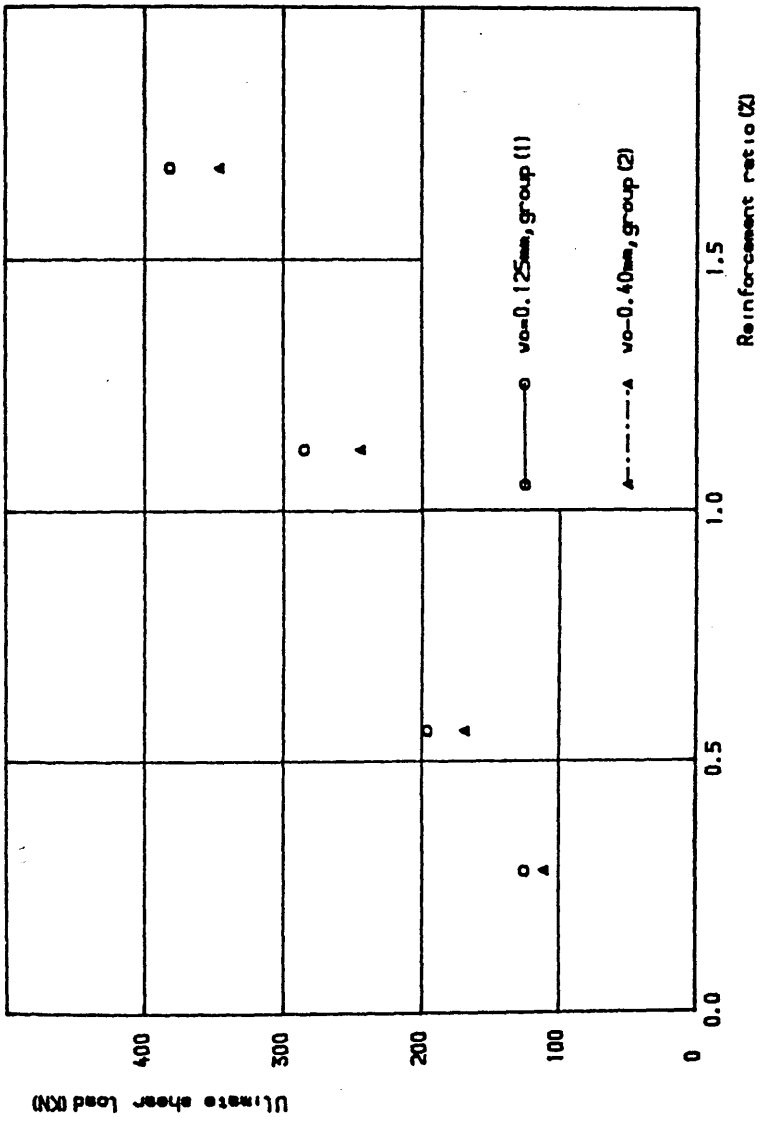

Figure(7.43) Effect of initial crack width on ultimate shear transfer strength by combined action under repeated load.

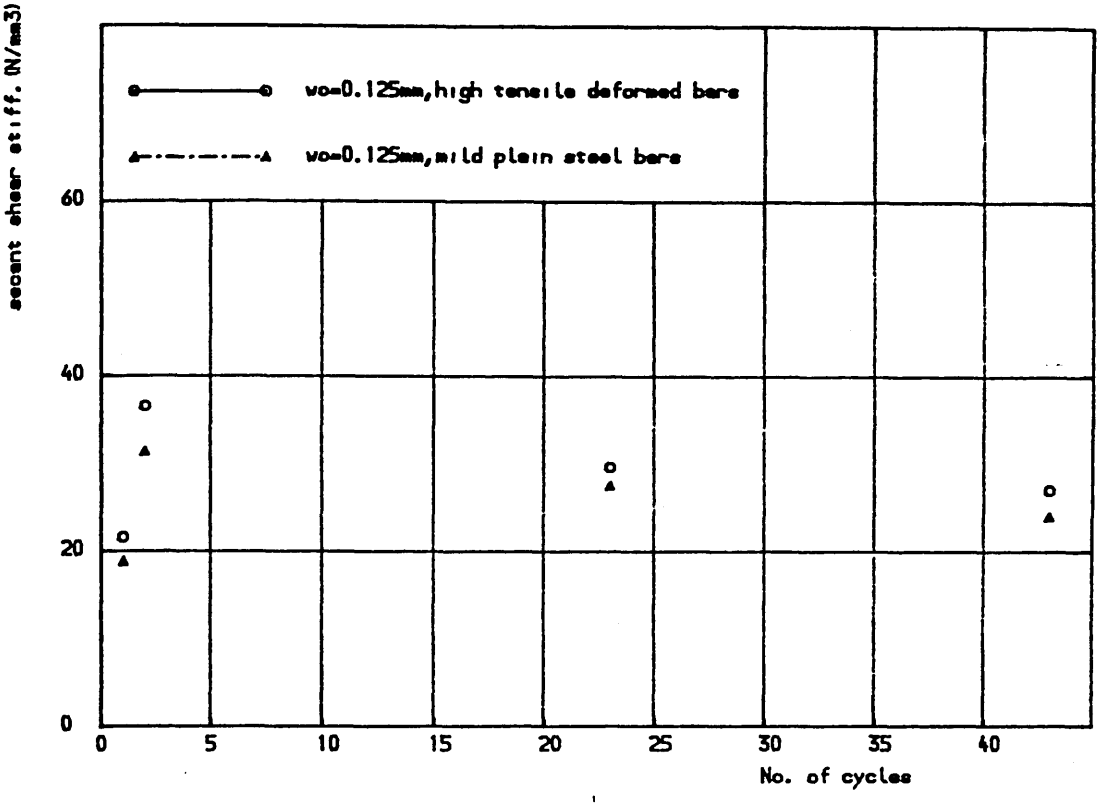

(a) Shear transverse reinforcement ratio 0.28 %

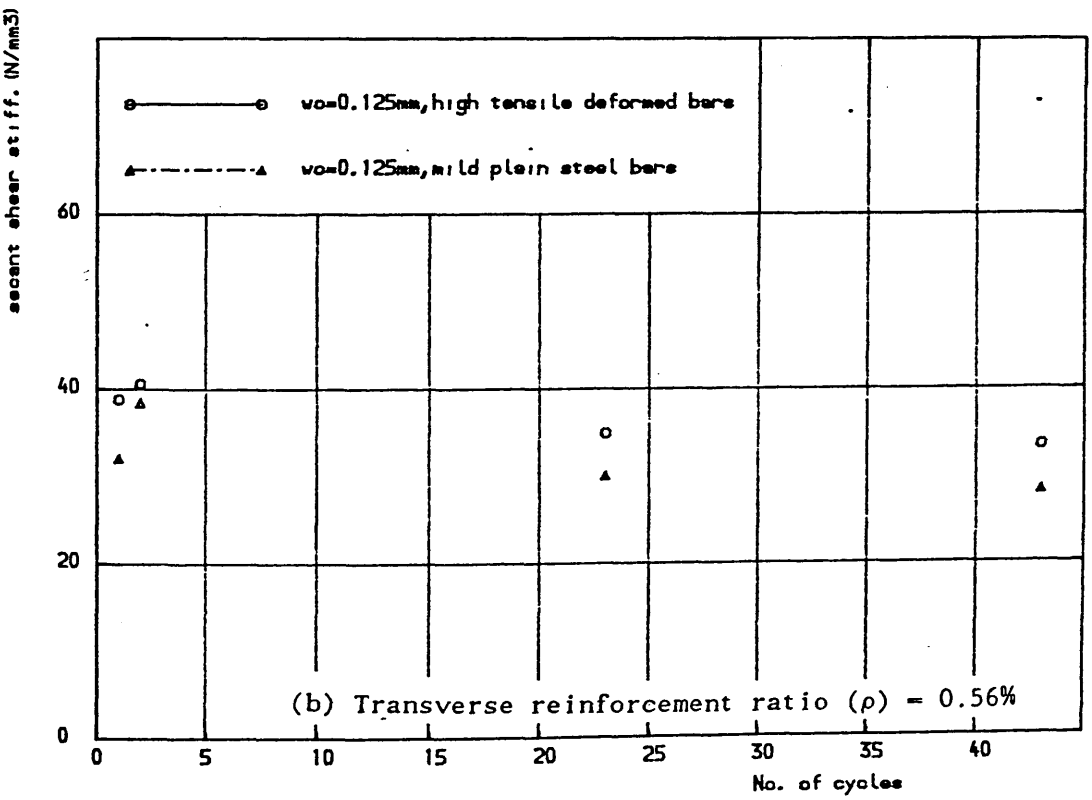

(b) Transverse reinforcement ratio (ρ) = 0.56%

Figure(7.44) Effect of travsverse reinforcement type on secant shear stiffness vs. number of load cycles for comb. action specimens

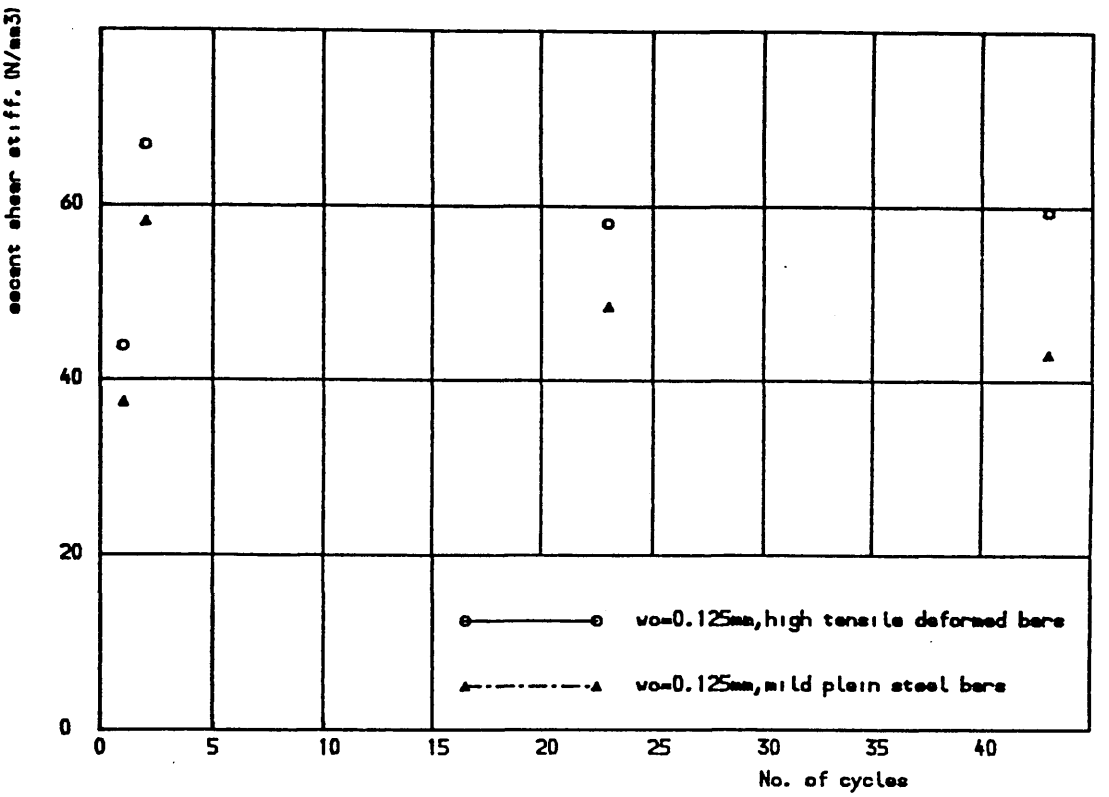

(c) Shear transverse reinforcement ratio 1.12 %

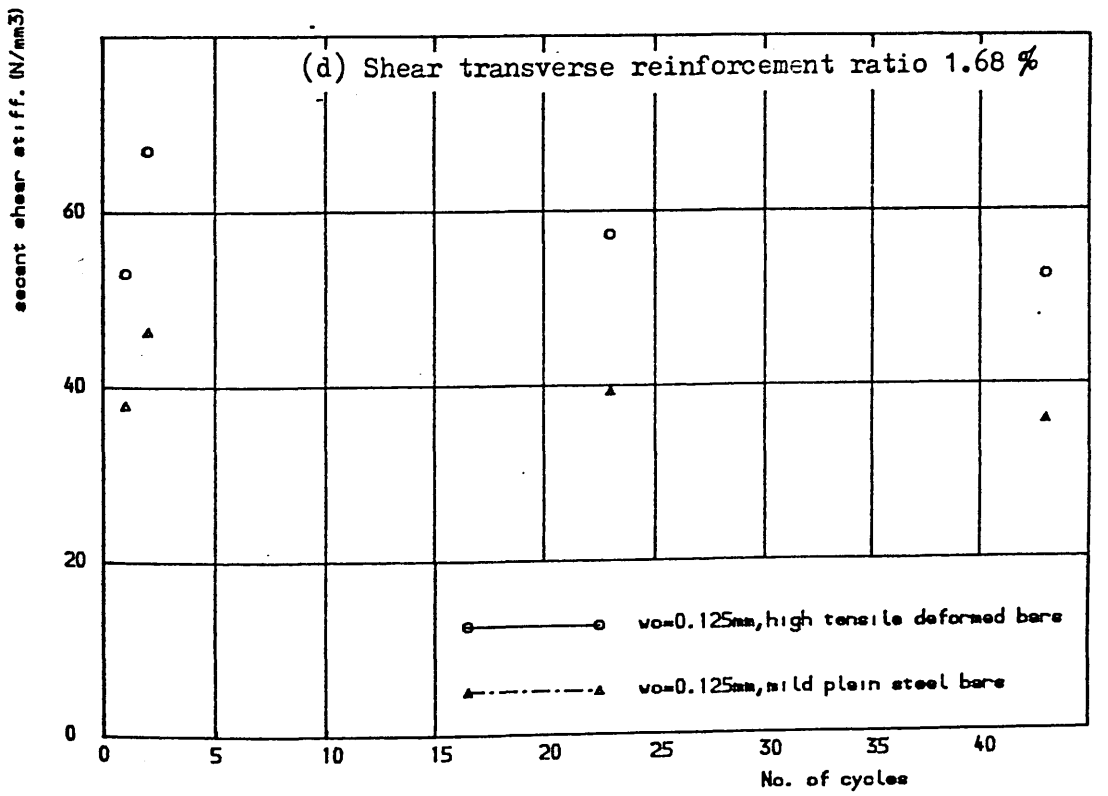

Figure(7.44)Cont. Effect of transverse reinforcement type on secant shear stiffness vs. number of load cycles for combined action specimens.

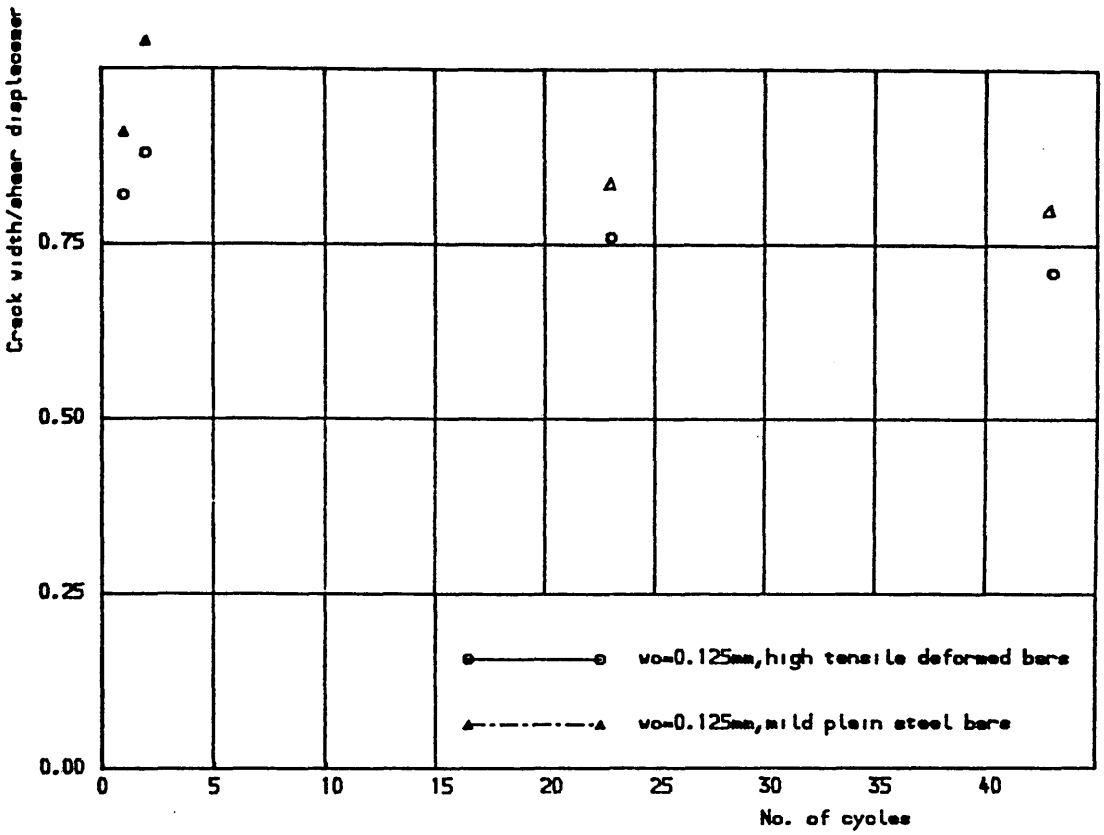

(a) Shear transverse reinforcement ratio 0.28 %

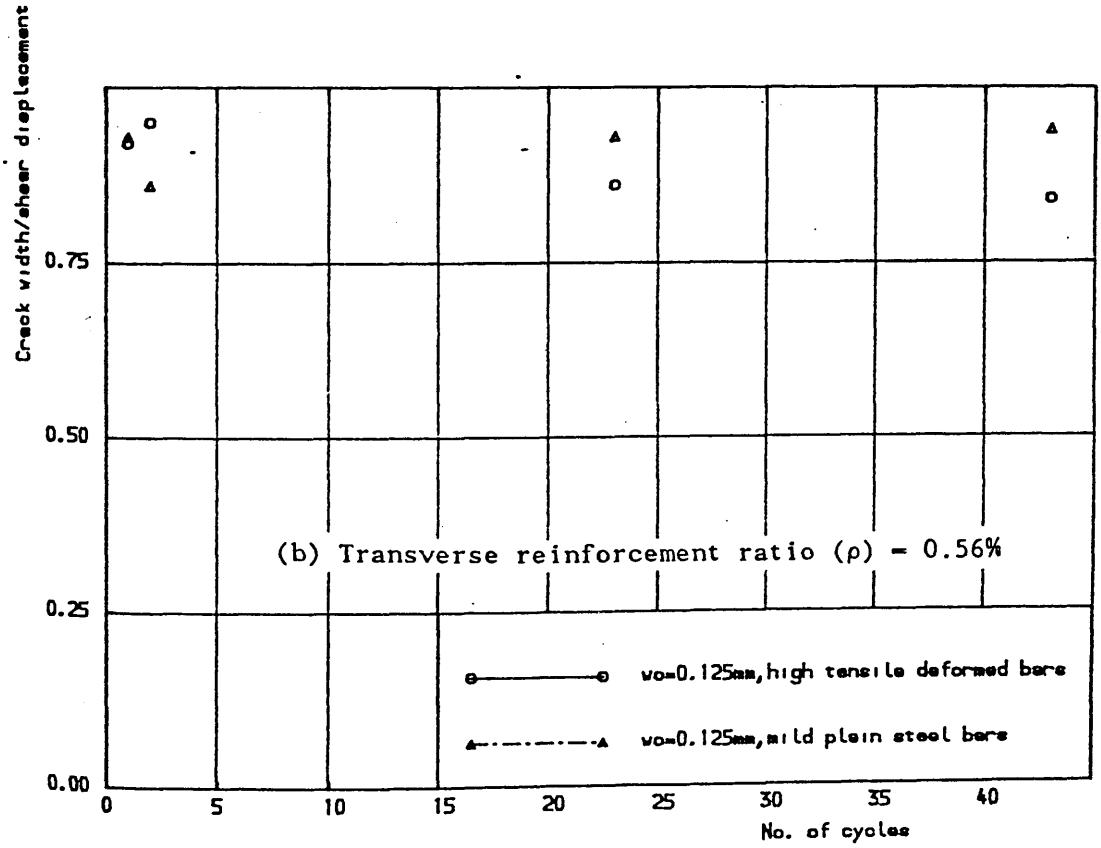

(b) Transverse reinforcement ratio (ρ) = 0.56%

Figure(7.45) Effect of transverse reinforcement type on crack width /shear displacement ratio vs. number of load cycles for combined action specimens.

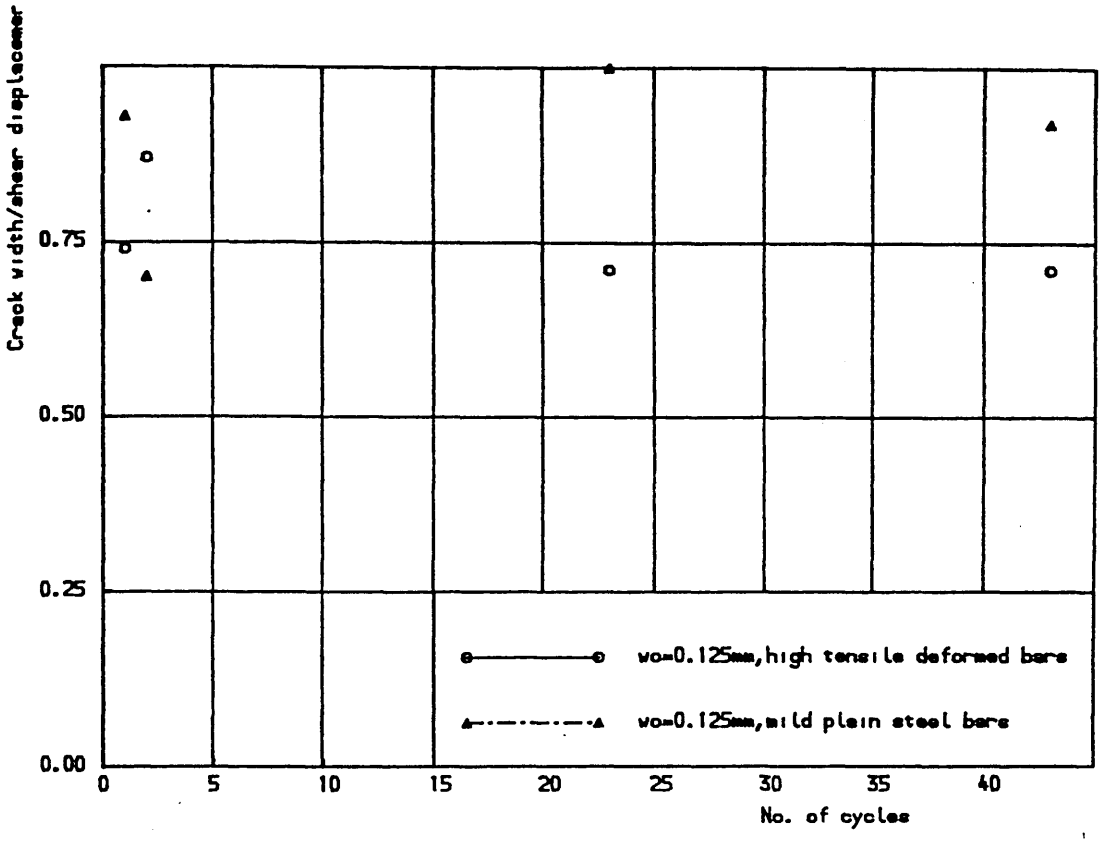

(c) Shear transverse reinforcement ratio 1.12 %

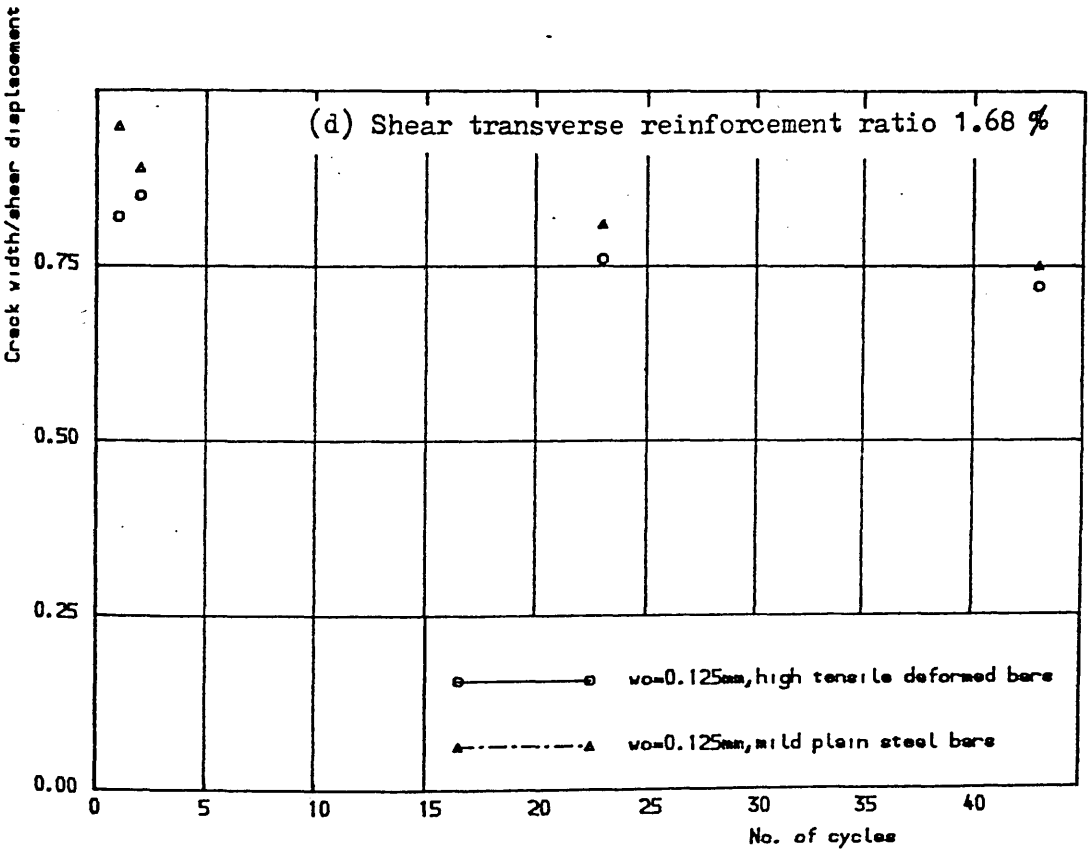

Figure(7.45 Cont)Effect of transverse reinforcement type on crack width /shear displacement ratio vs. number of load cycles for combined action specimens.

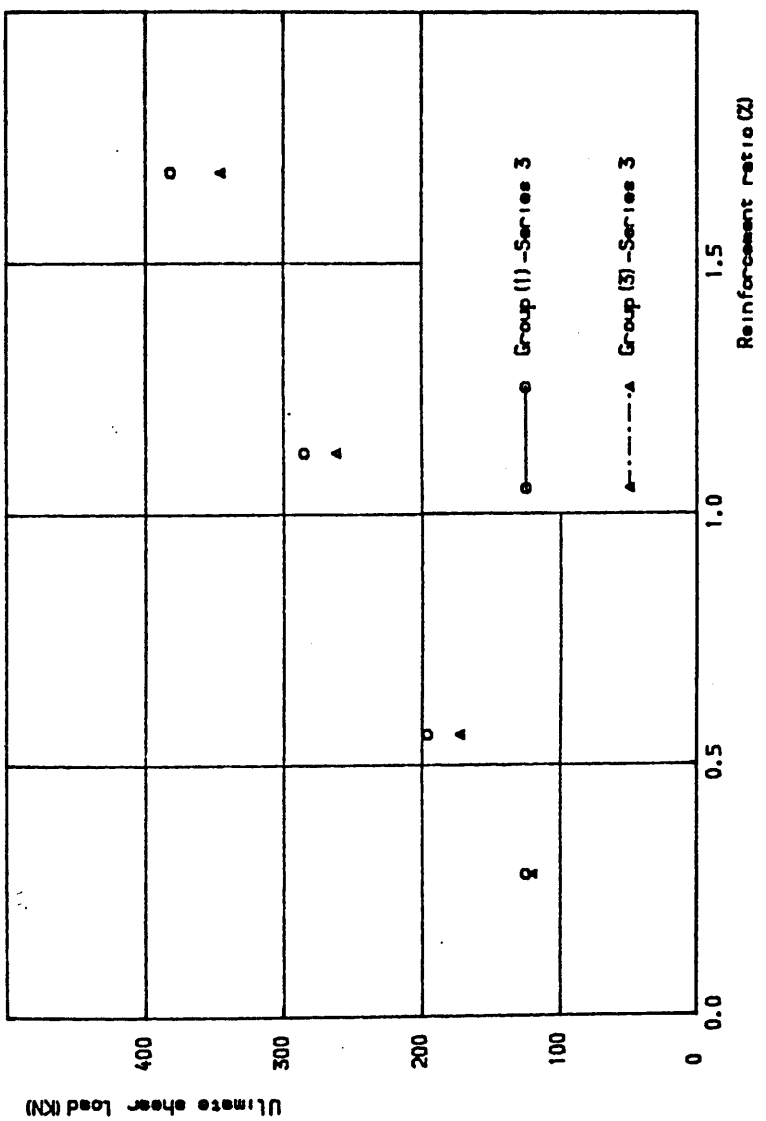

Figure(7.46) Effect of transverse reinforcement type on the ultimate shear transfer strength by combined action under repeated load

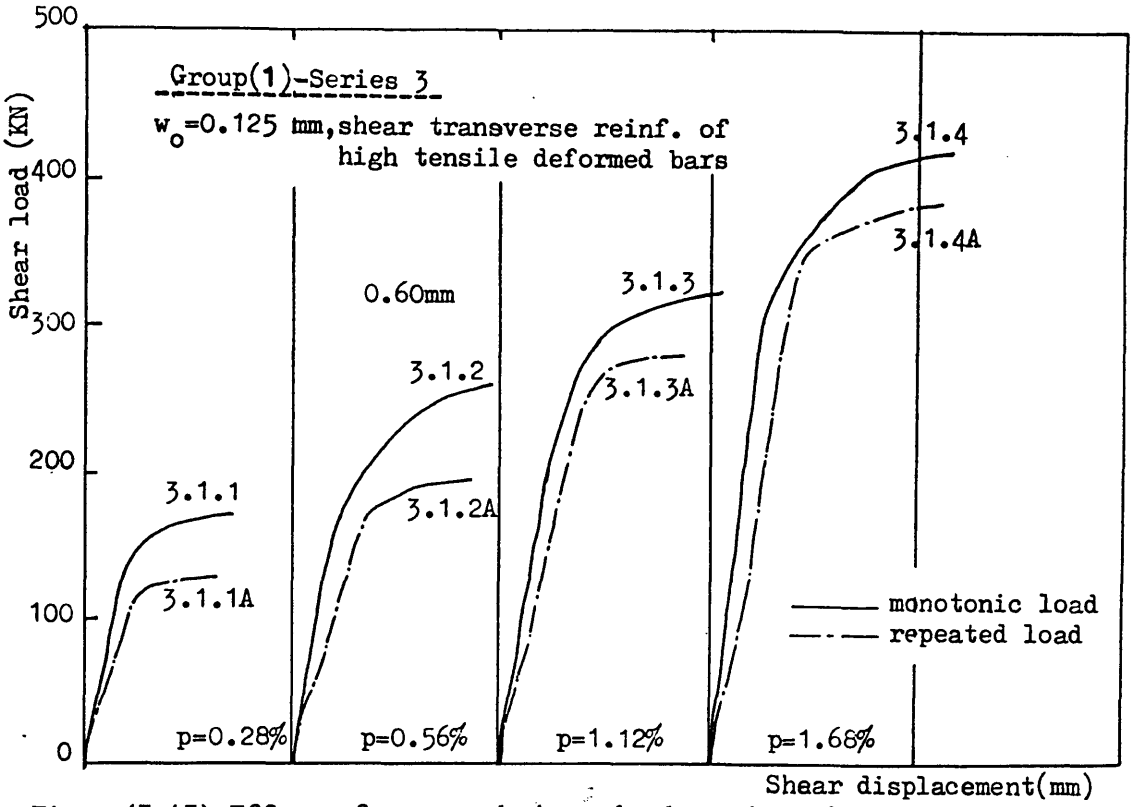

Figure(7.47) Effect of repeated shear load on shear load vs. shear displacement for combined action specimens with w=0.125 mm and high tensile deformed bars

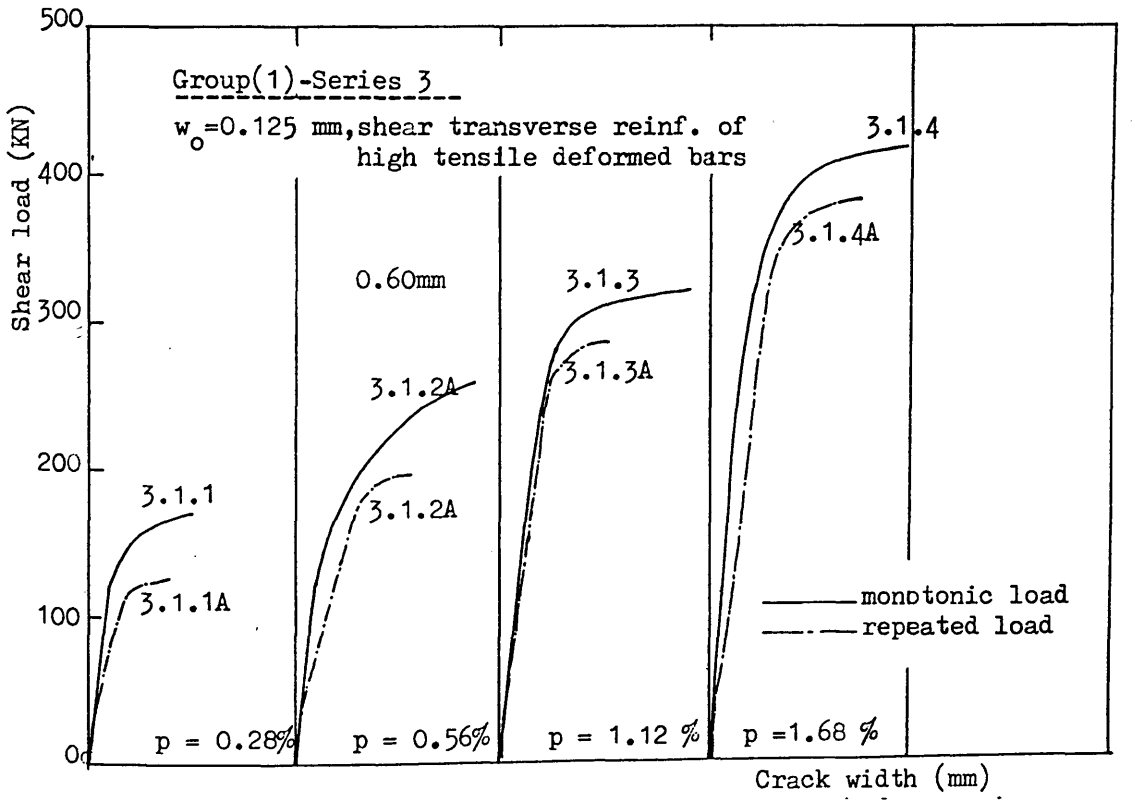

Figure(7.48) Effect of repeated shear load on shear load vs. crack width for combined action specimens with w_o=0.125mm and high tens. deformed bars

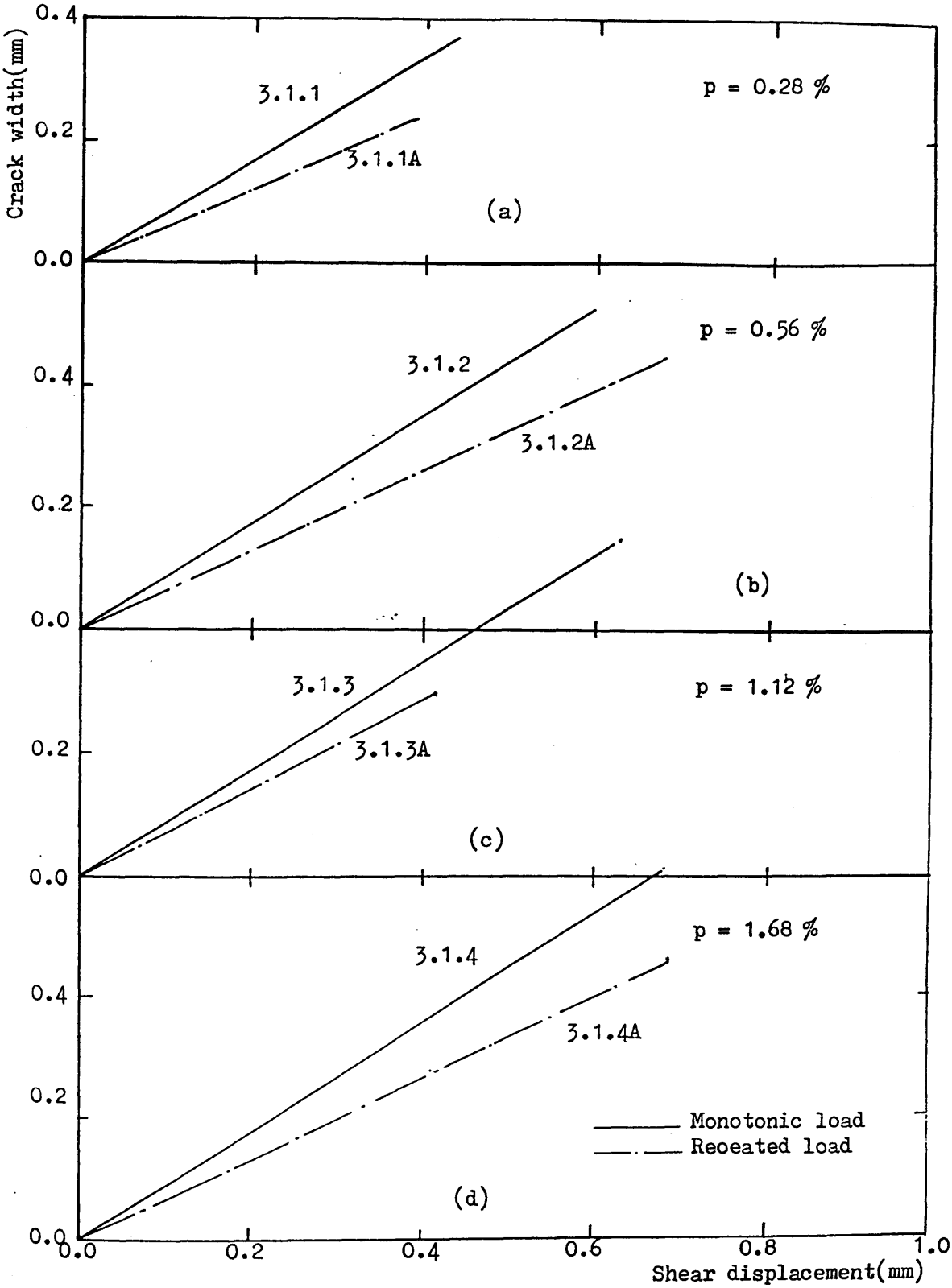

Figure(7.49) Effect of repeated shear load on crack width vs. shear displacement for combined action specimens with w_o=0.125 mm and high tesile deformed bars

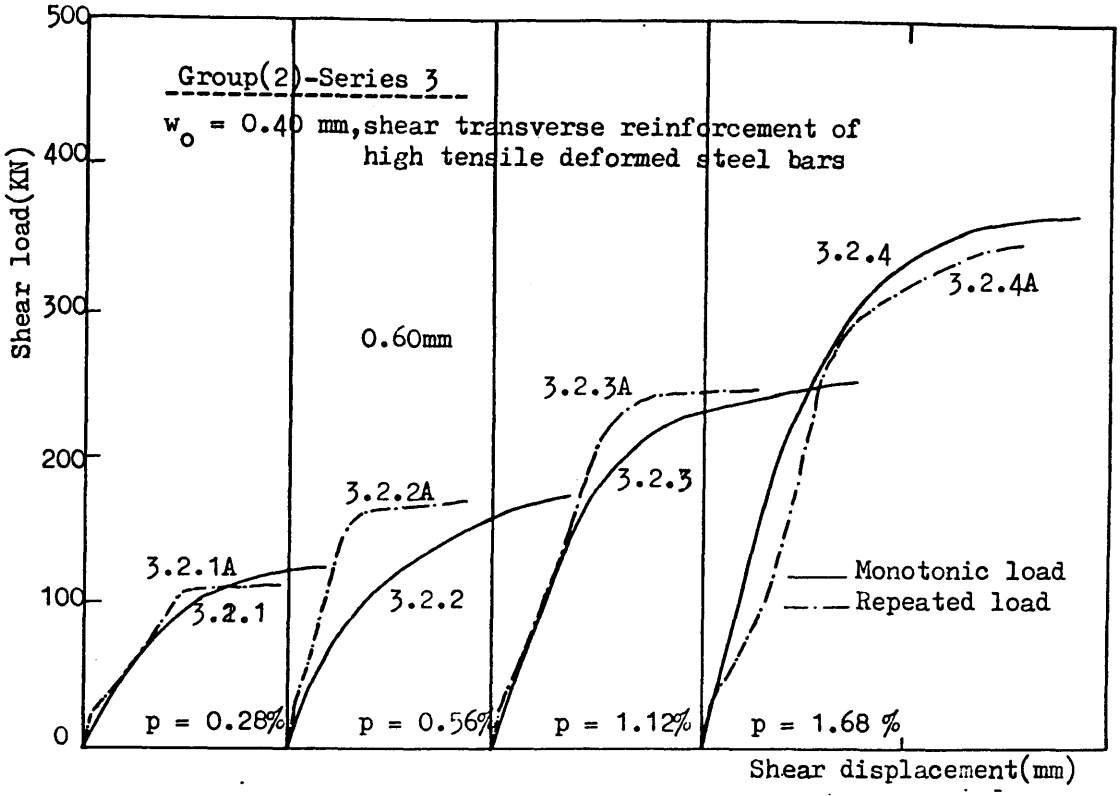

Figure(7.50) Effect of repeated shear load on shear load vs. shear displacement for combined action specimens with w_o=0.40 mm and high tensile deformed bars

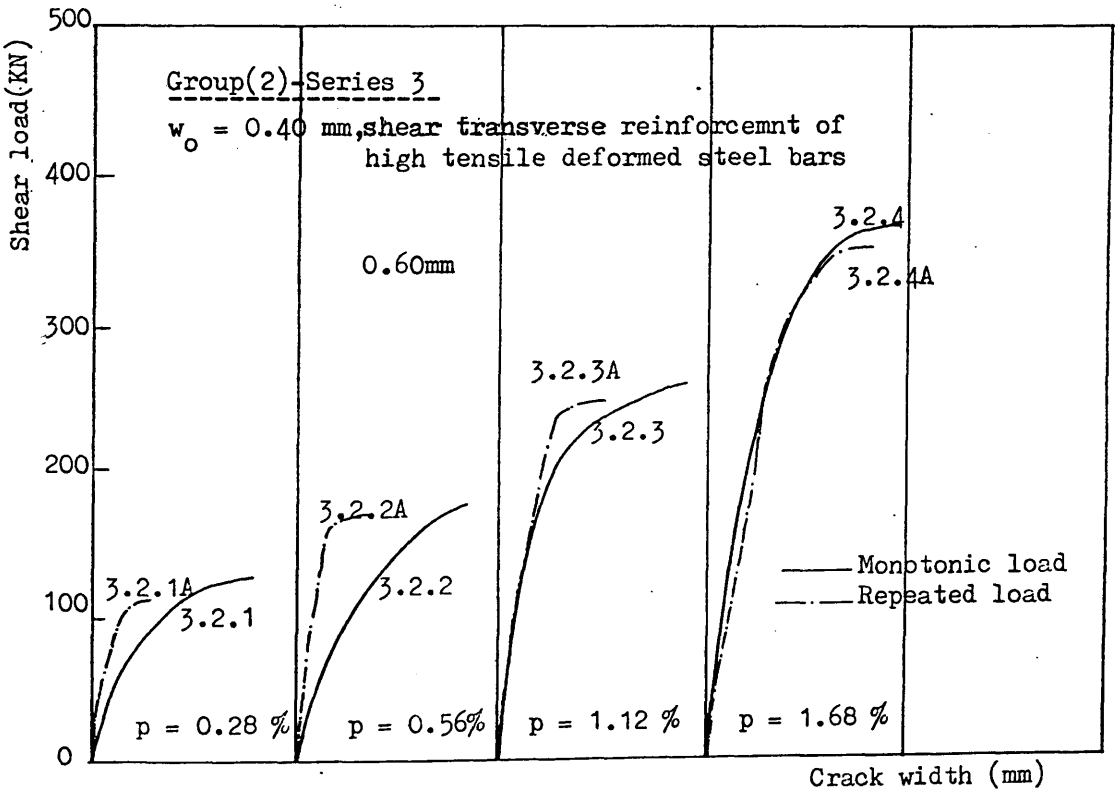

Figure(7.51) Effect of repeated shear load on shear load vs crack width for combined action specimens with w_o=0.40 mm and high tensile deformed bars

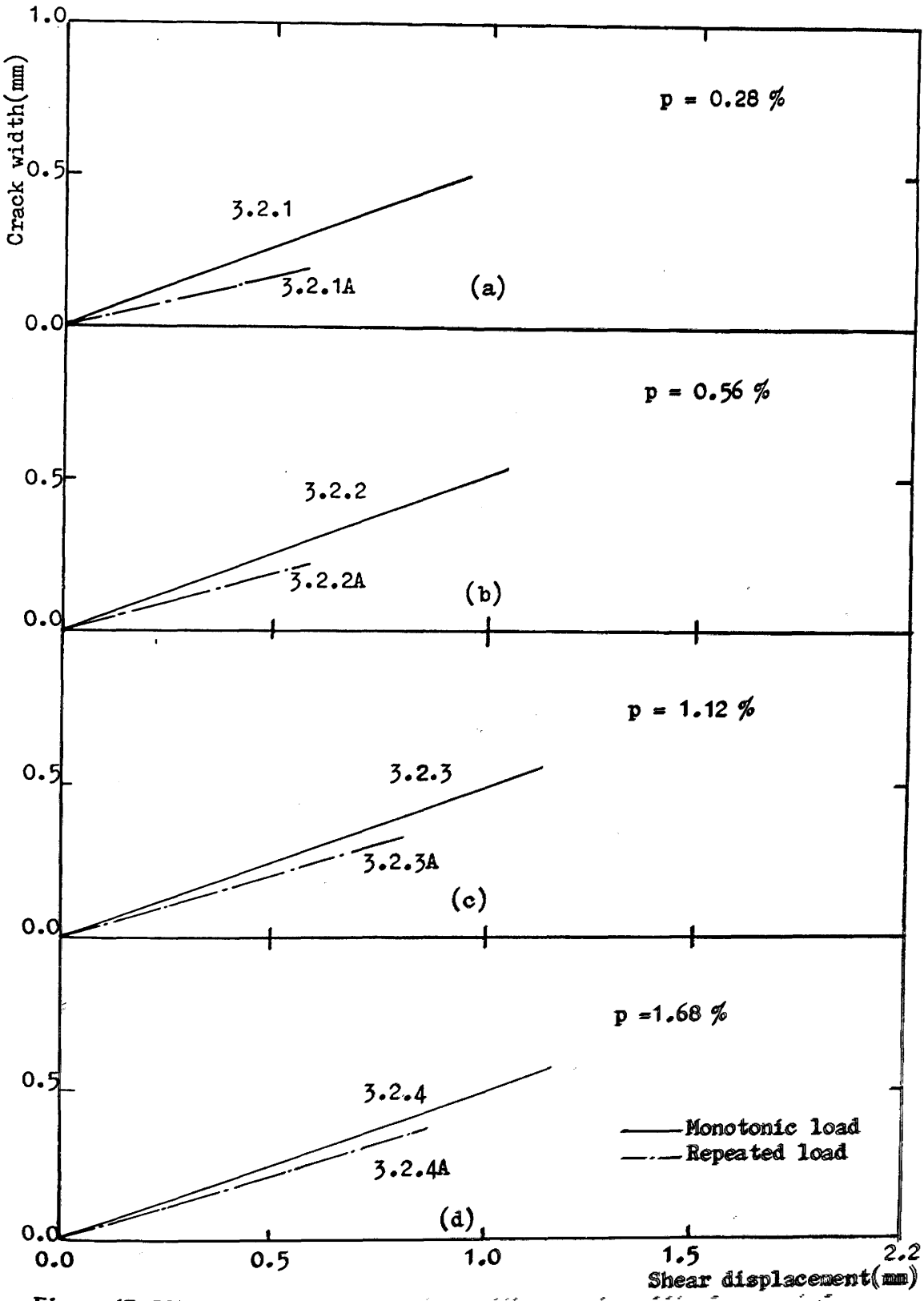

Figure(7.52) Effect of repeated shear load on crack width vs shear displacement for combined action specimens with w_o-0.4 mm and high tensile deformed bars

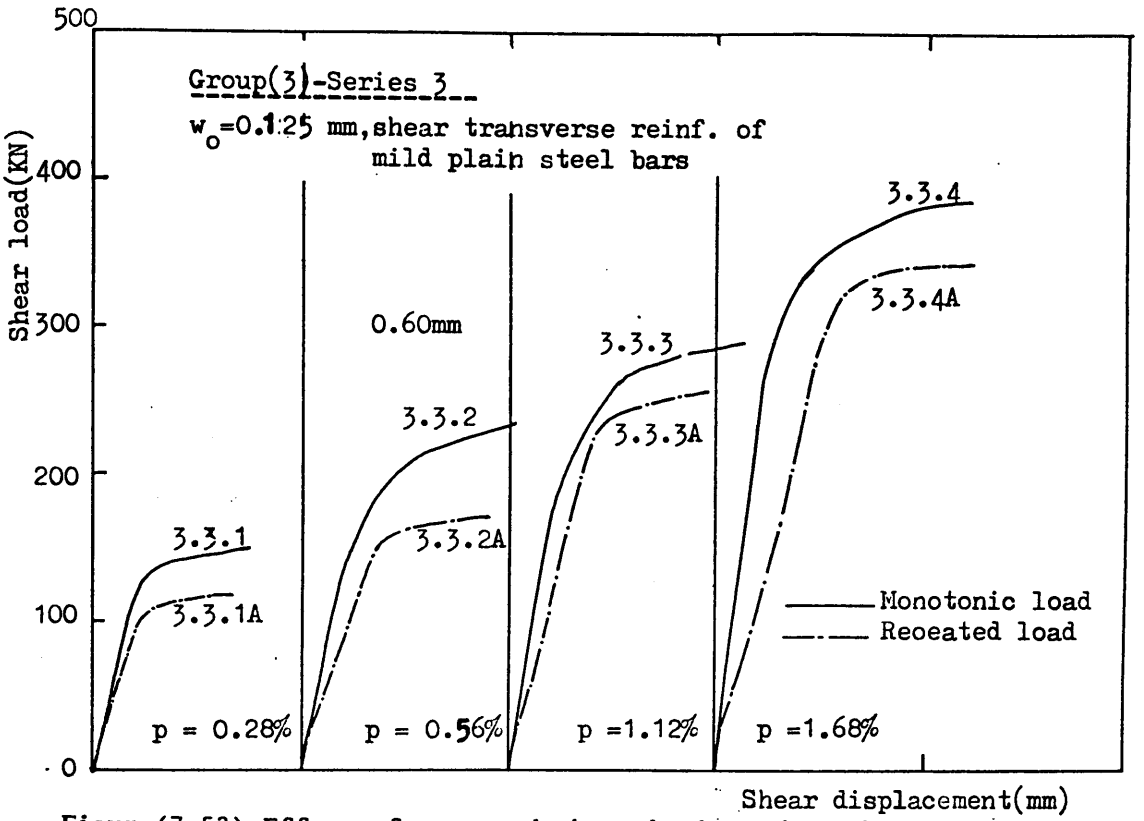

Figure(7.53) Effect of repeated shear load on shear load vs. shear displacement for combined action specimens with w_o=0.125 mm and mild tensile plain bars

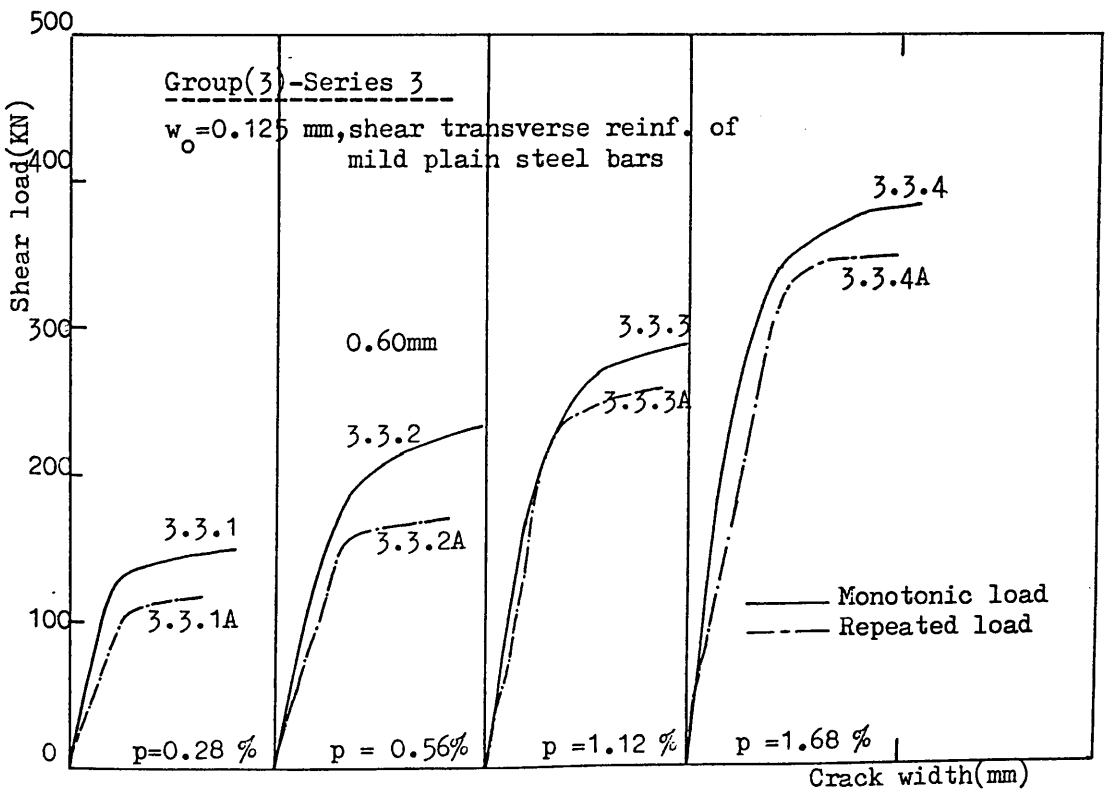

Figure(7.54) Effect of repeated shear load on shear load vs. crack width for combined action specimens with w_o=0.125 mm and mild tensile plain bars

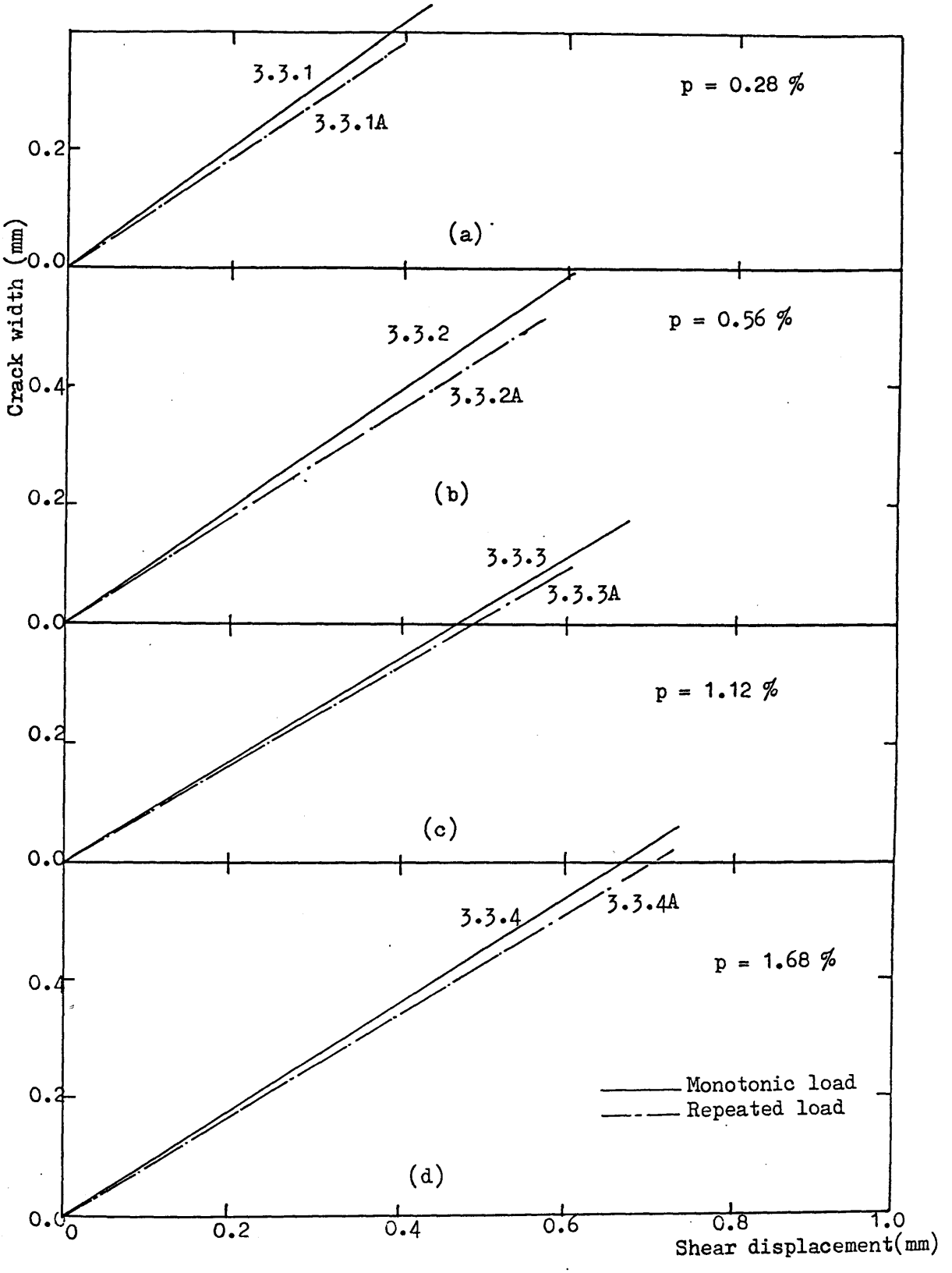

Figure(7.55) Effect of repeated shear load on crack width vs. shear displacement for combined action specimens with w_o=0.125 mm and mild tensile plain bars

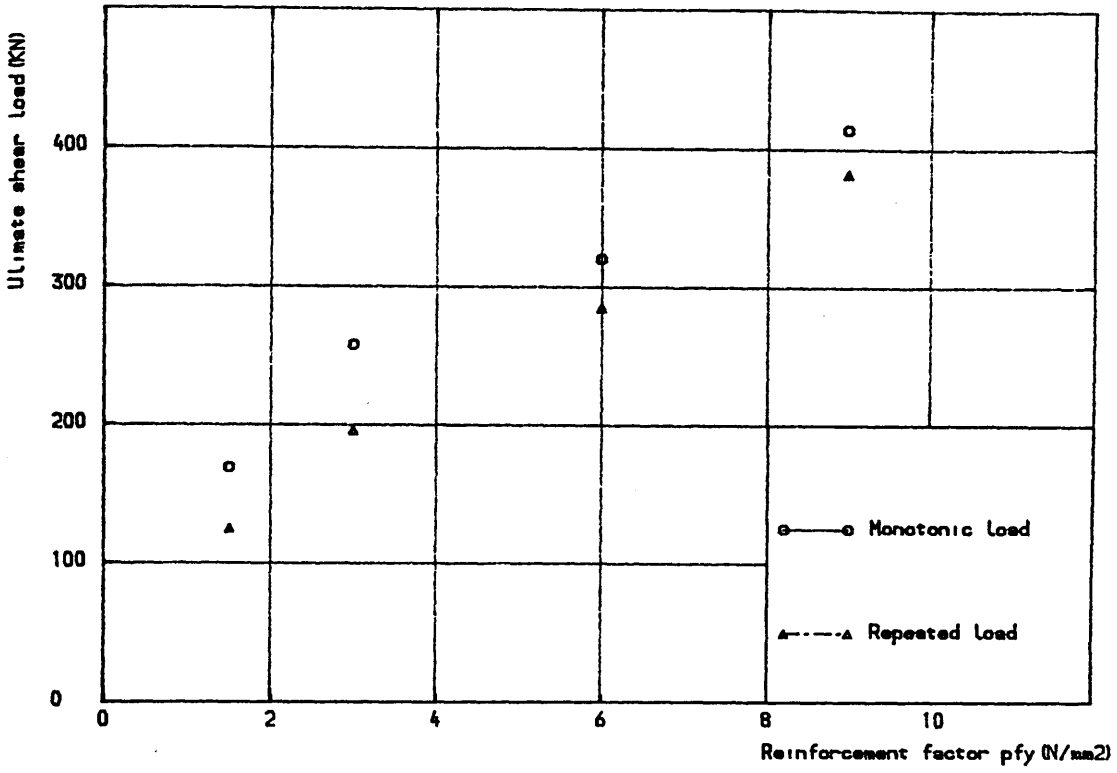

Figure(7.56) Effect of repeated shear load on ultimate shear transfer strength by combined action for specimens with w_o=0.125mm and high tensile deformed bars

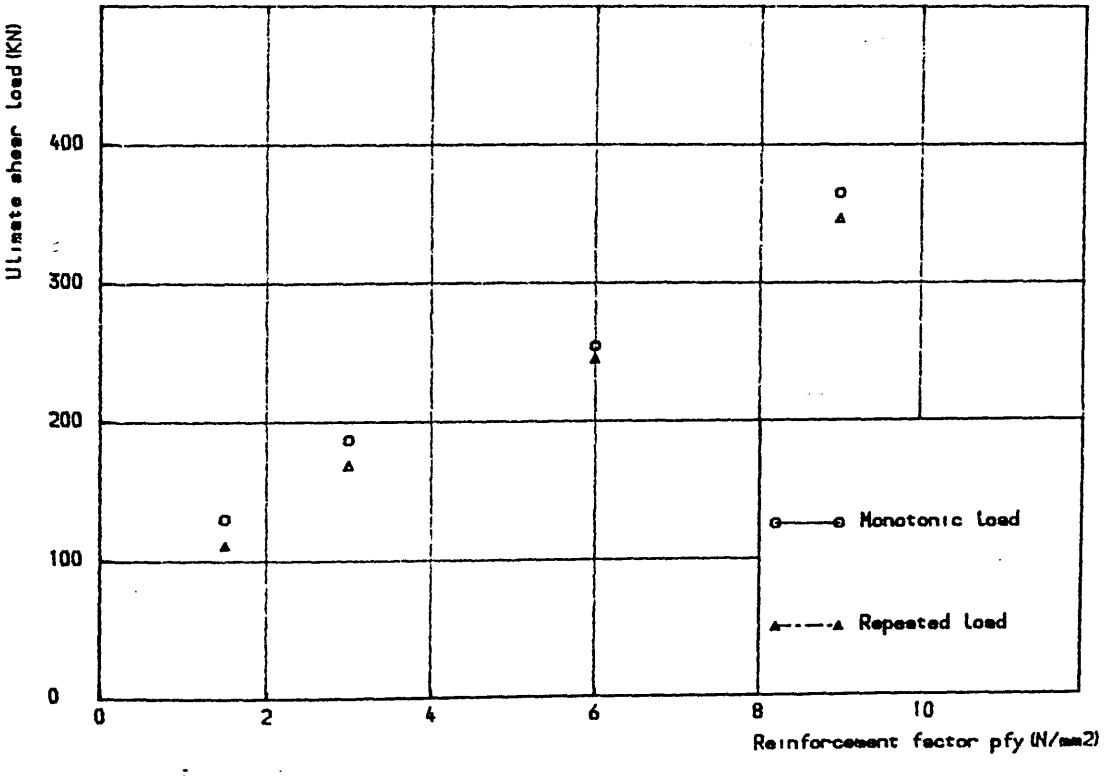

Figure(7.57) Effect of repeated shear load on ultimate shear transfer strength by combined action for specimens with w_o=0.40 mm and high tensile deformed bars

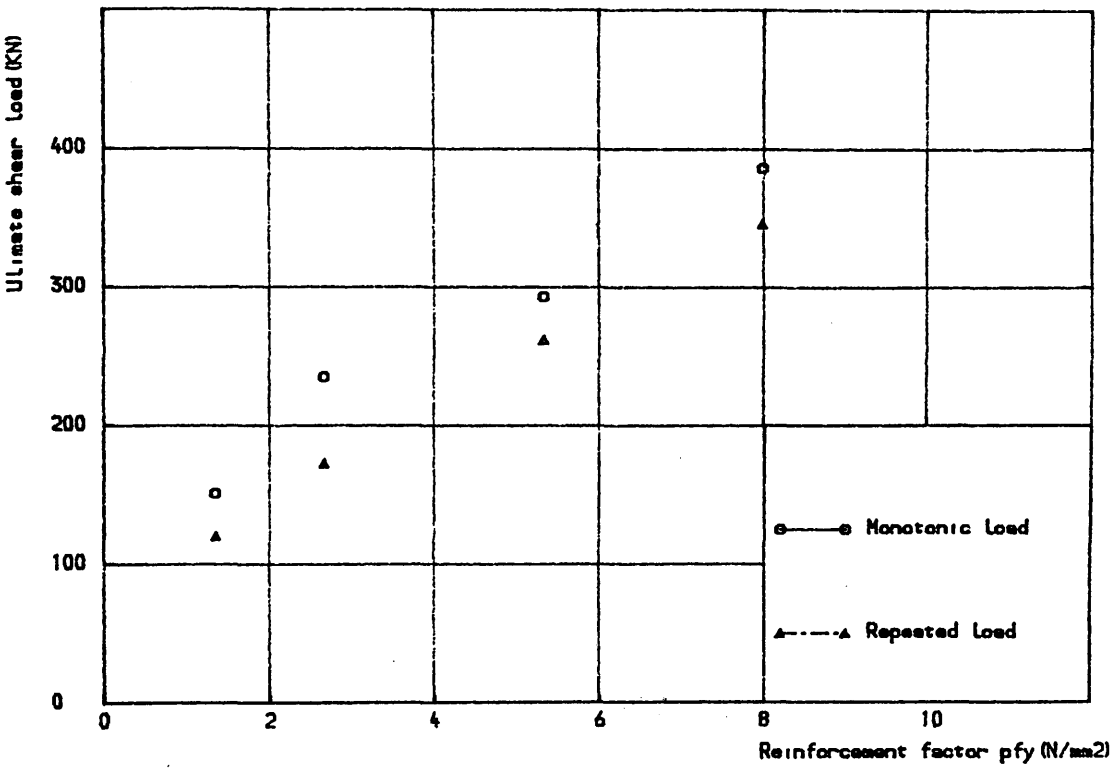

Figure(7.58) Effect of repeated shear load on ultimate shear transfer strength by combined action for specimens with w_o=0.125mm and mild tensile plain bars

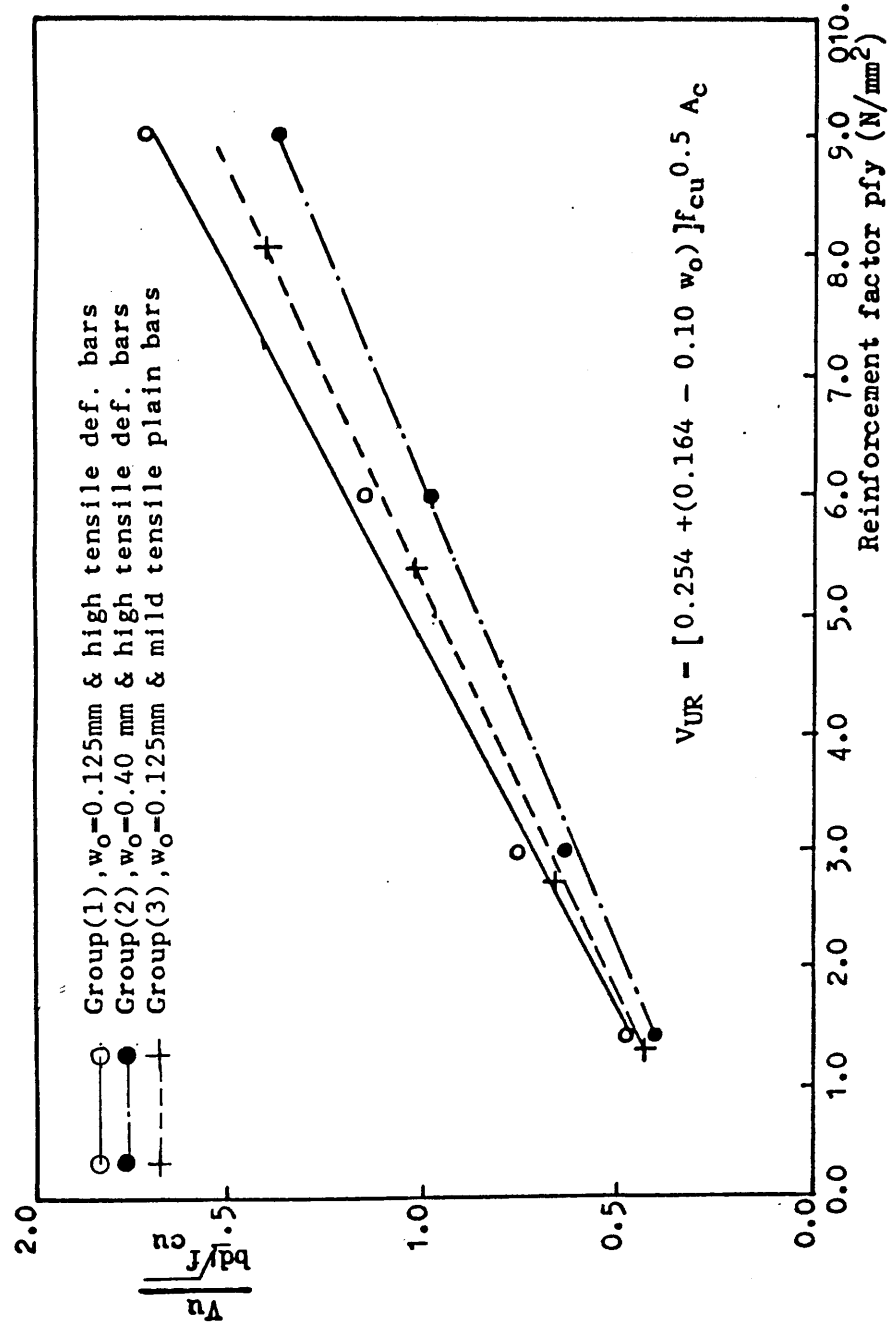

Figure(7.59) Comparison between the experimental and calculated ultimate shear transfer strength by combined action under repeated load using Equation(7.15)

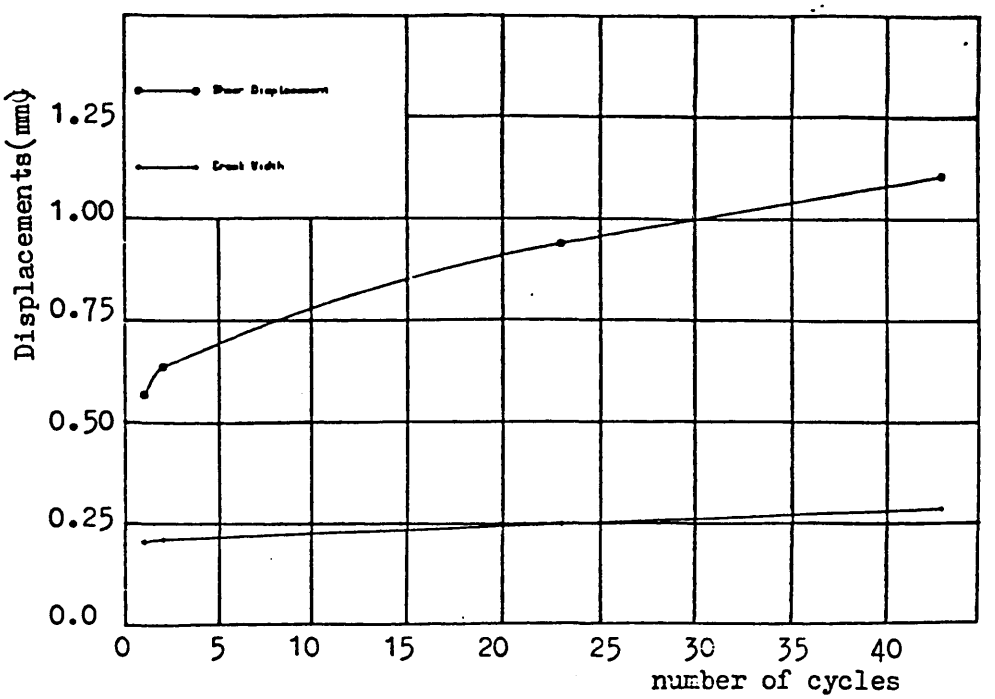

(a) Repeated load (specimen 3.2.4A)

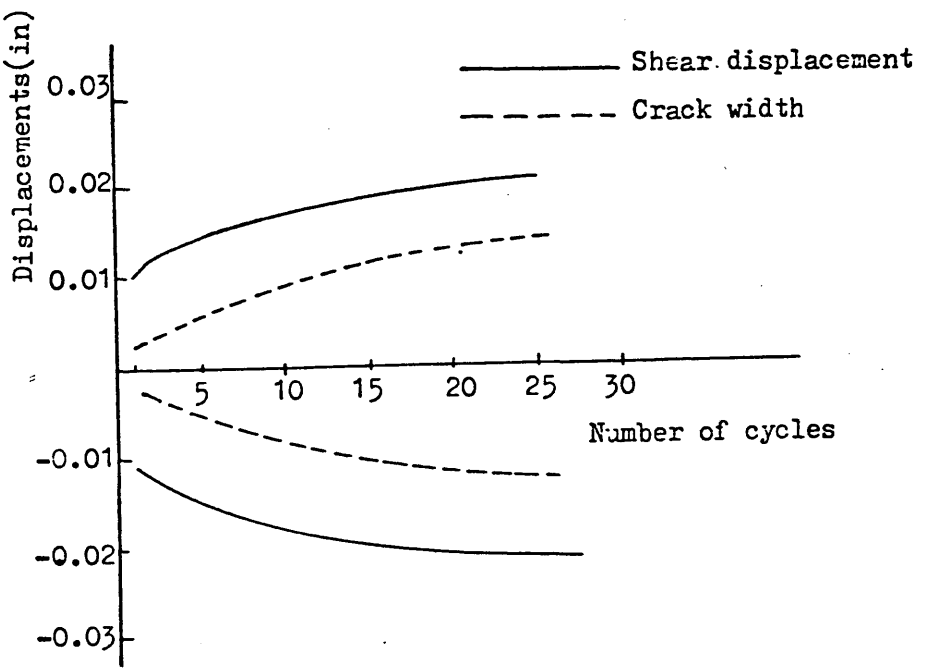

(b) Reversing cyclic load [27] (specimen C4-7)

ure(7.60) Comparison between displacements vs. number of load cycles for shear transfer tests by combined actions under repeated and reversing cyclic[27] loads

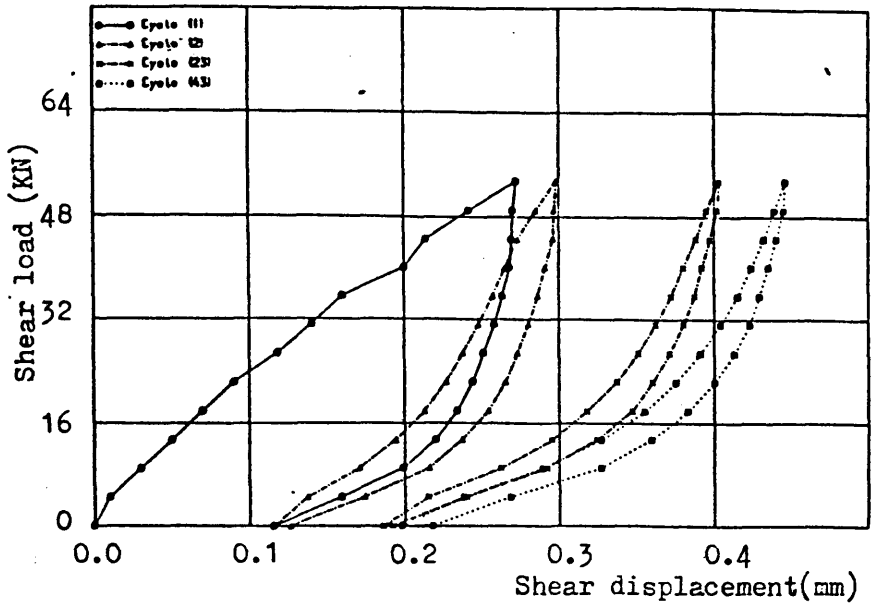

(a) Repeated load (specimen 2.1.4A)

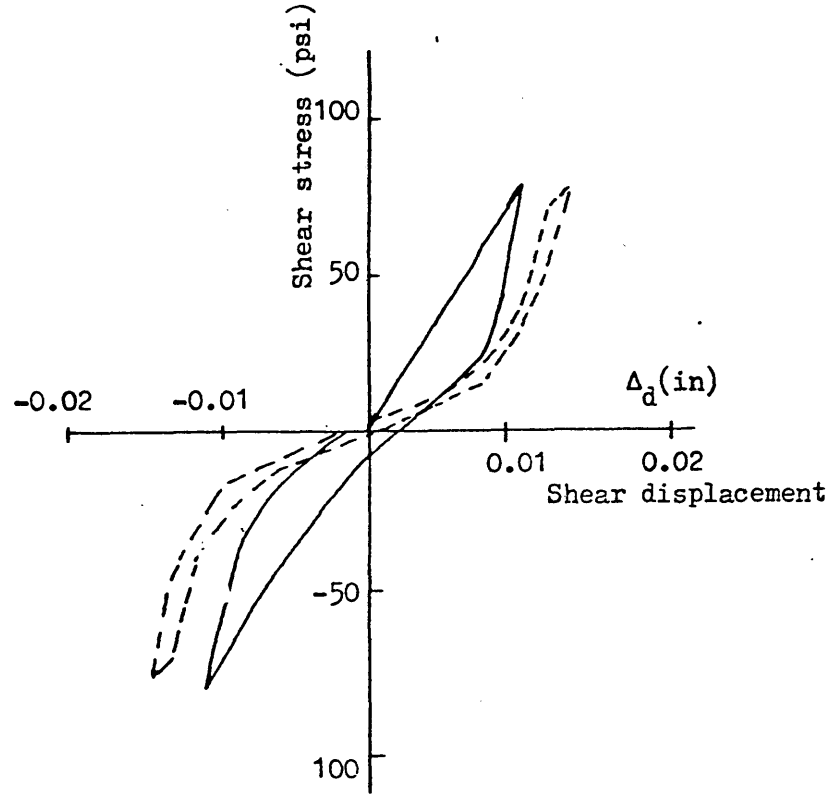

(b) Reversing cyclic load [27] (specimen D4-9)

Figure(7.61) Comparison between shear strength vs. shear displacement for shear transfer tests by dowel action under repeated and reversing cyclic[27] loads

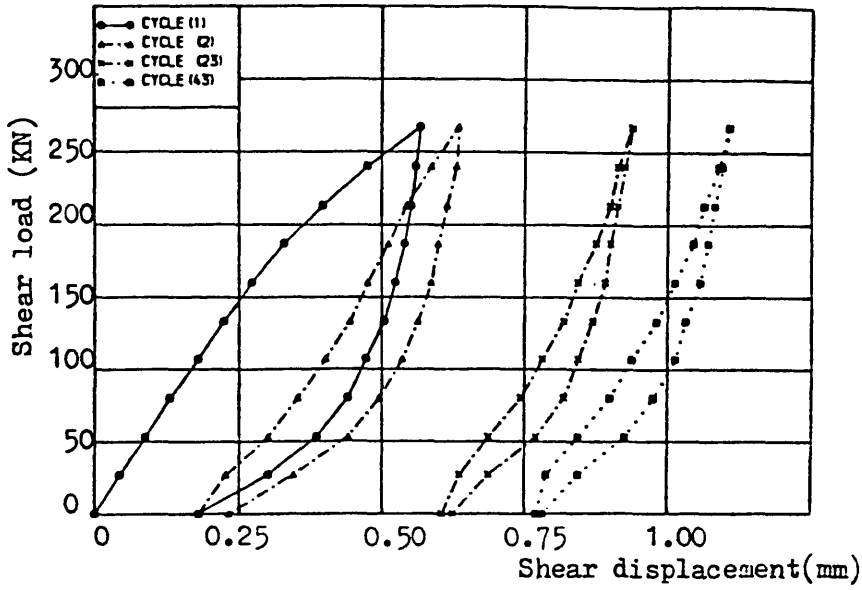

(a) Repeated load (specimen 3.24A)

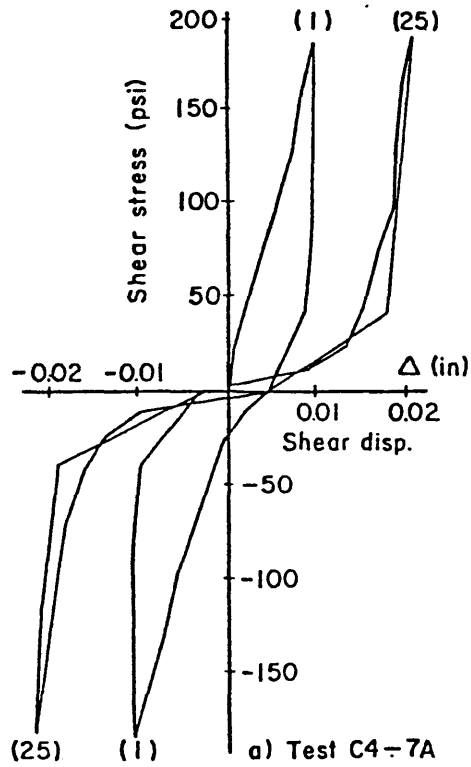

(b) Reversing cyclic load[27] (specimen C4-7A)

Figure(7.62) Comparison between shear strength vs. shear displacement for shear transfer tests by combined action under reptead and reversing cyclic [27] loads

REFERENCES

(1) Paulay, T., Park, R. and Phillips,M.H. "Horizontal construction joints in cast-in-place reinforced concrete", ACI, SP-42 "Shear in reinforced concrete", Vo.2, 1974, pp.599-616.

(2) Johansen, K.W. "Yield-Line Theory" Cement and Concrete Association, London, 1962.

(3) Wood, R.H. "Plastic and elastic design of slabs and plates". Thames and Hudson, London, M61, pp.344.

(4) Kwiecinski, M.W. "Yield Criterion for initially isotropic reinforced concrete slabs". Magazine of Concrete Research, Vol.17, No.51, June 1965, pp. 97-100.

(5) Prince, M.R. and Kemp, K.O. "A new approach to the yield criterion for isotropically reinforced concrete slabs". Magazine of Concrete Research, Vol.20, No.62, March 1968, pp. (13-20).

(6) Mills, G.M., "A practical kinking criterion for reinforced concrete slabs". Magazine of Concrete Research, Vo.27, No.90, Mar. 1975, pp. 13-22.

(7) Morley, C.T., "Experiments on the distortion of steel bars across cracks in reinforced concrete slabs". Magazine of Concrete Research, Nol.18, No.5, March 1966, pp.25-34.

(8) Marcus, H. "Load carrying capacity of dowels of transverse pavement joints". ACI Journa, Proc.V.48, No.2, October 1951.

(9) Finney, E.A., "Structural Design Consideration for pavement joint". ACI Journal, Proc. V.28, July 1956.

(10)Millard, S.G. and Johnson, R. "Shear transfer across cracks in reinforced concrete due to aggregate interlock and to dowel action.". Magazien of Concrete Research, Vo.36, No.126, March 1984, pp.9-21.

(11)Walraven, J.C. "Aggregate interlock : a theoretical and experimental analysis". Delft University Press, 1980.

(12)Stanton, J.F. "An investigation of dowel action of the reinforcement of nuclear containment vessels and their nonlinear dynamic response to earthquake loads". M.Sc. thesis, Cornell University.

(13)Krefield, W.J. and Thurston, C.W. "Contribution of longitudinal steel to shear resistance of reinforced concrete beams". Jnl. ACI., Vol.63, Mar.1966, pp.325-344.

(14)Taylor, H.P.J. "Investigation of the dowel shear forces carried by the tensile steel in reinforced concrete beams". C. & C.A., TRA.431, Nov. 1969.

(15)White, R.N. and Gergely, P. "Shear transfer in thick walled reinforced concrete structures under seismic loading". Report No.75-10, Cornell University, N.Y. 1973.

(16)Rasmussen, B.H., "Strength of transversely loaded bolts and dowels cast into concrete". Laboratoriet for Gygningssta Den. Tecn. Hoskole, Meddelelee, Vol.34, No.2, 1962 (in Danish).

(17)Dulaska, H. "Dowel action of reinforced crossing cracks in concrete". Journal of the American Institute, Vol.69, No.12, December 1972.

(18)Jacobsen, L.S. "Damping in composite structures". Proceedings of the 2nd World Conference on Earthquake Engineering, Tokyo and Kyoto , Japan, 1960, Vo.2, pp. 1029-1044.

(19)Hofbeck, J.A. Ibrahim, I.O. and Mattock, A.H. "Shear transfer in reinforced concrete". ACI Journal, Proc. V.66, No.2, February 1969.

(20)Mattock, A.H. and Hawkins,N.M. "Shear transfer in reinforced concrete. Recent Research". PCI Journal. Vol.17, March/April 1972.

(21)Mattock, A.H. "Effect of aggregate type on single direction shear transfer strength in monolithic concrete". Report SM74-2, Dept. of Civil Engineering, University of Washington, August, 1974.

(22)Walraven, J.C. "Experimental on shear trasnfer in cracks in concrete". Part 2: Analysis of test results, Report 5-79-10, Stevin Laboratory, Delft University of Technology.

(23)Walraven, J.C. "Experiments on shear transfer in cracks in concrete. Part I : Description of results", Report 5-79-3, January 1979, Stevin Laboratory, Delft University of Technology, The Netherlands.

(24)Millard, S.G. and Johnson, R., "Shear transfer in cracked reinforced concrete". Magazine of Concrete Research, Vol.137, No.130, March 1985.

(25)Goto, Y., "Cracks formed in concrete around deformed tension bars", ACI-Journal, Proceedings, Vol.68, No.4, April 1971, pp.241-251.

(26)Mattock, A.H. "The shear transfer behaviour of cracked monolithic concrete subject to cyclically reversing shear". Report 74-9 Dept. of Civil Engieering, University of Washington, Seattle, Washington 1974.

(27)Jimenez et al. "Shear transfer across cracks in reinforced concrete". Cornell University, Rep. 78-4, August 1978.

CHAPTER (8)

SHEAR TRANSFER MODELS FOR ANALYSIS AND DESIGN

8.1 Introduction

In this chapter firstly an attempt is made to provide information that might help to improve the modelling of shear transfer across cracks in nonlinear finite element analysis for structural concrete. Secondly, the different current international design codes, ACI318-83[1] and British Standard BS:8110[2], are examined by comparing their recommendations for shear transfer with the present test results and the equations proposed in the previous chapter. Other relevant formulations suggested by Mattock[3] and Walraven[4] are also examined and compared. Proposal is made for the improvement of the design procedures for shear transfer.

8.2 Cracking models for finite element analysis

Over the past 15 years a number of different models have been developed to represent cracking during a finite element analysis of reinforced concrete structures. The particular cracking model selected depends upon the purpose of the finite element study and the nature of the output desired from the study.

Two distinct approaches have been used to model cracking, namely, discrete crack models and distributed (smeared) crack models. A further distinction may be made, which may be based on the criterion adopted for crack initiation and propagation which can be based on limited tensile strength or fracture mechanics concepts.

The finite element method is a general discretization method for

solving continium problems governed by partial differential equation subjected to specified boundary constraints. The continium is subdivided into finite regions termed "elements", each of which possess a finite number of unknown parameters which approximate the values of the field variables which define the problem. These elements connect with each other through common points existing on their boundaries at which continuity and compatibility of the field variables are enforced. These common points are termed "nodes". In structural mechanics problems, the unknown field variables can be displacements, stresses, or both. The finite element method is unique in the way it can formulate the properties of individual elements of any type of problem. However, as, the finite element method is now so well documented, no attempt will be made to describe it in detail here.

Discrete cracks can be represented by eliminating the connection between nodes of adjacent elements, Figure (8.1). This can be done either by redefining the topology of the model [5] or reducing to zero stiffness of link elements connecting the nodes of adjacent concrete elements[6]. In the first case, one is faced with a task which is against the natural organization of finite element programs, in the second, one is obliged to put link elements at every concrete node. In both cases cracks may propagate only along the boundaries of concrete elements.

However, the use of discrete cracking representations has received only limited acceptance due to the difficulty involved in providing for an economical redefination of the structural topology following the formation of a crack. Furthermore, within the mechanics of finite elements, the trend has been to use higher order elements.

These elements, particularly the isoparameteric versions yield somewhat poor quality corner stress definitions which does not blend well with the edge cracking associated with the discrete crack concept.

With the changing of the topology in these models, the redefinition of the nodal points destroys the narrow band width in the structural stiffness matrix and greatly increases the computational effort required for the solution. The non-automatic method of defining cracks and the lack of generality in possible crack directions has made discrete cracking models unpopular for general application. However, in those cases in which local material behaviour at a particular stage during the life of a reinforced concrete structure is of interest, a discrete cracking model is likely to be the representation of choice and is especially useful for investigating the stresses in a structural member with a known crack location.

The need for a cracking model that offers (1) automatic generation of cracks without the redefinition of the finite element topology and (2) complete generality in possible crack direction has led a vast majority of investigators to adopt the so-called "smeared" cracking model. In smeared cracking model cracks may be considered over the finite area of an element, Figure (8.2). This assumption is physically reasonable, in view of the material inhomogeneity of concrete. Its representation can be achieved easily by changing the element stiffness matrix, assuming that the material becomes orthotropic.

8.3 Modelling of shear transfer across cracks

The modelling of shear transfer across reinforced concrete cracks in

the finite element method depends on the types of cracking models used. In discrete crack models two mechanisms of shear transfer, i.e. dowel action and interface shear transfer, can be represented by evaluating the stiffness of fictitious spring parallel to the crack plane k_h of a linkage element as shown in Figure (8.3). The stiffness characterization for such springs have been derived from analytical model in conjunction with experimental data which were reviewed earlier in chapter (2). However, these analytical models are dealt with either dowel action [7],[8],[9] or interface shear transfer mechanism[9],[10],[11] individually. Therefore, to represent shear transfer across a reinforced crack by adding the individual mechanisms might not lead to an accurate prediction because of neglecting the interaction between two shear transfer mechanisms[12].

In the smeared cracking approach shear transfer is most frequently modelled through the so-called "shear retention factor", β, which usually varies between 0 and 1, and is defined by:

$$\beta = G'/G \qquad (8.1)$$

where G' is the reduced shear modulus for cracked concrete and G is the modulus for uncracked concrete. Many investigators have used different values of the shear retention factor to give predictions closest to their experiments resultsas show in, Figure (8.4).

In the first nonlinear finite element of reinforced concrete the shear modulus of the uncracked state was still used after cracking[13],[14], Figure (8.4a). Other authors [15],[16] neglect the shear transfer across the cracks which may lead to numerical difficulties, Figure (8.4b).

In reality reinforced concrete after cracking is still able to transfer shear stresses across the cracks but the shear stiffness of the cracked concrete is less than the shear stiffness of the uncracked state. Therefore, in many publications the shear modulus of cracked concrete was obtained from the shear stiffness of uncracked concrete by using a constant value of β which was chosen rather arbitrarily[17],[18],[19],[20], Figure (8.4c). Others used a gradually decreasing value for β[21],[22],[24] following either linear or nonlinear curves, Figures (8.4d, e and f), and which are dependent on the strain normal to the crack.

In these cases it seems that the shear retention factor was used as much as a numerical device to obtain good results to match experimental data than as a real model of the physical phenomenon. Mohamed[23] argued that this was due to the actual contribution of shear transfer mechanisms, i.e. dowel action and interface shear transfer, not precisely yet known and hence more experimental data and a unification of existing data is needed. To achieve an aim of incorporating a realistic shear retention factor (β) to model shear transfer across cracked concrete, β was assumed by Phillips and Mohamed[24] to quadratic function of the fictitious direct strain "ϵ" normal to the crack as shown in Figure (8.4f), where β_1, β_2 and β_3 are shear retention parameters defining the shape of the curve. These factors can be interpreted as follows: β_1 represents the sudden loss of stiffness at crack formation, β_2 represents the residual stiffness due to dowel action of any steel crossing a crack once a crack has opened sufficiently for interface shear transfer to cease, and β_3 represents the rate of decay of stiffness as the crack widens and the crack surface deteriorates.

The question arises as to which of these formulations, if any, describe the shear transfer behaviour of cracked reinforced concrete element best. To answer this question, a study of the variation of the shear modulus of cracked reinforced concrete based on the present experimental results is undertaken in the next section.

8.4 Shear modulus of cracked reinforced concrete

In the formulations discussed in the previous section, the shear retention factor is specified as a function of strain normal to the crack plane. However, in real situation and as the present tests indicated shear transfer causes an increase in both crack width and shear displacement. Therefore, it is evident that the shear modulus of cracked reinforced concrete is not only a function of strain normal to the crack plane but also can be a function of shear strain. Accordingly, the relationships of shear modulus of crack section G' versus both normal and shear strain were investigated.

Figures (8.5-8.7) and (8.8-8.10) show these relationships for the combined action specimens with initial crack widths 0.125mm and 0.40mm and transverse reinforcement of high tensile deformed bars and those with initial crack width 0.125mm and mild tensile plain bars.

It is important to state that the main interest of this part of the study is focused on the manner of degradation of G' after crack occurs rather than how much the loss in the shear modulus of uncracked reinforced concrete would be once a crack occurs. Therefore, the least square method was used to obtain the best fit of the average of G' for the reinforcement ratios used which are ranged between 0.28% to 1.68%.

The following expressions are suggested for calculating the shear modulus of cracked reinforced concrete under monotonic load:

$$G' = A.B^{\epsilon/\epsilon u} \quad (N/mm^2) \qquad (8.2a)$$

where ϵ is the lateral strain normal to the crack plane, ϵ_u is the ultimate lateral strain measured at ultimate shear load, and A & B are parameters which depend on the initial crack width and type of transverse reinforcement. As was concluded in chapter (7), the type of transverse reinforcement had an insignificant effect on shear transfer behaviour compared to that of initial crack width which is indirect way the initial lateral strain. Hence, the parameters A and B can be expressed as a function of initial lateral strain (ϵ_o) as follows

$$A = 6.346 - 1.0550x10^3(\epsilon_o) \qquad (8.2b)$$

$$B = 0.206 + 0.0207x10^3(\epsilon_o) \qquad (8.2c)$$

An alternative equation for shear modulus of cracked reinforced concrete mainly as a function of shear strain can be expressed as follows:

$$G' = A_1.B_1^{(\gamma/\gamma_u)} \quad (N/mm^2) \qquad (8.3a)$$

where γ is shear strain, γ_u is the ultimate shear strain measured at ultimate shear load and the parameters A_1 & B_1 are given by

$$A_1 = 6.244 - 0.9887x10^3(\epsilon_o) \qquad (8.3b)$$

$$B_1 = 0.226 + 0.0034x10^3(\epsilon_o) \qquad (8.3c)$$

The fit of Equations (8.2) and (8.3) to the test results is shown in

Figures (8.5-8.7) and (8.8-8.10).

From a comparison between the currently measured variation of G' and those suggested by the previous investigators shown in Figure (8.4) the following conclusions can be drawn:

1. The shear retention factor "β" or G' is not only function of normal strain to the crack plane but also can be a function of shear strain.

2. The representation of shear transfer by the unchanged shear modulus of cracked sections[13],[14], Figure (8.4a) or by neglecting any shear transfer across the crack[15],[16] is completely unrealistic.

3. Constant reduction of shear stiffness after cracking[18],[19], Figure (8.4c) is rough simplification of the real behaviour.

4. Linear reduction of shear stiffness[21] after cracking, Figure (8.4d) is not accurate model. Moreover, the assumption of the inability of the cracked section to sustain any shear forces at ultimate load is not true.

5. Shear modulus of cracked reinforced concrete according to Al-Mahaidi[22] and Phillips/Mohamed[24] are consistent with the current test results of this study.

However, further analysis is made to provide additional information which might cover some aspects that are already raised by Mohamed[23] of the shortcoming of knowing the contribution of dowel action and

interface shear transfer mechanism. Also, the effect of initial crack width, type of transverse reinforcement and type of shear load on the shear modulus of cracked reinforced concrete is investigated.

8.4.1 Effect of studied parameters

(1) Effect of initial crack width

The effect of initial crack width on shear modulus of cracked reinforced concrete under both monotonic and repeated loading is investigated in this section. Under monotonic loading Equations (8.2) and (8.3) are used to compare the difference in G' due to the increase in initial crack width from 0.125mm to 0.40mm as shown in Figures (8.11) and (8.12). It can be seen that the increase in initial crack width from 0.125mm to 40mm resulted in an average reduction of 52% in the cracked shear modulus.

However, the difference between the shear modulus G' of specimens with different initial crack widths was decreased as the lateral or shear strain increase as shown in the above mentioned Figures and Table (8.1). This reflects the dominant contribution of interface shear transfer mechanism at the initial stage and its degradation at later stages where dowel action dominates. This explanation is evident from the case of repeated loading where such loading would affect the roughness of the crack surfaces as number of load cycles increased and a smaller influence would be expected compared to monotonic load.

However, before showing the effect of initial crack width under repeated load a least squares fit was made to the experimental results of the shear modulus G' versus both lateral and shear strains

under repeated load. The last cycle was used for this purpose. The following expressions were obtained:

$$G' = A_2.B_2^{(\epsilon/\epsilon_u)} \quad N/mm^2 \qquad (8.4a)$$

where A_2 and B_2 are coefficients which were derived using similar assumptions to the case of monotonic load and are given by

$$A_2 = 4.109 - 0.333x10^3(\epsilon_o) \qquad (8.4b)$$

$$B_2 = 0.397 - 0.0174x10^3(\epsilon_o) \qquad (8.4c)$$

and

$$G' = A_3.B_3^{(\gamma/\gamma_u)} \quad N/mm^2 \qquad (8.5a)$$

where the coefficients A_3 and B_3 are given by

$$A_3 = 4.26 - 0.354x10^3(\epsilon_o) \qquad (8.5b)$$

$$B_3 = 0.361 - 0.0179x10^3(\epsilon_o) \qquad (8.5c)$$

The fit of Equations (8.4) and (8.5) to the experimental results are shown in Figures (8.13)-(8.15) and (8.16)-(8.18).

The effect of initial crack width on G' under repeated load for the last cycle is shown in Figures (8.19) and (8.20) and Table (8.2). It can be seen that the increase in initial crack width from 0.125 to 0.40mm resulted in an average reduction of 30% compared to 50% under monotonic load. Also the difference between G' for the two different initial crack widths at the initial and later stages is significantly less than that found under monotonic loading.

(2) Effect of type of transverse reinforcement

Since an insignificant influence was expected on shear transfer when different types of transverse reinforcement was used, i.e. high

tensile deformed bars compared to mild tensile plain bars, Equations which fit the test results of specimens with these types of transverse reinforcement should be used rather than those equations previously suggested. Therefore, the following equations were used for studying the effect of this parameter under monotonic load and the last cycle of repeated load:

(1) Monotonic Load

(a) for high tensile deformed bars

$$G' = 5.439\ (.2327)^{\epsilon/\epsilon_u} \qquad (8.6)$$

$$G' = 5.396\ (.2288)^{\gamma/\gamma_u} \qquad (8.7)$$

(b) for mild tensile plain bars

$$G' = 4.616\ (.2318)^{\epsilon/\epsilon_u} \qquad (8.8)$$

$$G' = 4.622\ (.2322)^{\gamma/\gamma_u} \qquad (8.9)$$

(2) Repeated Load

(a) for high tensile deformed bars

$$G' = 4.238\ (.3394)^{\epsilon/\epsilon_u} \qquad (8.10)$$

$$G' = 4.4026\ (.2921)^{\gamma/\gamma_v} \qquad (8.11)$$

(b) for mild tensile deformed bars

$$G' = 3.148\ (.4116)^{\epsilon/\epsilon_u} \qquad (8.12)$$

$$G' = 3.233\ (.3864)^{\epsilon/\epsilon_u} \qquad (8.13)$$

A comparison of these equations is shown in Figures (8.21) & (8.22) and Table (8.3) under monotonic load and Figures (8.23) & (8.24) and Table (8.4) under repeated load.

It can be seen that under monotonic load the use of mild tensile plain bars results in an average reduction of 15% to the shear

modulus G' compared to high tensile deformed bars. This reflects the minor effect of bond condition between the transverse reinforcement and the surrounding concrete. In the case of repeated loading the average reduction in the shear modulus G' was approximately equal to that of the monotonic load. However, for repeated loading the difference between the shear modulus G' of the two different types of transverse reinforcement diminishes as the lateral or shear strain increases as shown in Figures (8.23) and (8.24) and Table (8.4). This reflects the greater damage to the bond between the deformed bars and the surrounded concrete due to a wedging action which would affect the dominant interface shear transfer mechanism at initial stages.

8.4.2. Relative contribution of dowel action and interface shear transfer mechanisms

Based on the combined and dowel actions test results an attempt is made in this section to highlight the relative contributions of interface shear transfer and dowel action on the total shear modulus of cracked reinforced concrete.

A least squares fitting of the experimental shear modulus of dowel action specimen versus lateral and shear strain resulted in the following expressions

$$G' = 0.4582 + \frac{0.00095}{\epsilon/\epsilon_u} \quad N/mm^2 \qquad (8.14)$$

$$G' = 0.43308 + \frac{0.0020}{\gamma/\gamma_u} \quad N/mm^2 \qquad (8.15)$$

where

G' = shear modulus of dowel action specimens

ϵ = lateral strain normal to the shear plane

ϵ_u = ultimate lateral strain

γ = shear strain

γ_u = ultimate shear strain.

These are illustrated in Figure (8.25) and (8.26). A comparison between the shear modulus G' for combined and dowel actions specimens versus lateral strain is shown in Figures (8.27) and (8.28).

It can be seen that for cracked sections with initial crack width of 0.125mm the interface shear transfer contributes approximately 90% in the initial stages. As the lateral strain increases the interface shear transfer degrades to 82% during the middle stage and to 63% at the final stage. At the same time dowel action develops in the opposite manner showing its increase as lateral strain increases, 10% at the initial stage and 18% and 34% during the middle and final stages.

In the case of the initial crack width of 0.40mm, it can be seen that relative contribution of the two mechanisms changes considerably compared to an initial crack width of 0.125mm. The dowel action exhibits a great responsibility for resisting the shear forces (about 25%) at the initial stages and 40% and 74% during the middle and final stages. Therefore, it can be recognized that the effect of initial condition of cracked reinforced concrete on the relative contribution of the interface shear transfer and dowel action is very important.

8.5 Design of shear transfer strength

The major international standards or codes of practices such as British Standard BS 8110:Part 1:1985[2], American Code ACI 813-83[1]

and PCI[25] provide design method for conditions where it is appropriate to consider shear transfer across a given plane, such as an existing or potential crack or an interface between two concretes cast at different times and joints transmitting shear. Other expressions have also been proposed by Mattock[3] and Walraven[4] to predict the ultimate shear transfer strength as described in chapter (2). These different formulations are summarized here for the purpose of comparison as follows:

ACI 813-83[1] Equation

$$V_u = \mu A_s f_y \qquad (8.16)$$

where

V_u is ultimate shear transfer strength

A_s is area of transverse reinforcement

μ is coefficient of friction which varies between 0.7 and 1.4.

In this equation provision is made that the shear strength shall not be taken greater than $0.20 f'_c A_c$ nor $800 A_c$ in pounds where A_c is the area of concrete section resisting shear transfer.

PCI[25] Equation

$$V_u = \mu A_s f_y \left[\frac{300}{\rho f_y} + 0.50 \right] \qquad (8.17)$$

where

V_u is ultimate shear transfer strength in pounds

A_s is area of transverse reinforcement (in^2)

f_y is yield stress of transverse reinforcement (psi)

ρ is transverse reinforcement ratio

μ is coefficient of friction.

This equation to be used if ρf_y exceeds 600 psi.

BS:8110[2] Equation

$$V_u = 0.6\ F_b \tan a_f \qquad (8.18)$$

where

F_b is $0.87\ f_y\ A_s$

A_s is area of transverse reinforcement

$\tan a_f$ is friction coefficient which can be taken 0.70, 1.4 and 1.70 depending on the surface condition of shear plane.

Mattock's[3] Equation

$$V_u = [400 + 0.80\ \rho f_y]A_c \qquad (2.21)$$

where

V_u is ultimate shear transfer strength in pounds.

f_y is yield stress of transverse reinforcement (psi)

A_c is area of shear plane (in^2

ρ is transverse reinforcement ratio.

A provision is made for this Equation which is that V_u should not be more than $0.3\ f_c'A_c$ where f_c' is concrete compressive stress.

Walraven's[4] Equation

$$v_u = C_1\ (\rho f_y)^{C_2} \qquad (2.22)$$

where

v_u is ultimate shear transfer stress (N/mm^2)

f_y is yield stress of transverse reinforcement (N/mm^2)

ρ is transverse reinforcement ratio

$c_1 = f_{cu}^{0.36}$

$c_2 = 0.09\ f_{cu}^{0.46}$.

Walraven suggested that this equation should be multiplied by a reduction factor 0.85.

A comparison between the calculated ultimate shear strength according to the above equations and the present experimental results for specimens with initial crack widths of 0.125mm and 0.40mm and with transverse reinforcement of high tensile deformed bars and mild tensile plain bars is shown in Figures (8.29a,b) and Tables (8.5a,b,c). Based on those comparisons the following observations can be made:

- The ACI Equation within its limits showed more conservative results for the reinforced cracked section with a small initial crack width of 0.125mm. The equation underestimated the experimental results of the specimens with initial crack widths 0.125mm and 0.40mm by an average 45% and 29% respectively.

- BS:8110 Equation also gave too conservative a prediction even when the recommended maximum shear coefficient of 1.70 was used. This can be attributed to the factor of 0.60 used in this equation. The equation underestimated the test results within the whole range of the reinforcement factor ρf_y used, i.e. 1.33 to 8.99 N/mm^2, by an average of 60% and 50% for the specimens with initial crack widths 0.125 and 0.40mm respectively.

- The PCI Equation shows a close similarity to Mattock's Equation. This can be seen if the PCI Equation is rearranged as follows

$$v_u = \mu 300 + 0.5\, \mu\rho f_y \text{ psi} \qquad (8.19a)$$

Substitute μ by 1.4, then

$$v_u = 420 + 0.7\rho f_y \text{ psi} \qquad (8.19b)$$

Both the PCI and Mattock equation showed a good agreement with test results of specimens with large initial crack width of

0.40mm. For specimens with smaller initial crack of 0.125mm the equations were rather conservative and underestimated the experimental results by an average of 18.5% and 15% for the high tensile deformed bars and 22% and 18.5% for mild tensile plain bars.

- Walraven's Equation predicted the experimental ultimate shear transfer strength quite reasonably for a small initial crack width of 0.125mm by an averagve 0.92. However, for specimen with the larger initial crack width of 0.40mm it showed poorer correlation and overestimated the test results by an average of 14%. This may be attributed to not considering the effect of the different condition between the crack surfaces.

From the above observations, it can be concluded that there is not one unified equation which is capable and flexible enough to predict the ultimate shear transfer strength for all the influential parameters such as initial crack width, concrete strength, reinforcement ratio and the type of transverse reinforcement.

Based on the results of this study Equation (7.14) was proposed by the author in an attempt to overcome this shortening as follows:

$$V_u = \left[[0.552 + 0.141\ \rho f_y] - [0.549 w_o (1+0.08 \rho f_y)] \right] \sqrt{f_{cu}} \cdot A_c$$

The calculated ultimate shear transfer strength according to this Equation showed good agreement with present test results as previously shown in Figure (7.25) and Table (7.11a). The Equation also predicted quite reasonably the test results of Walraven [27] and Mattock[28], where the initial crack width varies between 0.01-0.23mm and concrete strength of 19 N/mm-56 N/mm^2, as shown in Table (7.11b).

A general Equation (7.16) proposed by the author in section 7.5.7 of chapter (7) can be used to calculate the ultimate shear transfer strength under repeated load. The predicted ultimate shear strengths showed good agreement with the present test results as shown in Table (7.21).

Equation (7.16) was also used to predict the test results of Mattock[29] under reversed cyclic load as shown in Table (8.6) and Figure (8.30). The equation showed quite reasonable and safe prediction. Thus, the limitations made in section 7.5.7 in chapter (7) regarding this Equation can be modified to include both the repeated and reversible cyclic load.

Also, for design purpose under repeated loading it is recommended that the ultimate shear transfer strength can be taken as 0.7-0.9 of the shear transfer strength under monotonic load.

Table (8.1): Effect of initial crack width on the shear modulus of cracked reinforced concrete under monotonic load.

Type of strain	Strain ratio	Shear modulus G' (N/mm^2)		Difference (N/mm^2)
		w_o = 0.125	w_o = 0.40	
Lateral strain	0.0	5.027	2.126	2.90
	0.5	2.420	1.142	1.278
	1.0	1.160	0.613	0.550
Shear strain	0.0	5.009	2.292	2.71
	0.5	2.40	1.120	1.28
	1.0	1.152	0.547	0.60

Table (8.2): Effect of initial crack width on the shear modulus of cracked reinforced concrete G' under repeated load (last cycle).

Type of strain	Strain ratio	Shear modulus G' (N/mm^2)		Difference (N/mm^2)
		w_o = 0.125 mm	w_o = 0.40 mm	
Lateral strain	0.0	3.69	2.77	0.92
	0.50	2.259	1.58	0.675
	1.0	1.385	0.90	0.485
Shear strain	0.0	3.81	2.84	0.97
	0.50	2.21	1.52	0.69
	1.0	1.287	0.82	0.467

Table (8.3): Effect of type of transverse reinforcement on shear modulus of crack reinforced concrete G' monotonic load.

Type of strain	Strain ratio	Shear modulus G' (N/mm^2)		Difference (N/mm^2)
		High tensile def. bars	Mild tensile plain bars	
Lateral strain	0.0	5.439	4.616	0.823
	0.50	2.623	2.22	0.403
	1.0	1.265	1.06	0.205
Shear strain	0.0	0.396	4.622	0.774
	0.50	2.581	2.22	0.361
	1.0	1.234	1.073	0.161

Table (8.4): Effect of type of transverse reinforcement on shear modulus of cracked reinforced concrete G' under repeated load (last cycle).

Type of strain	Strain ratio	Shear modulus G' (N/mm^2)		Difference (N/mm^2)
		High tensile def. bars	Mild tensile plain bars	
Lateral strain	0.0	4.238	3.148	1.09
	0.5	2.468	2.019	0.449
	1.0	1.438	1.295	0.143
Shear strain	0.0	4.402	3.233	1.169
	0.50	2.379	2.009	0.37
	1.0	1.286	1.249	0.037

Table (8.5a): Comparison between calculated and experimental ultimate shear transfer strength under monotonic loading for specimen with high tensile deformed bars and initial crack width = 0.125 mm.

Specimen number	Reinforcement ratio	$v_{u\,cal.}/v_{u\,exp.}$					v_{u} Exp. (N/mm^2)
		ACI (1) Eq.	BS:8110 (2) Eq.	PCI (25) Eq.	Mattock (3) Eq.	Walraven (4) Eq.	
3.1.1	0.28	0.46	0.23	0.86	0.86	0.92	4.69
3.1.2	0.56	0.64	0.30	0.72	0.75	0.91	7.16
3.1.3	1.12	0.94	0.49	0.84	0.90	0.99	8.88
3.1.4	1.68	1.24	0.57	0.84	0.91	0.93	11.52

Table (8.5b): Comparison between calculated and experimental ultimate shear transfer strength under monotonic loading for specimen with high tensile deformed bars and initial crack width = 0.40 mm.

Specimen number	Reinforcement ratio	$v_{u\,cal.}/v_{u\,exp.}$					v_{u} Exp. (N/mm^2)
		ACI (1) Eq.	BS:8110 (2) Eq.	PCI (25) Eq.	Mattock (3) Eq.	Walraven (4) Eq.	
3.2.1	0.28	0.55	0.30	1.10	1.10	1.17	3.61
3.2.2	0.56	0.88	0.42	0.99	1.03	1.15	5.19
3.2.3	1.12	1.50	0.61	1.06	1.13	1.20	7.05
3.2.4	1.68	1.35	0.64	0.96	1.04	1.04	10.13

Table (8.5c): Comparison between calculated and experimental ultimate shear transfer strength under monotonic loading for specimens with mild tensile plain bars and initial crack width = 0.125 mm.

Specimen number	Reinforcement ratio	$v_{u\,cal.}/v_{u\,exp.}$					v_{u} Exp. (N/mm^2)
		ACI (1) Eq.	BS:8110 (2) Eq.	PCI (25) Eq.	Mattock (3) Eq.	Walraven (4) Eq.	
3.3.1	0.28	0.42	0.23	0.89	0.89	0.89	4.19
3.3.2	0.56	0.53	0.29	0.71	0.73	0.83	6.52
3.3.3	1.12	0.86	0.47	0.78	0.83	0.97	8.13
3.3.4	1.68	0.97	0.54	0.76	0.81	0.91	10.70

Table (8.6) Comparison between the experimental results[29] and the predicted ultimate transfer strength by combined action under reversed cyclic load using Equation (7.16).

Specimen No.	Reinf. parameter ρf_y (N/mm^2)	Initial crack width w_o (mm)	Reinf. yield stress f_y (N/mm^2)	Concrete comp. stress f_{cu} (N/mm^2)	Loading history		Exp. Ult. shear stress v_u (exp.) (N/mm^2)	Cal. Ult. shear stress v_u (cal.) (N/mm^2)	$\frac{v_u \text{ (cal.)}}{v_u \text{ (exp.)}}$
					No. of cycles	Range of load ±% of v_u*			
LC-1	2.523	0.254	420	32.7	1 - 10 11 - 15 16 - 20 21 - 25 26 - 30 31 - 35 36	50 58 66 74 82 90 98	4.96	3.60	0.72
LC-2	2.523	0.381	427	38.78	1 - 10 11 - 15 16 - 20 21 - 25 26 - 30 31 - 35 36 - 40 41 - 45 46	50 58 66 74 82 90 89 106 114	5.37	3.51	0.65

* v_u is calculated ultimate shear stress according to Mattock's Equation (2.21).

Table (8.6) (Cont'd). Comparison between the experimental results[29] and the predicted ultimate transfer strength by combined action under reversed cyclic load using Equation (7.16).

Specimen No.	Reinf. parameter ρf_y (N/mm^2)	Initial crack width w_o (mm)	Reinf. yield stress f_y (N/mm^2)	Concrete comp. stress f_{cu} (N/mm^2)	Loading history		Exp. Ult. shear stress v_u (exp.) (N/mm^2)	Cal. Ult. shear stress v_u (cal.) (N/mm^2)	$\frac{v_u \text{ (cal.)}}{v_u \text{ (exp.)}}$
					No. of cycles	Range of load ±% of v_u*			
LC-3	2.523	0.584	427	36.45	1 - 10 11 - 15 16 - 20 21 - 25 26	50 58 66 74 82	3.99	3.46	0.86
MC-1	3.03	0.279	344.75	33.4	1 - 10 11 - 15 16 - 20 21 - 25 26 - 30 31	50 58 66 74 82 90	4.67	4.0	0.86
MC-2	3.03	0.430	351.64	33.8	1 - 10 11 - 15 16 - 20 21 - 25 26 - 30 31	50 58 66 74 78 82	4.24	3.697	0.87

* v_u is calculated ultimate shear stress according to Mattock's Equation (2.21).

Table (8.6) (Cont'd.) Comparison between the experimental results[29] and the predicted ultimate transfer strength by combined action under reversed cyclic load using Equation (7.16).

Specimen No.	Reinf. parameter ρf_y (N/mm^2)	Initial crack width w_o (mm)	Reinf. yield stress f_y (N/mm^2)	Concrete comp. stress f_{cu} (N/mm^2)	Loading history		Exp. ult. shear stress v_u (exp.) (N/mm^2)	Cal. ult. shear stress v_u (cal.) (N/mm^2)	$\frac{v_u \text{ (cal.)}}{v_u \text{ (exp.)}}$
					No. of cycles	Range of load ±% of v_u*			
HC-1	4.55	0.254	337.85	34	1 - 10	50	7.17	5.10	0.71
					11 - 15	58			
					16 - 20	66			
					21 - 25	74			
					26 - 30	82			
					31 - 35	90			
					36 - 40	98			
					41 - 45	106			
					46	114			
HC-2	4.55	0.381	341	34	1 - 10	50	6.68	4.85	0.73
					11 - 15	58			
					16 - 20	66			
					21 - 25	74			
					26 - 30	82			
					31 - 35	90			
					36 - 40	98			
					41	106			

* v_u is calculated ultimate shear stress according to Mattock's Equation (2.21).

Table (8.6) (Cont'd.) Comparison between the experimental results[29] amd the predicted ultimate transfer strength by combined action under reversed cyclic load using Equation (7.16).

Specimen No.	Reinf. parameter ρf_y (N/mm^2)	Initial crack width w_o (mm)	Reinf. yield stress f_y (N/mm^2)	Concrete comp. stress f_{cu} (N/mm^2)	Loading history		Exp. Ult. shear stress v_u(exp.) (N/mm^2)	Cal. Ult. shear stress v_u (cal.) (N/mm^2)	$\frac{v_u \text{ (cal.)}}{v_u \text{ (exp.)}}$
					No. of cycles	Range of load ±% of v_u*			
HC-3	4.55	0.635	344	37	1 - 10 11 - 15 16 - 20 21 - 25 26 - 30 31	50 58 66 74 82 90	5.86	4.30	0.73

* v_u is calculated ultimate shear stress according to Mattock's Equation (2.21).

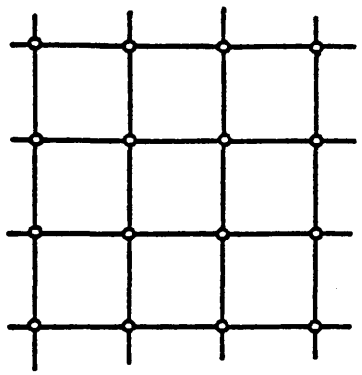

(a) mesh before cracking

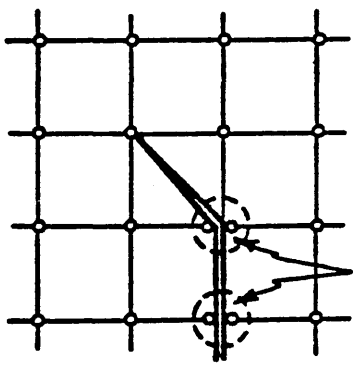

(b) mesh after cracking

Figure(8.1) Discrete crack representation

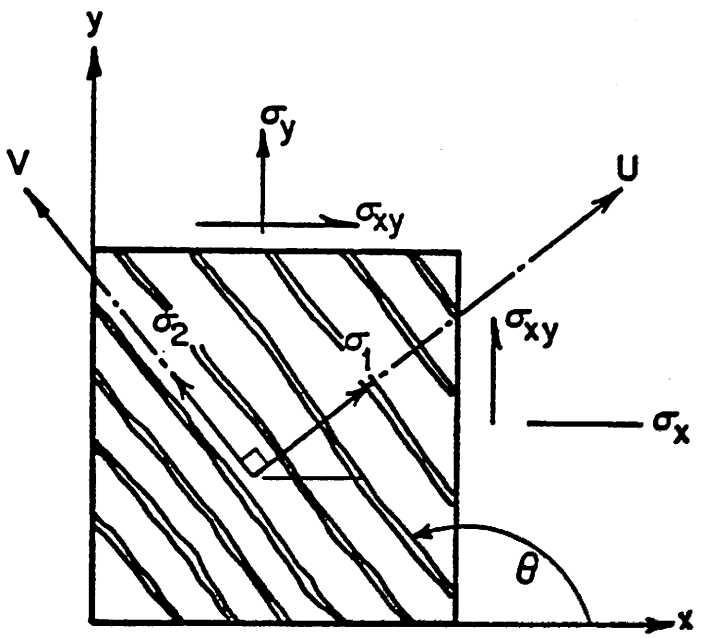

Figure(8.2) Smeared crack representation.

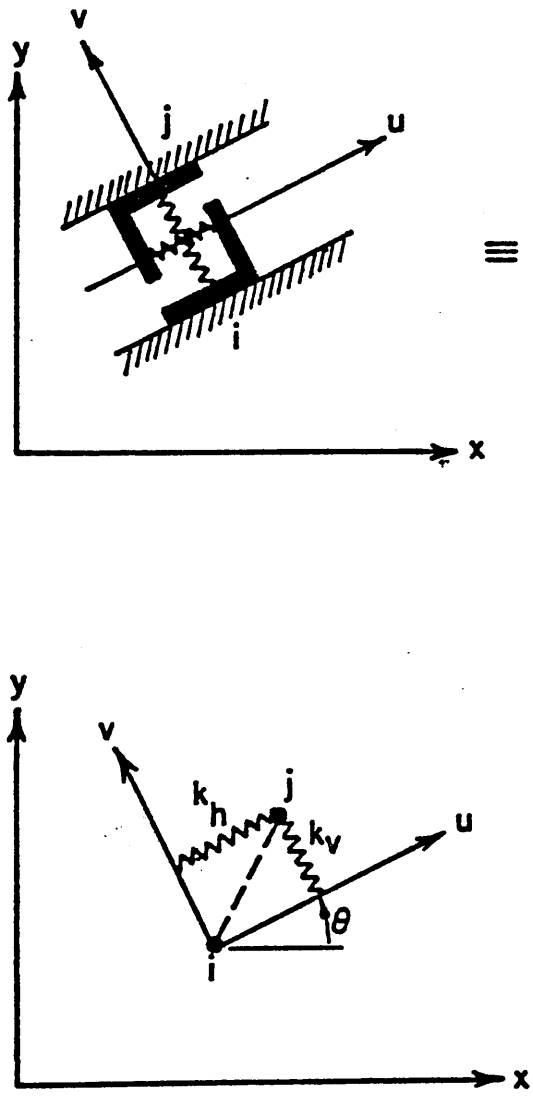

Figure(8.3) Linkage element.

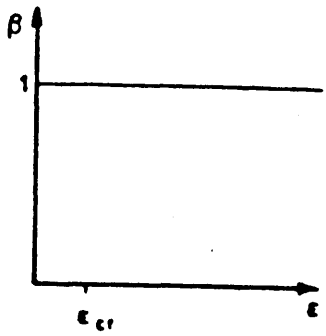

a) Franklin[13] and Isenberg/Adham[14]

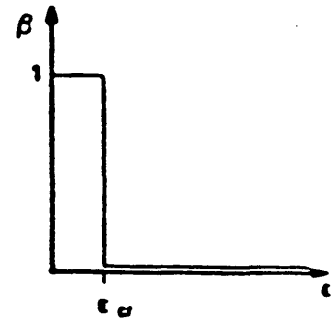

(b) Cervenka[15] and Loov[16]

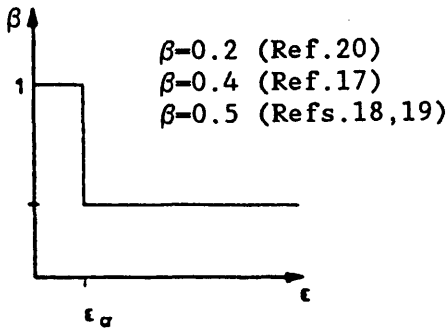

(c)Hand et al[17],Suidan/Schnobrich[18] Zienkiewics et al[19],and Yuzugullu[20]

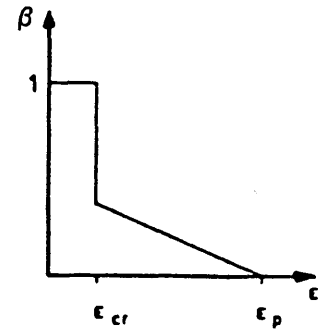

(d) Cedolin/Dei poli[21]

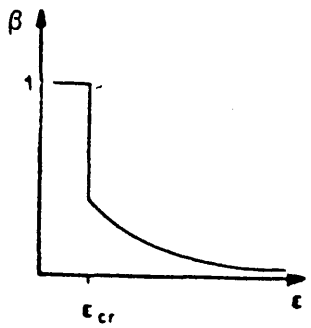

(e) Al-Mahidi[22]

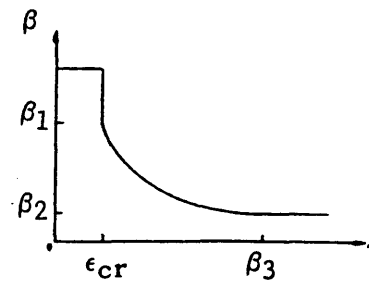

(f) Phillips/Mohamed[24]

Figure(8.4) Comparison between shear retention factor "β" used by previous investigators.

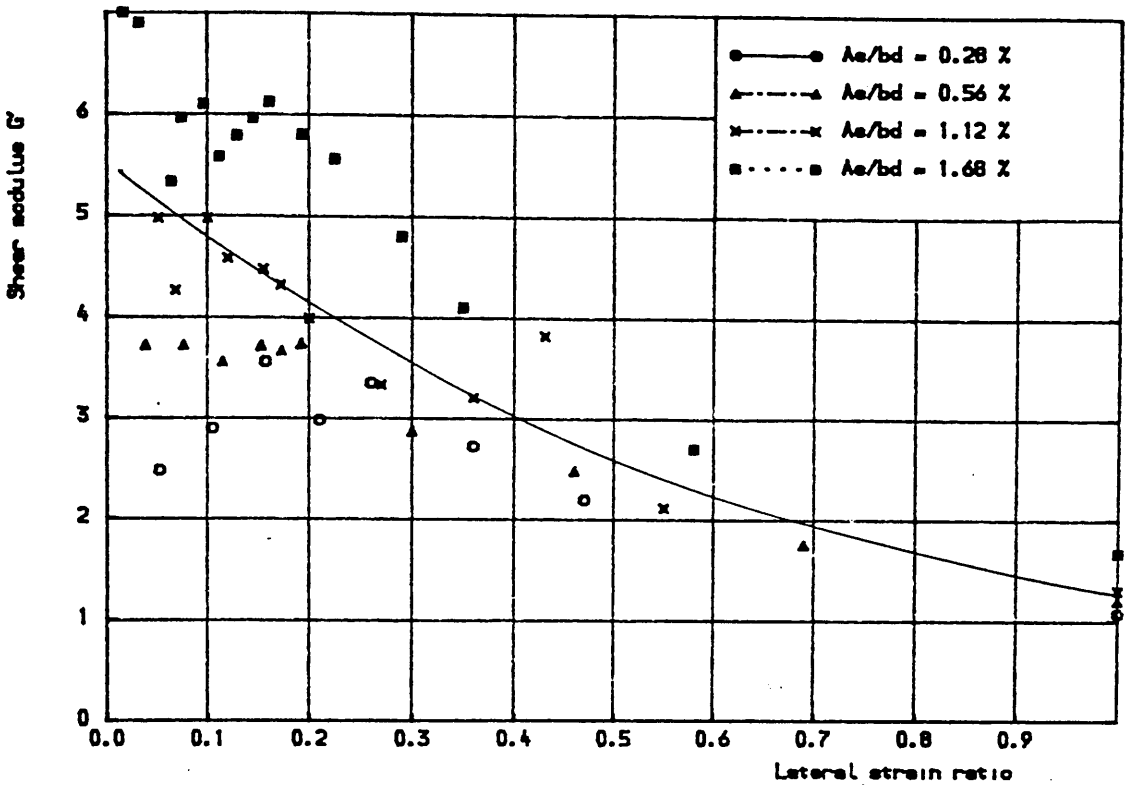

Figure(8.5) Shear modulus G' vs. lateral strain for the combined action specimens with w_o = 0.125mm and high tensile deformed bars tested under monotonic load.

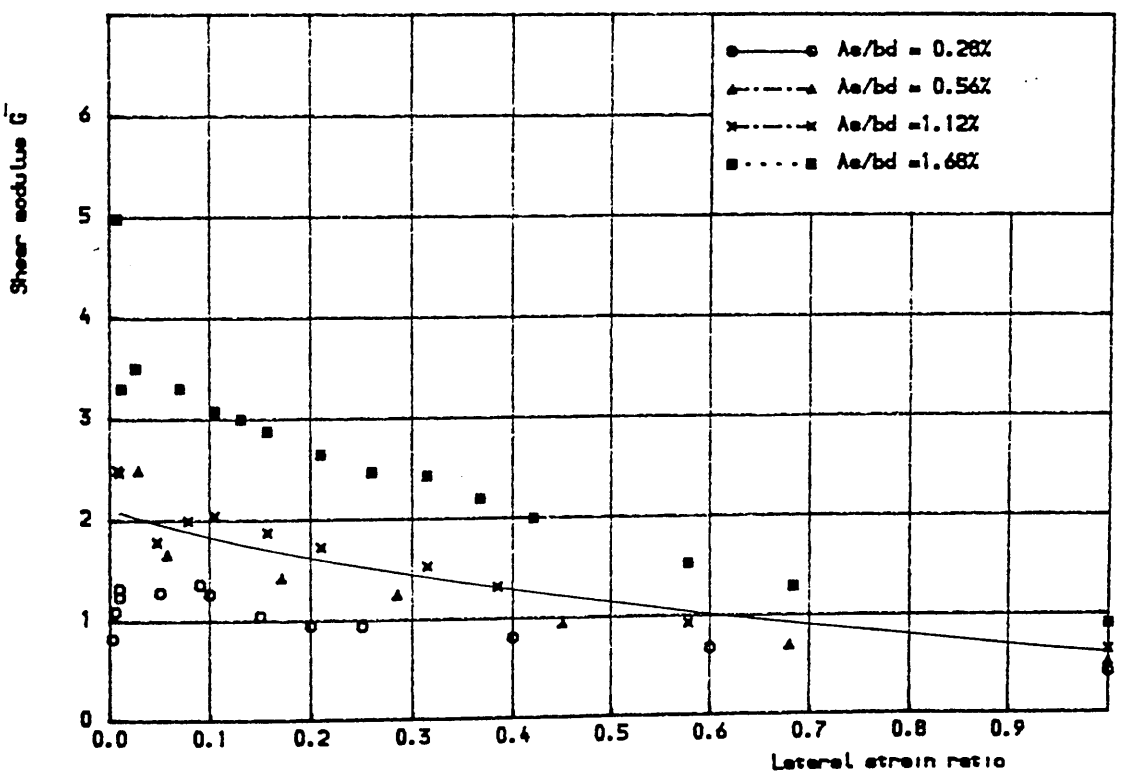

Figure(8.6) Shear modulus G' vs. lateral strain for the combined action specimens with w_o = 0.40mm and high tensile deformed bars tested under monotonic load.

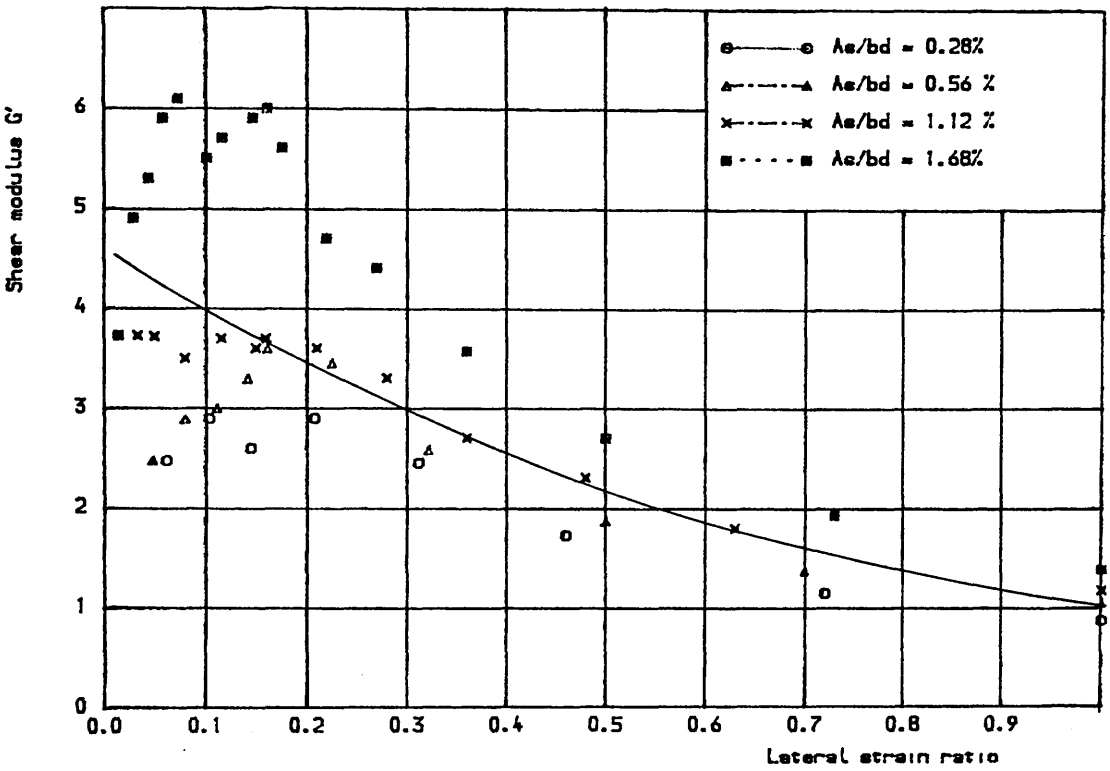

Figure(8.7) Shear modulus G' vs. lateral strain for the combined action specimens with w_o = 0.125mm and mild tensile plain bars tested under monotonic load.

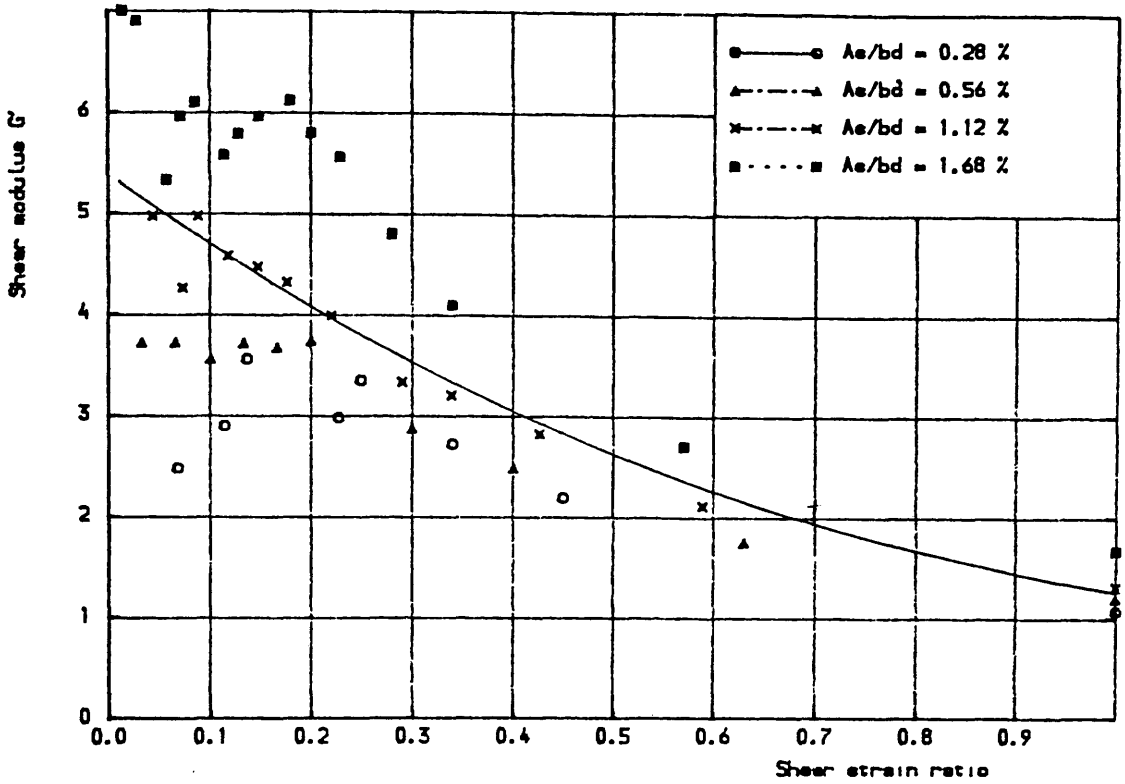

Figure(8.8) Shear modulus G' vs. shear strain for the combined action specimens with w_o = 0.125mm and high tensile deformed bars tested under monotonic load.

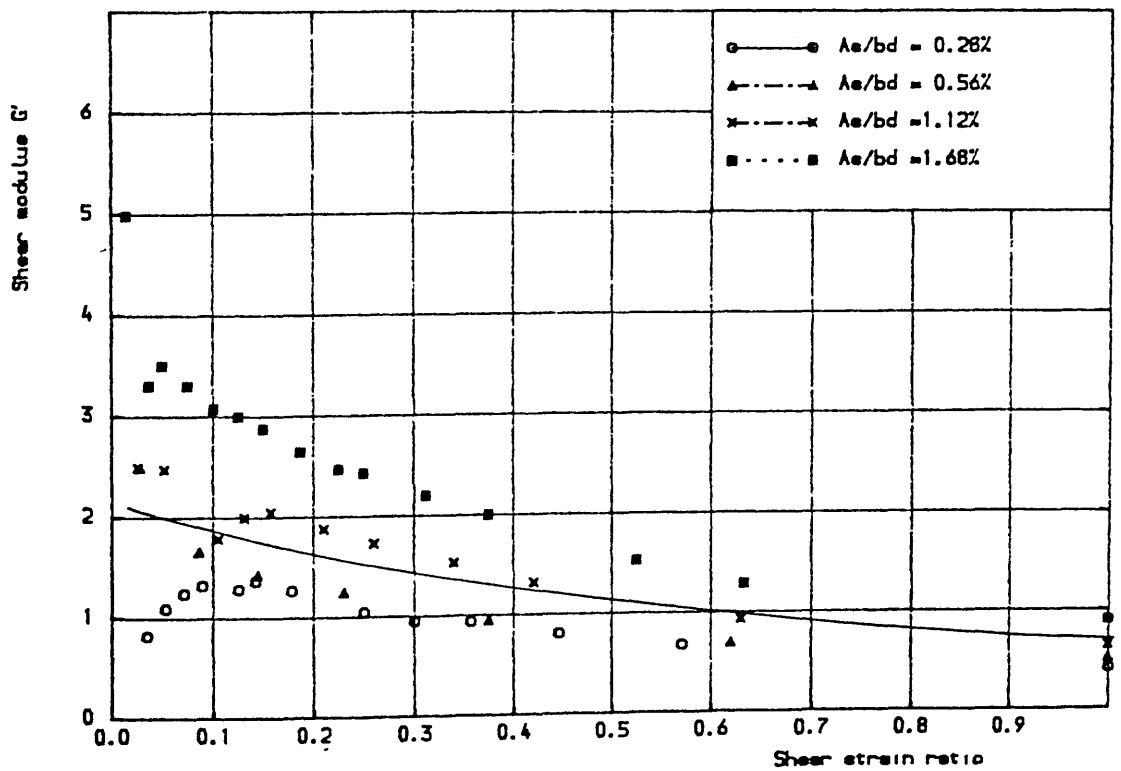

Figure(8.9) Shear modulus G' vs. shear strain for the combined action specimens with w_o = 0.40mm and high tensile deformed bars tested under monotonic load.

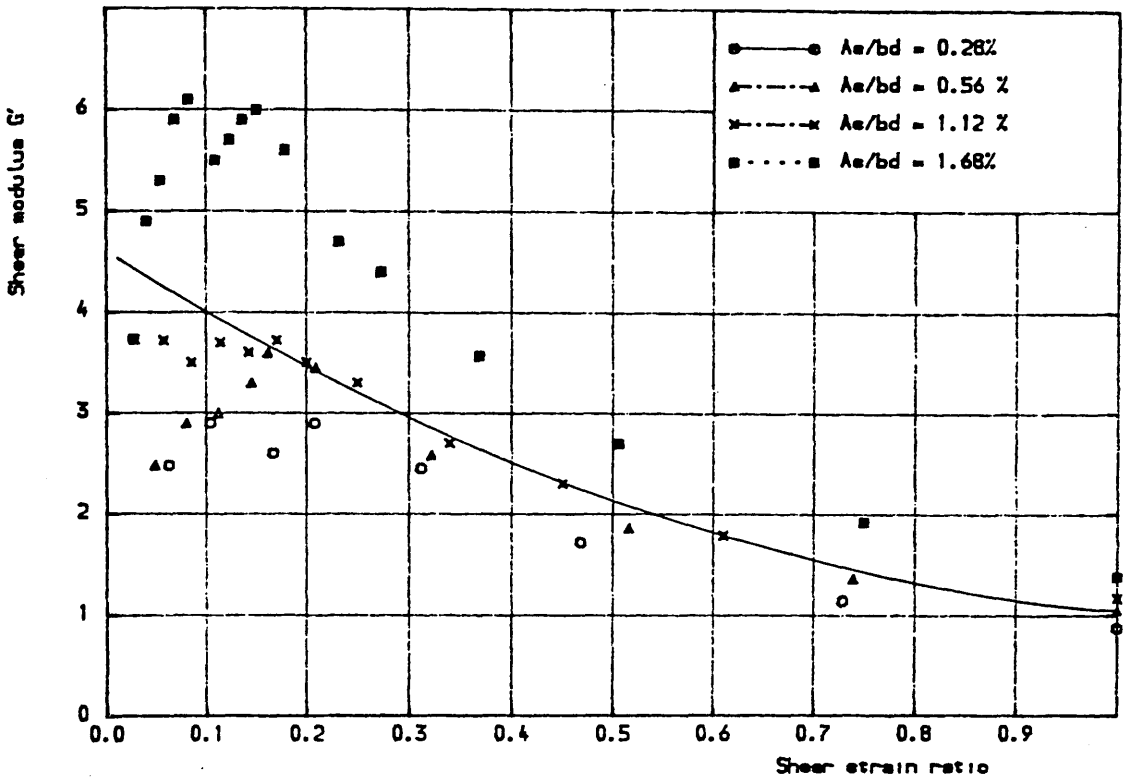

Figure(8.10) Shear modulus G' vs. shear strain for the combined action specimens with w_o=0.125 mm and mild tensile plain bars tested under monotonic load.

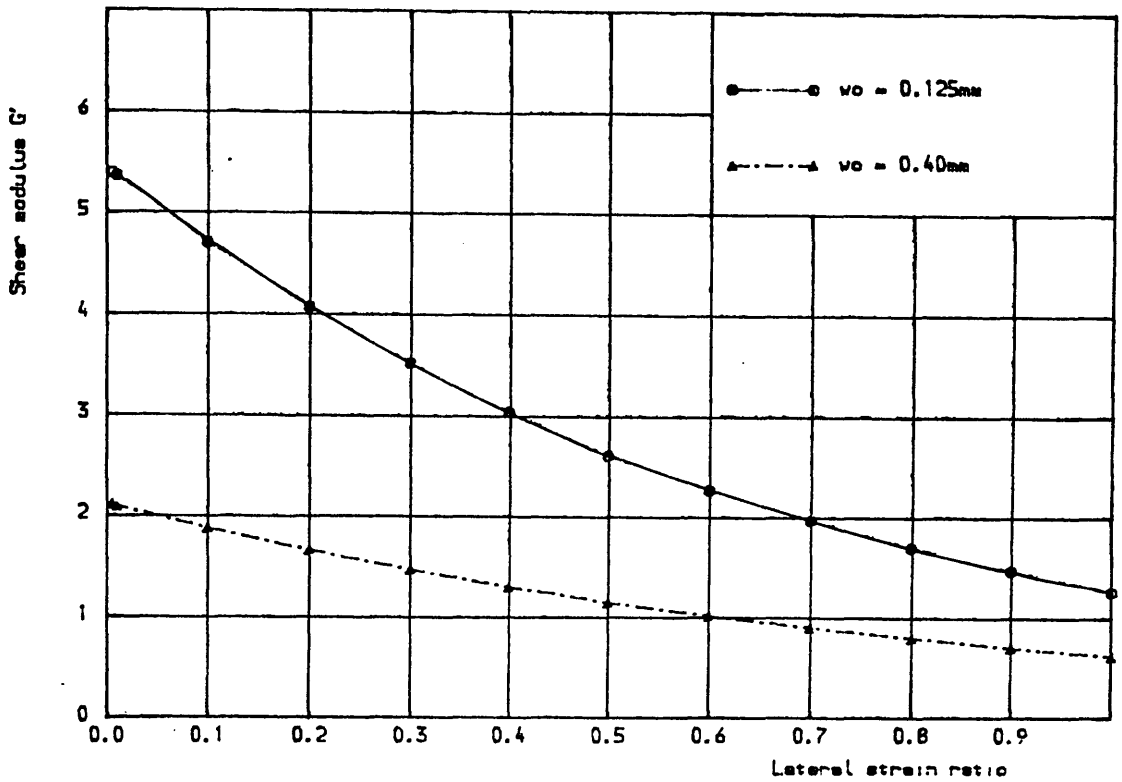

Figure(8.11) Effect of initial crack width (w_o) on shear modulus G' vs. lateral strain for the combined action under monotonic load.

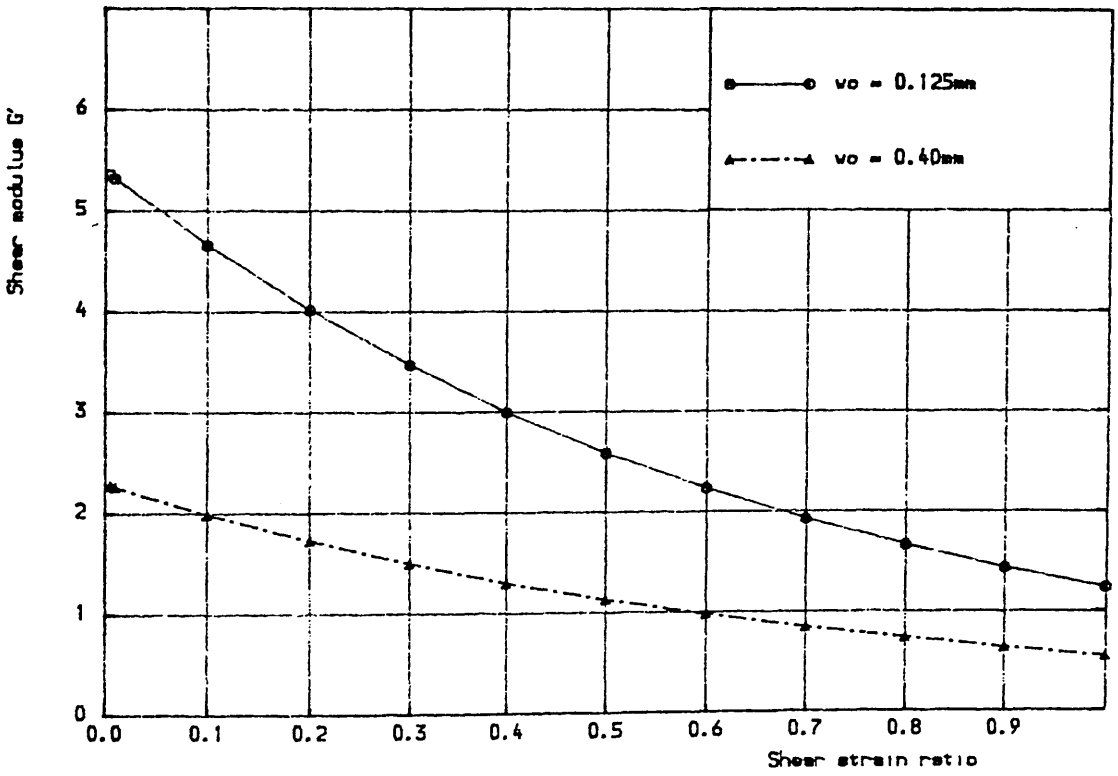

Figure(8.12) Effect of initial crack width (w_o) on shear modulus G' vs. shear strain for the combined action under monotonic load.

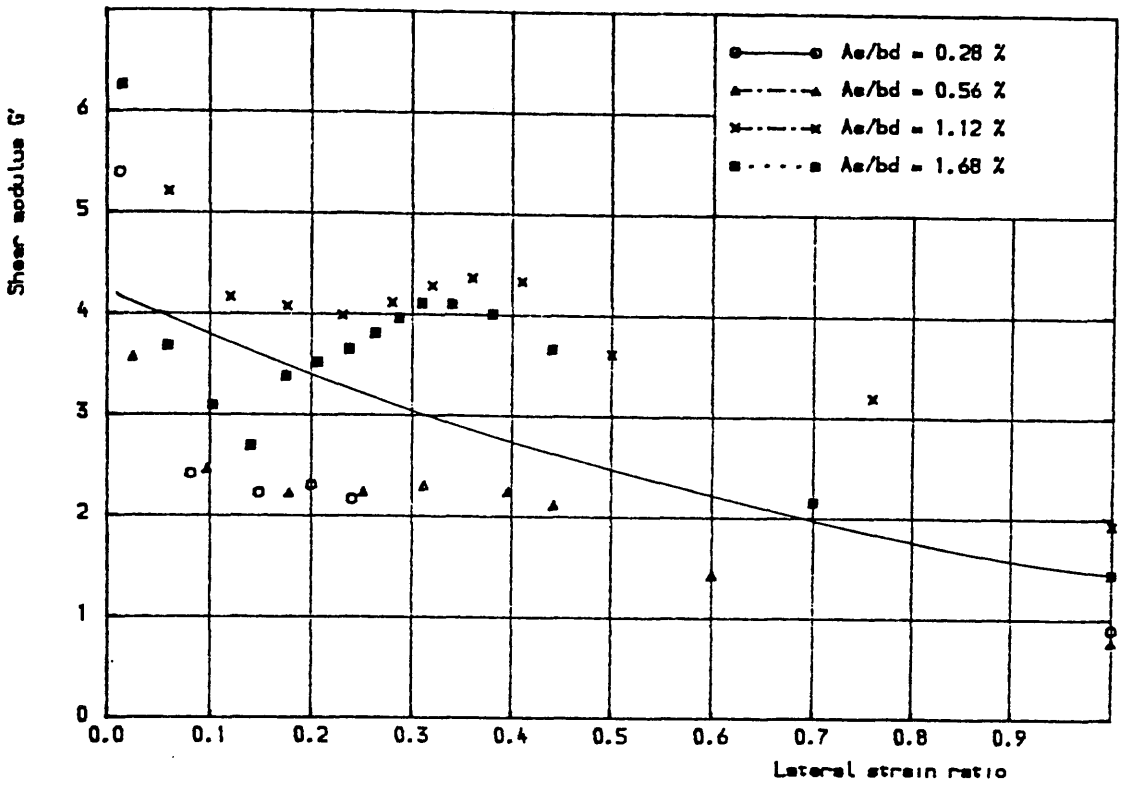

Figure(8.13) Shear modulus G' vs. lateral strain for the combined action specimens with w_o = 0.125mm and high tensile deformed bars tested under repeated load,last cycle.

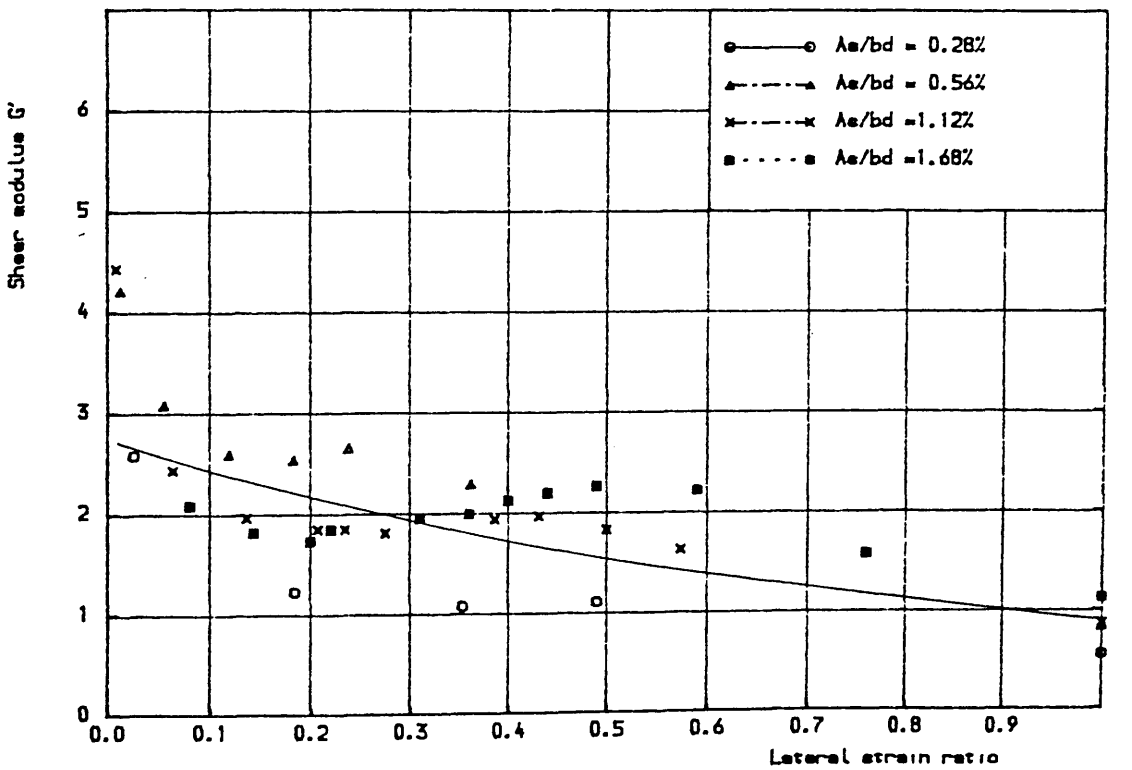

Figure(8.14) Shear modulus G' vs. lateral strain for the combined action specimens with w_o = 0.40mm and high tensile deformed bars tested under repeated load,last cycle.

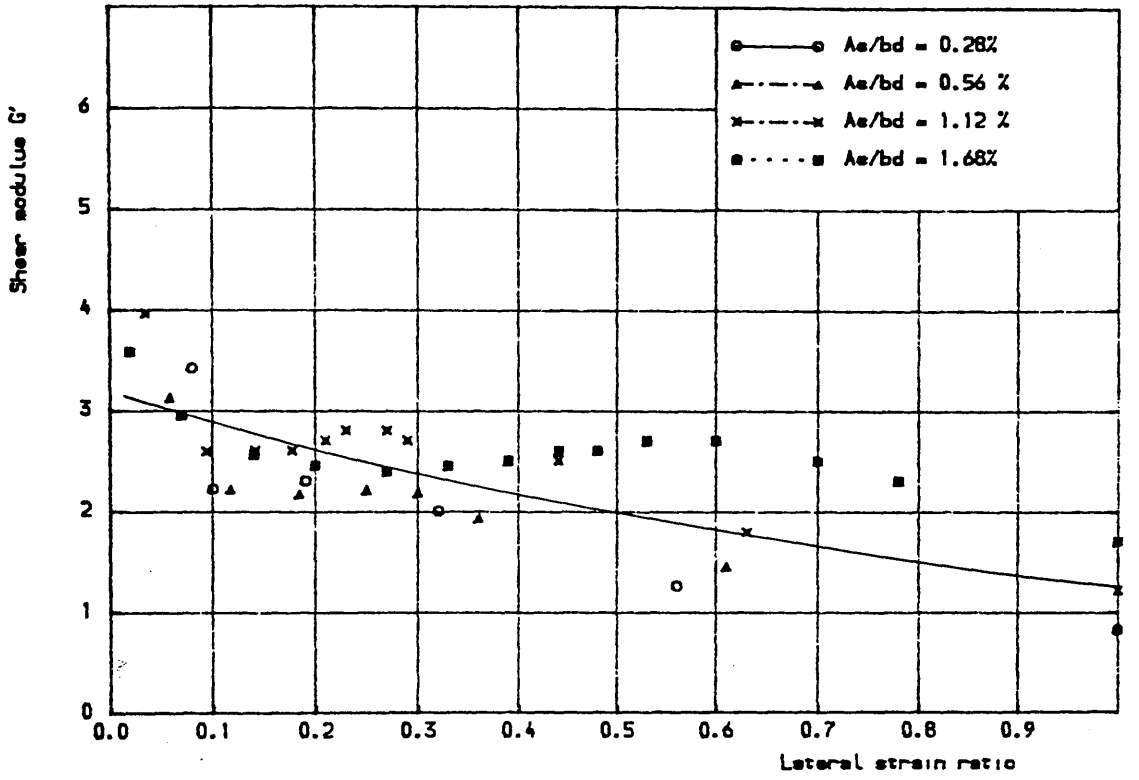

Figure(8.15) Shear modulus G' vs. lateral strain for the combined action specimens with w_o = 0.125mm and mild tensile plain bars tested under repeated load,last cycle.

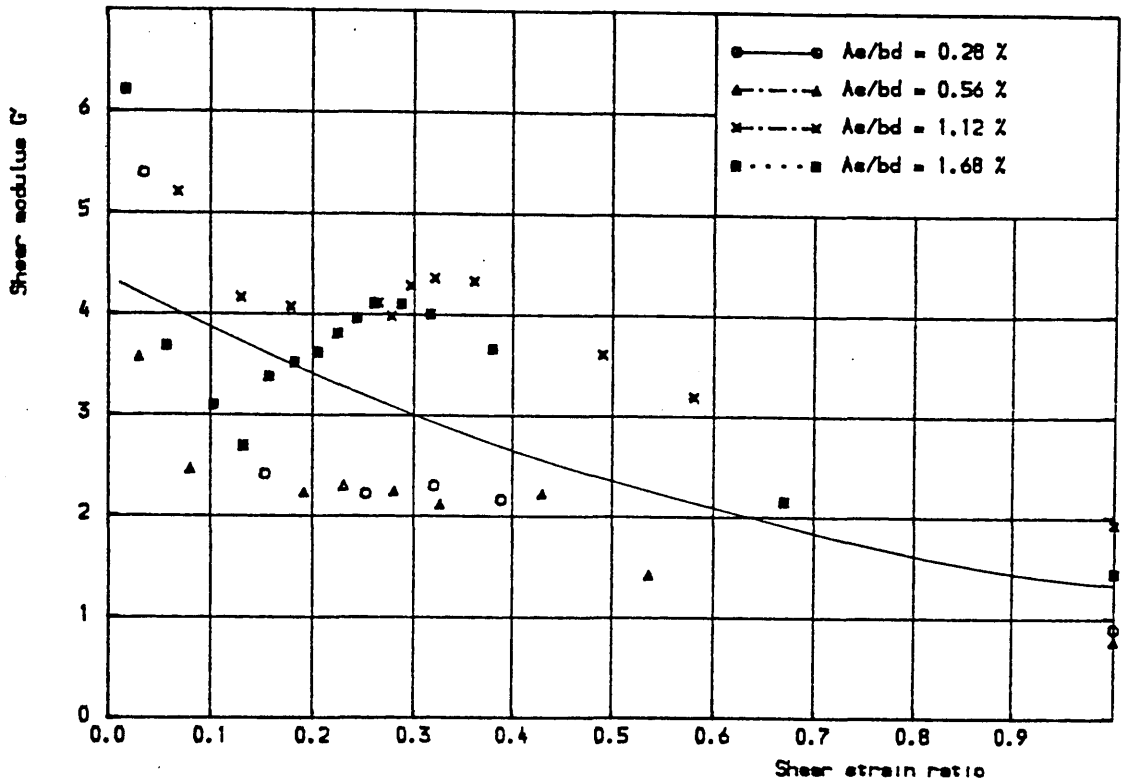

Figure(8.16) Shear modulus G' vs. shear strain for the comined action specimens with w_o = 0.125mm and high tensile deformed bars tested under repeated load,last cycle.

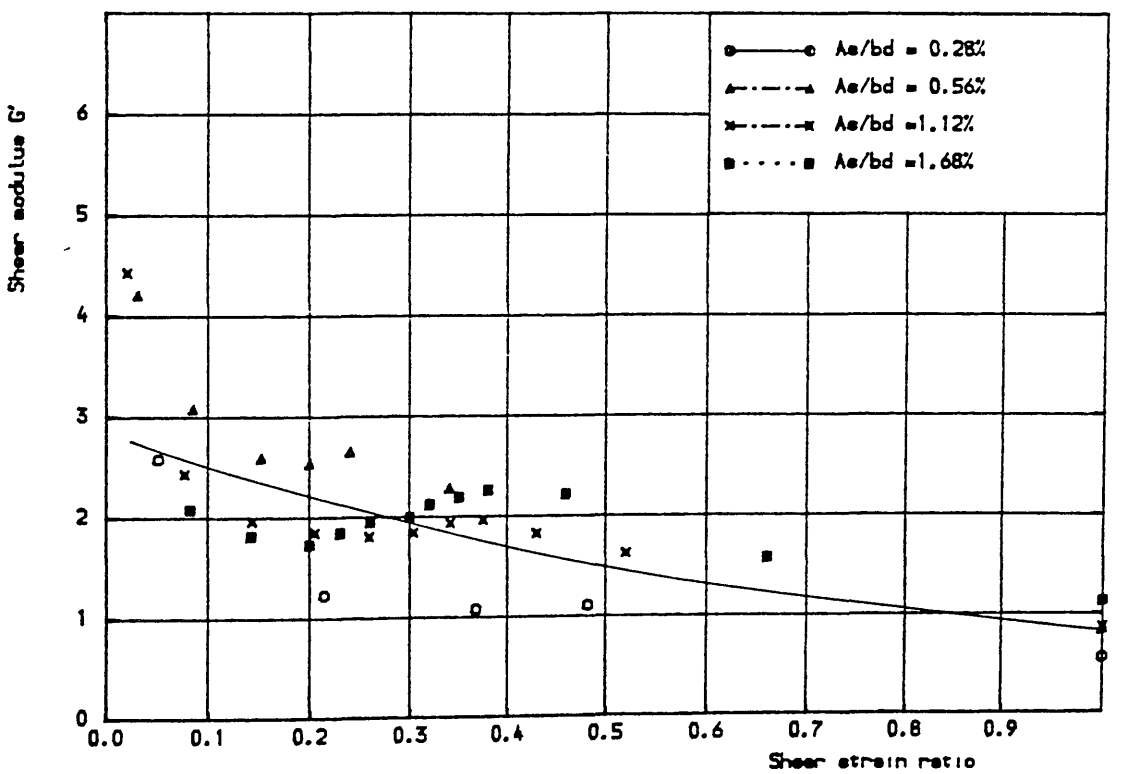

Figure(8.17) Shear modulus vs. shear strain for the combined action specimens with w_o = 0.40mm and high tensile deformed bars tested under repeated load,last cycle.

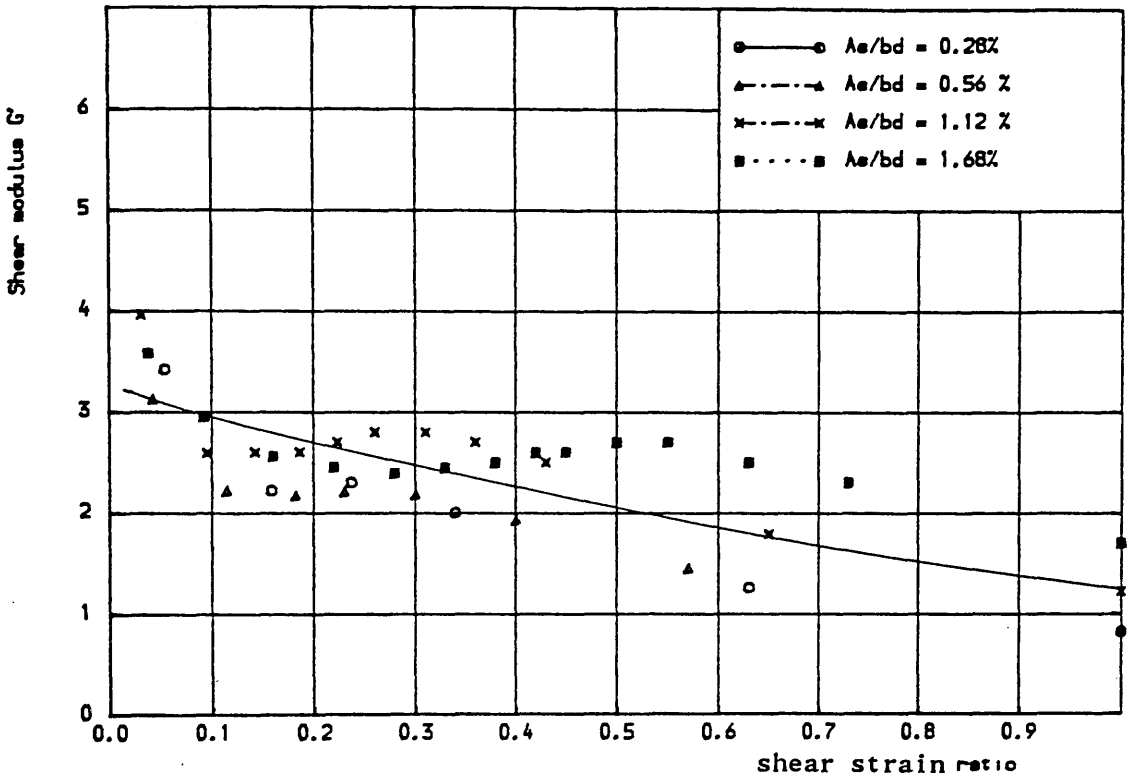

Figure(8.18) Shear modulus vs. shear strain for the combined action specimens with w_o = 0.125mm and mild tensile plain bars tested under repeated load,last cycle.

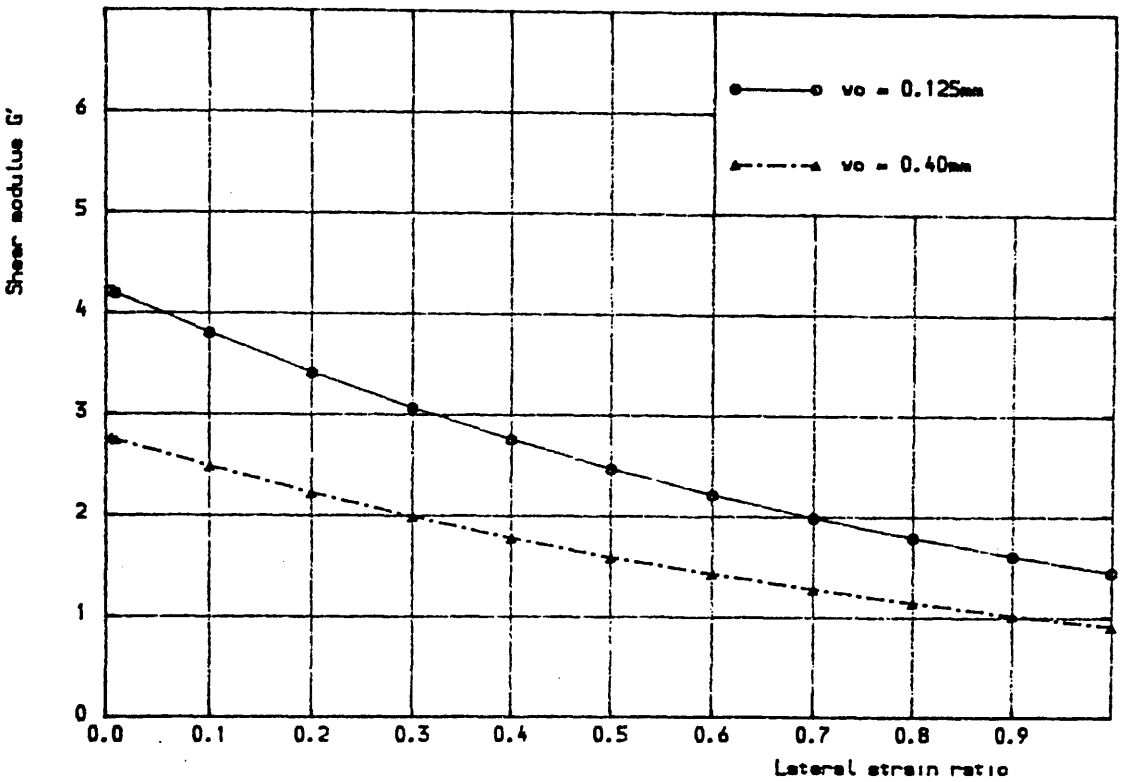

Figure(8.19) Effect of initial crack width (w_o) on shear modulus G' vs. lateral strain for the combined action under repeated load, last cycle.

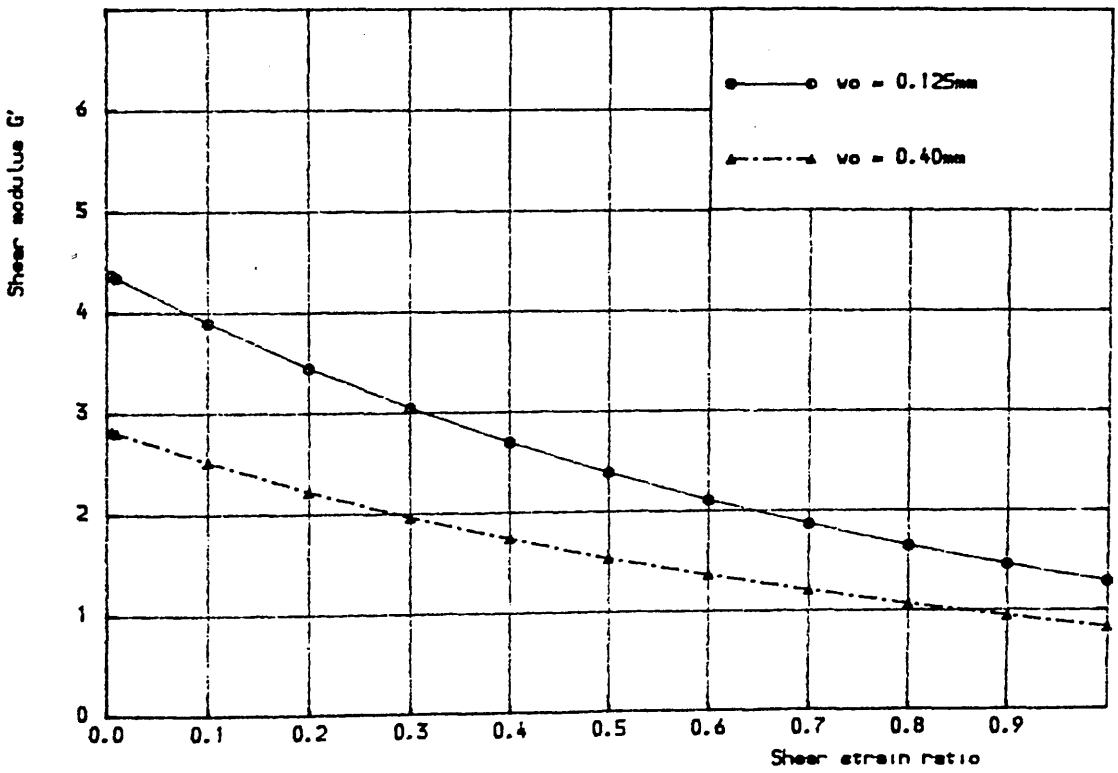

Figure(8.20) Effect of initial crack width (w_o) on shear modulus G' vs. shear strain for the combined action under repeated load, last cycle.

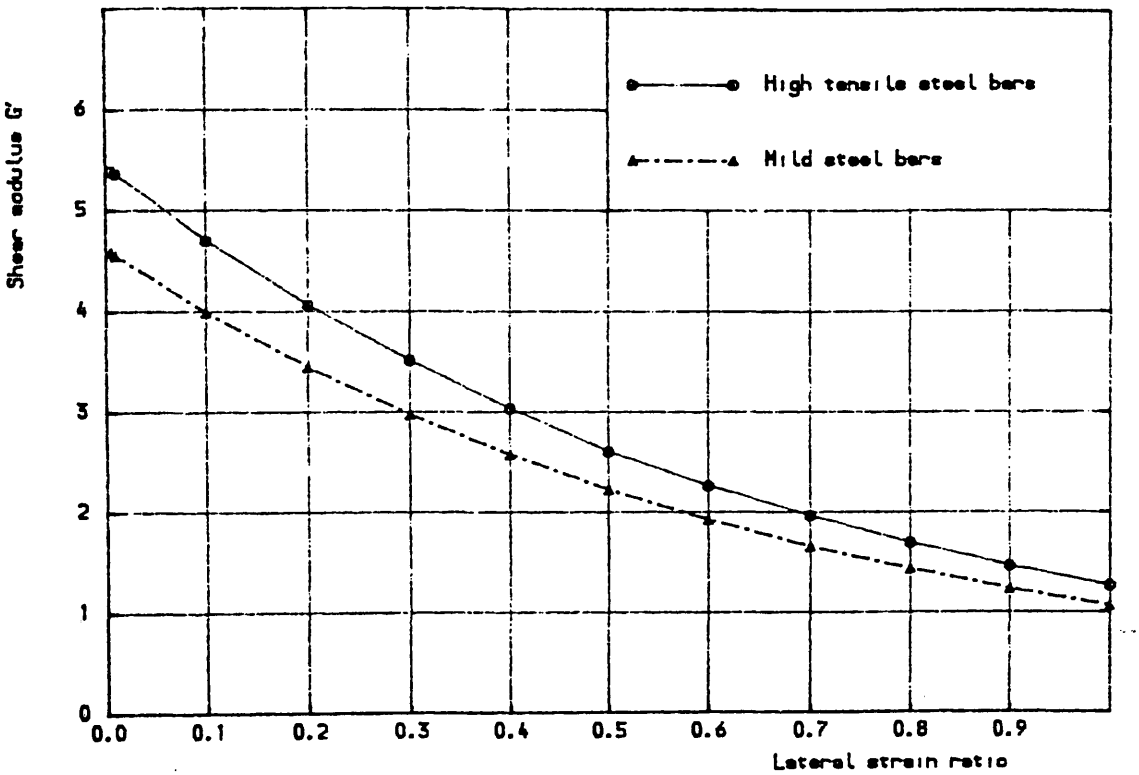

Figure(8.21) Effect of the transverse reinforcement type on shear modulus G' vs. lateral strain for combined action under monotonic load.

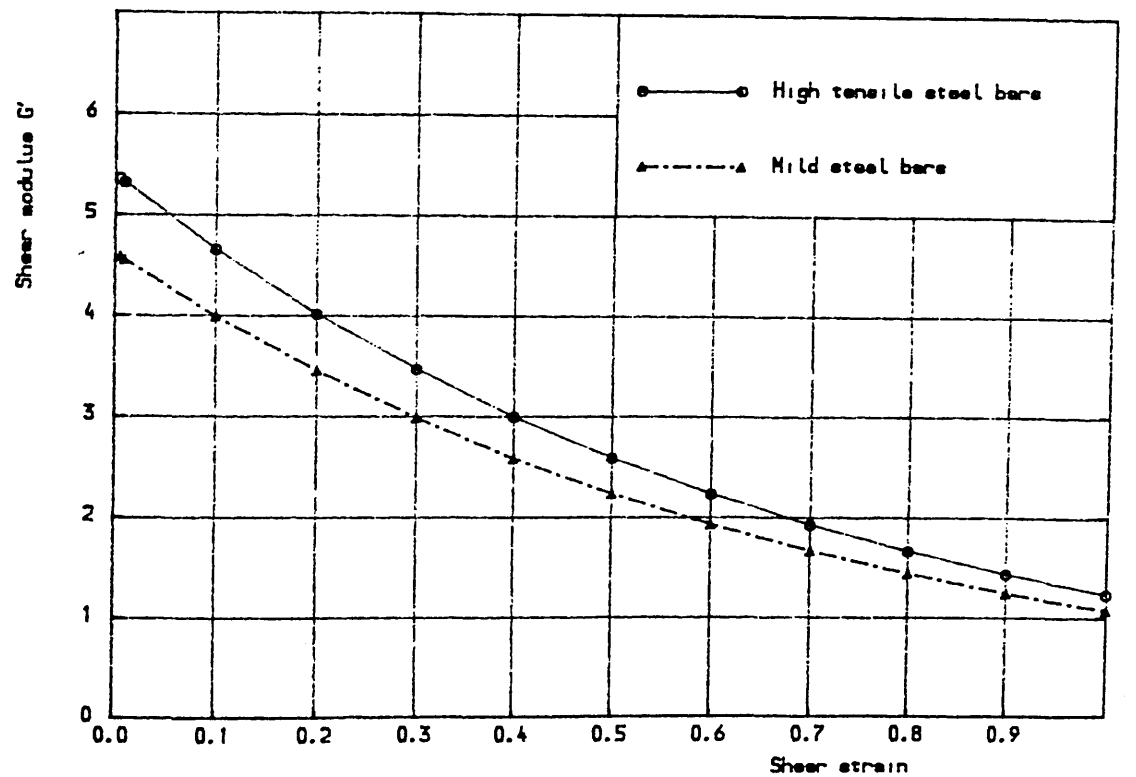

Figure(8.22) Effect of the transverse reinforcement type on shear modulus G' vs. shear strain for combined action under monotonic load.

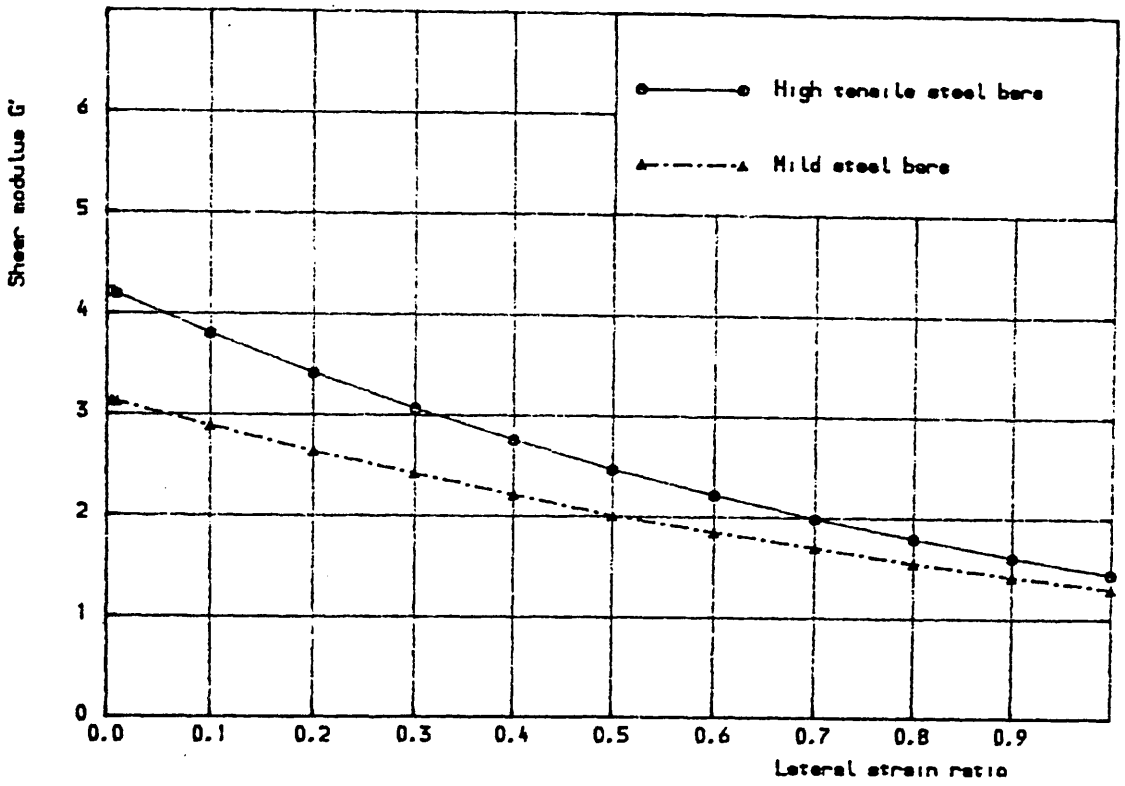

Figure(8.23) Effect of the transverse reinforcement type on shear modulus G' vs. lateral strain for combined action under repeated load, last cycle.

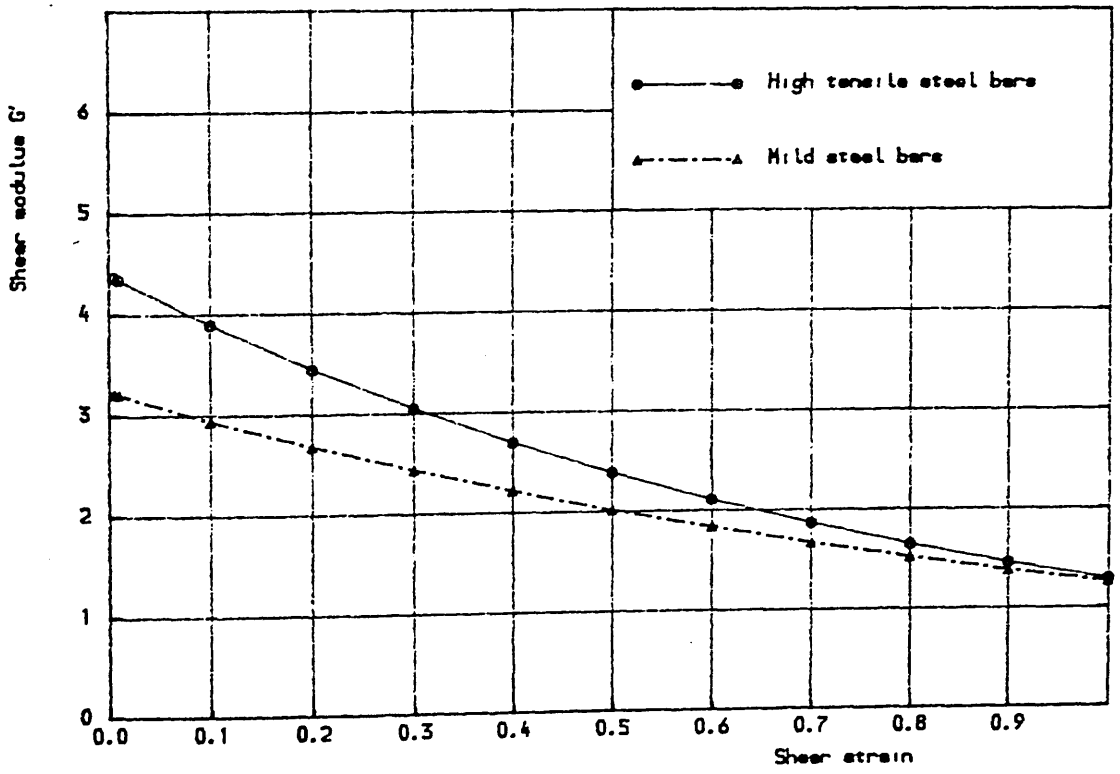

Figure(8.24) Effect of the transverse reinfocement type on shear modulus G' vs shear strain for combined action under repeated load, last cycle.

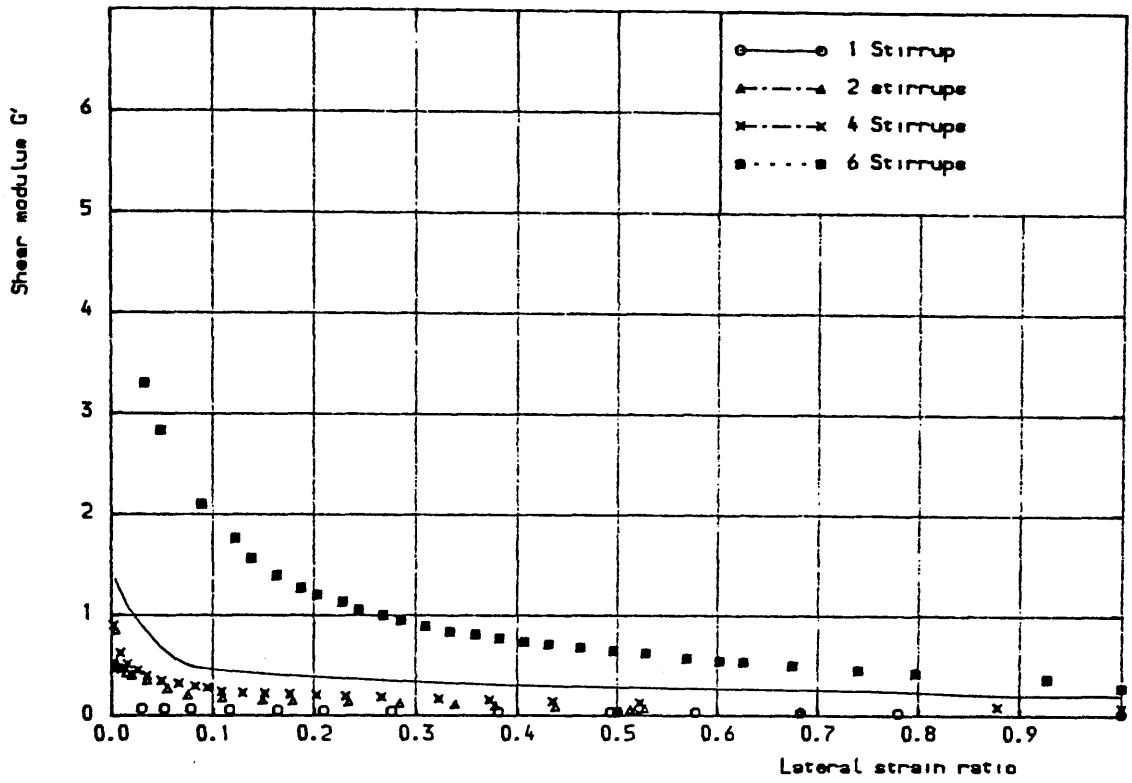

Figure(8.25) Shear modulus G' vs. lateral strain for dowel action specimens tested under monotonic load.

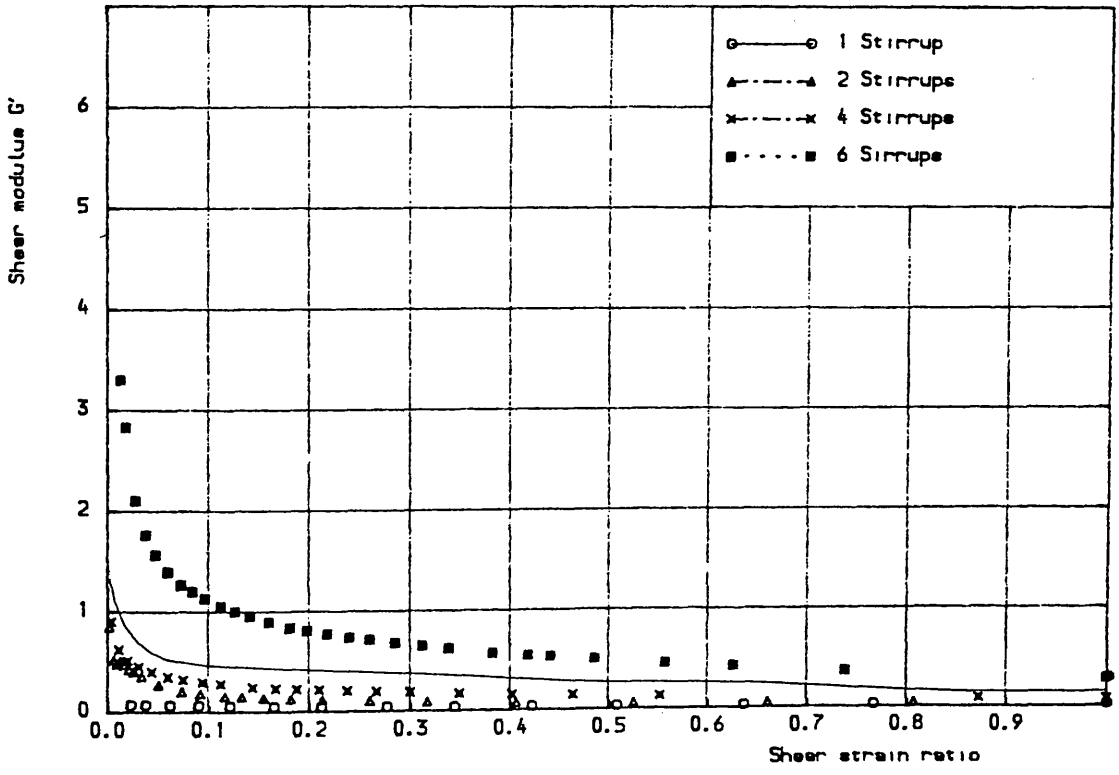

Figure(8.26) Shear modulus G' vs shear strain for dowel action specimens tested under monotonic load.

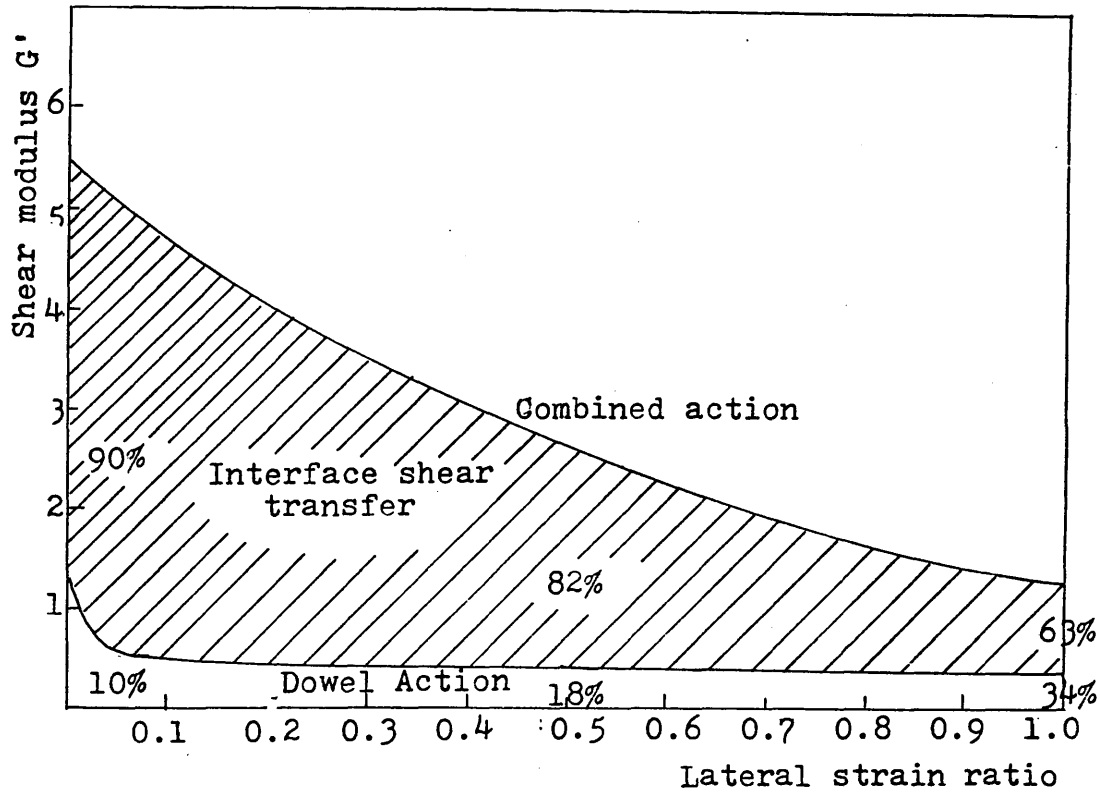

Figure(8.27) Relative contribution of interface shear transfer and dowel action to shear modulus G' of cracked section with w_o=0.125mm and reinforced with high tensile deformed bars.

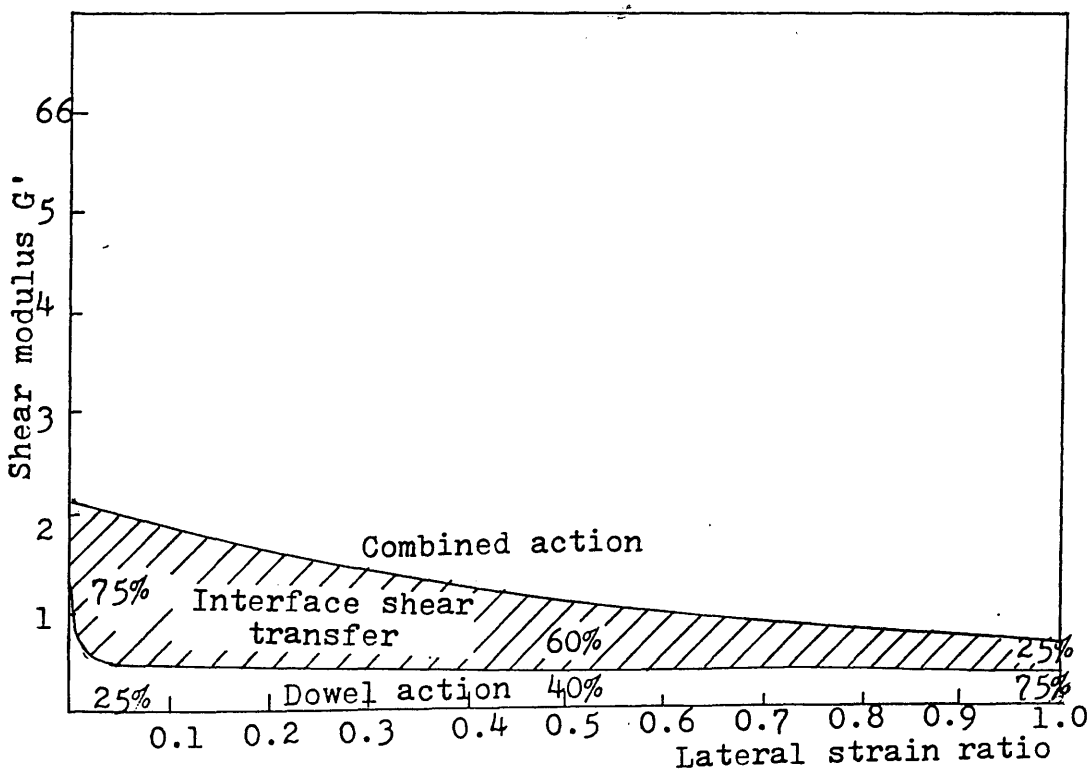

Figure(8.28) Relative contribution of interface shear transfer and dowel action to shear modulus G' of cracked section with w_o=0.40mm and reinforced with high tensile deformed bars.

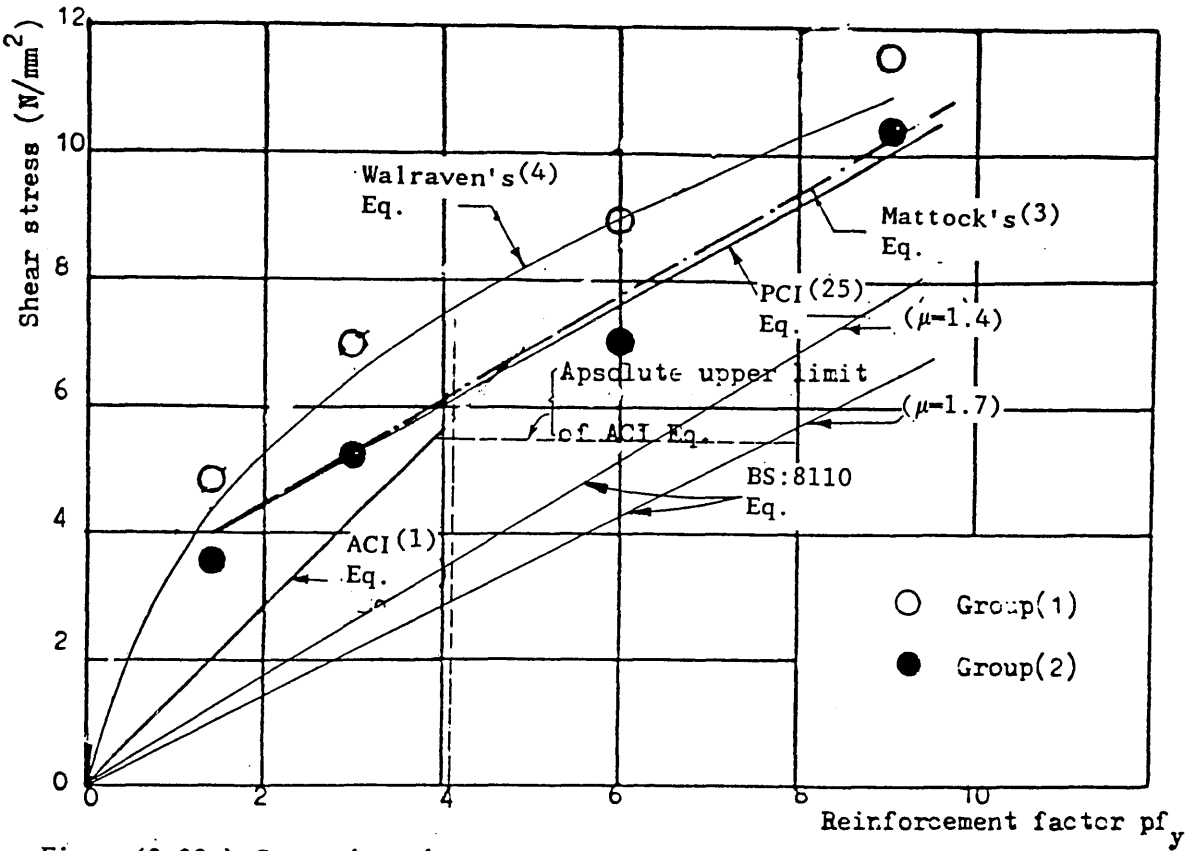

Figure(8.29a) Comparison between experimental ultimate shear stress for combimed action specimens with w_o=0.125mm & 0.40mm and high tensile deformed bars,and the calculated values according to References (1),(2),(3),(4)and(25)

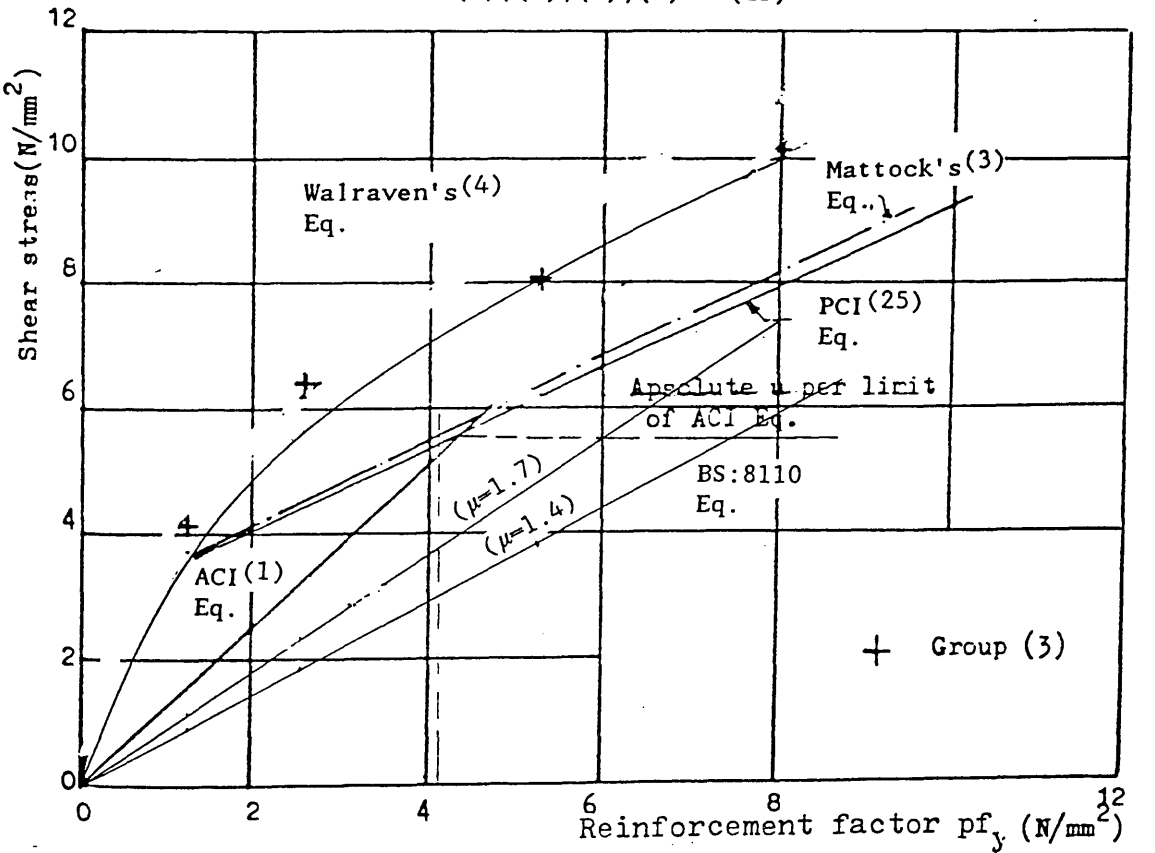

Figure(8.29b) Comparison between the experimental ultimate shear stress for combined action specimens with w_o=0.125mm and mild tensile plain bars ,and the calculated values according to References (1),(2),(3),(4),and (25).

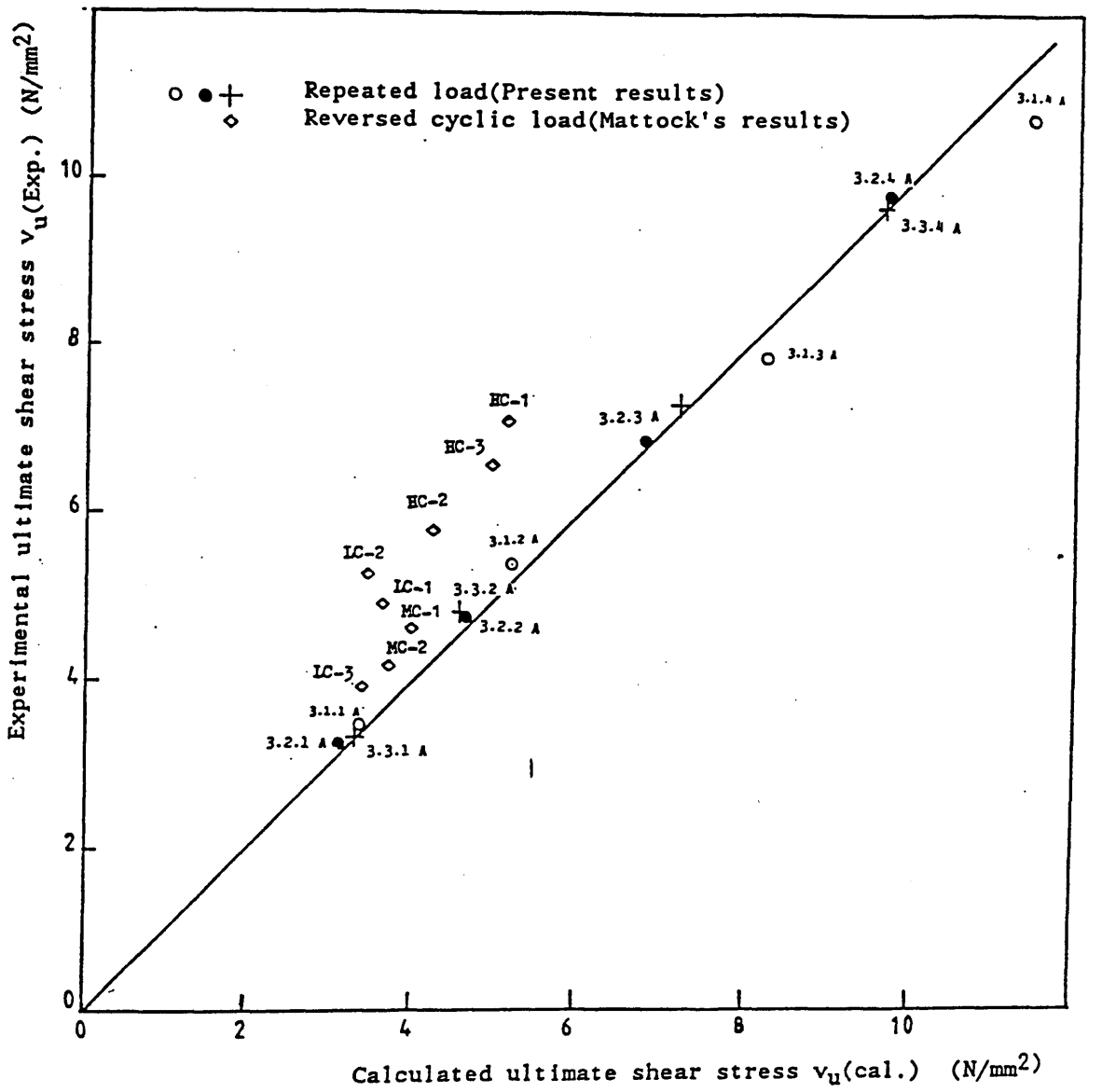

Figure(8.30) Comparison between the experimental results of this study & Mattock's[29] study and the calculated ult. shear transfer strength according to Equation (7.16)

REFERENCES

(1) Building Code Requirements for Reinforced Concrete, ACI 318-83, American Concrete Institute, 1983.

(2) British Standard Institution, BS:8110-1985, "British Standard Structural Use of Concrete", Part 1, Code of practice for design and construction, section 5.3.7.

(3) Mattock, A.H. and Hawkins, N.M., "Shear transfer in reinforced concrete-Recent Research", PCI Journal, Vol.17, March/April 1972.

(4) Walraven, J.C., "The behaviour of cracks in plain and reinforced concrete subject to shear", IABSE Colloquium, Delft 1981, Advanced Mechanics of Reinforced Concrete, pp.264

(5) Nilson, A.H., "Nonlinear analysis of reinforced concrete by the finite element method, "Journal of the American Concrete Institute, Vol.65, No.9, September, 1968.

(6) Ngo, D. and Scordelis, A.C., "Finite element analysis of reinforced concrete beams", Journal of the American Concrete Institute, Vol.64, No.3, March, 1967.

(7) Dulacska, H., "Dowel action of reinforcement crossing cracks in concrete", Journal of the American Concrete Institute, Vol.69, No.12, December, 1972.

(8) Walraven, J.C. "Aggregate interlock: a theoretical and experimental analysis", Delft University Press, 1980.

(9) Millard, S.G. and Johnson, R.P., "Shear transfer across cracks in reinforced concrete due to aggregate interlock and dowel action", Magazine of Concrete Research, Vol.36, No.126, March, 1984, pp.9-21.

(10)Fenwick, R.C. and Paulay, T., "Mechanism of shear resistance of concrete beams", Journal of the Structural Division, ASCE, Vol..94, No.ST10, Proceedings, paper 2325, October, 1968, pp.2325-2350.

(11)Houde, J. and Mirza, M.S., "A finite element analysis of shear strength of reinforced concrete beams", Shear in Reinforced Concrete, Vol.1, Special Publication SP-42, American Concrete Institute, Detroit, Michigan, 1974.

(12)Millard, S.G. and Johnson, R.P., "Shear transfer in cracked reinforced concrete", Magazine of Concrete Research, Vol.37, No.130, March, 1985.

(13)Franklin, H.A., "Non-linear analysis of reinforced concrete frames and panels", Dissertation, University of California, Berkeley, 1970.

(14)Isenberg, J. Adham, S., "Analysis of orthotropic reinforced concrete structures", Journal of the Structural Division, Proceedings of the ASCE, Vol.96, ST 12, December, 1970, pp.2607-2624.

(15)Cervenka, V., "Inelastic finite element analysis of reinforced concrete panels under in-plane loads", Doctor Thesis, University of Colorado, 1970.

(16)Loov, R., "The determination of stresses and deformations of reinforced concrete after cracking", Proceedings of the Southampton 1969 Civ. Eng. Materials Conference, pp.1257-1260.

(17)Hand, F.R., Pecknold, D.A., Schnobrich, W.C., "Non-linear layered analysis of RC plates and shells" Journal of the Structural Division, ASCE, Vol.99, ST 7, Proc. Paper 9860, July, 1973.

(18)Suidan, M. Schnobrich, W.C., "Finite element analysis of reinforced concrete", Journal of the Structural Division, Proceedings of the ASCE, Vol.99, No. ST 10, October, 1973, pp.2109-2122.

(19)Zienkiewics, O.C., Phillips, D.V., Owen, P.R.J., "Finite element analysis of some concrete non-linearities - Theory and examples", Proceedings of the Seminar "Concrete structures subjected to triaxial stresses", May, 1974, Bergamo, Italy.

(20)Yuzugullu, O., Schnobrich, W.C., "A numerical procedure for the determination of the behaviour of a shear wall frame system", ACI—Journal, Proceedings, Vol.70, No.7, July, 1973, pp.474-479.

(21)Cedolin, L., Dei Poli, S., "Finite element studies of shear critical reinforced concrete beams", Journal of the Engineering Mechanics Division, EM 3, June 1977, pp.395-410.

(22)Al-Mahaidi, R.S.H., "Nonlinear finite element analysis of reinforced concrete deep members", Rep. No.79-1, Cornell University, Ithaca, New York, 1979.

(23)Mohamed, M.S., "A finite element and experimental study of reinforced concrete in torsion", Ph.D. Thesis, University of Glasgow, 1986.

(24)Phillips, D.V., Mohamed, M.S., "Analysis of reinforced concrete beams in torsion" Proc.2nd. Int. Conf. on Civil Engineering computing, Vol.2, Institution of Civil Engineering, London 1985, pp.305-311.

(25)"PCI Design Handbook", Prestressed Concrete Institute, 1971.

(26)Birkland, P.W., Birkland, H.W., "Connect in Precast concrete construction", Journal of the American Concrete Institute, Proceedings, Vol.63, No.3, March, 1966.

(27)Walraven, J.C., Vos, E., Reinhardt, H.W., "Experimental on shear transfer in cracks in concrete. Part I:Description of results", Report No.5-79-3, January, 1979, Stevin Laboratory, Delft University of Technology, The Netherlands.

(28)Mattock, A.H., "Effect of aggregate type on single direction shear transfer strength in monolithic concrete", Report SM 74-2, Department of Civil Engineering, University of Washington, Seattle, Washington, August, 1974.

(29)Mattock, A.H., "The shear transfer behaviour of cracked monolithic concrete subject to cyclically reversing shear", Report No.SM 74-4, Department of Civil Engineering, University of Washington, Seattle, Washington, November, 1974.

CHAPTER (9)

CONCLUSIONS AND RECOMMENDATIONS FOR FUTURE WORK

9.1 Introduction

In this final chapter conclusions made within previous chapters are summarized together and will be presented under the following categories: (1) Shear transfer by dowel action alone and (2) by the combined mechanisms of dowel action and interface shear transfer. Finally, recommendations for future work are given.

9.2 Dowel action

9.2.1 Monotonic load

1. The experimental scatter in the test results was quite small and the test results were repeatable.

2. Flexure of dowel bars is the dominant mechanism of dowel action. The maximum moment is produced at a distance less than 1.25 bar diameter from shear plane. At shear load greater than 0.80 of the ultimate dowel load and up to the failure the kinking mechanism also played a more significant role and participates in resisting shear force.

3. The beam on an elastic foundation model is only adequate to describe the initial stage of dowel action behaviour.

4. Equation (2.17) proposed by Millard and Johnson showed that an exponential function is a better assumption to represent the dowel load-displacement relationship.

5. A new formulation to describe the overall behaviour of dowel action was proposed by the author and was based on idealizing the dowel load-displacement relationship to a quadrilinear curve. This compared well with the results of this investigation.

6. An increase in the reinforcement ratios of the dowel bars resulted in an increase in both dowel stiffness and ultimate dowel force.

7. The ultimate dowel force is reasonably predicted by the proposed semi-empirical equation (7.5), which was originally derived from the understanding of the internal mechanisms of dowel action, and the empirical equation (7.6) which obtained from the regression analysis of the test results. Both equation (7.5) and (7.6) can be used when failure occurs due to yielding of dowel bars.

9.2.2 Repeated load

1. The dominant modes of dowel action changes according to the magnitude of the applied shear loads, number of load cycles and the condition of concrete surrounding the dowel bars.

2. According to the history of repeated load used in this study the ultimate dowel force was approximately 0.6-0.80 of that under monotonic load.

3. The increase in reinforcement ratio resulted in a greater increase in the ultimate dowel force under repeated load compared with the monotonic loading. This increase was approximately 20% on average.

4. Dowel action behaviour under repeated load exhibited a close similarity to that under reversible cyclic load.

9.3 Combined action

9.3.1 Monotonic load

1. The scatter in the test results was small and tests were repeatable.

2. During the initial stages up to approximately 0.65 of the ultimate shear load (V_U) the majority of shear force is resisted by interface shear transfer. At higher shear loads interface shear transfer deteriorates and dowel action develops.

3. The interface shear transfer mechanism results in an increase in tensile strain at the transverse reinfordcement and a reduction in the flexural strain.

4. The idealized shear load-shear displacement proposed by the author showed reasonable agreement with test results of other investigations.

5. The initial crack width and the reinforcement ratio had a significant influence on the overall shear behaviour and on the

ultimate shear transfer strength.

6. The type of transverse reinforcement showed smaller effect on shear transfer behaviour and ultimate shear strength compared with that of initial crack width and reinforcement ratio.

7. The influence of initial crack width decreased with the increase of transverse reinforcement.

8. The reinforcement ratio exhibited a greater effect on shear stiffness during the nonlinear stage.

9. The bond condition between transverse reinforcing bars and the surrounding concrete has a smaller effect on interface shear transfer mechanisms compared to that of dowel action.

10. The relative contribution of dowel action and interface shear transfer mechanisms to the total shear transfer is significantly influenced by initial crack width and reinforcement ratio. The type of transverse reinforcement exhibited insignificant effect.

11. The increase in initial crack width and reinforcement ratio resulted in a reduction in the contribution of interface shear transfer and an increase in the dowel action contribution.

12. The relative contribution of dowel action and interface shear transfer mechanisms ranges between 20-35% and 80-65% respectively depends mainly on the initial crack width and reinforcement ratio.

13. The current method of BS : 8110 and ACI 813-83 gave a too conservative ultimate shear transfer strength. Other available equations were partially satisfactory in predicting the test results in this study.

14. Equation (7.14) proposed by the author to calculate ultimate shear strength showed good agreement with other available experimental results.

15. Shear retention factor can be presented in a nonlinear relationship as a function of lateral or shear strain.

9.3.2 Repeated load

1. The behaviour of the first load cycle is different from the second and subsequent cycles. For the first cycle behaviour is approximately linear. Response to the second and subsequent cycles is charaterized by a higher shear stiffness at low load level and a gradual decrease with the increase of the applied load.

2. The increase in reinforcement ratio results in an increase in shear stiffnesses at the different load cycles and ultimate shear transfer strength.

3. The reinforcement ratio seems not to have a significant effect on the ultimate shear transfer strength if the maximum applied repeated load is varied within a range less than 0.75 V_U and the number of load cycles as used in this study.

4. The reduction of initial crack width results in an increase in both the shear stiffnesses measured at maximum repeated load and the ultimate shear transfer strength.

5. The increase in reinforcement ratio had a smaller influence on the ultimate shear transfer strength with small initial crack width compared with large initial crack width.

6. Similar to monotonic load, the use of mild tensile plain bars instead of high tensile deformed bars did not show signficiant effect on shear stiffnesses or utlimate shear transfer strength.

7. A general Equation (7.16) was proposed by the author to assess the utlimate shear transfer strength under both monotonic and repeated load. At the present time this equation can be used if maximum repeated load is less than 0.75 of the ultimate shear transfer strength under monotonic load. This equation also showed its applicability to predict the ultimate shear strength under reversed cyclic load.

8. The ultimate shear transfer strength under the history of repeated load used here can be taken as 0.7-0.9 of V_U under monotonic load. However this depends principally on the initial crack width and reinforcement ratio.

9. The relative contribution of interface shear transfer and dowel action mechanisms to the total shear transfer strength is not significantly influenced by the type of transverse reinforcement and initial crack width. The contribution of dowel action and

interface shear transfer mechanism ranged between 15-24% and 85-76% respectively.

10. A qualitative similarity was found between shear transfer behaviour under repeated and reversed cyclic load.

9.4 Recommendation for future work

1. The present study revealed the sensitivity of steel strain measurements. The technique used here gave satisfactory measurements under monotonic load, but for more complicated shear loads, such as repeated loading, it could not be guaranteed to give full measurements for the whole history of loading, especially near to or at the shear plane. This was due to the redistribution of the stresses and changes in the bond condition between the steel bars and the surrounding concrete effecting the performance of the gauges. Also the fibres of the steel bar could be subjected to both tensile and compressive stresses, a condition which many types of strain gauges have difficulty in coping with. Therefore it would be worthwhile investigating other methods for measuring the steel strains so that more precise information can be obtained regarding the distribution of stresses in the bars, and the way they change under varying load conditions.

2. Further experimental work would be useful to confirm the validity of the idealized shear load versus shear displacement relationships under monotonic load, particularly for dowel action alone and to extend their limitations to include other additional

parameters such as different bar diameters, bar spacing, concrete cover, and variation in reifnorcement axial stresses.

3. In this study shear transfer under repeated loading was investigated for a regular history of loading, i.e. constant maximum repeated load for a fixed number of cycles. Further study is important which examines the variation in the magnitude of cyclic shear and the number of cycles. Thus it might be possible to establish a unified theoretical model which can predict overall behaviour, for a wider range of loading histories and which includes monotonic loading as a special case of cyclic loading.

4. The degradition of shear stiffness for cracked reinforced concrete had been investigated in this tudy for two different initial crack widths of 0.125 mm and 0.40 mm and reinforcement ratios ranging between 0.28% and 1.68%. Further investigation to assess the reduction in the shear stiffness once crack occurs in reinforced concrete would be a useful continuation of this study for modelling shear transfer in the finite elment method.

5. In general the study of shear transfer across cracks in reinforced concrete needs extending to include more complex situations such as cracking oblique to the reinforcement and cracks and reinforcement in two directions, particularly under repeated or reversed cyclic loading.